

# Defining dosimetry and implications for aerosol presentation for non-clinical development of respiratory drugs

A thesis submitted in accordance with the  
conditions governing candidates for the  
degree of

Philosophiae Doctor in Cardiff University

by

Graham R. Paul

December 2017

Cardiff School of Pharmacy and  
Pharmaceutical Science

Cardiff University

## ACKNOWLEDGEMENTS

I thank my supervisors Prof. Mark Gumbleton, Dr Graham Somers (GSK) and Prof. Glyn Taylor (retired) for their guidance during this project and GSK for sponsoring and resourcing this research.

I am grateful to colleagues for their technical assistance and expertise, who are too numerous to mention individually. Whilst I hereby confirm the designs of experiments, pre-treatment aerosol generation work and interpretation of all data are my own work, as too was single inhalation exposure of rats with associated head-out plethysmography, I am nevertheless indebted to colleagues for their contributions as follows:

- *DDS-NCE-MD* for physicochemical data and Chris Luscombe for his help with principal component analysis of these data (Chapter 2).
- Paula Chaffin and Thoralf Hartwig (*PDS-PPE-PSE*) for spray dried production of amorphous GSK-899.
- *PDS-ASD-PhysProps* for SEM of particles (Chapter 2).
- Martin Hingle (*PDS-DPDD*) for *in vitro* dissolution tests (Chapter 2).
- *IVSD* for formulations and analysis, help with pre-treatment aerosol trials, husbandry, licensed procedures e.g. repeat inhalation exposure (Chapter 5) and blood sampling; Doug Ball for LPS dosing (Chapter 4).
- *BIB/TBM* for bioanalysis of drug in blood/plasma and lung.
- Peter Marshall for MALDI-MSI of lung sections (Chapter 2).
- EMMS for loan of head-out plethysmography apparatus and Charles River Edinburgh for training in plethysmograph restraint (Chapter 3).
- Mike Denham for advice on statistical methods (Chapter 3) and Mark Lennon for determination of ED<sub>50</sub> values for efficacy (Chapter 4).
- *TMCP-CPD* for neutrophil counts and TNF $\alpha$  analyses (Chapter 4).
- *TMCP-Histology* for necropsies, histology (Chapters 2 to 5) and lung image analysis (Chapter 4); *Ex Vivo Bioimaging* for TEM (Chapter 5).
- *MSD-ISDM* for *in vitro* assay of particles in NR-8383 cells (Chapter 5).
- *Exploratory Biomarkers (US)* for lung image analysis (Appendix 10).
- *TMCP-Pathology* for evaluation of tissue sections by light microscopy and help in compiling figures (Chapter 5).

Dedicated to my mother, Doreen Paul, who died soon after submission of this thesis. Thanks to my family: Lynn Cook for her support on the home front, Thomas and Belinda (who changed so much during this project) and Pepé for being a welcome distraction. Thanks also to my parents Doreen (“flying free” and dearly missed) and Keith, my brother Martin and sister-in-law Goy for their encouragement throughout.

*Ignis aurum probat*

## ABSTRACT

Strategies for expediting preclinical development of drugs include using alternative (different to clinical) formulations or exposure routes to reduce compound usage. This may alter pharmacokinetics and hence efficacy and/or toxicopathology compared with the final formulation. Three p38 mitogen-activated kinase inhibitors (similar *in vitro* potency) with different physicochemical properties were administered to rats as dry powder or nebulised aerosols to investigate the influence of changes in particulate form on *in vivo* endpoints.

When rats settled in restraint tubes before aerosol administration, inhaled doses calculated from lung function measurements were consistent with values derived from body weights using a published algorithm. Drug-lung deposition was 12% of the inhaled dose, correlating with the rat deposition fraction (10%) used by US-FDA officials when reviewing regulatory submissions.

Drug persistence (GSK-899) in rat lung was associated with increased efficacy (inhibition of lipopolysaccharide-induced inflammation) four hours post challenge, compared with two readily absorbed drugs. However, administration of GSK-899 at a higher dose for 28 days resulted in accumulation of drug and alveolar macrophage aggregates in lungs with infiltration of neutrophils, a consequence of accumulating 'nuisance particles' and mild irritancy by GSK-899. GSK-361 (lipophilic; membrane permeable) resulted in lower lung exposure and efficacy, and no lung toxicopathology. Repeating experiments with compounds of different pharmacologies would confirm if these physicochemical properties support general trends for inhaled drugs or represent standalone results for these molecules. Changing aerosol form did not fundamentally change the nature of toxicopathology but presented technical limitations for evaluating the dose response.

This thesis demonstrated changes in aerosol form could modulate dose response without changing the nature of toxicopathology. Membrane permeability had a more profound effect on lung clearance and toxicopathology than aqueous solubility. Given technical limitations for drugs of low aqueous solubility, the aerosol form intended for clinical formulations should be used in early preclinical studies.

# TABLE OF CONTENTS

Declaration.....	ii
Acknowledgements.....	iii
Abstract.....	v
Table of Contents.....	vi
List of Tables.....	xi
List of Figures.....	xv
List of Abbreviations.....	xxii
Glossary of Terms.....	xxvi
<b>1. General introduction</b>	
1.1. Introduction.....	2
1.2. The respiratory tract.....	2
1.2.1. Proximal conductive airways.....	3
1.2.2. Distal respiratory region (lungs).....	10
1.2.3. Macrophages.....	11
1.3. Drug delivery devices.....	12
1.4. Challenges in non clinical lung delivery and respiratory drug development.....	16
1.4.1. Regulatory testing of drugs.....	18
1.4.2. Animal models for investigating efficacy.....	21
1.4.3. Animals and ethics in scientific research.....	22
1.4.4. Exposure of animals to inhaled materials and common practices in drug development.....	27
1.4.5. Animal exposure and understanding dosimetry.....	38
1.4.6. Fate of molecules post inhalation exposure.....	40
1.5. Chronic Obstructive Pulmonary Disease.....	45
1.5.1. p38 mitogen activated protein kinase inhibitors.....	46
1.6. Thesis aims and objectives.....	48
<b>2. Multivariate based selection of p38 mitogen-activated protein kinase inhibitors and investigation of pharmacokinetics in rats following a single inhalation exposure</b>	
2.1. Introduction.....	52
2.1.1. Principal component analysis of physicochemical properties of compounds.....	53
2.1.2. Aims and objectives.....	55
2.2. Materials and methods.....	57
2.2.1. Principal component analysis of the physicochemical properties of six p38 MAPK inhibitors.....	57
2.2.2. Test articles.....	61
2.2.3. Dissolution rates of p38 MAPK inhibitors in simulated lung fluid....	62
2.2.3.1. Sample preparation for dissolution testing.....	62
2.2.3.2. Preparation of simulated lung fluid.....	63
2.2.3.3. Evaluation of dissolution.....	63
2.2.4. Investigating the pharmacokinetics of p38 MAPK inhibitors in rats after a single inhaled dose.....	65

2.2.4.1.	Test system and animal husbandry .....	65
2.2.5.	Aerosol Generation and formulation details .....	66
2.2.5.1.	Dry powder formulations of p38 MAPK inhibitors.....	67
2.2.5.2.	Generation of dry powder aerosols of p38 MAPK inhibitors.....	68
2.2.5.3.	Liquid formulations of p38 MAPK inhibitors .....	69
2.2.5.4.	Nebulisation of droplet aerosols .....	72
2.2.5.5.	Rodent inhalation exposure system.....	73
2.2.5.6.	Aerosol characterisation .....	76
2.2.5.7.	Calculation of the estimated inhaled dose .....	82
2.2.5.8.	Pharmacokinetic profiling of p38 MAPK inhibitors in blood/plasma and lung.....	82
2.2.5.9.	Analysis of drug lung distribution by matrix assisted laser desorption/ionization (MALDI).....	85
2.3.	Results and discussion.....	87
2.3.1.	Principal component analysis of the physico chemical parameters of six p38 MAPK inhibitors .....	87
2.3.2.	X-ray powder diffraction of amorphous GSK-899 .....	95
2.3.3.	In vitro dissolution of p38 MAPK inhibitors.....	96
2.3.4.	Selection of p38 MAPK inhibitors for in vivo investigation of pharmacokinetics.....	97
2.3.5.	Scanning electron microscopy of particles.....	99
2.3.6.	Pharmacokinetics of p38 MAPK inhibitors in rats following a single inhaled dose .....	103
2.3.6.1.	Inhalation exposure of rats to p38 MAPK inhibitors and estimation of the inhaled dose .....	103
2.3.6.2.	Systemic and pulmonary pharmacokinetics and lung distribution of p38 MAPK inhibitors in rats.....	107
2.4.	Conclusion .....	125
<b>3.</b>	<b>Estimation of inhaled doses in rats from lung function data and refinement of tube restraint in scientific procedures</b>	
3.1.	Introduction .....	130
3.1.1.	Aims and objectives .....	132
3.2.	Materials and methods .....	133
3.2.1.	Head-out plethysmography and data capture of lung function measurements.....	133
3.2.2.	Investigating lung function and dosimetry in rats .....	134
3.2.2.1.	Preliminary analysis of lung function data.....	135
3.2.3.	Test system and animal husbandry .....	135
3.2.4.	Method acquisition (Design 1) .....	136
3.2.4.1.	Investigating lighting colour during tube restraint.....	138
3.2.4.2.	Statistical analysis of lung function data .....	139
3.2.4.3.	Methodological outcomes of Design 1 .....	139
3.2.5.	Colour of lighting and duration of acclimatisation protocols for tube restraint (Design 2) .....	139
3.2.5.1.	Data analysis of measured and body weight derived estimates of minute volume .....	142
3.2.5.2.	Data analysis of estimated lung deposited dose and measured drug-lung concentrations .....	142

3.2.5.3.	Statistical analysis of lung function data and drug-lung concentration in lung tissue.....	142
3.2.5.4	Methodological outcomes of Design 2 .....	143
3.2.6.	Settling rats before aerosol administration (Design 3) .....	143
3.2.6.1.	Statistical analysis of lung function data and drug-lung concentration in lung tissue.....	145
3.2.6.2.	Methodological outcomes of Design 3 .....	146
3.2.7.	Incorporation of lung function measurements into repeat-dose inhalation studies (Design 4).....	146
3.2.7.1	Statistical analysis of lung function data .....	147
3.2.8.	Aerosol generation of p38 MAPK inhibitors and inhalation exposure of rats .....	148
3.2.8.1.	Test articles.....	149
3.2.8.2.	Aerosol Generation and formulation details .....	149
3.2.8.3.	Aerosol characterisation .....	150
3.3.	Results and discussion.....	152
3.3.1.	Breath frequency and minute volume of rats restrained in tubes .	152
3.3.1.1.	Influence of lighting colour and duration of tube acclimatisation on breath frequency and minute volume of rats .....	157
3.3.1.2.	Breath frequency and minute volume of rats allowed to settle before aerosol administration.....	160
3.3.2.3.	Effect of neck restraint on breath frequency and minute volume of rats during repeat dose studies .....	163
3.3.2.	Relationship between measured minute volume and pre exposure body weight .....	169
3.3.3.	Comparison of measured lung concentrations and estimated pulmonary doses .....	172
3.4.	Conclusion .....	179
<b>4.</b>	<b>Suppression of lipopolysaccharide induced acute lung inflammation in rats by single prophylactic doses of p38 mitogen activated protein kinase inhibitors</b>	
4.1.	Introduction .....	184
4.1.1	Aims and objectives .....	188
4.2.	Materials and methods .....	190
4.2.1.	Test articles.....	190
4.2.2.	Investigating efficacy and exposure of inhaled p38 MAPK inhibitors in rats.....	191
4.2.2.1.	Efficacy of GSK-899 determined using neutrophil counts in BALF (Design A).....	193
4.2.2.2.	Evaluation of endpoints used to determine inhibition of lung inflammation by GSK-677 (Design B) .....	194
4.2.2.3.	Efficacy of GSK-899 measured using lung image analysis (Design C) .....	196
4.2.2.4.	Efficacy of GSK-361 using neutrophil counts in BALF and lung image analysis (Design D) .....	196
4.2.3.	Test system and animal husbandry .....	197
4.2.4.	Aerosol generation of p38 MAPK inhibitors and inhalation exposure of rats .....	197

4.2.4.1.	Dry powder formulations of p38 MAPK inhibitors.....	198
4.2.4.2.	Liquid formulations of p38 MAPK inhibitors .....	199
4.2.4.3.	Aerosol Generation and formulation details .....	201
4.2.4.4.	Inhalation exposure of rats .....	201
4.2.4.5.	Aerosol characterisation .....	201
4.2.4.6.	Calculation of the estimated inhaled dose .....	203
4.2.5.	Antigen challenge of rats .....	203
4.2.6.	Assessment of biomarkers for lung inflammation .....	204
4.2.6.1.	Bronchoalveolar lavage of lungs for analysis of TNF $\alpha$ and/or cell counts (Designs A, B and D) .....	204
4.2.6.2.	Lung sampling and processing for image analysis .....	205
4.2.6.3.	Determination of the 50% effective dose (ED50) for inhibition of LPS-induced lung inflammation .....	210
4.2.7.	Bioanalysis of p38 MAPK inhibitors in rat plasma and lung .....	210
4.2.7.1.	Plasma sampling for analysis of p38 MAPK inhibitors .....	210
4.2.7.2.	Lung sampling for homogenisation and analysis of p38 MAPK inhibitors .....	211
4.3.	Results and discussion.....	212
4.3.1.	Inhalation exposure of rats to p38 MAPK inhibitors .....	212
4.3.2.	Temporal variability of rat neutrophils in BALF four hours after an LPS challenge.....	216
4.3.3.	Pulmonary and systemic exposure of rats to GSK-677 and endpoints for investigating inhibition of acute lung inflammation (Design B).....	220
4.3.4.	Pulmonary and systemic exposure of rats to GSK-899 and inhibition of inflammation .....	226
4.3.5.	Pulmonary and systemic exposure of rats to GSK-361 and inhibition of inflammation (Design D).....	232
4.4.	Conclusion .....	236
<b>5.</b>	<b>Toxicopathology of p38 mitogen-activated protein kinase inhibitors in rats after inhalation of fixed doses for 28 days</b>	
5.1.	Introduction .....	242
5.1.1	Aims and objectives .....	244
5.2.	Materials and methods .....	246
5.2.1.	Test articles.....	246
5.2.2.	In vitro cytotoxicity and morphology of NR8383 rat macrophage cells incubated with particles.....	246
5.2.2.1.	Treatment of cells to investigate cytotoxicity and release of inflammatory cell mediators .....	247
5.2.2.2.	Analysis of cytotoxicity by measurement of lactate dehydrogenase leakage from treated cells.....	248
5.2.2.3.	Analysis of inflammatory cell mediators.....	249
5.2.2.4.	Treatment of cells to investigate cell morphology .....	249
5.2.2.5.	Processing cells for examination of morphology by transmission electron microscopy .....	250
5.2.3.	Investigating the toxicopathology and exposure of inhaled p38 MAPK inhibitors in rats.....	252

5.2.3.1. Dose selections for investigating pulmonary toxicopathology in rats .....	253
5.2.3.2. Investigating mechanisms of toxicopathology seen in rats inhaling p38 MAPK inhibitors .....	256
5.2.4. Test system and animal husbandry .....	260
5.2.5. Subcutaneous dosing of rats .....	261
5.2.6. Aerosol generation of p38 MAPK inhibitors and inhalation exposure of rats .....	261
5.2.6.1. Dry powder formulations of p38 MAPK inhibitors.....	261
5.2.6.2. Liquid formulations of p38 MAPK inhibitors .....	262
5.2.6.2. Aerosol Generation and formulation details .....	263
5.2.6.3. Inhalation exposure of rats .....	264
5.2.6.4. Aerosol characterisation .....	264
5.2.6.5. Calculation of the estimated inhaled dose .....	266
5.2.6.6. Bioanalysis of p38 MAPK inhibitors in rat plasma and lung .....	266
5.2.7. Terminal investigations.....	267
5.2.7.1. Bronchoalveolar lavage of lungs for transmission electron microscopy of macrophages .....	267
5.2.7.2. Histopathological examination of tissues .....	268
5.3. Results and discussion.....	273
5.3.1. In vitro analysis of cytotoxicity, cytokine release and morphology of cells incubated with particles .....	273
5.3.2. Toxicopathology of p38 MAPK inhibitors in rats following 28 days of inhalation exposure .....	276
5.3.2.1. Inhalation exposure of rats to p38 MAPK inhibitors and estimation of the inhaled dose .....	277
5.3.2.2. Pulmonary and systemic exposure of rats to GSK-899 and toxicopathology after 28 days .....	279
5.3.2.3. Pulmonary and systemic exposure of rats to GSK-677 and toxicopathology after 28 days .....	309
5.3.2.4. Pulmonary and systemic exposure of rats to GSK-361 and toxicopathology after 28 days .....	322
5.4. Conclusion .....	331
<b>6. General Discussion</b>	
6.1. General Discussion .....	340
6.2. Limitations and further work .....	353
6.3. Summary.....	356
<b>REFERENCES .....</b>	<b>361</b>
<b>APPENDICES.....</b>	<b>379</b>
<b>ADDENDA.....</b>	<b>449</b>

## LIST OF TABLES

### CHAPTER 1

- 1.1. Proportion of particles deposited in the lungs and respiratory tract of mice, rats, guinea pigs, dogs, monkeys and humans .... 40

### CHAPTER 2

- 2.1. Salt form and purity of p38 MAPK inhibitors used for dissolution testing (in vitro) and inhalation exposure of rats (in vivo)..... 62
- 2.2. Aqueous solutions of p38 MAPK inhibitors nebulised for single inhalation exposure of rats..... 70
- 2.3. Theoretical effective cut off diameter cut points (ECDs) for a Marple 296 cascade impactor ..... 81
- 2.4. 'In silico' physicochemical parameters for principal component analysis of six p38 MAPK inhibitors ..... 87
- 2.5. Scoring system used for pKa acid and base class definitions for *in silico* parameters listed in Table 2.4 ..... 89
- 2.6. Measured physicochemical parameters for principal component analysis of six p38 MAPK inhibitors ..... 90
- 2.7. Statistical summary data for principal component analysis of measured physicochemical parameters of six p38 MAPK inhibitors ..... 95
- 2.8. *In vitro* dissolution rates of five crystalline p38 MAPK inhibitors and amorphous GSK-899 in simulated lung fluid ..... 97
- 2.9. Key in vitro physicochemical parameters of p38 MAPK inhibitors selected for in vivo evaluation of lung exposure in rats ..... 98
- 2.10. Index of figures showing scanning electron microscopy (SEM) of input materials and aerosol samples..... 99
- 2.11. Estimated inhaled doses in rats and aerosol characterisation data for p38 MAPK inhibitors ..... 104
- 2.12. Estimation of fine particle fraction of aerosols of p38 MAPK inhibitors by interpolation of particulate size data ..... 106
- 2.13. Index of figures presenting concentrations of p38 MAPK inhibitors in lung and plasma, and relative lung distribution..... 107
- 2.14. Lung weights and estimated circulating blood volume of rats ..... 108
- 2.15. Distribution of drug between lung tissue and blood residing in vasculature, and indexing of appendices for individual data.... 109
- 2.16. Pharmacokinetics of mean p38 MAPK inhibitor concentrations in lung homogenate after single exposure of rats to test articles. 122
- 2.17. Pharmacokinetics of mean p38 MAPK inhibitor concentrations in plasma after single exposure to test articles ..... 123
- 2.18. Ranking of p38 MAPK inhibitors and aerosol forms for systemic and lung exposure ..... 124

### CHAPTER 3

3.1.	Tube restraint protocol for acclimatisation of rats to plethysmographs and a 31-day observation period (Design 1) .....	137
3.2.	Tube restraint protocol for acclimatisation of rats to plethysmographs and aerosol administration (Design 2).....	141
3.3.	Tube restraint protocol for acclimatisation of rats to plethysmographs and aerosol administration (Design 3).....	145
3.4.	Tube restraint protocol for acclimatisation of rats to head-out plethysmography and aerosol administration (Design 4).....	147
3.5.	Aqueous solutions of p38 MAPK inhibitors nebulised for single inhalation exposure of rats .....	149
3.6.	Duration of exposure, target doses and aerosol concentrations of p38 MAPK inhibitors for exposure of rats .....	150
3.7.	Aerosol sampling volumes for aerosol concentration and particle size analysis .....	151
3.8.	Index of figures and tables summarising lung function data, inhaled doses and lung concentrations of p38 MAPK inhibitors in rats.....	152
3.9.	Breath frequency (breaths per minute) of rats during a 60-minute inhalation exposure period .....	159
3.10.	Minute volume of rats during a 60-minute inhalation exposure period .....	160
3.11.	Breath frequency of rats during a 30-minute inhalation exposure period .....	162
3.12.	Minute volume of rats during a 30-minute inhalation exposure period .....	163
3.13.	Measured and body weight-derived estimates of minute volume of rats during a single 60-minute exposure period.....	170
3.14.	Measured and body weight-derived estimates of minute volume of rats during a single 30-minute exposure period.....	172
3.15.	Estimated inhaled doses in rats and aerosol characterisation data for crystalline GSK-899 .....	173
3.16.	GSK-899 concentration in rat lung homogenate after a single inhalation exposure (breakdown of groups) .....	174
3.17.	Estimated inhaled doses in rats and aerosol characterisation data for GSK-677 and GSK-361 .....	175

### CHAPTER 4

4.1.	Purity of crystalline p38 MAPK inhibitors used for inhalation exposure of rats .....	190
4.2.	Summary of aerosol particle sizes for amorphous GSK-899.....	190
4.3.	<i>In vitro</i> binding and potency of p38 MAPK inhibitors .....	197
4.4.	Dry powder formulations of p38 MAPK inhibitors, canister volumes, target doses and aerosol concentrations for exposure of rats .....	198
4.5.	Vehicles used for nebulisation of p38 MAPK inhibitors and repeated inhalation exposure of rats .....	199

4.6.	Formulation concentrations, target doses and aerosol concentrations for exposure of rats to p38 MAPK inhibitors ....	200
4.7.	Target aerosol concentrations and aerosol sampling volumes ....	202
4.8.	Aerosol characterisation data and inhaled doses of GSK-899 in rats (single 30-minute exposure).....	212
4.9.	Aerosol characterisation data and inhaled doses of GSK-899 in rats (single 30-minute exposure).....	213
4.10.	Aerosol characterisation data and inhaled doses of GSK-677 in rats (single 30-minute exposure).....	214
4.11.	Aerosol characterisation data and inhaled doses of GSK-361 in rats (single 30 or 60-minute exposure).....	215
4.12.	Estimated inhaled doses of GSK-677 to achieve 50% reduction (ED50) in inflammation endpoints evaluated using an acute lung inflammation model in rats .....	225
4.13.	Estimated inhaled dose of GSK-899 to achieve 50% reduction (ED50) in inflammation endpoints evaluated using an acute lung inflammation model in rats .....	232
4.14.	Estimated inhaled dose of GSK-361 to achieve 50% reduction (ED50) in inflammation endpoints evaluated using an acute lung inflammation model in rats .....	235
4.15.	Ranking of the exposure of rats to p38 MAPK inhibitors following a single inhaled administration .....	237
4.16.	Estimated inhaled doses of p38 MAPK inhibitors to achieve 50% reduction (ED50) in inflammation endpoints evaluated using an acute lung inflammation model in rats .....	238

## CHAPTER 5

5.1.	Purity of p38 MAPK inhibitors used for repeated administration to rats .....	246
5.2.	Volume of dust feed canisters, target doses and aerosol concentrations for exposure of rats to p38 MAPK inhibitors ....	262
5.3.	Vehicles used for nebulisation of p38 MAPK inhibitors and repeated inhalation exposure of rats .....	262
5.4.	Formulation concentrations, target doses and aerosol concentrations for exposure of rats to p38 MAPK inhibitors ....	263
5.5.	Target aerosol concentrations and aerosol sampling volumes ....	265
5.6.	Summary of inhaled doses, duration of treatment and sampling of lungs by bronchoalveolar lavage.....	268
5.7.	Summary of tissues examined by light microscopy after treatment of rats for 28 days .....	272
5.8.	In vitro cytotoxicity (EC50) data for p38 MAPK inhibitors.....	273
5.9.	Index of figures and tables for dosimetry, drug-lung and plasma concentrations and representative microscopy images in rats .....	276
5.10.	Estimated inhaled doses and characterisation of dry powder aerosols administered to rats over 28 days.....	278

5.11.	Estimated inhaled doses and characterisation of nebulised aerosols administered to rats over 28 days.....	279
5.12.	Pharmacokinetics of GSK-899 in plasma after inhaled administration of micronised crystals .....	282
5.13.	Histopathology of the respiratory tract of rats exposed to micronised crystalline GSK-899 for 28 days.....	285
5.14.	Pharmacokinetics of GSK-899 in plasma after inhaled administration of amorphous powder .....	291
5.15.	Histopathology of the respiratory tract of rats exposed to amorphous GSK-899 for 28 days.....	293
5.16.	Pharmacokinetics of GSK-899 in plasma after inhaled administration of nebulised solutions .....	298
5.17.	Histopathology of the respiratory tract of rats exposed to nebulised GSK-899 for 28 days .....	300
5.18.	Pharmacokinetics of GSK-899 in plasma after subcutaneous administration of a solution .....	304
5.19.	Histopathology of lungs and injection sites of rats dosed subcutaneously with GSK-899 for 28 days.....	305
5.20.	Pharmacokinetics of GSK-677 in plasma after inhaled administration of micronised crystals .....	311
5.21.	Histopathology of the respiratory tract of rats exposed to micronised crystalline GSK-677 for 28 days.....	313
5.22.	Pharmacokinetics of GSK-677 in plasma after inhaled administration of a nebulised solution .....	316
5.23.	Histopathology of the respiratory tract of rats exposed to nebulised GSK-677 for 28 days .....	318
5.24.	Pharmacokinetics of GSK-361 in plasma after inhaled administration of micronised crystals .....	325
5.25.	Pharmacokinetics of GSK-361 in plasma after inhaled administration of nebulised solution .....	330
5.26.	Key findings for in vitro and in vivo assessment of toxicopathology and exposure of p38 MAPK inhibitors.....	331

## CHAPTER 6

6.1.	Ranking of key findings for in vitro and in vivo assessment of p38 MAPK inhibitors .....	345
6.2.	Median effective dose (ED <sub>50</sub> ; single exposure) and non-effect levels (28 days) for inhaled p38 MAPK inhibitors administered to rats .....	350

# LIST OF FIGURES

## CHAPTER 1

1.1.	Fractional deposition of inhaled particles in humans .....	4
1.2.	Diagrammatic representation of the human and rodent respiratory tracts.....	5
1.3.	Comparison of the human respiratory epithelium at different lung locations .....	8
1.4.	Clinical inhalers and a nebuliser for dosing patients .....	15
1.5.	Total procedures performed in Great Britain during 2016 .....	24
1.6.	Refinement of drug development programmes to reduce animal use associated with drug attrition due to adverse lung pathology ....	25
1.7.	Dynamic single pass exposure systems for the non-clinical administration of aerosols .....	35
1.8.	Restraint of animals for snout only inhalation exposure .....	36
1.9.	Mechanisms of transmembrane absorption of molecules .....	42

## CHAPTER 2

2.1.	Illustration of principal component analysis .....	54
2.2.	Chemical structures of six p38 MAPK inhibitors shortlisted for potential investigation of in vivo endpoints .....	58
2.3.	Schematic of apparatus used to evaluate dissolution of p38 MAPK inhibitors in simulated lung fluid .....	64
2.4.	Design to investigate plasma and lung concentrations and lung distribution of p38 MAPK inhibitors in rats after a single inhaled dose .....	65
2.5.	Aerosol generator for dispersal of dry powder formulations .....	69
2.6.	Air jet nebuliser used to disperse solutions or suspensions .....	73
2.7.	Snout only inhalation exposure system incorporating a flow-through chamber for administration of aerosols to rats .....	75
2.8.	Apparatus for sampling the chamber atmosphere for measurement of aerosol concentration of drug analyte .....	78
2.9.	Sampling chamber air using a cascade impactor to determine the particle size distribution of drug analyte .....	79
2.10.	Score plot for principal component analysis of estimated ADME and physicochemical properties for six p38 MAPK inhibitors.....	93
2.11.	Loading plot for principal component analysis of calculated ADME and physicochemical properties for six p38 MAPK inhibitors.....	93
2.12.	Score plot for principal component analysis of the measured physicochemical properties for six p38 MAPK inhibitors .....	94
2.13.	Loading plot for principal component analysis of measured physicochemical parameters of six p38 MAPK inhibitors .....	94
2.14.	X-ray powder diffraction of amorphous and crystalline GSK-899 ...	95
2.15.	<i>In vitro</i> dissolution of five crystalline p38 MAPK inhibitors and amorphous GSK-899 in simulated lung fluid .....	96

2.16.	Scanning electron microscopy of ‘inhalation grade lactose’ used as excipient in dry powder formulations of p38 MAPK inhibitors ..	100
2.17.	Scanning electron microscopy of crystalline GSK-899.....	100
2.18.	Scanning electron microscopy of amorphous GSK-899.....	101
2.19.	Scanning electron microscopy of crystalline GSK-677.....	102
2.20.	Scanning electron microscopy of crystalline GSK-361.....	102
2.21.	Estimation of fine particle fraction (% mass <5µm aerodynamic diameter) by interpolation of particulate size data .....	106
2.22.	GSK-899 concentrations in lung homogenate sampled from rats after a single inhaled dose .....	110
2.23.	GSK-899 concentrations in plasma sampled from rats after a single inhaled or intravenous dose.....	111
2.24.	GSK-899 in lungs of rats inhaling crystalline drug imaged by matrix assisted laser desorption/ionization with mass spectrometry imaging.....	112
2.25.	GSK-899 in lungs of rats inhaling amorphous drug imaged by matrix assisted laser desorption/ionization with mass spectrometry imaging.....	112
2.26.	GSK-899 in lungs of rats inhaling nebulised drug imaged by matrix assisted laser desorption/ionization with mass spectrometry imaging.....	113
2.27.	GSK-677 concentrations in lung homogenate sampled from rats after a single inhaled dose .....	114
2.28.	GSK-677 concentrations in plasma of rats after a single inhaled or intravenous dose .....	115
2.29.	GSK-677 in lungs of rats inhaling crystalline drug imaged by matrix assisted laser desorption/ionization with mass spectrometry imaging.....	116
2.30.	GSK-677 in lungs of rats inhaling nebulised drug imaged by matrix assisted laser desorption/ionization with mass spectrometry imaging.....	116
2.31.	GSK-361 concentrations in lung homogenate sampled from rats after a single inhaled dose .....	117
2.32.	GSK-361 concentrations in plasma of rats after a single inhaled or intravenous dose .....	118
2.33.	GSK-361 in lungs of rats inhaling crystalline drug imaged by matrix assisted laser desorption/ionization with mass spectrometry imaging.....	118
2.34.	GSK-361 in lungs of rats inhaling nebulised drug imaged by matrix assisted laser desorption/ionization with mass spectrometry imaging.....	119
2.35.	SB-445 concentrations in lung homogenate sampled from rats after a single inhaled dose .....	120
2.36.	SB-445 concentrations in plasma sampled from rats after a single inhaled or intravenous dose.....	120

### CHAPTER 3

3.1.	Head-out plethysmography in rats.....	134
3.2.	Evolution of study designs for investigation of light, duration of tube acclimatisation and conditioning of rats on lung function .	135
3.3.	Design of a preliminary study to measure lung function over four weeks and consider the impact of lighting conditions .....	138
3.4.	Latin square design of study to investigate effects of lighting and duration of tube acclimatisation on lung function and dose .....	140
3.5.	Simple study design to investigate lung function measurements and drug-lung concentrations after a single inhaled dose of GSK-361 or GSK-677 .....	144
3.6.	Experimental design to investigate lung function of rats during a 28-day inhalation study .....	148
3.7.	Breath frequency of rats restrained in tubes once daily for 28 days.....	153
3.8.	Minute volume of rats restrained in tubes once daily for 28 days.....	154
3.9.	Breath frequency of rats restrained in tubes under red or white lighting.....	155
3.10.	Minute volume of rats restrained in tubes under red or white lighting .....	156
3.11.	Breath frequency of rats exposed to GSK-899 for 60 minutes after a tube acclimatisation protocol of two or six days and under red or white lighting.....	158
3.12.	Minute volume of rats exposed to GSK-899 for 60 minutes after a tube acclimatisation protocol of two or six days and under red or white lighting.....	159
3.13.	Breath frequency of rats exposed to crystalline or nebulised aerosols for 30 minutes.....	161
3.14.	Minute volume of rats exposed to crystalline or nebulised aerosols for 30 minutes.....	162
3.15.	Breath frequency of rats administered GSK-361 for 28 days .....	164
3.16.	Breath frequency of rats administered GSK-361 for 28 days .....	165
3.17.	Minute volume of rats administered GSK-361 for 28 days.....	166
3.18.	Minute volume of rats administered GSK-361 for 28 days.....	167
3.19.	Breath frequency in rats over a 28-day treatment period .....	168
3.20.	Measured minute volume and the body weight derived estimate in rats over a 28-day treatment period .....	169
3.21.	Measured minute volume and the body weight derived estimate against body weight of rats during a single exposure.....	170
3.22.	Measured minute volume and the body weight derived estimate against body weight of rats during a single exposure .....	171
3.23.	Measured minute volume and the body weight derived estimate against body weight of rats over 28 days.....	172

3.24.	Measured and predicted lung concentrations in rats after a single inhaled dose of GSK-899 and tube acclimatisation for two or six days under red or white light .....	174
3.25.	Measured and predicted lung concentrations in rats after a single inhaled dose of GSK-677 or GSK-361 .....	176
3.26.	Measured lung concentrations of GSK-899 as a proportion of the estimated inhaled dose in rats after a single exposure.....	177

#### **CHAPTER 4**

4.1.	Normal alveolus and injured alveolus in the acute phase of acute lung injury and acute respiratory distress syndrome .....	185
4.2.	Study design used for investigating inhibition of lipopolysaccharide induced lung inflammation after a single dose of an inhaled p38 MAPK inhibitor .....	192
4.3.	Inhibition of lipopolysaccharide induced lung inflammation in rats after prophylactic administration of GSK-899 .....	193
4.4.	Inhibition of lipopolysaccharide induced inflammation in rat lungs after prophylactic administration of GSK-677 .....	195
4.5.	Intratracheal instillation of a solution .....	204
4.6.	Example of image analysis of rat lungs for biomarkers of inflammation .....	209
4.7.	Neutrophil counts in bronchoalveolar lavage fluid sampled from control animals four hours after intratracheal instillation of lipopolysaccharide .....	217
4.8.	Neutrophils as a proportion of leukocytes in bronchoalveolar lavage fluid sampled from control rats four hours after intratracheal instillation of lipopolysaccharide.....	218
4.9.	Recovery of bronchoalveolar lavage fluid sampled from control animals .....	219
4.10.	GSK-677-concentrations in lung homogenate sampled from rats after a single inhaled dose (Study R31400N) .....	220
4.11.	GSK-677 concentrations in plasma sampled from rats after a single inhaled dose (Study R31400N).....	221
4.12.	Tumour necrosis factor-alpha in serum, relative to controls, sampled from an acute lung inflammation model in rats administered GSK-677 (Study R31400N) .....	222
4.13.	Tumour necrosis factor-alpha in broncho-alveolar lavage fluid, relative to controls, sampled from an acute lung inflammation model in rats administered GSK-677 (Study R31400N) .....	223
4.14.	Neutrophils in bronchoalveolar lavage fluid, relative to controls, harvested from an acute lung inflammation model in rats administered GSK-677 (Study R31400N) .....	223
4.15.	Proportion of lung tissue stained for myeloperoxidase or chloroacetate esterase, relative to controls, in an acute lung inflammation model in rats administered GSK-677 (Study R31400N) .....	224
4.16.	GSK-899 concentrations in lung homogenate sampled from rats after a single inhaled dose (Study R30820N) .....	227

4.17.	GSK-899 concentrations in plasma sampled from rats after a single inhaled dose (Study R30820N).....	228
4.18.	Neutrophils in bronchoalveolar lavage fluid, relative to controls, harvested from an acute lung inflammation model in rats administered GSK-899 (Study R30820N) .....	229
4.19.	GSK-899 concentrations in lung homogenate sampled from rats after a single inhaled dose (Study R31763N).....	230
4.20.	GSK-899 concentrations in plasma sampled from rats after a single inhaled dose (Study R31763N).....	231
4.21.	GSK-361 concentrations in lung homogenate sampled from rats after a single inhaled dose (Study R31765N).....	233
4.22.	GSK-361 concentrations in plasma sampled from rats after a single inhaled dose (Study R31765N).....	233
4.23.	Neutrophils in bronchoalveolar lavage fluid, relative to controls, harvested from an acute lung inflammation model in rats administered GSK-361 (Study R31765N) .....	234

## CHAPTER 5

5.1.	Generic outline of experimental design to investigate pulmonary toxicology following inhaled administration of p38 MAPK inhibitors for 28 days.....	252
5.2.	Chemical structures of two structurally similar isomers with different pharmacological potencies.....	257
5.3.	Outline of experimental design to investigate pulmonary toxicology after subcutaneous administration of GSK-899 for 28 days.....	259
5.4.	Trimming patterns for standardization of tissue sections for histopathological examination .....	270
5.5.	Cytotoxicity assessed by leakage of lactate dehydrogenase from NR8383 rat alveolar macrophage cells incubated with a p38 MAPK inhibitor .....	274
5.6.	Transmission electron microscopy of NR8383 rat alveolar macrophage cells incubated with a p38 MAPK inhibitor .....	275
5.7.	Drug-lung concentrations in rats following inhaled administration of crystalline GSK-899 for one or 28 days.....	280
5.8.	GSK-899 concentrations in rat plasma up to 24 hours after inhaled doses of crystalline GSK-899 on Days 1 and 28.....	281
5.9.	Normal macrophage sampled from a rat (control) after inhaled administration of lactose vehicle for 3 days.....	283
5.10.	Macrophages containing crystalline particles after inhalation of GSK-899 for 3 days .....	284
5.11.	Representative histology of control rat lung and treatment related changes after inhalation of crystalline GSK-899 for 28 days ...	286
5.12.	Representative histology of control rat bronchus associated lymphoid tissue (BALT) and increased cellularity after inhalation of crystalline GSK-899 for 28 days.....	287

5.13.	Representative histology of control rat larynx and changes after inhalation of crystalline GSK-899 for 28 days.....	287
5.14.	Drug-lung concentrations in rats following inhaled administration of amorphous GSK-899 for one or 28 days.....	288
5.15.	GSK-899 concentrations in rat plasma up to 24 hours after inhaled doses of amorphous GSK-899 on Days 1 and 28.....	290
5.16.	Macrophages containing amorphous particles after inhalation of GSK-899 for 3 days .....	292
5.17.	Representative histology of control rat lung and treatment related changes after inhalation of amorphous GSK-899 for 28 days .	294
5.18.	Representative histology of control rat larynx and treatment related changes after inhalation of amorphous GSK-899 for 28 days .....	295
5.19.	Drug-lung concentrations in rats following inhaled administration of nebulised GSK-899 for one or 28 days .....	296
5.20.	GSK-899 concentrations in rat plasma up to 24 hours after inhalation of nebulised doses on Days 1 and 28 .....	297
5.21.	Macrophages after inhalation of nebulised vehicle or GSK-899 for 3 days.....	299
5.22.	Representative histology of control rat lung and treatment related changes after inhalation of nebulised GSK-899 for 28 days .....	301
5.23.	Representative histology of rat lung and treatment related changes after inhalation of nebulised GSK-899 and/or vehicle for 28 days .....	301
5.24.	Drug-lung concentrations in rats after subcutaneous administration of GSK-899 for one or 28 days.....	302
5.25.	GSK-899 concentrations in rat plasma up to 24 hours after subcutaneous administration on Days 1 and 28.....	303
5.26.	Representative histology of control rat lung and after subcutaneous administration of GSK-899 for 28 days.....	304
5.27.	Representative histology of bronchus associated lymphoid tissue after subcutaneous administration of GSK-899 and/or vehicle for 28 days.....	306
5.28.	Representative histology of thymus after subcutaneous administration of GSK-899 and/or vehicle for 28 days.....	307
5.29.	Representative histology of subcutaneous injection site after administration of GSK-899 and/or vehicle for 28 days.....	308
5.30.	Drug-lung concentrations in rats following inhaled administration of crystalline GSK-677 for one or 28 .....	309
5.31.	GSK-677 concentrations in rat plasma up to 24 hours after inhaled doses of crystalline GSK-677 on Days 1 and 28.....	310
5.32.	Macrophages after inhalation of crystalline GSK-677 for 3 days..	312
5.33.	Drug-lung concentrations in rats following inhaled administration of nebulised GSK-677 for one or 28 days .....	314
5.34.	GSK-677 concentrations in rat plasma up to 24 hours after nebulised doses on Days 1 and 28 .....	315

5.35.	Macrophages after inhalation of nebulised vehicle or GSK-677 for 3 days.....	317
5.36.	Representative histology of control rat lung and treatment related changes after inhalation of nebulised GSK-677 for 28 days.....	319
5.37.	Representative histology of control rat nasal cavity and mild irritancy after inhalation of nebulised GSK-677 for 28 days.....	320
5.38.	Representative histology of control rat larynx and mild irritancy after inhalation of nebulised GSK-677 for 28 days.....	321
5.39.	Representative histology of control ventral pouch of rat larynx and mild irritancy after inhalation of nebulised GSK-677 for 28 days.....	322
5.40.	Drug-lung concentrations in rats following inhaled administration of crystalline GSK-361 for one or 28 days.....	323
5.41.	GSK-361 concentrations in rat plasma up to 24 hours after inhaled doses of crystalline GSK-361 on Days 1 and 28.....	324
5.42.	Macrophages after inhalation of lactose vehicle or crystalline GSK-361 for 28 days.....	326
5.43.	Representative histology of control rat lung and after inhalation of crystalline GSK-361 for 28 days.....	327
5.44.	Drug-lung concentrations in rats following inhaled administration of nebulised GSK-361 for one or 28 days.....	328
5.45.	GSK-361 concentrations in rat plasma up to 24 hours after nebulised doses on Days 1 and 28.....	329
5.46.	Representative histology of control rat lung and after inhalation of nebulised GSK-361 for 28 days.....	330
 <b>CHAPTER 6</b>		
6.1.	Chemical structures of three p38 MAPK inhibitors selected for investigation of in vivo endpoints.....	343

## LIST OF ABBREVIATIONS

AAPS	Association of Pharmaceutical Scientists
ABC	ATP-binding cassette transporter
ADA	anti-drug antibody
ANOVA	analysis of variance
AUC	area under the (drug) concentration time curve
A(SP)A	Animal (Scientific Procedures) Act, 1986 (UK)
ATP	adenosine triphosphate
BAL	bronchoalveolar lavage
BALF	bronchoalveolar lavage fluid
BALT	bronchus-associated lymphoid tissue
BC	before Christ
BF	breath frequency (by head-out plethysmography)
CAE	chloroacetate esterase
CCSP	club cell secretory protein
CD	cluster of differentiation (CD68, CD3 and CD79 glycoproteins expressed by macrophages, T- and B-lymphocytes respectively)
CFC	chlorofluorocarbon
CHI	chromatographic hydrophobicity index
CHCA	$\alpha$ -cyano-4-hydroxycinnamic acid
$C_{max}$	maximum (drug) concentration in stated medium
COPD	chronic obstructive pulmonary disease
$C_t$	target (aerosol) concentration
CV	coefficient of variation
DNA	deoxyribonucleic acid
DPI	dry powder inhaler
ECD	effective cut-point diameter
ED <sub>50</sub>	median effective dose
EDTA	ethylenediaminetetraacetic acid (anticoagulant)
EEC	European Economic Community
EMA, EMEA	European Medicines Agency
EPA	Environmental Protection Agency (USA)

EU	European Union
eRMV	estimated respired minute volume (calculated from body weight using an algorithm)
FDA	Food and Drug Administration (USA)
FTIH	first time in humans (first clinical trial)
GI-GOLD	Global Initiative for Chronic Obstructive Lung Disease
GRO	growth-regulated oncogene
GSD ( $\sigma$ )	geometric standard deviation
GSK	GlaxoSmithKline
GSK-340	GSK719340A (parent compound)
GSK-361	GSK678361A (parent compound)
GSK-677	GSK610677B (hydrochloride salt)
GSK-899	GSK258899B (mesylate salt)
HFA	hydrofluoroalkane
HOP	head-out plethysmography
HLOQ	higher limit of quantification
HPLC	high performance liquid chromatography
HLPC-MS/MS	HPLC with tandem mass spectrometry
HPLC-UV	HPLC with ultraviolet detection for quantification
HP $\beta$ CD	2-hydroxypropyl-beta-cyclodextrin
HRP	horseradish peroxidase
IAM	immobilised artificial membrane column
iCBS	inhalation Biopharmaceutics Classification System
ICH	International Council for Harmonisation of Technical Requirements for Pharmaceuticals for Human Use
ICS/LABA	inhaled corticosteroid and long-acting beta-2-agonist
IMS	industrial methylated spirits
LLOQ	lower limit of quantification
ID <sub>e</sub>	estimated inhaled dose
ID <sub>t</sub>	target inhaled dose
IL	interleukin
IMS	industrial methylated spirits
KC	keratinocyte chemoattractant
LDH	lactate dehydrogenase

LPS	lipopolysaccharide
MALDI-MSI	matrix assisted laser desorption/ionization with mass spectrometry imaging
MANOVA	multivariate analysis of variance (cited when three or more variables were analysed)
MAPK	mitogen-activated protein kinase
MCP-1	monocyte chemotactic protein 1
M-cell	microfold cells (antigen transport/presenting cells in mucosal membranes)
MHRA	Medicines and Healthcare Products Regulatory Agency (UK)
MMAD	mass median aerodynamic diameter
MV	minute volume (measured by plethysmography)
MVA	multivariate analysis
NGI	Next Generation Impactor
NHS	National Health Service (UK)
NICE	National Institute for Health and Care Excellence (UK)
MPO	myeloperoxidase
NIPALS	Nonlinear Iterative PARTial Least Squares (reiterative algorithm for approximating data for MVA or PCA)
NOAEL	no observed adverse effect level, defined as the highest evaluated dose that does not harm the test animals (Kerlin <i>et al.</i> , 2016)
NRC	National Research Council (USA)
OECD	Organisation for Economic Co-operation and Development
PCA	principal component analysis
Pgp	P-glycoprotein 1
pMDI	pressurised metered dose inhaler
PSD	particle size distribution
PVDF	polyvinylidene difluoride
QC	quality control
RMV	respired minute volume
RNA	ribonucleic acid
RPM	revolutions per minute
SB-323	SB-681323T (tosylate salt)

SB-445	SB-731445T (tosylate salt)
SIMS	secondary ion mass spectrometry
TEM	transmission electron microscope
TFA	trifluoroacetic acid
TNF	tumour necrosis factor
TOF	time of flight
T <sub>max</sub>	time to maximum (drug) concentration (C <sub>max</sub> )
UAR	Understanding Animal Research
UK	United Kingdom of Great Britain and Northern Ireland
USA	United States of America
USP	United States Pharmacopeia
VDSS	volume of distribution at steady state
VDUSS	unbound volume of distribution at steady state
v/v	volume for volume
WHO	World Health Organisation
w/v	weight for volume
w/w	weight for weight
XRPD	X-ray powder diffraction

#### **ABBREVIATIONS FOR GSK INFRASTRUCTURE**

ASD	Analytical Services and Development
BIB	Bioanalysis, Immunogenicity and Biomarkers
CPD	Clinical Pathology and Diagnostics
DDS	Drug Design and Selection
DPDD	Drug Product Design and Development
IVSD	<i>In Vivo</i> Science and Delivery
NCE-MD	New Chemical Entity - Molecular Discovery
MSD-ISDM	Mechanistic Safety and Disposition - Investigative Safety and Drug Metabolism
PDS	Product Development and Supply
PPE	Product and Process Engineering
PSE	Particle Sciences and Engineering
TBM	Toxicology and Biometabolism
TMCP	Translational Medicine and Comparative Pathobiology

## GLOSSARY OF TERMS

3Rs	Replacement, reduction, refinement: fundamental principles for the ethical use of animals in research.
<i>in silico</i>	Computational models ('in silicon [chips]') e.g. for chemistry or biological properties.
<i>in situ</i>	Latin: "in the situation"; situated in the natural or original place or position
<i>in utero</i>	Latin: "in the uterus"; unborn.
<i>in vitro</i>	Latin: "within the glass": procedures performed outside a living organism.
<i>in vivo</i>	Latin: "within the living": procedures performed using a living organism.
linear-up, log down	Calculation of AUC using linear trapezoidal rule up to $C_{max}$ (untransformed data for drug absorption) and log-trapezoidal rule after $C_{max}$ (log-transformed data for drug elimination phase).
Log D	Distribution coefficient of ionised plus non-ionised forms of a compound between aqueous and organic phases.
Log P	Partition coefficient of a non-ionised compound between aqueous and organic phases.
M1 macrophage	A "classically activated" macrophage with cytotoxic, inflammatory and antiproliferative properties.
M2 macrophage	Macrophage with anti-inflammatory properties; associated with remodelling and regeneration of damaged tissue.
NR8383	<i>In vitro</i> alveolar macrophage cell line.
pKa, pKb	Log <sub>10</sub> of acid and base dissociation constants.
pneumotach	Cell containing thin film across which changes in air pressure can be measured by a transducer (plethysmography).
transducer	Device that converts changes in air pressure into an analogue signal for data capture (plethysmography).

# **CHAPTER ONE**

## **General introduction**

## 1.1. Introduction

Ischaemic heart disease, stroke, lower respiratory infections and chronic obstructive lung disease (COPD) were the four major causes of death worldwide in 2015 (WHO, 2017), with an estimated three million people in the United Kingdom having COPD of whom 900,000 people have been diagnosed (NICE, 2010). GSK was the market leader in terms of revenue (\$9.4 billion) from respiratory disease products in 2015, accounting for 33.6% of this drug market (Research-Markets, 2016). Despite the successes of pharmaceutical corporations in developing inhaled medicines, there is still an unmet need for developing new respiratory medicines, particularly in the developing world where general access to healthcare is poor and resources are limited (Aït-Khaled *et al.*, 2001).

## 1.2. The respiratory tract

The primary functions of the respiratory tract are olfaction and gaseous exchange at an air-blood interface, to facilitate replenishment of oxygen supply for aerobic respiration and facilitate removal of volatile or gaseous waste products, most notably carbon dioxide (CO<sub>2</sub>). To facilitate gaseous exchange on the scale required to sustain large organisms such as mammals, reptiles and birds, a large permeable surface is required across which gases can readily traverse into a circulatory system. This represents a risk to the animal in terms of its internal exposure to inhaled environmental toxins, nuisance materials or airborne pathogens, and complex protective mechanisms have evolved to mitigate this. However, the functional nature of the lung also provides an opportunity for the deliberate and rapid exposure of a subject for better (anaesthetics and pharmaceuticals) or worse (pesticides and chemical or biological weapons). Utilising the inhaled route to administer drugs for the treatment of respiratory disease permits direct exposure of the target organ using small doses, particularly if drugs are designed to:

- have high potency, receptor affinity and protein binding
- slowly dissociate from its target receptor
- limit systemic exposure and hence the potential for 'off target' effects of a drug (Owen, 2013).

Air is a relatively harsh climate and detrimental to exposed cells. A secondary function of the respiratory tract is therefore to condition the inhaled air, filtering and/or humidifying it and modulating temperature before it reaches the epithelial cells in the lower respiratory tract.

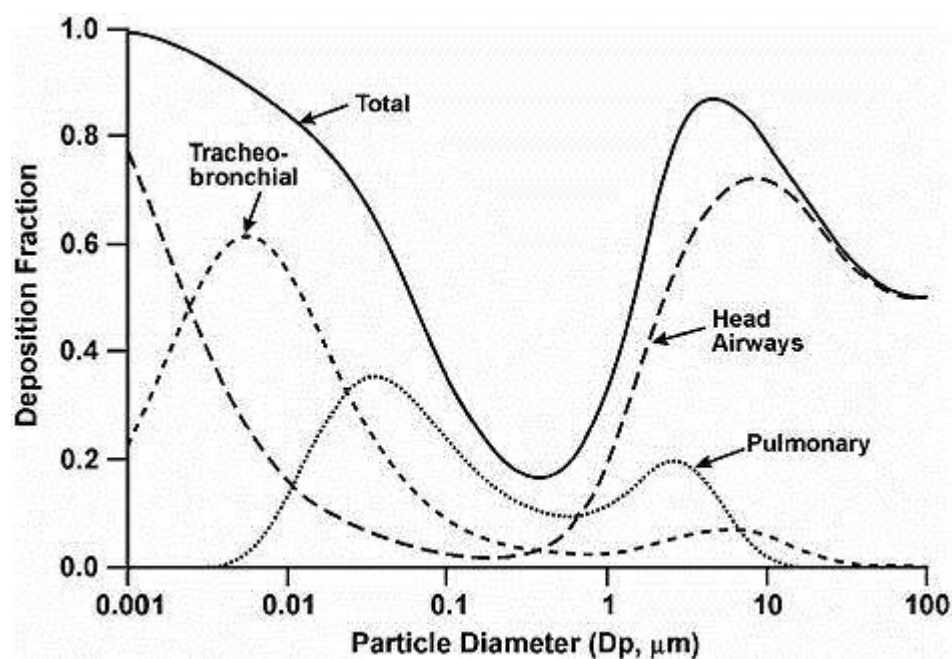
The respiratory tract thus consists of two functional regions, the proximal conductive airways to condition inhaled air and the distal respiratory region for gaseous exchange (Harkema *et al.*, 2013). The degree of particulate deposition in regions of the respiratory tract changes with particle size (Figure 1.1). There are anatomical differences between the respiratory tracts of mammals (Figure 1.2) with implications for an animal's breathing and aerosol deposition. Key differences are summarised for each respiratory tract tissue.

### **1.2.1. Proximal conductive airways**

The proximal conductive airways consist of the nasal cavity, pharynx, larynx, trachea and bronchi. The mucosa lining the conductive airways is very specialised, with the composition of cells in the epithelium changing throughout the respiratory tract to facilitate various functions.

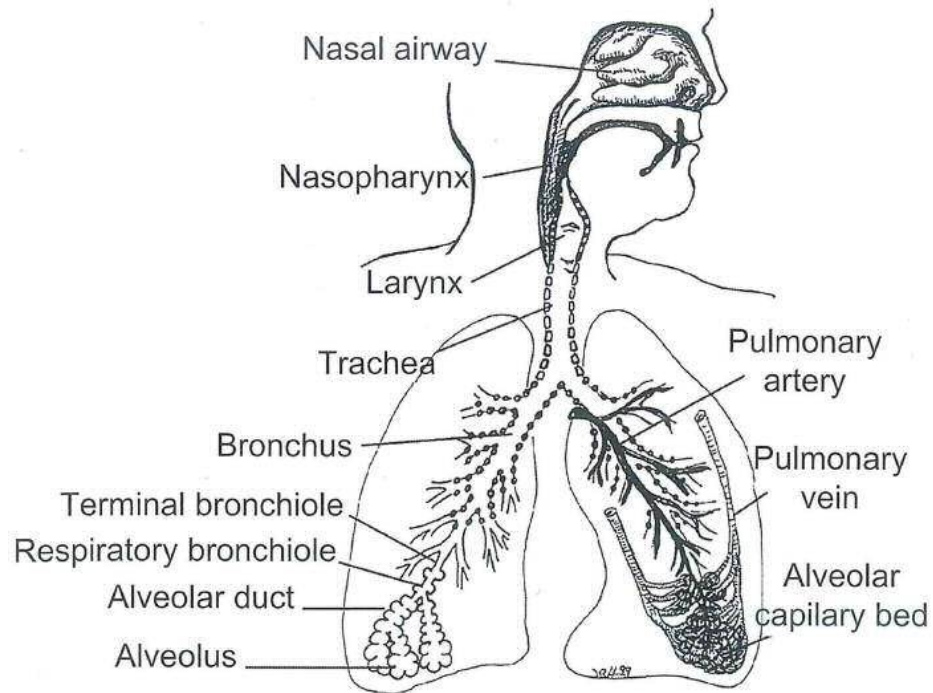
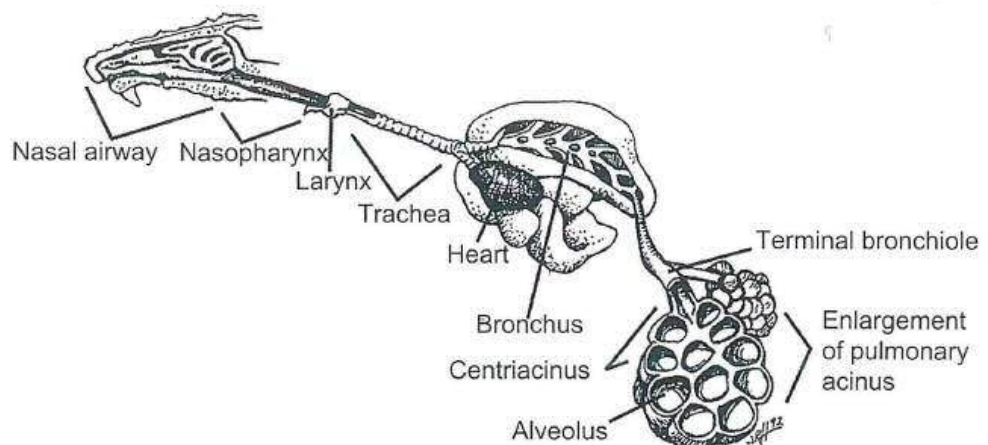
#### Nasal cavity

The nose or snout of land-based mammals accommodate the external nares (nostrils), which accommodate coarse hairs (vibrissæ) to trap large particulates. The nares open into the nasal cavity, which contains ridges of bone called turbinates that project into the nasal cavity.



**Figure 1.1:** Fractional deposition of inhaled particles in humans. Particulate of  $<0.5\mu\text{m}$  or 1 to  $10\mu\text{m}$  have the highest probability for deposition in the respiratory tract. Orally inhaled particles of  $\leq 5\mu\text{m}$  diameter and nasally inhaled particles of  $\leq 3\mu\text{m}$  diameter are thought to deposit in the lower airways of humans (NRC, 2006). *Snipes (1994) reproduced with permission of Medical Physics Publishing, Wisconsin, USA.*

The turbinates direct inhaled air over chemoreceptors in the olfactory neuroepithelium, which initiate a cascade of neuronal events when stimulated resulting in the transmission of signals to the olfactory bulb in the forebrain and the perception of odours (Ressler *et al.*, 1993). The nasal turbinates, which increase the surface area in the nasal cavity, are also an air conditioner (humidifying air and regulating temperature) and protect the delicate lung parenchyma by trapping inhaled particulates, absorbing water-soluble or reactive gases/vapours and metabolising xenobiotics (Harkema *et al.*, 2013). The complexity of the turbinates vary considerably between macrosmatic species (animals with highly developed olfaction) such as dogs, rodents and rabbits, and microsmatic species (animals with poor olfaction) such as primates (Lewis and McKeivitt, 2013).

**1.2A: human****1.2B: rodent**

**Figure 1.2:** Diagrammatic representation of the human and rodent respiratory tracts. Dots along the laryngeal and tracheobronchial airways indicate intramural cartilage. **1.2A:** human respiratory tract; breathing is nasally or orally, particularly with increased activity. **1.2B:** rodent respiratory tract. Rodents are obligate nasal breathers and their nasal turbinates are more convoluted than those of humans. *Harkema et al. (2013) reproduced with permission of Elsevier.*

Primates, cats and dogs readily breathe orally or nasally. However, prey species including rodents, rabbits, deer and equine species have evolved to breathe nasally (Lewis and McKevitt, 2013, Negus, 1927)

concurrently with grazing, in order to detect predators in their blind spot and to smell poisonous plants not visible to their laterally placed eyes during grazing (Negus, 1927). Obligate nasal breathing has implications for the deposition of aerosols in the respiratory tract of such prey species, including pigs (Larson and Herring, 1996, Moon and Smith, 1996, Jones *et al.*, 2001), with a higher proportion of particulate retained in the nasal cavities.

### Pharynx

The pharynx is cartilaginous and connects the nasal and oral cavities to the larynx; regions of the pharynx adjacent to these cavities are referred to as the oropharynx and nasopharynx respectively. The nasopharynx makes a downward bend as it progresses from the nasal cavity to the larynx, which varies for the natural posture of the animal. This bend is gradual in animals of a pronograde (horizontal) posture, such as rats (15°) and dogs (30°), and sharper in species of an orthograde (upright) posture such as the rhesus monkey (80°) (Schreider and Raabe, 1981).

### Larynx

The larynx is cartilaginous and connects the pharynx to the trachea. The glottis, the mid-section of the larynx, accommodates the vocal chords necessary for phonation. A key anatomical difference between species is the topography of the laryngeal diverticula (pouches), which are bilateral in dogs and primates and ventral in rodents; the function is unclear but the pouches may amplify vocalisations in some species (Lewis and McKeivitt, 2013).

The epiglottis is a cartilaginous structure at the anterior end of the larynx, and is generally more developed in macrosmatic species (species with highly developed olfaction) and deficient in microsmatic species (animals with poor olfaction). In obligate nasal breathers, the epiglottis seals the oral cavity ensuring inspired air enters via the nares and passes over the olfactory (Negus, 1927).

### Trachea and bronchi

The trachea is a conducting airway from the larynx to the carina, a ridge of cartilage where the airway bifurcates into two mainstem bronchi (Figure 1.2A), which in turn divide into smaller bronchi. This branching of airways is dichotomous in humans but monopodial in most mammalian species in which daughter branches are of unequal diameter (Harkema *et al.*, 2013).

U-shaped cartilaginous rings incorporated into the lateral and ventral walls of the trachea maintain an open airway; the dorsal wall consists of flexible fibroelastic and smooth muscle. The walls of the tracheal, bronchi and bronchioles consist of three layers, the mucosa (mucus membrane), submucosa (connective tissue) and the adventitia (loose connective tissue securing the airway to adjacent lung tissue). Smooth muscle between the mucosa and submucosa contracts and relaxes to constrict and dilate the respiratory airways respectively.

The cellular composition and thickness of the mucosa (pseudostratified respiratory epithelium) lining the lumen of the airways changes greatly from the proximal to the distal regions (Figure 1.3). The trachea consists of tall columnar ciliated cells, which progresses to cuboidal cells in the bronchioles and a thin squamous epithelium in the alveoli. Although the proportion of ciliated cells in the respiratory epithelium is consistent across species, differences are seen in the relative dimensions of the airways and the composition of other cell phenotypes. For example, the thickness of the epithelium at the trachea in humans is three times that of monkeys and ten times that of rodents (Harkema *et al.*, 2013).

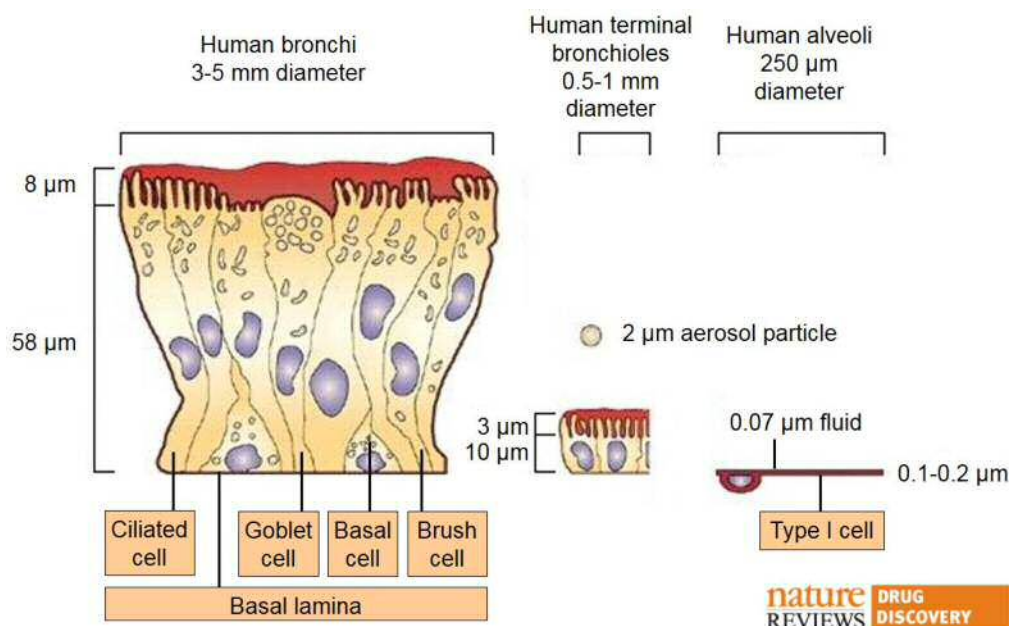


**Figure 1.3: Comparison of the human respiratory epithelium at different lung locations.** Epithelial cells from three regions of human lung are drawn to scale. As airborne particles penetrate deeper into the lung, the epithelium becomes thinner. A 2  $\mu\text{m}$  diameter particle typically contains hundreds of millions/billions of small molecules depending on whether it is a liquid droplet or solid particle. Solid particles are too large to be absorbed directly and must first dissolve to release their drug(s) for absorption. The dark orange colour in the figure represents the liquid layer, which gets progressively thinner as the airways become narrower until the thickness is  $<0.1 \mu\text{m}$  at the alveoli. The bronchial epithelium is constituted of basal cells (stem or progenitor cells for the epithelium that differentiate to form other cells in the event of injury or apoptosis), ciliated cells (facilitate migration of the mucus blanket), goblet cells (secrete mucous) and brush cells (involved in drug metabolism). These cell types persist in smaller airways but are shorter. The basal lamina is an extracellular matrix of various biopolymers to which the epithelial cells are attached. *Adapted from Patton and Byron (2007) and reproduced with permission of the Nature Publishing Group.*

Ciliated cells are the most common cell phenotype in the respiratory epithelium of mammals and, together with secretory cells, facilitate mucociliary clearance of foreign materials including particles and bacteria. The synchronised cilia (12 to 15 beats/second; 200 to 300 cilia/cell) move the mucous blanket towards the oesophageal opening at the larynx, where the material is constantly swallowed (Harkema *et al.*, 2013). The mucous blanket lines the airways and contains mucins

(glycoproteins), to form a gel-like fluid, and surfactants (mainly phospholipids) to reduce the surface tension and prevent airway collapse during exhalation. Both components also interact with viruses and pathogens respectively as part of the innate immune system to enhance macrophage and neutrophil responses (Lewis and McKeivitt, 2013). This layer is therefore an important physical barrier for trapping and facilitating removal of airborne particulates and pathogens.

Brush cells are uncommon in the respiratory epithelium but are found in the nasal and tracheobronchial epithelia. With chemoreceptors and basolateral contact with neurones, they appear to have a sensory role.

There are three key types of secretory cell in the respiratory epithelium:

- Mucous cells are the most common phenotype in the tracheobronchial airways of primates and dogs, but are restricted to the trachea and extrapulmonary bronchi of healthy pathogen-free rodents. These cells secrete the epithelial lining fluid containing glycoproteins (mucins), lipids, proteins and salts, a protective layer that moisturises and lubricates the airway. Exposure to irritants increases mucous production and, with repeated insult, may result in hyperplasia, an abnormal increase in the number of these cells (Harkema *et al.*, 2013).
- Club cells are found mainly in the terminal bronchioles of primates but are the primary secretory cell throughout the tracheobronchial airways of mice. The cells secrete proteins including the club cell secretory protein (CCSP; 10 kDa in size) and surfactants into the epithelial lung fluid. The cells also metabolise xenobiotics through cytochrome P<sub>450</sub>-dependent mixed-function oxidases and are progenitor cells for ciliated and other secretory cells (Harkema *et al.*, 2013).
- Serous cells are the predominant secretory cells in the trachea, extending to proximal intrapulmonary bronchioles of rats. They also occur in rodent nasal airways and human bronchi. Serous

cells produce mucous, antibacterial agents and lactoferrin, an iron-binding glycoprotein that degrades viral RNA as part of the innate immune system (McCormick *et al.*, 1974).

### **1.2.2. Distal respiratory region (lungs)**

The anatomical organisation of lungs into lobes varies significantly between species, with the lungs of non-human primates divided into six lobes (two off the left bronchus and four off the right bronchus). In rats, the left lung is a single lobe and the right lung consists of four lobes (Lewis and McKevitt, 2013). The upper airways in the lungs also contain several generations of non-respiratory bronchioles (conducting airways lacking alveolar ducts). The distal respiratory region, located in the lungs, consists of respiratory bronchioles, alveolar ducts and alveolar sacs, with the alveolar parenchyma (functional tissue) presenting a large surface area for gaseous exchange with the perfusing blood.

Respiratory bronchioles are poorly 'alveolised' and form the transitional airways between the non-respiratory bronchioles and the lung parenchyma. Several generations of respiratory bronchioles are seen in dogs and primates and are absent or present as a single generation in rodents and rabbits (Harkema *et al.*, 2013).

The lung parenchyma is approximately 90% of the total lung volume in mammals. An intricate clustering of alveoli (sacs), supported by the interstitium (mainly fibroblasts), optimises the surface area generated within the lung volume. The human lung contains approximately 500 million alveoli, equating to a surface area of 100 square meters. The ratio of surface areas for the alveolar and capillary lumens is near parity, with a mean separation between the two surfaces of just 0.4  $\mu\text{m}$  in rats and 0.6  $\mu\text{m}$  in humans facilitating efficient gaseous exchange. Alveoli are composed of two cell types:

- Type I pneumocytes, a water-tight but gas-permeable membrane of thin cells lining 95% of the alveolar air space;

- Type II pneumocytes cells produce, store and secrete alveolar secretions and regulate the composition and volume of the fluid in the lumen. In addition, these cells replenish damaged Type I pneumocytes (Harkema *et al.*, 2013).

The air in the alveolar sacs is ventilated tidally, with expansion and contraction of the lungs facilitated by movement of the diaphragm and ribcage. Gases diffuse across the thin epithelium from a higher concentration to a lower one, such that the haemoglobin in erythrocytes becomes re-oxygenated and CO<sub>2</sub> diffuses into the alveolar airspace. The waste air is then vented (exhaled) and replenished with inhalation of fresh air.

### **1.2.3. Macrophages**

Macrophages play a protective role as part of the innate immune system in the lung. They also play a key role in clearance of particles from the alveolar spaces of lungs, and migrate towards deposition sites and phagocytosed particles (Warheit and Hartsky, 1993).

Macrophages in the interstitium are derived from haematopoietic stem cells in the bone marrow and migrate to the lungs via the circulatory system (Geiser, 2010). Once in the interstitium, they phagocytose particulates that crossed the epithelium, or move into the alveolar space and differentiate to form alveolar macrophages. Although alveolar macrophages typically differentiate from circulating monocytes after migration into the alveoli, they undergo extensive proliferation *in situ* as part of an inflammatory response mediated by T-helper Type 2 cells (Murray and Wynn, 2011).

Activated macrophages can be classed as “classically activated” (M1), with inflammatory, cytotoxic and antiproliferative properties, and “alternatively activated” (M2), which are anti-inflammatory and involved in remodelling and regeneration of damaged tissue. A macrophage can change between the M1 and M2 states depending upon the stage of the inflammatory or disease process (Lewis and McKeivitt, 2013,

Murray and Wynn, 2011). Although much has been published about the activation state of macrophages in relation to immune function (Martinez and Gordon, 2014, Mosser and Edwards, 2008), the relationship between activation state and the endocytosis of drug particles is unclear. The time taken for macrophages to endocytose particles is fast but differs between species. Approximately 50% to 75% of particles are typically endocytosed within 2 to 3 hours of particle deposition,  $\geq 90\%$  by 10 hours and nearly 100% at 24 hours (Geiser, 2010). This has potential implications for inhaled medicines and their duration of action, since particles endocytosed by alveolar macrophages are compartmentalised, potentially impeding modulation of the target pharmacology.

Alveolar macrophages may leave the lung via mucociliary clearance, a key mechanism for clearance of inhaled particles, or transepithelial migration and subsequent movement into the lymphatic system. The latter route facilitates presentation of particles to dendritic (macrophage-like) cells specialised for antigen presentation (Lewis and McKevitt, 2013). The clearance time for macrophage-associated particles is relatively short in conducting airways (24 to 48 hours; primarily via muciliary clearance) and longer from the alveolar region (weeks to months). However, the time taken for macrophage clearance is species dependent; quickest in rodents and sheep but slower for primates, dogs and guinea pigs (Geiser, 2010).

### **1.3. Drug delivery devices**

The origins of inhaled therapies are most likely ubiquitous and date back at least 4000 years. The smoking of herbal preparations to treat respiratory diseases represents early attempts to target the drug at the diseased tissue. Ayurvedic therapies (India *circa* 2000 BC) included smoking *Datura* species containing potent alkaloids with anticholinergic bronchodilatory effects. Pipes (*circa* 1500 BC) for smoking tobacco and other herbal products were also found in Central and South America

(Anderson, 2005). Egyptian papyrus scrolls (*circa* 1554 BC) documented a method for smoking the fumes of black henbane (*Hyoscyamus niger*, which contains the muscarinic antagonist atropine) over a hot brick (Stein and Thiel, 2017) and described inhaled administration of nasal snuffs and vapours (Shehata, 2008).

*Circa* 400 BC, Hippocrates was credited with the design of an early inhaler consisting of a pot with a reed in the lid through which a patient could inhale the vapour (Anderson, 2005). However, little changed in respiratory medicine until the industrial revolution (1760), when new manufacturing processes and technical discoveries radically changed drug delivery. Previously, the inhaled drug was prepared by the physician or patient. With industrial practices, inhalers and medicines were mass produced remote from patients. Techniques developed to isolate active ingredients also enhanced the potency and safety of inhaled drugs. An English physician first described the “inhaler” for administration of opium to treat cough (Mudge, 1779); the device was a pewter tankard with an adapted lid incorporating a tube and valve through which the patient could inhale and exhale a steamed vapour (Anderson, 2005, Stein and Thiel, 2017).

Further innovations followed in the latter 1800s, with invention of the atomiser to disperse liquids as a fine spray, and then its modification to produce the nebuliser, an atomiser incorporating baffles to remove large non-respirable droplets (Nikander and Sanders, 2010). During this time, the first dry powder inhalers (DPIs) were developed and “asthma cigarettes” containing stramonium (from *Datura stramonium*), tea leaves, belladonna (contains atropine), kola nuts (contain caffeine) and lobelia (contains a toxicant similar to nicotine) were commercialised (Stein and Thiel, 2017). The revolution in modern inhaler design came in 1955, when Riker Labs (now 3M Drug Delivery Systems) developed the pressurised metered dose inhaler (pMDI) and launched the first pMDI-drug formulation in 1957 (Anderson, 2005). However, despite the development of hydrofluoroalkane (HFA)

propellants to replace the chlorofluorocarbon (CFC) propellants phased out by implementation of the Montreal protocol in 1989 (to safeguard against depletion of the ozone layer), initial uncertainty regarding the future of pMDIs prompted the modern development of DPIs (de Boer *et al.*, 2017). Nevertheless, the pMDI remains the predominant inhaler representing 80% of the global market for inhaled medicines (Telko and Hickey, 2005).

Today, nebulisers, pMDIs and DPIs are the devices commonly used for administering inhaled drugs. There are advantages and disadvantages for each of these devices and selection of the drug and inhaler device depends upon the clinical application, the cognitive and physical ability of the patient (Geller, 2005) and the available drug-inhaler products of pharmaceutical companies.

Many inhaled medicines are packaged into an inhaler, such as the pressurised metered dose inhaler (pMDI; Figure 1.4A) or a dry powder inhaler (DPI; Figure 1.4B). These portable devices are designed to dispense a fixed mass of drug that is inhaled by the patient within a few seconds. A pMDI contains a propellant that expels the aerosol when actuated by the patient. This requires considerable training by the patient to coordinate the actuation of the pMDI with their inspiratory flow. Whilst 40% to 60% of COPD patients adhere to the prescribed dosing regimen, just 10% of patients using pMDIs were able to perform all essential steps correctly; the most common error was failure to continue inhaling slowly after actuation of the pMDI (Restrepo *et al.*, 2008). Whilst a poor technique can be mitigated by using a spacer, a small chamber from which the expelled dose can be inhaled (recommended for children), these spacers are more bulky and unpopular with many adults.

1.4A:



1.4B:



1.4C:



**Figure 1.4: Clinical inhalers and a nebuliser for dosing patients.** **1.4A:** pressurized metered dose inhaler (pMDI). **1.4B:** dry powder inhaler (DPI). **1.4C:** nebuliser. Image c/o Understanding Animal Research, UK.

DPIs are generally easier to use than pMDIs because they are breath activated (Geller, 2005) and few patients develop a poor technique with chronic use. However, the peak inspiratory flow necessary to achieve a therapeutic effect is critical and DPIs cannot be used with spacers (Crompton, 1991). This is a disadvantage of some DPIs (inspiratory flow of 50 to 60 L/min) and patients achieving a low inspiratory flow rate, such as young children or COPD patients (Ashurst *et al.*, 2000); 17% of COPD patients in a study achieved an airflow of  $\geq 40$  L/min

(Dewar *et al.*, 1999). DPIs utilising powder doses from foil blister packs are resistant to high humidity and offer advantages over capsule-based DPIs for stability and dose delivery of the drug formulation in tropical climates.

Nebulisers are less portable, often requiring a pump or sonic device to generate a compressed air supply (Figure 1.4C) but can deliver higher doses than pMDIs or DPIs (Geller, 2005). The continuous delivery of a nebulised aerosol is better suited to rescue therapies, and nebulisers are typically used by paramedics on location, or at home or in healthcare centres to administer drugs over a longer dosing period.

#### **1.4. Challenges in non-clinical lung delivery and respiratory drug development**

Drug discovery and development are very time consuming and resource intensive processes. Estimates of the cost and time required to release a new drug onto the market vary, with seven to 12 years at a cost of \$1.2 billion cited by Shankar *et al.* (2006) and an estimate of \$0.87 to \$2.0 billion by Adams and Brantner (2006). Just five in 40,000 compounds tested in animals reach clinical (human) trials, of which just one eventually reaches the market (Kapetanovic, 2008). The pharmaceutical industry is under increasing pressure to reduce the cost of developing new drugs. Reducing the attrition of drug development programmes (increasing the success rate) and terminating non-viable assets sooner are two strategies for achieving this goal. Reducing the cost and resources to support non-clinical work is attractive if cost effective, and the use of surrogate formulations or administration routes to reduce compound usage in early drug development and thereby expedite preliminary evaluation of inhaled drugs in humans is sometimes proposed. However, such strategies defer de-risking potentially altered tolerability or toxicopathology of the final formulation and/or dose route until after the commitment of significant resources in support of the clinical development programme.

To improve patient compliance in treating chronic pulmonary diseases such as asthma and COPD, attempts have been made to simplify medication initially by combining drug products, and then by reducing the frequency of administration to the minimum. To this end, once daily dosing using inhalers have been evaluated (Buhl *et al.*, 2003, Cazzola and Matera, 2008). A clinical trial with 10,355 patients administered Trelegy Ellipta, the only FDA-approved once-daily triple therapy (containing an inhaled corticosteroid, a long-acting muscarinic antagonist and a long-acting beta2-adrenergic agonist) indicated a reduction in COPD exacerbations (RNS-LSE#1, 2017, RNS-LSE#2, 2017), *i.e.* the worsening of disease often associated with infection. Reducing the frequency of administration can be achieved through a variety of mechanisms to prolong the duration of action including:

- very low solubility (*e.g.* inhaled corticosteroids like fluticasone propionate for treatment of asthma);
- tissue retention due to hydrophobicity (*e.g.* salmeterol, a long-acting  $\beta$ 2-adrenergic receptor agonist) or positively charged moderately lipophilic molecules (*e.g.* verapamil for treatment of hypertension);
- particle engineering with excipients to slow the dissolution rate.

Hydrophobic molecules can be absorbed rapidly into the systemic circulation and away from the lungs, consequently eliciting short-lived efficacy at target receptors within the respiratory tract. Strategies to slow absorption or prolong lung retention are thus attractive for treating chronic respiratory disease (Patton and Byron, 2007).

Many inhaled drugs have been developed as dry powder formulations, notably as micronised crystals, to prolong physical stability and improve the control of clinical drug delivery (Crompton, 1991). In addition, inhaled drugs of relatively low aqueous solubility have been developed to limit systemic exposure after inhaled administration and to extend the duration of action for a single dose by slowing dissolution

of a drug in the lungs. A consequence of such drug design is the accumulation of undissolved drug in the lower respiratory tract with repeated administration, especially at higher doses typically employed in non-clinical toxicology studies conducted for safety assessment of inhaled molecules (Jones and Neef, 2012), with implications for the potential impairment of lung function (Fröhlich, 2017).

In the twentieth century, many published studies investigating respiratory tract clearance were conducted using inhaled particles containing radionuclides, in which the reported data pertained to both clearance of the administered particles and also any radionuclides that became dissociated following lung deposition (Cuddihy and Yeh, 1988). Adaptive lung changes and adverse lesions associated with lung burden have also been described in detail for nuisance particulates, e.g. minerals (Pauluhn, 2008), environmental pollutants (Miller, 2000) and pigments (Lee *et al.*, 1986), the mechanisms of which are independent of pharmacology-mediated toxicology. However, little has been published about the toxicopathology of inhaled pharmaceuticals.

#### **1.4.1. Regulatory testing of drugs**

The development of drugs as dry powder formulations for treatment of respiratory diseases has presented significant challenges. This is in part due to a relatively narrow therapeutic index, *i.e.* the multiple of the clinical dose in humans to the no observed adverse effect level (NOAEL), established from *in vivo* toxicity studies in animals; the NOAEL is the highest evaluated dose that does no harm to the test animals (Kerlin *et al.*, 2016). Regulatory authorities apply factors for safety margins between the animal NOAELs and human doses. The United States (US) Food and Drug Administration (FDA) arguably applies the most conservative margins for inter-species differences in lung deposited dose, by assuming 10% and 25% of an aerosol are deposited in the lungs of rats and dogs respectively, and assuming

100% of a clinical dose is retained in the lungs of humans. The publication of Snipes (1989), upon which these margins are believed to be based, is generally in line with the lung deposition fractions for animals but not humans (25% and 40% for nasally and orally inhaled aerosols of 2 $\mu$ m aerodynamic diameter respectively). An additional margin of 10-fold for rats and 6-fold for non-rodents is applied for unmonitorable findings (Lewis and McKeivitt, 2013, Owen, 2013, Forbes *et al.*, 2011, Jones and Baldrick, 2013) such as histopathological lung changes in animals that lack a clinical marker for humans. Taken together, the applied safety margins applied to therapeutic indices are 100-fold in rodents and 24-fold in non-rodents.

Regulation of non-clinical drug development has often been prompted by tragedies resulting in the death or suffering of humans (Kille, 2013), which identified gaps in the scientific knowledge and/or practices of the day. Regulatory agencies were initially founded by sovereign states to safeguard their citizens against consumer products. The FDA was founded in the USA in 1930 but can trace its origins back to the US Patent Office *circa* 1848 and its chemical analysis of agricultural products. In 1906, the “Pure Food and Drugs Act” prohibited the interstate trade in adulterated or misbranded food and drugs (FDA, 2017). The requirement for pre-market testing of pharmaceuticals as evidence of safety for new drugs was first enacted in the “Federal Food, Drug and Cosmetic Act” of 1938 (Kille, 2013).

Regulation of pharmaceuticals in the United Kingdom (UK) has similar origins to that in the USA; the “Adulteration of Food and Drugs Act, 1860” and the “Sale of Food and Drugs Act, 1875” were passed during the industrial revolution in response to industrialists infuriated by high absenteeism due to the consumption of adulterated foods. The Society of Public Analysts was founded after revision of the “Adulteration of Food and Drugs Act, 1872” made provision for the appointment of public analysts. Whilst the “Food and Drugs Act, 1938” introduced penalties for false or misleading labelling and advertising, it was not

until the “Medicines Act, 1968” that control of drugs for clinical and veterinary use were legislated separately to food (Dawson, 2014). This legislation followed outcry over birth defects after prescription of thalidomide to pregnant mothers in the late 1950s and early 1960s to alleviate morning sickness. To prevent reoccurrence of such a tragedy, the Committee on Safety of Drugs was established in 1963 and was superseded by the Committee on Safety of Medicines in 1968 and the Commission on Human Medicines in 2005 (MHRA, 2012).

There are two key elements to drug regulation. Firstly, there are guidelines outlining the data requirements necessary to support an application for the licenced marketing of a drug. Historically, these guidelines were implemented by each agency responsible for the control of drugs in the respective country. The harmonisation of guidelines was pioneered in Europe during the late 1980s with progression of the common market. During this period, the pharmaceutical industry and regulators for the three major pharmaceutical markets (USA, Europe and Japan) also discussed harmonisation of requirements for testing pharmaceuticals, with a view to eliminating unnecessary duplication of work, and ultimately reducing the resources, time, cost and number of animals required to bring drugs to various pharmaceutical markets (Jones and Baldrick, 2013). Since its inception in 1990, the International Council for Harmonisation of Technical Requirements for Pharmaceuticals for Human Use (ICH) has developed and maintained guidelines to generate comprehensive datasets to satisfy regulatory requirements for global licencing of drugs (ICH, 2017). Experimental protocols based on this guidance continue to evolve within pharmaceutical companies and contract research organisations to fulfil the regulatory obligations and accommodate the bespoke requirements of drug development programmes.

Secondly, there is a formal review of the data submission undertaken by a regulatory agency responsible for the market in question. This review includes characterisation of the drug product, hazard evaluation

(toxicology) and a complex risk assessment including consideration of toxicity observed in animals, the likelihood of an adverse outcome occurring in patients at anticipated doses, and a risk-benefit analysis of the potential side effects verses therapeutic prognosis of the disease.

Each nation is responsible for the regulatory approval and licensing of drugs administered to its resident population. In 1965, the European Economic Community mandated that “No proprietary medicinal product may be placed on the market in a Member State unless an authorisation has been issued by the competent authority of that Member State” (EEC, 1965), and this passed into British law with the “Medicines Act, 1968”. With funding from the European Union (EU), member states and the pharmaceutical industry, the European Medicines Agency (EMA) was founded in 1995 to harmonise the national medicine regulatory agencies of EU member states (EMA-1, 2017). Drawing on the resources of the regulatory agencies of member states, approval of new medicines for licensing in the European Economic Area (EEA) was facilitated under a reciprocal agreement without the need to obtain regulatory approval from each agency, reducing the cost of approving a new drug across the EEA and the time taken to prescribe new drugs to European patients. Following the UK announcement to leave the EU on 30-Mar-2017, implications for the reciprocal agreements between the Medicines and Healthcare Products Regulatory Agency (MHRA, UK) and the EMA or a need for duplicate reviews are unknown (Gulland, 2016, EMA-2, 2017). Nevertheless, the legal requirement for licensing new drugs will persist.

#### **1.4.2. Animal models for investigating efficacy**

Unlike non-clinical safety studies, there are no regulatory guidelines for animal models used to predict potential clinical efficacy *per se*. Animal models must be relevant to mechanism(s) of interest in patients. However, interspecies differences may present limitations for disease models such as asthma, which does not spontaneously develop in

laboratory species. Consequently, most animal 'asthma models' targeting the T-helper cell Type 2 response first require sensitisation of the species to an allergen that is subsequently used to challenge the airways and provoke an allergic response (Zosky and Sly, 2007). Development of suitable animal models may be hampered if the aetiology of the human disease is poorly understood; various animal models developed for pulmonary fibrosis mimic some but never all of the features of human idiopathic pulmonary fibrosis (Moeller *et al.*, 2008). Additional models may be technically challenging and costly, such as induction of a COPD-like disease in rodents after repeated inhaled administration of cigarette smoke. Underexposure of rodents to cigarette smoke may result in development of minimal disease or overexposure may result in effects associated with non-specific particle overload (Wright *et al.*, 2008). Researchers may therefore use a model to demonstrate engagement of a relevant mechanism in healthy animals, such as inhibition of inflammation, instead of using a disease model *per se*. Pre-clinical models are initially based upon available scientific literature or unpublished data, validated for novel pharmacological targets and may also be adapted for project requirements.

### **1.4.3. Animals and ethics in scientific research**

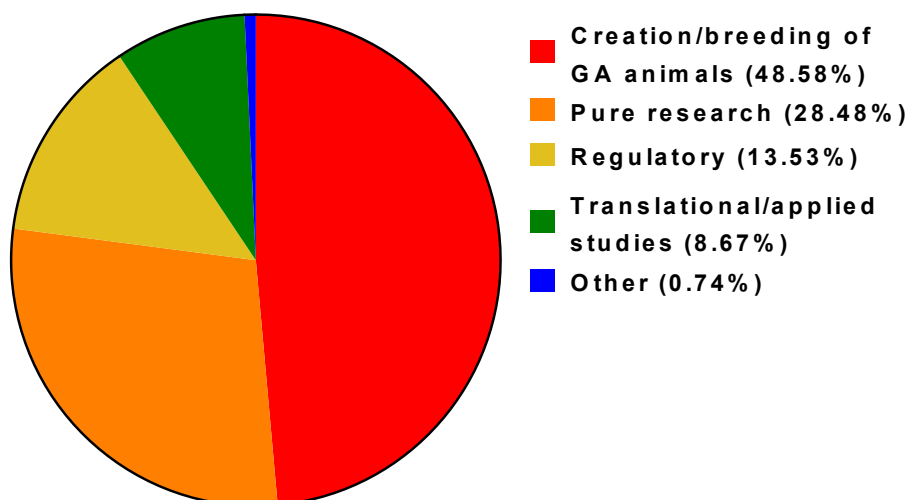
The use of animals in scientific research was essential to our understanding of diseases and underpinned major advances in modern medicine including development of vaccines, medicines, blood transfusion and dialysis, organ transplants and surgical procedures. Nevertheless, since domestication of dogs 15,000 years ago (Driscoll *et al.*, 2009), humans have shared an emotional attachment to companion animals (Dotson and Hyatt, 2008) and the use of animals in scientific research is consequently an emotive and contentious topic. Scientists have a moral obligation to use alternative investigations to animal experiments where possible (replacement), to design experiments that minimise the number of animals and/or licensed

procedures required to achieve the scientific objectives (reduction) and to use appropriate humane endpoints (Morton, 1999) to minimise the potential for suffering or distress (refinement). These concepts, known as the “3Rs”, were first described by Russel and Burch (1959) and are now fundamental to the ethical review process and regulation of *in vivo* experiments (Festing and Wilkinson, 2007). Whilst the EU ban on the animal testing of cosmetic products and marketing cosmetics tested on animals (Pauwels and Rogiers, 2007) represented a significant milestone in the application of the 3Rs, the complexity of respiratory drug delivery and the biological responses of intact animals to pharmaceuticals are such that the most complete assessment of pulmonary drug delivery, efficacy and toxicity is currently achieved *in vivo* (Fernandes and Vanbever, 2009, Holländer, 1988).

The “Cruelty to Animals Act, 1876” passed by the UK parliament was the world’s first legislation to set limits and instigate licensing for use of animals in scientific research. It was superseded by the “Animal (Scientific Procedures) Act, 1986” (A(SP)A), which probably represents the most stringent control of animal experimentation in the world (Wells, 2011). The act governs all scientific research in the UK using species of vertebrate (excluding humans) or cephalopod (Home Office, 2013), and outlines legal implications for scientists performing procedures in breach of licences for the named establishment, project and individual operator.

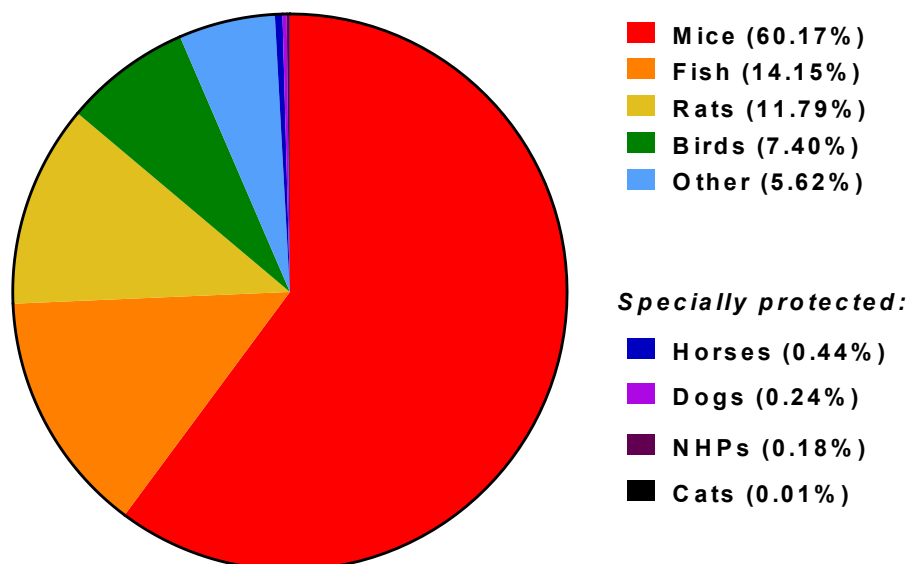
Statistics published annually by the UK Home Office are the most comprehensive dataset for animal research in the world and facilitate monitoring of trends in the numbers of animals used in the UK. Recent increases in animal procedures are mainly attributable to the creation and breeding of genetically altered animals, which accounted for 49% of procedures in 2016 (Figure 1.5A). Conversely, the number of experimental procedures in normal animals has declined steadily since 1987 (UAR, 2017), most of which were performed in rodents (Figure 1.5B).

**1.5A: Total procedures by purpose**



Total procedures = 3.932 million

**1.5B: Experimental procedures by species**

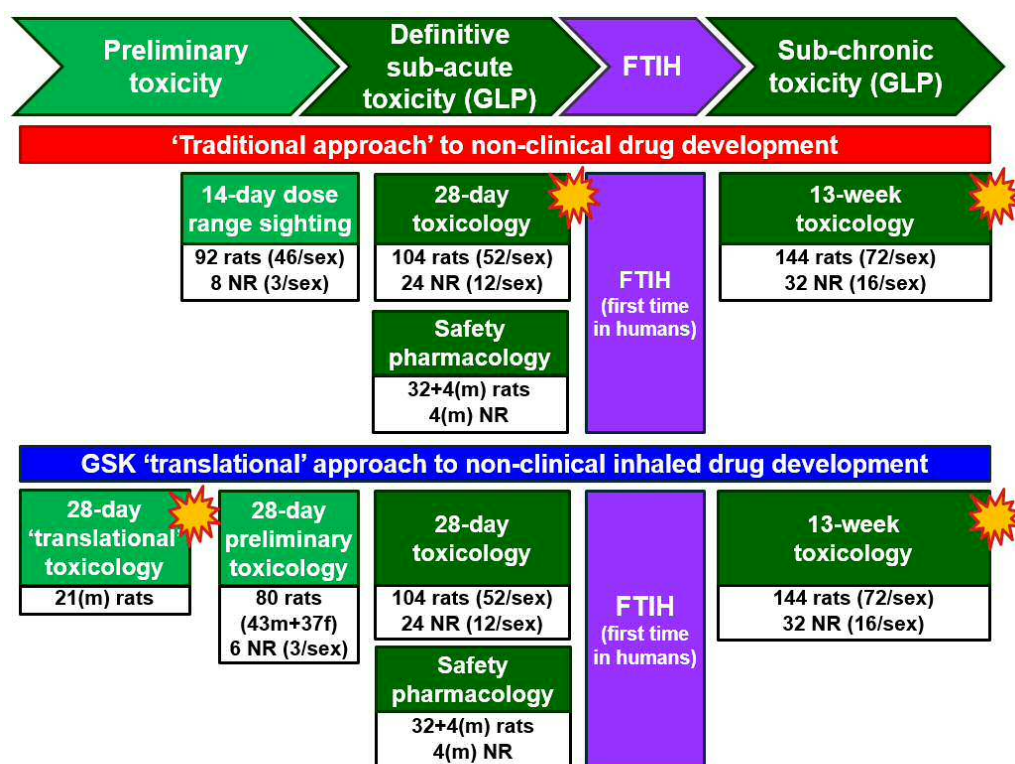


Total procedures = 2.028 million

**Figure 1.5: Total procedures performed in Great Britain during 2016 (Home Office, 2017).** **1.5A:** total procedures shown by purpose. **1.5B:** total experimental procedures shown by species (excludes creation or breeding of genetically altered animals); NHP = non-human primates.

The UK Home Office does not capture data in sufficient detail to indicate the use of animals by therapeutic areas in drug development or the exposure routes used for dose administration. The number of animals used to support development of a drug depends upon the therapeutic indication (e.g. short-term “rescue therapy” or long-term

treatment of chronic disease), differences between laboratory protocols or project plans, and the conventional or bespoke experiments required to address liabilities or further characterise results. Nevertheless, unpublished corporate guidance for drug development suggests at least 3000 animals are required to assess the non-clinical safety of a drug developed for chronic administration to humans. With just one in 8,000 drugs tested in animals progressing to clinical trials (Kapetanovic, 2008), pharmaceutical companies are adapting experimental designs to minimise animal use in research (Figure 1.6).



 point at which detection of adverse lung pathology is likely; subsequent studies assessing chronic, reproductive or immuno-toxicology, carcinogenicity or other endpoints are unlikely to be impacted by unforeseen lung toxicity.

**Figure 1.6: Refinement of drug development programmes to reduce animal use associated with drug attrition due to adverse lung pathology.** Review of attrition for inhaled drugs in the GSK portfolio indicated detection of adverse lung pathology increased significantly when administered to animals for 28 days or longer. Adaption of non-clinical safety programmes to include a ‘translational’ rat study designed to discharge this liability reduced animal usage by 211 rats and 36 non-rodents if adverse pathology developed over 28 days of treatment. **Key:** GLP = Good Laboratory Practice (audited studies for regulatory submission); FTIH = first time in humans; NR = non-rodents; m/f = male/female

Use of alternative dose forms and delivery platforms, e.g. nebulised solutions, are sometimes proposed to circumvent problems in early drug development, such as potentially time-consuming salt selection programmes or scaling-up chemical synthesis of sufficient drug for inhaled administration of dry powder formulations to animals. Although such an approach expedites preliminary evaluation of a drug in humans, this must be weighed against potential failure to discharge the risk of tolerability or toxicopathology of the final formulation resulting in use of additional animals. For example, if a drug was to be marketed as a dry powder inhaler product but early development of the drug was expedited using a nebulised solution to support “first time in humans”, nebulised delivery would also be applied during the non-clinical studies using approximately 265 animals (Figure 1.6). A preliminary bridging study using the final dry powder formulation would subsequently be undertaken using rodents by default, or the non-rodent species if more sensitive to the observed toxicopathology. If this bridging study (circa 56 rats or 6 non-rodents) identified adverse lung toxicopathology precluding development of a viable medicine, the ‘expedited strategy’ would arguably represent unnecessary use of 194 to 310 additional animals and exposure of healthy human volunteers when compared to evaluation of the dry powder formulation using GSK’s ‘translational’ approach. Increased understanding of the implications of changing aerosol form will thus inform decisions in early drug development programmes and ensure best practice in line with the 3Rs for non-clinical safety assessment of inhaled drugs.

All animal studies performed in support of this thesis were ethically reviewed and performed in accordance with the UK Animals (Scientific Procedures) Act 1986 and the GSK Policy on the Care, Welfare and Treatment of Animals.

#### **1.4.4. Exposure of animals to inhaled materials and common practices in drug development**

Non-clinical studies performed to characterise the general toxicology (and ideally efficacy) of a candidate drug typically administer compounds via the most clinically relevant route, *i.e.* the exposure route anticipated for dosing humans. Whilst the precise administration of a drug to animals by injection or orally (by intubation of the stomach) is relatively simple, inhaled administration presents considerably more technical and logistical challenges.

Selection of species in regulatory studies is often based upon guideline requirements for non-clinical safety, availability of historical baseline data, and the biological relevance of a species to humans. Animals must also be small enough to permit handling and inhalation exposure in sufficient numbers for the experiment, and large enough for measurement of the endpoints required to achieve the objectives. Development of new animal models for inhaled delivery is slower than for other exposure routes, not least because of the relatively small number of inhalation studies published and difficulties in engineering solutions for handling and exposing alternative species (Pauluhn and Mohr, 2000). The rat is the most commonly used rodent for non-clinical inhalation toxicology studies, with mice normally considered as a second rodent species for evaluation of carcinogenicity, or as a preferred alternate rodent species if the aetiology of toxicity observed in rats indicates the mouse is a more relevant species in comparison to humans, for example if metabolic or anatomical differences lead to toxicity. Historically, dogs and non-human primates were used as non-rodent species for inhalation toxicology studies. Since these species are specially protected under the EU and A(SP)A legislation, there is increasing pressure to consider the minipig as a non-rodent species for inhalation toxicology studies. Whilst the capability has been developed by at least one research organisation, no respiratory drug

development programmes to date have used the minipig as the non-rodent species.

Investigation of the effects of airborne materials (aerosols, vapours and gases) on animals dates back at least 150 years (MacFarland, 1983), with development of head-only exposure of animals first described almost 70 years ago (Princi *et al.*, 1949). Whilst inhalation exposure systems have improved with availability of new materials or development of ancillary apparatus, the basic methodological principles have hardly changed (MacFarland, 1983). Inhalation exposure systems used in non-clinical experiments consist of two key elements: the apparatus to generate a test atmosphere containing a compound or formulation in air, and apparatus designed to present the resultant test atmosphere to the animals.

Two fundamental elements are also found within the engineered infrastructure of the laboratory itself. The quality of air used for presentation of the test article to animals is immensely important. The air supply should be clean and is normally dried and filtered accordingly. Noteworthy considerations for air quality include relative humidity, temperature and contaminant foreign particles, which could have a direct effect on the animal or act as nuclei for the absorption of gaseous or liquid materials, concentrating a test material onto a particle. A system of valves and airflow meters are also required to control and monitor the compressed air supply and exhaust vacuum for an exposure system during generation of the test atmosphere. Exposure systems must also contain the test article to prevent passive exposure of the operators. Each exposure system should therefore be contained within a ventilated cabinet so that any test aerosol emitted from the exposure system is removed from the surrounding environment. Operators entering the cabinet should wear personal protective equipment including suitable face masks or respirators.

### Test atmosphere generation

Animals must be exposed to a test atmosphere containing the candidate drug for a longer period of time than human patients to achieve higher target doses, which are multiples of the anticipated human dose scaled for conservative factors applied for species-related differences in lung deposition (Degeorge *et al.*, 1997, Jones and Baldrick, 2013). Furthermore, the design of the clinical inhaler and/or composition of the clinical formulation are normally unknown in early drug development. Non-clinical laboratories therefore use custom or commercially available apparatus or adapt existing clinical devices to generate reproducible test atmospheres for sustained periods. Furthermore, given the conservative safety margins applied in dose selections, more 'industrial' devices such as atomisers may be used to achieve a higher feed rate than that achieved using clinical devices.

Test atmospheres can be broadly classified according to the physical properties of the constituent materials:

- solids, such as dusts, fibres (e.g. asbestos) and nanoparticles
- fluid droplets (non-volatile liquids)
- gases or vapour (generated from volatile liquids)
- pyrolysis products such as fumigants, tobacco or fire smoke.

A test atmosphere may be generated as a combination of these phases, such as droplets and vapour (from 'semi-volatile' liquids or a mixture of volatile and non-volatile liquids), a mixture of solids, liquids and vapour (nebulised suspensions), or particulate and vapour (sublimable solids). The apparatus used to generate a test atmosphere will therefore depend upon the physical state of the test article or formulation. Whilst inhaled anaesthetics are administered as gas or vapour mixtures with air or oxygen, most pharmaceuticals are solid at room temperature and were traditionally formulated as simple mixtures of drug(s) with excipients. Candidate drugs are thus typically presented to animals as powder aerosols or a nebulised solution or suspension.

Micronised crystalline drugs are robust and can generally be compressed and dispersed in air without compromising or impairing dissociation of primary particles in the formulation. However, with an increasing trend to develop biopharmaceuticals (biologically sourced drugs such as antibodies, peptides or oligonucleotides) for inhaled administration and increased use of engineered particles to stabilise, target and/or modulate release of drugs (Vehring, 2008), care must be taken to ensure such formulations and the drug activity are not compromised during aerosol generation.

When a test material is administered to animals via non-inhaled routes, the material is normally dissolved or dispersed in a vehicle and administered directly to the animals. Consequently, the concentration of the 'active drug' in the dosed formulation is normally the same as the nominal concentration prepared by the dispensary. This is not the case when formulations are dispersed in air for inhalation; a propellant (pMDI) will vaporise and particles of different densities, size or shape will have different aerodynamic properties and may sediment to differing degrees within the apparatus. Aerosols are therefore characterised for the concentration of the drug in the aerosol presented to animals; simple reverse phase high performance liquid chromatography may be sufficient for some biopharmaceuticals but indirect measurements such as absorbance may be necessary. In addition, biopharmaceutical particulates should also be evaluated to confirm that the large molecules remain active following aerosol generation and are not denatured by complications of the inhalation exposure procedure including shearing-stress, aggregation of proteins at air-liquid interfaces or 'extremes' of temperature (Hertel *et al.*, 2015).

A variety of dust generators are available for the dispersal of solid materials into an air stream. Some devices such as the Wright dust feed (Wright, 1950) introduce the powder into an air stream by scraping the powder from a canister containing compressed test material. Other devices avoid the need for compression, for example by drawing a

free-flowing powder into a stream of air using a venturi (Cheng *et al.*, 1989) or by expelling the powder from prefilled capsules using compressed air (Paul *et al.*, 2012). The selection of apparatus may be influenced by the properties of the powder formulation, which may preclude use of some devices suitable for aerosol generation. For example, particles of uniform size or mutually repelled by electrostatic charge may be unsuitable for compression into a canister, or adhesion of particles may impede the free-flowing movement of a powder.

Pharmaceuticals intended for respiratory indications are sometimes preformulated as a suspension in a pMDI, which contains a relatively insoluble drug maintained as a slurry in liquefied propellant, solvent and surfactant. Exposure of animals using pMDIs is relatively straight forward but apparatus used for discharging the test article must agitate the canisters between actuations to ensure adequate mixing of the propellant, drug and excipients. Care must also be taken to avoid frequent discharge resulting in excessive cooling or freezing of the valve due to evaporation of propellant/solvent; carousels are sometimes used to accommodate pMDIs for simultaneous discharge, increasing the total dose discharged each actuation.

For dispersal of liquid formulations, many devices are available commercially. Air jet nebulisers or atomisers are probably the most versatile because they disperse solutions or suspensions by directing compressed air through the liquid formulation, 'breaking the liquid mass up' into droplets. Clinical devices hold a reservoir of the liquid and are easily adapted so that this reservoir can be maintained at a constant volume for longer periods by dispensing the formulation from a larger storage vessel. A potential complication is that freshly nebulised particulates may be electrically charged, influencing deposition in the respiratory tract (NRC, 2006). Although published technical guidelines do not state an acceptable pH range for inhalation exposure of animals to aqueous formulations, it is common ethical practice for laboratories

to ensure formulations are neither too acidic nor alkaline; local practices vary but an accepted range of pH 3 to 9 is not uncommon.

### Exposure system

Non-clinical inhalation exposure systems are ultimately designed to present a test atmosphere to the snouts of animals. There are three fundamental concepts for presentation of a test atmosphere to animals: static (no airflow in chamber), dynamic single-pass exposure system and a dynamic recirculating exposure system (Cheng and Moss, 1995).

*Prima facie*, static and recirculating exposure systems appear to offer advantages for reducing the mass of test article required to sustain the target aerosol concentration. However, static atmospheres present challenges for simultaneous exposure of animals due to the depletion of oxygen, accumulation of CO<sub>2</sub> (limiting the exposure period) and homogenous mixing of particles inside the chamber. With recirculation of a test atmosphere, exposure of animals can be sustained if CO<sub>2</sub> is removed by passing the atmosphere through quicklime (CaO) or soda lime (Ca(OH)<sub>2</sub>) and supplementing the atmosphere with oxygen. However, recirculating chambers are better suited for exposing animals to gases or vapour atmospheres since particulates impact or sediment within the exposure system and are removed by the CO<sub>2</sub> scrubber. In addition, the presentation of pharmaceuticals to animals should be consistent with that intended for humans. Recycling of an aerosol that has been partially inhaled, exhaled and mixed with a supplementary aerosol supply is almost certainly not representative of the formulated drug product emitted from a clinical inhaler.

Conventional inhalation exposure systems commonly used for presentation of pharmaceutical aerosols to animals are thus of the dynamic single-pass design, in which the test atmosphere is continuously delivered and exhausted from the 'breathing zone'. The oxygen in the exposure system must be maintained at a minimum of 19% (v/v) and CO<sub>2</sub> must not increase excessively so as not to effect

animal physiology. This is achieved using an appropriate airflow to replenish the air within the 'breathing zone'. However, for test atmospheres containing a saturated vapour or gas, it may be necessary to supplement the atmosphere with oxygen to mitigate against the displacement of air by the test article and prevent the onset of hypoxia.

Inhalation exposure systems can also be broadly categorised as whole-body chambers and snout-only systems. Endotracheal tubes can also be used to expose larger species such as dogs and non-human primates individually for limited periods of time; this technique is analogous to oral inhalation of pMDI formulations in humans. Given the single-pass approach required for presentation of aerosols to animals, a proportion of particulate is inhaled by animals. Larger particulates dispersed from the aerosol generator impact or sediment within the exposure system and much of the finer particles are exhausted to waste. Inhaled administration of drugs to laboratory animals thus consumes a large mass of drug relative to other exposure routes for a given dose, which increases considerably with whole-body exposure.

Whole-body chambers are used primarily to expose rodents to industrial or agrochemicals and fumigants requiring exposure periods of six hours (US-EPA[3645], 1998, OECD[TG413], 2017, OECD[TG412], 2017). Animals are housed individually in cages within the chamber to minimise crowding and maximise exposure to the test atmosphere. The chamber must be well designed with a plenum to ensure even distribution of the test article within the chamber environment and hence uniform exposure of the animals. An advantage of this technique is that observation of animal behaviour during exposure is possible for those animals within view. However, individually housed animals may curl up and press their external nares against their body, filtering an aerosol through their fur, and particulates

are ingested orally when the animals groom themselves post exposure (Holländer, 1988, Princi *et al.*, 1949).

Snout-only inhalation exposure is most commonly used for both small and large species in pharmaceutical research. The potential for dermal and oral exposure is reduced by presenting an aerosol to an animal's nares. The internal volume of a snout-only system is considerably smaller than a whole-body chamber used to accommodate a given number of animals and the mass of test article required to maintain the target concentration in air is therefore considerably reduced.

Configurations of animal exposure systems are varied and are best considered in relation to the size of the test species, rodents and non-rodents (historically dogs and non-human primates). An exposure system consists of apparatus for dispersing the test article in air (aerosol generator, vaporiser or gas cylinder), a 'breathing zone' for exposure of animals and an exhaust system for the safe removal of waste atmosphere. For snout-only exposure of rats, animals are restrained in tubes and attached to a chamber through which the test atmosphere is directed (Figures 1.7A and 1.8A). Dogs and non-human primates are normally exposed using a mask attached to a breathing circuit conducting the test aerosol (Figure 1.7B); a rubber diaphragm (dogs) or foam edging may be used to achieve a seal around the snout of the animal to contain the test atmosphere during exposure. Provision (access ports and apparatus) must also be made for characterisation of the concentration in air and the particle size distribution if appropriate.

The duration of exposure may vary for local practices, but an exposure period of 30 to 60 minutes is common for snout-only administration of candidate drugs to both rodents and non-rodents.

1.7A:



1.7B:



**Figure 1.7: Dynamic single-pass exposure systems for the non-clinical administration of aerosols. 1.7A: snout-only inhalation chamber for exposure of rats in restraint tubes. A dust generator is mounted on top of the chamber and a vacuum attached at the base to vent the chamber. 1.7B: mask-based snout-only exposure system for dogs. Two nebulisers are seen attached to an expansion tank. The resultant aerosol is conducted via tubing to the masks or sampling port and returned to an exhaust manifold.**

Before undertaking aerosol administration, animals are acclimatised to the restraint and inhalation exposure procedures during which they are attached to the exposure system and exposed to air only. Local practices vary but this training typically takes approximately two days for rodents and two weeks for non-rodents. Pauluhn and Mohr (2000) described the need for tight-fitting masks and effective restraint of large species as a cause of stress that may alter breathing patterns and possibly make characterisation of the test atmosphere difficult or even impossible. Experience shows that, with sufficient pre-study training, dogs require minimal restraint during aerosol administration (Figure 1.8B). In fact, dogs have been observed sleeping during administration of drugs devoid of sedative activity. Nevertheless, it is important to frequently observe each animal during snout-only exposure to ensure it is inhaling the aerosol and that its condition is not compromised. For example, a rat may turn its head within a restraint tube presenting the risk of asphyxiation and necessitating intervention to reposition the rat. Tube restraint may also compromise a rodent's condition if a drug inhibits thermoregulation; whole-body exposure may

be a more appropriate method of exposure in the latter scenario (Lewis and McKeivitt, 2013).

**1.8A:**



**1.8B:**



**Figure 1.8: Restraint of animals for snout-only inhalation exposure.** **1.8A:** conscious rats lying in restraint tubes. **1.8B:** with sufficient pre-study training, dogs remain calm throughout inhalation exposure and require minimal restraint. A harness is attached to a pole towards the rear of the 'dosing table' but the animal is otherwise able to move freely whilst wearing the mask.

#### Particle size distribution and exposure of animals

Solid particulates are often of irregular shape and the density of materials may vary greatly. Aerodynamic equivalent diameter is a means of expressing particle size in terms of the diameter of a sphere of unit density that has the same settling velocity as the particle being studied (NRC, 2006). This relative measurement is a function of an airborne particle's shape, density and geometric size and thus provides a means of comparing a diverse range of airborne materials.

As the potentially most harmful particle size or most responsive region of the respiratory tract cannot be predicted for the species in question, non-clinical exposure systems designed to test chemicals are normally designed to administer polydisperse aerosols (particles of varied sizes) to animals to ensure exposure of the entire respiratory tract to generate general toxicology data suitable for risk assessment (Pauluhn, 2008).

For the testing of chemicals in rodents, regulatory technical guidance first issued in the early 1980s stipulated particulate size requirements of a mass median aerodynamic diameter (MMAD) of 1 to 3  $\mu\text{m}$  and

geometric standard deviation ( $\sigma_g$ ) of 1.5 to 3, although the regulatory guidance acknowledged that extenuating circumstances related to the physico-chemical properties of a test material may result in these ranges being exceeded (OECD[413], 2009, OECD[412], 2009, US-EPA[3645], 1998). In October 2017, the OECD revised its guidance primarily to accommodate the testing of nanomaterials. However, criteria revised for MMAD  $\leq 2 \mu\text{m}$  and  $\sigma_g$  of 1 to 3 were stipulated for all aerosol forms (OECD[TG413], 2017, OECD[TG412], 2017).

To date, pharmaceutical regulatory agencies have not issued technical guidance or expectations for aerosols administered to animals in non-clinical studies. This is perhaps because pharmaceutical development is focused on optimising drug delivery to humans and not laboratory species. Orally inhaled particles of  $\leq 5 \mu\text{m}$  diameter and nasally inhaled particles of  $\leq 3 \mu\text{m}$  diameter are thought to deposit in the lower airways of humans (NRC, 2006) and the optimal therapeutic response is reported to occur for a MMAD of 0.5 to 5  $\mu\text{m}$  (Tayab and Hochhaus, 2005). The test article supplied for non-clinical safety studies is representative of that subsequently administered to humans in clinical trials. This therefore presents practicing inhalation toxicologists with a dilemma insofar as the MMAD/ $\sigma_g$  of a pharmaceutical aerosol will be driven by the particle size range in the input material, which is optimised for humans. Whilst reasonable attempts are made to generate aerosols in line with the MMAD stipulated by regulators of the chemical industry, a smaller MMAD may not be technically feasible for exposure of rodents. The technical guidance issued by regulators of the chemical industry are therefore, in effect, reference documents for testing pharmaceuticals in rodent and non-rodent species.

### 1.4.5. Animal exposure and understanding dosimetry

When administering test articles to animals by inhalation, it is important to appreciate the technical limitations and implications for the achieved dose. Laboratory species are not dosed *per se*, but are exposed to an atmosphere containing test material mixed with air. Animals breathe passively from the test atmosphere; some material is retained in the respiratory tract but most is not. Although a breath-activated device may be employed to optimise dose delivery to larger species, this is impractical for smaller species such as rodents given the small volume of air inhaled relative to the internal volume of the 'dosing apparatus'.

The administered dose is thus unknown but is commonly calculated on a mass per unit body weight basis using the following equation:

$$\text{..... Equation 1}$$

Where  $ID_e$  = estimated inhaled dose (mg/kg),  $C$  = aerosol concentration (mg/L),  $RMV$  = respired minute volume (L/min),  $T$  = duration of inhalation exposure (30 minutes) and  $BW$  = body weight (kg; animals weighed pre-exposure).

The respired minute volume was historically estimated from various published algorithms (Guyton, 1947, McMahon *et al.*, 1975, Bide *et al.*, 2000) or occasionally measured directly. In 2008, the Association of Inhalation Toxicologists published an algorithm based on data collated from 10 laboratories constituting a total of 1983 observations in four species commonly used for inhalation toxicology studies at the time (rats, dogs, mice and cynomolgus monkeys). The working group recommended their algorithm be used for estimating doses to facilitate comparison of data generated at different research facilities.

Inhaled doses stated in this thesis are thus based on the respired minute volume estimated (eRMV) from body weight data using the published equation of Alexander *et al.* (2008) as follows:

$$\text{..... Equation 2}$$

However, use of such algorithms overlooks the potential for physiological or toxicological effects on lung function that can be induced by the test article's properties (Nirogi *et al.*, 2012, Vijayaraghavan *et al.*, 1993). Furthermore, predicted lung function does not permit correlation of data with other parameters such as the drug concentration in lung/plasma or animal behaviour.

Deposition of inhaled droplets or dust within the respiratory tract is dependent upon the aerodynamic properties of the particulate (a function of particle shape, mass and density), electrostatic charge (and hence potential for aggregation), the anatomy of the respiratory tract and the breathing pattern of the test subject (Snipes, 1989). Differences in the angle of bend in the pharynx of animals of pronograde (horizontal) and orthograde (upright) postures influence the proportion of particulate impacting against the wall of the airway. The nature of breathing also greatly influences the site of deposition. For example, rodents are obligate nasal breathing animals, which results in humidification of aerosols and filters out larger particles. However, human patients not only have larger airways but often inhale medicines orally, bypassing the nasal cavity and increasing the lung deposited dose 1.6-fold for particles of 2  $\mu\text{m}$  in aerodynamic diameter (Table 1.1). Approximately 85% of particles of aerodynamic diameter 2  $\mu\text{m}$  are 'inhalable' to rats (Miller, 2000) and Snipes (1989) reported that 7% of such particles are deposited in rat lung. Results of non-clinical studies must therefore consider the achieved particle size distribution and mass of drug likely to be retained by the animal. The US-FDA assumes lung deposition factors of 10% in rats, 25% in dogs and 100% in humans (Forbes *et al.*, 2011, Jones and Baldrick, 2013, Owen, 2013) based on the seminal publication of Snipes (1989). This article referenced historical data for industrial materials such as inorganic nuisance materials and radioactive particulates, which differ to the small organic molecules and biopharmaceuticals in drug development.

**Table 1.1: Proportion of particles deposited in the lungs and respiratory tract of mice, rats, guinea pigs, dogs, monkeys and humans<sup>A</sup>**

Species	Aerodynamic diameter									
	0.2 $\mu\text{m}$		0.5 $\mu\text{m}$		1 $\mu\text{m}$		2 $\mu\text{m}$		5 $\mu\text{m}$	
	Total	Lung	Total	Lung	Total	Lung <sup>B</sup>	Total	Lung	Total	Lung
Rat	-	-	<b>0.10</b>	<b>0.10</b>	NS	<b>0.10</b>	<b>0.60</b>	<b>0.07</b>	-	-
Guinea pig	0.50	0.35	0.50	0.35	NS	0.20	0.90	0.30	-	-
Dog	0.40	0.25	0.30	0.25	NS	0.25	0.60	0.20	-	-
Monkey	-	-	0.50	0.40	NS	0.30	0.75	0.20	0.90	0.10
Human <sup>C</sup>										
Nose	0.30	-	0.25	0.20	NS	0.25 <sup>D</sup>	0.80	0.25	1.00	0.10
Mouth	0.20	0.20	0.15	0.15			0.50	0.40	0.90	0.30

**Notes and references:**

- A Adapted by Snipes (1989) from Schlesinger (1985); “total” deposition equals the fraction of inhaled particles that deposit in the respiratory tract; “lung” deposition equals the fraction of inhaled particles that deposit in the lung.
- B Reproduced from Snipes (1989) table of “Respiratory Parameters for Selected Laboratory Animal Species and Humans”; total deposition not stated (NS).
- C Human data presented for nose breathing and mouth breathing.
- D Human exposure route not stated; adapted by Snipes (1989) from Schlesinger (1985) and from Snyder *et al.* (1975), data for adult man, “light activity”.

**1.4.6. Fate of molecules post inhalation exposure**

During inhalation of a polydisperse aerosol, larger particles are deposited predominantly in the upper respiratory tract (nasal cavity and/or pharynx) and are typically swallowed or may be expectorated. Finer particles will be drawn deeper into the lungs, a proportion of which will be deposited in the fluid or mucous lining the respiratory tract, and additional airborne particles will be deposited in the respiratory tract as the aerosol is exhaled (Figure 1.1). Once a particle has been deposited in the lung, there are initially two competing processes that govern the drug’s fate:

- Solvation and dissolution of the drug into the epithelial lung fluid, followed by transmembrane absorption into epithelial cells.
- Removal of particles by mucociliary clearance in the upper lung or endocytosis by macrophages in the alveolar region.

**Absorption**

Solid particles must undergo dissolution prior to transepithelial absorption. Dissolution can be described as a three-stage process. Firstly, the crystalline lattice (hydrogen bonds) of a solute must be

disrupted and, secondly, cavitation of the solvent must occur to 'host' dissolved molecules; both processes are endothermic. Thirdly, solvation or hydration of the molecules occurs (exothermic) in which the 'dissolved solute molecules' integrate with the 'solvent cavities' (Van den Mooter, 2012). The organization of molecules in an amorphous particle is random and the material is thus more soluble than the crystalline form because less energy is required to facilitate cavitation of the solvent alone. It is also reasonable to hypothesise that a drug presented as droplets of a nebulised aqueous solution will be absorbed even faster than its solid form because dissolution of the drug has already been achieved.

The rate at which a drug particle dissolves is influenced by the physicochemical properties of the drug molecule and the solvent, in this case epithelial lung fluid which is a complex mixture including water, salts, surfactant lipid and proteins. In the airways and alveoli, the epithelial lung liquid is also coated with a monolayer of lung surfactant in which the fatty acid chains of phospholipid molecules project towards the lumen (Patton, 1996). The rate of dissolution is also dependent upon the surface area of drug presented to the solvent, the degree to which the 'microclimate' around the particle becomes saturated with the drug, and the rate of transepithelial and then systemic absorption. The depth of epithelial lung fluid lining the respiratory tract becomes progressively thinner with progression from the upper to lower respiratory tract. In humans, the depth of fluid is 8  $\mu\text{m}$  at the bronchi, 3  $\mu\text{m}$  at terminal bronchioles and 0.07  $\mu\text{m}$  at the alveoli (Figure 1.3). Consequently, the surface area of a spherical particle of 2  $\mu\text{m}$  in diameter presented to the epithelial lung fluid will be significantly less in the alveoli than in the upper airways. Particle morphology may also potentially influence a particle's absorption or macrophage-mediated clearance from the lung and it is therefore likely that dissolution kinetics of aerosol particles on the lung surface are different to those of bulk material in aqueous media (Patton *et al.*, 2010).

Once dissolved in the epithelial lung fluid, a drug may then cross the epithelium via mechanisms influenced by the size of the molecule and its physicochemical properties (Figure 1.9). There are essentially two key mechanisms for the transepithelial absorption of small molecules: diffusion (transcellular and paracellular) and transcytosis (adsorption or receptor-mediated). Absorption may also occur through a compromised epithelium such as via apoptotic cells (Patton, 1996). In practice, transepithelial permeability will be a combination of these mechanisms.

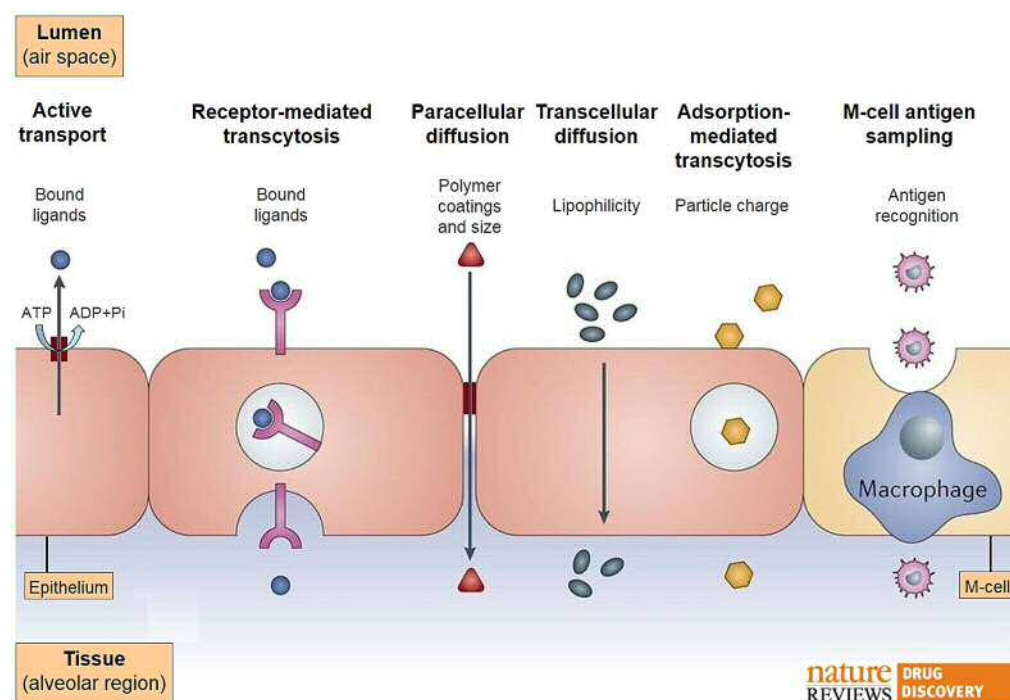


**Figure 1.9: Mechanisms of transmembrane absorption of molecules.** Adapted from Veisoh et al. (2015) and reproduced with permission of the Nature Publishing Group.

Diffusion, the non-specific net movement of molecules from an area of high concentration to an area of low concentration, occurs across cellular membranes (transcellular) or between adjacent cells by crossing tight junctions. Most aqueously soluble small molecules are absorbed from the lungs. Molecules that are more lipophilic are absorbed faster (within seconds or a few minutes), most likely across the cellular membrane. More hydrophilic molecules are absorbed at a

slower rate (within minutes to tens of minutes) and most likely via aqueous pores in the intercellular tight junctions (Patton *et al.*, 2004).

Transcytosis is a mechanism by which cells transport macromolecules from one membrane surface to another by formation of vesicles that maintain the membrane integrity or disrupt the electrochemical potential across a membrane. The movement of drugs can be receptor-mediated or non-specific if charged molecules adsorbed onto the membrane surface are captured during formation of the vesicles. Molecules may also potentially undergo non-specific migration if associated with fluid captured during vesicle formation, a process known as fluid phase transcytosis, although electron microscopy evidence for this was weak (Patton, 1996).

The transport of molecules across a membrane against a concentration gradient requires active transport, an ATP-dependent process facilitated by transmembrane proteins called ATP-binding cassette (ABC) transporters (Cole, 2014). Active transport can be competitively inhibited by common substrates for the binding site of the carrier protein, or inhibited non-competitively by binding elsewhere and altering the structure of the carrier protein (Alberts *et al.*, 2002). Whilst the absorption of drugs is normally considered from the apical to the basal surfaces of the respiratory epithelial membrane, the efflux transporter P-glycoprotein 1 (Pgp) antagonises this process. Often described as a “multidrug resistance protein pump”, Pgp is associated with the poor efficacy of glucocorticosteroids in some patients treated for inflammatory diseases (Barnes and Adcock, 2009). Pgp is generally restricted to the apical surface of cells in many tissues including the lung (Bellamy, 1996). Pgp appears to be well defined at the luminal surface of the bronchiolar epithelium (air interface), bronchial capillaries (blood interface) and alveolar macrophages, but evidence regarding the presence or absence of Pgp in alveolar epithelium is contradictory (Patton *et al.*, 2010). Substrates of Pgp crossing the apical membrane of epithelial cells are therefore pumped back into the

lumen of the airway, potentially impeding transepithelial migration of a drug on the one hand, and/or pumped into the capillaries expediting clearance from lung tissue into the systemic circulation.

Microfold cell (M-cell) antigen sampling is a mechanism for presenting particulates in the lumen to systemically circulating cells of the immune system, thereby effecting an immunological tolerance or suppression of the foreign material. M-cells are specialised epithelial cells that facilitate transcytosis of small particles, soluble macromolecules and microorganisms (Gebert *et al.*, 1996). The reduced efficacy and/or toxicity of biopharmaceuticals with repeated exposure may sometimes be attributable to the generation of anti-drug antibodies (ADAs). However ADAs may also illicit their own toxicity by cross-reacting with endogenous molecules in laboratory species (Koren *et al.*, 2008).

#### Macrophage and mucociliary clearance

Endocytic uptake of particles by macrophages is the primary mechanism for clearance of micron-sized particles at the lung epithelium. Macrophages may then leave the lung via transepithelial migration into the interstitium and subsequently the lymphatic system. However, the mucociliary escalator is the principal pathway for clearance of macrophage-associated particles (Geiser, 2010), which are conveyed to the larynx and swallowed. A proportion of an inhaled 'dose' may therefore be absorbed from the gastrointestinal tract and become systemically available depending upon its bioavailability (subject to the extent of hepatic first-pass metabolism). Tayab and Hochhaus (2005) claimed 10% to 60% of an orally inhaled drug entered the lungs, and 40% to 90% of the drug was swallowed when mucociliary clearance was considered. Whilst these ranges are broad, Bennett *et al.* (1999) showed that orally ingested Salmeterol accounted for approximately 28% and 36% of the increases in heart rate and plasma glucose concentration following an inhaled dose of 400mg (Salmeterol concentrations in plasma not presented).

## 1.5. Chronic Obstructive Pulmonary Disease

COPD is a 'generic disease' encompassing several inflammatory pulmonary conditions that impair lung function. These include emphysema and chronic bronchitis which affect the alveolar sacs and airways respectively (NHS, 2017). COPD is a debilitating disease in which patients present symptoms of dyspnoea (breathlessness), coughing, wheezing, sputum production and frequent chest infections (Celli *et al.*, 2004). COPD is most commonly found in smokers and administration of cigarette smoke to animals is used to induce an emphysema-like disease model (Wright and Churg, 2002, Churg *et al.*, 2008, Armstrong *et al.*, 2015, Shapiro, 2000). COPD is less commonly associated with exposure to irritant dusts, fumes and air pollution particles including the burning of biomass fuels (Churg *et al.*, 2008). Progression of COPD has also been reported in populations of workers in mining and construction (concrete) industries, in potato sorters exposed to diatomaceous earth (a soft, siliceous sedimentary rock) and in pottery workers (Hnizdo and Vallyathan, 2003). However, a genetic predisposition to COPD is also implicated, since 90% of COPD is associated with cigarette smoking but only 15% to 20% of heavy smokers develop this disease (Turato *et al.*, 2001).

The Global Initiative for Chronic Obstructive Lung Disease (GI-GOLD, 2006) defined COPD as:

“a preventable and treatable disease with some significant extrapulmonary effects that may contribute to the severity in individual patients. Its pulmonary component is characterized by airflow limitation that is not fully reversible. The airflow limitation is usually progressive and associated with an abnormal inflammatory response of the lung to noxious particles or gases.”

Diagnosis of COPD was historically based on clinical impairment of lung function using spirometry measurements, which does not capture

the aetiology of disease conditions resulting in the functional changes. COPD is characterised by the permanent destructive enlargement of air spaces in the lung parenchyma with fibrosis (emphysema) and inflammation of the distal airways (bronchiolitis) and central/proximal airways (chronic bronchitis). The structural changes include increased airway wall thickness (due to inflammation) and remodelling (fibrosis and smooth muscle hypertrophy) that collectively narrow or constrict the airways. In addition, emphysema results in a loss of elastic recoil of the airways (Turato *et al.*, 2001, Saetta *et al.*, 2001). T-lymphocytes (positive for CD4 and CD8 glycoproteins; clusters of differentiation at the cellular membrane of helper and killer immune cells), neutrophils and macrophages are implicated in the remodelling of airways and parenchymal destruction (Hnizdo and Vallyathan, 2003).

Glucocorticosteroids are the most effective anti-inflammatory drugs available to treat inflammatory and autoimmune diseases. However, some patients exhibit poor efficacy for treatment of asthma (1% of patients require oral steroids to supplement inhaled doses) and 90% of COPD patients do not respond to inhaled glucocorticosteroids (Barnes and Adcock, 2009). Activation of the mitogen-activated protein kinase (MAPK) pathways is one of the molecular mechanisms implicated in glucocorticoid resistance.

### **1.5.1. p38 mitogen-activated protein kinase inhibitors**

Mitogen-activated protein kinases (MAPKs) are part of conserved signalling pathways that facilitate relaying of extracellular stimulations to intracellular responses. p38 MAPK is more responsive to stress stimuli including ionizing radiation, osmotic shock and cytokine stimuli (Roux and Blenis, 2004). Located in the cytoplasm and nucleus (Cuenda and Rousseau, 2007), p38 MAPK performs a central regulatory function in a signal cascade that results in the synthesis and modulation of proinflammatory mediators. Consequently, inhibition of this mechanism represents a ubiquitous target for inflammatory

diseases including rheumatoid arthritis, Crohn's disease, psoriasis, COPD and asthma (Millan *et al.*, 2011, Mayer and Callahan, 2006). Research into potential mechanisms to inhibit inflammatory disease has focused on protein kinases, which are widely expressed in inflammatory cells and are activated by a variety of stresses. Activation (by phosphorylation) of the p38 MAPK pathways leads to changes in cell cycle or expression of key genes, including cytokines, chemokines, and growth factors (Chung, 2011). The alpha-isoform of p38 MAPK is expressed in airway smooth muscle cells, epithelial cells, and immune cells, and research into using p38 MAPK inhibitors to elicit an anti-inflammatory effect for treatment of COPD have focused on this isoform (Williams *et al.*, 2008, Mayer and Callahan, 2006).

To this end, GSK258899B, a p38 mitogen-activated protein kinase (MAPK) inhibitor of relatively low aqueous solubility, was initially developed as an anti-inflammatory drug designed to have a longer duration of action. Development of the candidate drug was terminated primarily due to inflammatory changes seen in the lungs of dogs after 28 days of treatment. However, an infiltration of inflammatory cells was also seen concurrently with accumulation of alveolar macrophages in the lungs of rats after 28 days (Freke, 2010). *Prima facie*, the inflammatory findings observed histopathologically appeared to be contradictory to the anticipated pharmacology for a p38 MAPK inhibitor. GSK258899B therefore represented a tool compound for investigation of inflammation and its potential modulation with a change in aerosol form. Selection of additional compounds of the same pharmacological class but with different physicochemical properties, such as higher solubility and/or membrane permeability, provided an opportunity to investigate the potential relevance of such parameters in drug design. Blood concentrations of drugs following inhaled administration are often cited but the persistence or location of a drug within the lung is rarely characterised (Patton *et al.*, 2010). Pauluhn (2008) stated differences in the toxic potency of relatively inert materials may be

associated with differences in particle clearance, dissolution rate in lung fluid or initiation of a self-perpetuating inflammation. Whilst potential therapeutic indications for p38 MAPK inhibitors in inflammatory diseases and rodent models for investigating mechanisms of inhibiting acute lung inflammation have been discussed in the literature (Banerjee *et al.*, 2012, Chung, 2011, Haddad *et al.*, 2001, Nick *et al.*, 2002, Underwood *et al.*, 2000, Williams *et al.*, 2008), little has been published about the toxicology of these biologically active organic molecules.

## 1.6. Thesis aims and objectives

Pharmaceutical companies are under increasing pressure to reduce the time and cost of developing new medicines. Expediting strategies for preclinical development of respiratory drugs include use of surrogate formulations or administration routes (different to intended clinical regimen) to facilitate *in vivo* experiments earlier in development, when candidate drugs are synthesised in small quantities. This research was undertaken to investigate potential implications of such expediting strategies. Accepted *in vivo* endpoints and methods for non-clinical assessment of efficacy and pulmonary toxicopathology were selected to profile the response of rats to dry powder or nebulised aerosols of three drugs of common pharmacology. The experimental objectives of this thesis were to:

- Select anti-inflammatory drugs of the same pharmacological class but with differing physicochemical properties, and to measure the systemic (plasma) and lung exposure in rats administered a dry powder aerosol or nebulised solution of each test article (Chapter 2).
- Evaluate the potential for environmental factors during inhalation exposure procedures to influence lung function and dosimetry of inhaled compounds (Chapter 3).

- Determine the median effective dose (ED<sub>50</sub>) of three compounds presented as dry powder and nebulised aqueous aerosols using a rat model to assess prophylactic inhibition of acute lung inflammation (Chapter 4).
- Determine the toxicopathology of three compounds presented as dry powder and nebulised aqueous aerosols for 28 days (Chapter 5).

Results of experimental objectives will be used to test the following key hypotheses:

- The physicochemical properties of a drug influence its lung or systemic exposure *in vivo*, and hence the resultant efficacy and/or toxicopathology.
- Changing the presentation of a drug to rats will affect its absorption and hence alter the resultant efficacy and/or toxicopathology *in vivo*.

Although the systemic and lung exposure of drugs are known to change for different formulations, less is currently known about the implications for potential changes in efficacy, toxicopathology and hence the therapeutic index between these endpoints. It is anticipated that the results of this thesis will indicate the potential opportunities or risks of administering surrogate formulations to animals in early respiratory drug development and identify key factors for drug design.



## **CHAPTER TWO**

**Multivariate-based selection of p38  
mitogen-activated protein kinase  
inhibitors and investigation of  
pharmacokinetics in rats following  
a single inhalation exposure**

## 2.1. Introduction

With just one in 40,000 compounds tested in animals eventually reaching the market (Kapetanovic, 2008), there is an ethical obligation and a compelling commercial argument for pharmaceutical companies to employ effective computational (“*in silico*”) models for lead optimisation and preselection of candidate drugs. *In silico* techniques are increasingly important in predicting chemical properties of new molecules and facilitating computer-aided drug design, considerably reducing the time and resources required for chemical synthesis and biological screening of new drugs (Kapetanovic, 2008). In 2015, a workshop of the American Association of Pharmaceutical Scientists (AAPS), US Pharmacopeia (USP) and Food and Drug Administration (FDA) identified a need to classify inhaled drugs modelled for physicochemical properties specific to lung physiology and drug delivery, similar to the Biopharmaceutics Classification System (BCS) developed in the 1990's for orally ingested drugs. However, workshop participants acknowledged that deriving inhalation BCS classifications would not be simple (Hastedt *et al.*, 2016). With a desire to extend the duration of pharmacological action for treatment of chronic pulmonary diseases (Buhl *et al.*, 2003, RNS-LSE#1, 2017), candidate drugs have been designed with relatively low aqueous solubility or high lipophilicity. However, strategies to slow absorption or prolong lung retention may have implications for safety as accumulation of insoluble material at the respiratory epithelium may impair lung function (Fröhlich, 2017). Aerosols are characterised for their particle size distribution, morphology and dissolution rate *in vitro*. Whilst much is also learnt from *in vitro* models used in high throughput screening of candidate drugs, for example with regards to the mechanisms and pharmacokinetics of absorption (including membrane permeability), receptor binding and occupancy, the most complete assessments of pulmonary drug delivery, efficacy and toxicity are determined *in vivo* using intact organisms (Fernandes and Vanbever, 2009).

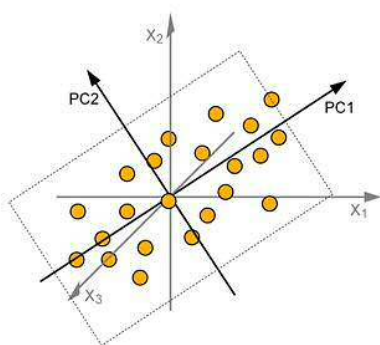
The pharmacokinetics of an inhaled drug can have profound implications for its efficacy and adverse effects, both locally and systemically. For example, the extent of systemic exposure to inhaled corticosteroids has implications for their pharmacodynamic effect of hypothalamic-pituitary-adrenal axis and cortisol suppression, which are associated with chronic adverse side effects such as thinning and bruising of skin, and reduced growth rate and bone density leading to fractures (Derendorf *et al.*, 2006). An understanding of the drug-lung concentration time profile following inhaled administration of a drug to animals immediately post exposure can provide an indication of the 'achieved lung dose' and the potential for accumulation in lungs with repeated administration. The pharmacokinetic parameters of selected p38 mitogen-activated protein kinase (MAPK) inhibitors in plasma and lung tissue and the pattern of lung deposition determined in this chapter will thus provide a context for investigation of efficacy and pulmonary toxicology in animal models described in subsequent chapters.

### **2.1.1. Principal component analysis of physicochemical properties of compounds**

Principal component analysis (PCA), also known as multivariate analysis (MVA), is a statistical method for evaluating complex multivariate data in which observations are described by several inter-correlated quantitative dependent variables (Abdi and Williams, 2010[A]). PCA was first outlined by Pearson in 1901 as an analysis for finding "lines and planes of closest fit to systems of points in space" and was introduced into chemistry by Malinowski in the 1960s (Wold *et al.*, 1987). Today, PCA is widely used by the pharmaceutical industry in conjunction with the concept of 'drug-like chemical space', a function of various physicochemical parameters calculated from a chemical structure or measured, to shortlist candidate drugs for high throughput screening (Mirza *et al.*, 2009). Three variables can be clearly represented using a three-dimensional plot. However, it is difficult for people to comprehend a greater number of variables represented mathematically. Multivariate

analysis provides a means of reducing the 'dimensionality' of large datasets to facilitate more manageable visualisation and interpretation of the information (Wheelock and Wheelock, 2013). This is achieved by representing data as a set of new orthogonal (perpendicular) variables called principal components used to project a pattern of similarity of the observations or variables as points in a two dimensional plot or map (Abdi and Williams, 2010[A]). The concept of multivariate analysis is illustrated in Figure 2.1.

**2.1A:**



**2.1B:**

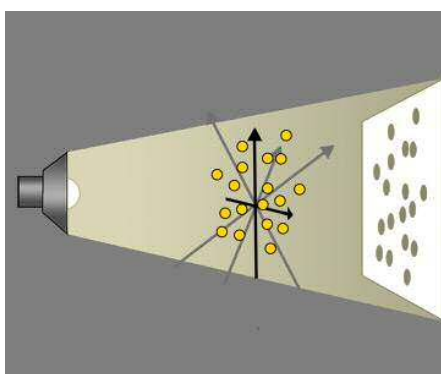


**Figure 2.1: Illustration of principal component analysis (Umetrics, 2013).** **2.1A:** A dataset of 22 observations are plotted for three variables (axes  $X_1$ ,  $X_2$  and  $X_3$ ). A line of best fit is plotted, representing the direction of maximum variation (principal component: PC1). A second axis, perpendicular to PC1, is plotted representing the next best line of fit (PC2). **2.1B:** The observations are projected onto a plane defined by the principal components (PC1 and PC2) to create score plot depicting separation of the observations in two dimensions.

By summarising the physicochemical properties of p38 MAPK inhibitors and plotting the relative similarities and differences of these molecules in the 'physchem space', PCA provides a means for selecting tool compounds of contrasting properties to investigate the systemic exposure, efficacy and toxicopathology, arising *in vivo* following inhaled administration to animals.

### 2.1.2. Aims and objectives

The experimental aims of this chapter are to:

- Select three p38 MAPK inhibitors of differing physicochemical properties by principal component analysis of predicted (*in silico*) and measured *in vitro* parameters.
- Characterise the particle forms for particulate aerosols of the p38 MAPK inhibitors selected for further investigation.
- Determine systemic (plasma) and lung exposure of the selected p38 MAPK inhibitors in rats after a single inhaled dose by chemical analysis of blood/plasma and lung homogenate samples taken up to 24 hours post exposure.
- Investigate drug-lung deposition of the selected p38 MAPK inhibitors in rats following a single inhaled dose, by matrix assisted laser desorption/ionization with mass spectrometry imaging (MALDI-MSI) analysis of lung sections.

Apparatus and procedures for inhalation exposure of rats described in this chapter will form the basis of core methodology in subsequent chapters. In addition, the following hypotheses will be tested:

- Compounds of faster dissolution *in vitro* are likely to be cleared more quickly *in vivo*, from the lungs of rats exposed to an aerosol of the test article.
- Presentation of the test article to rats as a nebulised solution will facilitate a quicker clearance from the lungs since dissolution of the particles is achieved prior to inhaled drug administration.

Results for the testing of these hypotheses will provide a context for investigations described in subsequent chapters. For example, the dissolution rate of a drug in simulated lung fluid (*in vitro*) may not necessarily translate to the *in vivo* model if dissolution in epithelial lung fluid was impeded by the layer of surfactant lining the respiratory tract. It is anticipated that the efficacy or incidence/severity of pulmonary

## *Chapter Two*

toxicopathology of a nebulised solution or compounds quickly cleared from the lungs will be less than for drugs persisting in lung tissue.

.

## 2.2. Materials and methods

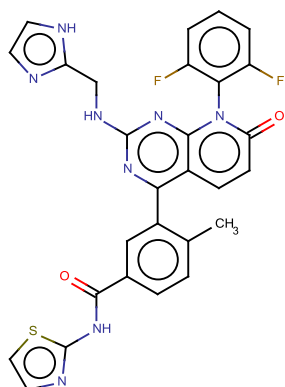
### 2.2.1. Principal component analysis of the physico-chemical properties of six p38 MAPK inhibitors

A shortlist of p38 MAPK inhibitors was compiled for further consideration. GSK development programmes associated with these compounds had been terminated but just six of these compounds (Figure 2.2) were available in sufficient quantity to support conduct of single exposure *in vivo* inhalation studies. Physicochemical data of preselected compounds were collated for PCA. Two datasets of parameters were selected for data mining with reference to panels commonly assessed during lead optimisation of compounds in early drug development by the sponsor (GSK). The parameters were interrelated but generally influenced lipophilicity, solubility and/or protein binding by molecules. Examples of general grouping for *in silico* parameters included:

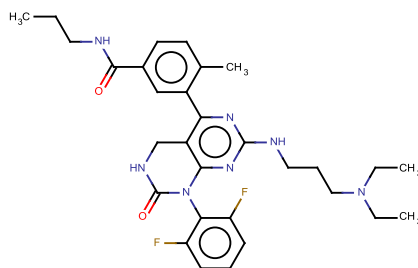
- Lipophilicity: high number of aromatic rings and fluorine groups; LogD (distribution coefficient between organic and aqueous media) and Log P (partition coefficient); membrane permeability.
- Solubility: high acid or base class (acidity/basicity), Abraham's hydrogen bond acidity/basicity; charge, number of positively ionisable groups; rotatable bonds, single bonds (sp<sup>3</sup>) and aliphatic rings (*i.e.* a lack of unsaturated bonds).
- Protein binding: high number of aromatic rings and double bonds (*i.e.* unsaturated bonds); higher proportion of oxygen, nitrogen and sulphur atoms versus carbon atoms ('hetero atoms').

These groupings are not mutually exclusive: basicity is associated with solubility and binding to alpha-1 acid glycoprotein (Urien *et al.*, 1993), a carrier of basic and neutral lipophilic compounds); acidity is associated with solubility and binding to human serum albumen via anionic or electronegative drug moieties (Simard *et al.*, 2006); aromatic rings are associated with lipophilicity and protein binding (Ritchie and Macdonald, 2009).

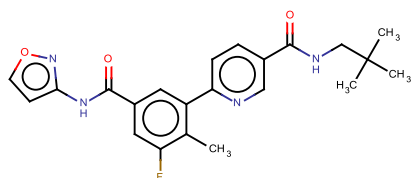
**A: GSK258899A (GSK-899)**



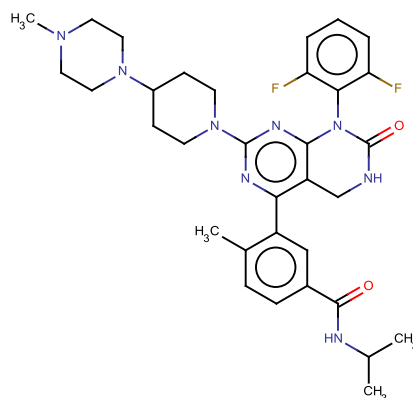
**B: GSK610677A (GSK-677)**



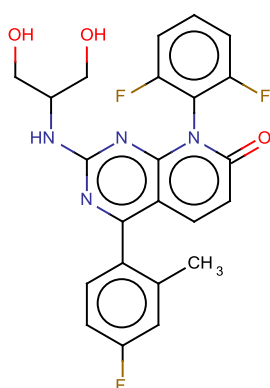
**C: GSK678361A (GSK-361)**



**D: GSK719340A (GSK-340)**



**E: SB-681323 (SB-323)**



**F: SB-731445 (SB-445)**

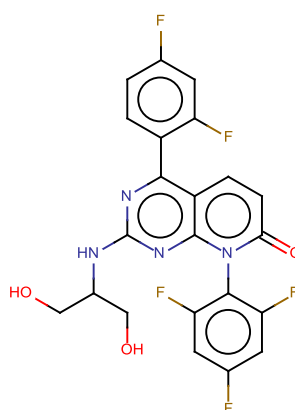


**Figure 2.2:** Chemical structures of six p38 MAPK inhibitors shortlisted for potential investigation of *in vivo* endpoints. Figures 2.2A to 2.2F show chemical structures for the parent compounds (free base). A criterion for compound selection was that all drug development programmes had been terminated.

The first data set consisted of 34 parameters calculated or derived (modelled *in silico*) from the molecular structure of each compound using Adamantis, an in-house web-based tool developed by GSK for the prediction of physicochemical properties and accessing ADME (absorption, distribution, metabolism and excretion) models (Ritchie *et al.*, 2009). The parameters included the following:

- Acid (pKa) and base (pKb) dissociation constants, ranked by range thresholds e.g. 0 = no acidic group; 1 = pKa>8.5 etc.
- Log P: partition coefficient of non-ionised compound between aqueous and organic phases (indication of lipophilicity).
- Log D: distribution coefficient of ionised plus non-ionised forms between aqueous and organic phases (indication of lipophilicity).
- Number of aromatic and non-aromatic rings in a molecule.
- The number of negatively ionisable groups and the number of positively ionisable groups in a molecule.
- The number of hydrogen bond donors and acceptors in a molecule.
- The number of rotatable bonds in a molecule.
- Average binding energy: derived for 10 common functional groups, where present, and used as an indicator of potential drug-receptor affinity (Andrews *et al.*, 1984).
- Polar surface area: calculated by the method of Ertl *et al.* (2000); only nitrogen and oxygen were considered as polar atoms.

The second data set consisted of 17 measured physicochemical parameters including but not limited to the following:

- Chromatographic Log P at pH 7.4: the partition coefficient of non-ionised compound between aqueous and organic phases (indication of lipophilicity).
- Chromatographic Log D at pH 7.4: the distribution coefficient of ionised plus non-ionised forms between aqueous and organic phases (indication of lipophilicity).

- Chromatographic hydrophobicity index (CHI), a rapid reverse-phase high performance liquid chromatography (HPLC) method used for measuring lipophilicity (Valkó *et al.*, 1997); CHI-values for Log P, Log D and the immobilised artificial membrane column (IAM) were determined.
- Logarithms of the steady state volume of distribution (VDSS) and estimated unbound volume of distribution (VDUSS).
- Estimated proportion of plasma protein-drug binding.
- Membrane permeability.
- Solubility after 0.5, 4 and 24 hours in simulated lung fluid; compounds were considered of low solubility for concentrations of <0.05 mg/mL and high solubility for >1 mg/mL. Simulated lung fluid consisted of 0.59 mg/mL lecithin and 1 mg/mL bovine serum albumin in aqueous 0.78% (w/v) sodium dihydrogen orthophosphate and 0.4% (w/v) sodium chloride, buffered to pH 6.9.

Although Log P and Log D were modelled (*in silico*) and measured (*in vitro*), these parameters were analysed separately by PCA, one dataset for Log P and Log D, and did not supersede one another.

Each dataset (X-matrix) was formatted as a table with the six p38 MAPK inhibitors (N=6 observations) and parameters (K=35 or 17 variables for the *in silico* and measured data respectively). Multivariate data analysis was performed using SIMCA software (version 13.0.3.0; Umetrics). The software extracted data from the “X-matrix” and the position of the compounds in the multidimensional space was visualised (multivariate projection) by drawing a new co-ordinate axis ( $t_{[1]}$ ) representing the line of best fit through the data points. This is known as the first principal component and all observations (compounds) were projected onto this new axis and the values scored. The programme then added a second principal component ( $t_{[2]}$ ), orthogonal to the first principal component, to define the next best direction for approximating the data. The compounds were projected onto a plane defined by the two principal

components to create a score plot representing the optimal two-dimensional view of the original multidimensional data. The new axes (first and second principal components) can be related back to each original variable (axis) by measuring the angles between them and the principal components. A small angle indicates a variable has a large impact because it is almost aligned with the principal component; conversely, a large angle indicates less influence. The influence of variables is summarised in the loadings plot, which can be superimposed on the score plot; the further a variable is from the origin of the loadings plot, the greater its influence on an observation appearing in the same quadrant of the score plot (Umetrics, 2013).

For each dataset, the scores and loadings plots were then compared to assess the relative distribution and separation of the compounds within the ' $t_{[1]}/t_{[2]}$  space' for each model. Statistical parameters for the PCA were also summarised as follows:

- Component index (1 or 2 for respective principal components).
- R2X: fraction of X variation modelled by the component.
- R2X (cum): cumulative R2X score for the stated component(s).
- Eigenvalue: the number of variables (K) multiplied by R2X.
- NIPALS iterations: number of Nonlinear Iterative PArtil Least Squares iterations until convergence, *i.e.* the point at which further iterations of the algorithm do not refine the outcome.

### 2.2.2. Test articles

The p38 MAPK inhibitors were supplied by GSK as micronised crystals (all compounds) and stored at ambient temperature, protected from light and moisture (Table 2.1).

Amorphous GSK-899 was produced by spray drying a saturated solution of GSK-899 (prepared from micronised crystals) in methanol. Harsh drying conditions were used in conjunction with atomisation to produce amorphous particles of a respirable size. Rapidly drying the droplets achieved a similar effect to rapidly cooling molten compounds, which

prevents adequate mobility of molecules to assume lattice positions (Telko and Hickey, 2005). The physical state of particles was confirmed using X-ray powder diffraction (XRPD), using crystalline GSK-899 as a reference material.

**Table 2.1: Salt form and purity of p38 MAPK inhibitors used for dissolution testing (*in vitro*) and inhalation exposure of rats (*in vivo*)**

Test article	Salt form	Purity	<i>In vivo</i> study number
GSK258899B	mesylate	95.4%	R30573N
SB-731445T	tosylate	99.9%	
GSK610677B	hydrochloride	98.5%	R30988N
GSK678361A	parent	99.7%	R31225N
SB-681323T	tosylate	99.6%	n/a

### 2.2.3. Dissolution rates of p38 MAPK inhibitors in simulated lung fluid

Prior to conducting experiments with animals, the *in vitro* dissolution of the crystalline forms of p38 MAPK inhibitors and amorphous GSK-899 were evaluated in simulated lung fluid using a flow-through apparatus.

#### 2.2.3.1. Sample preparation for dissolution testing

A filterete (Figure 2.3A) was prepared for powder sample collection, placed on a wire support mesh at Stage 3 of a Next Generation Impactor (NGI) and clamped in place using an O-ring seal. The filterete is a custom made total trap filter consisting of spun bound polypropylene in a cover-web design (3M, UK).

Approximately 1.5 mg of the test article was weighed into a size 3 capsule and loaded into a Cyclohaler® (Teva Pharmaceutical Industries, Israel). The powder was dispersed in air as two consecutive four-second bursts from the inhaler, at a flow rate of 60 L/min, and the respirable particles of the resultant aerosol (aerodynamic diameter  $\leq 4.46 \mu\text{m}$  (Marple *et al.*, 2003)) were collected onto the filterete.

The NGI was dismantled and the filterete removed and positioned on the lower half of a stainless steel filter holder with the powder orientated downwards, towards the inlet port (Figure 2.3B). A polyvinylidene difluoride

(PVDF) 0.22  $\mu\text{m}$  filter and then a stainless steel support were placed over the filter. The top of the filter holder was then screwed into place to form a tight seal, and the dissolution cell connected to HPLC tubing in an oven maintained at 37°C.

### **2.2.3.2. Preparation of simulated lung fluid**

Simulated lung fluid (0.59 mg/mL lecithin and 1 mg/mL bovine serum albumin in aqueous 0.78 % (w/v) sodium dihydrogen orthophosphate and 0.4% (w/v) sodium chloride, buffered to pH 6.9) was prepared the day before the dissolution experiment.

A phosphate buffer was first prepared by dissolving sodium dihydrogen orthophosphate (3.90g) and sodium chloride (2.0g) in deionised water (475 mL), adjusting the pH 6.9  $\pm$ 0.1 using 5M sodium hydroxide and made up to volume (500 mL) with deionised water. Simulated lung fluid was then formulated by dissolving lyophilised bovine serum albumin in the phosphate buffer at room temperature, and dispersing lecithin in the solution at 60°C over a period of two hours with constant stirring. The formulation was cooled to room temperature overnight.

### **2.2.3.3. Evaluation of dissolution**

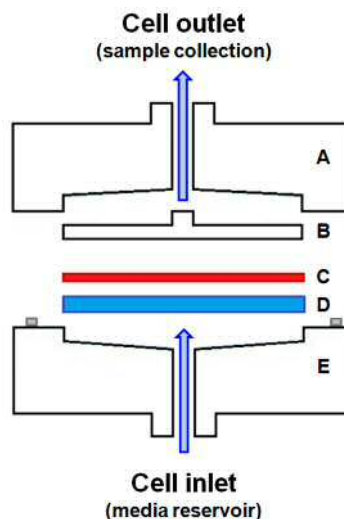
The flow-through design of apparatus used to perform dissolution experiments (Figure 2.3C) was based on a modified HPLC instrument. Simulated lung fluid was drawn at a constant flow of 1 mL/min from a reservoir of the media using an HPLC pump. The media was warmed via a coil and applied in an upward direction to the filter (clamped in an HPLC filter holder), both of which were accommodated in an oven maintained at 37°C. The dissolved test article which passed through the filter and the PVDF filter were collected for HPLC analysis with ultraviolet detection as a series of samples of 1.5 mL (*i.e.* over periods of 1.5 minutes) for up to three hours. On completion of the experiment, the filter was removed from the dissolution cell and any remaining test article was dissolved in 20 mL of 50:50 (v/v) acetonitrile in water.

The mass of analyte measured in each sample was used to calculate the cumulative percentage of test article recovered over the time course; the total mass of test article was calculated from the sum of analyte in each sample.

2.3A



2.3B



2.3C

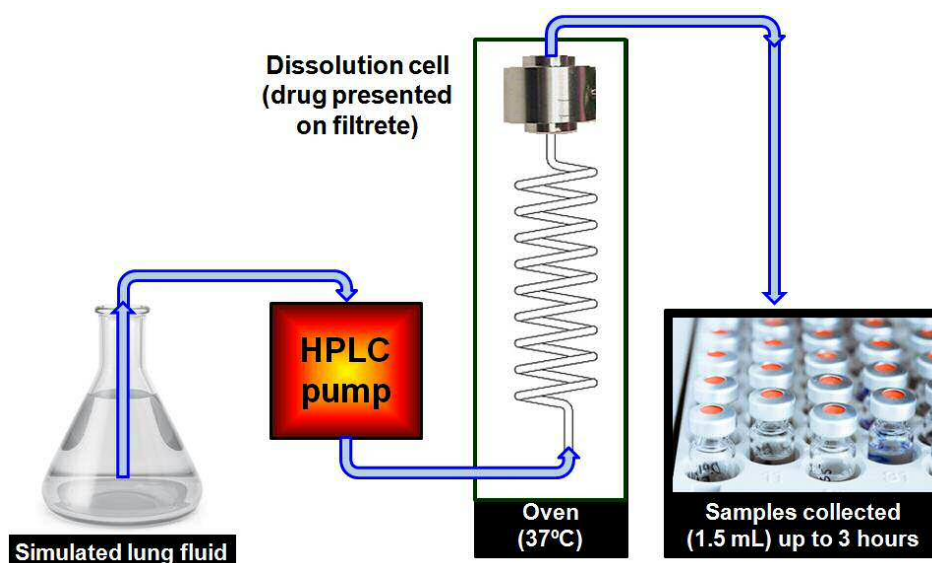


**Figure 2.3:** Schematic of apparatus used to evaluate dissolution of p38 MAPK inhibitors in simulated lung fluid. **2.3A:** filterrete (electrostatically charged polypropylene in spun bound cover-web design) used for presentation of respirable particles (aerodynamic diameter of  $<4.46\mu\text{m}$ ). **2.3B:** schematic of the dissolution cell showing the direction of media flow. Top to bottom: upper half of a stainless steel filter holder (A); stainless steel porous filter support (B); polyvinylidene fluoride (PVDF)  $0.22\ \mu\text{m}$  filter (C); filterrete (D) with loaded powder orientated towards the cell inlet; lower half of the stainless steel filter holder. **2.3C:** a constant flow ( $1\ \text{mL}/\text{min}$ ) of simulated lung fluid was drawn from a reservoir of the media using an HPLC pump, warmed to  $37^\circ\text{C}$  (via a heated coil) and applied to the filterrete in an upward direction. Serial samples ( $1.5\ \text{mL}$ ) were collected for HPLC-UV analysis over 3 hours.

### 2.2.4. Investigating the pharmacokinetics of p38 MAPK inhibitors in rats after a single inhaled dose

Rats were administered a p38 MAPK inhibitor, by inhalation, and then sampled for blood and/or lung tissue for chemical analysis by high performance liquid chromatography with mass spectrometry detection (HPLC-MS/MS) or assessment of drug-lung distribution by matrix assisted laser desorption/ionization with mass spectrometry imaging (MALDI-MSI) analysis (Figure 2.4). A target dose of 0.6 mg/kg was selected for single exposure of rats, which represents a 10-fold overage for a nominal clinical dose of 1 mg when a conservative scaling factor for inter-species differences in lung deposition is applied (Degeorge *et al.*, 1997, Jones and Baldrick, 2013).

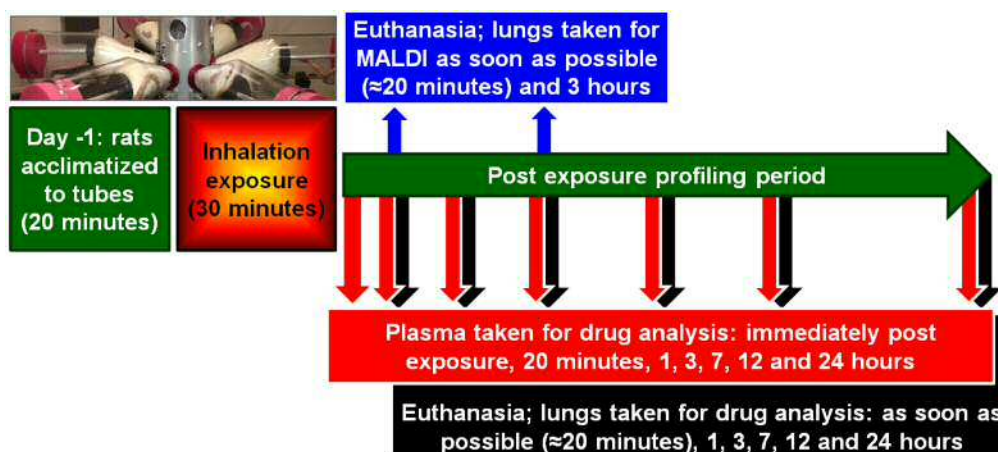


**Figure 2.4:** Design to investigate plasma and lung concentrations and lung distribution of p38 MAPK inhibitors in rats after a single inhaled dose. Rats were acclimatised to restraint tubes for 20 minutes (Day -1). The next day, rats were exposed to an aerosol for 30 minutes (target dose of 0.6 mg/kg) and sampled for plasma and lungs ( $n=3$ /time point) up to 24 hours post exposure. Additional rats ( $n=1$ /time point) were sampled for matrix assisted laser desorption/ionization (MALDI) analysis of drug-lung distribution.

#### 2.2.4.1. Test system and animal husbandry

Male Crl:WI(Han) rats (Charles River UK Ltd, Margate, Kent) were accommodated under standard laboratory conditions (Home Office, 2014) including room temperature of  $21\pm 2^{\circ}\text{C}$  and relative humidity of  $55\pm 10\%$  (excesses in relative humidity and temperatures of 18 to  $24^{\circ}\text{C}$  were acceptable for less than two consecutive days); a lighting cycle of

approximately 12 hours light to 12 hours dark was implemented. The animals were group housed (3/cage if practicable; same treatment group) in plastic solid bottom cages containing Aspen 4H bedding (Datesand Ltd, Manchester, UK) and given environmental enrichment including a fun tube and wood-chew (Lillico, Betchworth, UK) in each holding cage. Rats were accommodated for at least five days before undertaking the first licensed procedure (tube restraint) and were approximately 10 weeks old on the day of inhalation exposure (Day 1).

Rats had access to Purina Mills International (PMI) 5LF2 EURodent Diet and filtered mains water (Veolia Water plc, UK) *ad libitum*, except during inhalation exposure or blood sampling procedures.

For each experiment, animals were randomly allocated to treatment groups through arbitrary placement of the required number in each cage whilst unpacking the animals following delivery to the laboratory. Animals were identified by a number written in indelible ink on the tail.

### **2.2.5. Aerosol Generation and formulation details**

Groups of rats were administered a single dose of a p38 MAPK inhibitor, by snout-only inhalation exposure, presented as a dry powder formulation (all compounds) or as a nebulised aqueous solution (GSK-361, GSK-677 or GSK-899).

Aerosols were generated using commercially available aerosol generators for dry powder formulations (Section 2.2.5.2) or aqueous solutions (Section 2.2.5.4). Regulated airflow conducted the resultant aerosol from the apparatus into the top of a snout-only inhalation exposure chamber; volumetric flow of the compressed air supply and chamber exhaust (vacuum) were calibrated using a Bios Defender 510H airflow meter before initiating aerosol generation.

A target aerosol concentration of 0.028 mg/L was selected for exposure of animals and was calculated using the following equation:

\_\_\_\_\_ ..... Equation 3

Where  $C_t$  = target aerosol concentration (mg/L);  $ID_t$  = target inhaled dose (mg/kg); BW = predicted body weight (0.35 kg, based on unpublished historical data); RMV = respired minute volume (L/min) estimated using Equation 2 (Alexander *et al.*, 2008); T = duration of inhalation exposure (30 minutes).

'Pre-study' aerosol characterisation work was conducted without animals to establish the operating conditions needed to generate target aerosol concentrations and to ensure that the airborne particles or droplets were of a size suitable for exposure of rodents.

#### **2.2.5.1. Dry powder formulations of p38 MAPK inhibitors**

Each p38 MAPK inhibitor was blended nominally 5% (w/w) with 'inhalation grade lactose', which consisted mainly of large carrier particles but also included a small proportion of fine lactose particles; the mass median particle size of the lactose excipient was 66  $\mu\text{m}$ , with approximately 6% (w/w) of particles less than 4.5  $\mu\text{m}$ . The large lactose carrier particles are non-respirable and readily sediment out of the aerosol. These particles provide bulk to formulations for controlled dispersal of the drug(s) and minimise aggregations by reducing drug cohesiveness (Telko and Hickey, 2005).

For each of the blends of crystalline GSK-899, GSK-677 or GSK-361, the required masses of test article and lactose excipient were weighed into a suitable container and mixed using a bladed mixer (Donsmark QMM/I Mixing System; Donsmark Process Technology, Denmark) for 10 minutes at 600 revolutions per minute (RPM). For blends of amorphous GSK-899 or 5% (w/w) SB-445 (Study R31035N), the test article and excipient were mixed for four hours (GSK-899) or one hour (SB-445) respectively using a non-bladed inversion mixer (Turbula®; design similar to the contemporary T2F model by Glen Mills Inc, Clifton NJ, USA) at a nominal speed of 60 RPM. The resultant mixture was left to stand for one hour before samples were taken for chemical analysis.

### Chemical analysis of dry powder formulations

The concentration and homogeneity of each p38 MAPK inhibitor in its respective formulation were confirmed by chemical analysis. Six aliquots, each of 250 mg, were taken from each blend (2 samples from each of the top, middle and bottom) and dissolved in an appropriate diluent. The concentration of test article was measured using high performance liquid chromatography with ultraviolet detection (HPLC-UV), with reference to results of calibration standards and quality control (QC) samples that were prepared from independently prepared stock solutions of the reference material.

Dry powder formulations were packed into a canister (internal volume of 5 cm<sup>3</sup>) ready for aerosol generation. This was performed by compressing small aliquots of powder into the cylindrical canister using a bench press (applied force of 6 MPa) to build up thin layers of compressed powder of even density.

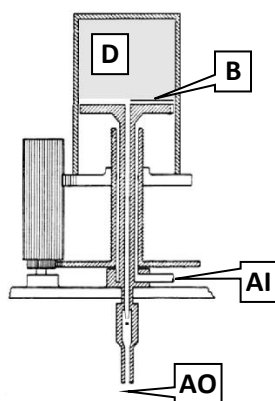
#### **2.2.5.2. Generation of dry powder aerosols of p38 MAPK inhibitors**

Aerosols were generated from the dry powder formulations using a Mk II Wright Dust Feed mechanism (Figure 2.5). The Wright dust feed (Wright, 1950) was designed to produce and maintain dust atmospheres by suspending material scraped from the surface of a compressed powder in a stream of dry air. A canister containing the powder was advanced along a screw thread so the formulation was presented to a radial blade at a consistent rate. The concentration of analyte in air can be altered by changing the cross-sectional area of powder presented to the blade (canisters of internal volume 1.3, 5 or 40 cm<sup>3</sup> are commercially available), the speed at which the radial section of powder is presented to the blade, and by varying the dilution of analyte in excipient. A regulated flow of compressed air (14 L/min) was used to disperse the powder into the exposure chamber.

The operational settings for the Wright dust feed were selected to facilitate controlled delivery of each p38 MAPK inhibitor at the required

powder feed rates to achieve the indicated dose. Speed settings were selected with reference to pre-study aerosol generation trials performed without rats. Operating conditions were adjusted as necessary during each experiment to target the aerosol concentrations for each dose.

### 2.5A



### 2.5B

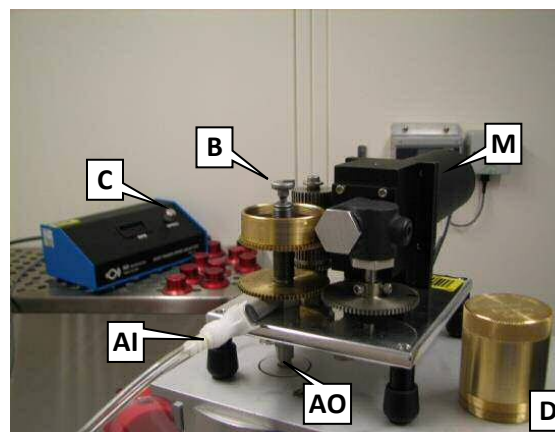


**Figure 2.5: Aerosol generator for dispersal of dry powder formulations.** **2.5A:** Schematic of a Wright dust feed (Wright, 1950) adapted from [www.researchgate.net](http://www.researchgate.net). **2.5B:** Mark II model used for generation of aerosols from p38 MAPK inhibitors blended with lactose vehicle. A blade (B) scrapes compressed powder (D), which is then suspended in a compressed air supply (AI) and dispersed downwards (AO) into the chamber. The motor (M) speed is adjusted by a variable rheostat (C).

### 2.2.5.3. Liquid formulations of p38 MAPK inhibitors

For exposure of animals to aqueous solutions of the p38 MAPK inhibitors, each micronised crystalline test article was dissolved in a vehicle to achieve a concentration (Table 2.2) anticipated to achieve an inhaled dose of 0.6 mg/kg. All mixtures were stirred magnetically throughout preparation and sonicated as required to aid formation of a solution. Solutol HS 15 is a non-ionic surfactant that inhibits P-glycoprotein 1 (Alani *et al.*, 2010), a multidrug resistance protein pump typically restricted to the apical surface of cells in many tissues including the lung (Bellamy, 1996). Solutol HS 15 has been shown to inhibit P-glycoprotein 1 (Pgp) and enhance membrane permeability (Alani *et al.*, 2010, Komarov *et al.*, 1996). Systemic absorption of the p38 MAPK inhibitors, as substrates of Pgp, may therefore be enhanced by Solutol HS 15 by inhibiting the active reflux of compounds back into the lumen.

**Table 2.2: Aqueous solutions of p38 MAPK inhibitors nebulised for single inhalation exposure of rats**

Study No.	Test article	Concentration in vehicle	Vehicle for nebulisation
R30573N	GSK-899	1.50 mg/mL	3% (v/v) Solutol HS 15 in 10% (w/v) aqueous 2-hydroxypropyl-beta-cyclodextrin
R30988N	GSK-677	2.50 mg/mL	3% (v/v) Solutol HS 15 in 0.9% (w/v) aqueous sodium chloride (pH 5.9)
R31225N	GSK-361	1.50 mg/mL	20:20:60 (v/v/v) Solutol HS 15, ethanol and 60 mM phosphate buffer (pH 7)

Cyclodextrins consist of a hydrophilic outer surface and a central lipophilic cavity. They form complexes with organic compounds via non-covalent bonds and are used to solubilise drugs of low solubility. Cyclodextrins improve the bioavailability of a drug by making it available at a biological interface such as a mucosa, from where the drug molecule transfers into the membrane without disrupting it (Challa *et al.*, 2005). Hydrophilic cyclodextrins including 2-hydroxypropyl-beta-cyclodextrin (HP $\beta$ CD) are unable to significantly permeate biological membranes but nevertheless enhance permeation of lipophilic drugs in aqueous environments (Loftsson *et al.*, 2007) by solubilising the molecule and facilitating its presentation at a membrane. Inclusion of HP $\beta$ CD could potentially enhance uptake of GSK-899 into the respiratory epithelium but may not necessarily promote its transfer into the systemic circulation. Ethanol is the most commonly used alcohol for enhancement of transdermal penetration of drugs (Sinha and Kaur, 2000). Kim and Chien (1996) demonstrated that skin permeation of three drugs increased with an increase in the proportion of ethanol in two cosolvent systems, achieving maximum skin permeability for 50% to 60% (v/v) ethanol. Gurtovenko and Anwar (2009) showed that insertion of ethanol into a lipid bilayer results in expansion and thinning of a membrane. Potential disruption of the membrane in concert with Solutol HS 15 may enhance the absorption of GSK-361, although the significance of enhanced absorption ascribed to ethanol in the nebulised formulation is uncertain,

given that volatile formulation components preferentially evaporate during aerosol generation, changing the composition of the droplets.

Solutol HS 15, HP $\beta$ CD and ethanol were used to solubilise p38 MAPK inhibitors of low solubility (GSK-899 and GSK-361). Solutol HS 15 was also formulated with GSK-677 for consistency with investigations comparing the toxicopathology of GSK-899 and GSK-677 described in Chapter 5. Whilst the potential for these vehicle components to enhance membrane permeability or systemic absorption of the p38 MAPK inhibitors in the lungs complicates elucidation of mechanisms for pulmonary absorption of nebulised test articles, this does not undermine the fundamental hypothesis that changing the aerosol form of a drug changes the kinetics of exposure and concomitant efficacy or toxicopathology.

Preparation of GSK-899 in 3% (v/v) Solutol HS 15 in 10% (w/v) aqueous 2-hydroxypropyl-beta-cyclodextrin

The required mass of GSK-899 for a given concentration and volume was weighed into a container and Solutol HS 15 (3% of final volume) was added. The resultant mixture was stirred and minimal heat applied using a stir/hot plate. The required volume (80% of final volume) of 10% (w/v) aqueous 2-hydroxypropyl-beta-cyclodextrin was added and the resultant mixture acidified using 11.6M hydrochloric acid to achieve a solution. The pH was adjusted to within a range pH 4 to 6 using 10M sodium hydroxide, and the solution was made up to the final volume using additional 10% (w/v) aqueous 2-hydroxypropyl-beta-cyclodextrin.

Preparation of GSK-677 in 3% (v/v) Solutol HS 15 in 0.9% (w/v) aqueous sodium chloride

The required mass of GSK-677 for a given concentration and volume was weighed into a container and Solutol HS 15 (3% of final volume) was added. The required volume of 0.9% (w/v) aqueous sodium chloride was then added and the resultant mixture stirred until a solution formed.

Preparation of GSK-361 in 20:20:60 (v/v/v) Solutol HS 15, ethanol and 60 mM phosphate buffer

The required mass of GSK-361 for a given concentration and volume was weighed into a container and ethanol (20% of final volume) added. The resultant mixture was stirred and minimal heat applied using a stir/hot plate until a solution formed. Solutol HS 15 (20% of final volume) was added and the resultant mixture was stirred, maintaining a solution. The solution was made up to the final volume with addition of 60 mM phosphate buffer (pH 7) and the resultant mixture stirred.

Evaluating physical stability of nebulised solutions

In order to minimise the potential for each test article to precipitate out of solution during dose administration or *in vivo*, its solubility in the vehicle was checked after a period of nebulisation and also after dilution in simulated lung fluid (0.59 mg/mL lecithin and 1 mg/mL bovine serum albumin in aqueous 0.78 % (w/v) sodium dihydrogen orthophosphate and 0.4% (w/v) sodium chloride, buffered to pH 6.9). Visual appraisal of nebulised formulations confirmed the test articles remained in solution. In addition, formulations were visually checked after dilution of the test solution 1:1 and 1:10 (v/v) in simulated lung fluid; absence of a precipitate was interpreted as an indication the p38 MAPK inhibitor would remain in solution after deposition of droplets in the epithelial lung fluid of rats exposed to the nebulised drug.

The concentration of each test article in solution was selected to facilitate controlled delivery of nebulised p38 MAPK inhibitor at the required feed rates to achieve the indicated dose. Formulation concentrations were selected with reference to pre-study aerosol generation trials performed without animals.

**2.2.5.4. Nebulisation of droplet aerosols**

Liquid aerosols were generated from aqueous solutions of each p38 MAPK inhibitor using the Pari LC<sup>®</sup> Sprint (Figure 2.6), a commercially available nebuliser used for clinical applications. Air jet nebulisers were designed to atomise liquids by directing compressed air at high velocity,

via a nozzle, through a reservoir of liquid. A baffle traps larger droplets, which return under gravity to the reservoir; smaller droplets are emitted from the device for presentation to the patient or test subject(s).

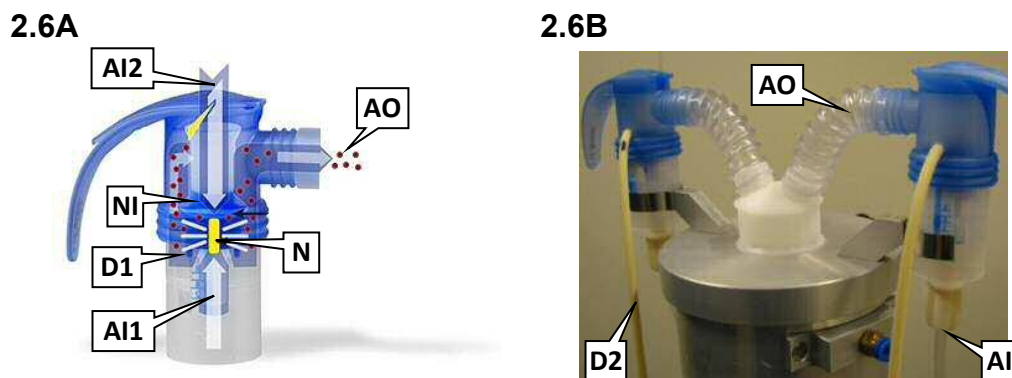


**Figure 2.6:** Air jet nebuliser used to disperse solutions or suspensions. **2.6A:** Schematic of a Pari LC Sprint adapted from [www.pari.com](http://www.pari.com). The compressed air (AI1) supplied to the nebuliser base passes through a nozzle (N), dispersing the liquid formulation (D1); small droplets are emitted from the aerosol outlet (AO). Ambient room air (AI2) can be drawn into the nebuliser via the nozzle insert (NI) during inspiration by a patient. **2.6B:** twin air jet nebulisers adapted for presentation of aqueous solutions of p38 MAPK inhibitors to rats. Tubing (D2) and a peristaltic pump were used to maintain the liquid formulation at a constant volume in the device during nebulisation.

The concentration of analyte in air was altered by varying its concentration in the solution or suspension used for atomisation. The Pari LC Sprints were modified to incorporate a tube for topping up the formulation from a bottle of the solution (using a peristaltic pump) and thus maintaining a constant volume of formulation in the device throughout the nebulisation period.

A single nebuliser was used for dispersal of GSK-677 and twin nebulisers for dispersal of the less soluble GSK-361 and GSK-899 to achieve the target dose. Calibrated flows of compressed air (nominally 6 to 7 L/min/nebuliser) supplemented with diluent air to deliver a total airflow of 14 L/min to the inhalation exposure chamber.

#### 2.2.5.5. Rodent inhalation exposure system

Aerosols were generated using the appropriate apparatus and directed into the top of a rodent snout-only inhalation exposure chamber (Figure 2.7). The chambers (ADG Developments Ltd, Holbeach,

Lincolnshire, UK) were of simple flow-through design (Figure 2.7C) and modular construction, consisting of a top section, three animal exposure sections (each accommodating two rows each of six animal exposure ports, and a single aerosol sampling port) and a base section to form a chamber with an internal diameter of four inches and volume of 7.5 litres. The chambers were operated under conditions of dynamic airflow such that animals could be sustained without compromising their physiology, *i.e.* to ensure oxygen was not depleted and carbon dioxide did not become excessive. The chamber exhaust (vacuum attached to the base section) was calibrated for airflow 16 L/min, which was slightly greater than the airflow emitted from the aerosol generation system (14 L/min). The diluent port in the chamber top section remained open to permit a draw of room air to balance airflow and maintain the chamber at near ambient pressure whilst ensuring airflow through the chamber. The chamber exhaust air was drawn through a filtration unit to remove particulates before the air was vented to atmosphere. For dry powder formulations, this consisted of two cartridges in series containing filters with cut-points of 5 µm followed by 0.5 µm.

For nebulised aerosols, the exhaust line upstream of the particle filters also incorporated a droplet trap (cartridge containing glass bumping granules and water) followed by an empty cartridge (to capture percolating fluid emitted from the droplet trap) and then a moisture trap (typically two cartridges filled with silica gel) to dry the air before it passed through the particle filters.

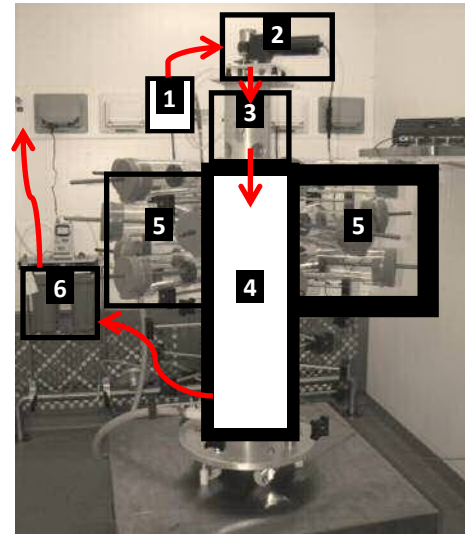
#### Acclimatisation of rats to inhalation exposure procedures

Rats were restrained in polycarbonate tubes for inhalation exposure procedures. On the day prior to aerosol administration, rats were placed into the restraint tubes, attached to the chamber and exposed to air only for 20 minutes (airflows were calibrated for a supply of 14 L/min supply and exhaust of 16 L/min).

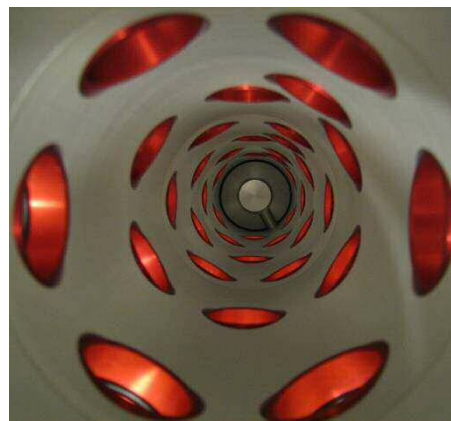
2.7A



2.7B



2.7C



2.7D



**Figure 2.7:** Snout-only inhalation exposure system incorporating a flow-through chamber for administration of aerosols to rats. **2.7A:** snout-only inhalation exposure system, which was operated dynamically (air constantly supplied to and extracted from the chamber). **2.7B:** schematic overlay of photograph showing a regulated air supply (1) connected to an aerosol generator (2), which dispersed test formulation into a chamber consisting of a mixing zone (3) and a 'dosing zone' (4) for presentation of the aerosol to rats restrained in tubes (5). Exhaled and waste aerosol were extracted from the base of the chamber and drawn through an exhaust filtration system (6) to remove particulate before being vented to atmosphere. **2.7C:** view down the centre of the flow-through design of exposure chamber. **2.7D:** presentation of a rat snout to the chamber, viewed through an open exposure port on the opposite side of the chamber.

#### Inhalation exposure of animals

Prior to exposure of animals, the aerosol generator was primed with the formulation. Rats were placed into the restraint tubes and attached to

the chamber; the vertical position (chamber level) of each animal on the chamber was documented.

It is not uncommon for an aerosol concentration gradient to form down an inhalation exposure chamber of flow-through design, as animals recycle the exhaled aerosol into the chamber atmosphere as it passes down the chamber (personal observations of unpublished data). This is less pronounced in chambers of narrower internal diameter, since the air velocity is faster for a given volumetric airflow. Nevertheless, in order to minimise a potential bias in achieved lung dose for animals sampled for blood and lung tissue (6 time points, each of 3 rats), one animal per time point was attached to each of the three chamber levels used. Unused animal exposure or sampling ports were closed using blanking plugs.

Aerosol generation was started by connection of the power supply to the Wright dust feed (powder formulations) or connection of the compressed air supply to the nebuliser (aqueous formulations), and the time was documented. Animals were exposed to the aerosol for a period of 30 minutes during which time operational settings (airflow and aerosol generation) and the animals were formally checked and documented at 10-minute intervals. Also for animal welfare purposes, an electronic probe (Rotronic HygroFlex HF53 transmitter and HC2-C05 probe) was used to monitor chamber air temperature during inhalation exposures (data not presented).

On completion of the 30-minute inhalation exposure period, aerosol generation was stopped (Wright dust feed power supply switched off or nebuliser air supply disconnected) and the time documented. The chamber was allowed to clear of aerosol and the condition of each animal was checked as it was returned to its holding cage.

#### **2.2.5.6. Aerosol characterisation**

'Pre-study' aerosol characterisation work was conducted without animals to establish the operating conditions needed to generate the aerosols at the target concentration, to confirm airborne particulates

were of suitable size for exposure of rats, and to select appropriate air sampling volumes for aerosol concentration and particle size analysis.

Aerosol samples were taken during exposure of rats to determine the aerosol concentration for estimation of inhaled doses, and particle size analysis to confirm administered aerosols were comparable for the test articles and appropriate for exposure of rats. Aerosol characterisation data are summarised (Table 2.10) for discussion in Section 2.3.6.1.

Additional samples of the test article and dry powder aerosols were taken during pre-study aerosol generation trials for imaging by scanning electron microscopy.

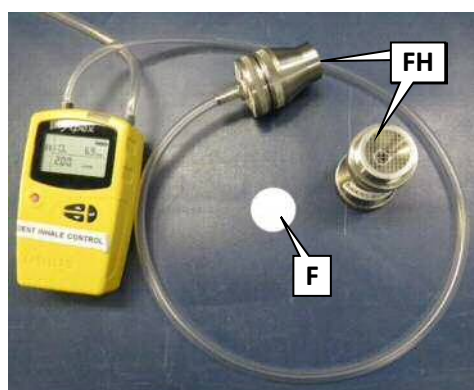
#### Aerosol concentration

The chamber aerosol concentration of each p38 MAPK inhibitor was determined twice during exposure of animals. The aerosol was sampled by drawing a measured volume of chamber air (6 litres for almost all aerosols; 4 litres for nebulised GSK-899 due to saturation of the filter with moisture) at a calibrated rate of 2.0 L/min through a glass fibre filter (Whatman GF/C). The filter was accommodated in an open-faced sampler (Figure 2.8A) that was attached to a sampling port adjacent to the rats (Figure 2.8B).

After sampling, each filter was transferred to a labelled glass vial and transferred to a laboratory for processing and analysis. A measured volume of diluent (solvent) was added for extraction of the analyte for chemical analysis using a validated method for high performance liquid chromatography with ultraviolet detection (HPLC-UV). The test article was used as reference material for preparation of analytical standards and QC samples.

Aerosol concentrations were calculated from the mass of analyte determined for each filter and the volume of chamber air sampled.

2.8A



2.8B

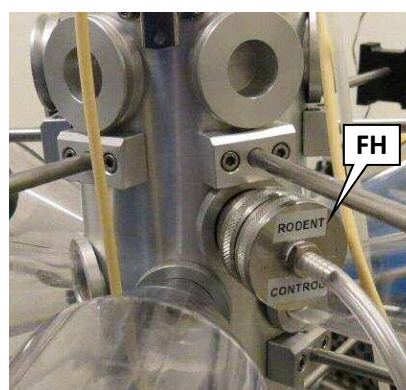


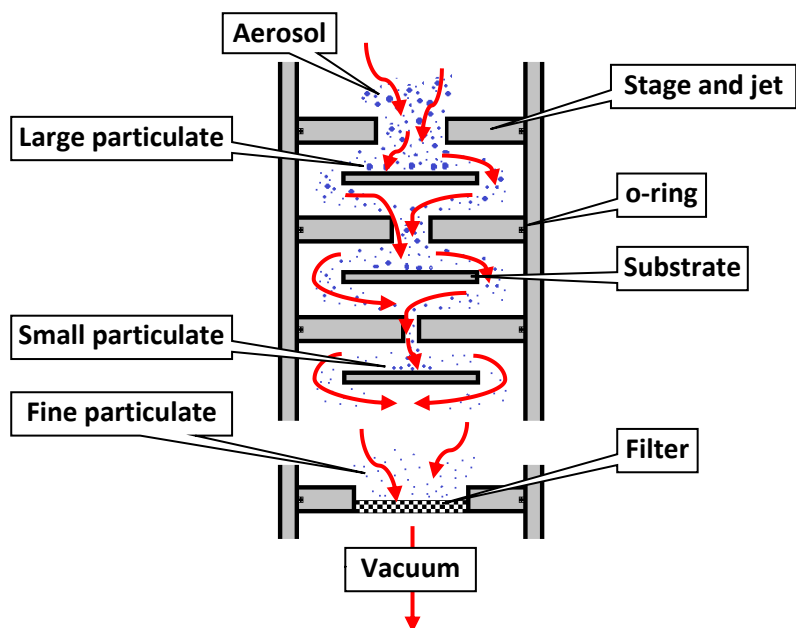
**Figure 2.8:** Apparatus for sampling the chamber atmosphere for measurement of aerosol concentration of drug analyte. **2.8A:** open-faced filter holder (FH) connected to a pump used for drawing a known volume of air (sampling rate of 2 L/min) through a glass fibre filter (F). Filters were processed for HPLC-MS/MS analysis of a test article. **2.8B:** filter holder (FH) attached to a chamber sampling port; sampled air was returned to the chamber exhaust to balance airflow during aerosol sampling.

Particulate Size Distribution

The size distribution of each p38 MAPK inhibitor was determined once during exposure of animals. A measured volume of air (6 litres for GSK-899 and SB-445; 20 litres for GSK-677 and GSK-361) was drawn from the exposure chamber, at a calibrated airflow of 2.0 L/min, through a Marple Personal Cascade Impactor (model 296) attached to a sampling port adjacent to the animals.

A Marple 296 cascade impactor (Figure 2.9) consists of six stages with cut-points of decreasing aerodynamic diameter (orifices of decreasing size) that are off-set from one stage to the next. An aerosol is fractionated into sub-populations of decreasing particle size by accelerating the particles through each orifice such that the larger particles with sufficient momentum are unable to follow a change in airflow direction and consequently impact upon a collection surface.

## 2.9A



## 2.9B



## 2.9C

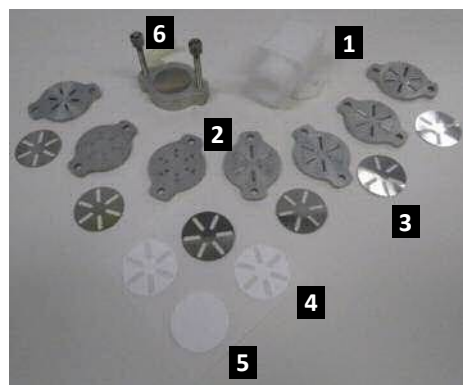


**Figure 2.9: Sampling chamber air using a cascade impactor to determine the particle size distribution of drug analyte. 2.9A:** schematic of a cascade impactor illustrating key design features, airflow (red) and deposition of particulate (blue) into fractions of decreasing size as the sampled aerosol is drawn through progressively smaller apertures. **2.9B:** Marple cascade impactor (Model No. 296) attached to a chamber port for aerosol sampling (airflow of 2 L/min) for HPLC-MS/MS analysis of the drug-analyte and determination of particle size distribution. **2.9C:** unassembled view of Marple cascade impactor showing the inlet cowl (1), slotted stages (2) and collection substrates (stainless steel (3) or glass-fibre (4) for powder or liquid aerosols respectively), a final glass fibre filter (5) which was supported on a wire mesh in the base section (6).

Dry powder aerosols were collected onto stainless steel plates and nebulised aerosols were collected onto glass fibre substrates (Whatman GF/A), with a final glass fibre filter (Whatman GF/A) for both aerosol forms. After sampling, each substrate was visually assessed to confirm

the presence or absence of a deposit and was transferred to an individually labelled glass vial. A measured volume of diluent was added to each vial to wash the stainless steel plate (dry powder aerosol) or extract the analyte from the glass fibre substrate. The washing or extract of the analyte was subjected to chemical analysis using a validated method for high performance liquid chromatography with ultraviolet detection (HPLC-UV) using the test article as reference material for preparation of analytical standards and quality control (QC) samples.

#### Analysis of particle size data

The percentage deposition on each stage was determined and used to calculate the cumulative percentage of particulate, by mass, smaller than each cut point (cumulative percentage undersize a stage).

Regression analysis of the probit of cumulative percentage undersize a stage versus the  $\text{Log}_{10}$  of the cut-point of the stage indicated that the log-transformed data were non-linear. Consequently, the mass median aerodynamic diameter (MMAD) was determined using a pragmatic method (Christopher *et al.*, 2010) by interpolation of the two central data points encompassing the median point of the distribution; the four central data points were used to estimate the geometric standard deviation ( $\sigma$ ), excluding the most outlying data points.

The European Medicines Agency Committee for Medicinal Products for Human Use define “fine particle mass” as the “particle size distribution of less than 5  $\mu\text{m}$ ” (EMA-3, 2006). Although this is described in a clinical context, it nevertheless provides another benchmark for comparing particle size. The fine particle fraction (percentage of mass <5 $\mu\text{m}$  aerodynamic diameter) was estimated by plotting the probit (probability function) of the cumulative proportion of aerosol mass less than each cut-point against  $\text{Log}_{10}$  of the cut-point. For each aerosol, the probit at  $\text{Log}_{10}(x)=0.70$  (aerodynamic diameter of 5  $\mu\text{m}$ ) was determined and back-transformed to a percentage using a probit table (Finney, 1952).

Theoretical cut-points for the Marple 296 at an airflow of 2.0 L/min (Rubow *et al.*, 1987) are reproduced for reference (Table 2.3). For determination of MMAD,  $\sigma_g$  and the fine particle fraction, the dynamically calibrated 'effective cut-point diameter' (ECD) for each individual device and stage were used to process data for each impactor sample.

**Table 2.3: Theoretical effective cut-off diameter cut-points (ECDs) for a Marple 296 cascade impactor**

	Marple 296 cascade impactor Stages and cut points						
Stage No.	3	4	5	6	7	8	Filter
ECD ( $\mu\text{m}$ )	9.8	6.0	3.5	1.55	0.93	0.52	0

#### Scanning electron microscopy of particles

Dry powder samples of lactose excipient, amorphous GSK-899 and crystalline GSK-899, GSK-677 and GSK-361 were sampled from the stock material and also from aerosols generated using the excipient alone or in combination with the p38 MAPK inhibitor (nominally 5% w/w) for imaging by scanning electron microscopy.

Aerosol samples were obtained by drawing a measured volume (1 litre) of the chamber atmosphere at a calibrated rate (1.0 L/min) through a polycarbonate isopore membrane filter (pore size 0.2  $\mu\text{m}$ ; 37 mm diameter; Millipore™), which was mounted in an open-face sampler and attached to the sampling port of the chamber. Following aerosol sampling, the filters were stuck to the lid of a petri dish or glass jar (to prevent contamination of the sampled aerosol) and stored at ambient temperature, protected from light and moisture pending image analysis. Reference (stock) material was deposited onto self-adhesive carbon discs using a brush; each carbon disc was mounted on an aluminium stub to facilitate manipulation of the sample and electron microscopy. Excess powder was carefully blown from the carbon disc.

For each aerosol sample, a square of approximately 50 mm length and width was excised from the centre of the filter and mounted onto a self-adhesive carbon disc, which was mounted on a stub.

The mounted samples were then coated with platinum for a total of 60 seconds (coating applied from three different angles each for 20 seconds).

#### **2.2.5.7. Calculation of the estimated inhaled dose**

Estimated inhaled doses were calculated using Equations 1 and 2 (Chapter 1, Section 1.3.4) for an exposure period of 30 minutes.

#### **2.2.5.8. Pharmacokinetic profiling of p38 MAPK inhibitors in blood/plasma and lung**

For logistical reasons, single dose experiments with GSK-899 and SB-445 were conducted first using analytical methods for blood samples diluted 1:1 in water. All subsequent experiments were performed using analytical methods established for plasma samples.

##### Sampling of blood for chemical analysis of GSK-899 or SB-445

A series of blood samples (60 $\mu$ L) were taken from groups of rats (3/dose/time point) immediately post exposure (30 minutes) and at 1.5, 3.5, 7.5, 12.5 and 24 hours relative to the start of inhalation exposure. Blood was sampled by jugular venepuncture or caudal venepuncture if further sampling from the jugular vein was not feasible; animals were warmed for up to 10 minutes at approximately 39°C to induce vasodilation in the tail for caudal venepuncture. Blood samples were taken into heparin (anticoagulant), mixed gently and placed on crushed wet-ice. As soon as practicable, duplicate aliquots (25  $\mu$ L) of the blood sample were mixed 1:1 with sterile water in a micronic tube. Samples were then frozen over solid carbon dioxide and stored in a freezer at approximately -20°C or below pending analysis.

Historically in drug development studies performed with GSK-899, sodium fluoride was used to inhibit endogenous esterases (Peirce, 1913) in plasma, which may otherwise hydrolyse an amide bond (Fukami and Yokoi, 2012) in the analyte (Figure 2.2A). The method of analysis using blood/water was developed by a second analytical group without inclusion of sodium fluoride. Retrospective work (aligned to study R30662N) using blood taken from GSK-899 treated rats demonstrated

that, under the experimental conditions, there was no difference in measured concentrations of GSK-899 in blood diluted 1:1 in water or 1:1 in aqueous sodium fluoride solution.

#### Sampling of plasma for chemical analysis of GSK-677 or GSK-361

Blood samples (400  $\mu\text{L}$ ) were taken from groups of rats (3/dose/time point) immediately post exposure (30 minutes) and at 1.5, 3.5, 7.5, 12.5 and 24 hours relative to the start of inhalation exposure. Blood was sampled by jugular venepuncture (immediately post exposure) or from the abdominal aorta, *i.e.* as a terminal sample taken during exsanguination of the animal under isoflurane anaesthesia. Blood samples were taken into EDTA (anticoagulant), mixed gently and placed on crushed wet-ice. As soon as practicable, duplicate aliquots (25  $\mu\text{L}$ ) of the blood sample were mixed 1:1 with sterile water in a micronic tube. Samples were then frozen over solid carbon dioxide and stored in a freezer at approximately  $-80^{\circ}\text{C}$  or below pending analysis.

#### Sampling of lung for homogenisation and chemical analysis of p38 MAPK inhibitors

Groups of rats (3/dose/time point) were euthanized (deep anaesthesia under isoflurane followed by exsanguination) as soon as possible after exposure and at 1.5, 3.5, 7.5, 12.5 and 24 hours relative to the start of inhalation exposure. The relative time of lung sampling for rats euthanized as soon as possible post exposure was approximately 50 minutes, *i.e.* 20 minutes after completion of the 30-minute inhalation exposure period, due to the logistics of transferring rats to the necropsy facility and the time taken for euthanasia and then isolation of lungs.

The lungs were exposed by excision of the sternum. The heart and thymus were removed and the lungs then isolated from the carcass and freed of as much connective tissue as possible. The trachea was removed and the lung lobes weighed. Right lung lobes were placed into a megacassette (GSK-899 or SB-445 treated rat lungs) or 7mL Precellys tube (GSK-677 or GSK-361 treated rat lungs) and snap frozen in liquid nitrogen. Samples were stored at  $-80^{\circ}\text{C}$  pending homogenisation.

Lung tissue presented in a megacassette (Fisher scientific, Reference No. 38VSP59042) was transferred to a 7mL Precellys tube (Precellys tissue homogenising CK28-7mL, Cat No. 0904-01). A volume of water was added to the lung tissue (one part water to one part lung tissue for GSK-361 and GSK-677; five parts water to one part lung tissue for GSK-899 and SB-445). At least two homogenisation cycles (15 seconds) were performed using a Precellys Tissue Homogenizer 24. The resultant tissue homogenate was centrifuged at 5500 RPM for 10 minutes and the supernatant transferred to a vial and stored at -80°C pending chemical analysis.

#### Chemical analysis of p38 MAPK inhibitors in lung homogenate and blood or plasma

Concentrations of GSK-899 or SB-445 in blood-water, GSK-677 or GSK-361 in plasma and all compounds in lung homogenate were quantified using a validated method for high performance liquid chromatography with mass spectroscopy detection (HPLC-MS/MS) using the respective p38 MAPK inhibitor and an internal standard as reference materials.

Results for analysis of blood-water samples were initially corrected for the 1:1 dilution to express concentrations in terms of GSK-899 in blood. Blood values were then converted to plasma-based values using a blood:plasma ratio of 2.10 for GSK-899 and 0.683 for SB-445 (unpublished data) to facilitate consistency of presentation for plasma data across all of the p38 MAPK inhibitors.

#### Determination of pharmacokinetic parameters

For each p38 MAPK inhibitor, statistical analysis of the drug-concentration profiles in lung and plasma was performed (Statistica, version 12.0.1133.40) using two-way analysis of variance (ANOVA), with post hoc analysis using Tukey's honestly significant difference test (Abdi and Williams, 2010[B]) to determine degrees of statistical significance between aerosol forms (crystals versus aqueous solution, and amorphous GSK-899).

Pharmacokinetic evaluations of plasma and lung concentration data for each p38 MAPK inhibitor were performed using a non-compartmental method to estimate the maximum observed concentration ( $C_{\max}$ ), time to  $C_{\max}$  ( $T_{\max}$ ) and the area under the concentration-time curve (AUC) approximated using the trapezoid rule (linear-up, log-down method). Statistical analysis was not performed for pharmacokinetic parameters because they were calculated from composite data and not for each animal individually.

#### **2.2.5.9. Analysis of drug-lung distribution by matrix assisted laser desorption/ionization (MALDI)**

For each p38 MAPK inhibitor, a rat was euthanized (deep anaesthesia under isoflurane followed by exsanguination) as soon as possible after the 30-minute inhalation exposure period (*i.e.* at 50 minutes) and at 3.5 hours relative to the start of inhalation exposure.

The lungs were exposed by excision of the sternum. The heart and thymus were removed and the lungs then isolated from the carcass and freed of as much connective tissue as possible. The lungs were carefully spread out on foil, with the trachea at the top and the front of the lungs uppermost, to permit identification of the individual lobes. The lungs were then placed in a megacassette, and frozen over solid carbon dioxide and stored at approximately  $-80^{\circ}\text{C}$  pending analysis.

Frozen lung samples were mounted onto a cryostat chuck and sections of nominally 12  $\mu\text{m}$  thickness were cut (LEICA CM3050S Cryostat) and thaw mounted onto indium tin oxide coated glass slides. Typically, five sections per lung were processed for matrix assisted laser desorption/ionization with mass spectrometry imaging (MALDI-MSI) including, where possible, a section selected for each lobe to include the main airway. Lung sections were coated with matrix, which consisted of approximately 2 mL of  $\alpha$ -cyano-4-hydroxycinnamic acid (CHCA; 7 mg/mL) matrix solution in 70:30 (v/v) methanol with 0.2% aqueous trifluoroacetic acid.

## *Chapter Two*

For GSK-899, GSK-677 and GSK-361, a Bruker UltrafleXtreme TOF-TOF mass spectrometer was used to construct an ion intensity map of the lung section by systematically vaporising focal points of the lung section and detecting the ionised analyte fragments by mass spectrometry. MALDI-MSI analysis of SB-445 was precluded by poor ionisation of the molecule.

## 2.3. Results and discussion

### 2.3.1. Principal component analysis of the physico-chemical parameters of six p38 MAPK inhibitors

Two datasets (X matrices) of physicochemical data were collated for principal component analysis. The first dataset (Tables 2.4 and 2.5) consisted of *in silico* parameters derived from molecular structures (Figure 2.2) and the second data set (Table 2.6) consisted of parameters measured *in vitro*.

**Table 2.4: 'In silico' physicochemical parameters for principal component analysis of six p38 MAPK inhibitors**

Physicochemical parameter	Test article					
	GSK-899	GSK-677	GSK-361	GSK-340	SB-323	SB-445
Pgp_v31.Pgp_Score <sup>A</sup> (sponsor's parameter; negative score indicates drug is Pgp substrate)	-1.57	-2.02	-0.23	-2.64	-0.54	-0.35
Chromatic distribution coefficient <sup>B</sup> (ChromLogD_v6.value)	3.77	2.29	4.84	2.85	3.87	3.52
Chromatic partition coefficient (ChromLogP_v1.value)	4.01	5.94	4.91	3.88	5.16	5.15
Property forecast index (PFI_v2.PFI_score)	9.77	5.29	7.84	5.85	7.87	7.52
perm_chrom_v4.perm_ score (function of ChromLogD vs cmr) <sup>C</sup>	-0.22	-0.64	0.5	-0.67	0.2	0.17
CXN_pKa.acid class;	1	1	2	1	1	1
CXN_pKa.base class See Table 2.5 for class score definition (CXN is software abbreviation)	2	7	1	6	1	1

#### Notes

- A Pgp (P-glycoprotein 1), a multidrug resistance protein pump often restricted to apical cell surface in tissues including lung (Bellamy, 1996). Model constructed from *in silico* data (LogD, charge, cLogP; Abraham's bond acidity and basicity) and validated for 442 non-substrates and 1201 substrates of Pgp (flux ratio of membrane permeability: basolateral to apical versus apical to basolateral).
- B Parameter used to derive Pgp\_v31.Pgp\_Score using an in-house *in silico* model.
- C Permeation model of ChromLogD plotted against CMR using a linear discriminant function. Compounds of larger positive values are more likely to be well absorbed; very large and lipophilic molecules (mw >500 and clogP >5) are likely to be poorly absorbed due to low solubility. Negative values indicate poor absorption.

## Chapter Two

Physicochemical parameter	Test article					
	GSK-899	GSK-677	GSK-361	GSK-340	SB-323	SB-445
Andrew's binding energy (abe); (Andrews <i>et al.</i> , 1984)	23.1	31.05	13.2	47.05	16.8	18.6
Net charge (charge) <sup>B</sup> <i>sum of positive/negative</i>	0	0	0	0	0	0
Calculated log partition coefficient (cLogP) <sup>B</sup>	3.750	5.287	3.746	2.063	3.758	3.847
Calculated molar refraction (cmr)	15.013	15.551	11.037	16.956	11.555	11.123
Ratio of rotatable to total bonds (flex)	15	27	15	12	16	16
Molecular weight (mw)	570.57	565.66	410.44	618.72	456.42	478.37
Molar volume (mv)	518	602	423.5	637	423.5	409.5
Polar surface area (tpsa); (Ertl <i>et al.</i> , 2000)	130.48	102.49	97.12	96.94	100.27	100.27
<b>Number of listed items in molecule</b>						
Aromatic rings (aring)	6	3	3	3	4	4
Halogen groups (halgrps)	1	1	0.5	1	1.5	2.5
Hydrogen bond acceptors (hba)	6	4	4	4	5	5
Hydrogen bond donors (hbd)	3	3	2	2	3	3
Non-hydrogen atoms (heavy)	41	41	30	45	33	34
Hetero atoms (hetrat); <i>ratio of O, N and S vs C</i>	0.39	0.30	0.32	0.30	0.30	0.32
Hydrogen bond acceptor (liphba); (Lipinski <i>et al.</i> , 1997)	10	9	7	10	7	7
Hydrogen bond donor (liphbd); (Lipinski <i>et al.</i> , 1997)	3	3	2	2	3	3
Aliphatic rings (naring)	0	1	0	3	0	0
Negatively ionisable groups (neg)	0	0	0	0	0	0
Positively ionisable groups (pos)	0	1	0	1	0	0
Rotatable bonds (rb)	7	12	5	6	6	6
sp2 carbons (sp2); <i>aromatic or double bond</i>	35	22	21	22	23	23
sp3 carbons (sp3); <i>saturated bonds</i>	6	19	9	23	10	11

### Notes

B Parameter used to derive Pgp\_v31.Pgp\_Score using an in-house *in silico* model.

Physicochemical parameter	Test article					
	GSK-899	GSK-677	GSK-361	GSK-340	SB-323	SB-445
<b>Abraham's descriptors</b> (Abraham, 1993)						
Hydrogen bond acidity (alpha) <sup>B</sup>	1.0841	0.7658	0.8446	0.572	0.3989	0.3989
Hydrogen bond basicity (betah) <sup>B</sup>	2.6653	2.9075	1.7470	3.4886	2.1699	2.0209
Dipolarity/ polarizability (pi)	5.2771	3.6982	3.5739	4.078	3.3452	3.3558
Excess molar refraction (r2)	4.8492	3.6563	2.2754	4.2079	3.5091	3.2663
McGowan characteristic scaled molar volume (vx2); (McGowan, 1978)	3.8289	4.2796	3.0456	4.5849	3.0703	2.9648

**Notes**

B Parameter used to derive Pgp\_v31.Pgp\_Score using an in-house *in silico* model.

**Table 2.5: Scoring system used for pKa acid and base class definitions for *in silico* parameters listed in Table 2.4**

Value	Acid class	Base class
0	No acidic group	No basic group
1	pKa >8.5	pKa ≤6.0
2	pKa 7.5 - 8.5	pKa 6.0 - 7.0
3	pKa 7.0 - 7.49	pKa 7.01 - 7.5
4	pKa 6.5 - 6.99	pKa 7.51 - 8.0
5	pKa 6.0 - 6.49	pKa 8.01 - 8.5
6	pKa 5.5 - 5.99	pKa 8.51 - 9.0
7	pKa <5.5	pKa >9.0

**Table 2.6: Measured physicochemical parameters for principal component analysis of six p38 MAPK inhibitors**

Physicochemical parameter	Test article					
	GSK-899	GSK-677	GSK-361	GSK-340	SB-323	SB-445
Apparent membrane permeability of compound in MDCKII-MDR1 cells <sup>A</sup> (Cmpd_Papp nm/sec)	97.2	71.4	350.1	13.348	146.605	209.62
Solubility in SLF (µg/mL)						
0.5 hours	3	878	29	100	347	280
4 hours	4	957	9	130	352	294
24 hours	6	865	14	220	393	314
Acid or Base	Weak Base	Basic	Neutral	Basic	Neutral	Neutral
Property forecast index (PFI); sum of the number of aromatic rings and ChromLogD	9.29	4.90	7.96	5.83	7.57	7.90
Artificial membrane permeability <sup>B</sup> (PERM_NUM) at pH 7.05	160	6.33	540	31	470	-
% human serum albumin protein binding (HSA_PCT_BIND)	94.8	81.0	88.8	90.3	88.8	91.2
Alpha-1-acid glycoprotein binding (AGP_PCT_BIND)	90.2	79.4	76.0	86.2	74.6	77.0
% plasma protein binding (PCT_PPB)	99.5	96.1	96.3	99.0	-	96.5
VDSS (steady state volume of distribution)	1.19	2.86	1.89	3.20	1.04	0.758
LogVDSS	0.0767	0.456	0.276	0.506	0.0152	-0.12
LogVDUSS (log of unbound volume of distribution at steady state)	1.53	1.18	1.28	1.58	1.03	1.04
Chromatographic (CHROM) LogD at pH 7.4	3.29	1.9	4.96	2.83	3.57	3.90
CHI_LogD at pH 7.4	1.77	0.92	2.80	1.48	1.95	2.15
CHI_LogP	1.77	2.48	2.81	2.30	2.00	2.15
CHI_IAM	39.7	39.7	39.06	43.7	33.7	32.2

**Notes**

- A MDCKII-MDR1: cell line of Madin-Darby canine kidney cells transfected with human Pgp (Agarwal *et al.*, 2007). For measurement of passive membrane permeability, Pgp was inhibited by GF120918 (Ward and Azzarano, 2004).
- B Passive permeability across lipid bilayer of egg phosphatidyl choline (1.8%) and cholesterol (1%) in n-decane; buffer (50mM Na<sub>2</sub>HPO<sub>4</sub> with 0.5% HPβCD; pH 7.05) of donor (bottom) and acceptor (top) compartments analysed for drug concentration at 3 hours of incubation (Kansy *et al.*, 1998, Veber *et al.*, 2002).
- SLF simulated lung fluid
- LogD distribution coefficient in organic-aqueous phases
- LogP partition coefficient in organic-aqueous phases
- CHI chromatographic hydrophobicity index (data obtained from HPLC method)
- IAM immobilised artificial membrane (HPLC column for phospholipidotic potential)

Principal component analysis of the *in silico* data generated a score plot (Figure 2.10) in which the compounds formed three equidistant groups within the 't<sub>[1]</sub>/t<sub>[2]</sub> space'. GSK-899 lay close to the t<sub>[1]</sub> axis, with a dual cluster (GSK-677 and GSK-340) in the lower left quadrant and a second cluster (SB-323, SB-445 and GSK-361) in the lower right quadrant. The two principal components accounted for 74% of the data variability in the dataset (Table 2.7). The influence of parameters (variables) on the distribution of the compounds is summarised in the loading plot (Figure 2.11); variables with a narrow angle to an axis have a more predominant relationship with that principal component (t<sub>[1]</sub> or t<sub>[2]</sub>), and the further a variable is from the origin of the loading plot, the greater its significance for a compound (observation) appearing in the same quadrant of the score plot (Umetrics, 2013).

The loading plot (Figure 2.11) indicated the *in silico* parameters most influencing the relative distribution of the three groups of compounds from one another included the following:

1. GSK-899: number of aromatic rings, sp<sup>2</sup> hybridised carbons (double or aromatic bonds) and hydrogen bond acceptors, a higher proportion of oxygen, nitrogen and sulphur atoms relative to carbon ("heterat") and polar surface area ("tpsa");
2. GSK-677 and GSK-340: pKa base class, hydrogen bond basicity ("betah"), Andrew's average binding energy ("abe"), molar volume, number of aliphatic rings ("naring") and positively ionisable groups, hydrogen bond basicity ("betah") and McGowan's scaled molar volume ("vx2");
3. GSK-361, SB-323 and SB-445: Pgp score (the smaller negative scores suggested these three compounds were less likely to be substrates of P-glycoprotein 1 and would not be actively returned to the lumen); positive scores for the permeation model of ChromLogD plotted against calculated molar refraction ("perm\_chrom\_v4.perm\_score") indicated the compounds may be better absorbed.

Principal component analysis of the measured physicochemical data (Table 2.6) produced a similar distribution of compounds in the 't<sub>[1]</sub>/t<sub>[2]</sub> space' (Figure 2.12) suggesting the information embedded within the *in silico* model was reasonably well aligned to experimental data. There was limited separation of the three compounds clustered in the lower right quadrant (SB-323, SB-445 and GSK-361) but a clear separation of the other three compounds, with GSK-340 plotted in the upper left quadrant between GSK-677 and GSK-899. The variances of the two principal components (R<sup>2</sup>X<sub>[1]</sub> and R<sup>2</sup>X<sub>[2]</sub>) accounted for 80% of the variance in the dataset (Table 2.7).

The distribution of variables in the loading plot (Figure 2.13) indicated the *in vitro* parameters most influencing the relative distribution of the compounds from one another in the score plot included the following:

1. GSK-899: binding of plasma protein ("Pct\_PPB") and alpha-1-acid glycoprotein ("AGP\_Pct\_Bind") and log of the unbound volume of distribution at steady state ("LogVDUSS");
2. GSK-677: solubility in simulated lung fluid;
3. GSK-361, SB-445 and SB-323: apparent (passive) membrane permeability ("Cmpd\_Papp\_nm\_sec"), artificial membrane permeability ("Perm\_Num\_pH7.05") and chromatographic LogD ("Chrom\_LogD\_pH7.4").
4. GSK-340: chromatographic hydrophobicity index for the immobilised artificial membrane column ("CHI-IAM").

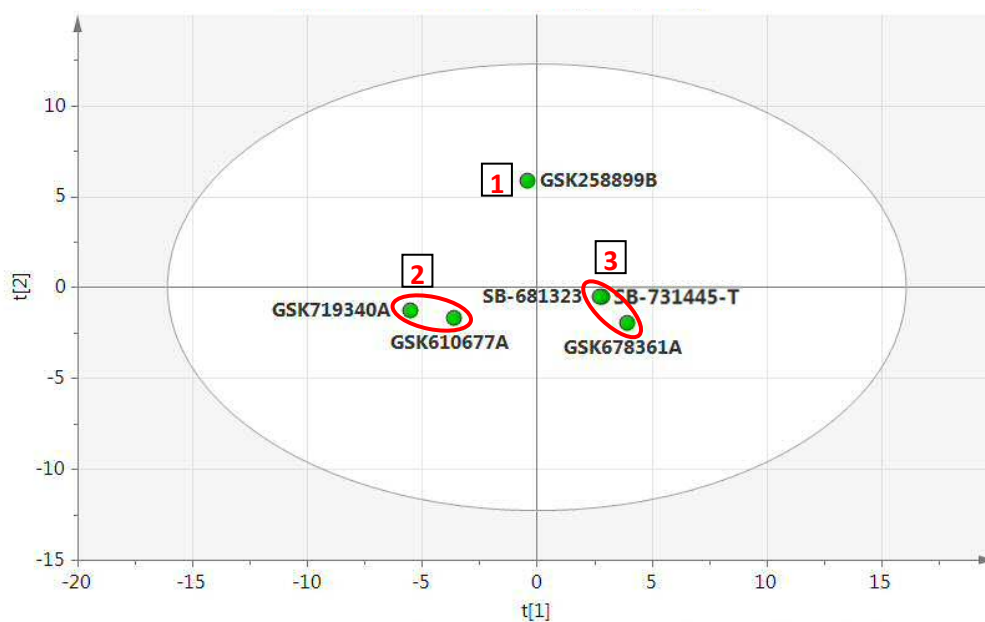


**Figure 2.10:** Score plot for principal component analysis of estimated ADME and physicochemical properties for six p38 MAPK inhibitors: 34 parameters were derived for each molecular structure shown in Figure 2.2 using Adamantis, a predictive web-based tool for characterising compounds.

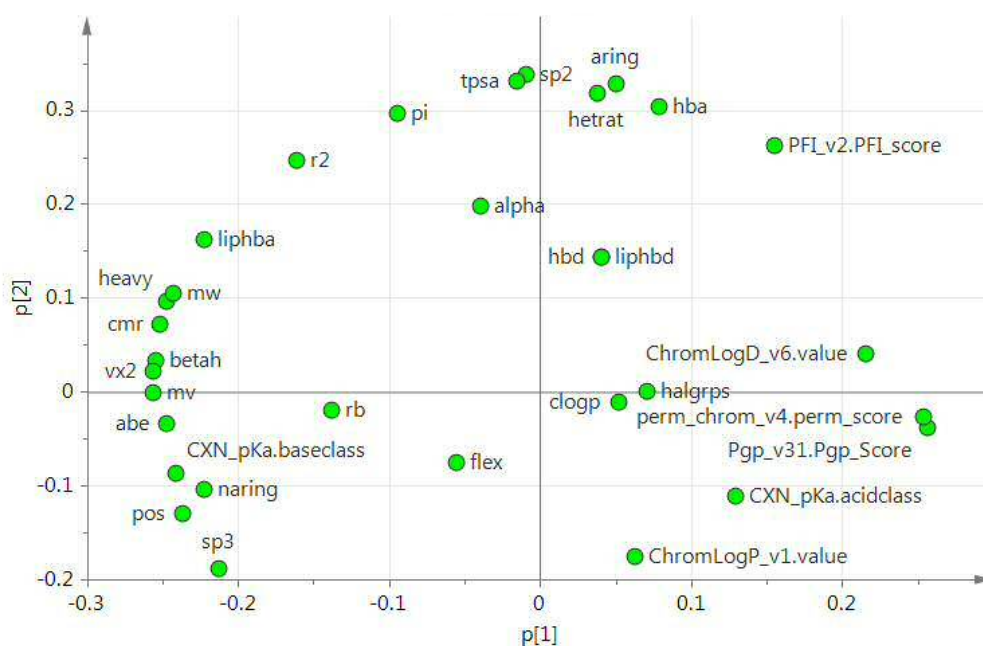


**Figure 2.11:** Loading plot for principal component analysis of calculated ADME and physicochemical properties for six p38 MAPK inhibitors. Most noteworthy parameters appear furthest from the origin and, in terms of its contribution to a principal component, has the narrowest angle from the respective axis ( $p[1]$  or  $p[2]$ ).

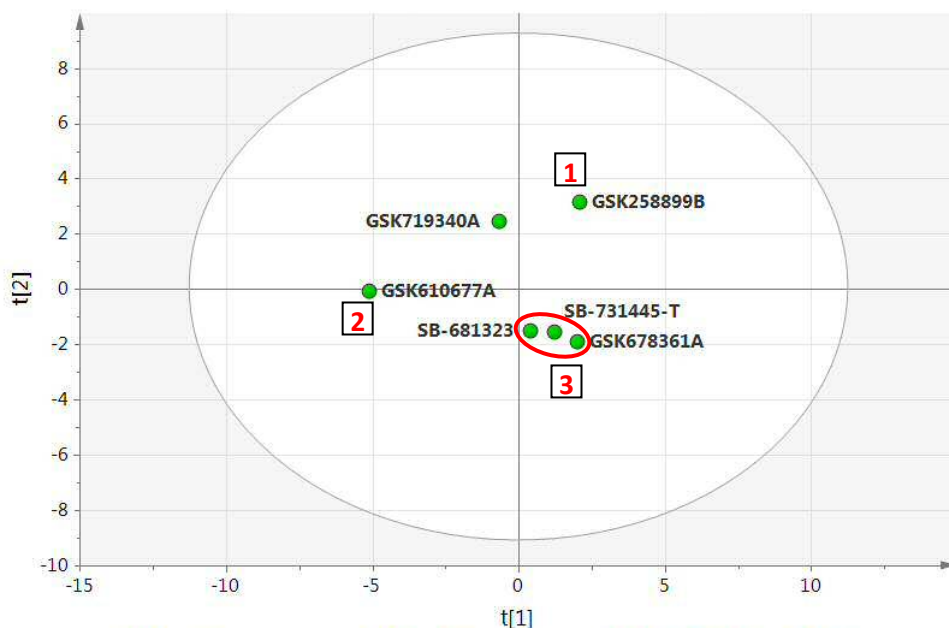


**Figure 2.12:** Score plot for principal component analysis of the measured physicochemical properties for six p38 MAPK inhibitors: 14 *in vitro* parameters and solubility (0.5, 4 and 24 hours in simulated lung fluid) were measured for each molecular structure shown in Figure 2.2.

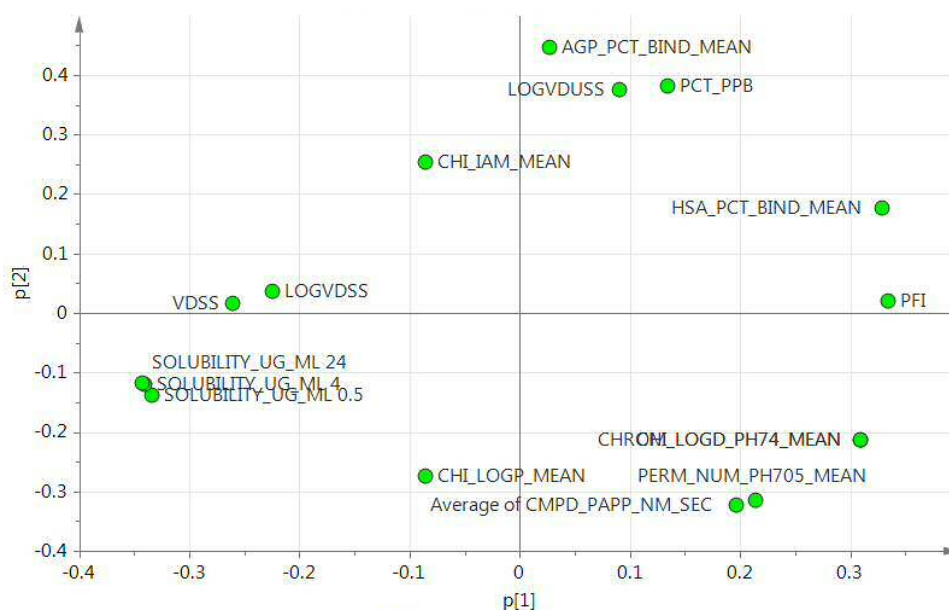


**Figure 2.13:** Loading plot for principal component analysis of measured physicochemical parameters of six p38 MAPK inhibitors. Most noteworthy parameters appear furthest from the origin and, in terms of its contribution to a principal component, has the narrowest angle from the respective axis ( $p[1]$  or  $p[2]$ ).

**Table 2.7: Statistical summary data for principal component analysis of measured physicochemical parameters of six p38 MAPK inhibitors**

Dataset	Component	R2X	R2X(cum)	Eigenvalue	Iterations
<i>In silico</i>	1	0.466	0.466	2.8	20
	2	0.272	<b>0.738</b> <sup>A</sup>	1.63	19
<i>In vitro</i>	1	0.505	0.505	3.03	20
	2	0.294	<b>0.799</b> <sup>B</sup>	1.77	19

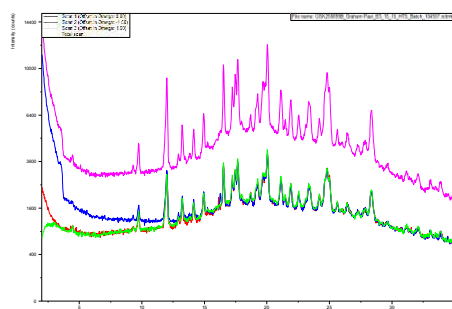
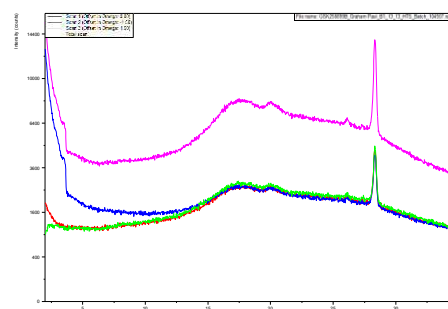
**Notes**

A *In silico* data: cumulative R2X value of 0.738 indicates the two principal components (R2X[1] and R2X[2]) account for 74% of variance in the data set.

B *In vitro* data: cumulative R2X value of 0.799 indicates the two principal components (R2X[1] and R2X[2]) account for 80% of variance in the data set.

**2.3.2. X-ray powder diffraction of amorphous GSK-899**

Before conducting *in vitro* dissolution testing and *in vivo* experiments, and again following completion of most *in vivo* experiments, samples of spray dried GSK-899 were analysed by X-ray powder diffraction (XRPD) to confirm the material was amorphous and had not reverted to the more stable crystalline state. The characteristic diffraction pattern for crystalline GSK-899 (Figure 2.14A) was not evident for amorphous GSK-899 (Figure 2.14B), which exhibited a broad baseline characteristic of randomly orientated molecules (Bates *et al.*, 2006).

**2.14A****2.14B**

**Figure 2.14: X-ray powder diffraction of amorphous and crystalline GSK-899.** Replicate scans (red, blue and green) shown with a total scan (pink) as a plot of signal intensity (counts) against scattering angle ( $2\theta$ ). **2.14A:** GSK-899 crystals (Lot 051087156) exhibit a reproducible peak 'signature' for diffracted X-rays consistent with atomic spacing in crystals. **2.14B:** amorphous GSK-899 (batch EE666025D) shows a broad baseline devoid of peaks indicative of randomly orientated molecules.

### 2.3.3. *In vitro* dissolution of p38 MAPK inhibitors

The cumulative mass of dissolved drug, expressed as a percentage of total mass, plotted against time (Figure 2.15) showed dissolution of crystalline GSK-899 and GSK-361 in simulated lung fluid was considerably slower than crystalline GSK-677, SB-323 or SB-445. The dissolution-time curve for amorphous GSK-899 was sigmoid but the rate from 12 minutes was much faster than for crystalline GSK-899, which is consistent with the findings of Hancock and Parks (2000).

Dissolution rates expressed as the percentage of dissolved mass against time (%/min) were calculated for the steepest approximately linear portion of each compound profile (Table 2.8). The ranking of dissolution rates for the crystalline compounds was broadly in line with measured solubility data. The dissolution rate for amorphous GSK-899 was faster than that of crystalline GSK-899 but slower than crystalline GSK-677, SB-323 and SB-445.

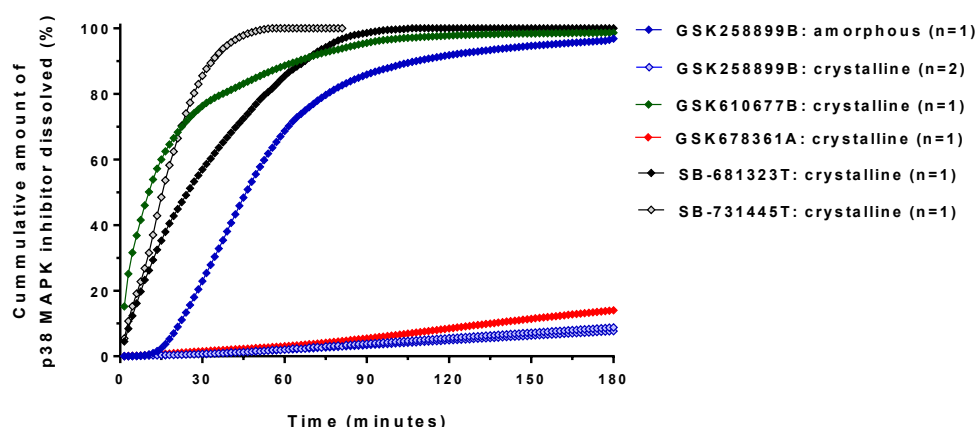


**Figure 2.15:** *In vitro* dissolution of five crystalline p38 MAPK inhibitors and amorphous GSK-899 in simulated lung fluid. The cumulative proportion of each test article dissolved plotted against time (individual data). GSK performs dissolution testing of respirable aerosols on a risk-benefit basis. Experiments for investigative purposes, including this thesis, are performed once given the observed robustness of the test methodology and chemical analyses (unpublished data; duplicate data for crystalline GSK-899 were consistent with this assertion). Data in support of strategic decisions for commercial assets (drug development) and regulatory submissions are generated in triplicate for reporting mean dissolution and standard deviation.

**Table 2.8: *In vitro* dissolution rates of five crystalline p38 MAPK inhibitors and amorphous GSK-899 in simulated lung fluid**

PCA group <sup>A</sup>	Test article	Particle form	Dissolution rate (%/min)	Period of analysis (min) <sup>B</sup>	Measured solubility (µg/mL) <sup>C</sup>
1	GSK258899B	crystalline	0.0459	1.5 - 180	4.33
		amorphous	1.47	15 - 60	
2	GSK610677B	crystalline	2.85	1.5 - 19.5	900
3	GSK678361A	crystalline	0.0783	1.5 - 180	17.3
	SB-681323T	crystalline	2.13	1.5 - 19.5	364
	SB-731445T	crystalline	3.17	1.5 - 19.5	296

**Notes**

- A Nominal grouping identified in PCA score plots in Figures 2.10 and 2.12.  
 B Period selected for initial linear portion of the curve before slowing of rate.  
 C Mean for 0.5, 4 and 24 hours (values for timepoints presented in Table 2.6).

### 2.3.4. Selection of p38 MAPK inhibitors for *in vivo* investigation of pharmacokinetics

The aim of PCA was to select three from six p38 MAPK inhibitors with contrasting physicochemical properties within the ' $t_{11}/t_{12}$  space'. For both *in silico* and *in vitro* data, PCA clearly separated GSK-899 from the other compounds and can be considered a more aromatic molecule (Figure 2.11) with a propensity for protein binding (Figure 2.13). Although GSK-677 and GSK-340 were clustered in the *in silico* ' $t_{11}/t_{12}$  space', a clear separation of these compounds was evident for the *in vitro* dataset and GSK-677 was selected as a readily soluble, more polar and basic molecule.

For both PCA analyses, SB-323, SB-445 and GSK-361 were clustered with high passive membrane permeability (Figure 2.13). SB-323 and SB-445 were indistinguishable in the score plot for *in silico* data, with GSK-361 plotted slightly towards the periphery from these compounds. *In vitro* dissolution rates in simulated lung fluid separated these compounds, with GSK-361 exhibiting a slow rate and SB-323 and SB-445 faster rates. GSK-361 was selected as a membrane permeable molecule of low solubility and high lipophilicity. Given its limited supply, SB-445 (high solubility, high lipophilicity and high membrane

permeability) was only included in the single dose study described in this chapter to investigate its pharmacokinetics after inhaled administration.

A plot of the solubility versus dose in conducting airways for marketed pulmonary drugs was considered at a workshop of the AAPS, US-FDA and USP, with a view to considering development of an inhalation Biopharmaceutics Classification System (iBCS). The plot included a threshold representing critical solubility of small molecule drugs for a given dose above which drugs had sufficient solubility to be dissolved and below which drugs were dissolution limited; most of the marketed drugs plotted were not dissolution limited (Hastedt *et al.*, 2016). Key *in vitro* measurements and descriptors for selected p38 MAPK inhibitors in keeping with this convention included solubility in simulated lung fluid and passive membrane permeability (Table 2.9).

**Table 2.9: Key *in vitro* physicochemical parameters of p38 MAPK inhibitors selected for *in vivo* evaluation of lung exposure in rats**

Test article	Physicochemical parameter			Key descriptors
	Solubility in SLF at 4 hours (µg/mL)	Apparent membrane permeability of drug in MDCKII-MDR1 cells <sup>A</sup> (nm/sec)	% plasma protein binding (PCT_PPB)	
GSK-899	4	97.2	99.5	Low solubility; low membrane permeability
GSK-677	957	71.4	96.1	High solubility; low membrane permeability
GSK-361	9	350.1	96.3	Low solubility; high membrane permeability
SB-445	294	209.62	96.5	High solubility; high membrane permeability

**Notes**

A MDCKII-MDR1: cell line of Madin-Darby canine kidney cells transfected with human Pgp (Agarwal *et al.*, 2007). For measurement of passive membrane permeability, Pgp was inhibited by GF120918 (Ward and Azzarano, 2004).

SLF simulated lung fluid

### 2.3.5. Scanning electron microscopy of particles

Aerosols generated from lactose excipient alone or in combination with nominally 5% (w/w) p38 MAPK inhibitor were sampled for scanning electron microscopy, with reference to the input materials (indexed in Table 2.10).

**Table 2.10: Index of figures showing scanning electron microscopy (SEM) of input materials and aerosol samples**

Input material		Figure number
Lactose	n/a	2.16
GSK-899	crystalline	2.17
	amorphous	2.18
GSK-677	crystalline	2.19
GSK-361	crystalline	2.20

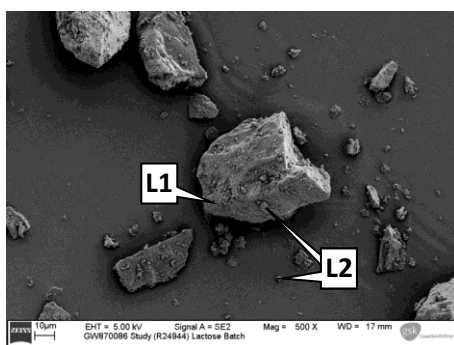
**Notes**

P38 MAPK inhibitors used for investigation of efficacy (Chapter 4) and repeat dose toxicity (Chapter 5) were sampled; SB-445 not sampled for SEM.

Particles of the excipient, “inhalation grade lactose”, were irregular in shape with both angular and smooth edges (Figure 2.16). The lactose excipient was supplied as a mixture of mainly large carrier particles with 6% (w/w) fine particles (<4.5 µm aerodynamic diameter). Large carrier particles (50 to 100 µm aerodynamic diameter) are commonly used as excipient in dry powder inhaler formulations to facilitate manipulation of small clinical doses and to improve dispersal of the drug in air (Healy *et al.*, 2014).

Comparison of supplied excipient (Figure 2.16A) with sampled aerosol (Figure 2.16B) shows enrichment of the fine particles of lactose during aerosol generation, with primary particles and agglomerates evident on the isopore membrane filter. Enrichment of fine lactose particles (and a respirable drug if present) in aerosols generated from dry powder formulations occurs as the large lactose particles impact or sediment within the exposure system.

2.16A:



2.16B:

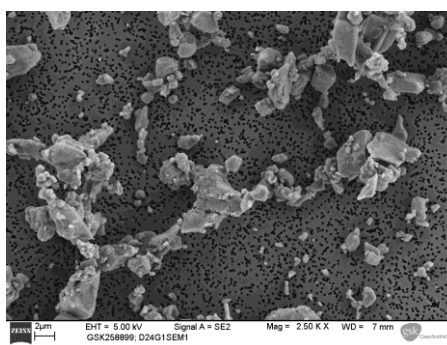
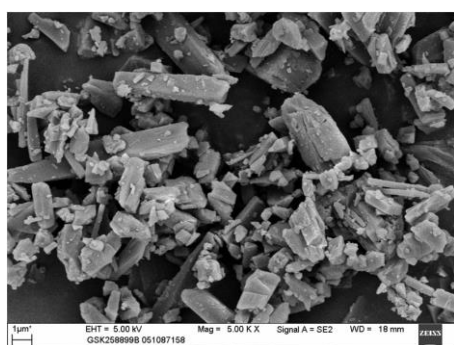


**Figure 2.16:** Scanning electron microscopy of ‘inhalation grade lactose’ used as excipient in dry powder formulations of p38 MAPK inhibitors. **2.16A:** excipient supplied for preparation of drug-lactose blends. Particles were irregular in shape, with angular and smooth edges. Large particles (L1) are visible, with smaller particles of lactose (L2) adhered to their surface. **2.16B:** lactose particles sampled from an aerosol onto an isopore filter; the pores are visible as black spots on the membrane.

Crystalline drugs manufactured for non-clinical (*in vitro* and *in vivo*) and clinical (human) development are commonly micronised using a jet mill to reduce particle size for inhaled delivery. Micronised crystals of the p38 MAPK inhibitors were angular and irregular in appearance with GSK-899 (Figure 2.17A) and GSK-361 (Figure 2.20A) of columnar appearance with elongated crystals of medium aspect ratio; crystals of GSK-361 appeared more slender than GSK-899. Micronised crystals of GSK-677 (Figure 2.19A) were more plate-like and less distinct from lactose.

2.17A:



2.17B:

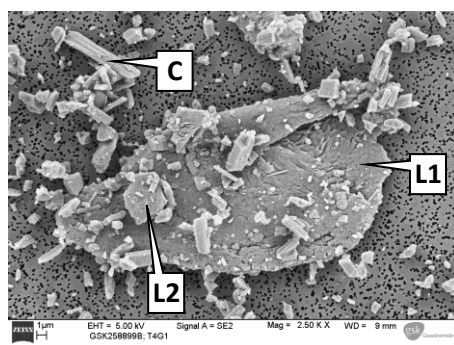
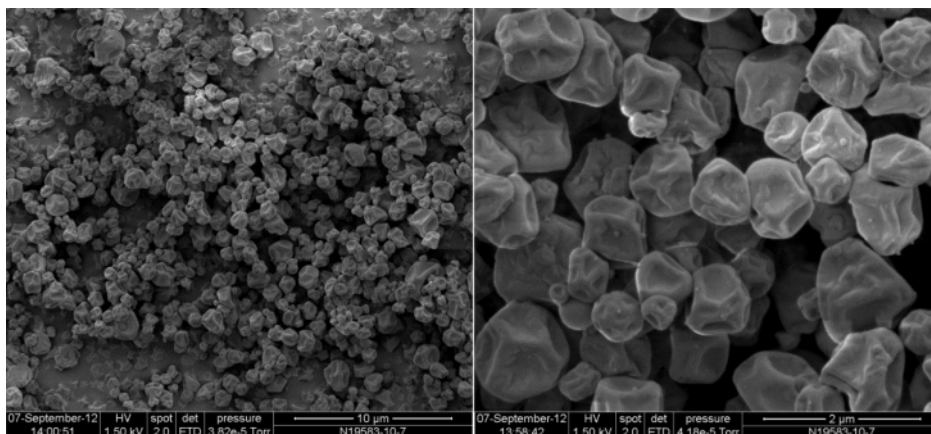


**Figure 2.17:** Scanning electron microscopy (SEM) of crystalline GSK-899. **2.17A:** jet milled (micronised) crystals of angular and irregular appearance. **2.17B:** particles sampled from an aerosol generated from 5% (w/w) crystalline GSK-899 in lactose onto an isopore filter. A large lactose particle (L1) is clearly visible but the irregular angular appearance of crystalline GSK-899 (C) and small lactose particles (L2) makes differentiation of species by SEM uncertain.

Amorphous GSK-899 was produced by spray drying a saturated solution of the drug in methanol, a volatile solvent that rapidly evaporated to produce particles of randomly orientated GSK-899 molecules. Particles resembled shrunken spheres of dimpled appearance (Figure 2.18A).

### 2.18A



### 2.18B

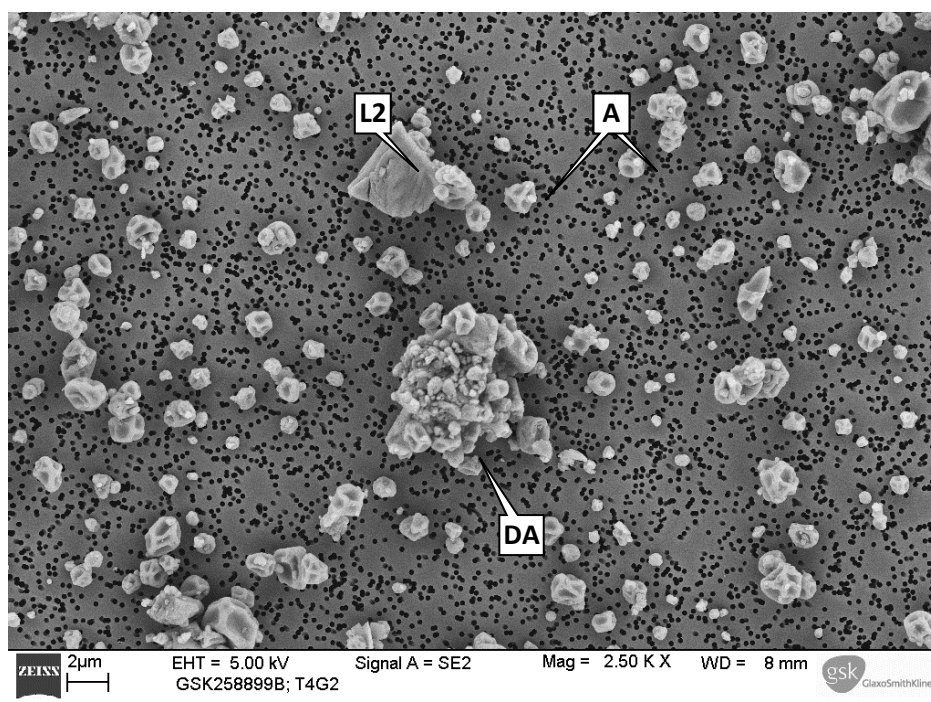
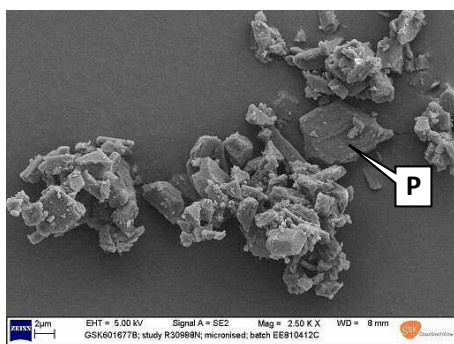


**Figure 2.18: Scanning electron microscopy of amorphous GSK-899.** **2.18A:** amorphous powder was produced by spray drying a saturated solution of GSK-899 in methanol to produce ‘dimpled spheres’. **2.18B:** particles sampled from an aerosol generated from 4% (w/w) amorphous GSK-899 in lactose onto an isopore filter. A larger lactose particle (L1) and primary amorphous particles (A) are distinct. A drusy agglomeration (DA) of particles represents a large lactose particle coated with small lactose particles and amorphous GSK-899.

Aerosols generated from powder formulations of p38 MAPK inhibitors showed the drug and lactose as primary particles and also as drusy agglomerations, *i.e.* large particle (lactose) coated with fine particulates. Given the particle shapes for the input materials, distinction of the p38 MAPK inhibitor from lactose was readily apparent for amorphous GSK-899 (Figure 2.18B) and, to a lesser extent, crystalline GSK-361 (Figure 2.20B) but was indistinguishable for crystalline GSK-677.

**2.19A:**



**2.19B:**

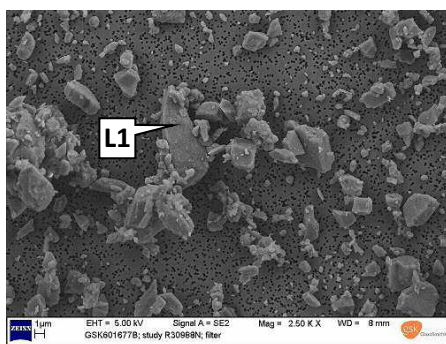
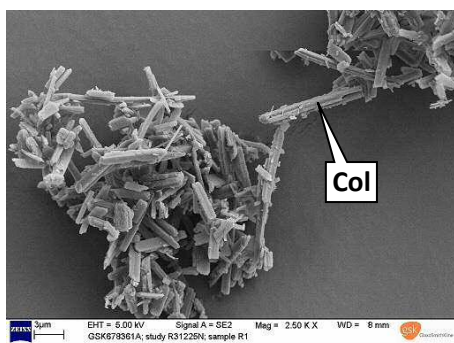


**Figure 2.19: Scanning electron microscopy (SEM) of crystalline GSK-677.** **2.19A:** crystals were micronised using a jet mill, producing smaller crystals of an angular and irregular or plate-like (P) appearance. **2.19B:** particles sampled from an aerosol generated from 5% (w/w) crystalline GSK-677 in lactose onto an isopore filter. A large lactose particle (L1) is distinct but the irregular and plate-like appearance of crystalline GSK-677 and small lactose particles precludes differentiation of these two species by SEM.

**2.20A:**



**2.20B:**

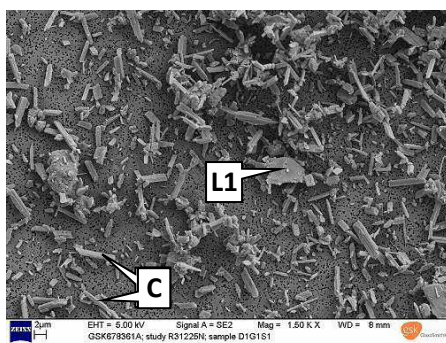


**Figure 2.20: Scanning electronic microscopy of crystalline GSK-361.** **2.20A:** crystals were micronised using a jet mill, producing smaller crystals of an angular and irregular or columnar (Col) appearance. **2.20B:** particles sampled from an aerosol generated from 5% (w/w) crystalline GSK-361 in lactose onto an isopore filter. Plate-like lactose particles (L1) and columnar GSK-361 crystals (C) can be distinguished in the image.

SEM of aerosols revealed no indication that fine particles had fused to form larger aggregates in the aerosol and that compression of dry powder formulations to facilitate aerosol generation would not compromise presentation of the p38 MAPK inhibitors to animals.

### **2.3.6. Pharmacokinetics of p38 MAPK inhibitors in rats following a single inhaled dose**

It was anticipated the rate of clearance of p38 MAPK inhibitors from rat lungs after inhalation exposure would be driven by high solubility and lipophilicity, facilitating transmembrane migration of the molecules and uptake into the systemic circulation (blood). Compounds presenting a faster dissolution rate were expected to achieve higher plasma concentrations immediately after inhalation exposure, and for lung concentrations to be significantly reduced at 24 hours post exposure.

Based on the results of PCA and *in vitro* dissolution, it was hypothesised that exposure in terms of area under the drug-concentration time curve may be ranked as follows:

- Plasma: SB-445 > GSK-678 > GSK-361 > GSK-899
- Lung: GSK-899 > GSK-361 > GSK-678 > SB-445

It was also hypothesised that:

- Nebulised solutions of p38 MAPK inhibitors would be cleared from the lungs quicker than for the corresponding crystalline aerosol form, as crystalline particles must first undergo dissolution prior to transmembrane absorption.
- Presentation of GSK-899 as amorphous powder would achieve higher plasma concentrations and show faster lung clearance than for the crystalline form of GSK-899.

#### **2.3.6.1. Inhalation exposure of rats to p38 MAPK inhibitors and estimation of the inhaled dose**

Generally, achieved mean aerosol concentrations were in good agreement with target ( $\pm 10\%$  of 24  $\mu\text{g}/\text{L}$ ), with crystalline GSK-899 and nebulised GSK-361 slightly higher ( $\pm 15\%$  of target). Mean estimated

inhaled doses for each p38 MAPK inhibitor and aerosol form were generally  $\pm 15\%$  of the target dose of 0.6 mg/kg (0.51 to 0.69 mg/kg), with GSK-677 doses below this range (Table 2.11). This was primarily due to lower body weights for rats exposed to GSK-677 (target dose assumed a mean body weight of 350g) and depletion of the GSK-677 solution in the nebuliser reservoir resulting in a reduced aerosol concentration for the latter period of animal exposure.

**Table 2.11: Estimated inhaled doses in rats and aerosol characterisation data for p38 MAPK inhibitors**

Study number	Test article	Aerosol form and test article concentration in vehicle	Estimated inhaled dose <sup>A</sup> (mg/kg)	Mean (n=2) drug aerosol concentration ( $\mu\text{g/L}$ )	Particle size distribution	
					MMAD ( $\mu\text{m}$ )	$\sigma\text{g}$
R30573N	GSK-899	Crystalline (4.9% w/w)	0.681	31.6	2.4	1.9
		Amorphous (4.0% w/w)	0.527	24.4	2.7	2.1
		Nebulised solution (1.5 mg/mL)	0.529	24.4	4.2	1.8
	SB-455	Crystalline (4.9% w/w)	0.517	23.9	2.7	2.0
R30988N	GSK-677	Crystalline (4.4% w/w)	0.490	22.2	2.8	2.0
		Nebulised solution (2.5 mg/mL)	0.422	19.1	1.3	2.2
R31225N	GSK-361	Crystalline (4.8% w/w)	0.554	26.0	2.0	2.4
		Nebulised solution (1.5 mg/mL)	0.570	27.0	2.5	2.4

**Notes**

MMAD mass median aerodynamic diameter

$\sigma\text{g}$  geometric standard deviation

A Estimated inhaled doses calculated for a 30-minute exposure period using mean data (body weight and aerosol concentration) and a body-weight derived estimate of respired minute volume (Alexander *et al.*, 2008).

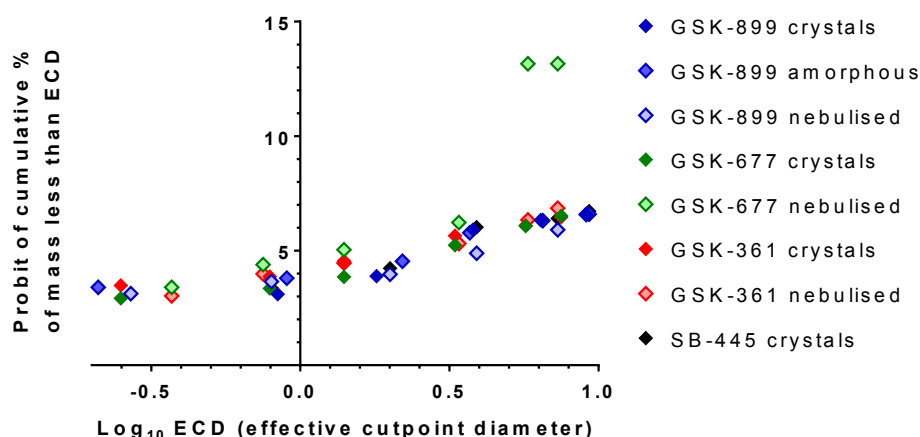
The mass median aerodynamic diameter (MMAD) for nebulised GSK-899 (4.2  $\mu\text{m}$ ) was on the cusp of the range 1 to 4  $\mu\text{m}$  recommended for acute (single exposure) inhalation toxicity testing (US-EPA[1300], 1998, OECD[403], 2009). Otherwise, the MMAD and estimated

geometric standard deviation ( $\sigma_g$ ) for all aerosols were within ranges stipulated to ensure exposure of the respiratory tract of rodents during repeat exposure studies, *i.e.* MMAD of 1 to 3  $\mu\text{m}$  and  $\sigma_g$  of 1.5 to 3.0 (OECD[412], 2009, OECD[413], 2009, US-EPA[3645], 1998). The MMAD for nebulised GSK-899 and GSK-361 was higher than for powder aerosols of the respective compounds, and also nebulised GSK-677. This is at least in part due to utilisation of two nebulisers to disperse the solution into the chamber to achieve the target aerosol concentration, which was necessitated by low aqueous solubility of the compounds.

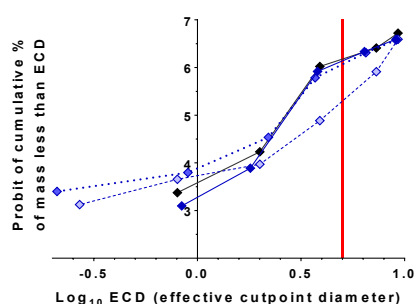
Significant differences between droplet or particle size distributions will have implications for the mass of an aerosol deposited in the lower respiratory tract. However, the MMAD is a median value of particle size and not an absolute threshold of respirability, with a proportion of larger particulates being inhaled by animals. Miller (2000) reported the probability of rats inhaling particles of 4  $\mu\text{m}$  aerodynamic diameter was 71%, and of inhaling particles of 7  $\mu\text{m}$  aerodynamic diameter was 55%.

The fine particle fraction (percentage mass less than 5  $\mu\text{m}$  aerodynamic equivalent diameter (EMA-3, 2006)) was determined for each compound and aerosol form (Figure 2.21). Values (Table 2.12) were similar for most of the aerosols (81% to 87%), lower for nebulised GSK-899 (62%) and higher for nebulised GSK-677 (>99.9%).

2.21A:



2.21B: GSK-899 and SB-445



2.21C: GSK-677 and GSK-361

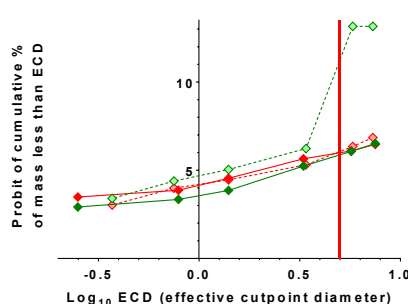


**Figure 2.21: Estimation of fine particle fraction (% mass <5µm aerodynamic diameter) by interpolation of particulate size data.** **2.21A:** probit (probability function) of cumulative mass less than a cut-point plotted against Log<sub>10</sub>(cut-point). The probit at x=0.70 (aerodynamic diameter of 5 µm) was determined for back-transformation of the fine particle fraction (Table 2.12). **2.21B:** GSK-899 and SB-445. **2.21C:** GSK-677 and GSK-361.

**Table 2.12: Estimation of fine particle fraction of aerosols of p38 MAPK inhibitors by interpolation of particulate size data**

Study number	P38 MAPK inhibitor and particle form		Probit at Log <sub>10</sub> (5µm)	Fine particle fraction (%<5µm) <sup>A</sup>
R30573N	GSK-899	crystalline	6.15	87%
		amorphous	6.08	86%
		nebulised	5.30	62%
R30988N	GSK-677	crystalline	5.90	81%
		nebulised	11.1	>99.9%
R31225N	GSK-361	crystalline	6.00	84%
		nebulised	6.05	85%

Notes

A Probit at x=0.70 (equating to 5µm effective cut-point aerodynamic diameter) transformed to probability (percentage mass less than cut-point) using Finney's table (Finney, 1952).

### 2.3.6.2. Systemic and pulmonary pharmacokinetics and lung distribution of p38 MAPK inhibitors in rats

Lung and plasma concentration profiles and representative MALDI-MSI images for drug-lung deposition are presented for each p38 MAPK inhibitor (Table 2.13). Summary pharmacokinetic parameters for lung and plasma data are tabulated together following the figures (Tables 2.16 and 2.17).

**Table 2.13: Index of figures presenting concentrations of p38 MAPK inhibitors in lung and plasma, and relative lung distribution**

Study number	p38 MAPK inhibitor and particle form		Figure number		
			Concentration (HPLC-MS/MS)		Lung distribution (MALDI-MSI)
			Lung	Plasma	
R30573N	GSK-899	crystalline	2.22	2.23	2.24
		amorphous			2.25
nebulised	2.26				
	SB-445	crystalline	2.35	2.36	n/a
R30988N	GSK-677	crystalline	2.27	2.28	2.29
		nebulised			2.30
R31225N	GSK-361	crystalline	2.31	2.32	2.33
		nebulised			2.34

Although rats were exsanguinated before isolation of lung samples, the mass of p38 MAPK inhibitor measured in lung homogenate would be a combination of drug associated with lung tissue *per se* and residual blood in the vasculature of the lungs post mortem. Triplett *et al.* (1985) reported that blood accounted for 30% of the mass of wet lung. However, the Sprague Dawley rats used for these investigations were euthanized under urethane anaesthesia (at a dose not expected to affect blood pressure (Field and Lang, 1988)) by injection of potassium chloride, which is used to induce cardiac arrest in murine models (Abella *et al.*, 2004). The lung weights of the exsanguinated animals used for investigations described in this chapter were similar to the published mean value but body weights were higher than the published range (Triplett *et al.*, 1985). Estimation of the circulating blood volume from body weights using a published conversion factor (Diehl *et al.*, 2001) and comparison of the ratio of lung weight to circulating blood volume

suggested there was 33% less blood residing in the lung tissue of the exsanguinated rats (Table 2.14).

**Table 2.14: Lung weights and estimated circulating blood volume of rats**

Compound and aerosol form		No. rats (n)	Lung weight (g)		Body weight (g)		Circulating blood volume <sup>A</sup> (mL)	Ratio LWT:CBV
			Mean (total)	sd	Mean	sd		
GSK-899	crystalline	18	1.126	0.079	321.8	16.2	20.6	0.055
	amorphous	18	1.096	0.065	320.4	13.6	20.5	0.053
	nebulised	18	1.114	0.066	316.0	14.1	20.2	0.055
GSK-677	crystalline	18	1.000	0.056	272.8	16.4	17.5	0.057
	nebulised	18	1.013	0.062	271.6	16.2	17.4	0.058
GSK-361	crystalline	18	1.176	0.092	348.8	15.6	22.3	0.053
	nebulised	18	1.369	0.104	378.5	26.9	24.2	0.057
SB-445	crystalline	18	1.159	0.084	320.2	11.9	20.5	0.057
All groups combined (p38 MAPK inhibitors)		144	1.132	0.131	318.7	37.2	20.4	0.056
Triplett <i>et al.</i> (1985)		40	1.32	0.92	250 <sup>B</sup>	n/a	16.0	0.083

#### Notes

LWT Lung weight

A Circulating blood volume (CBV) calculated from body weight using value of 64 mL/kg for rats (Diehl *et al.*, 2001)

B Body weight: median value of published range (225 to 275g) used for calculation of CBV

In order to determine the potential distribution of p38 MAPK inhibitors between lung tissue and blood residing in the lung vasculature, lung and blood concentrations of each p38 MAPK inhibitor were used to estimate the proportion of analyte associated with the tissue *per se*. Results indicate that, when quantifiable,  $\geq 99\%$  of the p38 MAPK inhibitor was associated with lung tissue for most aerosols. For GSK-361, it was estimated  $\leq 20\%$  of the analyte was associated with residual blood in the wet lung sample (Table 2.15). Given the general prevalence of p38 MAPK inhibitors in the lung tissue following inhaled administration, correction of lung concentration data for residual blood was considered unnecessary for evaluation of lung pharmacokinetics.

The mean GSK-899 concentration in lungs sampled as soon as practicable after inhaled administration of crystals to rats was approximately three-fold higher than that of animals administered

amorphous powder and 15-fold higher than for the nebulised solution (Figure 2.22), achieving statistical significance for all comparisons of aerosol form ( $p < 0.01$ ). Although the MMAD for nebulised GSK-899 was higher than for crystalline and amorphous particulates, the observed differences in lung concentration cannot be ascribed to differences in the fine particle fraction alone (Table 2.12) or a difference in estimated inhaled doses for crystalline and nebulised GSK-899 (Table 2.11).

**Table 2.15: Distribution of drug between lung tissue and blood residing in vasculature, and indexing of appendices for individual data**

Compound	Aerosol form	No. rats (n)	Proportion of drug associated with lung tissue		Maximum proportion of drug in blood <sup>A</sup>
			mean <sup>A</sup>	sd	
GSK-899	crystalline	13	100%	0%	0%
	amorphous	16	100%	0%	1%
	nebulised	15	100%	0%	1%
GSK-677	crystalline	14	100%	0%	0%
	nebulised	13	100%	0%	0%
GSK-361	crystalline	15	92%	5%	18%
	nebulised	13	88%	7%	20%
SB-445	crystalline	18	99%	1%	3%

**Notes**

A Assumes 20% of lung weight is attributable to residual blood, based on differences between the ratio of lung weight to circulating blood volume for exsanguinated and non-exsanguinated rats (Table 2.14)

It is worth noting isolation of lungs at the first timepoint occurred approximately 20 minutes after the end of the 30-minute inhalation exposure period. This was due to logistics for transferring animals to a necropsy facility, euthanasia (exsanguination under anaesthesia) and removal of lungs from the carcass. A drug-lung residence period of 20 to 50 minutes thus elapsed before lungs were isolated, during which time particles underwent dissolution and absorption. Systemic uptake and elimination of drug in plasma normally achieves steady state during aerosol administration (personal observation of unpublished pharmacokinetic data), with a decline in plasma concentration seen post exposure. For low solubility drugs, the 20-minute period elapsing post exposure may, at least in part, account for differences in lung dose

measured after cessation of aerosol generation. For nebulised solutions, a drug would be available for absorption after deposition but this would be delayed for crystals of relatively low solubility first undergoing dissolution.

The drug-lung concentration profiles show a persistence of crystalline GSK-899 in rat lung after single exposure, with mean concentrations at 24 hours just 74% of the post exposure mean for rats administered crystals, 10% for amorphous powder and 3% for the nebulised solution. This shows a potential for drug accumulation with repeated once daily administration of crystalline and perhaps amorphous GSK-899.

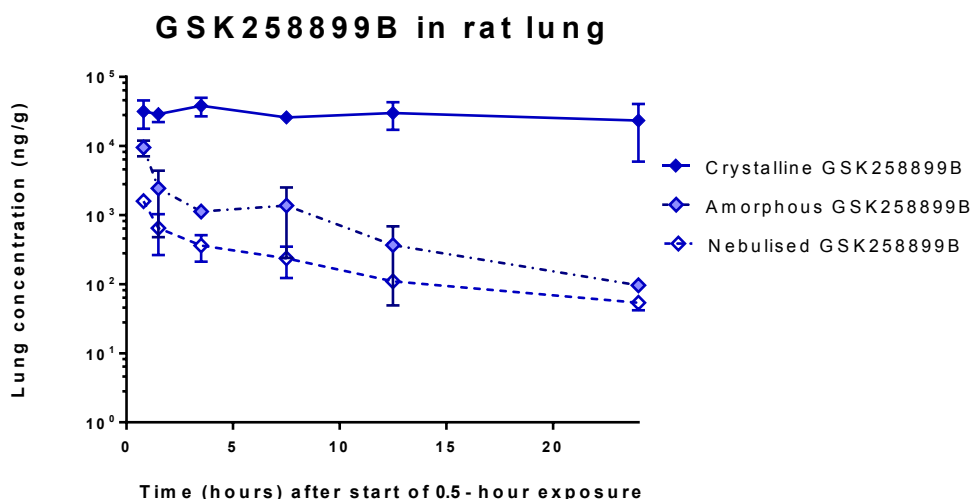


**Figure 2.22: GSK-899 concentrations in lung homogenate sampled from rats after a single inhaled dose.** Rats inhaled crystalline, amorphous or aqueous (nebulised) GSK-899 for 30 minutes (target dose of 0.6 mg/kg). Mean GSK-899 concentrations in lungs are shown with standard deviations (error bars; n=3) up to 24 hours from the start of exposure. Statistical analysis (2-way ANOVA with post hoc analysis using Tukey's honestly significant difference test (Abdi and Williams, 2010[B])) of  $\log_{10}$ -transformed data indicated each aerosol was significantly different from one another ( $p < 0.01$ ).

Drug-plasma concentrations of GSK-899 following inhalation exposure were highest in rats administered amorphous or nebulised GSK-899 (Figure 2.23). Although the profiles appeared similar for these aerosol forms, differences achieved statistical significance ( $p < 0.05$ ). The profile following exposure of rats to crystalline GSK-899 was more variable with a time of peak concentration ( $T_{max}$ ) at 7.5 hours. This profile was

significantly different ( $p < 0.01$ ) to the profiles following exposure of rats to amorphous or nebulised aerosol forms. Plasma concentrations after a 30-minute intravenous infusion of GSK-899 (Petri, 2004) showed an initial distribution phase characterized by a steep gradient (Shargel *et al.*, 2005) that was not seen after inhalation exposure of rats.

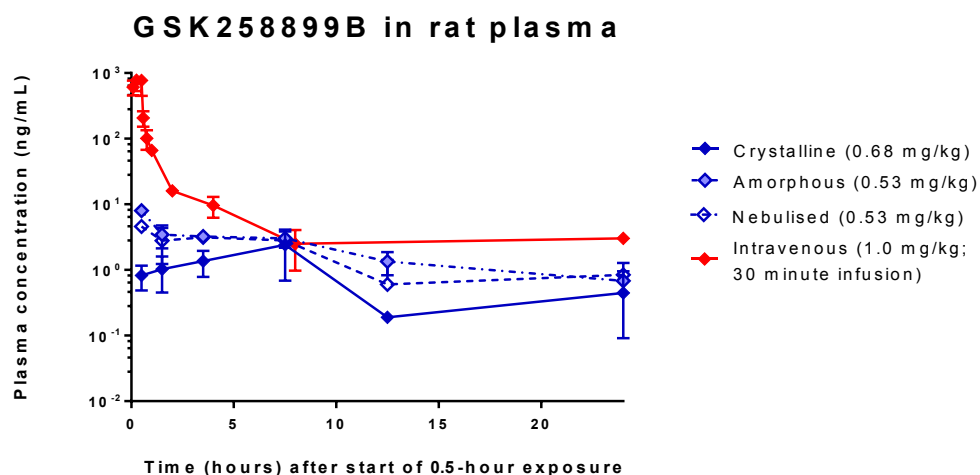
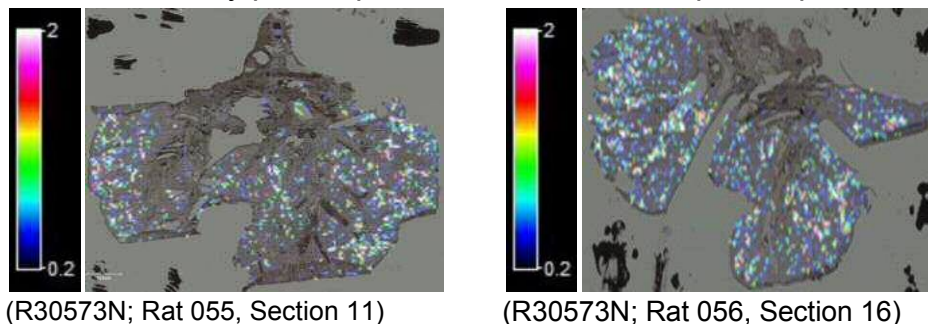


**Figure 2.23: GSK-899 concentrations in plasma sampled from rats after a single inhaled or intravenous dose.** Rats inhaled crystalline, amorphous or aqueous (nebulised) GSK-899 for 30 minutes (target dose of 0.6 mg/kg). Data (in red) also plotted for rats administered GSK-899 by a 30-minute intravenous infusion (Petri, 2004). Mean GSK-899 plasma concentrations shown with standard deviations (error bars;  $n=3$ ) up to 24 hours from start of exposure. Statistical analysis (2-way ANOVA with post hoc analysis using Tukey's honestly significant difference test (Abdi and Williams, 2010[B])) of concentrations indicated each aerosol form was significantly different from one another ( $p < 0.01$  for crystalline versus amorphous/nebulised GSK-899;  $p < 0.05$  for amorphous versus nebulised GSK-899). *No result for samples at 1.5 hours (1/3 crystalline), 7.5 hours (1/3 crystalline, 1/3 amorphous and 2/3 nebulised) and 12.5 hours (2/3 crystalline) due to no response for internal standard; insufficient sample for re-analysis.*

MALDI-MSI analysis of lung sections from rats administered crystalline GSK-899 showed foci of peak concentrations distributed relatively evenly across the tissue as soon as practicable post exposure and three hours later (Figure 2.24). The signal intensity of GSK-899 for rats administered amorphous powder was less pronounced than for crystalline GSK-899 post exposure, but also showed no obvious drug localisation within the lung section (Figure 2.25A). GSK-899 was barely perceptible after nebulised administration (Figure 2.26A), relative to the

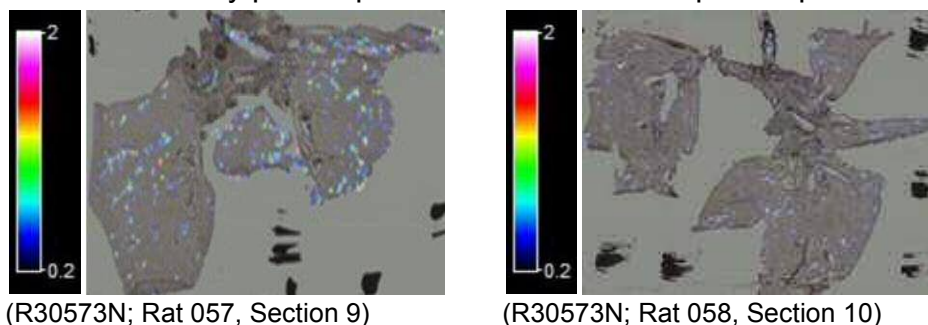
amorphous and crystalline aerosol forms. Imaged sections at three hours post exposure indicated drug clearance of the amorphous (Figure 2.25B) and nebulised (Figure 2.26B) aerosol forms.

**2.24A:** immediately post exposure    **2.24B:** 3 hours post exposure

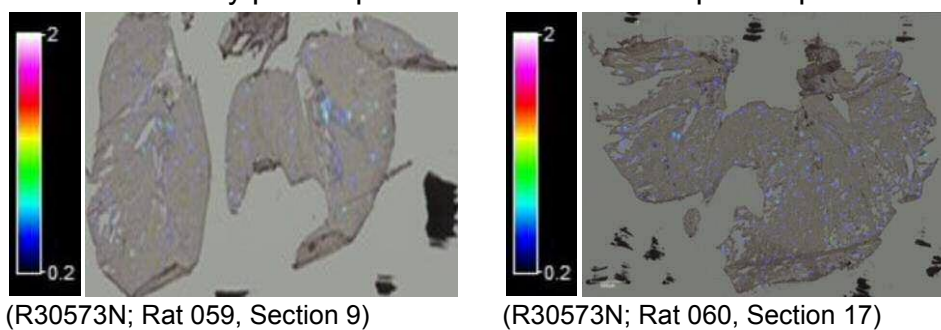


**Figure 2.24:** GSK-899 in lungs of rats inhaling crystalline drug imaged by matrix assisted laser desorption/ionization with mass spectrometry imaging (MALDI-MSI). Rats inhaled crystalline GSK-899 for 30 minutes (target dose of 0.6 mg/kg). A matrix was applied to frozen sections of tissue (12  $\mu$ m thick) for MALDI-MSI; coloured scaling of the relative amount of GSK-899 is shown (arbitrary units). **2.24A:** rat lung taken as soon as possible (20 minutes) after a single exposure. **2.24B:** rat lung taken 3 hours post exposure.

**2.25A:** immediately post exposure    **2.25B:** 3 hours post exposure



**Figure 2.25:** GSK-899 in lungs of rats inhaling amorphous drug imaged by matrix assisted laser desorption/ionization with mass spectrometry imaging (MALDI-MSI). Rats inhaled amorphous GSK-899 for 30 minutes (target dose of 0.6 mg/kg). A matrix was applied to frozen sections of tissue (12  $\mu$ m thick) for MALDI-MSI; coloured scaling of the relative amount of GSK-899 is shown (arbitrary units). **2.25A:** rat lung taken as soon as possible (20 minutes) after exposure. **2.25B:** rat lung taken 3 hours post exposure.

**2.26A:** immediately post exposure    **2.26B:** 3 hours post exposure

**Figure 2.26:** GSK-899 in lungs of rats inhaling nebulised drug imaged by matrix assisted laser desorption/ionization with mass spectrometry imaging (MALDI-MSI). Rats inhaled aqueous (nebulised) GSK-899 for 30 minutes (target dose of 0.6 mg/kg). A matrix was applied to frozen sections of tissue (12  $\mu\text{m}$  thick) for MALDI-MSI; coloured scaling of the relative amount of GSK-899 is shown (arbitrary units). **2.26A:** rat lung taken as soon as possible (20 minutes) after exposure. **2.26B:** rat lung taken 3 hours post exposure.

These observations correlate with the drug-lung concentration profiles. GSK-899 persistence after inhalation of micronised crystals and depletion of amorphous GSK-899 was consistent with the hypothesis that materials exhibiting a faster dissolution rate *in vitro* are likely to be cleared more quickly *in vivo* following inhalation exposure of rats.

Solubilisation of crystalline solutes first requires disruption of the crystal lattice (Van den Mooter, 2012). A faster dissolution rate for amorphous powder may thus occur due to the disrupted, random organisation of molecules in the inhaled particles, making GSK-899 more available for solvation and subsequent absorption from the lung surface. Nebulised GSK-899 was presented in solution, facilitating absorption from lungs.

GSK-677 concentration profiles in lung tissue (Figure 2.27) and plasma (Figure 2.28) were indistinguishable for the crystalline and nebulised aerosols forms. Mean lung concentrations of GSK-677 following exposure were similar to that of nebulised GSK-899 (Figure 2.22) and GSK-677 plasma concentrations were initially higher than those of GSK-899 (Figure 2.23) but had decreased by at least one order of magnitude within one hour post exposure. This supports the hypothesis that a faster *in vitro* dissolution rate would lead to faster absorption and systemic exposure after inhaled administration of GSK-677 to rats and that dissolution of crystalline GSK-677 was not rate limiting. Plasma concentrations after a 30-minute intravenous infusion of GSK-677 followed a similar profile to those evident after inhalation exposure, indicating an initial distribution phase characterized by a steep gradient followed by a slower elimination phase (Shargel *et al.*, 2005).

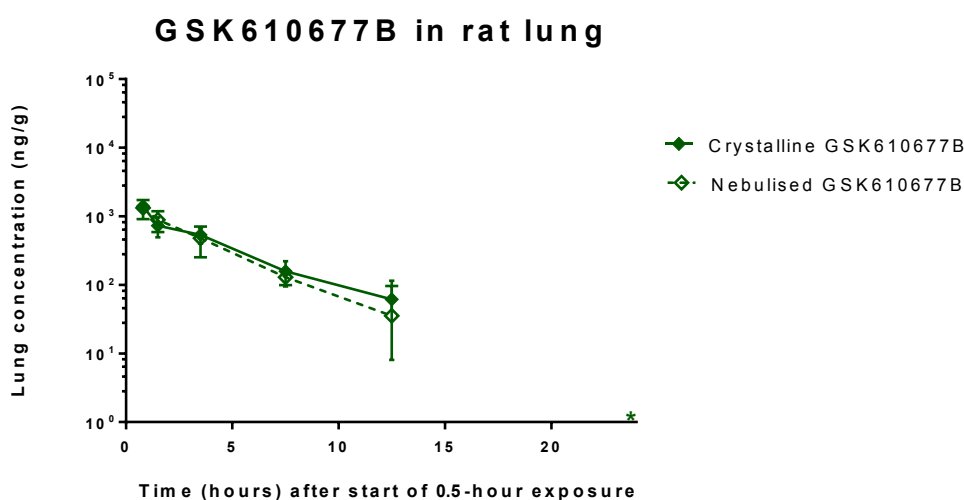


**Figure 2.27: GSK-677 concentrations in lung homogenate sampled from rats after a single inhaled dose.** Rats inhaled an aerosol of crystalline or aqueous (nebulised) GSK-677 for 30 minutes (target dose of 0.6 mg/kg). Mean GSK-677 concentrations are shown with standard deviations (error bars; n=3) up to 24 hours from the start of exposure. Lung concentrations at 24 hours post exposure (\*) were below the limit of quantification (<40 ng/g lung tissue). No differences of statistical difference (2-way ANOVA with post hoc analysis using Tukey's honestly significant difference test (Abdi and Williams, 2010[B])) for log<sub>10</sub>-transformed data.

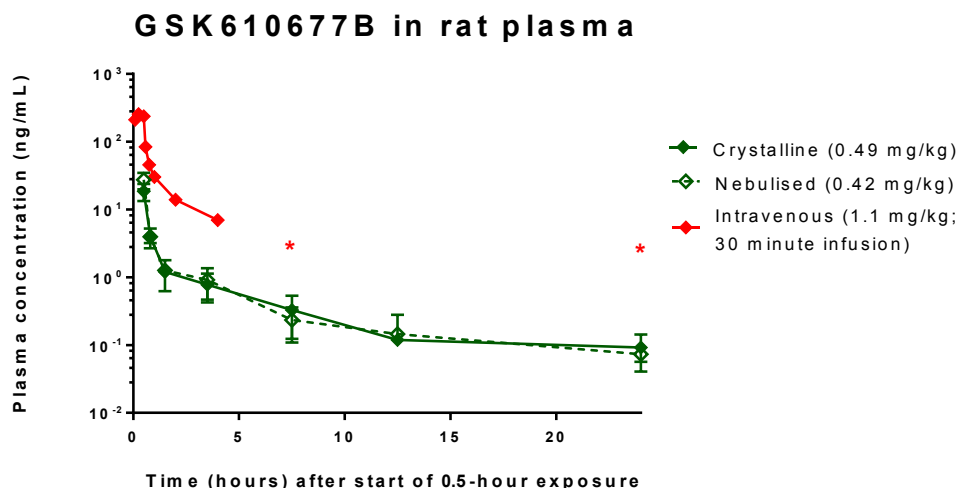


**Figure 2.28: GSK-677 concentrations in plasma of rats after a single inhaled or intravenous dose.** Rats inhaled an aerosol of crystalline or aqueous (nebulised) GSK-677 for 30 minutes (target dose of 0.6 mg/kg). Data (in red) also plotted for rats administered GSK-677 a 30-minute intravenous infusion (Umbrecht, 2007); plasma concentrations at  $\geq 8$  hours (\*) were not quantifiable ( $< 5$  ng/mL). Mean GSK-677 concentrations in plasma are shown with standard deviations (error bars;  $n=3$ ) up to 24 hours from the start of exposure. No differences of statistical difference (2-way ANOVA with post hoc analysis using Tukey's honestly significant difference test (Abdi and Williams, 2010[B])) for  $\log_{10}$ -transformed data.

MALDI-MSI analysis of rat lung sections showed 'hot areas' of GSK-677 in the main airways, with relatively even distribution of foci corresponding to peak drug concentrations across peripheral tissue (Figures 2.29A and 2.30A). For each aerosol form, a decreased signal intensity of GSK-677 was seen three hours post exposure (Figures 2.29B and 2.30B) but it was difficult to draw conclusions regarding relative differences in signal intensity for crystalline or nebulised GSK-677 given differences in the coloured scaling applied for image analysis in each experiment.

**2.29A:** immediately post exposure **2.29B:** 3 hours post exposure

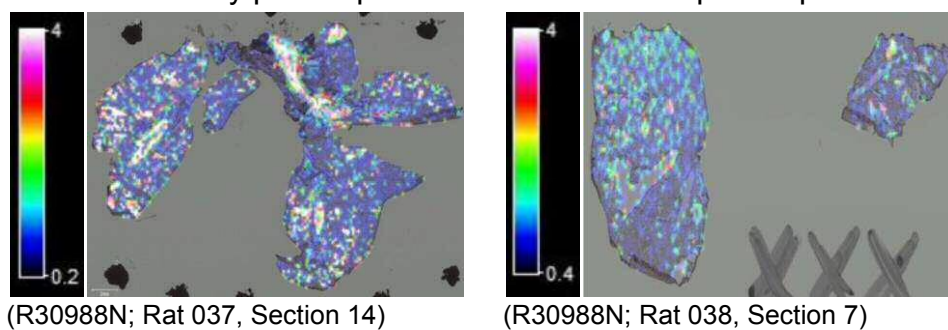


**Figure 2.29: GSK-677 in lungs of rats inhaling crystalline drug imaged by matrix assisted laser desorption/ionization with mass spectrometry imaging (MALDI-MSI).** Rats inhaled crystalline GSK-677 for 30 minutes (target dose of 0.6 mg/kg). A matrix was applied to frozen sections of tissue (12  $\mu\text{m}$  thick) for MALDI-MSI; coloured scaling of the amount of GSK-677 is shown (arbitrary units). **2.29A:** rat lung taken as soon as possible (20 minutes) after a single exposure. **2.29B:** rat lung taken 3 hours post exposure.

**2.30A:** immediately post exposure **2.30B:** 3 hours post exposure

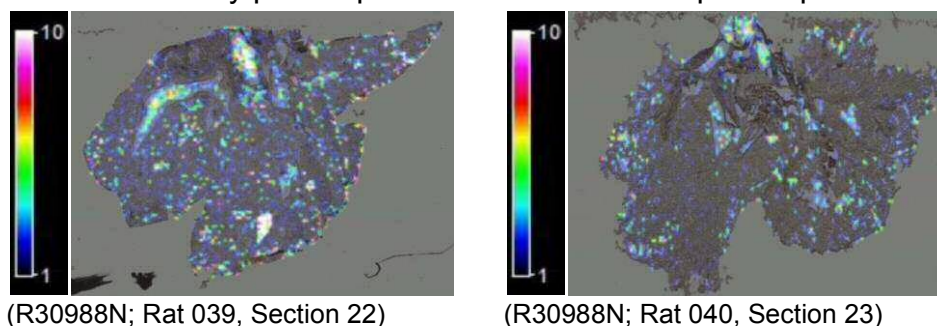


**Figure 2.30: GSK-677 in lungs of rats inhaling nebulised drug imaged by matrix assisted laser desorption/ionization with mass spectrometry imaging (MALDI-MSI).** Rats inhaled aqueous (nebulised) GSK-677 for 30 minutes (target dose of 0.6 mg/kg). A matrix was applied to frozen sections of tissue (12  $\mu\text{m}$  thick) for MALDI-MSI; coloured scaling of the amount of GSK-677 is shown (arbitrary units). **2.30A:** rat lung taken as soon as possible (20 minutes) after a single exposure. **2.30B:** rat lung taken 3 hours post exposure.

GSK-361 lung concentrations were higher in rats following inhaled administration of crystals than for the nebulised solution (Figure 2.31), achieving statistical significance ( $p < 0.01$ ), and were similar to concentrations of GSK-899 in rats administered the amorphous powder (Figure 2.22). Plasma concentrations were variable and, although mean values for crystalline GSK-361 appeared higher than nebulised GSK-361 (Figure 2.32), no statistical significance was achieved.

As with GSK-899, a particle-lung residence time of 20 to 50 minutes occurred and a slow dissolution rate may have given rise to short-term formation of a lung depot of micron-sized GSK-361 crystals, accounting for the difference in drug-lung concentration evident at the first time point (Figure 2.31). Plasma concentrations following inhaled administration of GSK-361 initially increased, indicating an absorption phase. Thereafter, plasma concentration profiles were similar to an essentially linear profile seen after administration of an intravenous bolus of GSK-361 (Ioannou, 2005) indicating the distribution phase was rapid (Shargel *et al.*, 2005). MALDI-MSI of the lungs of rats administered GSK-361 showed even distribution of foci corresponding to peak drug concentrations across lung sections, with a greater signal intensity in rats administered crystals in rats administered crystals (Figure 2.33A) than nebulised GSK-361 (Figure 2.34A). This finding correlated with the lung concentration data (Figure 2.31). A decreased signal intensity was evident for both aerosol forms of GSK-361 at three hours post exposure (Figures 2.33B and 2.34B).

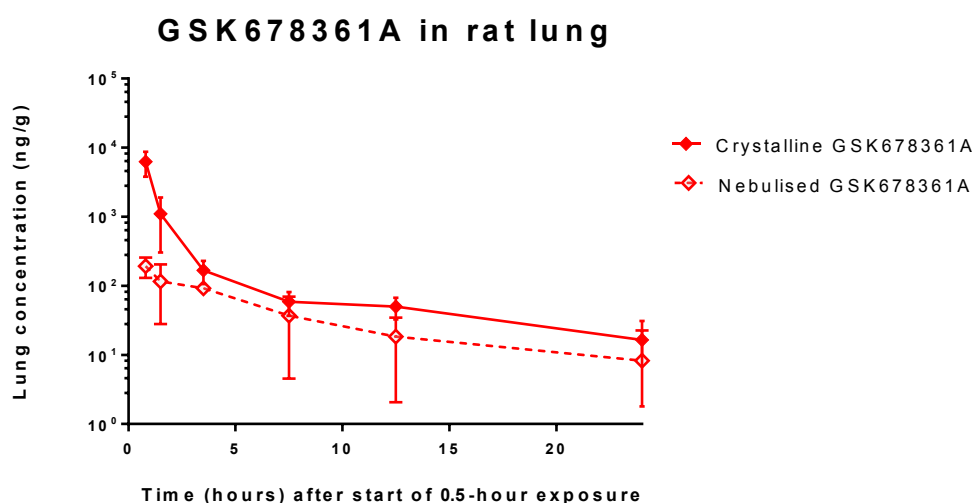


**Figure 2.31: GSK-361 concentrations in lung homogenate sampled from rats after a single inhaled dose.** Rats inhaled an aerosol of crystalline or aqueous (nebulised) GSK-361 for 30 minutes (target dose of 0.6 mg/kg). Mean GSK-361 concentrations are shown with standard deviations (error bars; n=3) up to 24 hours from the start of exposure. Statistical analysis (2-way ANOVA with post hoc analysis using Tukey's honestly significant difference test (Abdi and Williams, 2010[B])) of log<sub>10</sub>-transformed data indicated a significant difference between crystalline and nebulised aerosols (p<0.01).

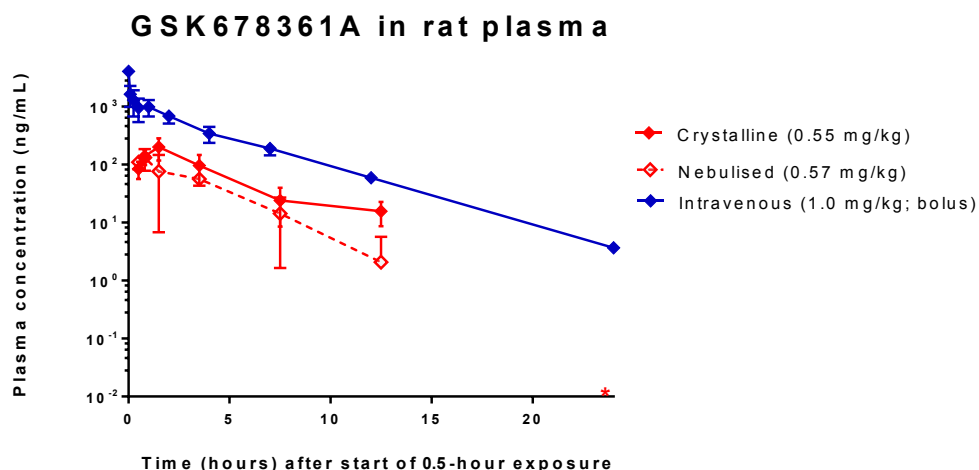
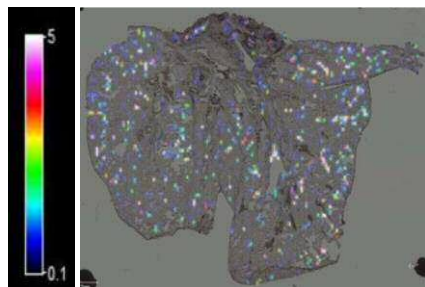


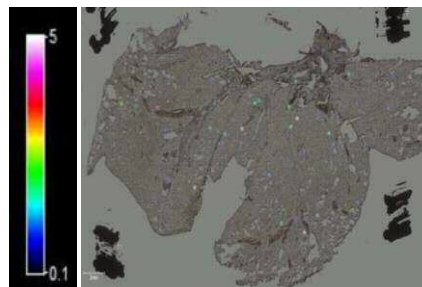
**Figure 2.32: GSK-361 concentrations in plasma of rats after a single inhaled or intravenous dose.** Rats inhaled an aerosol of crystalline or aqueous (nebulised) GSK-361 for 30 minutes (target dose of 0.6 mg/kg). Data (in blue) also plotted for rats administered GSK-677 as an intravenous bolus (Ioannou, 2005). Mean GSK-361 concentrations in plasma are shown with standard deviations (error bars;  $n=3$ ) up to 24 hours from the start of exposure. Plasma concentrations at 24 hours (\*) were not quantifiable ( $<5$  ng/mL). No differences of statistical difference (2-way ANOVA with post hoc analysis using Tukey's honestly significant difference test (Abdi and Williams, 2010[B])) for  $\log_{10}$ -transformed data.

**2.33A:** immediately post exposure

**2.33B:** 3 hours post exposure



(R31225N; Rat 019, Section 25)



(R31225N; Rat 020, Section 19)

**Figure 2.33: GSK-361 in lungs of rats inhaling crystalline drug imaged by matrix assisted laser desorption/ionization with mass spectrometry imaging (MALDI-MSI).** Rats inhaled crystalline GSK-361 for 30 minutes (target dose of 0.6 mg/kg). A matrix was applied to frozen sections of tissue (12  $\mu\text{m}$  thick) for MALDI-MSI; coloured scaling of the amount of GSK-361 is shown (arbitrary units). **2.33A:** rat lung taken as soon as possible (20 minutes) after a single exposure. **2.33B:** rat lung taken 3 hours post exposure.

**2.34A:** immediately post exposure      **2.34B:** 3 hours post exposure

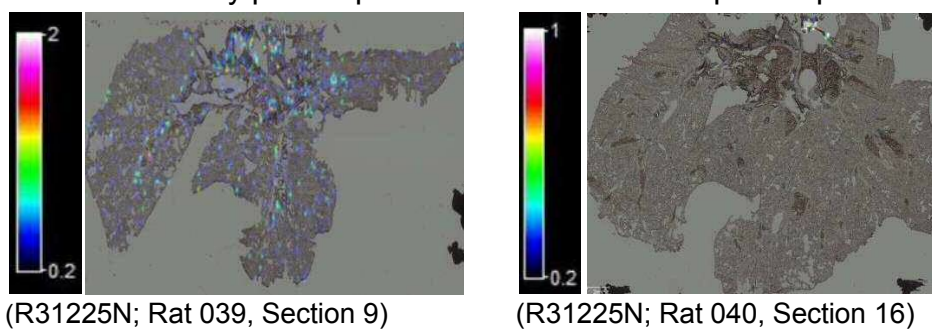


**Figure 2.34: GSK-361 in lungs of rats inhaling nebulised drug imaged by matrix assisted laser desorption/ionization with mass spectrometry imaging (MALDI-MSI).** Rats inhaled aqueous (nebulised) GSK-361 for 30 minutes (target dose of 0.6 mg/kg). A matrix was applied to frozen sections of tissue (12  $\mu$ m thick) for MALDI-MSI; coloured scaling of the amount of GSK-361 is shown (arbitrary units). **2.34A:** rat lung taken as soon as possible (20 minutes) after a single exposure. **2.34B:** rat lung taken 3 hours post exposure.

Lung concentrations of SB-445 (Figure 2.35) were similar to values for respective analytes after administration of GSK-677 (Figure 2.27) or nebulised GSK-899 (Figure 2.22). SB-445 in plasma followed a similar profile to SB-445 in lung, with peak values at 1.5 hours and quantifiable values persisting at 24 hours (Figure 2.36). MALDI-MSI was not possible due to poor ionisation of SB-445.

Pharmacokinetic parameters for p38 MAPK inhibitors, *i.e.* area under the drug concentration-time curve (AUC), the maximum concentration ( $C_{max}$ ), time to  $C_{max}$  ( $T_{max}$ ) and half-life, are summarised for lung (Table 2.16) and plasma (Table 2.17).

Generally, lung exposure (AUC and  $C_{max}$ ) in rats administered the crystalline aerosol form of each p38 MAPK inhibitor was higher than for the corresponding nebulised form (Table 2.16). This was marked for GSK-899, reflecting the persistence of crystals in rat lungs post exposure, with an AUC that was three-fold higher than for amorphous powder and 127-fold higher than for the nebulised solution. AUC for crystalline GSK-361 was 10-fold higher than the nebulised form and AUCs for crystalline and nebulised GSK-677 were essentially the same.

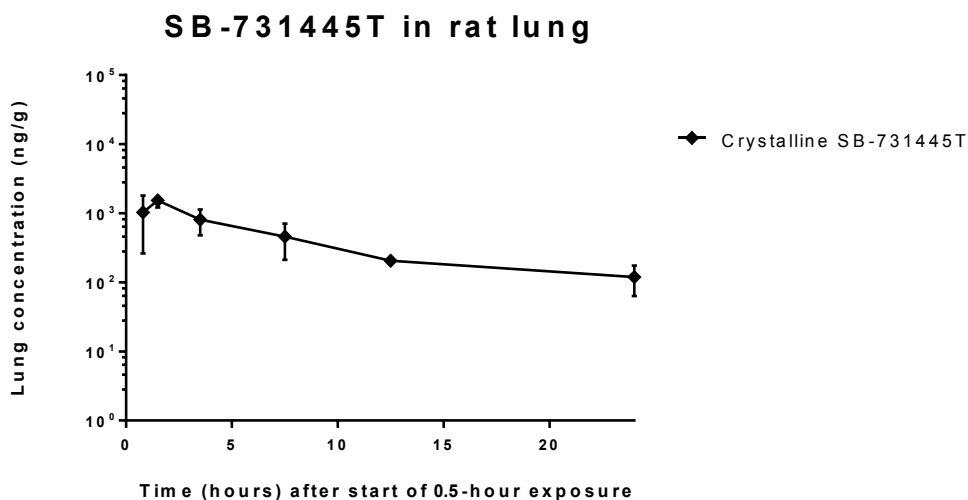


**Figure 2.35:** SB-445 concentrations in lung homogenate sampled from rats after a single inhaled dose. Rats inhaled crystalline SB-445 for 30 minutes (target dose of 0.6 mg/kg). Mean concentrations are shown with standard deviations (error bars; n=3) up to 24 hours from the start of exposure.

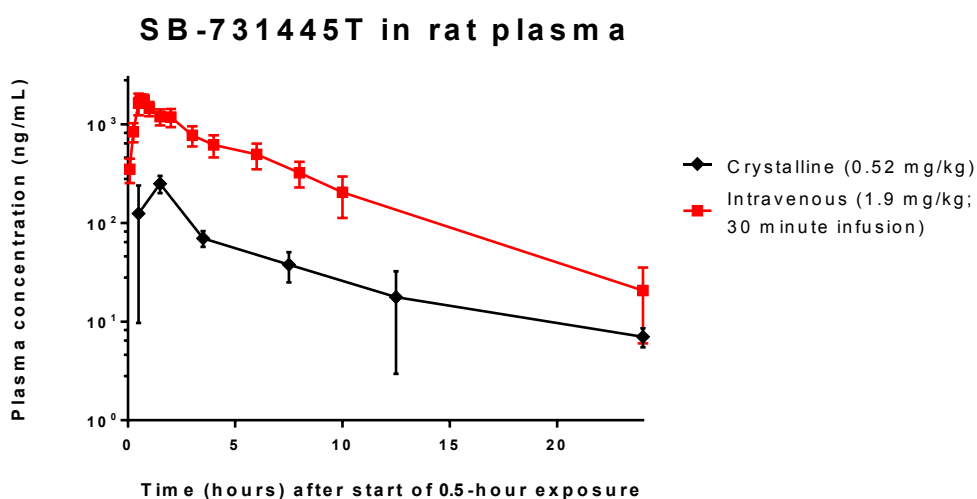


**Figure 2.36:** SB-445 concentrations in plasma sampled from rats after a single inhaled or intravenous dose. Rats inhaled crystalline SB-445 for 30 minutes (target dose of 0.6 mg/kg). Data (in red) also plotted for rats administered SB-445 by a 30-minute intravenous infusion (Zhang, 2003). Mean concentrations in plasma are shown with standard deviations (error bars; n=3) up to 24 hours from the start of exposure.

Generally,  $C_{max}$  was observed at the end of the inhalation exposure period but crystalline SB-445 showed a slight peak at 1.5 hours (one hour after cessation of aerosol generation) and crystalline GSK-899 peaked at 3.5 hours. The later  $T_{max}$  for crystalline SB-445 and GSK-899 are likely to be associated with inter-animal variability, a relatively flat

concentration profile shortly after inhalation exposure and, especially for GSK-899, formation of a depot of test article in the lungs. Plasma concentrations following inhaled and intravenous administration of GSK-361 (Zhang, 2003) initially increased indicating a fast absorption phase followed by elimination (Shargel *et al.*, 2005).

Systemic exposure (AUC and  $C_{\max}$ ) was highest in rats inhaling crystalline SB-445, followed by GSK-361. The ranking of the third and fourth compounds showed differences in parameters, with a higher  $C_{\max}$  for GSK-677 compared with GSK-899 and lower AUC for a given aerosol form (Table 2.18). Relative differences between the crystalline and nebulised aerosol forms were evident. For GSK-677, systemic exposure was similar following inhalation of crystalline and nebulised aerosols and is consistent with the hypothesis that an onset of systemic absorption is dependent upon dissolution. For GSK-899, systemic exposure was lowest in rats administered the crystalline form, higher for the nebulised solution but highest for amorphous powder. This is again consistent with the hypothesis regarding the relationship between dissolution and absorption; the low solubility for crystalline GSK-899 impedes disruption of the crystal lattice (Van den Mooter, 2012). Dissolution of amorphous powder was quicker given the disrupted, random organisation of molecules in the inhaled particles. Systemic exposure of GSK-361 in plasma, as with lungs, appeared to be higher in rats administered the crystals than nebulised solution. However the apparent difference in AUC is influenced by the mean values at 12.5 hours post exposure used for the calculation. For rats administered nebulised GSK-677, 2/3 plasma concentrations were below the limit of quantification (<5 ng/mL) and values of zero were used for calculation of a mean value, exaggerating the apparent difference to the mean value for rats inhaling crystalline GSK-677; there were no differences of statistical significance between the concentration profiles (Figure 2.32).

Although the partition of p38 MAPK inhibitors in plasma or cellular components of blood differs for each compound, their ranking was not

affected when AUC and  $C_{max}$  were converted to values in terms of whole blood using rat blood:plasma concentration ratios (Table 2.17).

**Table 2.16: Pharmacokinetics of mean p38 MAPK inhibitor concentrations in lung after single exposure of rats to test articles**

Compound	Aerosol form	Inhaled Dose (mg/kg)	Toxicokinetic parameter (lung)			
			AUC <sub>0-t</sub> (h.ng/g)	C <sub>max</sub> (ng/g)	T <sub>max</sub> (h) <sup>A</sup>	T <sub>1/2</sub> (h) <sup>A</sup>
GSK-899	Crystalline	0.680	678000	38390	3.5	74.7
	Amorphous	0.528	22100	9527	0.8	5.0
	Nebulised	0.521	5340	1592	0.8	7.5
GSK-677	Crystalline	0.490	3770	1410	0.8	3.0
	Nebulised	0.421	3690	1320	0.8	2.3
GSK-361	Crystalline	0.554	6250	6250	0.8	8.4
	Nebulised	0.570	633	193	0.8	7.8
SB-445	Crystalline	0.516	9680	1530	1.5	7.6

**Notes**

- A T<sub>1/2</sub> and median T<sub>max</sub> relative to the start of the 30-minute exposure period; time point at 0.8h includes a 20-minute period post exposure to isolate lungs.  
 CV Coefficient of variation (%) = sd/mean

There were differences in the relationship between half-lives in lung tissue and plasma and between aerosol forms of the p38 MAPK inhibitors (Tables 2.16 and 2.17). The half-life of crystalline GSK-899 in lung was at least 10-fold longer than for the other aerosol forms reflecting previous discussion about its low solubility and persistence in lung tissue. The half-life of GSK-899 in plasma following intravenous infusion was approximately half that following aerosol administration which was consistent with slower systemic absorption associated with a pulmonary depot of GSK-899. Half-lives of GSK-361 in lung were also longer than for plasma following inhaled administration. However, half-lives in plasma were similar after inhaled or bolus intravenous administration. The half-lives of GSK-677 in lung were lower than for plasma following aerosol administration, and lower again in plasma following intravenous infusion. The plasma profiles of GSK-677 (Figure 2.27) indicated an initial distribution phase, which may account for a shorter half-life in lung tissue with a longer elimination phase from plasma. The half-lives of

crystalline SB-445 in lung and plasma were similar following inhaled administration and slightly lower in plasma following intravenous infusion suggesting that the soluble membrane permeable SB-445 was not retained in tissues.

**Table 2.17: Pharmacokinetics of mean p38 MAPK inhibitor concentrations in plasma after single exposure to test articles**

Compound	Aerosol form	Dose (mg/kg)	Toxicokinetic parameter (plasma)			
			AUC <sub>0-t</sub> (h.ng/mL)	C <sub>max</sub> (ng/mL)	T <sub>max</sub> (h) <sup>A</sup>	T <sub>1/2</sub> (h) <sup>A</sup>
GSK-899	Crystalline	0.680	19.0 <sup>B</sup>	2.4 <sup>B</sup>	7.5	9.5
	Amorphous	0.528	48.1 <sup>B</sup>	8.0 <sup>B</sup>	0.5	9.0
	Nebulised	0.521	38.1 <sup>B</sup>	4.6 <sup>B</sup>	0.5	10.2
	Intravenous	1.0 (infus) <sup>C</sup>	455	807	0.25	4.7
GSK-677	Crystalline	0.490	15.4	18.6	0.5	6.0
	Nebulised	0.421	18.5	27.4	0.5	10.1
	Intravenous	1.1 (infus) <sup>C</sup>	166	256	0.25	1.5
GSK-361	Crystalline	0.554	760	200	1.5	3.5
	Nebulised	0.570	387	131	0.8	1.9
	Intravenous	1 (bolus) <sup>C</sup>	4877	1620	0.083	3.0
SB-445	Crystalline	0.516	977 <sup>D</sup>	250 <sup>D</sup>	1.5	6.3
	Intravenous	1.91 (infus) <sup>C</sup>	463	1902	0.58	4.0

**Notes**

- A T<sub>1/2</sub> and median T<sub>max</sub> relative to the start of the 30-minute exposure period.
- B GSK-899: blood in water (1:1 w/w) was analysed; parameters converted to plasma using blood:plasma ratio of 2.1 (unpublished data).
- C Intravenous administration as a bolus or 30-minute infusion.
- D SB-445: blood in water (1:1 w/w) was analysed; parameters converted to plasma using blood:plasma ratio of 0.683 (unpublished data).
- CV Coefficient of variation (%) = sd/mean

Whilst ranking of lung exposure for the three lead compounds (GSK-899, GSK-361 and GSK-677) following inhaled administration of the crystalline aerosol form supported the hypothesis that a faster dissolution rate would facilitate depletion of lung concentration, it did not necessarily follow that the observed systemic exposure would be relatively higher (Table 2.18). In addition, SB-455 (high solubility, high lipophilicity) ranked second highest for lung exposure and highest for systemic exposure. However, the volume of distribution was highest for GSK-677 and lowest for SB-445 (Table 2.6) indicating that GSK-677 was

distributed more into the tissues and this may account for the lower systemic exposure observed following inhaled administration. The biphasic kinetics of GSK-677 in plasma (Figure 2.27) also indicates distribution of the compound in secondary tissues following systemic absorption (Rowland and Tozer, 1995).

**Table 2.18: Ranking of p38 MAPK inhibitors and aerosol forms for systemic and lung exposure**

Sample medium	Particulate category	AUC or C <sub>max</sub>	Ranking of p38 MAPK inhibitors and aerosol form
Lung	Crystalline	both	GSK-899 > SB-445 > GSK-361 > GSK-677
	Nebulised	both	GSK-899 > GSK-677 > GSK-361
	GSK-899	both	crystalline > amorphous > nebulised
	GSK-677	both	crystalline ≈ nebulised
	GSK-361	both	crystalline > nebulised
Plasma	Crystalline	AUC C <sub>max</sub>	SB-445 > GSK-361 > GSK-899 <sup>A</sup> ≥ GSK-677 <sup>A</sup> SB-445 > GSK-361 > GSK-677 > GSK-899
	Nebulised	AUC C <sub>max</sub>	GSK-361 > GSK-899 > GSK-677 GSK-361 > GSK-677 > GSK-899
	GSK-899	both	amorphous > nebulised > crystalline
	GSK-677	both	nebulised ≈ crystalline
	GSK-361	both	crystalline > nebulised

**Notes**

- A Ranking of compounds for plasma AUC and C<sub>max</sub> was not changed with transformation to blood-based values<sup>B</sup>; an equivocal difference for two crystalline forms was more distinct in AUC<sub>blood</sub> (GSK-899 > GSK-677)
- B Blood:plasma concentration ratios (unpublished data) used to estimate C<sub>max</sub> and AUC: GSK-899 (2.10), GSK-677 (1.02), GSK-361 (1.30) SB-445 (0.683)

## 2.4. Conclusion

Principal component analysis (PCA) was used to select p38 MAPK inhibitors of differing physicochemical properties, using datasets of predicted (*in silico*) parameters derived from molecular structures or measured *in vitro* parameters. The score plot for each model grouped six p38 MAPK inhibitors into three distinct populations. The ranking of *in vitro* dissolution rates for five crystalline (cr) p38 MAPK inhibitors and amorphous (am) GSK-899 was as follows: SB-445(cr) > GSK-677(cr) > SB-323(cr) > GSK-899(am) > GSK-361(cr) > GSK-899(cr). A compound from each of the populations defined by PCA was selected for *in vivo* evaluation of exposure (lung and plasma) in rats, with GSK-899 (low solubility, aromatic and protein bound), GSK-677 (soluble, polar and basic) and GSK-361 (low solubility and high lipophilicity) representing the most diverse compounds within the 'physicochemical space'. SB-445 (high solubility and lipophilicity) was included to contrast with the low solubility and dissolution of GSK-361.

Ranking of lung exposure for the three lead compounds following inhaled administration of crystals (GSK-899 > GSK-361 > GSK-677) supported the hypothesis that a faster dissolution rate would facilitate quicker lung clearance. However, this did not necessarily translate to a higher systemic exposure observed post dose (GSK-361 > GSK-899 ≥ GSK-677), most likely due to differences in distribution and elimination of the compounds from plasma. Differences in relative exposure between the aerosol forms were evident, with GSK-899 lung exposure ranked crystalline > amorphous > nebulised. This was again consistent with the hypothesis regarding the relationship between dissolution and absorption. Systemic exposure of GSK-677, and GSK-361 (notwithstanding data variability at 12.5 hours and the analytical limit of quantification), were more similar for the two aerosol forms. Although fast dissolution may account for similarity of concentration profiles for GSK-677, the lipophilicity of GSK-361 may explain the higher systemic

exposure *in vivo* versus comparable aerosol forms of GSK-899. Particles deposited in the lung must first dissolve into the epithelial lung fluid, which may become locally saturated with drug if clearance from this 'compartment' is slower than the rate of dissolution. This local effect may be exacerbated by extreme variations in regional deposition that can affect pharmacokinetics of the inhaled drug (Gray, 2015). This contrasts with the *in vitro* dissolution test in which a continuous flow of simulated fluid is applied to the powder preventing saturation of the local fluid environment, maintaining the undissolved test article in sink conditions. Secondly, the principal fluid lining the conducting airways is mucous (85% water) but surfactant (85% phospholipid, 5% cholesterol and 10% surfactant proteins) is predominant in the respiratory region (Eixarch *et al.*, 2010), varying solubility of particles throughout the respiratory tract. *In vivo*, a lipophilic compound will cross a cell membrane, maintaining sink conditions and facilitating further dissolution of the particle into the fluid. Measurement of drug concentrations in plasma during inhalation exposure of rats and more rapid isolation of lungs on cessation of aerosol generation would present technical challenges. However, future work in this area would refine characterisation of drug concentration profiles in lung and plasma during inhaled administration of the p38 MAPK inhibitors and improve understanding of the relationship between the kinetics of exposure for these two compartments.

In addition to transfer of 'free drug' from the epithelial lung fluid to lung tissue to blood, which are in equilibrium between these compartments, there are other mechanisms influencing the fate of particles deposited in the lungs. All compounds are likely to be, to a greater or lesser extent (GSK-677 > GSK-899 > GSK-361 > SB-445) substrates for P-glycoprotein 1, an efflux pump found on apical membranes that is involved in the energy (ATP) dependent expulsion of xenobiotics as a multidrug resistance mechanism against cytotoxicity (Bellamy, 1996). Lysosomes play a key role in autophagy, the breakdown of endogenous molecules such as phospholipids and waste products. Amphiphilic drugs

(containing both lipophilic and hydrophilic moieties) are prone to lysosomal trapping (Kazmi *et al.*, 2013). Alveolar macrophages are rich in lysosomes and lung surfactant, and their presence in lung accounts for high uptake of basic lipophilic drugs. Values for lysosomal trapping in lungs vary for drugs, with 25% reported for the anti-depressant Perazine (Daniel and Wójcikowski, 1999) and 60% to 90% for psychotropic drugs also investigated by Daniel and Wójcikowski (1997). Macrophages also play a key role in clearance of particles from the lungs. Geiser (2010) stated that typically 50% to 75% of micron-sized particles are phagocytosed after two to three hours,  $\geq 90\%$  of particles by 10 hours and almost all particles phagocytosed by 24 hours. The macrophages are in turn cleared from the conducting airways via the mucociliary escalator within 24 to 48 hours, and may take weeks or months to clear from alveoli (Geiser, 2010). Under the conditions of the *in vivo* experiments, it is likely GSK-899 crystals would have been endocytosed by macrophages but did not have sufficient time to facilitate mucociliary clearance.

Drug-lung concentration profiles were consistent with the hypothesis that GSK-361 (low solubility; high passive membrane permeability) is maintained under sink conditions *in vivo* but GSK-899 (low solubility; low passive membrane permeability) becomes saturated in epithelial lung fluid due to a slower rate of transmembrane clearance. However, relatively little is known about transporter systems and efflux pumps in the lung (Patton *et al.*, 2010) and such mechanisms could also play a role in the pulmonary pharmacokinetics of GSK-899 and/or GSK-361 resulting in the observed differences in drug-lung concentration profiles. Quantification of drug concentrations in various lung compartments, such as epithelial lung fluid, epithelial cells and macrophages throughout the distal respiratory region of rat lung may elucidate key mechanisms pertinent to the pulmonary pharmacokinetics of the p38 MAPK inhibitors. MALDI-MSI showed a concentration of GSK-677 in the main airways and a relatively even distribution of GSK-361 and GSK-899 across lung

sections immediately post exposure and at three hours where still present, irrespective of aerosol form. Chaurand *et al.* (2007) described use of MALDI-MSI capable of achieving irradiation areas down to 7  $\mu\text{m}$ . However, this lacks the lateral resolution required to differentiate between compartments within the lung section such as the epithelium and fluid (<0.2  $\mu\text{m}$  and 0.07  $\mu\text{m}$  thick at alveoli; 10  $\mu\text{m}$  and 3  $\mu\text{m}$  thick at terminal bronchioles; (Patton and Byron, 2007)) and macrophages (13  $\mu\text{m}$  diameter; (Krombach *et al.*, 1997)). Secondary ion mass spectrometry (SIMS), is capable of lateral resolution down to 50 nm for elemental ions (Benabdellah *et al.*, 2010) and a resolution of 80 to 100 nm was reported for imaging of melanin stained using iodine-125 labelled iodobenzamide (Guerquin-Kern *et al.*, 2004). SIMS may therefore provide an opportunity for ultrastructural investigations in concert with MALDI-MSI to determine the location of p38 MAPK inhibitors within cell types or fluid compartments of the lung sections.

This chapter characterised the lung and systemic exposure following administration of a single inhaled dose of p38 MAPK inhibitors to rats. The observed differences in exposure and a potential for accumulation in lungs with repeated daily administration will be considered for investigations of efficacy following a single dose (Chapter 4) and for toxicopathology evident after 28 days of treatment (Chapter 5).

# **CHAPTER THREE**

**Estimation of inhaled doses in rats  
from lung function data and  
refinement of tube restraint in  
scientific procedures**

### 3.1. Introduction

Inhaled administration of substances to animals is technically challenging for quantitative dosimetry. Animals are not “dosed” *per se* but are exposed to an atmosphere containing a test substance or formulation mixed with air. Non-clinical “doses” reported for animals inhaling such atmospheres are commonly calculated using the following equation:

$$\text{—————} \dots\dots\dots \text{Equation 1}$$

Where  $ID_e$  = estimated inhaled dose (mg/kg),  $C$  = aerosol concentration (mg/L),  $RMV$  = respired minute volume (L/min)  $T$  = duration of inhalation exposure and  $BW$  = body weight (kg). The minute volume (MV) can be measured but is more commonly estimated by calculation from body weight using a published algorithm. Various algorithms (Guyton, 1947, McMahon *et al.*, 1975, Bide *et al.*, 2000) or minute volume data for a variety of species (Snipes, 1989) have been published. Given a lack of consensus within the regulatory toxicology and research communities for the method of estimating inhaled doses in drug safety studies, a working party (Alexander *et al.*, 2008) reviewed 18 datasets generated by 10 contributing laboratories in conscious animals of species used in non-clinical research (mice, rats, beagle dogs and cynomolgus monkeys) and published the following algorithm:

$$\dots\dots\dots \text{Equation 2}$$

Where  $eRMV$  = estimated respired minute volume (L/min) and  $BW$  = body weight (kg). This equation is commonly used in respiratory drug development as it was derived from a larger volume of data in toxicologically relevant species. However, use of such an algorithm overlooks the physiological effects on lung function that can be induced by a substance’s properties (Nirogi *et al.*, 2012, Vijayaraghavan *et al.*, 1993). Furthermore, variability in MV measurements may have

occurred between datasets due to differences in habituation of animals to the restraint procedures between species and protocols used by the 10 participating laboratories (Alexander *et al.*, 2008).

Lung-homogenate concentration data for small groups of rats (typically  $n=3$ ) attached to adjacent ports on a snout-only inhalation exposure chamber, and thus breathing from the same aerosol, sometimes vary up to three-fold (personal observation of unpublished data). Little is known about the ways environmental factors may affect lung function and hence the inhaled dosimetry for individual animals subjected to “standard procedures” during non-clinical studies. For example, manipulation or disturbance of animals may excite them to varying degrees and the implications of this for lung dose are uncertain. In addition, rats are insensitive to red light (Szél and Röhlich, 1992). Amber or red-coloured transparent polycarbonate shelters for rodents are marketed with the claim that they “provide security and shelter for the animal by reducing the level of perceived light” (Datesand, 2017, Scanbur, 2017), although the efficacy of such products do not appear to have been determined independently (Burn, 2008). It was hypothesised that conducting snout-only inhalation exposure procedures under red-filtered lighting may maintain rats in a calmer state during the tube restraint procedure.

Plethysmography is a technique used for measuring changes in the volume of an organ or body, typically due to changes in the volume of blood (Pointel *et al.*, 1981) or air (Pennock *et al.*, 1979) contained therein. A head-out plethysmograph (Vijayaraghavan *et al.*, 1993, Glaab *et al.*, 2001) is a vessel that encloses the body of a subject to facilitate lung function measurements derived from changes in ambient pressure due to changes in body volume as the subject breathes. Since the head of an animal is outside this compartment, its snout or head can be presented simultaneously to an atmosphere for inhaled administration of a test substance, e.g., aerosol, vapour or smoke.

Protocols for acclimatisation of animals to tube restraint vary between laboratories, and may also vary within institutions depending upon the species and experimental objectives. Nirogi *et al.* (2012) described acclimatisation of rats to plethysmograph chambers for two hours, twice daily over three days before investigating the effect of respiratory stimulants or depressants on lung function. Renninger (2006) described acclimatisation of rats for up to 15 minutes on three consecutive days in preparation for safety pharmacology (single dose) investigations, whilst other laboratories acclimatise rodents daily and progressively increase the tube residence time up to the required duration over five days (Hoymann, 2012) or a week. In addition, the tube acclimatisation protocols applied in toxicology studies employing inhaled administration or intravenous infusion also varies considerably. This has implications for dosimetry and the translation of results between studies, such as respiratory pharmacology and toxicology.

### **3.1.1. Aims and objectives**

The experimental aims of this chapter are to measure breath frequency (BF) and minute volume (MV) in conscious rats using head-out plethysmography to test the following hypotheses:

- lighting colour (red or white) and duration of restraint tube acclimatisation protocols influence BF and MV of rats;
- the degree of restraint (use of neck seal) during a repeat dose study artefactually affects the BF and MV measurements of rats;
- measured MV is consistent with the pre-dose body weight derived estimate (eRMV) calculated using the algorithm of Alexander *et al.* (2008).

On the basis of lung function data generated to test these hypotheses, which can be interpreted as a surrogate indicator of activity or stress (Williams *et al.*, 1988, Barone *et al.*, 1990), the influence of conditioning rats on their welfare and dosimetry of inhaled drugs will be considered.

## 3.2. Materials and methods

### 3.2.1. Head-out plethysmography and data capture of lung function measurements

Minute volume and breath frequency of conscious rats were measured non-invasively using a body plethysmograph (Model PLY22L; Electro-Medical Measurement Systems (EMMS), UK), a restraint tube designed to accommodate rats and facilitate measurement of lung function parameters. The plethysmograph was similar to that described by Glaab *et al.* (2001) but differing insofar as only the snout of a rat would be presented to a test atmosphere contained within an exposure chamber. The animal's body was enclosed in the tube, using a rubber diaphragm to form a seal around its neck (Figure 3.1A). Two diaphragms were used during capture of lung function data, with holes pre-cut at the centre of each disc to allow the animal's head to pass through (holes of 20 mm or 25 mm diameter were typically cut for rats of 240 g to 270 g). A thin latex diaphragm (0.25 mm thick) was used to form the seal around the neck of the rat facilitating lung function measurement. A second latex diaphragm was thicker (0.63 mm thick) and used as a support for the thinner diaphragm. A sensor (pneumotach and pressure transducer) facilitated detection of changes in air pressure inside the tube as the animal breathes.

Using Boyle's law (absolute pressure and the volume of a fixed mass of gas are inversely proportional at constant temperature), lung function parameters derived from the changes in pressure inside the body plethysmograph were captured using software (eDacq version 1.8.4b; EMMS) that facilitated rejection of anomalous breath-wave signals ascribed to a compromised neck seal, typically associated with an animal's movement in the plethysmograph; approximately 700 to 1,000 breaths per hour were captured for each animal. During data capture, the breath wave, tidal volume and minute volume for each animal were displayed on a monitor (Figure 3.1B). Each plethysmograph containing a rat was attached to a simple, flow-through

design of a snout-only inhalation exposure chamber to facilitate exposure of the animals to air only or in combination with an aerosol of a p38 MAPK inhibitor as described in Chapter 2 (Section 2.2.5.5).

### 3.1A



### 3.1B

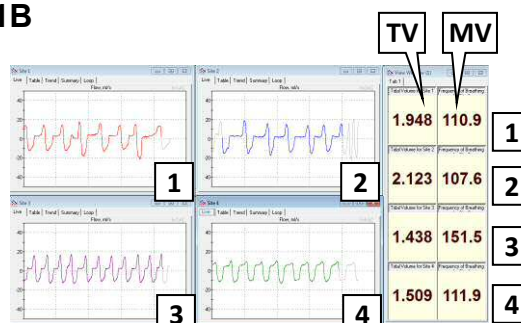


**Figure 3.1: Head-out plethysmography in rats. 3.1A:** restraint of a rat in a plethysmograph. **3.1B:** real-time monitoring of breath waves for four rats and monitoring of tidal volume (TV) and minute volume (MV) for each rat (1 to 4).

### 3.2.2. Investigating lung function and dosimetry in rats

Four experiments were conducted during which procedures for acclimatisation of rats to the plethysmographs and data capture were refined. Given an ethical obligation to minimise the degree of restraint applied to rats repeatedly undergoing inhalation exposure procedures, consideration was given to inclusion or omission of the neck seal on days when lung function data were not recorded. The protocol for acclimatising rats to plethysmographs evolved from one experiment to the next and key features or refinements for lung function measurements introduced for subsequent experiments included improvements in data quality by allowing rats to settle in the plethysmographs before aerosol generation, and reducing potential stimuli by limiting nearby activities or incursions into the area surrounding the chamber (Figure 3.2). For Designs 2 to 4, rats were exposed to an aerosol of a p38 MAPK inhibitor; the pharmacology was not expected to affect the lung function measurements. Key outcomes for each experimental design are summarised in the methods (Section 3.2) for clarity of the evolving methodology but are

subsequently described in detail in the results and discussion (Section 3.3).

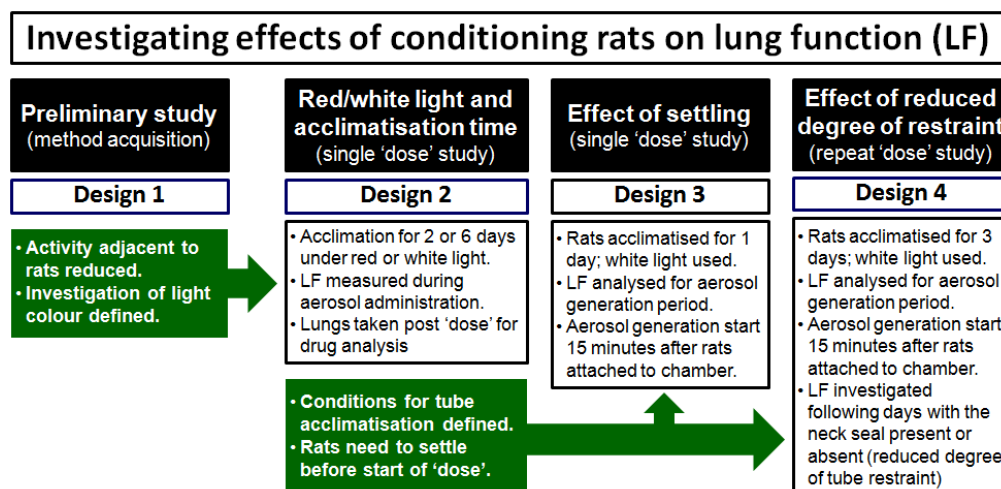


**Figure 3.2: Evolution of study designs for investigation of light, duration of tube acclimatisation and conditioning of rats on lung function.**

### 3.2.2.1. Preliminary analysis of lung function data

In order to facilitate analysis of group trends for the continuous data ( $\leq 1000$  breaths/hour for each animal), mean minute volume (MV) and breath frequency (BF) were calculated for each rat for 5-minute periods at intervals throughout each data capture period.

### 3.2.3. Test system and animal husbandry

Male rats (Charles River UK Ltd, Margate, Kent) were randomly allocated to groups and accommodated under standard laboratory conditions (Home Office, 2014) with access to food and water as described in Chapter 2 (Section 2.2.4.1). Rats were accommodated for at least five days before undertaking the first licensed procedure (tube restraint) and were approximately 10 or 11 weeks old on the (first) day of aerosol administration and/or observation as applicable (Day 1).

Two strains of rat were used to investigate lung function. The CrI:WI(Han) rat is currently the sponsors strain of choice for non-clinical safety studies, and was used for the first three experiments (Designs 1 to 3). The CrI:CD(SD) rat was formerly used for non-clinical safety studies including the first toxicity studies performed using p38 MAPK

inhibitors before termination of the respective drug development programmes. For logistical reasons, investigation of lung function in the fourth experiment (Design 4) was performed using the same animals designated for the toxicokinetic investigations described in Chapter 5, for which the Crl:CD(SD) rat was selected for continuity with and reference to historical pathology data for p38 MAPK inhibitors.

#### **3.2.4. Method acquisition (Design 1)**

A preliminary study was performed to implement methodology and confirm satisfactory data capture by head-out plethysmography. Rats (2 groups; n=4) were acclimatised to plethysmographs over a six-day period, using a protocol similar to those adopted by other laboratories preparing rodents for respiratory pharmacology investigations using head-out plethysmography (Hoymann, 2012). Rats were restrained in tubes each day for progressively longer periods of time and were first restrained using a latex neck seal from the fourth day of acclimatisation (Table 3.1). Rats were then maintained for a 31-day observation period (Days 1 to 31). Rats were restrained in plethysmographs, attached to the inhalation chamber and exposed to air only, once daily, throughout the acclimatisation and 31-day observation periods. For lung function measurements, rats were restrained in plethysmographs for 90 minutes with the neck seal incorporated.

**Table 3.1: Tube restraint protocol for acclimatisation of rats to plethysmographs and a 31-day observation period (Design 1)**

Days of observation period <sup>A</sup>	Tube	Group A		Group B		Comment or figure number for presentation of BF / MV
		Neck seal present	Time in tube (min)	Neck seal present	Time in tube (min)	
<b>Acclimatisation to tube restraint</b>						
-6	PLY22L	No	n/a	No	n/a	Rat 'run up' tube  3.7A / 3.9A 3.7B / 3.9B 3.7C / 3.9C
-6 <sup>B</sup>	PLY22L	No	20	No	20	
-5	PLY22L	No	45	No	45	
-4	PLY22L	No	60	No	60	
-3	PLY22L	Yes	30 <sup>C</sup>	Yes	30 <sup>C</sup>	
-2	PLY22L	Yes	60	Yes	60	
-1	PLY22L	Yes	90	Yes	90	
<b>Observation period</b>						
1	PLY22L	Yes	90	Yes	90	3.7D / 3.9D
2 to 6	PLY22L	No	60	No	60	
7	PLY22L	Yes	90 <sup>D</sup>	No	60	
8	PLY22L	Yes	90	Yes	90	3.7E / 3.9E
9 to 13	PLY22L	No	60	No	60	
14	PLY22L	Yes	90	No	60	
15	PLY22L	Yes	90 <sup>D</sup>	Yes	90	3.7F / 3.9F  3.8A / 3.10A
16 to 26	PLY22L	No	60	No	60	
27	PLY22L	Yes	90 <sup>D</sup>	No	60	
28	PLY22L	Yes	90	Yes	90	
29	PLY22L	No	60	No	60	3.8B / 3.10B 3.8C / 3.10C
30	PLY22L	Yes	90	Yes	90	
31	PLY22L	Yes	90	Yes	90	

**Notes**

BF/MV Breath frequency; minute volume

A Days of acclimatisation to tube restraint, conventionally preceding the first aerosol administration, are designated by a negative number.

B 20-minute restraint period performed during afternoon (all other procedures were conducted during the morning).

C 30-minute acclimatisation performed with tubes on non-slip table surface (15 minutes) followed by attachment of tubes to chamber (15 minutes).

D Lung function data were captured on Days 7, 14 and 27 for Group A only. These profiles (not reported) were very similar to those presented for Days 8, 15 and 28, for which data are also available for Group B.

In order to consider the potential influence of infrequent restraint using the neck seal after Day 1, rats allocated to Group B were subjected to

the neck seal for single occasions (Days 8, 15 and 28) and rats of Group A were subjected to restraint with the neck seal for two consecutive days (Days 7/8, 14/15 and 27/28). On days when data capture was not performed, rats were restrained in the plethysmographs for 60 minutes without a neck seal (Table 3.1; Figure 3.3).

### Design 1

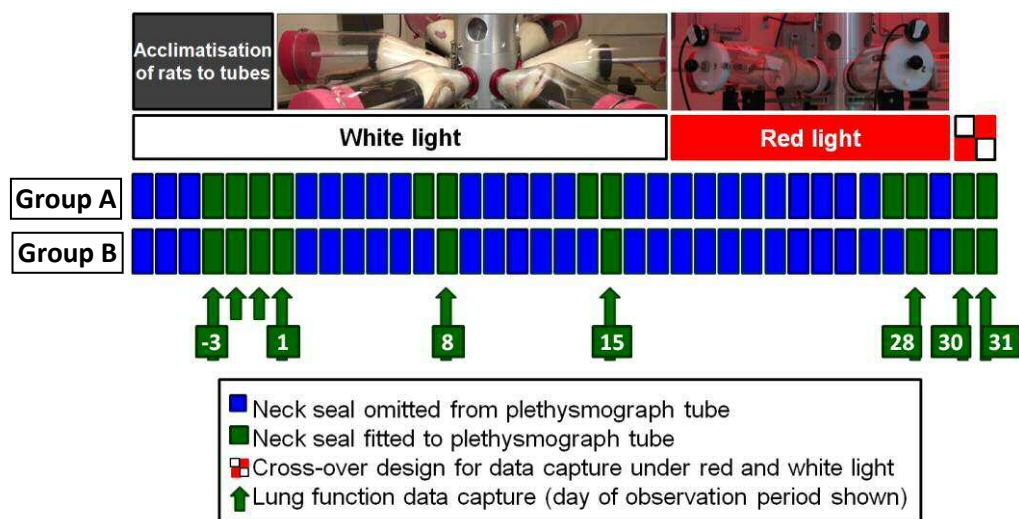


**Figure 3.3:** Design of a preliminary study to measure lung function over four weeks and consider the impact of lighting conditions. Rats (n=4; two groups designated A and B) were acclimatised to plethysmograph tubes over six days and maintained under normal fluorescent lighting for 17 days. From Days 18 to 29, rats were restrained under red-filtered lighting and a cross-over design for red and white lighting was implemented on Days 30 and 31.

#### 3.2.4.1. Investigating lighting colour during tube restraint

Tube restraint of animals during the acclimatisation period (Day -6 to Day -1) and Days 1 to 17 of the observation period were performed under normal fluorescent ('white') lighting. The potential influence of lighting colour on activity and hence breathing of rats during inhalation exposure procedures was first considered during this experiment. From Days 18 to 29, restraint procedures were performed under red-filtered lighting ( $\lambda \geq 600$  nm) and a cross-over design was implemented with half of the rats (n=2/group) subjected to white light and the other half to red light on Day 30, and *vice versa* on Day 31 (Figure 3.3).

#### **3.2.4.2. Statistical analysis of lung function data**

Multivariate analysis of variance (MANOVA) was conducted (Statistica, version 12.0.1133.40) using pooled data (n=8 for Groups A/B and Days 30/31) with post hoc analysis using Tukey's honestly significant difference test (Abdi and Williams, 2010[B]).

#### **3.2.4.3. Methodological outcomes of Design 1**

Variability in MV and BF values indicated a need to minimise disturbances adjacent to rats undergoing plethysmography data capture. Anecdotal observations in activity and the presence of faeces suggested rats may be calmer under red light, although these apparent observations may have been a consequence of repeated conditioning of the rats from Day 19, irrespective of lighting colour.

#### **3.2.5. Colour of lighting and duration of acclimatisation protocols for tube restraint (Design 2)**

In Design 1, animals were acclimatised to the plethysmographs over six days, in line with the practices of other laboratories investigating respiratory pharmacology in rodents. For inhaled administration of candidate drugs for pharmacokinetics and/or toxicopathology investigations, rodents are typically acclimatised to the restraint tubes over shorter periods. At the sponsor's laboratory, rodents were commonly acclimatised for 20 minutes and then 45 minutes over the two days preceding the first 60-minute inhalation exposure, or for 20 minutes the day before the first 30-minute inhalation exposure. This raised a question regarding the implications for breathing patterns of animals prepared specifically for pharmacology investigations versus routine administration of inhaled drugs in non-clinical studies, and potential differences in the resultant lung deposited doses of a drug. In addition, anecdotal observations for Design 1 suggested red lighting may maintain animals in a calmer state when restrained for head-out plethysmography. However, this needed to be evaluated more robustly.

Design 2

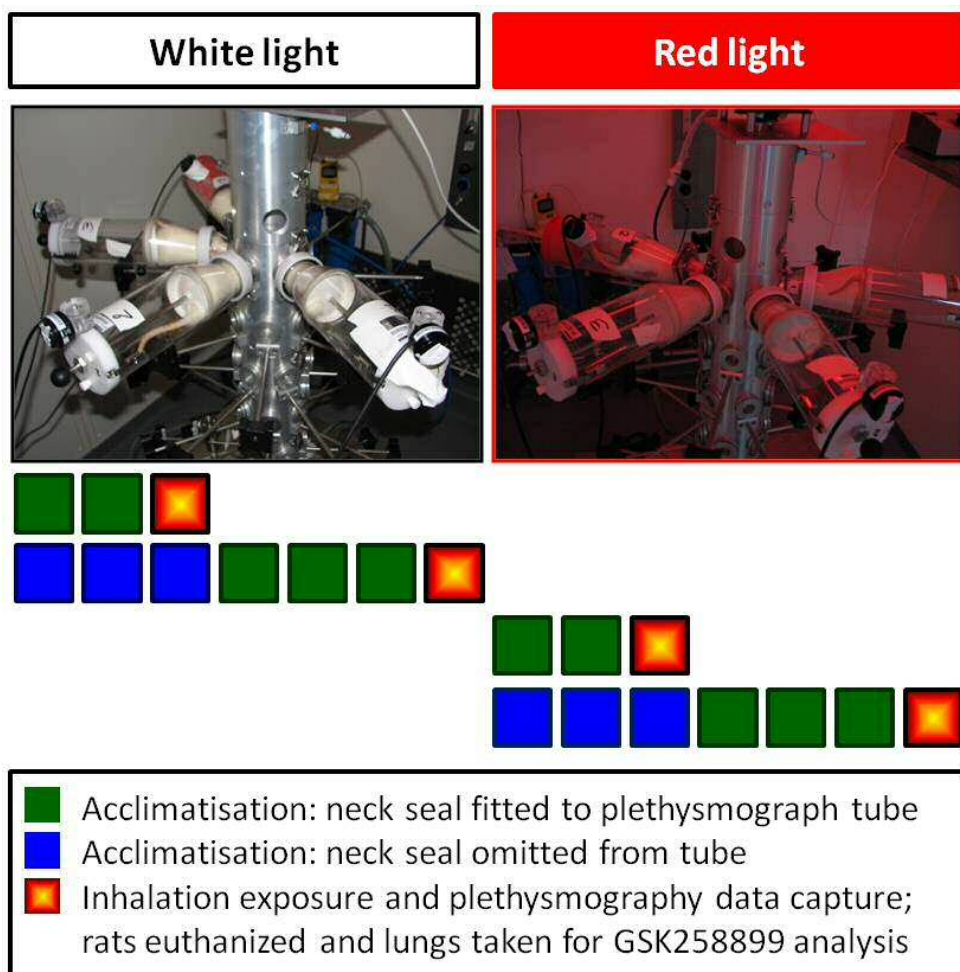


**Figure 3.4: Latin square design of study to investigate effects of lighting and duration of tube acclimatisation on lung function and dose.** Groups of rats (n=8) were acclimatised to plethysmograph tubes over two or six days and under normal fluorescent ('white') or red-filtered lighting. All rats (32 in total) were exposed to crystalline GSK-899 for 60 minutes concurrently with lung function measurements, euthanized and lungs taken for analysis of GSK-899. For logistical reasons (limited capacity for respiratory data capture), acclimatisation and inhalation exposures were conducted over four weeks using two sub-groups of rats (n=4/treatment), duplicating the outlined design.

A Latin square design was used to investigate the potential influence of lighting colour and duration of pre-treatment acclimatisation protocols on MV and BF during inhalation exposure of rats to an aerosol (Figure 3.4).

Rats (4 groups; n=8/group) were acclimatised to plethysmographs under either normal fluorescent (white) lighting or red-filtered lighting ( $\lambda \geq 600$  nm) by progressively extending restraint periods over two or

six days (Table 3.2). BF and MV were measured during inhaled administration of crystalline GSK-899 (600 µg/kg; 60 minutes) under white or red light. Rats were restrained in plethysmographs, attached to the snout only chamber and exposed to 5% GSK-899 (w/w) in lactose for 60 minutes as summarised in Section 3.2.8.

**Table 3.2: Tube restraint protocol for acclimatisation of rats to plethysmographs and aerosol administration (Design 2)**

Days of observation period	Tube	2-day protocol		6-day protocol	
		Neck seal present	Time in tube (min)	Neck seal present	Time in tube (min)
<b>Acclimatisation to tube restraint</b>					
-6	ADG <sup>B</sup>	-	-	No	20
-5	ADG <sup>B</sup>	-	-	No	45
-4	ADG <sup>B</sup>	-	-	No	60
-3	PLY22L	-	-	Yes	30
-2	PLY22L	Yes	20	Yes	60
-1	PLY22L	Yes	45	Yes	60
<b>Treatment (aerosol administration)</b>					
1	PLY22L	Yes	60	Yes	60

**Notes**

- A Days of acclimatisation to tube restraint are designated by a negative number  
 B “Standard” restraint tube (ADG Developments Ltd, UK) routinely used for inhalation exposure of rats

Rats were euthanized (exsanguination under isoflurane anaesthesia) as soon as practicable post exposure and the lungs removed (right and intermediate lobes pooled) and homogenised for analysis of GSK-899 using a validated HPLC-MS/MS method as described in Chapter 2 (Section 2.2.5.8), but with addition of an equal volume of 10 mg/mL aqueous sodium fluoride added to the tissue to prevent potential hydrolysis of an amide bond in GSK-899. Results of Chapter 2 showed the crystalline form of GSK-899 was of relatively low solubility *in vitro* and there was no appreciable decrease in drug-lung concentrations up to 24 hours post exposure. Crystalline GSK-899 was therefore selected for this experiment to enable investigation of lung dose post exposure

whilst minimising the potential for drug-lung clearance prior to isolation of lung tissue for analysis by HPLC-MS/MS.

The plethysmography apparatus permitted simultaneous data capture from four subjects. Consequently, for Design 2, a group size of  $n = 8$  for each of four treatments (white versus red light; two versus six days of acclimatisation) necessitated inhalation exposure of animals as two sub-groups. In order to reduce potential bias, the experiment was performed over four weeks with the first sub-group of each treatment conducted first (Figure 3.4) before repeating the cycle of treatments and inhalation exposure procedures for the second sub-groups.

#### **3.2.5.1. Data analysis of measured and body weight derived estimates of minute volume**

The inhaled dose is proportional to the minute volume (Equation 1). There is potential for differences between measured MV and the body weight derived estimate (eRMV), and hence potential discrepancies in dose estimation, were investigated by comparing the mean measured minute volumes for the 60-minute inhalation exposure period with eRMV values calculated from the corresponding pre-dose body weight for each animal using Equation 2 (Alexander *et al.*, 2008).

#### **3.2.5.2. Data analysis of estimated lung deposited dose and measured drug-lung concentrations**

Drug-lung concentrations measured by HPLC-MS/MS were compared with estimates of the lung deposited dose. The lung dose was calculated from the estimated inhaled dose (Equation 1), calculated using MV (measured) or eRMV (Equation 2), and assuming 7% of inhaled GSK-899 was deposited in the rat lung (Snipes, 1989).

#### **3.2.5.3. Statistical analysis of lung function data and drug-lung concentration in lung tissue**

Statistical analysis of lung function and concentration data were performed using Statistica software (version 12.0.1133.40) as follows:

#### MV and BF: comparison of acclimatisation protocols

MANOVA was conducted using pooled data (n=16 for duration of acclimatisation or lighting colour) with post hoc analysis using Tukey's honestly significant difference test (Abdi and Williams, 2010[B]).

#### Comparison of measured MV and body weight-derived eRMV when plotted against body weight

One-way analysis of variance (ANOVA) was conducted using pooled animal-specific mean data for the 60-minute inhalation exposure period. Data were pooled for both the duration of acclimatisation and lighting colour (n=32).

#### Lung concentrations for measured (HPLC-MS/MS) or estimated (MV or eRMV) data

MANOVA was conducted using pooled data (n=16 for duration of acclimatisation or lighting colour) with post hoc analysis using Tukey's honestly significant difference test (Abdi and Williams, 2010[B]).

### **3.2.5.4 Methodological outcomes of Design 2**

A shorter acclimatisation period, with inclusion of the neck seal throughout, was sufficient provided animals were allowed to settle in the restraint tubes for 15 minutes before the start of aerosol generation. MV and BF for rats maintained under red or white light were similar and normal fluorescent lighting was acceptable for further experiments.

### **3.2.6. Settling rats before aerosol administration (Design 3)**

In Design 2, the MV and BF of rats acclimatised over two days appeared to settle during the first 15 minutes of inhalation exposure.

The design of two single dose experiments performed to investigate the pharmacokinetics of inhaled GSK-677 or GSK-361 (Figure 3.5; Chapter 2) were adapted such that rats were allowed to settle in their restraint tubes before aerosol generation was initiated (Table 3.3) and selected rats were used to capture lung function measurements.

### Design 3

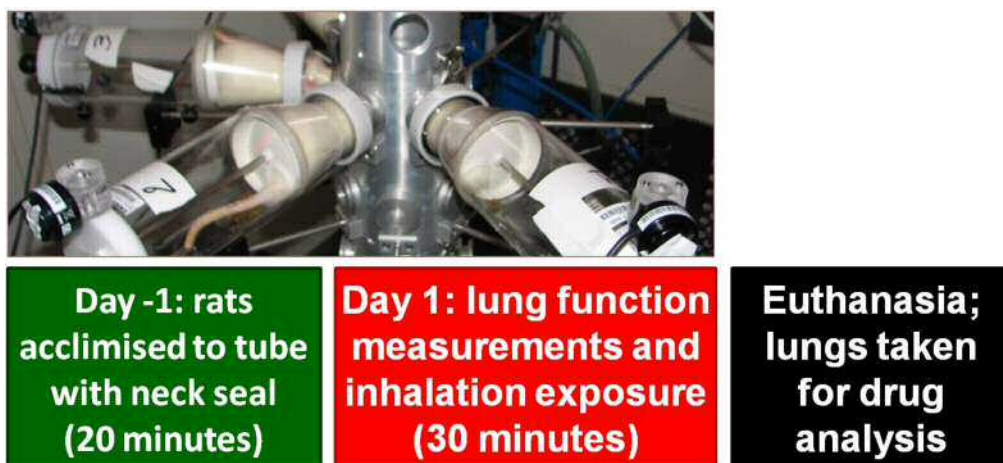


**Figure 3.5:** Simple study design to investigate lung function measurements and drug-lung concentrations after a single inhaled dose of GSK-361 or GSK-677. Groups of rats (n=3) were acclimatised to plethysmograph tubes for 20 minutes (Day -1). The following day, lung function was measured whilst rats settled in the tubes for 15 minutes and then during aerosol administration for 30 minutes. Rats were euthanized as soon as possible after exposure and the lungs taken for drug analysis.

The day before aerosol administration, rats (4 groups; n=3/group) were acclimatised to tube restraint for 20 minutes using plethysmographs fitted with the neck seal. The following day, rats were restrained in plethysmographs, attached to the snout only chamber and allowed to settle for 15 minutes before exposure to crystalline or aqueous nebulised aerosols of GSK-677 or GSK-361 for 30 minutes (see Section 3.2.8). Lung function data were captured throughout the pre-exposure and aerosol administration periods, with the erroneous exception of a period preceding administration of crystalline GSK 361. All procedures were performed under normal fluorescent lighting.

**Table 3.3: Tube restraint protocol for acclimatisation of rats to plethysmographs and aerosol administration (Design 3)**

Days of observation period <sup>A</sup>	Tube model	2-day protocol	
		Neck seal present	Time in tube (min)
<b>Acclimatisation to tube restraint</b>			
-1	PLY22L	Yes	20
<b>Treatment (aerosol administration)</b>			
1	PLY22L	Yes	15 <sup>B</sup> +30

**Notes**

A Day of acclimatisation to tube restraint is designated by a negative number.

B Rats allowed to settle in restraint tubes before starting aerosol generation.

Rats were euthanized (exsanguination under isoflurane anaesthesia) as soon as practicable post exposure and the lungs removed (right and intermediate lobes pooled) and homogenised for analysis using a validated HPLC-MS/MS method for GSK-677 or GSK-361 as described in Chapter 2 (Section 2.2.5.8).

### 3.2.6.1. Statistical analysis of lung function data and drug-lung concentration in lung tissue

Statistical analysis of lung function and concentration data were performed using Statistica software (version 12.0.1133.40) as follows:

#### MV and BF: comparison of aerosol forms

Two-way ANOVA was applied to the animal specific mean data for each time point, and also for the 30-minute inhalation exposure period.

#### Comparison of measured MV and body weight-derived eRMV when plotted against body weight

One-way ANOVA was conducted using pooled animal-specific mean data for the 30-minute inhalation exposure period. Data were pooled for both the aerosol form and test articles (n=12).

#### Lung concentrations for measured (HPLC-MS/MS) or estimated (MV or eRMV) data

MANOVA was conducted using pooled data (n=6 for aerosol form or compound) with post hoc analysis using Tukey's honestly significant difference test (Abdi and Williams, 2010[B]).

### **3.2.6.2. Methodological outcomes of Design 3**

It was confirmed a shorter acclimatisation period, with application of the neck seal, was sufficient when animals were allowed to settle in the restraint tubes for 15 minutes before the start of aerosol generation.

### **3.2.7. Incorporation of lung function measurements into repeat-dose inhalation studies (Design 4)**

The fourth experiment was designed to consider technical implications for incorporating lung function measurements into repeated exposure inhalation toxicology studies. Given the degree of restraint required to facilitate data capture using the design of head-out plethysmograph, a 28-day experiment was conducted to investigate the effect on lung function measurements when the neck seal was included or omitted during inhalation exposure procedures on days preceding data capture. For logistical reasons, MV and BF were measured using animals assigned to two inhalation toxicology studies, one administering crystalline GSK-361 and the other aqueous nebulised GSK-361.

Rats (2 groups; n=3/group) were acclimatised to the plethysmographs for 20 minutes, then 45 minutes and finally 60 minutes over three consecutive days preceding the first aerosol administration (Table 3.4). Rats were then restrained in plethysmographs, attached to the snout only chamber and allowed to settle for 15 minutes before exposure to a crystalline or aqueous nebulised aerosol of GSK-361 for 60 minutes once daily for 28 days (see Section 3.2.8). Lung function data were captured throughout the pre-exposure and aerosol administration periods on Day -1 (acclimatisation) and Days 1, 4, 14 and 26 to 28 of treatment. On Days 5 to 13 and 15 to 25, rats were restrained without a neck seal and exposed to the aerosol for 60 minutes (Figure 3.6). All procedures were performed under normal fluorescent lighting.

After the last administration of GSK-361 (Day 28), rats were sampled for plasma up to 24 hours post exposure and then euthanized (by

exsanguination under isoflurane anaesthesia) and the lungs taken for toxicokinetic investigations described in Chapter 5.

**Table 3.4: Tube restraint protocol for acclimatisation of rats to head-out plethysmography and aerosol administration (Design 4)**

Days of observation period <sup>A</sup>	Tube model	Group A		Figure number for presentation of BF / MV	Comment
		Neck seal present	Time in tube (min)		
<b>Acclimatisation to tube restraint</b>					
-3	PLY22L	Yes	20		
-2	PLY22L	Yes	45		
-1	PLY22L	Yes	60	3.15A / 3.17A	
<b>Treatment period (aerosol administration)</b>					
1	PLY22L	Yes	15 <sup>B</sup> +60	3.15B / 3.17B	First day of aerosol administration
2 to 3	PLY22L	Yes	15 <sup>B</sup> +60		
4	PLY22L	Yes	15 <sup>B</sup> +60	3.15C / 3.17C	
5 to 13		No	60		
14	PLY22L	Yes	15 <sup>B</sup> +60	3.15D / 3.17D	
15 to 25	PLY22L	No	60		
26 to 28	PLY22L	Yes	15 <sup>B</sup> +60	3.16 (3.15E) / 3.18 (3.17E)	

**Notes**

BF/MV Breath frequency; Minute volume

A Days of acclimatisation to tube restraint designated by a negative number.

B Rats allowed to settle in restraint tubes before starting aerosol generation.

### 3.2.7.1 Statistical analysis of lung function data

Statistical analysis of lung function data was performed using Statistica software (version 12.0.1133.40) as follows:

#### Comparison of the measured and body weight derived estimates of minute volume

The potential for differences between measured MV and the body weight derived estimate (eRMV), and hence potential discrepancies in dose estimation, were investigated by comparing the mean measured minute volumes for the 60-minute inhalation exposure period with eRMV values calculated from the corresponding pre-dose body weight for each animal using Equation 2 (Alexander *et al.*, 2008).

## Design 4

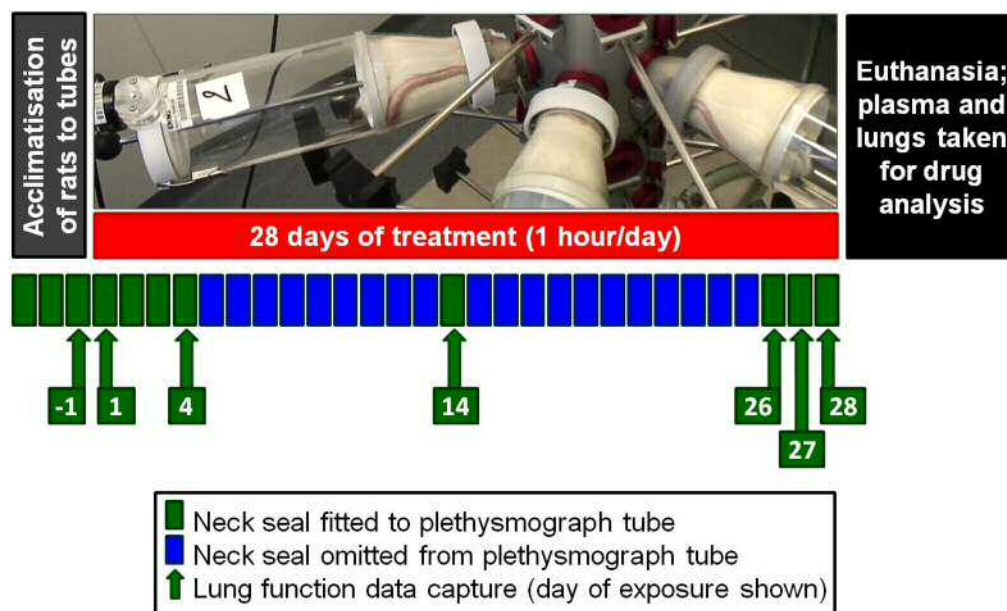


**Figure 3.6: Experimental design to investigate lung function of rats during a 28-day inhalation study.** Rats ( $n=3$ ) were acclimatised to plethysmograph tubes (with neck seals) over three days and exposed (60 minutes/day) to crystalline or nebulised GSK-361 for 28 days. Lung function data were captured on the last day of acclimatisation (Day -1) and during inhalation exposures on Days 1, 4, 14 and 26 to 28 of treatment. Neck seals were omitted from plethysmograph tubes for exposure of rats on Days 5 to 13 and 15 to 25 of treatment (shown as blue rectangles).

#### Comparison of BF for two aerosol forms

Two-way ANOVA was applied to the animal specific mean data for the 60-minute inhalation exposure period ( $n=3$ ).

#### Comparison of measured MV and body weight-derived eRMV for two aerosol forms

MANOVA was conducted using pooled data ( $n=6$ ) with post hoc analysis using Tukey's honestly significant difference test (Abdi and Williams, 2010[B]).

### **3.2.8. Aerosol generation of p38 MAPK inhibitors and inhalation exposure of rats**

For experiments requiring aerosol administration to rats (Designs 2 to 4), aerosols were generated and directed into the top of the snout-only inhalation exposure chamber as described in Chapter 2 (Section 2.2.5).

### 3.2.8.1. Test articles

The p38 MAPK inhibitors were supplied as micronised crystals and stored at ambient temperature, protected from light and moisture.

#### Dry powder formulations of p38 MAPK inhibitors

For aerosol administration of crystalline p38 MAPK inhibitors, aliquots of dry powder formulations prepared for use in Chapter 2 (nominally 5% drug (w/w) in lactose) were packed into the dust feed canisters (internal volume of 5 cm<sup>3</sup>). These methods were described in Chapter 2 (Section 2.2.5.1).

#### Liquid formulations of GSK-677 and GSK-361

For nebulisation of aqueous solutions of GSK-677 or GSK-361, each micronised crystalline test article was dissolved in a vehicle to achieve a concentration (Table 3.5) anticipated to achieve the target inhaled dose. Methods for preparation of the formulations are stated in Chapter 2 (Section 2.2.5.3).

**Table 3.5: Aqueous solutions of p38 MAPK inhibitors nebulised for single inhalation exposure of rats**

Test article	Study No.	Concentration in vehicle	Vehicle for nebulisation
GSK-677	R30988N	2.50 mg/mL	3% (v/v) Solutol HS 15 in 0.9% (w/v) aqueous sodium chloride (pH 5.9)
GSK-361	R31225N R31036N	1.50 mg/mL 1.60, 1.70 or 1.75 mg/mL	20:20:60 (v/v/v) Solutol HS 15, ethanol and 60 mM phosphate buffer (pH 7)

### 3.2.8.2. Aerosol Generation and formulation details

Groups of rats were administered an aerosol of the p38 MAPK inhibitor once (Designs 2 and 3) or repeatedly (Design 4), by snout-only inhalation exposure, as a dry powder aerosol or nebulised solution as appropriate (Chapter 2, Sections 2.2.5.2 and 2.2.5.4 respectively). The same design of apparatus was used for both single and repeated exposure of rats to nebulised GSK-361 (Designs 3 and 4), *i.e.* with the output of two nebulisers directed into a common exposure chamber.

For single inhalation exposure of rats (Designs 2 and 3), a target dose of 0.6 mg/kg was selected in line with non-clinical studies representing

a 10-fold overage for a nominal clinical dose of 1 mg when a conservative scaling factor for inter-species differences in lung deposition is applied (Degeorge *et al.*, 1997, Jones and Baldrick, 2013). Rats undergoing repeated inhalation exposure to GSK-361 (Design 4) were administered the target dose of 1 mg/kg/day selected for toxicopathology investigations described in Chapter 5.

Target aerosol concentrations (Table 3.6) for exposure of animals were calculated from the required doses using Equation 2 (Chapter 1, Section 1.3.4) and Equation 3 (Chapter 2, Section 2.2.5), assuming a predicted body weight of 350g (unpublished data) and an inhalation exposure period of 30 or 60 minutes as appropriate.

**Table 3.6: Duration of exposure, target doses and aerosol concentrations of p38 MAPK inhibitors for exposure of rats**

Test article	Study No.	Experimental design for lung function	Target dose (mg/kg)	Duration of exposure period (minutes)	Target aerosol concentration (mg/L)
GSK-899	R31125N	2	0.6	60	0.014
GSK-677	R30988N	3	0.6	30	0.028
GSK-361	R31225N	3	0.6	30	0.028
	R31035N	4	1	60	0.024
	R31036N	4	1	60	0.024

### 3.2.8.3. Aerosol characterisation

'Pre-study' aerosol characterisation work was conducted without animals to establish the operating conditions needed to generate target aerosol concentrations and to ensure aerosols were in line with particulate size criteria for exposure of rodents (OECD[412], 2009, OECD[413], 2009, US-EPA[3645], 1998). For repeat exposure studies, the operating conditions of the dust generator (speed of canister advancement) or concentration of GSK-361 in the nebulised solution were adjusted as necessary during the course of the study, with reference to HPLC-UV analysis results of aerosol concentration, to maintain the desired aerosol concentration on target.

Aerosols were also taken during exposure of animals using the stated air sampling volumes (Table 3.7) to determine aerosol concentrations

of the p38 MAPK inhibitors for dose estimation using Equation 1, and to determine particle size parameters, as described in Chapter 2 (Section 2.2.5.6). For repeat exposure studies, aerosol concentration was determined for representative days (approximately half of the exposure occasions) and particle size distribution was determined once in Weeks 1 and 3 of treatment.

**Table 3.7: Aerosol sampling volumes for aerosol concentration and particle size analysis**

Test article	Aerosol form	Study No.	Air sampling volume (L)	
			Aerosol concentration	Particle size distribution
GSK-899 <sup>A</sup>	crystalline	R31125N	4	8
GSK-677 <sup>B</sup>	crystalline nebulised	R30988N	6	20
			6	24
GSK-361 <sup>C</sup>	crystalline nebulised	R31225N	6	20
	crystalline nebulised	R31035N	6	6
		R31036N	6	6

**Notes**

- A Diluent for HPLC-UV analysis (Appendix 28): methanol: 0.1% formic acid (50:50 v/v)
- B Diluent for HPLC-UV analysis (Appendix 31): acetonitrile: 0.1% formic acid (50:50 v/v)
- C Diluent for HPLC-UV analysis (Appendix 33): acetonitrile: methanol: water (40:40:20 v/v/v)

### 3.3. Results and discussion

Lung function data (breath frequency and minute volume) and dosimetry (inhaled dose and lung concentration) are presented for each experimental design (Table 3.8) and discussed in the context of lung function, effect of animal handling, correlation of lung function with body weight-derived predictions and implications for lung deposition.

**Table 3.8: Index of figures and tables summarising lung function data, inhaled doses and lung concentrations of p38 MAPK inhibitors in rats**

Experiment design	Study number		Figure/table number			
			Breath frequency	Minute volume	Inhaled doses	Lung concentration
1	R30657N	Figures	3.7, 3.9	3.8, 3.10	-	-
2	R31125N	Figures	3.11	3.12, 3.21	-	3.24
		Tables	3.9	3.10, 3.13	3.15	3.16
3	R30988N	Figures	3.13	3.14, 3.22	-	3.25
	R31225N	Tables	3.11	3.12, 3.14	3.17	-
4	R31035N R31036N	Figures	3.15, 3.16, 3.19	3.17, 3.18, 3.20, 3.23	-	-

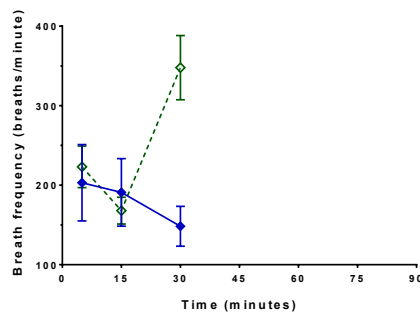
#### 3.3.1. Breath frequency and minute volume of rats restrained in tubes

Mean breath frequency (BF) and minute volume (MV) of rats generally decreased over the first 15 minutes of restraint for all experiments.

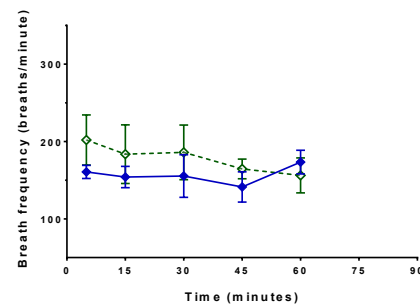
In the preliminary study, Design 1, transient increases in BF (Figure 3.7) and MV (Figure 3.8) were likely to be associated with stimulation of the animals during the observation period. It is common practice during non-clinical studies to perform visual checks on the condition of restrained animals for animal welfare reasons. It is likely the transient increases in BF and MV coincided with visual checks on the restrained animals and operational parameters such as chamber airflow and temperature, or when repositioning animals with a compromised neck seal (e.g. to remove an animal's forepaw from between its neck and the latex diaphragm).

### Design 1: breath frequency

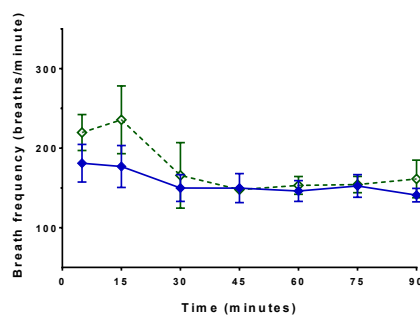
#### 3.7A: Day -3 (white light)



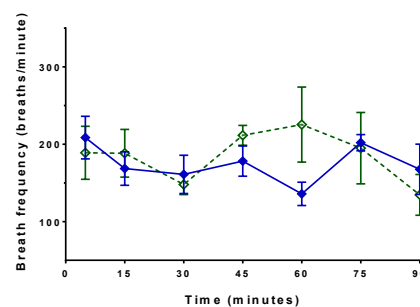
#### 3.7B: Day -2 (white light)



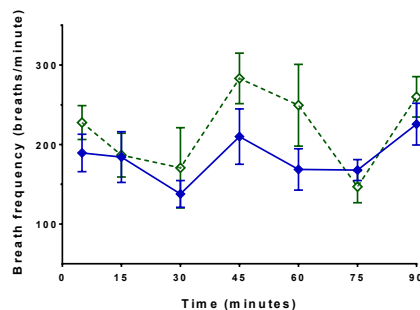
#### 3.7C: Day -1 (white light)



#### 3.7D: Day 1 (white light)



#### 3.7E: Day 8 (white light)



#### 3.7F: Day 15 (white light)

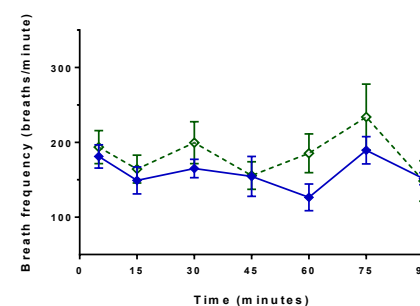
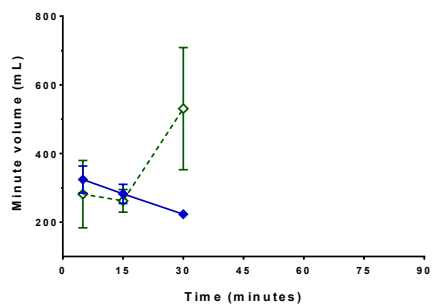


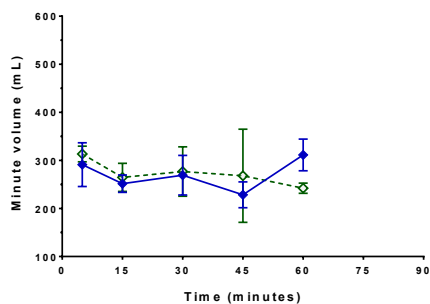
**Figure 3.7:** Breath frequency of rats restrained in tubes once daily for 28 days. Mean data plotted with standard deviations ( $n=4$ ). Rats were acclimatised to plethysmographs with neck seals (30, 60 and 90 minutes) and monitored for an additional 17 days under normal fluorescent light (see Figure 3.3 for study design); all rats (Groups A and B) were restrained with neck seals on days of BF measurement and Group A were also subjected to neck seals on Days 7 and 14. The same rats were used for Group A (blue solid line) and Group B (green dotted line) throughout the experiment. Generally, breath frequency decreased during the first 15 minutes of restraint suggesting that animals were calmer after a settling period. Time courses on each day of observation nevertheless showed transient increases, with no obvious improvement (*i.e.* reduced variability) of data for Group A.

**Design 1: minute volume**

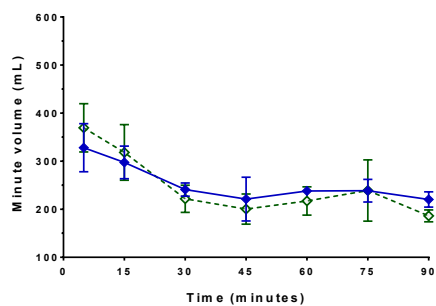
**3.8A: Day -3 (white light)**



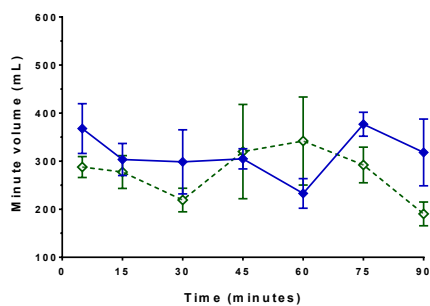
**3.8B: Day -2: (white light)**



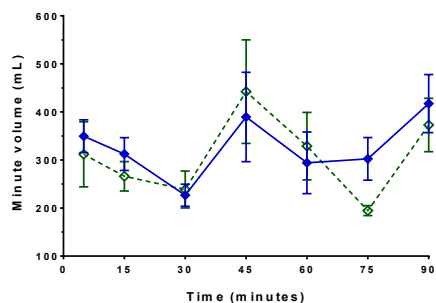
**3.8C: Day -1 (white light)**



**3.8D: Day 1 (white light)**



**3.8E: Day 8 (white light)**



**3.8F: Day 15 (white light)**

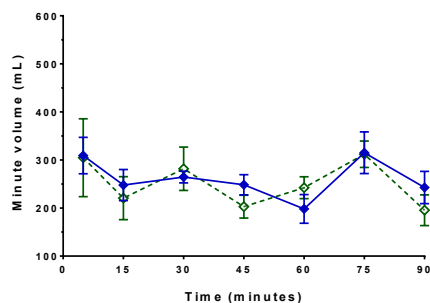
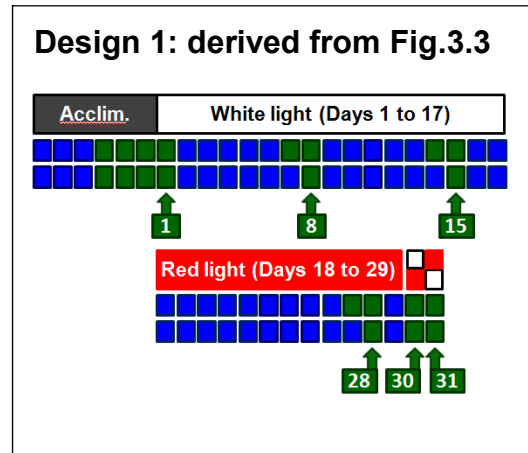
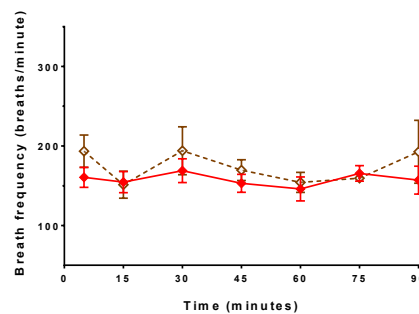


**Figure 3.8: Minute volume of rats restrained in tubes once daily for 28 days.** Mean data plotted with standard deviations (n=4). Rats were acclimatised to plethysmographs with neck seals (30, 60 and 90 minutes) and monitored for an additional 17 days under normal fluorescent light (see Figure 3.3 for details of design); all rats (Groups A and B) were restrained with neck seals on days of BF measurement and Group A were also subjected to neck seals on Days 7 and 14. The same rats were used for Group A (blue solid line) and Group B (green dotted line) throughout the experiment. Generally, minute volume decreased during the first 15 minutes of restraint suggesting animals were calmer after a settling period. Time courses on each day of observation nevertheless showed transient increases, with no obvious improvement (*i.e.* reduced variability) of data for Group A.

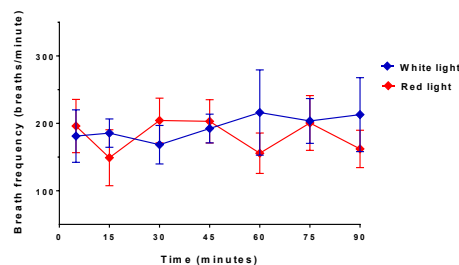
Under the conditions of this experiment, no improvement (reduced variability) in the BF or MV was evident on Days 8 and 15 of the observation period for rats also restrained with neck seals on the day preceding each data capture period (Group A), relative to comparator rats (Group B) not subjected to the neck seal on Days 7 and 14.

### Design 1: breath frequency

#### 3.9A: Day 28 (red-filtered light)



#### 3.9B: Day 30 (cross-over)



#### 3.9C: Day 31 (cross-over)

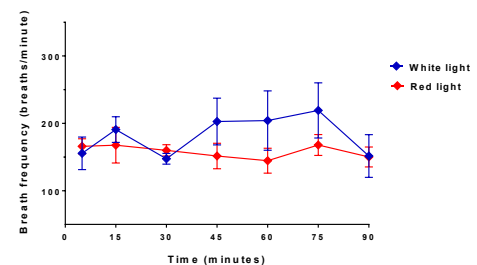
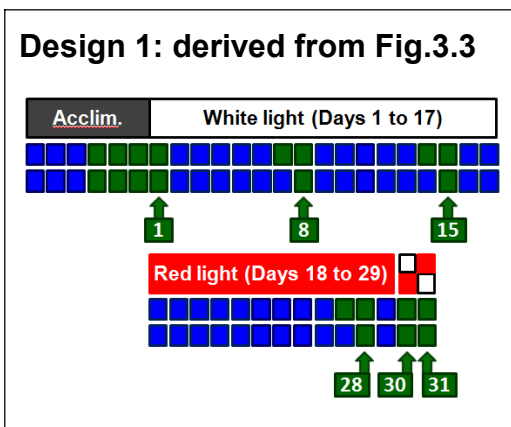
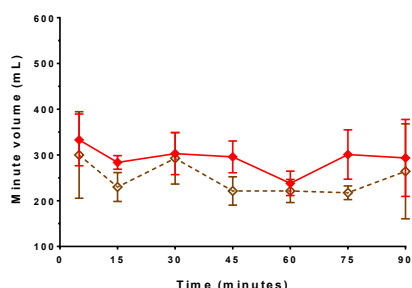


**Figure 3.9: Breath frequency of rats restrained in tubes under red or white lighting.** Mean data plotted with standard deviations ( $n=4$ ). Rats were restrained under red light (Days 18 to 29) and then under red or white light according to a cross-over design as extension to the experiment in Figure 3.7. **3.9A:** Day 28; Group A (red solid line) and Group B (brown dotted line) were subjected to restraint under red light for 10 days. Breath frequency appeared less variable than for the same rats maintained under white light (Figure 3.7). **3.9B:** Day 30; half of Groups A and B restrained under white light and half under red light. **3.9C:** Day 31; repetition with light colour switched for sub-groups. Statistical analysis (MANOVA with post hoc analysis using Tukey's honestly significant difference test (Abdi and Williams, 2010[B]);  $n=8$  with pooling of data) indicated a significant difference ( $p<0.01$ ) between rats under red and white light, and between Days 30 and 31. No differences of statistical significance between time points during the 90-minute observation period.

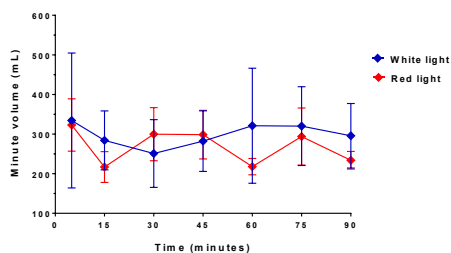
Fewer faecal pellets were seen in plethysmographs when rats were restrained under red light from Day 18, suggesting rats may be calmer (Williams *et al.*, 1988, Barone *et al.*, 1990) than under white light. This subjective observation was apparently consistent with less variable BF (Figure 3.9A) and MV (Figure 3.10A) data on Day 28.

**Design 1: minute volume**

**3.10A: Day 28 (red-filtered light)**



**3.10B: Day 30**



**3.10C: Day 31**

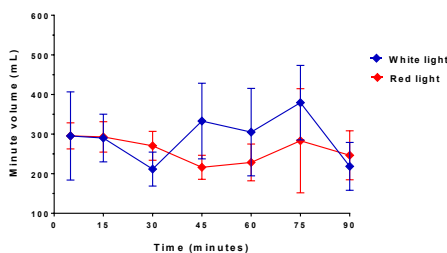


**Figure 3.10: Minute volume of rats restrained in tubes under red or white lighting.** Mean data plotted with standard deviations (n=4). Rats were restrained under red light (Days 18 to 29) and then according to a cross-over design or red and white light as an extension to the experiment shown in Figure 3.8. **3.10A:** Day 28; Group A (red solid line) and Group B (brown dotted line) were subjected to tube restraint under red light for 10 days. Minute volume appeared less variable than that observed for the same rats when maintained under white light (Figure 3.9). **3.10B:** Day 30; half of Groups A and B restrained under white light and the other half of Groups A and B under red light. **3.10C:** Day 31; repetition with lighting colour switched for cohorts of Groups A and B. Statistical analysis (MANOVA with post hoc analysis using Tukey's honestly significant difference test (Abdi and Williams, 2010[B]); n=8 with pooling of data) indicated no differences of significant difference between red or white light, day or time of measurement.

Statistical analysis of data pooled for investigation of light colour on Days 30 and 31 suggested BF (Figure 3.9B/C) of rats under red light

was lower than for white light ( $p < 0.01$ ). However, significant differences were also evident between Days 30 and 31 suggesting data variability. There were no significant differences in MV (Figure 3.10B/C) for rats under red or white light nor between Days 30 or 31. The error bars (standard deviations) indicated data for Days 30 and 31 were more variable than for the same animals on Day 28 of the observation period. Furthermore, apparent differences in measurements taken under white and then red light may also have been attributable to further procedural conditioning of rats as the observation period progressed. A more robust experimental design was thus required to further investigate these preliminary observations.

#### **3.3.1.1. Influence of lighting colour and duration of tube acclimatisation on breath frequency and minute volume of rats**

BF and MV measurements for the preliminary study (Design 1) showed a potential for interventions or activities near rats undergoing plethysmography data capture to induce erratic increases in BF and MV. Checks made on the condition of restrained rats for Designs 2 to 4 were performed less intrusively to limit the potential for excitation of animals during data capture, achieving a more stable baseline with fewer transient increases in BF and/or MV during the plethysmography data capture periods (Figures 3.11 to 3.18).

When considering the potential for lighting colour to affect the excitability of animals during restraint, measurements of BF in Design 1 were equivocal. In a more robust study (Design 2), BF (Figure 3.11A) or MV (Figure 3.12A) measurements for rats restrained under red or white light were similar during inhalation exposure, with no significant difference between mean values for the 60-minute exposure period (Table 3.9 for BF; Table 3.10 for MV). The profile for BF showed a trend for a gradual reduction throughout the 60-minute exposure period and MV appeared to decrease from five minutes of exposure, establishing a baseline thereafter.

Investigation of the duration of the acclimatisation protocol showed no significant differences in mean BF (Table 3.9) or MV (Table 3.10) for animals acclimatised to restraint tubes over two or six days. Nevertheless, transient but statistically significant elevations in BF (Figure 3.11B;  $p < 0.01$ ) and MV (Figure 3.12B;  $p < 0.05$ ) were evident for rats acclimatised over two days compared with rats acclimatised over six days. BF and MV for rats acclimatised over six days followed a stable baseline with no elevation at the start of the exposure period.

## Design 2: breath frequency

### 3.11A: lighting conditions

### 3.11B: acclimatisation period

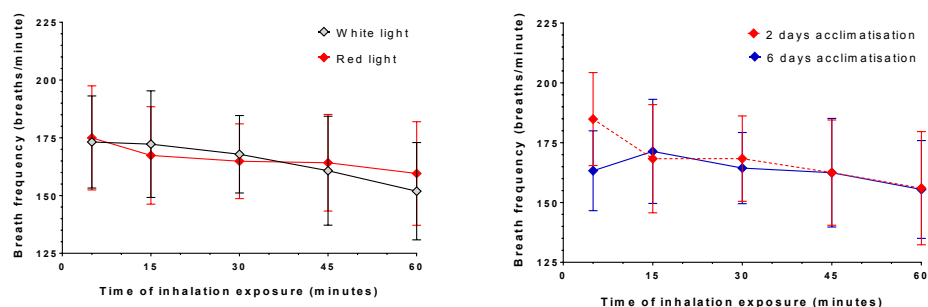


**Figure 3.11:** Breath frequency of rats exposed to GSK-899 for 60 minutes after a tube acclimatisation protocol of two or six days and under red or white lighting. Latin square design ( $n=8$  rats/group) used for statistical analyses (MANOVA with post hoc analysis using Tukey's honestly significant difference test (Abdi and Williams, 2010[B]); mean data with standard deviations ( $n=16$ ) are plotted against time of inhalation exposure. Breath frequencies at 5 minutes ( $p < 0.01$ ) and 15 minutes ( $p < 0.05$ ) were significantly different to those at 60 minutes. **3.11A:** light colour used during restraint for acclimatisation and inhalation exposure (2-day and 6-day acclimatisation data pooled); no differences of statistical significance. **3.11B:** duration of acclimatisation period (red and white light data pooled); no differences of statistical significance.

**Table 3.9: Breath frequency (breaths per minute) of rats during a 60-minute inhalation exposure period**

Design 2 (R31125N)	Lighting conditions <sup>A</sup>		Tube acclimatisation <sup>A</sup>	
	White	Red	2 days	6 days
Mean (bpm)	169.2	170.3	168.3	169.0
sd	15.7	5.93	17.9	19.2
CV	9%	10%	11%	11%
n	16	16	16	16

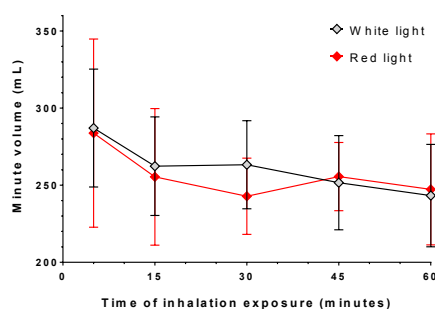
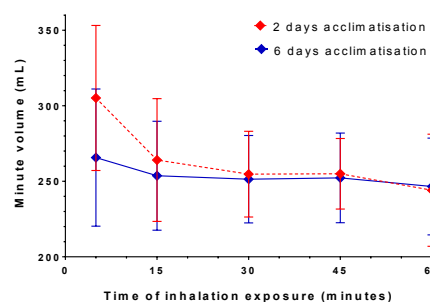
**Notes**

sd standard deviation

CV coefficient of variation (ratio of standard deviation to mean)

n number of animals/group in statistical comparison

A No differences of statistical difference (2-way ANOVA); Latin square design (n=8 rats/group) for statistical analyses of acclimatisation period (red and white light data pooled) and lighting (2-day and 6-day acclimatisation data pooled).

**Design 2: minute volume****3.12A: lighting conditions****3.12B: acclimatisation period**

**Figure 3.12: Minute volume of rats exposed to GSK-899 for 60 minutes after a tube acclimatisation protocol of two or six days and under red or white lighting.** Latin square design (n=8 rats/group) used for statistical analyses (MANOVA with post hoc analysis using Tukey's honestly significant difference test (Abdi and Williams, 2010[B])); mean data with standard deviations (n=16) are plotted against time of inhalation exposure. Minute volumes at 5 minutes were significantly different to the rest of the profile ( $p < 0.05$  relative to 15 minutes;  $p < 0.01$  relative to 30, 45 and 60 minutes). **3.12A:** light colour used during restraint for acclimatisation and inhalation exposure (2-day and 6-day acclimatisation data pooled); no differences of statistical significance. **3.12B:** duration of acclimatisation period (red and white light data pooled); no differences of statistical significance.

**Table 3.10: Minute volume of rats during a 60-minute inhalation exposure period**

Design 2	Lighting conditions <sup>A</sup>		Tube acclimatisation <sup>A</sup>	
	White	Red	2 days	6 days
MV (mL)	262.0	254.6	258.1	253.8
sd	22.2	25.2	18.4	25.2
CV	8%	10%	7%	10%
n	16	16	16	16

**Notes**

A No differences of statistical difference (2-way ANOVA); Latin square design (n=8 rats/group) for statistical analyses of acclimatisation period (red and white light data pooled) and lighting (2-day and 6-day acclimatisation data pooled).

These data indicated the red filtration of light did not reduce BF or MV and, by inference, did not induce a calmer state for animals undergoing inhalation exposure to a dry powder aerosol. A shorter acclimatisation protocol (two days) did not significantly affect mean respiratory parameters for the 60-minute period. However, reductions in BF and MV early in the exposure period suggests modification of the procedure to allow rats to settle in the restraint tubes before aerosol generation may facilitate a more consistent exposure of rats to the test aerosol.

### **3.3.1.2. Breath frequency and minute volume of rats allowed to settle before aerosol administration**

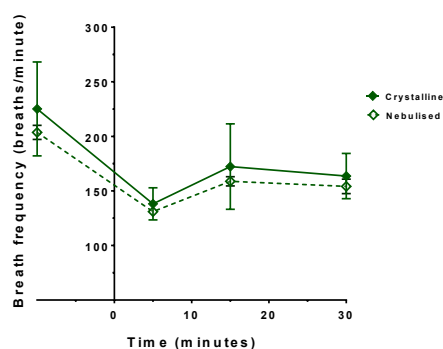
Procedures including checks on animal condition and aerosol sampling were performed less intrusively, where practicable, to limit the potential for excitation of animals during plethysmography data capture. A pre-exposure period of nominally 15 minutes was also applied for rats to settle in plethysmographs before aerosol administration. Statistically significant ( $p < 0.01$ ) reductions in BF (Figure 3.13; Table 3.11) and MV (Figure 3.14; Table 3.12) were evident after the pre-exposure period.

Statistical analysis of the time courses indicated the BF of rats inhaling crystalline p38 MAPK inhibitors was significantly higher than for the nebulised aerosol forms, but with no significant difference between compounds. However, there was no significant difference in mean values for the 30-minute exposure period (Table 3.11). This apparent

difference was driven by generally higher BF values for rats administered crystalline GSK-361 (Figure 3.13B) and the time profiles were similar for crystalline and nebulised GSK-677 (Figure 3.13A). Similarly, the MV of rats administered GSK-361 was significantly higher than for GSK-677 but there was no significant difference between aerosol forms (Figure 3.14; Table 3.12).

### Design 3: breath frequency

#### 3.13A: GSK-677



#### 3.13B: GSK-361

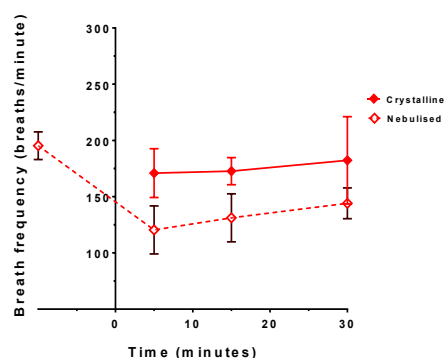


**Figure 3.13: Breath frequency (BF) of rats exposed to crystalline or nebulised aerosols for 30 minutes.** Mean BF with standard deviations (n=3) against time of inhalation exposure (30 minutes). **3.13A:** GSK-677 treated rats settled for 20 minutes before exposure. **3.13B:** GSK-361 treated rats settled for 15 minutes before exposure (data not captured before exposure to crystalline GSK-361). Statistical analysis (MANOVA with post hoc analysis using Tukey's honestly significant difference test (Abdi and Williams, 2010[B]) indicated significant differences ( $p < 0.01$ ) between pre-exposure (-10 minutes) data and during exposure, and between crystalline and nebulised aerosols; no significant difference between GSK-677 and GSK-361.

**Table 3.11: Breath frequency (breaths per minute) of rats during a 30-minute inhalation exposure period**

Design 3 Period <sup>A</sup>	Summary parameters	Compound <sup>A</sup>		Aerosol form <sup>A</sup>	
		GSK-677	GSK-361	Crystalline	Nebulised
Pre-exposure (-10 min)	Mean (bpm)	214.4	195.3	225.2	199.5
	sd	29.9	12.4	43.0	9.9
	CV	14%	6%	19%	5%
	n	6	3 <sup>B</sup>	3 <sup>B</sup>	6
Aerosol administration <sup>**</sup> (0 to 30 min)	Mean (bpm)	156.4	150.8	163.9	143.3
	sd	17.2	29.3	25.6	16.2
	CV	11%	19%	16%	11%
	n	6	6	6	6

**Notes**

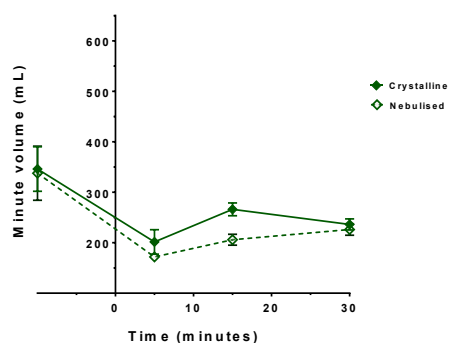
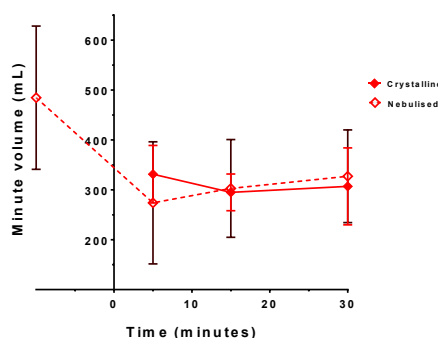
sd standard deviation

CV coefficient of variation (ratio of standard deviation to mean)

n number of animals/group in statistical comparison

A Statistical analysis (MANOVA with post hoc analysis using Tukey's honestly significant difference test (Abdi and Williams, 2010[B]) indicated reduced MV from pre-exposure to aerosol exposure periods (\*\* p<0.01; drug and aerosol form data pooled); no significant difference between drugs or aerosol forms.

B Data for nebulised GSK-361 treated rats only (data not captured in error before administration of crystalline GSK-361).

**Design 3: minute volume****3.14A: GSK-677****3.14B: GSK-361**

**Figure 3.14: Minute volume (MV) of rats exposed to crystalline or nebulised aerosols for 30 minutes.** Mean MV with standard deviations (n=3) against time of inhalation exposure (30 minutes). **3.14A:** GSK-677 treated rats settled for 20 minutes before exposure. **3.14B:** GSK-361 treated rats settled for 15 minutes before exposure (data not captured before exposure to crystalline GSK-361). Statistical analysis (MANOVA with post hoc analysis using Tukey's honestly significant difference test (Abdi and Williams, 2010[B])) indicated significant differences (p<0.01) between MV pre-exposure (-10 minutes) and during exposure, and between GSK-677 and GSK-361; no significant difference between crystalline and nebulised aerosol forms.

**Table 3.12: Minute volume of rats during a 30-minute inhalation exposure period**

Design 3 Period <sup>A</sup>	Summary parameters	Compound <sup>A</sup>		Aerosol form <sup>A</sup>	
		GSK-677	GSK-361	Crystalline	Nebulised
Pre-exposure (-10 min)	MV (mL)	341.9	484.5	346.0	411.1
	sd	44.1	143.7	44.2	126.0
	CV	13%	30%	13%	31%
	n	6	3 <sup>B</sup>	3 <sup>B</sup>	6
Aerosol administration <sup>**</sup> (0 to 30 min)	MV (mL)	224.7	295.0 *	265.2	254.4
	sd	18.3	71.2	43.3	80.2
	CV	8%	24%	16%	32%
	n	6	6	6	6

**Notes**

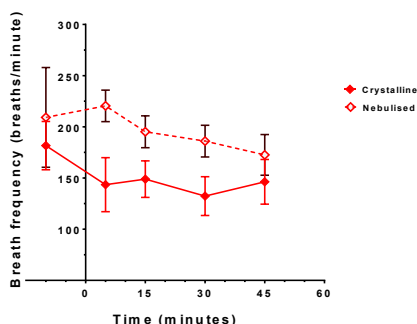
- A Statistical analysis (MANOVA with post hoc analysis using Tukey's honestly significant difference test (Abdi and Williams, 2010[B])) indicated reduced MV from pre-exposure to aerosol administration periods (\*\* p<0.01; aerosol form and drug data pooled) and significant difference between GSK-677 and GSK-361 treated rats (\* p<0.05; aerosol form data pooled); no significant difference between aerosol forms (drug data pooled).
- B Data for nebulised GSK-361 treated rats only (data not captured in error before administration of crystalline GSK-361).

### 3.3.2.3. Effect of neck restraint on breath frequency and minute volume of rats during repeat dose studies

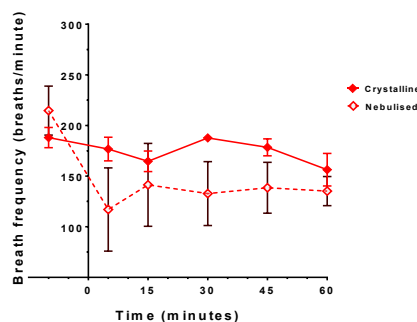
Procedures including checks on animal condition and aerosol sampling were performed less intrusively, where practicable, to limit the potential for excitation of animals during plethysmography data capture. Generally, BF (Figures 3.15 and 3.16) and MV (Figures 3.17 and 3.18) decreased during the pre-exposure settling period but remained elevated for rats administered crystalline GSK-361 on Day 1, the first day that animals inhaled an aerosol. This finding appears consistent with the apparent elevation observed for rats administered a single dose of GSK-361 (Figures 3.13 and 3.14). BF and MV data appeared less variable on Day 4 (Figures 3.15C and 3.17C respectively) and Day 28 (Figures 3.16C and 3.18C respectively), which followed repeated administration of aerosols concurrent with conditioning of the rats with neck seals incorporated into the plethysmographs.

**Design 4: breath frequency**

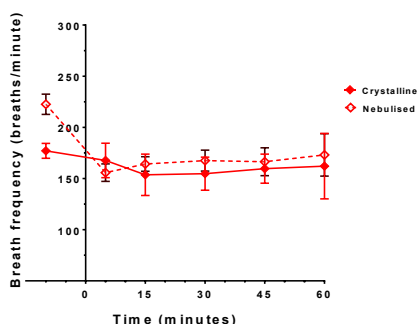
**3.15A: Day -1 (acclimatisation)**



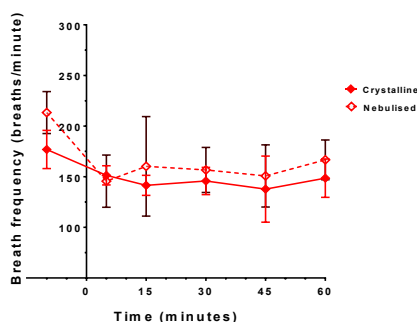
**3.15B: Day 1**



**3.15C: Day 4**



**3.15D: Day 14**



**3.15E: Day 26**

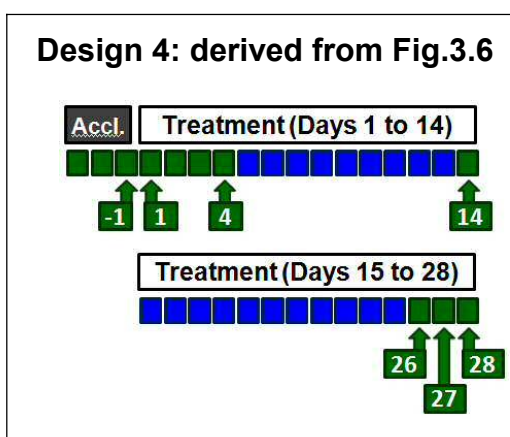
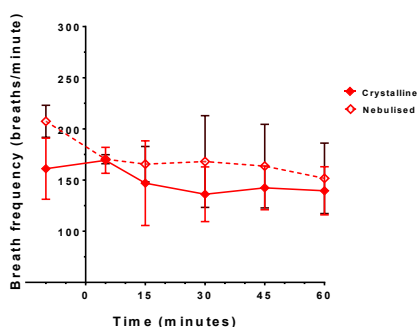
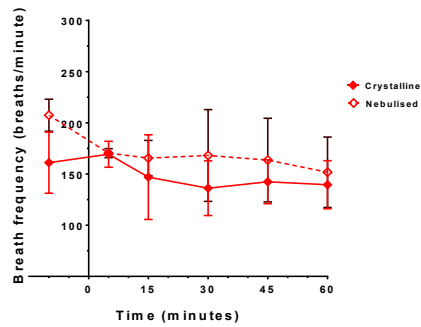


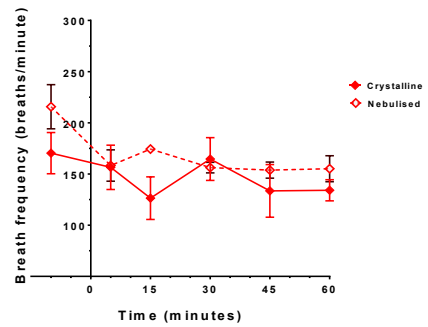
**Figure 3.15: Breath frequency of rats administered GSK-361 for 28 days.** Mean data with standard deviations (n=3). Rats were allowed to settle for 15 minutes before aerosol administration (60 minutes). **3.15A:** Day -1; third and final day of tube acclimatisation. **3.15B:** Day 1; first inhaled dose. Variability of data was greater for rats administered the nebulised aerosol. **3.15C:** Day 4; data less variable than for Day 1. **3.15D:** Day 14 (neck seal omitted from tubes on Days 5 to 13); data are more variable than for Day 4. **3.15E:** Day 26 (neck seal omitted from tubes on Days 15 to 25); data variability similar to Day 14, when data were also captured after a routine of tube restraint without the neck seal present.

**Design 4: breath frequency**

**3.16A: Day 26**



**3.16B: Day 27**



**3.16C: Day 28**

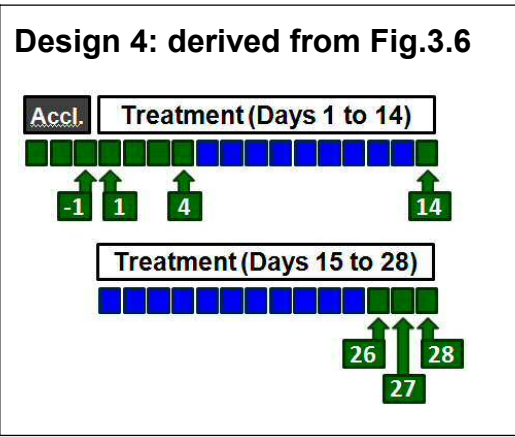
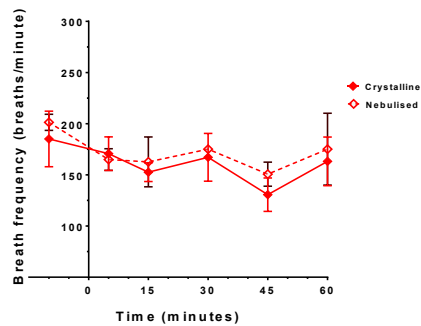
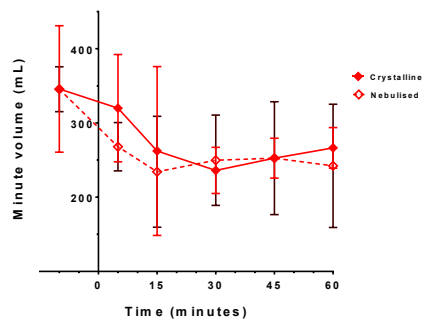


**Figure 3.16: Breath frequency of rats administered GSK-361 for 28 days.** Mean data with standard deviations (n=3). Rats were allowed to settle for 15 minutes before aerosol administration (60 minutes). **3.16A:** Day 26 (neck seal omitted from tubes on Days 15 to 25); Figure 3.15E reproduced for reference. **3.16B:** Day 27. **3.16C:** Day 28; a progressive reduction in data variability was apparent over three days with reintroduction of the neck seal from Day 26.

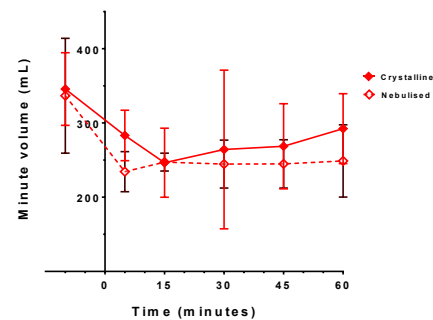


## Design 4: minute volume

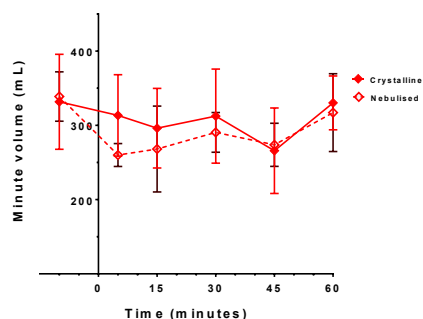
## 3.18A: Day 26



## 3.18B: Day 27



## 3.18C: Day 28



## Design 4: derived from Fig.3.6

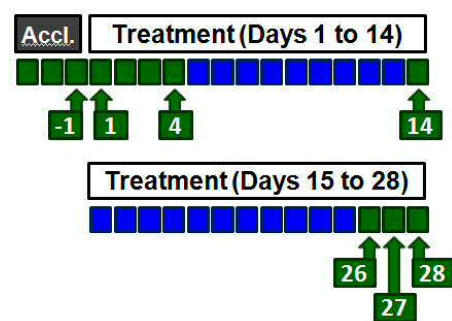


**Figure 3.18:** Minute volume of rats administered GSK-361 for 28 days. Mean data with standard deviations ( $n=3$ ). Rats were allowed to settle for 15 minutes before aerosol administration (60 minutes). **3.18A:** Day 26 (neck seal omitted from tubes on Days 15 to 25); Figure 3.17E reproduced for reference. **3.18B:** Day 27. **3.18C:** Day 28; a slight reduction in data variability was apparent over three days with reintroduction of the neck seal from Day 26.

Mean BF (Figure 3.19) and MV (Figure 3.20) values for the 60-minute exposure period were most variable on Day 1, when rats were first exposed to an aerosol, and on Days 14 and 26 following a treatment period in which the neck seal was omitted from the body plethysmograph for aerosol administration. It is noteworthy that mean MV was similar to or slightly greater than the body weight-derived estimate (eRMV) when the neck seal was used during days of restraint preceding data capture on Days 1, 4 and 28. However, with omission of the neck seal from Day 5 (excluding days of data capture), the mean MV decreased with an increase in eRMV (Days 14 and 26). With reintroduction of the neck seal from Day 26, the variability in measured

BF and MV progressively reduced and mean MV attained parity with eRMV on Day 28, suggesting rats may require at least two days of reacclimatisation to the neck seal before the mean measured MV is representative of eRMV.

#### Design 4: breath frequency

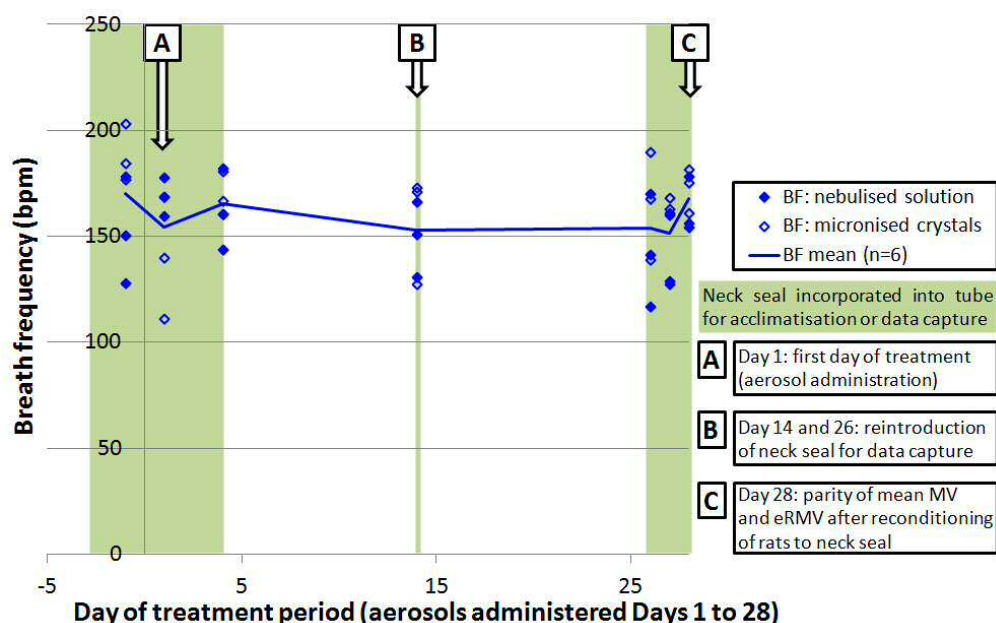


**Figure 3.19: Breath frequency (breaths per minute) in rats over a 28-day treatment period.** Mean data points (n=6) are joined by a blue line. There was no obvious difference for rats administered a crystalline or nebulised aerosol of GSK-361. Statistical analysis (2-way ANOVA) indicated no significant differences between crystalline and nebulised aerosol forms, or days of measurement.

Alternatively, this raises the possibility of an observer effect, *i.e.* that minute volume may change as a consequence of using the neck seal to facilitate measurement of this parameter. Nirogi *et al.* (2012) published baseline minute volumes for male Wistar rats (body weight range of 250 g to 300 g) of  $173 \pm 15.7$  mL when measured by whole body plethysmography of 'unrestrained' rats and  $228 \pm 14.8$  mL when measured by head-out plethysmography, suggesting a potential for procedural-related differences in lung function measurements between techniques with differing degrees of animal restraint.

## Design 4: minute volume

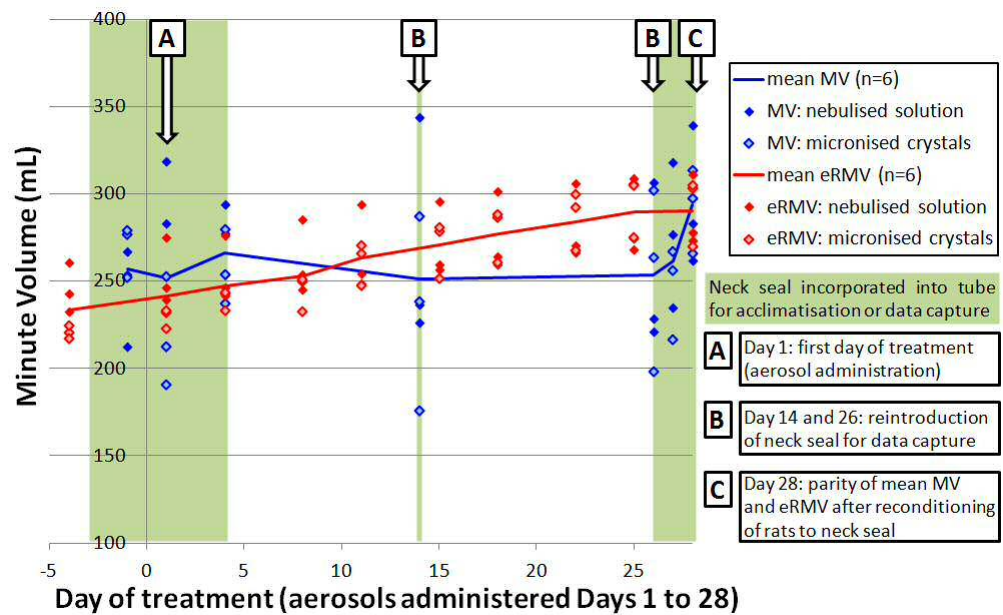


**Figure 3.20: Measured minute volume (MV) and the body weight derived estimate (eRMV) in rats over a 28-day treatment period.** Measured MV data are shown in blue, with corresponding body weight derived eRMV data in red. Mean data points are joined by a blue or red line, respectively. Statistical analysis (MANOVA with post hoc analysis using Tukey's honestly significant difference test (Abdi and Williams, 2010[B])) for Days 1, 4, 14/15, 26/25 and 28 indicated no significant differences between MV and eRMV or crystalline and nebulised aerosol forms; MV and eRMV values were significantly higher on Day 28 ( $p < 0.05$ ) compared with Day 1.

### 3.3.2. Relationship between measured minute volume and pre-exposure body weight

In Design 2, rats were acclimatised to tube restraint over two or six days, and plethysmography data were captured during administration of crystalline GSK-899 for 60 minutes; no settling period was applied before starting aerosol generation. Figure 3.21 indicates there was no clear proportional relationship between the body weight-derived and measured MV of rats under the conditions of this experiment. The measured MV data were considerably more variable than the body weight-derived estimates but also generally and significantly ( $p < 0.01$ ) higher; mean MV  $\approx 1.17x$  eRMV (Table 3.13).

## Design 2: minute volume

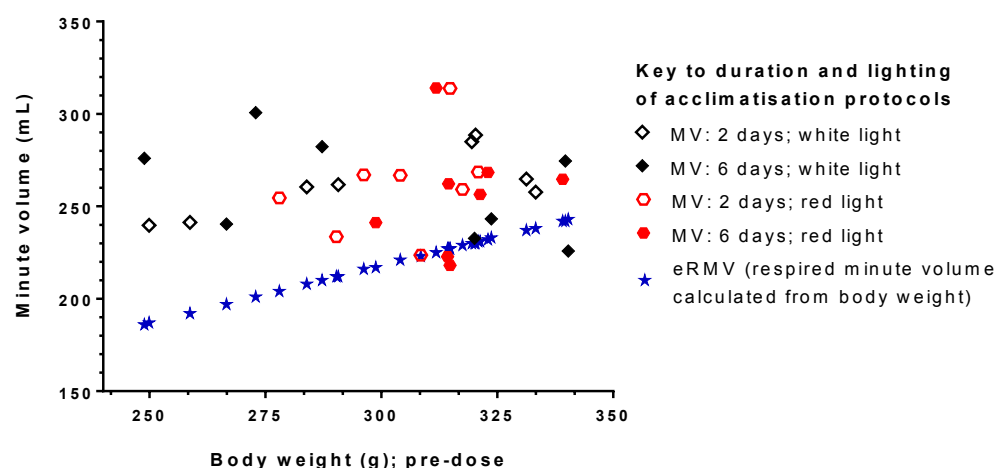


**Figure 3.21: Measured minute volume (MV) and the body weight derived estimate (eRMV) against body weight of rats during a single exposure.** Rats were administered GSK-899 for 60 minutes, starting immediately after their attachment to the chamber. Data plotted against pre-dose body weights.

**Table 3.13: Measured and body weight-derived estimates of minute volume (mL) of rats during a single 60-minute exposure period**

Design 2 (R31125N)	Respired minute volume (body weight derived estimate)	Minute volume (measured)
Mean	221	260**
sd	15.9	24.8
CV	7%	10%
n	32	32

## Notes

\*\* indicates statistical difference ( $p < 0.01$  using 1-way ANOVA) for measured minute volume versus the body weight-derived estimate (eRMV).

In contrast, when rats were allowed to settle in the plethysmographs for 15 minutes before the start of aerosol generation, the MV and eRMV for a given body weight were generally similar (Figure 3.22) although 3/6 rats administered GSK-361 were outliers and increased the overall mean (Table 3.14) in line with rats that did not settle before exposure (Table 3.13). In addition, when rats were acclimatised to the neck seal in days preceding data capture during the repeat dose study, the MV and eRMV for a given body weight were also generally similar and a change in MV (23% increase) was in line with the body weight development (30% gain) of rats from Days 1 to 28 of treatment (Figure 3.23). This finding supports use of an algorithm for estimating

the inhaled dose of a test article in healthy rats provided animals are adequately conditioned to the procedure and allowed to settle in restraint tubes before initiating aerosol generation. However, the rats used for MV measurements were not adversely affected by repeated administration of GSK-361 and, consequently, the potential relationship between MV and adverse body weight changes (reduced gain or loss) was not addressed in this experiment. Nevertheless, it is reasonable to hypothesize that MV and body weight may not be proportional for a compromised animal. For example, depletion of adipose tissue is unlikely to influence lung architecture and lung function may be affected by the onset of inhalation toxicity (Sung *et al.*, 2008).

### Design 3: minute volume

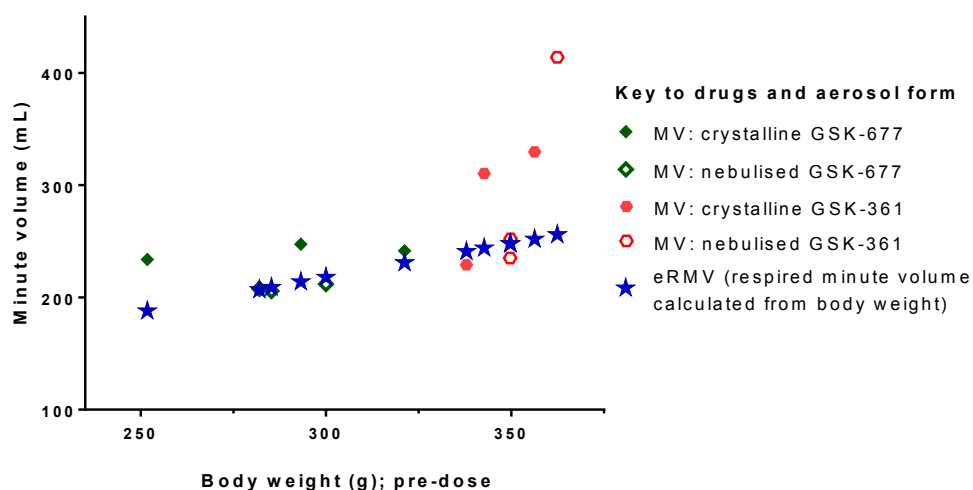


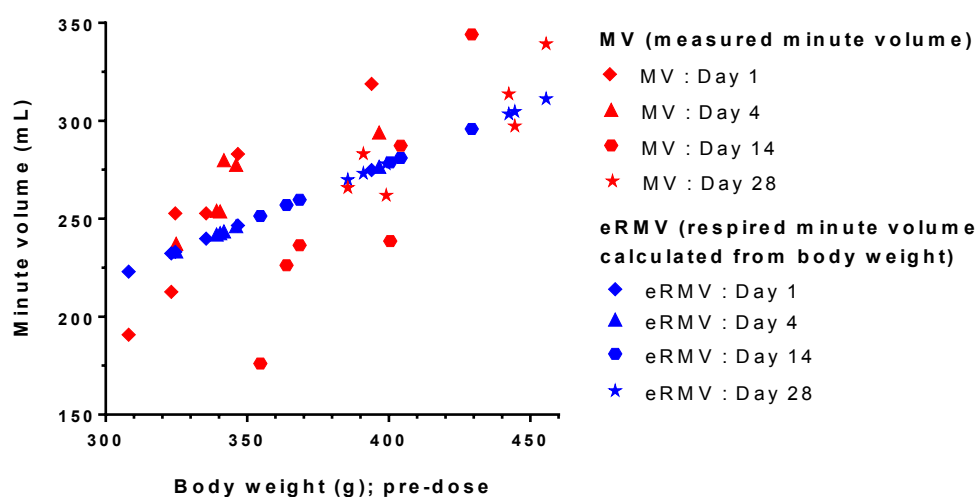
**Figure 3.22:** Measured minute volume (MV) and the body weight derived estimate (eRMV) against body weight of rats during a single exposure. Rats were allowed to settle in plethysmographs for 15 minutes and then administered GSK-677 or GSK-361 for 30 minutes. Data plotted against pre-exposure body weights.

**Table 3.14: Measured and body weight-derived estimates of minute volume (mL) of rats during a single 30-minute exposure period**

Design 3 (R30988N and R31225N)	Respired minute volume (body weight derived estimate)	Minute volume (measured)
Mean	229.7	259.8
sd	21.9	61.7
CV	10%	24%
n	12	12

**Notes**

No differences of statistical difference (1-way ANOVA) for measured minute volume versus the body weight-derived estimate (eRMV).

**Design 4: minute volume**

**Figure 3.23: Measured minute volume (MV) and the body weight derived estimate (eRMV) against body weight of rats over 28 days.** Rats were administered GSK-361 for 60 minutes, starting 15 minutes after attachment of rats to the chamber. Minute volumes for Days 1, 4, 14 and 28 of the study data are plotted against pre-dose body weights for each rat (Day 14 MV data plotted against the Day 15 body weight).

### 3.3.3. Comparison of measured lung concentrations and estimated pulmonary doses

For logistical reasons in Design 2, rats were administered GSK-899 as sub-groups (n=4) for each of the four treatments. Mean aerosol concentrations for the second cycle of inhalation exposures were at least 30% higher than for the first corresponding sub-group, with a consequent difference in estimated inhaled doses between each of the

paired sub-groups. The particle size distributions were similar between treatment groups and the two cycles (Table 3.15).

**Table 3.15: Estimated inhaled doses in rats and aerosol characterisation data for crystalline GSK-899**

**Design 2**

Study number	Acclimatisation duration and lighting colour	Estimated inhaled dose <sup>A</sup> (mg/kg)		Mean (n=2) aerosol concentration of GSK-899 (µg/L)	Particle size distribution	
		sub-group	group		MMAD (µm)	σg
R31125N	2 days; white	0.741	0.843	16.7	2.0	2.0
		0.944		21.9	2.3	2.0
	6 days; white	0.717	0.876	16.2	1.9	2.1
		1.034		24.1	1.9	2.0
	2 days; red	0.813	0.997	18.5	1.7	2.0
		1.181		27.3	2.3	1.9
	6 days; red	0.744	0.972	17.2	2.4	2.0
		1.201		29.4	2.3	1.9

**Notes**

MMAD mass median aerodynamic diameter

σg geometric standard deviation

A Estimated inhaled doses calculated for a 60-minute exposure period using mean data (aerosol concentration and body weight) and a body-weight derived estimate of respired minute volume (Alexander *et al.*, 2008).

Drug concentrations for lungs taken immediately post-exposure (Table 3.16) appeared to be slightly more variable than MV measured in the same animals (Table 3.10). This was attributable, at least in part, to differences in aerosol concentration achieved for the two sub-groups for each treatment (light colour and duration of acclimatisation protocol). With pooling of group data to investigate the light colour or duration of acclimatisation as appropriate (Figure 3.24), an apparent difference in lung-homogenate concentrations for red versus white lighting was evident and in contrast to trends observed in BF and MV, and hence the “achieved lung dose.” Although the variability observed in lung-homogenate concentrations was not unexpected (personal observation of unpublished data), the apparent differences between these data types suggest the reason for a difference in lung concentrations between the treatment groups cannot be ascribed to

differences in aerosol concentration alone or inter-animal differences of MV and thus the deposited lung dose *per se*.

**Table 3.16: GSK-899 concentration in rat lung homogenate ( $\mu\text{g/g}$ ) after a single inhalation exposure (breakdown of groups)**

Design 2 (R31125N)	GSK-899 concentration in lung homogenate immediately post exposure			
	White light; 2 days	Red light; 2 days	White light; 6 days	Red light; 6 days
Mean ( $\mu\text{g/g}$ )	33.3	44.6	33.7	36.8
sd	6.46	5.38	2.55	5.93
CV	19%	12%	8%	16%
n	8	8	8	8

#### Notes

sd standard deviation

CV coefficient of variation (ratio of standard deviation to mean)

n number of animals/group in statistical comparison

### Design 2: drug-lung concentrations

#### 3.24A: acclimatisation period

#### 3.24B: lighting conditions

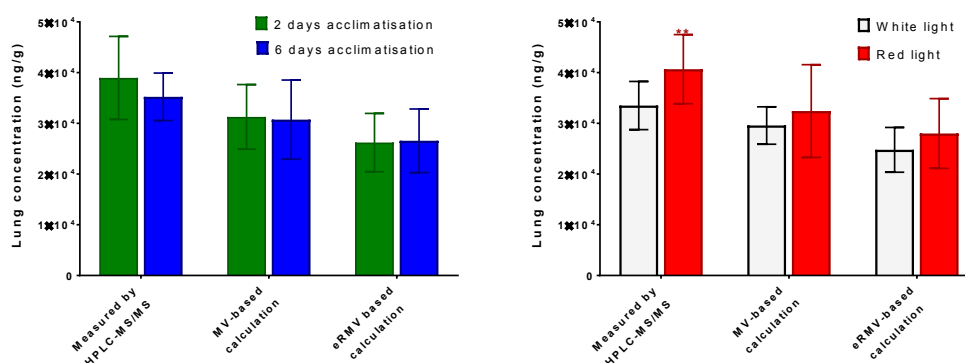


**Figure 3.24: Measured and predicted lung concentrations in rats after a single inhaled dose of GSK-899 and tube acclimatisation for two or six days under red or white light.** Latin square design (n=8 rats/group) used for statistical analyses (MANOVA with post hoc analysis using Tukey's honestly significant difference test (Abdi and Williams, 2010[B]); n=16; data pooled). Means with standard deviations shown for GSK-899 lung concentrations and predicted from measured minute volume (MV) and body weight (eRMV). Post hoc statistical analysis indicated all methods of drug-lung determinations were significantly different ( $p < 0.0101$ ). **3.24A:** no significant difference between two or six days of acclimatisation (data pooled for light colour). **3.24B:** lighting colour during tube acclimatisation and inhalation exposure (data pooled for acclimatisation periods); \*\* statistical significance ( $p < 0.01$ ) for light colour.

Possible explanations for discrepancies or imprecision in drug-lung homogenate concentrations include processing of lung-homogenate samples for HPLC-UV analysis e.g. non-uniform drug-lung deposition in conjunction with pooling of selected lung lobes, the degree of homogenization and incomplete solvent extraction of the drug. Statistical analysis of GSK-899 lung concentrations measured by HPLC-MS/MS or estimated from minute volume indicated that all methods were significantly different from one another, with mean values ranked HPLC-MS/MS > MV > eRMV.

Estimated inhaled doses and aerosol characterisation data for GSK-677 and GSK-361 (Table 3.17) were discussed in Chapter 2 (Section 2.3.6.1). The estimated doses for these compounds achieved over a 30-minute exposure were lower than the estimated inhaled doses of GSK-899 achieved over 60 minutes (Table 3.15).

**Table 3.17: Estimated inhaled doses in rats and aerosol characterisation data for GSK-677 and GSK-361**

**Design 3**

Study number	Test article	Aerosol form and test article concentration in vehicle	Estimated inhaled dose <sup>A</sup> (mg/kg)	Mean (n=2) drug aerosol concentration (µg/L)	Particle size distribution	
					MMAD (µm)	σg
R30988N	GSK-677	Crystalline (4.4% w/w)	0.487	22.2	2.8	2.0
		Nebulised solution (2.5 mg/mL)	0.418	19.1	1.3	2.2
R31225N	GSK-361	Crystalline (4.8% w/w)	0.555	26.0	2.0	2.4
		Nebulised solution (1.5 mg/mL)	0.574	27.0	2.5	2.4

**Notes**

MMAD mass median aerodynamic diameter

σg geometric standard deviation

A Estimated inhaled doses calculated for a 30-minute exposure period using mean data (aerosol concentration and body weight) and a body-weight derived estimate of respired minute volume (Alexander *et al.*, 2008).

Statistical analysis of GSK-677 and GSK-361 lung concentrations (Figure 3.25) measured by HPLC-MS/MS or estimated from minute volume indicated that measured values were significantly lower ( $p < 0.01$ ) than estimated values. There were no significant differences between estimates derived from measured MV or body weight-derived estimates (eRMV), which was consistent with the change in procedure allowing rats to settle in the plethysmographs for approximately 15 minutes prior to the start of aerosol administration.

### Design 3: drug-lung concentrations

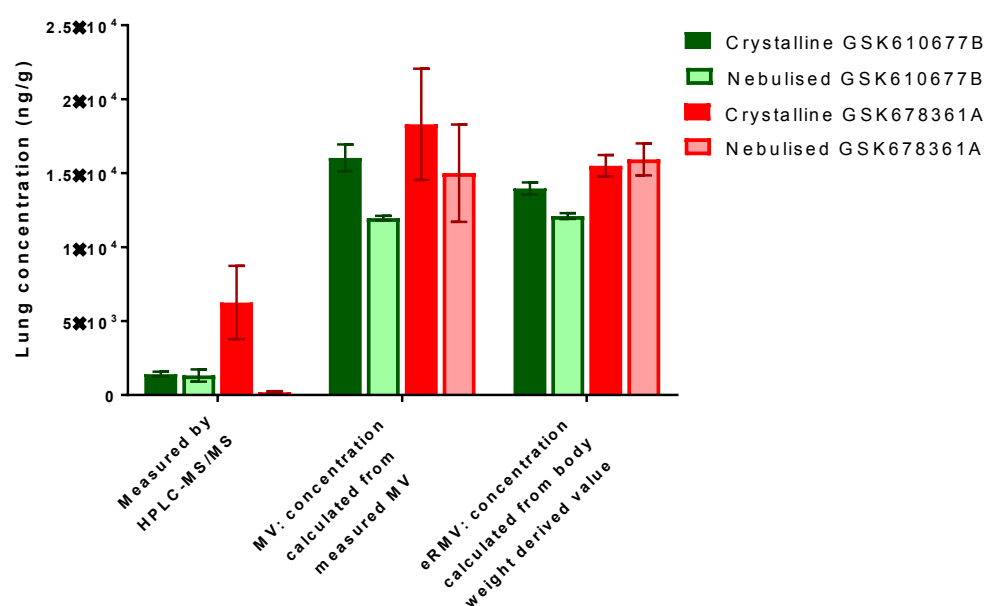


**Figure 3.25: Measured and predicted lung concentrations in rats after a single inhaled dose of GSK-677 or GSK-361.** Mean data with standard deviations ( $n=3$ ) are shown for drug concentrations in lung homogenate (analysis by HPLC-MS/MS) and estimated from the measured minute volume (MV) and body weight-derived estimate (eRMV). Statistical analysis (MANOVA with post hoc analysis using Tukey's honestly significant difference test (Abdi and Williams, 2010[B]);  $n=6$  with pooling of data) indicated significant differences between lung concentrations measured by HPLC-MS/MS and those estimated from MV or eRMV ( $p < 0.01$ ), with no significant difference between MV or eRMV-derived values. Lung concentrations after exposure to crystalline or nebulised aerosol forms were also significantly different ( $p < 0.01$ ). There was no significant difference between GSK-361 or GSK-677.

The persistence of GSK-899 in lung tissue up to 24 hours post exposure and comparatively fast reduction in drug-lung concentrations of GSK-677 or GSK-361 post exposure were described in Chapter 2

(Section 2.6.3.2). The discrepancy between lung concentrations of GSK-677 or GSK-361 and the higher estimates based on MV are attributable to the kinetics of dissolution/absorption and systemic distribution of the analyte during exposure (30 minutes) and the off-dose period before isolation of lungs (approximately 20 minutes).

Mean measured lung concentrations of GSK-899 were approximately 20% higher than the estimated lung deposited doses derived from measured MV. Since no appreciable change in GSK-899 concentration is evident immediately post exposure, these data indicate that approximately 12% of GSK-899 administered as an aerosol of mass median aerodynamic diameter (MMAD) 2  $\mu\text{m}$  was deposited in the lungs of exposed rats (Figure 3.26).

### Design 2: drug-lung concentrations

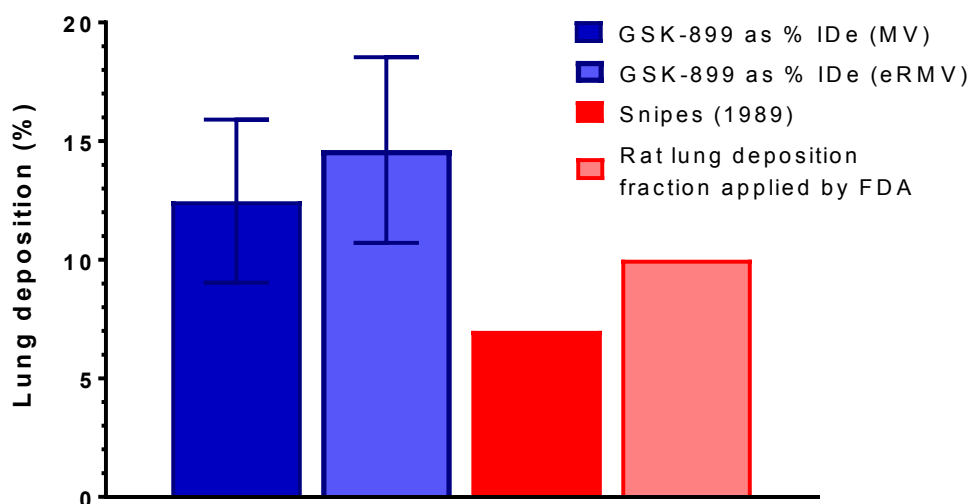


**Figure 3.26:** Measured lung concentrations of GSK-899 as a proportion of the estimated inhaled dose (IDe) in rats after a single exposure. Lung deposition (n=32) was calculated as the measured mass of GSK-899 in lung (by HPLC-MS/MS) as a percentage of the lung dose predicted from the inhaled dose calculated from measured minute volume (MV) or body weight-derived estimate (eRMV). Rat lung deposition fractions reported by Snipes (1989) and applied by US-FDA (Lewis and McKeivitt, 2013, Owen, 2013, Forbes *et al.*, 2011, Jones and Baldrick, 2013) are also shown.

### *Chapter Three*

This is slightly higher than the pulmonary deposition value of 7% published by Snipes (1989) and similar to the deposition factor of 10% in rats applied by the US Food and Drug Administration when evaluating regulatory submissions for the clinical approval of inhaled drugs (Lewis and McKeivitt, 2013, Owen, 2013, Forbes *et al.*, 2011, Jones and Baldrick, 2013).

### 3.4. Conclusion

This work illustrated the importance of considering the experimental design and procedural conduct for acclimatising animals to restraint procedures and data acquisition by head-out plethysmography, a technique used for assessing lung function and estimating doses in non-clinical inhalation studies.

The plethysmography data indicated 15 minutes was sufficient for rats to achieve a settled state, in terms of BF or MV measurements with little change in these parameters thereafter. On the basis of these data, which were interpreted as a surrogate indicator of activity or stress (Williams *et al.*, 1988, Barone *et al.*, 1990), procedures were harmonised for routine non-clinical studies performed by the sponsor, with rodents acclimatised to restraint tubes for 30 minutes on each of two consecutive days preceding the first dose, irrespective of the dose route (typically intravenous infusion or inhalation exposure) or the duration of treatment (single or repeated administrations). This represented refinement of procedures on two fronts:

- Firstly, by considerably reducing the duration and frequency of pre-treatment tube acclimatisation applied to rats before the first dose. The need to subject rats to progressively longer restraint periods up to four hours to match the intravenous infusion period was subsequently proven unnecessary (personal observation of unpublished data).
- Secondly, by extending the tube restraint period to 30 minutes and applying this on each of two pre-treatment occasions to ensure rats achieved a settled state before being returned to their holding cages.

Key conclusions of work described in this chapter were:

- Two days of acclimatisation of rats (or reacclimatisation after a reduced level of restraint) to plethysmographs was sufficient to achieve parity of mean MV (measured) with mean eRMV (body

weight-derived estimate) when rats were allowed to settle for 15 minutes before initiating aerosol generation.

- Changes in MV were in line with the normal body weight gain of rats over a 28-day period supporting use of an algorithm for estimating the inhaled dose of a drug in healthy rats. However, the relationship between MV and body weight following an adverse effect of treatment, *i.e.* weight loss or reduced gain due to toxicity, is uncertain.
- There were no differences in BF or MV for rats illuminated by red or white light during acclimatisation and inhalation exposure procedures.
- MV measurements were more variable than corresponding body weight-derived estimates (eRMV), especially when animals were exposed to an aerosol for the first time.
- The lung deposited fraction of GSK-899 (12%) was consistent with the fraction applied by US-FDA regulators (10%) for drug safety assessment (Lewis and McKeivitt, 2013, Owen, 2013, Forbes *et al.*, 2011, Jones and Baldrick, 2013).

Although rats were successfully acclimatised for a 60-minute exposure period over two days, experiments requiring detection of subtle changes in lung function (*e.g.* a dose response in respiratory pharmacology) may require a modified and possibly more prolonged approach for acclimatisation. An ethical desire to minimise the degree of restraint applied to animals during repeated inhalation exposure studies must be weighed against a potentially deleterious effect on the precision and accuracy of lung function measurements.

These conclusions are limited by the small group sizes, which were nevertheless typical of those used during non-clinical studies in early drug development. Given the desire and ethical obligation to minimise the number of animals used in non-clinical research, measurement of lung function may therefore provide a tool for understanding anomalies

in quantitative lung doses and potential effects on inhaled dosimetry associated with the properties of a test substance, but also for refining procedures for inhaled administration of test articles or other procedures requiring tube restraint.



# **CHAPTER FOUR**

**Suppression of  
lipopolysaccharide-induced acute  
lung inflammation in rats by single  
prophylactic doses of p38 mitogen  
activated protein kinase inhibitors**

## 4.1. Introduction

Signalling pathways activated during acute lung inflammation are also activated by acute lung injury and acute respiratory distress syndrome (Figure 4.1), a diffuse but critical lung injury resulting in 40% mortality for affected patients (Matthay and Zemans, 2011). p38 mitogen activated protein kinase (MAPK) performs a central regulatory function in the synthesis and modulation of proinflammatory mediators. p38 $\alpha$  MAPK is expressed in the cytoplasm and nucleus of cells (Cuenda and Rousseau, 2007) in the airway smooth muscle, respiratory epithelium and immune system (Williams *et al.*, 2008, Mayer and Callahan, 2006), thus representing a ubiquitous target in the respiratory tract for suppressed expression of cytokines, chemokines and growth factors.

Bacterial lipopolysaccharide (LPS) provokes a potent immunological response resulting in local or systemic inflammation (Van Helden *et al.*, 1997, Ulich *et al.*, 1994). In the late 1980s, a series of small molecules were found to inhibit LPS-induced production of interleukin-1 (IL-1) and tumour necrosis factor (TNF) in human monocytes, and were subsequently shown to selectively inhibit p38 MAPK (Lee *et al.*, 1999). Beardmore *et al.* (2005) demonstrated normal LPS-induced cytokine release in a p38 $\beta$  MAPK knockout murine model, indicating the p38 $\alpha$  MAPK isoform was a major component of the pathway and hence a principal target for inhibition (Mayer and Callahan, 2006).

Bronchoalveolar lavage (flushing of lungs with isotonic fluid), was developed in the early 1980s as a method for investigating pulmonary toxicity. The application of this technique is based on the premise that exposure of the respiratory epithelium to inhaled toxicants will result in the release of markers including cellular contents (such as enzymes or total protein) from injured cells, inflammatory mediators and subsequent recruitment of inflammatory cells to the epithelial-air surface and associated fluid.

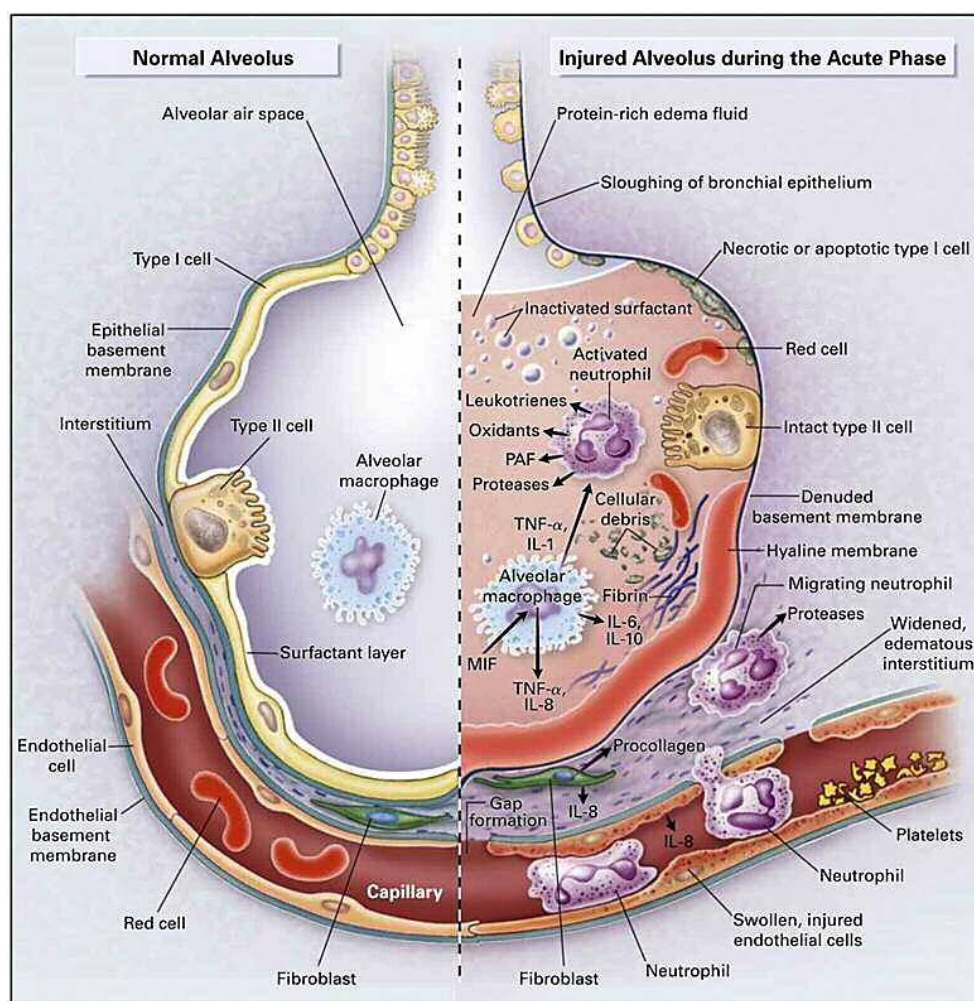


**Figure 4.1:** Normal alveolus (left) and injured alveolus in the acute phase of acute lung injury and acute respiratory distress syndrome (right). Neutrophils adhere to the injured capillary endothelium and migrate through the interstitium into the air space filled with protein-rich oedema fluid. Alveolar macrophages secrete cytokines (IL-1, 6, 8 and 10) and TNF $\alpha$  that locally stimulate chemotaxis and activate neutrophils, which release proinflammatory molecules (oxidants, proteases, leukotrienes and platelet-activating factor (PAF)). Anti-inflammatory mediators in the alveolus include IL-1 receptor antagonist, anti-IL-8 autoantibodies, soluble TNF receptor and cytokines (such as IL-10 and IL-11). With the syndrome (diffuse, critical lung injury), sloughing of bronchial and alveolar epithelial cells also occurs and protein-rich hyaline membranes form on the basement membrane; IL-1 stimulates production of extracellular matrix by fibroblasts. The influx of protein-rich oedema fluid into the alveolus leads to inactivation of surfactant. *Matthay and Zemans (2011) reproduced with permission of Annual Reviews, USA.*

These inflammatory markers in the epithelial lung fluid or lumen can be sampled for analysis by flushing the lung with an isotonic salt solution (Henderson, 1984, Henderson *et al.*, 1985); an influx of neutrophils is the most sensitive indicator of inflammation (Henderson, 2005). Conversely, a reduction or suppression of these markers in animals with prophylactic treatment of a drug provides a non-clinical model for assessing the efficacy of a drug (Underwood *et al.*, 2000, Mayer and Callahan, 2006, Haddad *et al.*, 2001).

Efficacy models used for the screening of drugs need to be consistent; the biological response of animals to LPS and its suppression by a prophylactic dose of a drug should both be reproducible, without high inter-animal variability and not susceptible to temporal or genetic drift. The nature of the bronchoalveolar lavage (BAL) sampling process (flushing of lungs with saline) has the potential to exacerbate experimental error due to partial recovery of the lavageate and the efficiency of harvesting cells in the airways and alveoli. Ettensohn *et al.* (1988) reported the proportion of lavageate recovered from human lung with each sample was generally consistent ( $64.8 \pm 9.8\%$ , with 3/16 subjects presenting high variability) but considerable variability was evident in leukocyte counts between individuals (inter-subject variability) and between successive lavages recovered from each subject (intra-subject variability). Work described by Hoshino *et al.* (1999) indicated no significant difference in the proportion of lavageate recovered for groups of rats (variability of leukocyte counts not specified) but unpublished data (GSK) suggested a potential for variability in rat leukocyte counts and pro-inflammatory mediators harvested in bronchoalveolar lavage fluid (BALF).

Biomarkers for quantifying acute lung inflammation and the application of alternative techniques may present opportunities for adapting and developing non-clinical efficacy models. Quantification of inflammatory cell infiltration cannot be done easily using routine histological sections and stains; the phenotype of inflammatory cells must be determined and

representative areas of lung tissue cannot be surveyed and readily quantified without automation. Cell counting could be performed following digestion of lung tissue with collagenase but this technique is also labour intensive and time consuming. Quantification of cell infiltration by gamma-counting leukocytes (radiolabelled *ex vivo*) also carries the risk that *in vitro* manipulation of cells (purification and radiolabelling) may activate cells and compromise the experiment (Schneider *et al.*, 1997). Schneider and Issekutz (1996) described a method for assaying the activity of myeloperoxidase (MPO; a biomarker for neutrophils) in extracts of lung tissue sampled from Brown Norway rats challenged with ovalbumin. Sugiyama *et al.* (2001) described the immunostaining of MPO in histological sections of human arteries. Image analysis has potential applications for the automation and standardisation of high throughput screening of cell morphology or phenotypes in samples (such as tissue biopsies, cell swabs or blood) for the diagnosis of diseases (Loukas *et al.*, 2003, Ross *et al.*, 2006), although some reviews suggest further research is required before automated image analysis systems can be recommended for healthcare screening (Willis *et al.*, 2005). Nevertheless, image analysis could potentially facilitate quantification of LPS-induced inflammation in rat lung sections provided neutrophils can be distinguished from the lung tissue and other cells in section.

Factors influencing the biological response of a subject to an inhaled drug include the achieved dose, location of the pharmacological target receptor within the respiratory tract and cross-reactivity with 'off-target receptors'. Since the p38 MAPK receptor is expressed throughout the respiratory tract and in inflammatory cells migrating to the site of insult, efficacy of this pharmacological class can be investigated by determining the degree of prophylactic inhibition of the infiltration of neutrophils following a pulmonary challenge by LPS. Given the ubiquitous nature of the target, inhaled administration and/or intratracheal instillation of the

drug and LPS can be performed without the need to target a specific region of the respiratory tract.

Administration of LPS in acute lung models is often performed via intratracheal administration (Van Helden *et al.*, 1997, Ulich *et al.*, 1994, Spond *et al.*, 2004, Shanley *et al.*, 1995) and is a technique that can be performed under light anaesthesia without the technical infrastructure and engineering required to support inhalation exposure systems. Non-clinical evaluation of the efficacy of drugs is normally conducted early in drug development, when candidate drugs are initially produced in small quantities. Drugs eventually intended for inhaled administration to humans are therefore often administered to non-clinical models using a surrogate exposure route, typically intratracheal instillation. However, intratracheal instillation is not a clinical route of exposure and the pattern of particle lung deposition is different to that achieved following inhalation exposure to aerosols (Osier and Oberörster, 1997). Whilst aerosol generators have been designed to expose individual or small groups of rodents using small quantities of test article (Paul *et al.*, 2012, Gerde, 1999), intratracheal instillation is commonly used in non-clinical research.

#### **4.1.1 Aims and objectives**

Using three p38 MAPK inhibitors of differing physicochemical properties, the experimental aims of this chapter are to:

- Determine the utility of biomarkers of inflammation in BALF (neutrophils and TNF $\alpha$ ) or image analysis (neutrophil infiltration evident in lung sections) to evaluate a dose response for the prophylactic inhibition of LPS-induced acute lung inflammation.
- For each of three p38 MAPK inhibitors, determine the median effective dose (ED<sub>50</sub>) in rats for prophylactic inhibition of LPS-induced acute lung inflammation.
- Determine the systemic and/or lung exposure of each p38 MAPK inhibitor in rats after a single inhalation exposure to contextualise

the dose responses for inhibition of LPS-induced acute lung inflammation.

By comparing the data generated following administration of the p38 MAPK inhibitors as nebulised solutions or dry powder aerosols, the following hypotheses will be tested:

- Changes in the presentation of a drug to rats may affect lung exposure and consequently the drug concentration at the pharmacological target, resulting in modulation of dose response for efficacy (ED<sub>50</sub>).
- Differences in physicochemical properties may affect the compartmentalisation of a drug in cells or fluid compartments within the respiratory tract, affecting the drug concentration at the pharmacological target, influencing the dose response for efficacy (ED<sub>50</sub>).

Although the systemic and lung exposure of drugs are known to change for different formulations, less has been published about the potential implications for efficacy. It is anticipated that results of these investigations will permit ranking of p38 MAPK inhibitors and/or aerosol forms for their relative efficacy. Identification of potential limitations or opportunities for modulating efficacy may also have implications for experimental design in early non-clinical development of inhaled drugs.

## 4.2. Materials and methods

### 4.2.1. Test articles

The p38 MAPK inhibitors were supplied by GSK as micronised crystals and stored at ambient temperature, protected from light and moisture. (Table 4.1).

**Table 4.1: Purity of crystalline p38 MAPK inhibitors used for inhalation exposure of rats**

Test article	Salt form	Purity	<i>In vivo</i> study number
GSK258899B	mesylate	95.4%	R30820N R31763N
GSK610677B	hydrochloride	98.5%	R31400N
GSK678361A	parent	99.7%	R31675N

Two batches of amorphous GSK-899 were produced by spray drying a saturated solution of GSK-899 (prepared from micronised crystals) in methanol. The amorphous state of the resultant material was confirmed by X-ray powder diffraction analysis (XRPD; Chapter 2, Section 2.3.2). One batch (amorphous-2) was used for single exposure experiments described in Chapter 2. A larger batch (amorphous-1) was supplied for repeat exposure experiments described in Chapter 5 and was of slightly larger particle size (Table 4.2). Both batches were selected for experiments described in this chapter to investigate the potential influence of particle size on achieved lung dose and efficacy.

**Table 4.2: Summary of aerosol particle sizes for amorphous GSK-899**

Test article	Batch identification	Aerosol concentration (µg/L)	Particle size		<i>In vivo</i> study number
			MMAD (µm)	σg	
GSK-899	Amorphous-2	24.4	2.7	2.1	R30573N (Chapter 2)
	Amorphous-1	0.592	3.9	2.0	R30662N (Chapter 5)
		26.9	4.2	1.9	
		380	3.7	2.3	

#### Notes

MMAD mass median aerodynamic diameter  
 σg geometric standard deviation

#### 4.2.2. Investigating efficacy and exposure of inhaled p38 MAPK inhibitors in rats

For investigating the efficacy of p38 MAPK inhibitors in the respiratory tract of rats and to put potential findings in context with concomitant pharmacokinetics, groups of rats were administered a single prophylactic 'dose' of the test aerosol, by snout-only inhalation exposure. Rats were then challenged with LPS and evaluated for inhibition of acute lung inflammation (Figure 4.2). Additional animals (satellite groups) were concurrently administered an inhaled dose of the p38 MAPK inhibitor and sampled for plasma and lung tissue for HPLC-MS/MS analysis of the drug. Blood and tissue samples were thus obtained for three key investigations as follows:

- Assessment of biomarkers for the inflammatory cell infiltration in lungs of rats challenged with LPS, with reference to a vehicle control for the drug (n=6 rats/treatment).
- Drug concentration measured in rat plasma sampled post exposure (n=3 rats/timepoint).
- Drug concentrations in lungs sampled post exposure (n=3 rats/timepoint).

Following optimisation of the LPS challenge (Appendix 1), four large experiments were performed to determine the median effective dose (ED<sub>50</sub>) of each MAPK inhibitor in each aerosol form. Experimental Design A, the first of four principal experiments, was based on a protocol developed and validated at GSK (unpublished data) in which neutrophils are evaluated in BALF four hours after a single challenge with LPS (2 µg/rat); other research facilities also implement a four-hour interval between the LPS challenge and sampling of BALF for analysis of cytokines and/or neutrophils (CRL, 2017, Eutamene *et al.*, 2005). The design evolved from one experiment to the next, mainly simplifying technical logistics for experimental conduct (data comparisons were not compromised). Additional parameters were considered following review

of the dose response data for the inflammatory responses. The rationale for dose selections and experimental design features are summarised with methodological outcomes for each experiment (Sections 4.2.2.1 to 4.2.2.4). Details of the biomarkers for inflammation and associated methodology are described in Section 4.2.6.

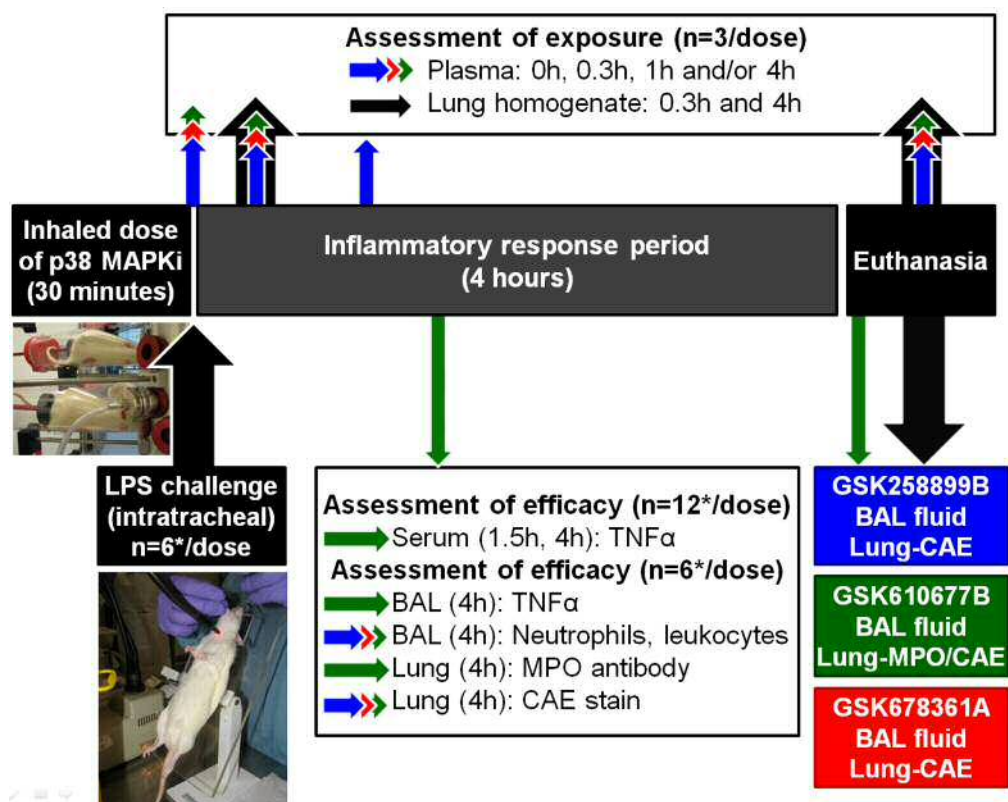
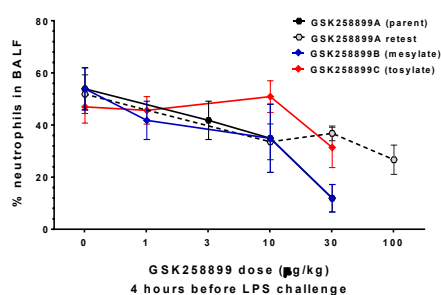


**Figure 4.2:** Study design used for investigating inhibition of lipopolysaccharide induced lung inflammation after a single dose of an inhaled p38 MAPK inhibitor. Rats (n=6/dose) inhaled an aerosol of the p38 MAPK inhibitor (dry powder or aqueous formulations) or vehicle (control) for 30 minutes and were immediately challenged by intratracheal instillation of lipopolysaccharide (LPS); a 'negative' control group for baseline data was instilled with phosphate buffered saline. Four hours post challenge, rats were euthanized and the lungs removed to evaluate markers for inflammation: histological staining of lung sections for myeloperoxidase (MPO) and/or chloroacetate esterase (CAE), or bronchoalveolar lavage (BAL) using saline to facilitate measurement of TNFα (GSK-677 study only) and neutrophils in lung. Serum was sampled 1.5 and 4 hours after administration of GSK-677 and LPS for analysis of TNFα (\* n=2x 6/dose; lung histology and lavage groups). Additional rats (n=3/dose) were sampled immediately post exposure (all p38 MAPK inhibitors) and after four hours (GSK-899 only) for analysis of drug concentrations in plasma and lung homogenate.

#### 4.2.2.1. Efficacy of GSK-899 determined using neutrophil counts in BALF (Design A)

This study was performed in two phases. Firstly, blends of GSK-899 micronised crystals or amorphous powders ('batches' 1 and 2) in lactose were administered a target dose of 30 µg/kg. This dose was based on unpublished data (Figure 4.3) indicating an ED<sub>50</sub> of 3 µg/kg GSK-899 when administered as an aqueous suspension by intratracheal instillation, adjusted to allow for 10% deposition of an aerosol in rat lungs (Forbes *et al.*, 2011, Jones and Baldrick, 2013, Owen, 2013).

##### 4.3A: dry powder



##### 4.3B: wet suspension

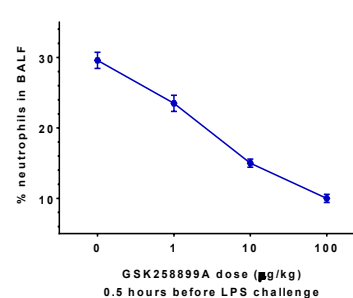


**Figure 4.3:** Inhibition of lipopolysaccharide induced lung inflammation in rats after prophylactic administration of GSK-899 (unpublished data). Rats were administered micronised GSK-899 by intratracheal instillation before whole body inhalation exposure to a nebulised aerosol of lipopolysaccharide (LPS; 15 minutes). Lungs were lavaged four hours after LPS challenge and the harvested neutrophils counted (expressed as a percentage of total cell count). **4.3A:** dry powder formulations dosed four hours before LPS challenge. **4.3B:** aqueous suspension of GSK-889A (parent) dosed 30 minutes before LPS challenge. A median effective dose (ED<sub>50</sub>) of 3 µg/kg was cited (data circa 2004; method of calculation not stated).

Subsequently, one dose for each particle form of GSK-899 was selected following review of the neutrophil counts in BALF for the previously administered dose. Nebulised doses of GSK-899 were administered in a second experimental phase with a concurrent vehicle control; doses were selected with reference to neutrophil counts for rats administered dry powder formulations. An additional dose (maximum practicable for solubility) was subsequently administered with a concurrent control.

#### Methodological outcomes of Design A

Although progressive selection of doses for each aerosol form was expected to achieve a dose range that encompassed the ED<sub>50</sub>, an

observed day to day variability in the neutrophil cell counts in BALF sampled from the LPS-dosed control animals complicated data analysis (dose response expressed relative to the concurrent LPS controls). Further experiments would administer a range of doses for one aerosol form on a given day, with duplicate cohorts (if necessary) and alternative aerosol forms administered on separate days.

#### **4.2.2.2. Evaluation of endpoints used to determine inhibition of lung inflammation by GSK-677 (Design B)**

Given the temporal variability in neutrophil counts noted in BALF samples during Design A, additional endpoints were evaluated concurrently with the BAL neutrophil count following LPS challenge as follows:

- Leukocytes and neutrophils in BALF
- TNF $\alpha$  in serum and BALF
- Image analysis of biomarkers for neutrophils in lung sections: myeloperoxidase (MPO) and chloroacetate esterase (CAE).

Inhaled target doses (1, 10, 100 and 1000  $\mu$ g/kg) were selected as a logarithmic progression based on unpublished data (Figure 4.4) indicating an ED<sub>50</sub> of 5  $\mu$ g/kg GSK-677 when administered as an aqueous suspension by intratracheal instillation. The selected doses were adjusted for 10% lung deposition in rats (Forbes *et al.*, 2011, Jones and Baldrick, 2013, Owen, 2013) and the dose range was anticipated to encompass the inhaled ED<sub>50</sub>.

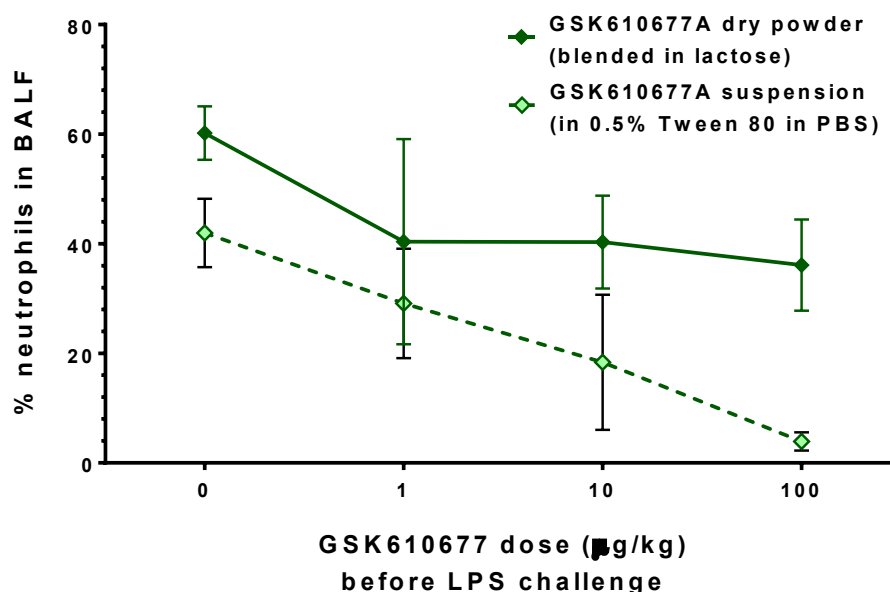


**Figure 4.4:** Inhibition of lipopolysaccharide induced inflammation in rat lungs after prophylactic administration of GSK-677 (unpublished data). Rats were dosed micronised GSK-677 in lactose or aqueous suspension (drug in 0.5% Tween 80 in phosphate buffered saline) by intratracheal instillation. Animals were challenged with a nebulised aerosol of lipopolysaccharide (LPS; 15 minutes; whole body inhalation exposure) four hours after instillation of dry powder formulations or 30 minutes after instillation of aqueous suspensions. Lungs were lavaged four hours post LPS-challenge and harvested neutrophils counted (expressed as a percentage of total cell count); linear regression analysis of the dose response was used to determine a median effective dose (ED<sub>50</sub>) of 5 µg/kg as aqueous suspension.

#### Methodological outcomes of Design B

TNFα concentrations in serum and BALF were more variable than for neutrophils in BALF. Image analysis of rat lung sections indicated MPO lacked the specificity for neutrophils required to assess LPS-induced inflammation in the non-clinical model. Further experiments would evaluate neutrophils in BALF (Design D) and/or lung image analysis of CAE-stained sections (Designs C and D).

#### **4.2.2.3. Efficacy of GSK-899 measured using lung image analysis (Design C)**

Inhaled target doses (3, 30, 300 and 1000 µg/kg) were selected as a logarithmic progression anticipated to encompass the ED<sub>50</sub>. Experimental design was standardized for each of the aerosol forms based on results for Design A (Figures 4.16 to 4.18). This experiment was performed to evaluate inhibition of LPS-induced acute lung inflammation in rats by GSK-899 using image analysis of CAE-stained lung sections.

#### **4.2.2.4. Efficacy of GSK-361 using neutrophil counts in BALF and lung image analysis (Design D)**

Inhaled target doses (3, 30, 300 and 1000 µg/kg) were selected as a logarithmic progression in line with Design C. Unpublished data (Table 4.3) indicated *in vitro* potency for inhibition of p38 MAPK was similar for GSK-899, GSK-677 and GSK-361. This experiment was performed to evaluate inhibition of LPS-induced acute lung inflammation in rats by GSK-361, as determined by neutrophil counts in BALF and image analysis of CAE-stained lung sections. In addition, histology sections of lungs subjected to BAL sampling were prepared for image analysis to assess the extent to which the BAL sampling procedure depleted neutrophils from the lungs.

#### Methodological outcomes of Designs C and D

A series of artefacts were observed during preparation of lung sections that compromised image analysis; the aetiology of the artefacts, which were not evident in Design B, were investigated (Appendix 2). Although methodology was modified and lung sections were successfully scanned, the significant delays prevented completion of image analysis for the assessment of lung inflammation at the time of thesis submission.

**Table 4.3: *In vitro* binding and potency of p38 MAPK inhibitors**

p38 MAPK isoform	Parameter (pKi)	GSK-899	GSK-677	GSK-361
p38 $\alpha$	Binding	8.8 $\pm$ 0.2	8.6 $\pm$ 0.1	8.6 $\pm$ 0.2
	Inhibition	8.9 $\pm$ 0.2	8.3 $\pm$ 0.2	8.8 $\pm$ 0.2
	Competition	8.7	pKi = 8.7	pKi = 8.7
	Reversibility	-	pKi' = 8.1	pKi' = 8.1
		NS <sup>A</sup>	NS <sup>A</sup>	"rapid"
p38 $\beta$	Binding	8.2	NS	NS
	Inhibition	8.3 $\pm$ 0.3	7.8	7.4
	Competition	8.7	NS	NS
	Reversibility	NS	NS	NS
Comments	p38 $\gamma$ and p38 $\delta$	p38 $\alpha$ 400-fold more potent	p38 $\alpha$ >2000-fold more potent	p38 $\alpha$ 1000-fold more potent

**Notes**

Ki dissociation constant for inhibitor binding

Ki' dissociation constant for inhibitor binding to a site distinct from the substrate binding site

NS not stated or determined

A no significant return in enzymatic activity observed

**4.2.3. Test system and animal husbandry**

Male Crl:WI(Han) rats (Charles River UK Ltd, Margate, Kent) were randomly allocated to groups and accommodated under standard laboratory conditions (Home Office, 2014) with access to food and water as described in Chapter 2 (Section 2.2.4.1). Rats were identified by a number written in indelible ink on the tail.

Rats were accommodated for at least five days before undertaking the first licensed procedure (tube restraint) and were approximately 10 weeks old on the day of aerosol administration (Day 1).

Clinical observations and body weight measurements were maintained for all animals to ensure their general wellbeing during the experiment and to facilitate key procedures or investigations such as dosing.

**4.2.4. Aerosol generation of p38 MAPK inhibitors and inhalation exposure of rats**

Groups of rats were administered an aerosol of the p38 MAPK inhibitor for 30 minutes by snout-only inhalation exposure. Aerosols were

generated from dry powder formulations or aqueous solutions and directed into the top of the snout-only inhalation exposure chamber as described in Chapter 2 (Section 2.2.5). Target aerosol concentrations (Tables 4.4 and 4.6) for the exposure of animals were calculated from the required doses using Equation 3 (Chapter 2, Section 2.2.5).

#### 4.2.4.1. Dry powder formulations of p38 MAPK inhibitors

Aliquots of dry powder formulations used for prophylactic exposure of rats to crystalline p38 MAPK inhibitors or amorphous GSK-899 were packed into the dust feed canisters (Table 4.4) using the method described in Chapter 2 (Section 2.2.5.1).

**Table 4.4: Dry powder formulations of p38 MAPK inhibitors, canister volumes, target doses and aerosol concentrations for exposure of rats**

Study number	Test article	Target dose (µg/kg)	Test article in lactose (% w/w)	Aerosol generator canister size (cm <sup>3</sup> )	Target aerosol concentration (µg/L) <sup>A</sup>
R30820N	GSK-899 (crystalline)	3	0.1%	5	0.14
		30	0.1%	5	1.4
		300	1%	5	14
		1000	1%	40	45
	GSK-899 (amorphous-1)	3	0.5%	1.3	0.14
		30	0.5%	1.3	1.4
		300	5%	5	14
		1000	5%	40	45
R30820N	GSK-899 (amorphous-2)	0.3	0.4%	1.3	0.014
		3	0.4%	5	0.14
		30	0.4%	5	1.4
		300	4%	5	14
R31763N	GSK-899 (crystalline)	3	0.05%	5	0.15
		30	1%	5	1.5
		300	1%	5	15
		1000	5%	5	50
	GSK-899 (amorphous-1)	3	0.05%	5	0.15
		30	0.5%	5	1.5
		300	5%	5	15
		1000	5%	5	50
	GSK-899 (amorphous-2)	3	0.08%	5	0.15
		30	0.08%	5	1.5
		300	2.6%	5	15
		1000	2.6%	5	50

Study number	Test article	Target dose (µg/kg)	Test article in lactose (% w/w)	Aerosol generator canister size (cm <sup>3</sup> )	Target aerosol concentration (µg/L) <sup>A</sup>
R31400N	GSK-677 (crystalline)	1	0.01%	5	0.047
		10	0.1%	5	0.47
		100	1%	5	4.7
		1000	10%	5	47
R31765N	GSK-361 (crystalline)	3	0.05%	5	0.15
		30	1%	5	1.5
		300	1%	5	15
		1000	5%	5	50

**Notes**

A Calculation of target aerosol concentration: R30820N assumed body weight of 240g; R31763N, R31400N and R31765N assumed body weight of 350g

**4.2.4.2. Liquid formulations of p38 MAPK inhibitors**

For nebulisation of aqueous solutions, each p38 MAPK inhibitor was dissolved in the vehicle (Table 4.5) to prepare concentrations anticipated to achieve target aerosol concentrations and inhaled doses (Table 4.6). Methods of preparing solutions are stated in Chapter 2 (Section 2.2.5.3).

**Table 4.5: Vehicles used for nebulisation of p38 MAPK inhibitors and repeated inhalation exposure of rats**

Test article	Study No.	Vehicle for nebulisation
GSK-899	R30820N	3% (v/v) Solutol HS 15 in 10% (w/v) aqueous 2-hydroxypropyl-β-cyclodextrin
	R31763N	3% (v/v) Solutol HS 15 in 0.9% (w/v) aqueous sodium chloride (pH 5.9)
GSK-677	R31400N	3% (v/v) Solutol HS 15 in 0.9% (w/v) aqueous sodium chloride (pH 5.9)
GSK-361	R31765N	20:20:60 (v/v/v) Solutol HS 15, ethanol and 60 mM phosphate buffer (pH 7)

**Table 4.6: Formulation concentrations, target doses and aerosol concentrations for exposure of rats to p38 MAPK inhibitors**

Test article	Study number	Target dose (µg/kg)	Concentration in vehicle (mg/mL)	Number of nebulisers per system	Target aerosol concentration (µg/L)
GSK-899	R30820N	3	0.01	1	0.14
		30	0.15	1	1.4
		300	2.0	1	14
		MP	3.0	1	MP
	R31763N	3	0.025	1	0.15
		30	0.25	1	1.5
		300	1.5	1	15
		1000	4.0	2	50
GSK-677	R31400N	1	0.0049	1	0.047
		10	0.044	1	0.47
		100	0.40	1	4.7
		1000	4.0	1	47
GSK-361	R31765N	3	0.027	1	0.15
		30	0.15	1	1.5
		300	2.0	1	15
		1000	2.0	2	50

**Notes**

MP Maximum practicable dose based on limited solubility of GSK-899 in vehicle

Solutol HS 15 and 2-hydroxypropyl-β-cyclodextrin or ethanol were used to solubilise p38 MAPK inhibitors of low solubility (GSK-899 and GSK-361). Solutol HS 15 was formulated with GSK-677 for exposure of rats to nebulised GSK-899 or GSK-677 for comparison of the efficacy for these compounds. Potential implications for the enhanced absorption of p38 MAPK inhibitors were discussed in Chapter 2 (Section 2.2.5.3) and inclusion of these reagents in the vehicle does not undermine the fundamental hypothesis that changing the aerosol form of a drug changes the kinetics of exposure and concomitant efficacy.

Each experiment included a group of control rats that inhaled the vehicle of the p38 MAPK inhibitor (30 minutes) and was then challenged by intratracheal instillation of phosphate buffered saline (PBS; vehicle for LPS). Neutrophil counts in BALF for PBS-control s were approximately zero, confirming the nebulised vehicles did not cause inflammation.

#### **4.2.4.3. Aerosol Generation and formulation details**

Groups of rats were administered an aerosol of the p38 MAPK inhibitor, by snout-only inhalation exposure, as a dry powder aerosol or nebulised solution (Chapter 2, Sections 2.2.5.2 and 2.2.5.4 respectively).

Generally, a single nebuliser of nominal airflow 6 L/min was used to disperse each solution at the target aerosol concentration; a chamber exhaust of 16 L/min was applied to vent the test atmosphere. For the highest doses of GSK-899 and GSK-361 at the highest dose (studies R31763N and R31765N), dual nebulisers (6 L/min/nebuliser) were used to disperse the formulations and mitigate against limited solubility of the test article in its vehicle to achieve the target aerosol concentration.

#### **4.2.4.4. Inhalation exposure of rats**

Animals were exposed to test aerosols using the apparatus and methods described in Chapter 2 (Section 2.2.5.5). The chambers were operated under conditions of dynamic airflow, with a chamber exhaust flow of 16 L/min.

Rats were restrained for exposure in polycarbonate restraint tubes and attached to the chamber; the vertical position (chamber level) of each animal was documented. Unused animal exposure or sampling ports were closed using blanking plugs.

Animals were exposed to the aerosol for 30 minutes, during which time operational settings (airflow and aerosol generation) and animals were formally checked and documented at 10-minute intervals.

#### **4.2.4.5. Aerosol characterisation**

'Pre-study' aerosol characterisation work was conducted without animals to establish the operating conditions needed to generate target aerosol concentrations and to ensure aerosols were in line with particulate size criteria for exposure of rodents (OECD[412], 2009, OECD[413], 2009, US-EPA[3645], 1998). For Design A (study R30820N), selection of chamber settings was based upon time of flight analysis (ToF) of particulates using a TSI Aerosol Particle Sizer; these

data were referenced against a calibration curve of particulate concentration (ToF analysis) against GSK-899 concentration (chemical analysis by HPLC-UV) generated for each dry powder formulation.

**Table 4.7: Target aerosol concentrations and aerosol sampling volumes**

Test article	Study number	Aerosol form	Target aerosol concentration (µg/L)	Sampling volume		
				Aerosol concentration	Particle size using cascade impactor	
				Aerosol (L)	Aerosol (L)	Solvent (mL)
GSK-899	R30820N	crystalline amorphous-1	0.14	20	[120]	3
			1.4	10		3
			14	4		3
		45	6	8	3	
		amorphous-2	0.014	60	[120]	3
			0.14	10	NS	NS
	1.4		10	8	3	
	nebulised	0.14	10	[40]	5	
		1.4	10	[10]	5	
		14	6	10	5	
MP		6	8	5		
R31763N	crystalline amorphous-1	0.15	20	[120] <sup>A</sup>	5	
		1.5	8	20	5	
	amorphous-2 nebulised	15	4	8	5	
		50	2	4	5	
	GSK-677	R31400N	crystalline nebulised	0.047	40	NS
			0.47	8	[60]	5
			4.7	4	16	5
			47	4	6	5
GSK-361	R31765N	crystalline nebulised	0.15	20	[120]	5
			1.5	8	20	5
			15	4	8	5
			50	2	4	5

**Notes**

MP Maximum practicable dose based on limited solubility of GSK-899 in vehicle

NS Not sampled

[ ] Particle size distribution sampled during pre-study trials (aerosol sampling period exceeded duration of inhalation exposure)

[ ]<sup>A</sup> Aerosol sampling volume: 120 L for crystalline and amorphous-2 GSK-899 aerosols; 24L for amorphous-1 aerosol (sampling pump stalled prematurely); 72L for nebulised aerosol (sampling pump stalled prematurely)

Aerosols were sampled using predefined air sampling volumes (Table 4.7) during exposure of rats to determine the aerosol concentration and particle size distribution of p38 MAPK inhibitors as described in Chapter 2 (Section 2.2.5.6). For aerosol concentration, filter samples were taken in duplicate when practicable. An additional sample

was taken, if practicable, using a cascade impactor for determination of the particle size distribution; cascade impactor samples were not taken during exposure of animals to the lower doses because the aerosol sampling period required to capture sufficient analyte for quantification exceed the duration of animal exposure.

#### **4.2.4.6. Calculation of the estimated inhaled dose**

Estimated inhaled doses were calculated using Equations 1 and 2 (Chapter 1, Section 1.3.4) for an exposure period of 30 minutes.

#### **4.2.5. Antigen challenge of rats**

Immediately following inhalation exposure of the p38 MAPK inhibitor or vehicle alone, groups of rats (n=6/treatment) were challenged with LPS obtained from *Escherichia coli* 0127:B8 (product number L3129; Sigma Aldrich). Additional control rats ( $\leq 6$ ) exposed to the inhalation formulation vehicle alone were challenged with phosphate buffered saline (vehicle for LPS) as a negative control for determination of baseline data.

Methodology for LPS challenge of rats was optimised (Appendix 1). LPS was instilled into the trachea as a bolus (2  $\mu\text{g}/\text{rat}$ ; 0.2 mL/rat; 10  $\mu\text{g}/\text{mL}$  LPS in phosphate buffered saline) using a Penn Century microsyringe (Figure 4.5A) with the device placed transorally under light anaesthesia; when practicable, all instillations were performed by the same operator.

Rats anaesthetised with 5% (v/v) isoflurane in oxygen (2 L/min) were held supine and angled at approximately 45°C to enable visualisation of the pharynx via a cold light source placed over the animal's throat (Figure 4.5B). A loop was placed over the upper incisors and used to hold the mouth open and maintain the rat's head in a stable position. The tongue was manipulated to aid visualisation of the vocal chords. The cannula (Penn Century microsyringe) was inserted into the mouth parallel to the hard palate and guided towards the vocal folds. When the epiglottis was deemed to be open, the cannula was directed into the trachea through the vocal folds. Once in position, the dose was

dispensed and the device carefully removed. Post challenge, rats fully recovered from anaesthesia before being returned to the holding cages.

**4.5A**



**4.5B**



**Figure 4.5: Intratracheal instillation of a solution.** **4.5A:** Penn Century microsprayer (without syringe). **4.5B:** intratracheal dosing of a rat under light anaesthesia; a cold light source was used to visualize the vocal folds to facilitate passage of the cannula into the trachea.

#### **4.2.6. Assessment of biomarkers for lung inflammation**

Design B (GSK-677): 0.6 mL of blood was sampled at 1.5 hours and 4 hours post challenge. The blood was sampled by caudal venepuncture or from the abdominal aorta under deep isoflurane anaesthesia into a BD SST Serum Microtainer and allowed to stand for at least two hours before centrifugation (5250 rpm; 3 minutes) for separation of serum.

Rats were euthanized four hours after the LPS challenge (4.5 hours after the start of aerosol generation) or post inhalation exposure to sample lungs for assessment of inflammation (Sections 4.2.6.1 or 4.2.6.2) or drug concentration (Section 4.2.7.2) respectively. Rats were euthanized by exsanguination via the abdominal aorta under isoflurane anaesthesia. Death was confirmed by cutting major blood vessels (cessation of circulation).

##### **4.2.6.1. Bronchoalveolar lavage of lungs for analysis of TNF $\alpha$ and/or cell counts (Designs A, B and D)**

The thoracic cavity was opened by excision of the sternum and the lungs removed. A cannula was inserted into the trachea and tied in place with thread. The lungs were gently lavaged with 3 $\times$  5 mL fresh ice cold 0.9% aqueous sodium chloride and the lobes gently massaged prior to

removal of each lavageate. Lavageates were pooled in a centrifuge tube for each rat and kept on ice pending analysis of TNF $\alpha$  or cell counting. BALF samples were centrifuged for five minutes at 1500 rpm (approximately 395 $\times$ g), at approximately 4°C with no brake. The supernatant was transferred to a separate tube for analysis of TNF $\alpha$  (Design B) or discarded (Designs A and D). The cell pellet was resuspended in 1 mL fresh ice cold 0.9% sodium chloride and transferred to a 1.5 mL eppendorf tube.

#### Cell counts (Designs A, B and D)

An aliquot of the cell suspension was counted for leukocytes using an Advia 2120 analyser and reagents supplied by Siemens Diagnostics.

A second aliquot ( $\leq$ 0.5 mL) was applied to the cytofunnel (filling port) of a Shandon Cytospin Cyto centrifuge for preparation of a cyto spin slide. Approximately  $5 \times 10^4$  cells in the cyto spin chamber were air-dried and stained with Wright-Giemsa stain (Sigma Aldrich) using a Hematek stainer; the stain includes methylene blue and azure B to stain nuclei blue/purple and eosin to stain cytoplasm pink. The cells were viewed by light microscopy and the neutrophils and leukocytes counted manually.

#### TNF $\alpha$ (Design B)

BALF supernatant or serum was aliquoted (50  $\mu$ L) into a 96-well plate. A duplicate plate was prepared as a contingency for repeat analysis. The plates were stored at -80°C or colder pending quantification of TNF $\alpha$  using the multiplex Meso Scale Discovery (MSD) protocol supplied with the kit (Plate Catalogue Number N153A41).

#### **4.2.6.2. Lung sampling and processing for image analysis**

The thoracic cavity was opened by excision of the sternum and the lungs removed, inflated with 10% buffered formalin and preserved in this fixative for at least 24 hours before further processing was performed.

After fixation, lungs were trimmed to expose areas of interest and placed into labelled cassettes according to a predefined pattern to orientate the lobes presented for examination; a total of seven sections were

organised into two cassettes to present representative sections of all lung lobes. The cassettes containing lung samples were stored in 10% buffered formalin until processed.

#### Tissue processing for preparation of slides

Tissues were processed using an automated schedule during which the tissues were immersed in a series of reagents, each for one hour. The tissues were first dehydrated by immersing the cassettes in 70% industrial methylated spirits (IMS; one cycle), 90% IMS (one cycle) and then absolute IMS (five cycles). The cassettes were immersed in xylene (three cycles). Xylene is miscible with paraffin wax and was used to “clear” the dehydrant (IMS) from the tissue. The tissues were then impregnated with molten paraffin wax maintained at  $\leq 63^{\circ}\text{C}$  (four cycles). For embedding, a mould base was filled with molten paraffin wax in a working area (“embedding centre”) maintained at  $60^{\circ}\text{C}$ . The trimmed tissues in a cassette were transferred to the mould and orientated in accordance with a blocking pattern with the surface of interest downwards. The mould was chilled on a cold plate, the position of the tissues adjusted if necessary, and the lid of the mould closed using the labelled cassette base. The mould was further cooled until the paraffin wax had set, and the mounted wax block removed from the mould.

#### Preparation of slides for lung image analysis

The wax blocks were mounted onto a microtome, coarse trimmed to expose the area of interest and cooled on ice. After removing any ‘coarse trimming artefacts’, sections of 3 to 5  $\mu\text{m}$  thickness were cut and floated onto warm distilled water ( $47$  to  $50^{\circ}\text{C}$ ), and picked up onto a clean glass slide pre-labelled with study, animal and block identification numbers.

Design B (MPO and CD68): sections mounted on Colormark™ Plus microscope slides were immunohistochemically labelled for MPO (product number A0398; Dako) or CD68 (product number MCA341R; Serotec). Slides were processed using an automated sequence using a Ruo Discovery Multimer V2 protocol on a Discovery Ultra instrument with associated reagents (Ventana Medical Systems; VMS) as follows: slides

warmed in oven (60°C; 8 minutes); deparaffinised in VMS solvent (65°C; 12 minutes); incubated in “CC1 Pretreatment Solution” (95°C; 52 minutes); incubated in primary antibody (MPO or CD68; 37°C; 32 minutes); “CM inhibitor” applied (8 minutes); labelled with OMap anti-Rb HRP secondary antibody (16 minutes; anti-rabbit antibody linked to horseradish peroxidase). Staining of the immunolabelled cells was developed by incubation (4 minutes; room temperature) of sections with 3,3'-diaminobenzidine, which is metabolised by HRP to produce a dark stain in the immunolabelled cells. Lung sections were counterstained with haematoxylin II, dehydrated in 70% IMS (2× 3 minutes) and cleared in xylene (3× 3 minutes). A coverslip was then applied and set using Entellan® rapid mounting medium (Sigma Aldrich). Extra sections cut from an arbitrarily selected block from the treated group were processed as an isotype negative (background labelling) control for the primary antibodies.

Designs B to D (CAE): lung sections were stained for CAE (biomarker of neutrophils) and counterstained with haematoxylin (stains cell nuclei blue) to contrast definition of the lung tissue with the neutrophils. Slides with mounted lung sections were warmed in an oven (60°C; 60 minutes) to melt the paraffin wax and then immersed in xylene, ethanol and then water (1 cycle; timings not specified) to deparaffinize the sections. Slides were rinsed in deionised water and stood in warmed deionised water (37°C) until required for further processing. Slides were fixed (30 seconds; room temperature) in a solution of formaldehyde, acetone and water (3:66:31 v/v/v) containing 7 mM citrate (catalogue number 915; Sigma Aldrich), rinsed in deionised water (2 changes) and stood in warmed deionised water (1×3 minutes; agitated at 30-second intervals). Slides were then incubated (37°C; protected from light; 15 minutes for Design B; 7 minutes for Designs C and D;) in Naphthol AS-D Chloroacetate staining solution (Product code 91C-1KT; Sigma Aldrich), rinsed in warmed deionised water (5 changes), and counterstained in 5% Harris' Haematoxylin (1× 20 seconds), rinsed in

cold running tap water (15 seconds) followed by warm water (15 seconds) to develop the blue stain. The slides were briefly rinsed in deionised water and dried in an oven at 50°C. A coverslip was then applied and set using Entellan® rapid mounting medium (Design B: catalogue number 1079610100; Sigma Aldrich) or permanent aqueous mounting medium (Designs C and D: catalogue number BUF058B; Bio-Rad).

#### Lung image analysis

Stained slides were wiped clean with tissue, loaded onto a ScanScope XT brightfield scanner (Leica, formerly Aperio) and digitalised (×40 magnification) to produce 1020 pixel-wide strips that were automatically ‘stitched together’ to form a single SVS-formatted image (ScanScope Virtual Slide). Any scans of “quality factor” less than 95% were rejected and the slide rescanned; scans passing this criterion were visually inspected to ensure no visible seams between the stitch stripes, variable illumination or poor focus were evident.

Design B (MPO/CD68 and CAE): The digitalised images (Figure 4.6A) were imported into Architect XD Tissue Studio (version 2.1.1; Definiens). Lung sections were demarcated by manually drawing around their boundaries (bronchus associated lymphoid tissue excluded) and areas of stained tissue and cells delineated (Figure 4.6B). All pixels that represented the physical lung structure (such as alveolar/bronchiolar walls, bronchi and blood vessels) were segmented into a class for ‘lung structure’ and all pixels representing lumens of alveoli and airways *etc* were segmented into a second class for ‘air spaces’. All pixels representing the brown stain (MPO or CD68-positive) or red stain (CAE-positive) were segmented by adjusting the intensity (optical density) threshold for the detection of the biomarker area. The quality of segmentation was evaluated by inspecting the accuracy of coloured overlays representing each class: yellow for biomarker; blue for nuclei; green for cytoplasm (Figures 4.6C and 4.6D). If segmentation appeared

robust, the optimised settings ('image analysis solution') were saved for batch processing all scans for the experiment.

Designs C and D (CAE): modified lung image analysis method not available at time of thesis submission.

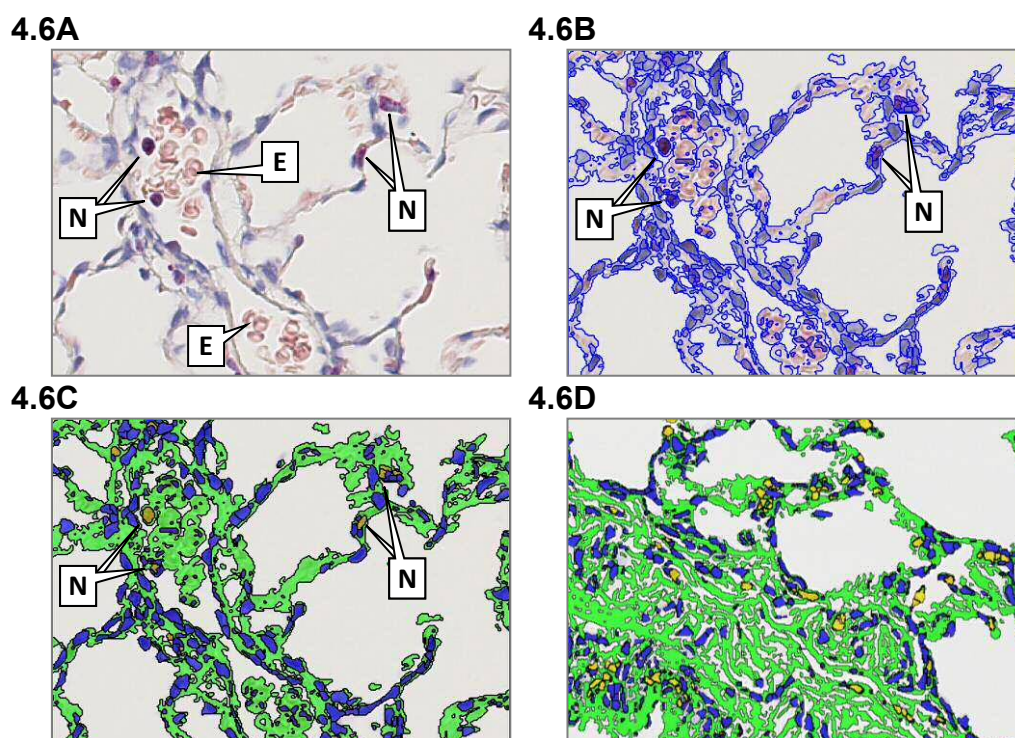


**Figure 4.6: Example of image analysis of rat lungs for biomarkers of inflammation.** Rats ( $n=6/\text{treatment}$ ) were administered lipopolysaccharide in phosphate buffered saline by intratracheal instillation ( $2 \mu\text{g}/\text{rat}$ ; bolus). Lungs were taken four hours later, fixed in 10% buffered formalin and embedded in paraffin wax. Lung sections were stained for myeloperoxidase (MPO) or chloroacetate esterase (CAE), biomarkers of neutrophils, and the lung tissue counterstained with haematoxylin and eosin. **4.6A:** lung section with neutrophils stained by CAE (N) and erythrocytes (E); cell nuclei counterstained blue by haematoxylin and cytoplasm pink by eosin. **4.6B:** the lung was demarcated (not shown) and areas of stained tissue and cells delineated. **4.6C:** colour overlays were applied to the areas of interest: CAE-stained neutrophils (yellow), nuclei (blue) and lung tissue (green). **4.6D:** another representative lung section showing CAE-stained neutrophils (yellow) distinct from lung tissue and nuclei. The ratio of CAE-stained area to the remaining tissue area is determined; air spaces are excluded.

The area of MPO or CAE-positive staining in each scan was expressed as a proportion of the surface area of the lung structure. The area of 'air spaces' was omitted from this calculation to minimise artefactual inter-animal variation due to lung inflation on the calculation of the lung

area. Since MPO was stained in both neutrophils and macrophages, the CD68-positive area was also deducted from the MPO-positive area to improve the neutrophil specificity for evaluation of this biomarker.

#### **4.2.6.3. Determination of the 50% effective dose (ED<sub>50</sub>) for inhibition of LPS-induced lung inflammation**

For each biomarker of inflammation, the baseline value (mean for PBS-challenged rats) was deducted from the datum for each animal. This value was then expressed as a percentage of the similarly adjusted mean biomarker value for LPS-challenged rats. Relative biomarker values (% of LPS control) were plotted against Log<sub>10</sub> of the estimated inhaled dose of the p38 MAPK inhibitor and a linear regression line was fitted. The regression line was then used to estimate the inhaled dose that gives a 50% response (ED<sub>50</sub>) along with the corresponding 95% confidence interval of this estimate. This analysis was conducted using SAS (version 9.3).

#### **4.2.7. Bioanalysis of p38 MAPK inhibitors in rat plasma and lung**

Groups of rats were sampled for plasma and lungs following exposure to the p38 MAPK inhibitor for HPLC-MS/MS analysis of the test article.

##### **4.2.7.1. Plasma sampling for analysis of p38 MAPK inhibitors**

Blood samples were taken from groups of rats (3/dose/timepoint) by jugular venepuncture or from the abdominal aorta under isoflurane anaesthesia for the final (terminal) sample at the following timepoints after inhalation exposure to a p38 MAPK inhibitor:

- Design A: 60 µL immediately post exposure (0.5 hours) and at 1.5 and 4.5 hours after the start of aerosol administration; blood was mixed 1:1 with sodium fluoride (10 mg/mL).
- Designs B to D: 400 µL immediately post exposure (0.5 hours) and at euthanasia (0.8 hours following the start of aerosol administration). Blood was processed for preparation of plasma.

Blood/plasma was processed for chemical analysis by HPLC-MS/MS as described in Chapter 2 (Section 2.2.5.8); samples were stored in a freezer at approximately -20°C or below prior to analysis.

GSK-899 concentrations in blood (Design A) were converted to plasma-based values using a blood:plasma ratio of 2.10 (unpublished data).

#### **4.2.7.2. Lung sampling for homogenisation and analysis of p38 MAPK inhibitors**

Groups of rats (3/dose/timepoint) were euthanized as soon as practicable after a single exposure (all p38 MAPK inhibitors) or 4.5 hours relative to the start of a single inhalation exposure (GSK-899 only; study R30820N). The lungs were taken and processed for HPLC-MS/MS analysis of p38 MAPK inhibitor in lung homogenate as described in Chapter 2 (Section 2.2.5.8).

### 4.3. Results and discussion

#### 4.3.1. Inhalation exposure of rats to p38 MAPK inhibitors

Achieved aerosol concentrations (Tables 4.8 to 4.11), and hence the estimated inhaled doses of p38 MAPK inhibitors, deviated from the respective targets but nevertheless achieved a series of doses suitable for evaluating the dose response of p38 MAPK inhibitors for inhibition of LPS-induced acute lung inflammation in rats.

**Table 4.8: Aerosol characterisation data and inhaled doses of GSK-899 in rats (single 30-minute exposure)**

Study number	Aerosol form	Formulation concentration in vehicle	Estimated inhaled dose <sup>A</sup> (µg/kg)	Mean (n=2) drug aerosol concentration (µg/L)	Particle size distribution	
					MMAD (µm)	og
R30820N	Crystalline	0.89% (w/w)	1.07	0.0499	[2.6] <sup>B</sup>	[2.5]
		0.89% (w/w)	18.4	0.846	NS	NS
		1.0% (w/w)	305	14.0	2.2	2.2
		1.0% (w/w)	533	24.1	2.0	2.5
	amorphous-1	0.50% (w/w)	2.58	0.120	[4.4] <sup>B</sup>	[1.9]
		0.50% (w/w)	12.5	0.582	[5.3] <sup>B</sup>	[1.9]
		5.0% (w/w)	210	9.65	3.8	2.3
		5.0% (w/w)	2349	106	7.2	NC <sup>C</sup>
	amorphous-2	0.082% (w/w)	0.658	0.0288 (n=1)	NS	NS
		0.082% (w/w)	3.95	0.183	NS	NS
		0.082% (w/w)	37.7	1.77	[2.0] <sup>B</sup>	[2.1]
		4.0% (w/w)	366	16.7	[2.2] <sup>B</sup>	[2.3]
		4.0% (w/w)	915	42.7	NS	NS
	Nebulised solution	0.01 mg/mL	1.28	0.0590	-	-
		[0.02 mg/mL]	-	-	[2.6] <sup>B</sup>	NC <sup>D</sup>
		0.15 mg/mL	22.7	1.05	-	-
		[0.20 mg/mL]	-	-	[2.7] <sup>B</sup>	[2.3]
		2.0 mg/mL	279	12.9	2.5	2.0
		3.0 mg/mL	845	38.1	1.8	2.1

#### Notes

MMAD mass median aerodynamic diameter

og geometric standard deviation

A Estimated inhaled doses calculated for a 30-minute exposure period using mean data (aerosol concentration and body weight) and a body-weight derived estimate of respired minute volume (Alexander *et al.*, 2008).

[ ]<sup>B</sup> Aerosol sample taken during aerosol generation trial without rats (required aerosol sampling period at 2 L/min exceeded 30-minute exposure period).

NC og not calculable

C MMAD between two largest cut-points of 6.1 and 8.2 µm

D At least 3 of 7 stages below limit of quantification (insufficient data)

NS Not sampled

Deviations from target were particularly evident for Design A (Table 4.8), in which exposure system settings were based upon time of flight analysis data for particulates (referenced against a calibration curve of particulate versus GSK-899 aerosol concentrations). For subsequent experiments (Tables 4.9 to 4.11), settings were based upon chemical analysis data measured in more extensive pre-study trials, in line with the approach used for experiments described in Chapters 2, 3 and 5. This more conservative approach achieved a greater proportion of achieved aerosol concentrations in line with the respective targets.

**Table 4.9: Aerosol characterisation data and inhaled doses of GSK-899 in rats (single 30-minute exposure)**

Study number	Aerosol form	Formulation concentration in vehicle	Estimated inhaled dose <sup>A</sup> (µg/kg)	Mean (n=2) drug aerosol concentration (µg/L)	Particle size distribution	
					MMAD (µm)	σg
R31763N	Crystalline	0.053% (w/w)	3.03	0.135	[4.0] <sup>B</sup>	[2.9]
		0.95% (w/w)	28.9	1.34	2.1	2.2
		0.95% (w/w)	244	11.3	2.7	2.2
		4.9% (w/w)	1156	53.7	2.4	2.2
	amorphous-1	0.045% (w/w)	3.01	0.135	[5.9] <sup>B</sup>	[2.0]
		0.50% (w/w)	31.5	1.48	4.2	2.0
		5.0% (w/w)	259	11.9	3.2	2.2
		5.0% (w/w)	1038	48.8	3.2	2.2
	amorphous-2	0.082% (w/w)	2.15	0.100	[3.3] <sup>B</sup>	[2.1]
		0.082% (w/w)	30.5	1.41	3.7	2.4
		2.5% (w/w)	288	13.4	2.3	2.2
		2.5% (w/w)	1171	55.1	3.0	2.1
	Nebulised solution	0.024 mg/mL	2.59	0.115	[0.9] <sup>B</sup>	NC
		0.24 mg/mL	24.3	1.12	1.1	2.5
		1.5 mg/mL	304	14.2	2.7	2.3
		3.5 mg/mL	891	42.1	4.0	2.0

**Notes**

MMAD mass median aerodynamic diameter

σg geometric standard deviation

A Estimated inhaled doses calculated for a 30-minute exposure period using mean data (aerosol concentration and body weight) and a body-weight derived estimate of respired minute volume (Alexander *et al.*, 2008).

[ ]<sup>B</sup> Aerosol sample taken during aerosol generation trial without rats (required aerosol sampling period at 2 L/min exceeded 30-minute exposure period).

NC og not calculable (3 of 7 stages below limit of quantification)

**Table 4.10: Aerosol characterisation data and inhaled doses of GSK-677 in rats (single 30-minute exposure)**

Study number	Aerosol form	Formulation concentration in vehicle	Estimated inhaled dose <sup>A</sup> (µg/kg)	Mean (n=2) drug aerosol concentration (µg/L)	Particle size distribution	
					MMAD (µm)	σg
R31400N	Crystalline	0.012% (w/w)	1.00	0.0463 (n=1)	NS	NS
			1.11	0.0513 (n=1)		
		0.11% (w/w)	8.82	0.410	[4.3] <sup>B</sup>	[2.3]
			9.66	0.447		
	1.1% (w/w)	81.6	3.76	3.9	1.9	
		306	14.3			
	11 % (w/w)	1034	48.3	3.6	2.5	
		775	35.9			
	Nebulised solution	0.0050 mg/mL	1.36	0.0638 (n=1)	NS	NS
			1.39	0.0650 (n=1)		
0.044 mg/mL		14.3	0.699	[2.6] <sup>B</sup>	[2.1]	
		13.7	0.641			
0.40 mg/mL	144	6.71	2.7	2.3		
	95.3	4.48				
3.9 mg/mL	1249	58.4	2.2	2.5		
	973	45.2				

**Notes**

MMAD mass median aerodynamic diameter

σg geometric standard deviation

NS Not sampled

A Estimated inhaled doses calculated for a 30-minute exposure period using mean data (aerosol concentration and body weight) and a body-weight derived estimate of respired minute volume (Alexander *et al.*, 2008).[ ]<sup>B</sup> Aerosol sample taken during pre-study aerosol generation trial without rats (aerosol sampling period at 2 L/min exceeded 30-minute exposure period).

Particle size distribution data were generally compliant with criteria stipulated in the contemporary guidance for testing chemicals in rodents: mass median aerodynamic diameter (MMAD) 1 to 3 µm and geometric standard deviation 1.5 to 3 (OECD[412], 2009, OECD[413], 2009, US-EPA[3645], 1998). The MMAD for aerosols of GSK-899 amorphous-1 were higher (Tables 4.8 and 4.9) but were generally in line with particle size data for aerosols administered to rats during a repeat dose study (Table 4.2). Although the anomalous MMAD (7.2 µm) determined for the amorphous-1 high dose (Table 4.8) was inconsistent with that achieved

in the subsequent experiment (Table 4.9) and during repeated administration (Table 4.2), the lung concentration data confirmed the lung deposited dose was relatively lower for rats administered 2350 µg/kg (Figure 4.16A) than 1038 µg/kg (Figure 4.19). Although differences in MMAD were evident for GSK-899 amorphous-1 and amorphous-2 aerosols in the first experiment (Table 4.8), values determined for the higher doses in the second experiment performed to investigate the utility of lung image analysis (Table 4.9) were similar.

**Table 4.11: Aerosol characterisation data and inhaled doses of GSK-361 in rats (single 30 or 60-minute exposure)**

Study number	Aerosol form	Formulation concentration in vehicle	Estimated inhaled dose <sup>A</sup> (µg/kg)	Mean (n=2) drug aerosol concentration (µg/L)	Particle size distribution	
					MMAD (µm)	σg
R31765N	Crystalline	0.042% (w/w)	3.52 4.61	0.155 0.205	[1.7] <sup>C</sup>	[3.8]
		0.95% (w/w)	31.1 28.1	1.41 1.28	1.7 1.2	3.4 5.1
		0.95% (w/w)	282 283	12.8 12.9	1.9 2.2	3.1 2.8
		5.0% (w/w)	883 958	40.2 43.6	1.7 2.7	2.6 2.7
	Nebulised solution	0.027 mg/mL	3.51 4.17	0.155 0.193	[1.8] <sup>C</sup>	[2.3]
		0.15 mg/mL	36.1 10.5	1.65 0.471	2.6 1.3	2.2 2.5
		1.9 mg/mL	236 100	10.8 4.58	2.0 1.4	2.3 2.7
		1.9 mg/mL	1006 <sup>B</sup> 1232 <sup>B</sup>	23.0 28.2	2.3 2.0	2.5 2.2

**Notes**

MMAD mass median aerodynamic diameter

σg geometric standard deviation

A Estimated inhaled doses calculated for a 30-minute exposure period using mean data (aerosol concentration and body weight) and a body-weight derived estimate of respired minute volume (Alexander *et al.*, 2008).

B Nebulised high dose: limited solubility of GSK-361 in vehicle necessitated exposure of rats for 60 minutes to achieve the target dose (all other groups were exposed for 30 minutes).

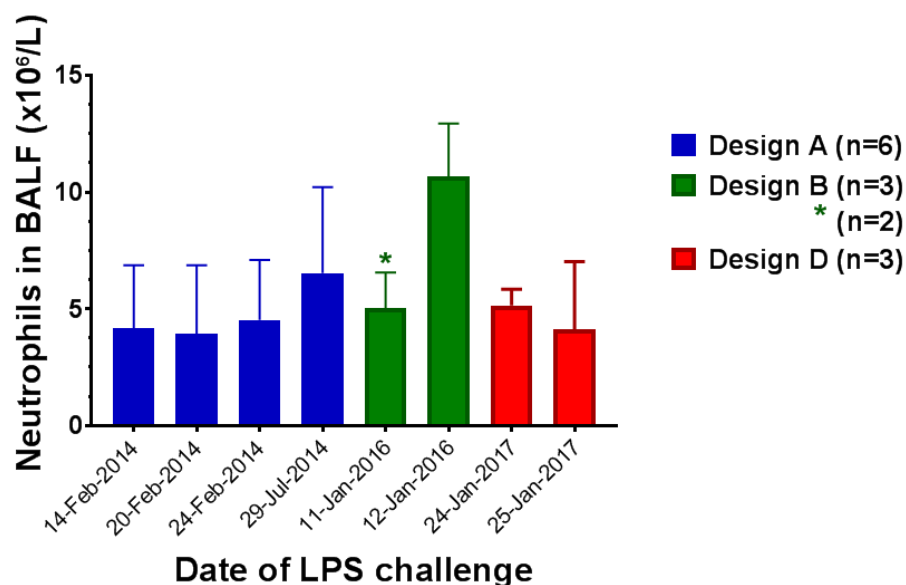
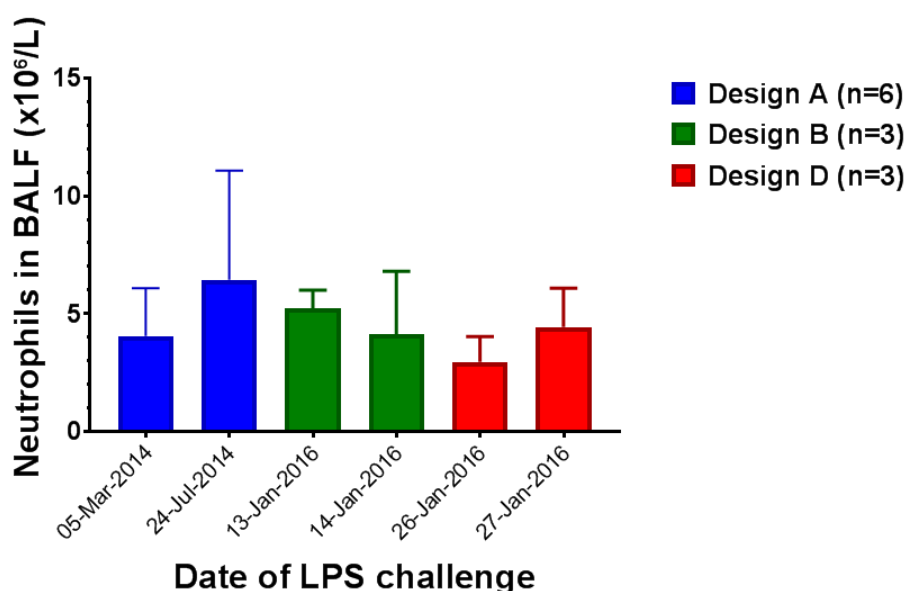
[ ]<sup>C</sup> Aerosol sample taken during pre-study aerosol generation trial without rats (aerosol sampling period at 2 L/min exceeded 30-minute exposure period).

### 4.3.2. Temporal variability of rat neutrophils in BALF four hours after an LPS challenge

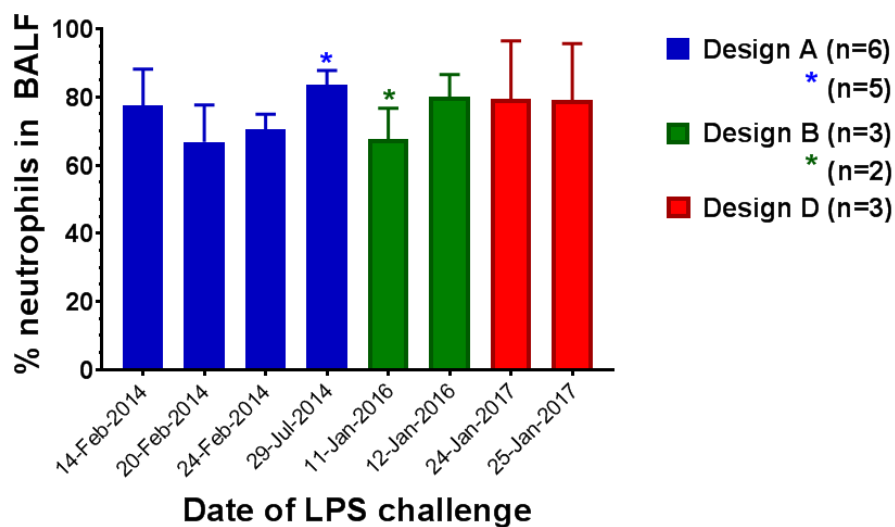
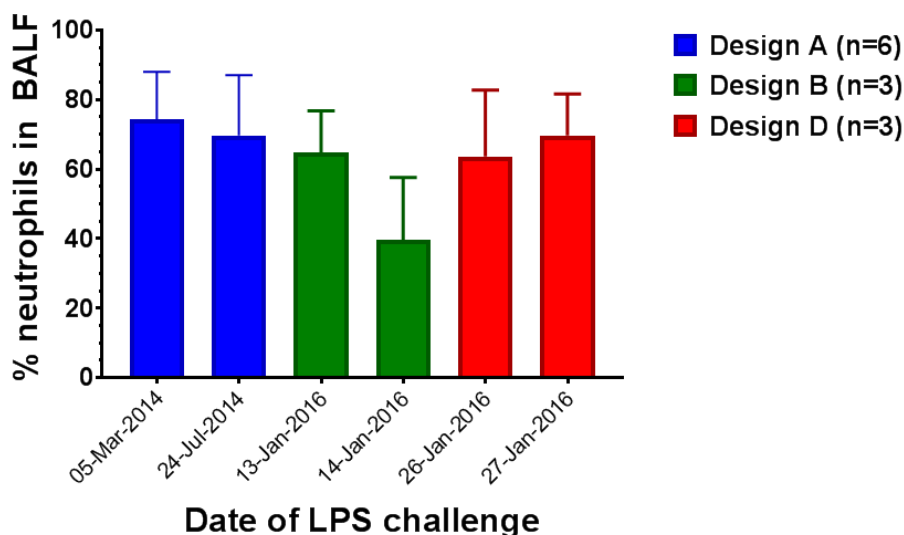
Neutrophil counts in BALF obtained from control rats four hours after intratracheal instillation of LPS showed variability between sampling occasions (Figure 4.7). Relative mean neutrophil counts (Figure 4.8) expressed as a percentage of leukocytes were 75% with a range of 67% to 84% for lactose-control rats, and 66% with a range of 40% to 75% for control rats administered a nebulised vehicle; the mean for 14-Jan-2016 (n=3; nebulised vehicle) was skewed by a low result (18%) for 1/3 rats.

This day to day variability in control neutrophil counts complicated data analysis, since dose response was expressed relative to the response of control rats to the LPS challenge. The source of such variability has implications for the integrity of the p38 MAPK inhibitor dose responses. Ettensohn *et al.* (1988) reported recovery of  $64.8 \pm 9.8\%$  of BALF from humans with 3/16 outliers. A similar recovery of BALF was achieved from isolated lungs of the control rats challenged with LPS, with a mean recovery of  $71 \pm 10\%$  and 12/60 outliers. The total recovered volumes were consistent between sampling occasions with no obvious correlation between peak or trough neutrophil counts (Figures 4.7 and 4.8) and high or low BALF yields (Figure 4.9) respectively. It is therefore unlikely that variability in neutrophil counts is attributable to the recovery volumes *per se*. However, it is plausible the variability may be attributable, at least in part, to partial recovery of neutrophils from lungs during the flushing procedure. The potential for differential recovery of neutrophils in BALF was to be investigated further by image analysis of CAE-stained neutrophils in lungs that had undergone BAL sampling or were 'naïve' for this procedure (Design D).

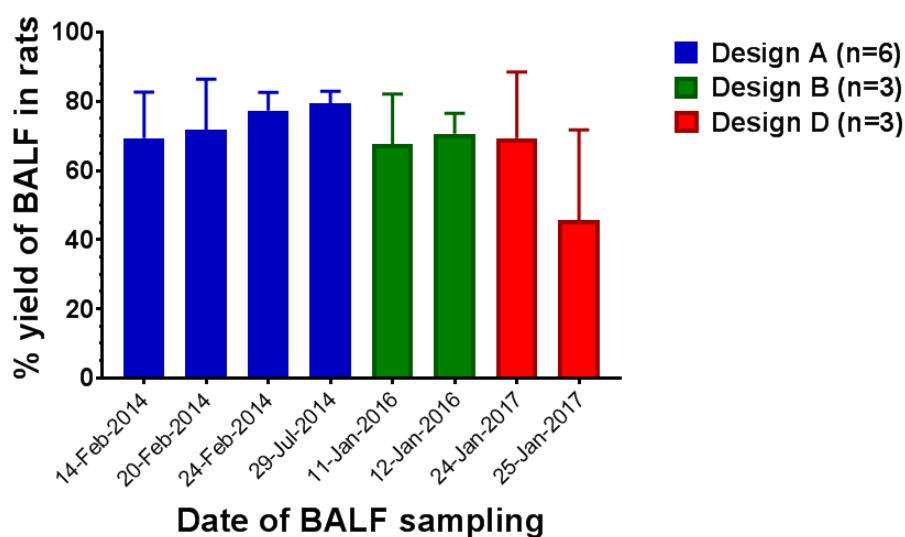
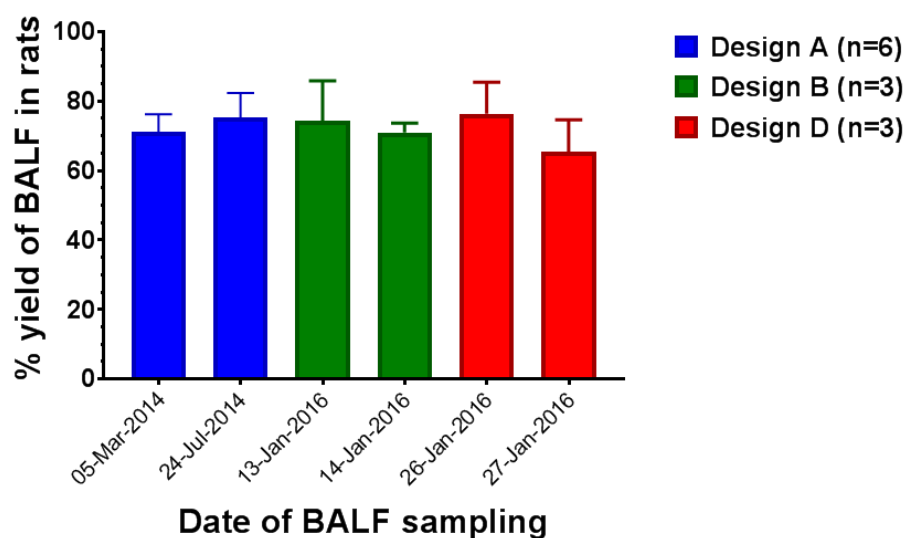
In addition, the day to day variability may be temporal and potentially influenced by differences in the sub-clinical immune status and/or antigen challenge responses for batches of animals.

**4.7A: lactose vehicle control****4.7B: nebulised vehicle control**

**Figure 4.7: Neutrophil counts in bronchoalveolar lavage fluid (BALF) sampled from control animals four hours after intratracheal instillation of lipopolysaccharide (LPS).** Rats inhaled an aerosol of lactose or the vehicle for nebulization of GSK-899 (Design A), GSK-677 (Design B) or GSK-361 (Design D) for 30 minutes and challenged by intratracheal instillation of LPS. Four hours later, rats were euthanized and sampled for BALF to determine neutrophil counts (mean presented with standard deviation as error bars). **4.7A:** rats administered lactose before LPS challenge. **4.7B:** rats administered a nebulised aqueous vehicle before LPS challenge.

**4.8A: lactose vehicle control****4.8B: nebulised vehicle control**

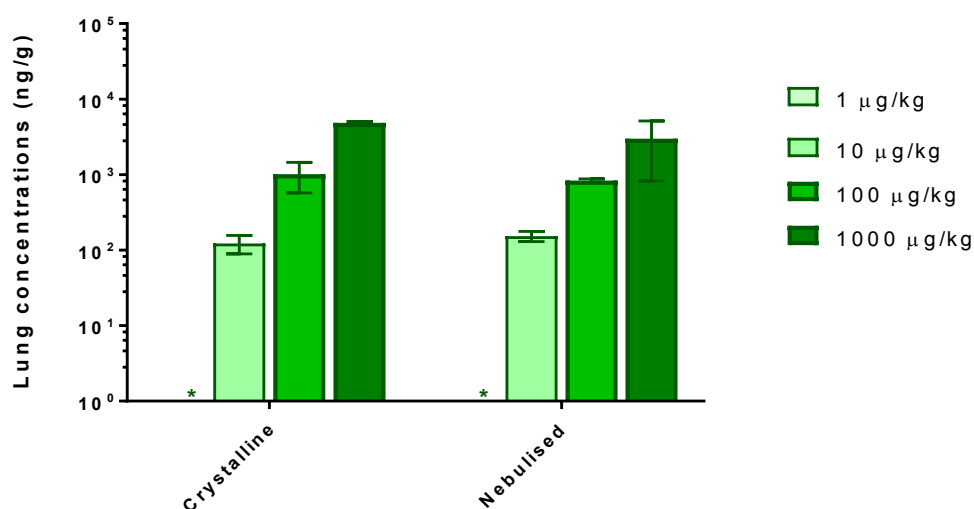
**Figure 4.8:** Neutrophils as a proportion of leukocytes in bronchoalveolar lavage fluid (BALF) sampled from control rats four hours after intratracheal instillation of lipopolysaccharide (LPS). Rats inhaled an aerosol of lactose or the vehicle for nebulization of GSK-899 (Design A), GSK-677 (Design B) or GSK-361 (Design D) for 30 minutes and challenged by intratracheal instillation of LPS. Four hours later, rats were euthanized and sampled for BALF to determine neutrophil counts (relative mean presented with standard deviation as error bars). **4.8A:** rats administered lactose before LPS challenge. **4.8B:** rats administered a nebulised aqueous vehicle before LPS challenge.

**4.9A: lactose vehicle control****4.9B: nebulised vehicle control**

**Figure 4.9: Recovery of bronchoalveolar lavage fluid (BALF) sampled from control animals.** Rats were euthanized, the lungs removed and a cannula inserted into the trachea and secured with thread. Lungs were gently lavaged with 3×5mL ice cold saline (0.9%); lobes were gently massaged prior to removal of each aliquot, which were pooled for each animal (mean yield presented with standard deviation as error bars). **4.9A:** rats administered lactose before LPS challenge. **4.9B:** rats administered a nebulised aqueous vehicle before LPS challenge.

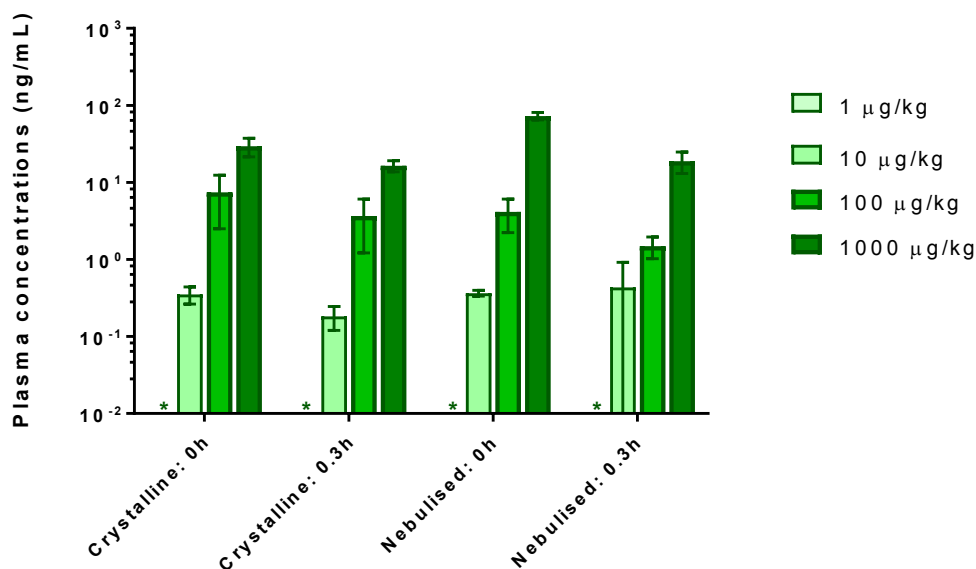
### 4.3.3. Pulmonary and systemic exposure of rats to GSK-677 and endpoints for investigating inhibition of acute lung inflammation (Design B)

Concentrations of GSK-677 in lungs (Figure 4.10) and plasma (Figure 4.11) after aerosol administration increased with dose and were similar for crystalline and nebulised aerosol forms, with clear separation of the doses. Lung and plasma concentrations at the low dose of 1 µg/kg were non-quantifiable (<120 ng/g lung tissue; <0.05 ng/mL plasma).



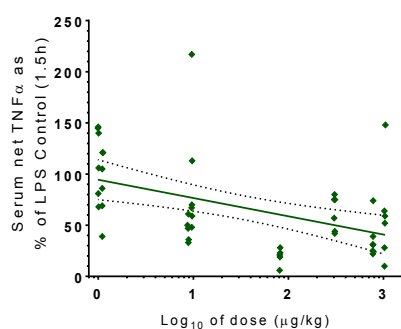
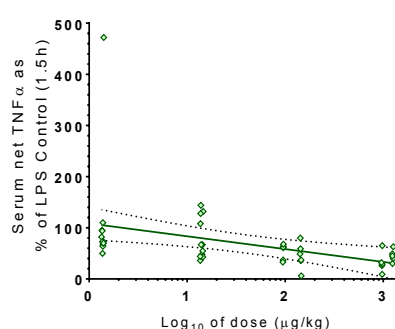
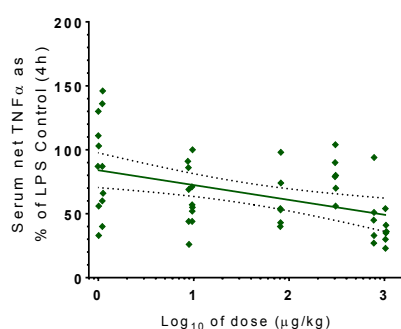
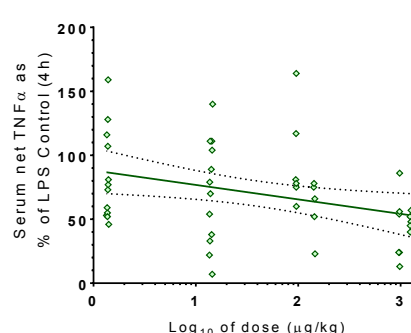
**Figure 4.10: GSK-677 concentrations in lung homogenate sampled from rats after a single inhaled dose (Study R31400N).** Rats inhaled an aerosol of crystalline or aqueous (nebulised) GSK-677 for 30 minutes. Mean GSK-677 concentrations with standard deviations (error bars; n=3) are shown for lung homogenate samples taken as soon as practicable (approximately 20 minutes) after the inhalation exposure. \* indicates concentrations were below the limit of quantification (<120 ng/g).

A decrease in plasma concentration was evident during the 20-minute period elapsing between removal of the rats from the inhalation exposure chamber and their euthanasia for lung sampling (Figure 4.11). These data are consistent with the results described in Chapter 2.

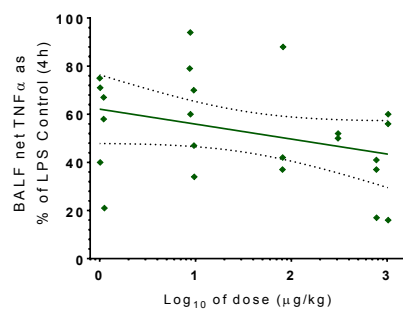
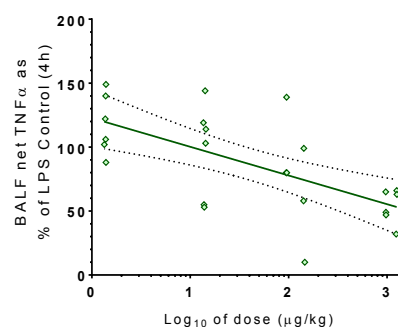


**Figure 4.11: GSK-677 concentrations in plasma sampled from rats after a single inhaled dose (Study R31400N).** Rats inhaled an aerosol of crystalline or aqueous (nebulised) GSK-677 for 30 minutes. Mean GSK-677 concentrations with standard deviations (error bars; n=3) are shown for plasma samples taken immediately after inhalation exposure and during exsanguination for lung tissue sampling (approximately 20 minutes later). \* indicates concentrations were below the limit of quantification (<0.05 ng/mL).

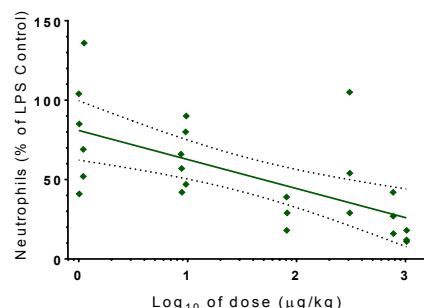
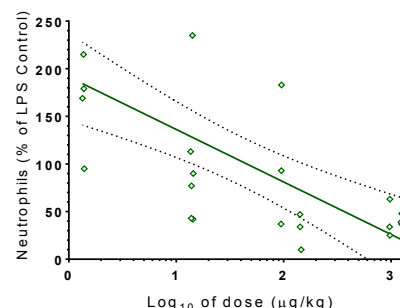
Plotted data and the linear regression lines for evaluated biomarkers showed a more pronounced suppression of LPS-induced inflammation with an increase in the inhaled dose of GSK-677. However, concentrations of TNF $\alpha$  in serum (n=12/dose) at 1.5 or 4 hours post challenge (Figure 4.12) or BALF (n=6/dose) at 4 hours post challenge (Figure 4.13) were most variable, with outliers particularly evident in serum at 1.5 hours (Figures 4.12A and 4.12B). Relative neutrophil counts in BALF (Figure 4.14) and the relative proportion of MPO or CAE-stained lung sections (Figure 4.15) appeared less variable than TNF $\alpha$ . However, the relative MPO data for rats administered GSK-677 (especially nebulised aerosols) were higher than corresponding data for CAE, suggesting elevation of the baseline associated with a potential lack of specificity of the antibody for MPO in the rat lung sections.

**4.12A: Crystals (1.5 hours)****4.12B: Nebulised (1.5 hours)****4.12C: Crystals (4 hours)****4.12D: Nebulised (4 hours)**

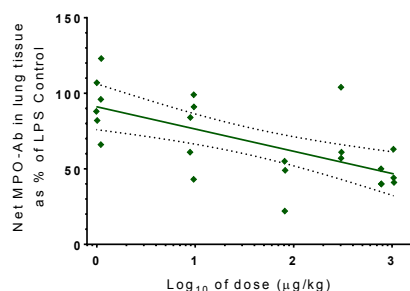
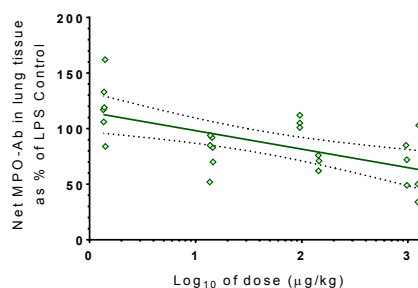
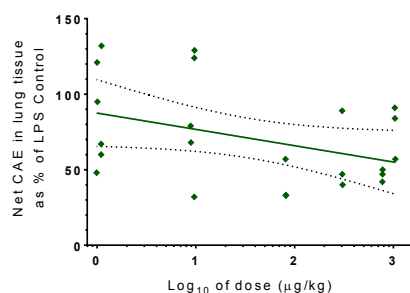
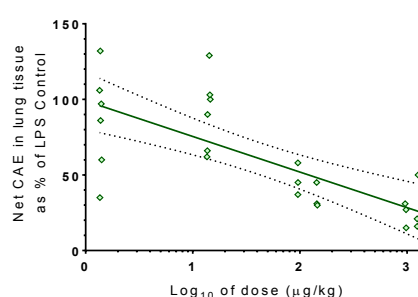
**Figure 4.12: Tumour necrosis factor-alpha (TNF $\alpha$ ) in serum, relative to controls, sampled from an acute lung inflammation model in rats administered GSK-677 (Study R31400N).** Rats ( $n=6/\text{dose}$ ) were exposed to an aerosol of GSK-899 or vehicle (control) for 30 minutes and then challenged with lipopolysaccharide (LPS) by intratracheal instillation; a control group for baseline data was instilled with phosphate buffered saline (PBS;  $n=4$ ). Serum samples were obtained at 1.5 and 4 hours post challenge. Net TNF $\alpha$  concentrations (individual value less the mean concentration for PBS-challenged controls) were expressed relative to LPS-challenged controls and plotted against  $\log_{10}$  dose of GSK-677. Individual data, a linear regression line and the corresponding 95% confidence interval (dotted lines) are plotted for each aerosol form and time point. **4.12A:** crystalline doses: 1.00-1.11, 8.82-9.66, 81.6-306 and 775-1034  $\mu\text{g}/\text{kg}$ ; serum sampled at 1.5 hours post challenge. **4.12B:** nebulised doses: 1.36-1.39, 13.7-14.3, 95.3-144 and 973-1249  $\mu\text{g}/\text{kg}$ ; serum sampled at 1.5 hours post challenge. **4.12C:** crystalline doses: 1.00-1.11, 8.82-9.66, 81.6-306 and 775-1034  $\mu\text{g}/\text{kg}$ ; serum sampled at 4 hours post challenge. **4.12D:** nebulised doses: 1.36-1.39, 13.7-14.3, 95.3-144 and 973-1249  $\mu\text{g}/\text{kg}$ ; serum sampled at 4 hours post challenge.

**4.13A: Crystals (4 hours)****4.13B: Nebulised (4 hours)**

**Figure 4.13: Tumour necrosis factor-alpha (TNF $\alpha$ ) in broncho-alveolar lavage fluid (BALF), relative to controls, sampled from an acute lung inflammation model in rats administered GSK-677 (Study R31400N).** Rats (n=6/dose) were exposed to an aerosol of GSK-899 or vehicle (control) for 30 minutes and then challenged with lipopolysaccharide (LPS) by intratracheal instillation; a control group for baseline data was instilled with phosphate buffered saline (PBS; n=4). Four hours post challenge, rats were euthanized and lungs lavaged with saline. Net TNF $\alpha$  concentrations (individual value less the mean concentration for PBS-challenged controls) were expressed relative to LPS-challenged controls and plotted against log<sub>10</sub> dose of GSK-677. Individual data, a linear regression line and the corresponding 95% confidence interval (dotted lines) are plotted for each aerosol form and time point. **4.13A:** crystalline doses: 1.00-1.11, 8.82-9.66, 81.6-306 and 775-1034  $\mu\text{g}/\text{kg}$ . **4.13B:** nebulised doses: 1.36-1.39, 13.7-14.3, 95.3-144 and 973-1249  $\mu\text{g}/\text{kg}$ .

**4.14A: Crystals****4.14B: Nebulised**

**Figure 4.14: Neutrophils in bronchoalveolar lavage fluid, relative to controls, harvested from an acute lung inflammation model in rats administered GSK-677 (Study R31400N).** Rats (n=6/dose) were exposed to an aerosol of GSK-677 or vehicle (control) for 30 minutes and then challenged with lipopolysaccharide (LPS) by intratracheal instillation; a control group for baseline data was instilled with phosphate buffered saline (PBS; n=4). Four hours post challenge, rats were euthanized and lungs lavaged with saline to harvest neutrophils. Neutrophils (expressed as net proportion of leukocytes for each rat, *i.e.* less mean count for PBS-challenged controls, and relative to LPS-challenged controls) were plotted against log<sub>10</sub> dose of GSK-677. Individual data, a linear regression line and the corresponding 95% confidence interval (dotted lines) are plotted for each aerosol form. **4.14A:** crystalline doses: 1.00-1.11, 8.82-9.66, 81.6-306 and 775-1034  $\mu\text{g}/\text{kg}$ . **4.14B:** nebulised doses: 1.36-1.39, 13.7-14.3, 95.3-144 and 973-1249  $\mu\text{g}/\text{kg}$ .

**4.15A: Crystals (MPO)****4.15B: Nebulised (MPO)****4.15C: Crystals (CAE)****4.15D: Nebulised (CAE)**

**Figure 4.15: Proportion of lung tissue stained for myeloperoxidase (MPO) or chloroacetate esterase (CAE), relative to controls, in an acute lung inflammation model in rats administered GSK-677 (Study R31400N).** Rats ( $n=6$ /dose) were exposed to an aerosol of GSK-899 or vehicle (control) for 30 minutes and then challenged with lipopolysaccharide (LPS) by intratracheal instillation; a control group for baseline data was instilled with phosphate buffered saline (PBS;  $n=6$ ). Four hours post challenge, rats were euthanized, lungs preserved for histology; sections 3  $\mu$ m thick were stained for MPO or CAE and imaged. The proportion of lung tissue stained for MPO or CAE (less mean value for PBS-challenged controls) relative to LPS-challenged controls was plotted against  $\log_{10}$  dose of GSK-677. Individual data, a linear regression line and the corresponding 95% confidence interval (dotted lines) are plotted for each aerosol form. **4.15A:** crystalline doses: 1.00-1.11, 8.82-9.66, 81.6-306 and 775-1034  $\mu$ g/kg; lung stained for MPO. **4.15B:** nebulised doses: 1.36-1.39, 13.7-14.3, 95.3-144 and 973-1249  $\mu$ g/kg; lung stained for MPO. **4.15C:** crystalline doses: 1.00-1.11, 8.82-9.66, 81.6-306 and 775-1034  $\mu$ g/kg; lung stained for CAE. **4.15D:** nebulised doses: 1.36-1.39, 13.7-14.3, 95.3-144 and 973-1249  $\mu$ g/kg; lung stained for CAE.

The 95% confidence limits of the median effective dose ( $ED_{50}$ ) for each biomarker of inflammation reflected high variability in the datasets; confidence limits increased dramatically when the extrapolated  $ED_{50}$  was outside the evaluated range of inhaled doses. Confidence limits for  $TNF-\alpha$  measurements and lung image analysis of net MPO (MPO less CD68-positive areas) were particularly variable, together with the CAE

data for rats administered crystalline GSK-677, with estimated ED<sub>50</sub> values exceeding doses at which pulmonary toxicopathology was observed (Chapter 5). The ED<sub>50</sub> was approximately 360 µg/kg for both aerosol forms based on neutrophil counts in BALF, and 126 µg/kg for nebulised GSK-677 CAE staining of lung sections. Both estimates are higher than that predicted from intratracheal instillation of an aqueous suspension of GSK-677 (ED<sub>50</sub> = 5 µg/kg; Figure 4.4B) after a lung deposition fraction of 10% was considered (Forbes *et al.*, 2011, Jones and Baldrick, 2013, Owen, 2013).

**Table 4.12: Estimated inhaled doses of GSK-677 to achieve 50% reduction (ED<sub>50</sub>) in inflammation endpoints evaluated using an acute lung inflammation model in rats**

Parameter and medium	Presentation of GSK-677	ED <sub>50</sub> estimate (µg/kg) <sup>A</sup>	95% confidence interval (µg/kg)		ED <sub>50</sub> outside dose range? <sup>B</sup>
			lower	upper	
TNFα (1.5h) serum	crystalline	1709	230	1.45 x10 <sup>6</sup>	Yes
	nebulised	863	153	1.94 x10 <sup>5</sup>	No
TNFα (4h) serum	crystalline	6525	701	7.17 x10 <sup>6</sup>	Yes
	nebulised	90101	1471	NC	Yes
TNFα (4h) BALF	crystalline	17377	286	NC	Yes
	nebulised	7389	685	7.55 x10 <sup>7</sup>	Yes
Neutrophils (4h) BALF	crystalline	366	95.5	5744	No
	nebulised	356	102	4356	No
MPO stain (4h) lung	crystalline	3893	569	6.32 x10 <sup>5</sup>	Yes
	nebulised	47044	2137	1 x10 <sup>10</sup>	Yes
CAE stain (4h) lung	crystalline	42701	286	NC	Yes
	nebulised	126	40.4	714	No

**Notes**

- A ED<sub>50</sub> values extrapolated from net data (mean value for PBS control deducted from result for LPS-challenged animal) expressed relative to the mean of LPS-challenged controls (see Figures 4.12 to 4.15).
- B 95% confidence limits increase dramatically when the extrapolated ED<sub>50</sub> was outside the evaluated range of estimated inhaled doses.
- NC Not calculable

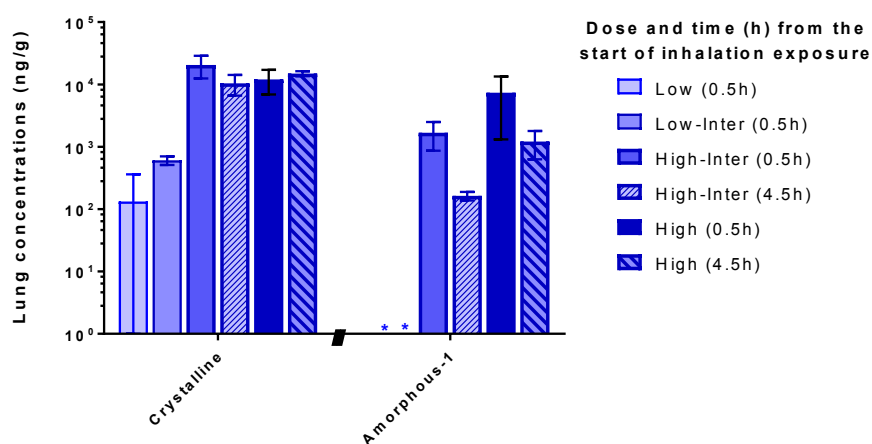
#### **4.3.4. Pulmonary and systemic exposure of rats to GSK-899 and inhibition of inflammation**

Design A: lung concentrations of GSK-899 after inhaled administration of crystals increased with dose  $\leq 308$   $\mu\text{g}/\text{kg}$ . Concentrations were similar for crystalline doses of 308 and 531  $\mu\text{g}/\text{kg}$  with no difference at 0.5 and 4.5 hours (Figure 4.16). Lung concentrations for rats inhaling amorphous or nebulised GSK-899 were lower than those of rats administered the crystalline form at a given dose, with the amorphous-1 preparation achieving the lowest relative lung concentration when normalisation of dose was considered. This is consistent with the higher MMAD noted for the latter aerosol form (Table 4.8) and the trends in results described in Chapter 2. GSK-899 was not quantifiable at low doses (amorphous-1  $\leq 18.9$   $\mu\text{g}/\text{kg}$ ; amorphous-2 at 0.653  $\mu\text{g}/\text{kg}$ ; nebulised at 1.30  $\mu\text{g}/\text{kg}$ ).

GSK-899 concentrations in plasma evaluated at the two highest doses for each aerosol form showed an increase with dose, and declined from 0.5 hours (immediately post inhalation exposure) to 1.5 and 4.5 hours (Figure 4.17). For comparable doses, amorphous-2 GSK-899 achieved the highest plasma concentration and crystalline GSK-899 the lowest.

Suppression of LPS-induced inflammation was evident with an increase in inhaled dose for each of the aerosol forms of GSK-899 (Figure 4.18). *Prima facie*, the plotted data and linear regression lines for neutrophils in BALF showed a similar variability in data points for GSK-899 to that evident for GSK-677 (Figure 4.14).

## 4.16A:



## 4.16B:

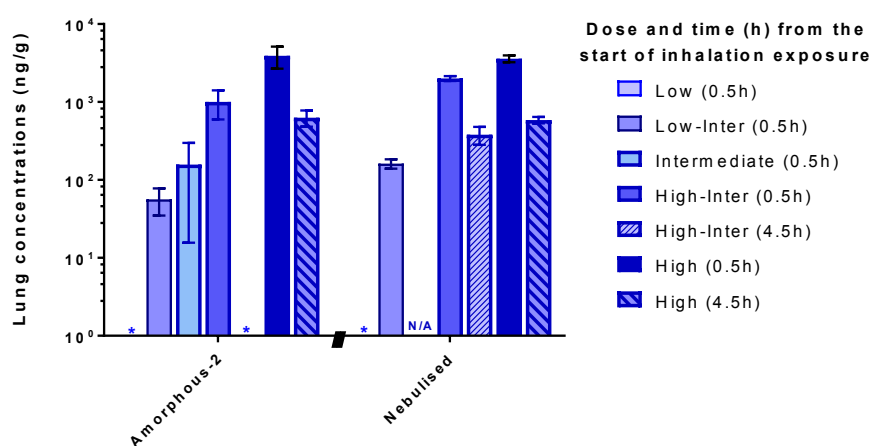
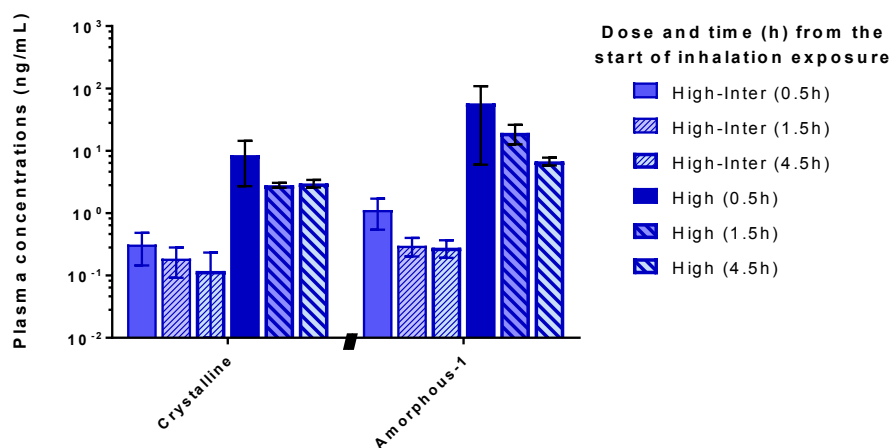
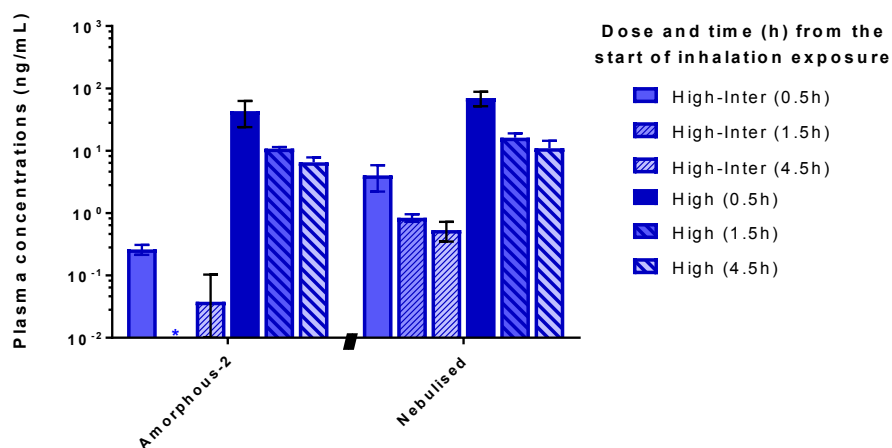


**Figure 4.16: GSK-899 concentrations in lung homogenate sampled from rats after a single inhaled dose (Study R30820N).** Rats inhaled an aerosol of crystalline, amorphous or aqueous (nebulised) GSK-899 for 30 minutes. Mean GSK-899 concentrations with standard deviations (error bars; n=3) are shown for lung homogenate samples taken as soon as practicable (approximately 20 minutes) after inhalation exposure (0.5h) and for higher doses at 4.5 hours (4 hours post exposure). \* indicates concentrations were below the limit of quantification (<120 ng/g). **4.16A:** rats administered crystalline GSK-899 (1.07, 22.5, 308 and 531 µg/kg for low to high dose groups respectively) or amorphous-1 powder (2.60, 18.9, 213 and 2350 µg/kg respectively). **4.16B:** rats administered amorphous-2 powder (0.653, 4.00, 22.4, 36.3 and 364 µg/kg respectively) or nebulised GSK-899 (1.30, 22.6, 280 and 844 µg/kg respectively; “intermediate dose” designation not applicable).

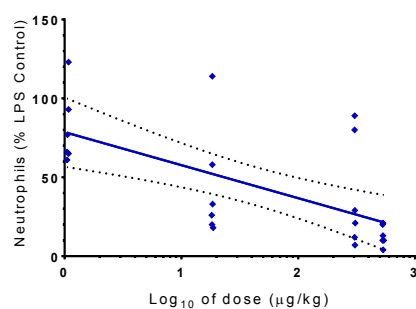
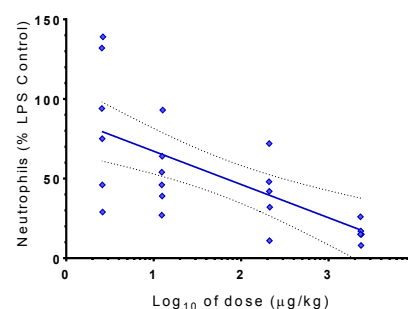
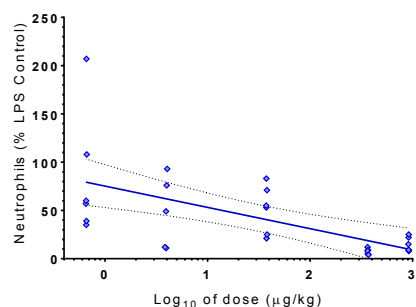
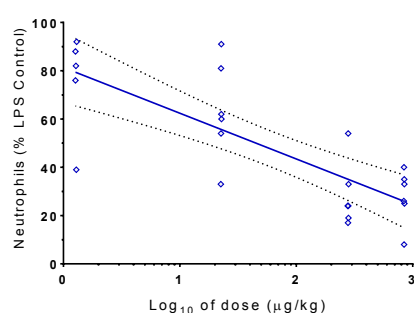
## 4.17A:



## 4.17B:



**Figure 4.17: GSK-899 concentrations in plasma sampled from rats after a single inhaled dose (Study R30820N).** Rats inhaled an aerosol of crystalline, amorphous or aqueous (nebulised) GSK-899 for 30 minutes. Mean GSK-899 concentrations with standard deviations (error bars; n=3) are shown for plasma samples taken as soon as practicable (approximately 20 minutes) after inhalation exposure (0.5h) and at 1.5 and 4.5 hours (1 and 4 hours post exposure). \* indicates concentrations were below the limit of quantification (<0.05 ng/mL). **4.17A:** rats administered crystalline GSK-899 (308 and 532 µg/kg for high-intermediate and high dose groups respectively) or amorphous-1 powder (215 and 2340 µg/kg respectively). **4.17B:** rats administered amorphous-2 powder (34.6 and 363 µg/kg respectively) or nebulised GSK-899 (282 and 840 µg/kg respectively).

**4.18A: Crystals****4.18B: Amorphous-1****4.18C: Amorphous-2****4.18D: Nebulised**

**Figure 4.18:** Neutrophils in bronchoalveolar lavage fluid, relative to controls, harvested from an acute lung inflammation model in rats administered GSK-899 (Study R30820N). Rats ( $n=6$ /dose) were exposed to an aerosol of GSK-899 or vehicle (control) for 30 minutes and then challenged with lipopolysaccharide (LPS) by intratracheal instillation; a control group for baseline data was instilled with phosphate buffered saline (PBS;  $n=4$ ). Four hours post challenge, rats were euthanized and lungs lavaged with saline to harvest neutrophils. Neutrophils (expressed as net proportion of leukocytes for each rat, *i.e.* less mean count for PBS-challenged controls, and relative to LPS-challenged controls) were plotted against  $\log_{10}$  dose of GSK-899. Individual data, a linear regression line and the corresponding 95% confidence interval (dotted lines) are plotted for each aerosol form. **4.18A:** crystalline doses: 1.07, 18.4, 305 and 533  $\mu\text{g}/\text{kg}$ . **4.18B:** amorphous-1 doses: 2.58, 12.5, 210 and 2349  $\mu\text{g}/\text{kg}$ . **4.18C:** amorphous-2 doses: 0.658, 3.95, 37.7, 366 and 915  $\mu\text{g}/\text{kg}$ . **4.18D:** nebulised doses: 1.28, 22.7, 279 and 845  $\mu\text{g}/\text{kg}$ .

Design C: lung concentrations of GSK-899 after inhaled administration of each aerosol form increased with dose, with clear separation of the doses (Figure 4.19). Lung concentrations for rats inhaling amorphous or nebulised GSK-899 were generally similar for a given dose and lower than that for the corresponding dose of crystalline GSK-899. These findings are consistent with results described in Chapter 2.

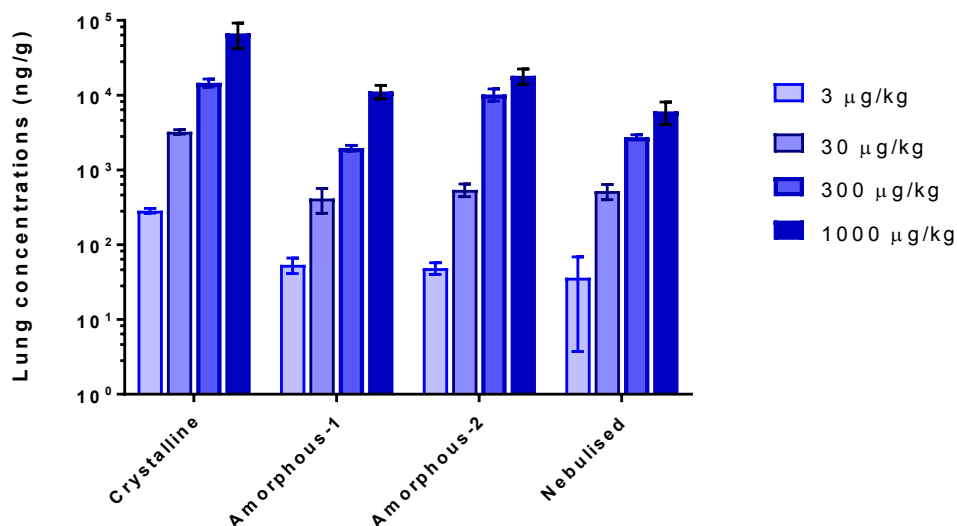


**Figure 4.19: GSK-899 concentrations in lung homogenate sampled from rats after a single inhaled dose (Study R31763N).** Rats inhaled an aerosol of crystalline, amorphous or aqueous (nebulised) GSK-899 for 30 minutes. Mean GSK-899 concentrations with standard deviations (error bars; n=3) are shown for lung homogenate samples taken as soon as practicable (approximately 20 minutes) after the inhalation exposure.

GSK-899 concentrations in plasma were only quantifiable (>0.05 ng/mL) in samples taken immediately following administration of amorphous or nebulised GSK-899 at the highest administered dose of 1000 µg/kg (Figure 4.20). GSK-899 was not quantifiable in plasma samples taken approximately 20 minutes later, during exsanguination of animals for lung sampling. Systemic exposure of rats to GSK-899 was therefore lower than that apparent for GSK-677.

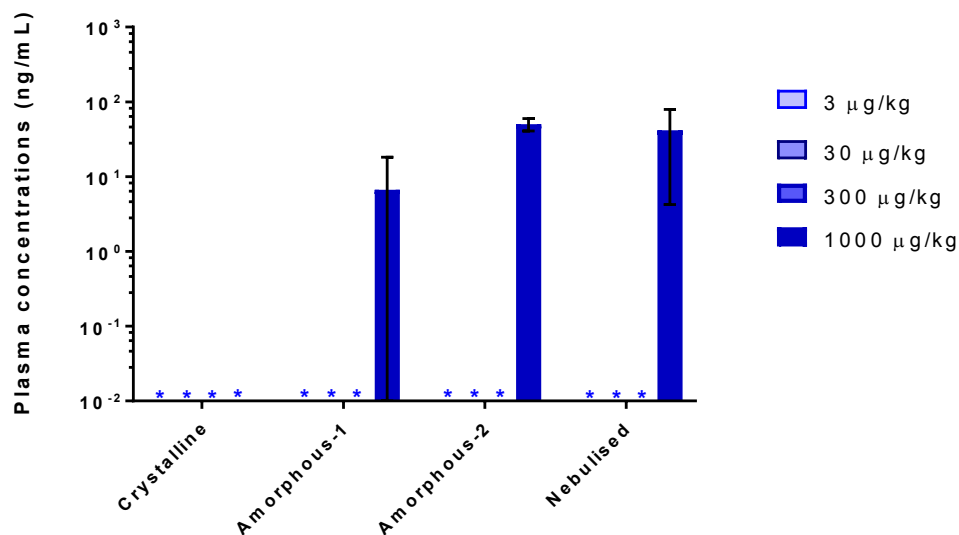


**Figure 4.20: GSK-899 concentrations in plasma sampled from rats after a single inhaled dose (Study R31763N).** Rats inhaled an aerosol of crystalline, amorphous or aqueous (nebulised) GSK-899 for 30 minutes. Mean GSK-899 concentrations with standard deviations (error bars; n=3) are shown for plasma samples taken immediately post inhalation exposure; all plasma samples taken during exsanguination (approximately 20 minutes later) were not quantifiable. \* indicates concentrations below the limit of quantification (<0.05 ng/mL).

The 95% confidence limits of ED<sub>50</sub> determined from GSK-899 dose responses for reduction of neutrophils in BALF (Table 4.13) were considerably narrower than confidence limits for GSK-677 (Table 4.12). The ED<sub>50</sub> values for GSK-899 aerosols were notably lower than for GSK-677 and outside the confidence limits for GSK-677 (and *vice versa*) indicating a significant difference between the two compounds.

The ED<sub>50</sub> for amorphous-1 GSK-899 was six-fold higher than for the amorphous-2 batch, with confidence limits also indicating a significant difference between aerosols generated from amorphous batches. This trend was anticipated given differences in the aerosol particle size distribution and hence a potential difference in lung deposited dose. The ED<sub>50</sub> for nebulised amorphous-2 was also significantly lower than for nebulised GSK-899 but the confidence limits and ED<sub>50</sub> values for each aerosol form overlapped sufficiently to preclude a clear ranking relative to crystalline GSK-899.

**Table 4.13: Estimated inhaled dose of GSK-899 to achieve 50% reduction (ED<sub>50</sub>) in inflammation endpoints evaluated using an acute lung inflammation model in rats**

Parameter and medium	Presentation of GSK-899	ED <sub>50</sub> estimate (µg/kg) <sup>A</sup>	95% confidence interval (µg/kg)		ED <sub>50</sub> outside dose range?
			lower	upper	
Neutrophils (4h) BALF	crystalline	23.38	3.54	95.28	No
	amorphous-1	65.88	15.23	292.8	No
	amorphous-2	10.08	0.86	44.52	No
	nebulised	44.66	15.79	114.6	No

**Notes**

A ED<sub>50</sub> values extrapolated from net data (mean value for PBS control deducted from result for LPS-challenged animal) expressed relative to the mean of LPS-challenged controls (see Figures 4.18).

**4.3.5. Pulmonary and systemic exposure of rats to GSK-361 and inhibition of inflammation (Design D)**

Concentrations of GSK-361 in lungs (Figure 4.21) and plasma (Figure 4.22) after aerosol administration increased with dose. The lung concentrations measured in rats administered crystalline GSK-361 were higher than for the corresponding nebulised dose, in line with results described in Chapter 2. Separation of GSK-361 exposure in rats for the doses was less pronounced than for GSK-677 and GSK-899. GSK-361 was not quantifiable in lung (<30 ng/g lung tissue) for nebulised doses ≤30 µg/kg or plasma (<5 ng/mL) for either aerosol form at these doses. Where quantifiable (doses ≥300 µg/kg), plasma concentrations of GSK-361 for each aerosol form were similar at the time rats were removed from the inhalation exposure chamber and at euthanasia for lung sampling (Figure 4.22).

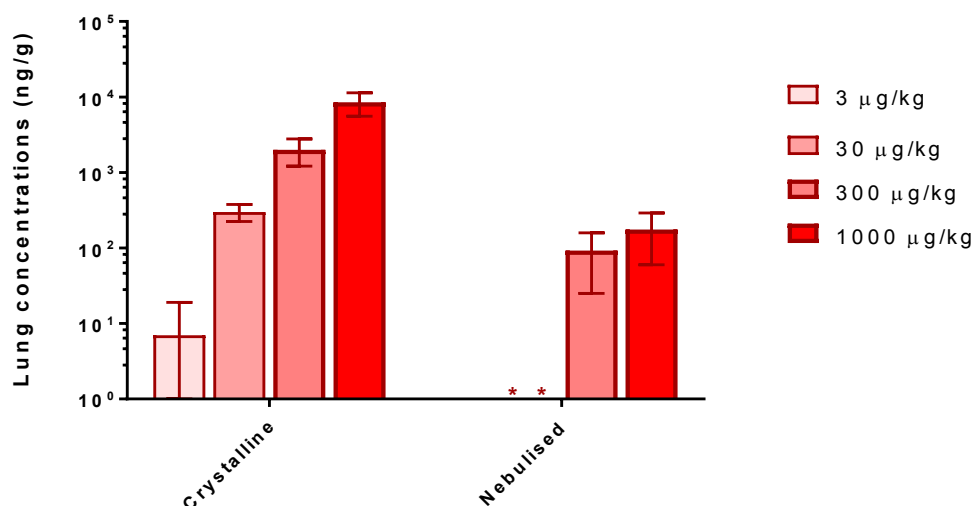


**Figure 4.21: GSK-361 concentrations in lung homogenate sampled from rats after a single inhaled dose (Study R31765N).** Rats inhaled an aerosol of crystalline or aqueous (nebulised) GSK-361 for 30 minutes. Mean GSK-361 concentrations with standard deviations (error bars; n=3) are shown for lung homogenate samples taken as soon as practicable (approximately 20 minutes) after the inhalation exposure. \* indicates concentrations were below the limit of quantification (<30 ng/g).

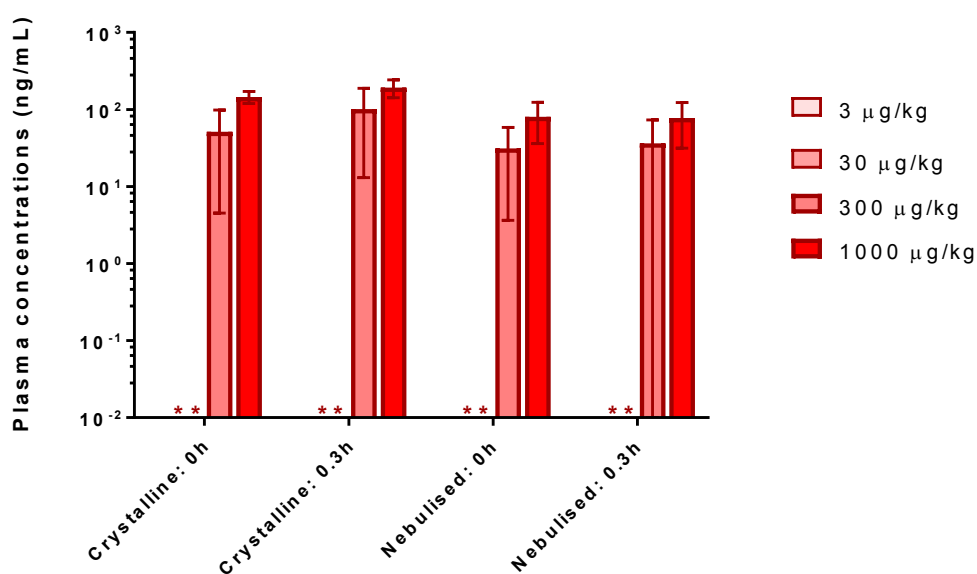
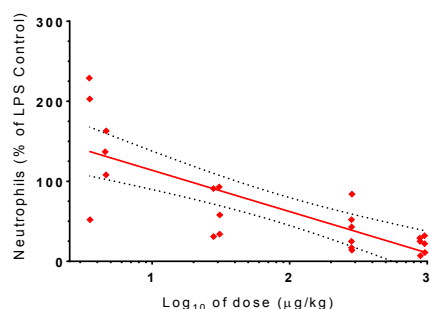


**Figure 4.22: GSK-361 concentrations in plasma sampled from rats after a single inhaled dose (Study R31765N).** Rats inhaled an aerosol of crystalline or aqueous (nebulised) GSK-361 for 30 minutes. Mean GSK-361 concentrations with standard deviations (error bars; n=3) are shown for plasma samples taken immediately after inhalation exposure and during exsanguination for lung tissue sampling (approximately 20 minutes later). \* indicates concentrations were below the limit of quantification (<5 ng/mL).

Suppression of LPS-induced inflammation was evident with an increase in inhaled dose for each of the aerosol forms of GSK-361 (Figure 4.23). Neutrophil counts were most variable at the lowest dose, when relative neutrophil counts were highest, and least variable at the highest dose.

#### 4.23A: Crystals



#### 4.23B: Nebulised

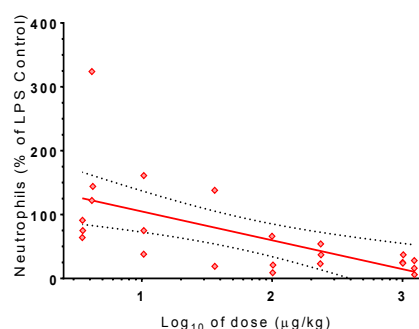


**Figure 4.23: Neutrophils in bronchoalveolar lavage fluid, relative to controls, harvested from an acute lung inflammation model in rats administered GSK-361 (Study R31765N).** Rats (n=6/dose) were exposed to an aerosol of GSK-361 or vehicle (control) for 30 minutes and then challenged with lipopolysaccharide (LPS) by intratracheal instillation; a control group for baseline data was instilled with phosphate buffered saline (PBS; n=6). Four hours post challenge, rats were euthanized and lungs lavaged with saline to harvest neutrophils. Neutrophils (expressed as net proportion of leukocytes for each rat, *i.e.* less mean count for PBS-challenged controls, and relative to LPS-challenged controls) were plotted against  $\log_{10}$  dose of GSK-361. Individual data, a linear regression line and the corresponding 95% confidence interval (dotted lines) are plotted for each aerosol form. **4.23A:** Crystalline doses: 3.52-4.61, 28.1-31.1, 282-283 and 883-958  $\mu\text{g}/\text{kg}$ . **4.23B:** Nebulised doses: 3.51-4.17, 10.5-36.1, 236-100 and 1006-1232  $\mu\text{g}/\text{kg}$ .

The 95% confidence limits of  $\text{ED}_{50}$  determined from GSK-361 dose responses for reduction of neutrophils in BALF (Table 4.14) were narrower than the confidence limits for GSK-677 (Table 4.12) and broader than those for GSK-899 (Table 4.13).  $\text{ED}_{50}$  values determined for the two aerosol forms of GSK-361 were similar despite differences in the lung concentrations following inhaled administration of the crystalline and nebulised aerosols. The  $\text{ED}_{50}$  values for GSK-361 ranked between GSK-677 and GSK-899, with confidence intervals indicating a significant difference between GSK-361 and GSK-899.

**Table 4.14: Estimated inhaled dose of GSK-361 to achieve 50% reduction (ED<sub>50</sub>) in inflammation endpoints evaluated using an acute lung inflammation model in rats**

Parameter and medium	Presentation of GSK-361	ED <sub>50</sub> estimate (µg/kg) <sup>A</sup>	95% confidence interval (µg/kg)		ED <sub>50</sub> outside dose range?
			lower	upper	
Neutrophils (4h) BALF	Crystalline Nebulised	172.2	79.4	476.5	No
		164.6	45.4	1595.7	No

**Notes**

- A ED<sub>50</sub> values extrapolated from net data (mean value for PBS control deducted from result for LPS-challenged animal) expressed relative to the mean of LPS-challenged controls (see Figure 4.23).

## 4.4. Conclusion

The objectives of this chapter were to assess the efficacy of three p38 MAPK inhibitors using a non-clinical model for the prophylactic inhibition of LPS-induced acute lung inflammation. Following review of preliminary data for neutrophil counts in BALF, additional biomarkers for inflammation were incorporated into experiments for evaluation.

Optimisation of the exposure route used for LPS challenge using small numbers of rats ( $n=3/\text{treatment}$ ) indicated that, for the administered doses, successful intratracheal instillation of the antigen achieved a higher and more consistent increase in neutrophils in BALF within a dosing session than for the more diffuse delivery achieved by inhalation exposure. However, a successful outcome was dependent upon the operator being able to ensure the catheter was placed within the trachea and not the oesophagus before dispensing the dose volume of LPS.

Key experiments were designed to compare endpoints such as neutrophil counts in BALF versus biomarkers for neutrophils in lung sections. However, given the total number of animals required for each experiment and the time taken to perform the required procedures for each animal, it was necessary to design each experiment with sub-groups treated on consecutive days. Aerosol delivery and hence inhalation exposure procedures are more susceptible to day-to-day variability in delivered doses than exposure routes simply dispensing measured volumes of liquid (oral gavage or parenteral injection). Whilst temporal variability has little impact for assessing changes after repeated administration (changes related to mean doses), the potential for data variability is higher for cohorts of single inhaled doses. Experiments were therefore designed with sub-groups of animals for each treatment (BALF sampling or lung histology) administered a common aerosol on one of two days such that potential differences in lung deposited doses of p38 MAPK inhibitors would not bias the results for one of the principal endpoints under investigation.

Data variability was evident for the neutrophil counts in BALF taken from control rats challenged with LPS (Designs A, B and D). Experiments were modified (Designs C and D) to determine if lung image analysis of CAE-stained neutrophils in LPS-treated control rats showed a similar pattern of variability to that observed for neutrophil counts in BALF (data not available at thesis submission). If data variability had proven to be of a temporal nature then this would illustrate the importance of prioritising variables and minimising parameters to accommodate all procedures within a series of succinct experiments, each with its own control group. Results described in Chapter 2 were used to rank the systemic (plasma) and lung exposure of rats to p38 MAPK inhibitors in terms of the AUC over 24 hours and  $C_{max}$  after a single inhalation exposure (Table 4.15). Drug-lung and plasma concentrations of p38 MAPK inhibitors measured in rats exposed concurrently with animals used to evaluate efficacy (challenged with LPS) were consistent with these rankings of  $C_{max}$ .

**Table 4.15: Ranking of the exposure of rats to p38 MAPK inhibitors following a single inhaled administration**

Sample medium	Pharmacokinetic parameter	Ranking of p38 MAPK inhibitors
Lungs	AUC <sub>0-t</sub>	GSK-899 > GSK-361 > GSK-677
	$C_{max}$ crystals nebulised	GSK-899 > GSK-361 > GSK-677
		GSK-899 > GSK-677 > GSK-361
Plasma	AUC <sub>0-t</sub>	GSK-361 > GSK-899 > GSK-677
	$C_{max}$	GSK-361 > GSK-677 > GSK-899

For a drug to be efficacious, it must be available at the target receptor or site of action. p38 $\alpha$  MAPK is expressed in the cytoplasm and nucleus of cells (Cuenda and Rousseau, 2007) in the airway smooth muscle, respiratory epithelium and immune system (Williams *et al.*, 2008, Mayer and Callahan, 2006). The median effective dose (ED<sub>50</sub>) extrapolated from the linear regression lines of dose responses for suppression of neutrophils in BALF ranked the compounds GSK-899 < GSK-361 <

GSK-677, with a significant difference between GSK-899 and the other compounds. This was consistent with the higher lung concentrations of GSK-899 measured post exposure, *i.e.* at the time of LPS challenge. However, similar lung concentrations of GSK-361 (crystalline) and GSK-677 (both forms) and their less significant ranking of ED<sub>50</sub> allude to potential implications for physicochemical properties of a drug to enhance or impair access of a molecule to the pharmacological target. It could be hypothesised a receptor in the cytoplasm or nucleus (p38 MAPK) is more accessible to a membrane permeable molecule (GSK-361) than a readily soluble molecule (GSK-677).

**Table 4.16: Estimated inhaled doses of p38 MAPK inhibitors to achieve 50% reduction (ED<sub>50</sub>) in inflammation endpoints evaluated using an acute lung inflammation model in rats**

Parameter and medium	Compound	Aerosol form	ED <sub>50</sub> estimate (µg/kg)	95% confidence interval (µg/kg)	
				lower	upper
Neutrophils (4h) BALF	GSK-899	crystalline	23.38	3.54	95.28
		amorphous-1	65.88	15.23	292.8
		amorphous-2	10.08	0.86	44.52
		nebulised	44.66	15.79	114.6
	GSK-677	crystalline	366	95.5	5744
		nebulised	356	102	4356
GSK-361	crystalline	172	79.4	476.5	
	nebulised	165	45.4	1596	
CAE stain (4h) lung	GSK-677	Crystalline	42701 <sup>AB</sup>	286	NC
		Nebulised	126 <sup>A</sup>	40.4	714

**Notes**

- A ED<sub>50</sub> values extrapolated from net data (mean value for PBS control deducted from result for LPS-challenged animal) expressed relative to the mean of LPS-challenged controls (see Figures 4.16 to 4.19).
- B 95% confidence limits increase dramatically when the extrapolated ED<sub>50</sub> was outside the evaluated range of estimated inhaled doses.
- NC Not calculable

A significant decrease in aerosol particle size (MMAD) with an increase in lung concentration for amorphous GSK-899 was consistent with an increase in ED<sub>50</sub>. However, the variability of data indicated by the 95% confidence limits precluded clear ranking of all aerosol forms of

GSK-899, and limited general conclusions with regards to ranking of the compounds.

Measurements of TNF $\alpha$  in serum and BALF showed high variability and appeared unsuitable for evaluating a dose response for inhibition of acute lung inflammation in the rat model used. It is noteworthy that, for the three administered volumes of lavageate (5 mL/lavage), mean recoveries of 58%, 76% and 80% were achieved for successive cycles. Although the lung lobes were massaged prior to removal of each BALF volume, retention of fluid from the first lavage cycle in the distal lung may potentially impair access of successive volumes of lavageate to the distal lung and/or poor mixing of the administered and residual lavageates may give rise to incomplete sampling of TNF $\alpha$  and neutrophils from the lower respiratory tract.

Schneider *et al.* (1997) described a method for determining neutrophil counts in BALF based upon the enzymatic activity of MPO. However, a high baseline achieved for immunostaining of MPO (even after redaction of CD68-positive areas, *i.e.* macrophages) indicated this biomarker lacked sufficient specificity for identifying neutrophils in rat lung sections without further method development. Standalone image analysis results for CAE-stained lung sections from rats exposed to GSK-677 were equivocal. However, results for rats exposed to GSK-899 or GSK-361 (Appendix 10) subsequently confirmed CAE also lacked sufficient specificity to identify neutrophils in rat lung sections (no obvious inhibitory dose response; 95% confidence limits not calculable).

This chapter describes experiments undertaken to characterised the efficacy of three p38 MAPK inhibitors using a rat model for acute lung inflammation, when administered as nebulised solutions, amorphous (GSK-899) or crystalline dry powder formulations. Key conclusions of experiments described in this chapter are:

- The observed variability in biomarkers limited the conclusions that could be drawn from the data. Nevertheless, attempts to stain

histology sections of lung for biomarkers of neutrophils produced insufficient contrast for quantitative image analysis. Assessment of acute lung inflammation by counting neutrophils in BALF, although variable, was thus the best of the biomarkers evaluated.

- A larger particle size of amorphous GSK-899 (MMAD  $\geq 3.8 \mu\text{m}$  versus  $2.1 \mu\text{m}$ ) and hence a less respirable aerosol resulted in a less effective dose (higher ED<sub>50</sub>). Differences in drug particle size and hence the lung deposited dose therefore modulated drug efficacy for inhibition of acute lung inflammation.
- The median effective dose (ED<sub>50</sub>) for suppression of neutrophils in BALF ranked compounds GSK-899 < GSK-361 < GSK-677, with confidence limits indicating a significant difference between GSK-899 and the other compounds.
- ED<sub>50</sub> values were similar for respective nebulised and crystalline aerosol forms of GSK-361 (high passive membrane permeability) and GSK-677 (high solubility). However, dry powder formulations of GSK-899 were more effective at four hours post LPS-challenge (ED<sub>50</sub> values lower) than for a nebulised solution consistent with an increased lung residence time (Hastedt *et al.*, 2016).
- GSK-899, a drug of relatively low solubility and consequently more persistent in lung tissue, inhibited LPS-induced lung inflammation more effectively than GSK-361 (low solubility; high passive membrane permeability) and GSK-677 (high solubility).

Image analysis could potentially facilitate quantification of LPS-induced acute lung inflammation in histological sections but identification of a robust biomarker of neutrophils and development of histology methods is required to achieve the tighter confidence limits necessary for a more robust ranking of p38 MAPK inhibitors and aerosol forms for efficacy. In addition, comparison of lung sections stained for such a biomarker of neutrophils from rats administered a p38 MAPK inhibitor with or without being sampled for BALF four hours post LPS-challenge would indicate the efficiency with which neutrophils are harvested from lungs by lavage.

# **CHAPTER FIVE**

**Toxicopathology of p38 mitogen-  
activated protein kinase inhibitors  
in rats after inhalation of fixed  
doses for 28 days**

## 5.1. Introduction

Non-clinical studies performed to characterise the general toxicology of candidate drugs typically administer compounds via the clinically relevant route, *i.e.* the anticipated exposure route for dosing humans. However, inhaled administration of drugs to laboratory animals consumes large masses of test material, relative to other exposure routes. This is especially true of conventional inhalation exposure systems used for presentation of dry powder aerosols, in which airflow is normally operated dynamically without recycling the test aerosol. A proportion of the particulate impacts or sediments within the exposure system. Furthermore, published estimates of the lung deposited dose indicate that only 7% to 10% of an inhaled aerosol of 2  $\mu\text{m}$  aerodynamic diameter is deposited in the lungs of rats (Snipes, 1989, Jones and Baldrick, 2013). This is in stark contrast to the straightforward administration of drugs orally or via parental routes involving injection, which permits precise delivery of dose volumes with little wastage of the liquid formulation.

The pharmaceutical industry is coming under increasing pressure to reduce the cost of developing new drugs and, by implication, minimising expenditure associated with early development of candidate drugs that subsequently fail to achieve regulatory approval. In early drug development, synthesis of a candidate drug is performed on a small scale at relatively high cost. In 2016, it took 6 to 9 months and a cost of £200,000 to £300,000 to synthesise approximately 30g of drug to support doses of  $\leq 2.3$  mg/kg/day for the first inhalation toxicity studies of a respiratory drug in rats (28 days treatment) and dogs (14 days treatment). Less than 4% of this amount of drug would have been required to dose these animals orally (conservative estimate from unpublished data). The use of surrogate exposure routes and/or formulations (differing from intended clinical presentation) to reduce compound usage and thereby expedite preliminary evaluation of drugs

to “first time in humans” (FTIH) would thus be attractive if effective. However, such strategies defer de-risking potentially altered tolerability or toxicopathology of the final formulation and dose route until later in development.

The requirement for pre-market testing of pharmaceuticals as evidence of safety for new drugs was enacted in US legislation in 1938 (Kille, 2013) and was formally instigated in the United Kingdom following outcry over birth defects following the prescription of thalidomide to pregnant mothers in the late 1950s and early 1960s (MHRA, 2012). Today, the International Council for Harmonisation of Technical Requirements for Pharmaceuticals for Human Use (ICH) maintains oversight of its safety guidelines outlining investigations to generate comprehensive datasets to satisfy regulatory requirements for market approval of drugs. Experimental designs based on such guidance continue to evolve within pharmaceutical and contract research organisations.

The principals of reduction, refinement and replacement of the use of animals in scientific research (3Rs) are fundamental to the ethical review process and regulation of *in vivo* experiments (Festing and Wilkinson, 2007). However, the most complete assessments of pulmonary drug delivery, efficacy and toxicity are still provided by *in vivo* investigations (Fernandes and Vanbever, 2009). Understanding the relationship between endpoints for *in vitro* and *in vivo* experiments and the extent to which the former can predict the latter are thus key to implementation of the 3Rs.

Haematoxylin (Titford, 2005) and eosin (Bancroft and Cook, 1994) were first used for dyeing fabrics in the early 1500s and 1875 respectively. Amateur microscopists started using these dyes in the mid-1800s to stain cellular components, which was a milestone in medical research because the two stains have become the main diagnostic technique for histopathologists today (Bancroft and Cook,

1994); haematoxylin stains basophilic substances blue (e.g. calcified structures, DNA in the nucleus and RNA in the endoplasmic reticulum) and eosin is a pink counter stain that binds to acidophilic moieties such as lysine or arginine side chains in proteins, which are prevalent in tissue fibres and the cytoplasm. Other histological stains or techniques such as immunohistochemical staining of clusters of differentiation may be used to determine the phenotypes of inflammatory cells seen in section (Saetta *et al.*, 1999, Fehrenbach *et al.*, 2003).

Although histopathology evaluation of tissues is the 'gold standard' for evaluating toxicopathology, an understanding of dosimetry, exposure and fate of a test article are also key to understanding the context for toxicopathology findings, particularly when comparing formulations or compounds. For example, the severity or potential absence of a lesion observed histopathologically could be a function of differences in the achieved dose, systemic exposure and/or the rate of elimination of a compound from the affected tissue.

Experiments described in this chapter were designed with reference to a generic protocol designed to investigate the general toxicity of pre-candidate drugs in rodents. Unpublished toxicopathology data in rats administered crystalline GSK-899 (Freke, 2010) or GSK-677 (Freke, 2007) were used to select suitable doses for the *in vivo* toxicity studies.

### **5.1.1 Aims and objectives**

Using three p38 MAPK inhibitors of differing physicochemical properties, the experimental aims of this chapter are to:

- Investigate the potential cellular toxicity, release of inflammatory cell mediators and particle uptake by macrophages *in vitro*.
- Determine histopathological changes in the respiratory tract of rats administered one of three p38 MAPK inhibitors for 28 days.
- Determine the systemic (plasma) and lung exposure of each p38 MAPK inhibitor in rats after single and repeated exposure.

- Investigate the particle uptake of macrophages *in vivo*, following inhaled administration of three p38 MAPK inhibitors for 28 days

By comparing the data generated following administration of the p38 MAPK inhibitors as nebulised solutions or dry powder aerosols, the following hypotheses will be tested:

- Changes in aerosol presentation to rats will affect exposure of tissues and systemic absorption of the drug, resulting in modulation of toxicopathology after repeated administration due to pulmonary drug clearance or persistence/accumulation.
- Differences in physicochemical properties between compounds may affect drug-lung clearance or compartmentalisation of a drug in cells or fluid compartments within the respiratory tract, which in turn influence adaptive changes (e.g. lung clearance) and/or toxicopathology following repeated administration.

It is anticipated that results of these investigations will contrast the toxicopathology of molecules with differing physicochemical properties and illustrate potential limitations of using surrogate formulations. Increased understanding of such limitations could optimise experimental design in early non-clinical development of inhaled drugs.

## 5.2. Materials and methods

### 5.2.1. Test articles

The p38 MAPK inhibitors were supplied by GSK as micronised crystals and stored at ambient temperature, protected from light and moisture (Table 5.1).

**Table 5.1: Purity of p38 MAPK inhibitors used for repeated administration to rats**

Test article	Salt form	Purity	<i>In vivo</i> study numbers
GSK258899B	mesylate	95.4%, 98.7%	R29413
		98.7%	R29739
		95.4%	R30353N, R30662N, R31038N, R31039N
		95.5%	R31697N, R31711N
GSK610677B	hydrochloride	98.5%	R31037N, R31038N
GSK678361A	parent	99.7%	R31034N, R31035N, R31036N
SB-681323T	tosylate	99.6%	n/a

Amorphous GSK-899 was produced by spray drying a saturated solution of GSK-899 (prepared from micronised crystals) in methanol. The amorphous state of the resultant material was confirmed by X-ray powder diffraction analysis (XRPD; Chapter 2, Section 2.3.2).

### 5.2.2. *In vitro* cytotoxicity and morphology of NR8383 rat macrophage cells incubated with particles

The NR8383 cell line was established from normal alveolar macrophages obtained from Sprague Dawley rats by bronchoalveolar lavage (Helmke *et al.*, 1987, Helmke *et al.*, 1989) and obtained from American Type Culture Collection (ATCC, Manassas, USA) care of LGC (Middlesex, UK).

The NR8383 cells were grown in Kaighn's modification of Ham's F12 medium (Kaighn *et al.*, 1981) with 2mM glutamine, supplemented with 15% heat-inactivated foetal bovine serum (Invitrogen catalogue number 10108-157) and 100 units/mL penicillin and 100 µg/mL streptomycin serum (Invitrogen catalogue number 15140-122). The cells were incubated in T75 cm<sup>2</sup> (20 mL) or T175 cm<sup>2</sup> (50 mL) tissue

culture flasks, which were maintained at 37°C in a humidified atmosphere containing 5% CO<sub>2</sub>; cell culture media was changed twice weekly. Approximately 0.5 × 10<sup>5</sup> cells/mL were seeded (40 mL into a T175 cm<sup>2</sup> flask), of which approximately half adhered to the flask and half remained as a floating population of cells.

#### **5.2.2.1. Treatment of cells to investigate cytotoxicity and release of inflammatory cell mediators**

Cytotoxicity was assessed by measurement of the enzymatic activity of lactate dehydrogenase (LDH) in the extracellular medium. LDH is a cytosolic enzyme and leakage of the enzyme into the medium is an indication of cell membrane damage (Fotakis and Timbrell, 2006). All treatments (p38 MAPK inhibitor concentrations and controls) were performed in triplicate.

Cells were seeded into wells (48-well tissue culture plates (Costar™ 3548); 6 × 10<sup>4</sup> cells in 125 µL), incubated for two to four hours. An equal volume of medium containing p38 MAPK inhibitor was added (typically six concentrations to cover a range of 6.25 to 400 µg/mL) and the treated cells were incubated for 72 hours.

Controls were similarly treated, by addition of an equal volume of media alone (negative control) or appropriate reagent in media (positive control) as follows:

- Untreated control (addition of media only at 0 hours).
- Triton X-100 (catalogue number T9284; Sigma Aldrich, Dorset, UK): positive control for LDH (cytotoxicity). Triton X-100 was added to cells at 71.5 hours to achieve a final concentration of 0.1% (v/v), to solubilise cellular membranes and release intracellular lactate dehydrogenase into the media.
- Lipopolysaccharide (catalogue number L2654-1MG; Sigma Aldrich, Dorset, UK): positive control for cytokine/chemokine release. Lipopolysaccharide was added to cells at 0 hours to achieve final concentrations of 5 and 10 ng/mL.

On completion of the 72-hour treatment period, the 48-well plates were centrifuged (805×g for 10 minutes) and aliquots of 50 µL supernatant were transferred to flat-bottomed 96-well plates for LDH analysis. Remaining supernatant (approximately 200 µL) was transferred to wells in a 'v-bottomed' 96-well plate for analysis of cytokines. The pelleted cells were lysed at room temperature with addition of 250 µL of cell lysis agent (CellLytic™ Sigma C2978) for 15 minutes. The 48-well plates were then centrifuged (805×g for 10 minutes) and aliquots of 50 µL supernatant were transferred to flat-bottomed 96-well plates for measurement of total LDH from the lysed cells.

#### **5.2.2.2. Analysis of cytotoxicity by measurement of lactate dehydrogenase leakage from treated cells**

LDH in the media supernatant was analysed using a colourimetric technique. A reaction mixture was prepared in accordance with the protocol supplied with the Cytotoxicity Detection Kit (Roche, 2016) and 50 µL transferred to each well. The media-reaction mixture stood for 30 minutes at room temperature, protected from light, and was then transferred to a cuvette and the absorbance of the sample was measured at wavelength 490 nm using a Spectramax absorbance plate reader (wavelength correction applied at 650 nm).

The proportion of LDH leaking from the NR8383 cells was calculated using the following equation:

$$\text{-----} \quad \text{..... Equation 4}$$

The median effective concentration (EC<sub>50</sub>) was extrapolated from the dose response curve, which was scaled for a maximum response value of 100% relative to the total LDH value determined for the lysed cells.

p38 MAPK inhibitors were categorised for their potential cellular toxicity as low risk (EC<sub>50</sub> >100 µg/mL), medium risk (EC<sub>50</sub> of 10 to 100 µg/mL) or high risk (EC<sub>50</sub> <10 µg/mL). Categorisation of compounds as low or medium risk was made with reference to a threshold of 100 µg/mL, representing a maximum theoretical drug concentration in rat epithelial

lung fluid to cover a clinical dose of 1 mg. This was derived from a published estimate of the volume of epithelial lung fluid in rats (Cheng *et al.*, 1995), an assumed body weight of 350 g and reference dose of 0.6 mg/kg to cover a nominal clinical dose of 1 mg/kg (rationale defined in Chapter 2, Section 2.2.4). The “high risk” category was based upon unpublished *in vivo* data indicating foamy macrophages are more likely to occur in animals retaining more than 10% of the lung deposited dose at 24 hours post exposure.

#### **5.2.2.3. Analysis of inflammatory cell mediators**

The remaining supernatant prepared at 72 hours was centrifuged (340×g for 5 minutes) to remove debris, and the resultant supernatant aliquoted into a 96-well plate. A duplicate plate was prepared as a contingency for repeat analysis. The plates were stored at -80°C or colder pending quantification of cytokines/chemokines using the multiplex Meso Scale Discovery (MSD) protocol supplied with the kit (Plate Catalogue Number N75CA-1) for the following parameters:

- Interleukins: IL-1 $\alpha$  and IL-1 $\beta$
- Tumour necrosis factor (TNF)
- Chemokine: CXCL1 (C-X-C motif, ligand 1) otherwise known as keratinocyte chemoattractant (KC) or growth-regulated oncogene (GRO)
- MCP-1 (monocyte chemotactic protein 1)

#### **5.2.2.4. Treatment of cells to investigate cell morphology**

Cells were seeded into wells (six-well tissue culture plates (Costar™ 3506);  $7.6 \times 10^5$  cells in 1.5 mL), incubated for two to four hours. An equal volume of medium containing p38 MAPK inhibitor was added (final concentrations of 50 or 400  $\mu\text{g}/\text{mL}$ ) and the treated cells were incubated for 72 hours. Controls were similarly treated, by addition of an equal volume of media alone (untreated control) or chloroquine diphosphate (final concentration 10  $\mu\text{g}/\text{mL}$ ; catalogue number C6628; Sigma Aldrich, Dorset, UK) as a positive control for phospholipidosis.

On completion of the 72-hour treatment period, cells were harvested from the six-well plates by gently scraping the cells using a plunger from a syringe and then transferring the cells to a 15 mL tube. The contents of replicate wells for a given treatment were pooled. The harvested cells were centrifuged (340×g for five minutes) and the supernatant discarded. The cells were resuspended and fixed in 1 mL of phosphate buffered 4% formaldehyde with 1% glutaraldehyde and the cells processed for transmission electron microscopy.

#### **5.2.2.5. Processing cells for examination of morphology by transmission electron microscopy**

Cells fixed in 4% formaldehyde and 1% glutaraldehyde (v/v) were transferred to a 1.5 mL eppendorf tube and centrifuged. For each of the washings or manipulations stated below, the supernatant was carefully removed (by pipette) and discarded, taking care not to disturb the pellet of cells, and approximately 1 mL of reagent was added.

The fixed cells were washed with three changes of Millonig's phosphate buffer (Millonig, 1961), which was prepared as follows:

Stock solutions of 2.26% (w/v) sodium dihydrogen orthophosphate ( $\text{NaH}_2\text{PO}_4$ ) in distilled water, and 2.52% (w/v) sodium hydroxide (NaOH) in distilled water were prepared and stored refrigerated (approximately 4°C for up to three months).

Millonig's phosphate buffer was prepared by mixing 83 mL of 2.26% (w/v)  $\text{NaH}_2\text{PO}_4$ , 17 mL of 2.52% NaOH, 10 mL of distilled water and 0.54g of sucrose. The resultant formulation was mixed well and accepted for use if pH was within 7.0 to 7.4.

The Millonig's phosphate buffer was carefully removed and the cells treated for 60 minutes with 1% aqueous osmium tetroxide ( $\text{OsO}_4$ ) reduced with 1.5 % aqueous potassium ferrocyanide ( $\text{K}_4[\text{Fe}(\text{CN})_6]$ ); the reaction mixture was prepared shortly before use by mixing stock solutions (1:1 v/v) of 2% (w/v)  $\text{OsO}_4$  and 3% (w/v)  $\text{K}_4[\text{Fe}(\text{CN})_6]$ .

The  $\text{OsO}_4$  and  $\text{K}_4[\text{Fe}(\text{CN})_6]$  reaction mixture was carefully removed and the cell pellet washed with two changes of distilled water (each of five minutes). The cells were then treated with 0.1% (w/w) aqueous sodium thiocarbohydrazide for 10 minutes and again washed with two changes of distilled water (each of five minutes). The water was removed and discarded, and the cell pellet treated with aqueous 1%  $\text{OsO}_4$  reduced with aqueous 1.5 %  $\text{K}_4[\text{Fe}(\text{CN})_6]$  for 15 minutes.

The  $\text{OsO}_4$  and  $\text{K}_4[\text{Fe}(\text{CN})_6]$  reaction mixture was discarded and the cell pellet washed with three to four changes of distilled water, and dehydrated in two washes of 30% ethanol (five minutes each), one wash with 70% ethanol (five minutes), one wash in 90% ethanol (five minutes), three washes in absolute ethanol (10 minutes each) and two washes in dried acetone (each of five minutes; moisture was removed from acetone through storage over a molecular sieve).

The acetone was discarded and cell pellet was treated with 50% Agar 100 resin (product code AGR1031; Agar Scientific Ltd, Essex, UK) in acetone (v/v) for two hours, 80% Agar 100 resin in acetone (v/v) overnight, and then four changes of 100% Agar 100 resin for a total period of at least seven hours. The resin embedded cells were then cured in an oven at 65°C for 24 hours.

#### Preparation of slides and transmission electron microscopy

Sections approximately 1  $\mu\text{m}$  thick were cut using a microtome and stained with 1% toluidine blue in 1% aqueous sodium tetraboratetoluidine (w/w/v) and examined by light microscopy to locate areas of interest for electron microscopy. Ultra-thin sections (80 to 90 nm thick) were then prepared, stained with 0.5% uranyl acetate and 3% lead citrate using an automated grid stainer and examined using a Hitachi H7500 transmission electron microscope (TEM), operated at 80KV. The AMT XR41 Digital Camera System was used to capture representative TEM digital images and 100 cells were assessed for

morphological changes including vacuolation. Representative images of the macrophages are shown in Section 5.3.

### 5.2.3. Investigating the toxicopathology and exposure of inhaled p38 MAPK inhibitors in rats

In order to investigate the toxicopathology of p38 MAPK inhibitors in the respiratory tract of rats and to put potential findings in context with concomitant pharmacokinetics, groups of rats were administered fixed 'doses' of the test aerosol, once daily by snout-only inhalation exposure, for up to 28 consecutive days (Figure 5.1).

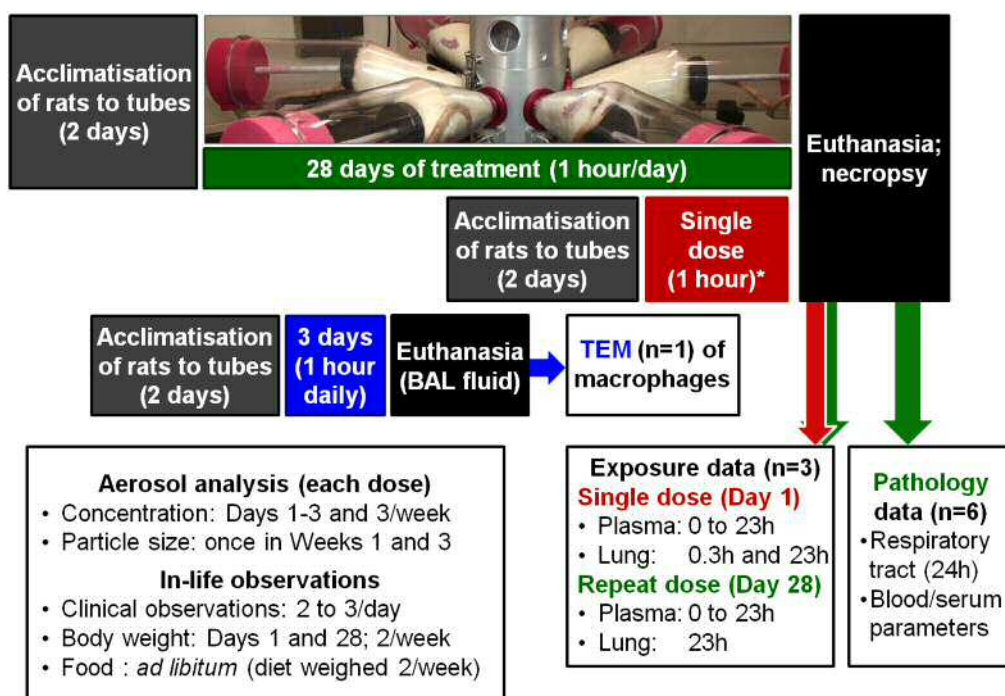


**Figure 5.1: Generic outline of experimental design to investigate pulmonary toxicology following inhaled administration of p38 MAPK inhibitors for 28 days.** Rats (n=6/dose) inhaled a p38 MAPK inhibitor (dry powder or aqueous formulation) or vehicle (control) for 1 hour daily for 28 days. Rats were euthanized on Day 29 and the respiratory tract was preserved in formalin for histological processing and examination by light microscopy. Satellite groups (3 rats/dose/timepoint) were sampled for plasma and lung for analysis of drug concentrations after a single dose and 28 days of treatment (\* rats administered a single dose were exposed concurrently with repeat dose animals on Day 28 of treatment). In most instances, an additional rat for each aerosol form was treated for 3 days and euthanized (Day 4) for bronchoalveolar lavage (BAL) of lungs with saline to harvest macrophages for examination by transmission electron microscopy (TEM).

Blood and tissue samples were obtained for three key investigations as follows:

- Toxicopathology changes in the respiratory tract after 28 days of treatment, with reference to a vehicle control (n = 6 rats/group).
- Systemic exposure measured in rat plasma sampled post exposure on Days 1 and 28 of treatment (n = 3 rats/group/day).

Drug concentrations in lungs taken as soon as practicable after exposure on Day 1, and 24 hours post exposure on Days 1 and 28 of treatment (n = 3 rats/group/timepoint).

In addition, the lungs of a few animals at selected doses were sampled by bronchoalveolar lavage (BAL; flushing of lungs with saline) and the harvested macrophages were examined by TEM for particle uptake.

Datasets were generated from a series of experiments, in which one of the p38 MAPK inhibitors (GSK-899, GSK-677 or GSK-361) was administered to rats as a given aerosol form, *i.e.* crystalline powder (or amorphous GSK-899) or nebulised aqueous formulation.

#### **5.2.3.1. Dose selections for investigating pulmonary toxicopathology in rats**

Target doses ( $\leq 45$  mg/kg/day GSK-899) were initially selected with reference to unpublished toxicopathology data for inhaled GSK-899 and then dose range studies conducted in support of this research. Where practicable, target doses of 1 and 15 mg/kg/day were applied for each p38 MAPK inhibitor for each aerosol form. Nebulised doses of GSK-899 and GSK-361 were limited by the relatively low solubility of each test article in aqueous vehicle, and the maximum practicable dose for these experiments was 1 mg/kg/day. A dose of 1 mg/kg/day in rats equated to a 17-fold overage for a nominal clinical dose of 1 mg with application of conservative scaling factors for lung deposition (Degeorge *et al.*, 1997, Jones and Baldrick, 2013). Details of dose selections for each experiment are summarised below.

GSK-899 (crystalline): 1 and 15 mg/kg/day

Doses of 1 and 45 mg/kg/day were initially selected for evaluation of crystalline GSK-899. A high dose of 45 mg/kg/day was based on unpublished data (Freke, 2010) and was expected to induce adverse (harmful) toxicopathology in rat lungs (findings consistent with interstitial pneumonia were seen in rats administered 49.7 mg/kg/day for 28 days). A low dose of 1 mg/kg/day was anticipated to be a non-adverse dose, *i.e.* a dose that does no harm to the test animals (Kerlin *et al.*, 2016).

Whilst defining compound requirements to support this research, it became clear insufficient GSK-899 was available to prepare the mass of amorphous GSK-899 required to sustain doses up to 45 mg/kg/day for 28 days. Dose range experiments performed using crystalline GSK-899 indicated toxicopathology findings at 15 or 45 mg/kg/day after three days were similar (Appendix 5) and a dose of 15 mg/kg/day was adopted as the high dose for further investigations of toxicopathology.

GSK-899 (amorphous): 0.02, 1 and 15 mg/kg/day

Doses of 1 and 15 mg/kg/day were selected for comparison with toxicopathology findings in rats administered crystalline GSK-899. A low dose of 0.02 mg/kg/day was included for the amorphous powder and represented a theoretical threshold above which accumulation of GSK-899 may occur, based on the solubility of GSK-899 in simulated lung fluid and published estimates for the volume of epithelial lung fluid in rats (Rennard *et al.*, 1986).

GSK-899 (nebulised): 1 mg/kg/day

Nebulised doses were limited by the relatively low aqueous solubility of GSK-899. Rats were first exposed using a solution of GSK-899 in 3% (v/v) Solutol HS 15 in 10% (w/v) aqueous 2-hydroxypropyl- $\beta$ -cyclodextrin (Solutol-HP $\beta$ CD). However, lung pathology changes in control animals examined after 28 days of treatment were ascribed to the vehicle and exacerbated by GSK-899. The experiment was repeated using another vehicle, 3% (v/v) Solutol HS 15 in 0.9% (w/v)

aqueous sodium chloride (Solutol-NaCl), to determine what findings could be ascribed to GSK-899 alone when administered in solution. Before undertaking this second experiment, a preparatory study was performed in which rats (n=6) were exposed to the latter vehicle alone for 14 days; an absence of lung pathology changes after 14 days of treatment indicated vehicle-related changes would be unlikely after completion of the 28-day treatment period in the main experiment.

GSK-677 (crystalline): 1, 6.7 and 15 mg/kg/day

Doses of 1 and 15 mg/kg/day were selected to facilitate comparison of systemic and lung exposure following inhaled administration of crystalline GSK-677 to rats, with comparable data for GSK-899. An intermediate dose of 6.7 mg/kg/day represented a theoretical threshold above which accumulation may potentially occur, again based on the solubility of GSK-677 in simulated lung fluid and published estimates for the volume of epithelial lung fluid in rats (Rennard *et al.*, 1986). Additional animals were not used to evaluate the inhalation toxicity of crystalline GSK-677 because unpublished data (Freke, 2007) were available to the sponsor, citing a no observed adverse effect level of 67.8 mg/kg/day (Table 5.22).

GSK-677 (nebulised): 1, 6.5 and 15 mg/kg/day

Nebulised doses of 1, 6.5 and 15 mg/kg/day were selected to compare systemic and lung exposure data for GSK-677 with comparable data for the crystalline form, and for comparison of potential toxicopathology findings with changes seen following administration of GSK-899 to rats.

GSK-361 (crystalline): 0.25, 1 and 15 mg/kg/day

Doses of 1 and 15 mg/kg/day were selected to facilitate comparison of potential findings in rats administered crystalline GSK-361 with the lung changes and exposure (drug concentrations in lung tissue and plasma) after administration of GSK-899 to rats for 28 days. A low dose of 0.25 mg/kg/day was included and represented a theoretical threshold above which accumulation of GSK-361 may potentially occur, based on the solubility of GSK-361 in simulated lung fluid and published

estimates for the volume of epithelial lung fluid in rats (Rennard *et al.*, 1986).

GSK-361 was not developed for clinical administration via the inhaled route. In the absence of inhalation toxicology or exposure data, a dose range study (R31034N) was performed in which doses of 5 or 15 mg/kg/day were administered to groups of rats (n=4) for 14 days. Doses were well tolerated with no lung changes to preclude progression of the 28-day study (Appendix 6), *i.e.* no indication that an onset of toxicity would prevent completion of the treatment period.

#### GSK-361 (nebulised): 0.25 and 1 mg/kg/day

The high dose of nebulised GSK-361 was limited by its relatively low solubility in vehicle (20:20:60 (v/v/v) Solutol HS 15, ethanol and 60 mM phosphate buffer). Doses of 0.25 and 1 mg/kg/day were selected to facilitate comparison of potential lung changes and exposure in rats administered crystalline GSK-361 or aerosols of p38 MAPK inhibitors (1 mg/kg/day) at these doses.

#### **5.2.3.2. Investigating mechanisms of toxicopathology seen in rats inhaling p38 MAPK inhibitors**

Key findings for the 28-day inhalation toxicology studies included toxicopathology findings observed in the lungs of rats administered GSK-899 or GSK-677, not only as dry powder formulations but also as nebulised solutions (Section 5.3). Although these p38 MAPK inhibitors were administered as aqueous formulations that remained in solution when diluted in simulated lung fluid, it is possible the airborne drug may have precipitated prior to deposition of droplets in the respiratory tract. In order to investigate the mechanism of action, *i.e.* to determine if the lung changes were attributable to the presence of particulate material or the chemical (pharmacological) action of the compound *per se*, two experimental approaches were considered for further evaluation.

#### Inhaled administration of a pharmacologically 'inert' analogue

Histopathological examination of the lungs of rats administered an inert analogue of GSK-899 for 28 days would facilitate a means of

determining if lung toxicopathology observed following repeated exposure of rats to GSK-899 was attributable to the molecular action of the drug *per se* (pharmacology or ‘off-target toxicity’) or due to a more generic mechanism such as the presence of drug particulate in the lungs of affected rats; a reduced incidence and/or severity of lung findings would implicate a molecular mechanism for the p38 MAPK inhibitors. GSK2656081A (GSK-081) is a p38 MAPK inhibitor and an isomer of GSK-899 (Figure 5.2), with a potency approximately 100-fold lower than the latter compound.

**5.2A: GSK2656081A (GSK-081)**      **5.2B: GSK258899A (GSK-899)**

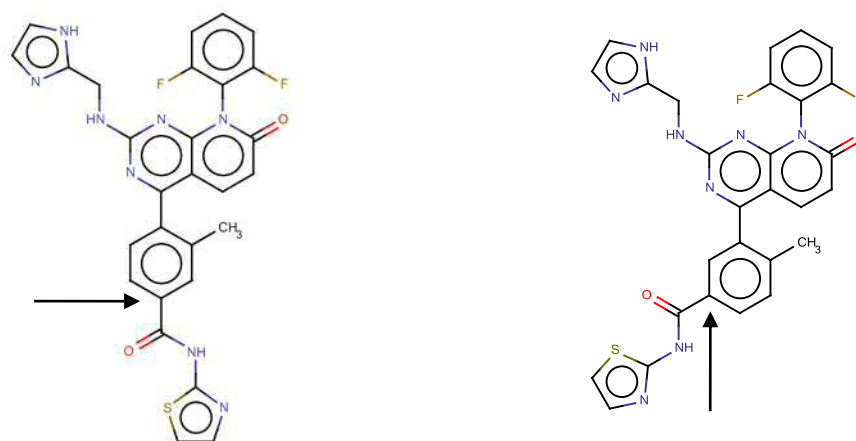


**Figure 5.2:** Chemical structures of two structurally similar isomers with different pharmacological potencies. Differences in the position of the carbonyl group are shown by an arrow. **Fig 5.2A:** GSK2656081A (free base). **Fig 5.2B:** GSK258899A (free base) is approximately 100-fold more potent.

Approximately 1 kg of crystalline GSK-081 was required to produce sufficient micronised material for the comparative target inhaled doses for a 28-day inhalation toxicology study. However, the cost of production in 2013 was estimated at £186,000 and prohibitive for this research project.

Examination of rat lungs following repeated systemic exposure

Administration of GSK-899 or GSK-677 to rats using an alternative route remote from the respiratory tract would provide a means for *in situ* perfusion of lungs by the p38 MAPK inhibitors. An absence of toxicopathology findings after 28 days of treatment would imply the

changes observed in lungs after 28 days of inhalation exposure were attributable to a localised effect of deposited aerosol particulates.

Intravenous infusion of the p38 MAPK inhibitor into the caudal vein, for one hour daily, was initially considered as the surrogate exposure route of choice to achieve a similar drug-time concentration profile in plasma to that anticipated for a one-hour inhalation exposure period, *i.e.* a profile with steady state achieved during a one-hour dosing period followed by a post dose decline in plasma concentration. However, intravenous infusion of aqueous formulations for 28 days presents significant technical challenges including surgical preparation of rats and maintaining the patency of cannulae throughout the treatment period. Such studies require extensive experience in the use of this technique for prolonged treatment periods, a capability that was not available locally. The cost of funding the proposed experiment at a contract research organisation (\$169,600 CDN in 2016, equating to £106,000) was prohibitive for this research project.

Subcutaneous injection was subsequently evaluated as an alternative exposure route. A single dose of GSK-899 or GSK-677 (5 mg/kg) in Solutol-NaCl was administered dorsally as a bolus injection to groups of rats (n=3) to evaluate the systemic exposure (Appendix 7) and tolerability of the test article at the injection site (Appendix 8). Rats were euthanized after a four-day off-dose period and the injection site taken for histopathological examination. The injection site was sampled after an off-dose period to evaluate the potential degree of recovery between consecutive injections at a site if repeated dosing (injection once daily) was rotated across four dorsal injection sites. Observations indicated subcutaneous administration of GSK-899 was likely to be tolerated for 28 days according to the proposed dosing regimen. However, degenerative and inflammatory changes at the injection site of two rats administered a single subcutaneous dose of GSK-677 precluded progression of this compound for repeated administration.

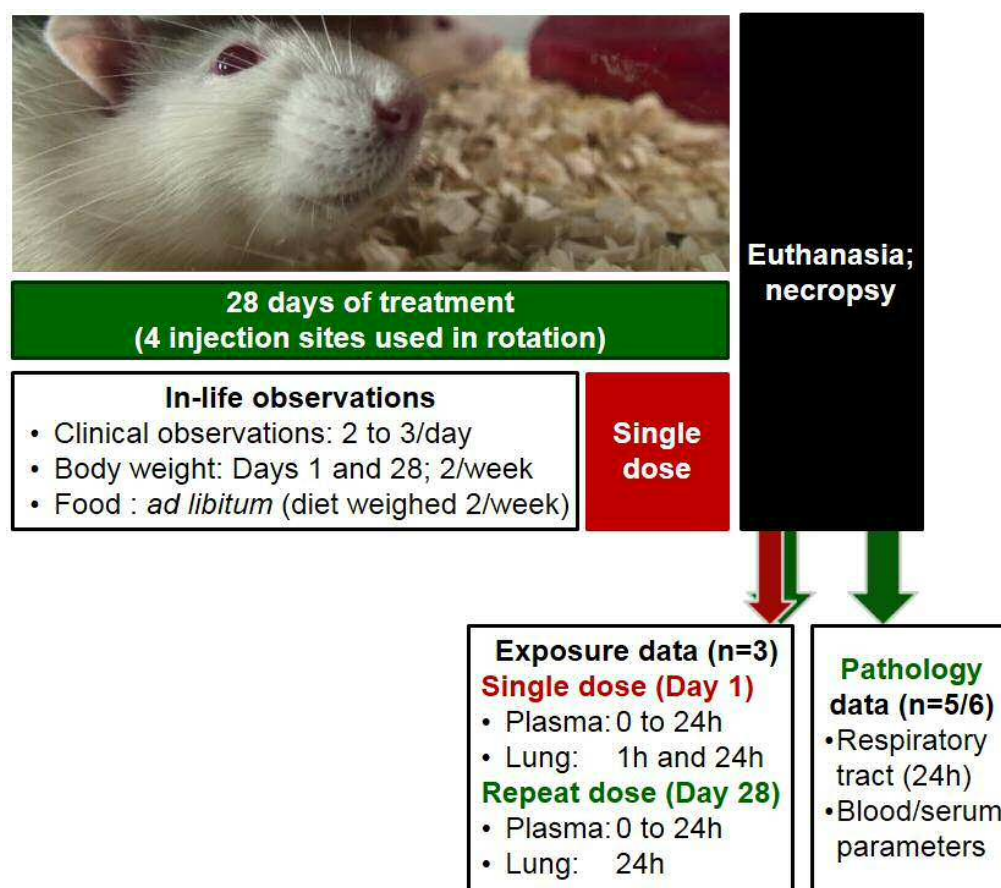


**Figure 5.3: Outline of experimental design to investigate pulmonary toxicology after subcutaneous administration of GSK-899 for 28 days.** Rats were dosed 5 mg/kg/day (n=6 rats) or the vehicle (control; n=5 rats) once daily for 28 consecutive days; four dorsal injection sites were used in rotation (7 injections/site with off-dose periods of 3 consecutive days). Rats were euthanized on Day 29 and the respiratory tract was preserved in formalin for histological processing and examination by light microscopy. Satellite groups (3 rats/dose/timepoint) were sampled for plasma and lung for analysis of drug concentrations after a single dose and 28 days of treatment.

In order to investigate the pulmonary toxicopathology of systemically exposed rats and to put potential findings in context with concomitant pharmacokinetics, groups of rats were dosed GSK-899 at 5 mg/kg/day subcutaneously, once daily, for up to 28 consecutive days (Figure 5.3).

Blood and tissue samples were obtained for three key investigations as follows:

- Toxicopathology changes in the respiratory tract after 28 days of treatment, with reference to vehicle controls (n = 6 rats/group).

- Systemic exposure measured in rat plasma sampled post exposure on Days 1 and 28 of treatment (n = 3 rats/group/day).
- Drug concentrations in lungs taken one hour post dose on Day 1, and 24 hours post dose on Days 1 and 28 of treatment (n = 3 rats/group/timepoint).

A dose of 5 mg/kg/day was selected with reference to pharmacokinetic plasma data in rats sampled after a single subcutaneous dose of 5 mg/kg (Appendix 7), equating to systemic exposure at least 6-fold higher than that achieved following inhaled doses of 15 mg/kg/day.

#### **5.2.4. Test system and animal husbandry**

Male Crl:CD(SD) rats (Charles River UK Ltd, Margate, Kent) were randomly allocated to groups and accommodated under standard laboratory conditions (Home Office, 2014) with access to food and water as described in Chapter 2 (Section 2.2.4.1). Rats were identified by a number written in indelible ink on the tail, except for animals of the first study performed using crystalline GSK-899 (study R29413) in which rats were tattooed in line with local practices at that time.

Rats were accommodated for at least five days before undertaking the first licensed procedure (tube restraint) and were approximately 10 weeks old on the first day of aerosol administration (Day 1). Satellite animals administered a single inhaled exposure for measurement of p38 MAPK inhibitor in plasma and/or lung tissue were maintained in the animal holding room and then exposed concurrently with repeat dose animals on Day 28 of treatment; single dose animals were thus approximately 14 weeks old on the day of exposure.

The Crl:CD(SD) strain of rat was used for non-clinical safety studies performed using GSK-899 and GSK-677 before termination of the respective drug development programmes. This strain of rat was thus selected for continuity with and reference to historical (unpublished) toxicopathology data for these p38 MAPK inhibitors.

Clinical observations and body weight measurements were maintained for all animals to ensure their general wellbeing during the experiment and to facilitate key procedures or investigations such as dosing.

### **5.2.5. Subcutaneous dosing of rats**

Rats were dosed GSK-899 (1 mg/mL in Solutol-NaCl adjusted to within pH 4 to 6; dose volume of 5 mL/kg) for up to 28 days. Rats were injected at one of four dorsally located sites, used in rotation, such that a period of three days elapsed between consecutive injections at the same location. This facilitated a degree of recovery from any trauma associated with the dosing procedure. Chemical analysis (HPLC-UV) of samples taken from formulations dosed on Days 1 and 28 confirmed satisfactory accuracy of preparation.

### **5.2.6. Aerosol generation of p38 MAPK inhibitors and inhalation exposure of rats**

Groups of rats were administered an aerosol of the p38 MAPK inhibitor for 60 minutes, either once or repeatedly for up to 28 days, by snout-only inhalation exposure. Aerosols were generated from dry powder formulations or aqueous solutions and directed into the top of the snout-only inhalation exposure chamber as described in Chapter 2 (Section 2.2.5).

Target aerosol concentrations (Tables 5.2 and 5.4) for the exposure of animals were calculated from the required doses using Equation 3 (Chapter 2, Section 2.2.5).

#### **5.2.6.1. Dry powder formulations of p38 MAPK inhibitors**

For aerosol administration of crystalline p38 MAPK inhibitors or amorphous GSK-899, aliquots of dry powder formulations were packed into the dust feed canisters (Table 5.2) using the method described in Chapter 2 (Section 2.2.5.1).

**Table 5.2: Volume of dust feed canisters, target doses and aerosol concentrations for exposure of rats to p38 MAPK inhibitors**

Test article	Study number	Target dose (mg/kg)	Test article concentration in lactose (% w/w)	Aerosol generator canister size (cm <sup>3</sup> )	Target aerosol concentration (µg/L)
GSK-899 (crystalline)	R29413	1	40	5	24
	R29739	45	40	40	1080
	R30353N	15	40	5	360
	R30662N	15	40	5	360
GSK-899 (amorphous)	R30662N	0.02	0.5	1.3	0.5
		1	5	5	24
		15	40	5	360
GSK-677 (crystalline)	R31037N	1	5	5	24
		6.7	40	5	160
		15	40	5	360
GSK-361 (crystalline)	R31034N	5	40	5	120
		15	40	5	360
	R31035N	0.25	1	5	6
		1	5	5	24
		15	40	5	360

**5.2.6.2. Liquid formulations of p38 MAPK inhibitors**

For nebulisation of aqueous solutions of each p38 MAPK inhibitor, the crystalline test article was dissolved in vehicle (Table 5.3) to achieve a concentration anticipated to achieve the target aerosol concentration and inhaled dose (Table 5.4). Methods for preparing formulations are stated in Chapter 2 (Section 2.2.5.3).

**Table 5.3: Vehicles used for nebulisation of p38 MAPK inhibitors and repeated inhalation exposure of rats**

Test article	Study No.	Vehicle for nebulisation
GSK-899	R31038N	3% (v/v) Solutol HS 15 in 0.9% (w/v) aqueous sodium chloride (pH 5.9)
	R31039N	3% (v/v) Solutol HS 15 in 10% (w/v) aqueous 2-hydroxypropyl-β-cyclodextrin
GSK-677	R31038N	3% (v/v) Solutol HS 15 in 0.9% (w/v) aqueous sodium chloride (pH 5.9)
GSK-361	R31036N	20:20:60 (v/v/v) Solutol HS 15, ethanol and 60 mM phosphate buffer (pH 7)

Solutol HS 15 and 2-hydroxypropyl-β-cyclodextrin or ethanol were used to solubilise p38 MAPK inhibitors of low solubility (GSK-899 and GSK-361). Solutol HS 15 was also formulated with GSK-677 for

concurrent exposure of rats to nebulised GSK-899 or GSK-677 for comparison of the toxicopathology for these compounds. Potential implications for the enhanced absorption of p38 MAPK inhibitors were discussed in Chapter 2 (Section 2.2.5.3) and inclusion of these reagents in the vehicle does not undermine the fundamental hypothesis that changing the aerosol form of a drug changes the pharmacokinetics of exposure and concomitant toxicopathology.

**Table 5.4: Formulation concentrations, target doses and aerosol concentrations for exposure of rats to p38 MAPK inhibitors**

Test article	Study number	Target dose (mg/kg)	Concentration in vehicle (mg/mL)	Target aerosol concentration (µg/L)
GSK-899	R31038N	1	1.4 to 2.9	24
	R31039N	1	1.9 to 2.5	24
GSK-677	R31038N	1	1.4 to 2.4	24
		6.5	8.5 to 14.0	130
		15	25.0 to 35.0	360
GSK-361	R31036N	0.25	0.8 to 1.0	6
		1	1.6 to 1.75	24

#### 5.2.6.2. Aerosol Generation and formulation details

Groups of rats were administered an aerosol of the p38 MAPK inhibitor once or for up to 28 consecutive days, by snout-only inhalation exposure, as a dry powder aerosol or nebulised solution as appropriate (Chapter 2, Sections 2.2.5.2 and 2.2.5.4 respectively).

For nebulisation of GSK-899 and GSK-677 (study R31038N) in Solutol-NaCl, a single nebuliser of nominal airflow 6 L/min was used to disperse each solution at the target aerosol concentration; a chamber exhaust of 15 L/min was applied to vent the test atmosphere. For dispersal of GSK-899 in Solutol-HPβCD (study R31039N) or GSK-361 in 20:20:60 (v/v/v) Solutol HS 15, ethanol and 60 mM phosphate buffer (study R31036N), dual nebulisers were used to disperse the formulations and mitigate against limited solubility of each test article in the respective vehicle to achieve the target aerosol concentration.

### **5.2.6.3. Inhalation exposure of rats**

Animals were exposed to test aerosols using the apparatus and methods described in Chapter 2 (Section 2.2.5.5). The chambers were operated under conditions of dynamic airflow, with a chamber exhaust flow of typically 15 to 16 L/min. For logistical reasons, different airflows were used for the experiments employing dual nebulisers: an exhaust airflow of 12 L/min was applied during nebulisation of GSK-899 in Solutol-HP $\beta$ CD (study R31039N) and an exhaust flow of 18 L/min was applied during nebulisation of GSK-361 in 20:20:60 (v/v/v) Solutol HS 15, ethanol and 60 mM phosphate buffer (study R31036N).

Rats were restrained for exposure in polycarbonate restraint tubes and attached to the chamber; the vertical position (chamber level) of each animal was documented. It is not uncommon for a gradient in aerosol concentration to form down a flow-through design of snout-only exposure chamber, as animals recycle the exhaled aerosol into the chamber atmosphere as it progresses down the chamber. This is less pronounced in chambers of narrower internal diameter, since the air velocity is faster for a given volumetric airflow. Nevertheless, in order to minimise a potential bias in achieved lung dose for treatments requiring repeated concurrent exposure of more than six rats per chamber (*i.e.* loading more than one chamber level), animals were rotated through the chamber levels day by day such that mean doses would be similar for all animals over the 28-day treatment period. Unused animal exposure or sampling ports were closed using blanking plugs.

Animals were exposed to the aerosol for 60 minutes each day, during which time operational settings (airflow and aerosol generation) and animals were formally checked and documented at 15-minute intervals.

### **5.2.6.4. Aerosol characterisation**

'Pre-study' aerosol characterisation work was conducted without animals to establish the operating conditions needed to generate target aerosol concentrations and to ensure aerosols were in line with

particulate size criteria for exposure of rodents (OECD[412], 2009, OECD[413], 2009, US-EPA[3645], 1998). The operating conditions of the dust generator (speed of canister advancement) or concentration of p38 MAPK inhibitor in the solution for nebulisation were adjusted as necessary during the study, with reference to HPLC-UV analysis results of aerosol concentration, to maintain the desired aerosol concentration on target.

Aerosols were also sampled using predefined air sampling volumes (Table 5.5) during exposure of rats to determine the aerosol concentration and particle size distribution of p38 MAPK inhibitors as described in Chapter 2 (Section 2.2.5.6). For aerosol concentration, filter samples were taken in duplicate on representative days of treatment (approximately half of the exposure periods including days of blood sampling for pharmacokinetic investigations).

**Table 5.5: Target aerosol concentrations and aerosol sampling volumes**

Test article	Aerosol form	Study No.	Target aerosol concentration (µg/L)	Sampling volume (L)		
				Aerosol concentration		Particle size using cascade impactor
				Aerosol (L)	Aerosol (L)	Solvent (mL)
GSK-899	crystalline	R29413	24	10	10	5
		R29739	1080	2	2	5
		R30353N	360	6	10	3
		R30662N	360	4	6	3
	amorphous	R30662N	0.5	30	50	3
			24	6	10	3
			360	4	6	3
nebulised	R31038N	24	4	30	5	
	R31039N	24	4	8	5	
GSK-677	crystalline	R31037N	24	4	8	3
			160	4	8	3
			360	4	8	3
	nebulised	R31038N	24	4	30	5
			130	4	8	5
			360	4	8	5
GSK-361	crystalline	R31034N	120	4	8	5
			360	4	4	5
		R31035N	6	8	8	5
			24	6	6	5
	nebulised	R31036N	360	4	4	5
			6	8	8	5
			24	6	6	5

Additional samples were taken using cascade impactors, typically once for each dose level in Weeks 1 and 3 of treatment, for determination of the particle size distribution; some cohorts of animals (e.g. single dose animals) were exposed concurrently with repeat dose animals but not necessarily on days of aerosol sampling for particle size analysis.

#### **5.2.6.5. Calculation of the estimated inhaled dose**

The estimated inhaled dose was calculated using Equations 1 and 2 (Chapter 1, Section 1.3.4) for an inhalation exposure period of 60 minutes.

#### **5.2.6.6. Bioanalysis of p38 MAPK inhibitors in rat plasma and lung**

Groups of rats (n=3/dose) were sampled for plasma following a single exposure or after the final exposure (Day 28). In addition, lungs (n=3/dose/timepoint) were taken as soon as practicable after a single exposure and at 24 hours, relative to the start of a single exposure (Day 1) or the end of treatment (Day 28) for HPLC-MS/MS analysis of the test article.

#### Plasma sampling for chemical analysis of p38 MAPK inhibitors

A series of blood samples (approximately 400 $\mu$ L) were taken from groups of rats (3/dose/timepoint) immediately post exposure (60 minutes) and at 1.5, 2.5, 4.5, 8.5 and 24 hours relative to the start of inhalation exposure, or 0.5, 1, 2, 4, 8 and 24 hours after a subcutaneous dose as appropriate. Blood was sampled by jugular venepuncture or caudal venepuncture (tail warmed to induce vasodilation) if further sampling from the jugular vein was not technically feasible, or from the abdominal aorta under isoflurane anaesthesia for the final (terminal) sample. The blood was processed for preparation of plasma and analysed by HPLC-MS/MS as described in Chapter 2 (Section 2.2.5.8); plasma was stored in a freezer at approximately -20°C or below prior to analysis.

### Sampling of lung for homogenisation and chemical analysis of p38 MAPK inhibitors

Groups of rats (3/dose/timepoint) were euthanized (deep anaesthesia under isoflurane followed by exsanguination) at one hour on Day 1 (as soon as possible after inhalation exposure, or one hour post subcutaneous dose) or at 24 hours on Days 1 and 28. The lungs were taken and processed for HPLC-MS/MS analysis of p38 MAPK inhibitor in lung homogenate as described in Chapter 2 (Section 2.2.5.8).

### Determination of pharmacokinetic parameters

For each p38 MAPK inhibitor, statistical analysis of the drug-concentration profiles in lung and plasma was performed (Statistica, version 12.0.1133.40) using two-way analysis of variance (ANOVA) for lung concentrations and multivariate analysis of variance (MANOVA) for plasma concentrations, with post hoc analysis using Tukey's honestly significant difference test (Abdi and Williams, 2010[B]) to determine degrees of statistical significance between doses and timepoints.

Pharmacokinetic evaluations of plasma concentration data for each p38 MAPK inhibitor were performed using a non-compartmental method to estimate the maximum observed concentration ( $C_{max}$ ), time to  $C_{max}$  ( $T_{max}$ ) and the area under the concentration-time curve (AUC) approximated using the trapezoid rule (linear-up, log-down method).

## **5.2.7. Terminal investigations**

On completion of the required treatment period (approximately 24 hours after the final dose), rats were euthanized by exsanguination via the abdominal aorta under isoflurane anaesthesia. Death was confirmed by cutting major blood vessels (cessation of circulation).

### **5.2.7.1. Bronchoalveolar lavage of lungs for transmission electron microscopy of macrophages**

Methodology for the harvesting of macrophages for transmission electron microscopy (TEM) was adapted for incorporation into

experiments as the research progressed. Differences in experimental design or techniques are summarised in Table 5.6.

**Table 5.6: Summary of inhaled doses, duration of treatment and sampling of lungs by bronchoalveolar lavage**

Test article	Aerosol form	Study No.	Inhaled dose (mg/kg/day)	Days of treatment	Lung lobes sampled	Volume of BALF
GSK-899	crystalline	R29413	1, 45	3	all	4× 5mL
	amorphous	R30662N	15	3	intermediate	3× 1mL
	nebulised	R31038N	1	3	all	3× 5mL
GSK-677	crystalline	R31037N	15	3	all	3× 5mL
	nebulised	R31038N	15	3	all	3× 5mL
GSK-361	nebulised	R31035N	0.25, 1, 15	28	left	3× 2mL

#### Notes

BALF bronchoalveolar lavage fluid: volume of aqueous 0.9% (w/v) sodium chloride used to flush lungs

The thoracic cavity was opened by excision of the sternum and the lungs removed. For sampling the left lung of GSK-361 treated rats, the right bronchi were first clamped. The trachea (or bronchus of the intermediate lobe for rats administered amorphous GSK-899) was cannulated, with the cannula securely tied in place with thread.

The lung/lobe was gently lavaged with an appropriate volume of ice cold aqueous 0.9% (w/v) sodium chloride. The lobe(s) were gently massaged prior to removal of the lavageate (BALF), which was transferred to a tube suitable for centrifugation. BALF samples were kept chilled on ice between processing steps and successive washes were pooled to form one sample per animal.

BALF samples were centrifuged for five minutes at 1500 rpm (approximately 395×g), at approximately 4°C with no brake. The supernatant was discarded and the pellet of cells resuspended in 1 mL formaldehyde glutaraldehyde (4% formaldehyde and 1% glutaraldehyde in a phosphate buffer; pH 7.2 to 7.4) and processed for TEM as described in Section 5.2.2.5.

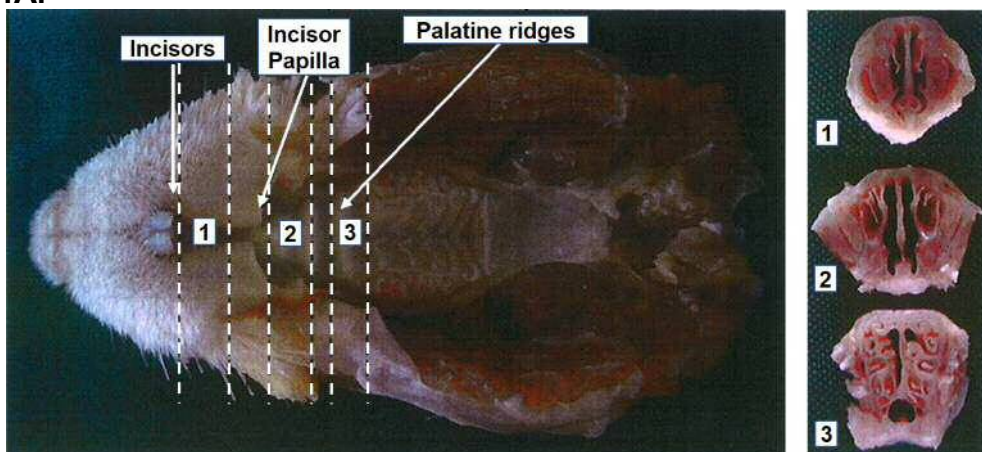
#### 5.2.7.2. Histopathological examination of tissues

Animals were subjected to a macroscopic examination (visual appraisal) during necropsy. The thoracic cavity was opened by excision

of the sternum and tissues required for preservation were systematically removed and preserved in an appropriate fixative. A generic tissue preservation list for rodent inhalation toxicology studies was used and included but was not limited to the respiratory tract (including head for nasal cavities), vital organs, gastrointestinal tract, reproductive organs, lymphoid tissues, skeletal muscle, nerves, femur, skin and animal identification. Eyes and optic nerves were preserved in Davidson's fixative (2:35:10:53 (v/v) 40% formaldehyde solution, ethanol, glacial acetic acid and distilled water). Testes were preserved in modified Davidson's fixative (30:15:5:50 (v/v) 40% formaldehyde solution, ethanol, glacial acetic acid and distilled water) for approximately 24 hours and were then transferred to 70% industrial methylated spirits (IMS) in water. Otherwise, tissues were fixed in 10% buffered formalin for at least 4 days (liver), 24 hours (other soft tissues) or 48 hours (hard tissues) before further processing was performed; lungs were inflated with fixative prior to immersion.

After fixation, tissues required for examination by light microscopy were trimmed in accordance with standardised procedures to expose areas of interest, ready for further processing (Figure 5.4). The head (for examination of nasal cavities) was decalcified in Kristenson's fluid (43 mg/mL (w/v) sodium formate in 19.6% (v/v) formic acid) for eight days, with trimming of tissue performed half way through the decalcification process (Figure 5.4A). Trimmed tissues were placed into labelled cassettes, in accordance with an embedding guide (Figure 5.4B) to standardise orientation of the tissues presented for examination. The cassettes containing tissues were stored in 70% IMS (eyes, optic nerves or testes) or 10% buffered formalin until processed.

5.4A:



5.4B:

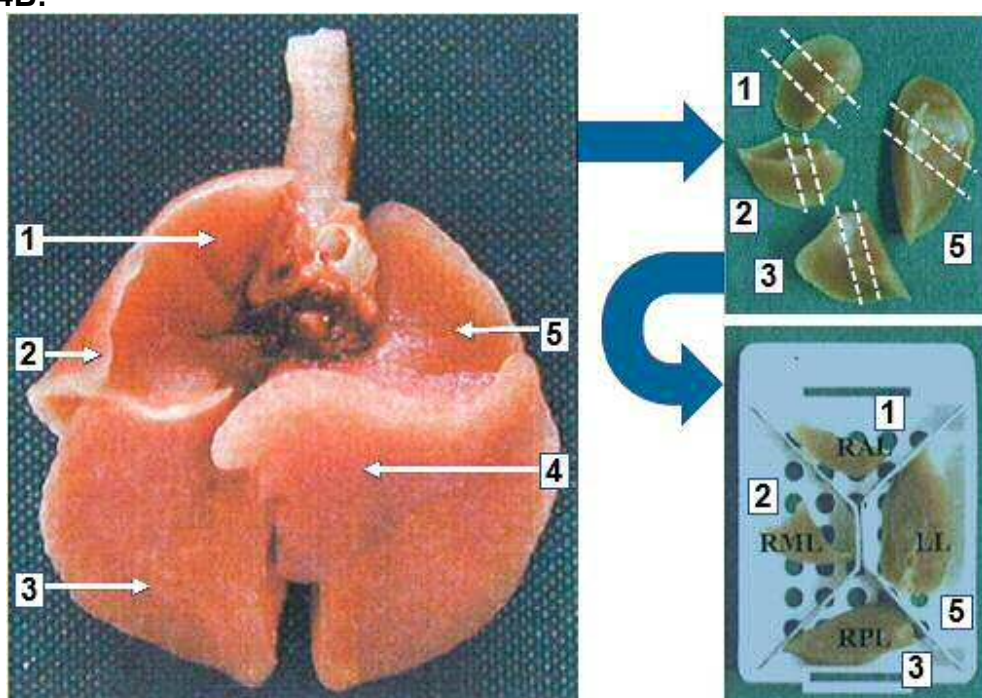


**Figure 5.4:** Trimming patterns for standardization of tissue sections for histopathological examination. **5.4A:** rat head trimmed to expose three standard sections of the nasal cavities. **5.4B:** rat lungs inflated with fixative showing the right anterior lobe (1), right mid lobe (2), right posterior lobe (3), intermediate lobe (4) and left lung (5). The trimming pattern of fixed lung tissue and arrangement in a cassette for embedding in paraffin wax (intermediate lobe not routinely processed) are also shown.

Tissue processing for preparation of slides

Tissues were processed using an automated schedule during which the tissues were immersed in a series of reagents, each for one hour. The tissues were first dehydrated by immersing the cassettes in 70% IMS (once), 90% IMS (once) and then absolute IMS (five cycles). The

cassettes were then immersed in xylene (three cycles). Xylene is miscible with paraffin wax and is used to “clear” the dehydrant (IMS) from the tissue. The tissues were then impregnated with molten paraffin wax maintained at  $\leq 63^{\circ}\text{C}$  (four cycles). For embedding, a mould base was filled with molten paraffin wax in a working area (“embedding centre”) maintained at  $60^{\circ}\text{C}$ . The trimmed tissues in a cassette were transferred to the mould and orientated in accordance with a blocking pattern with the surface of interest downwards. The mould was then chilled on a cold plate, the position of the tissues adjusted if necessary, and the lid of the mould closed using the labelled cassette base. The mould was then further cooled until the paraffin wax had set, and the mounted wax block removed from the mould.

#### Preparation of slides for microscopic examination

The wax blocks were mounted onto a microtome, coarse trimmed to expose the area of interest and cooled on ice. After removing any ‘coarse trimming artefacts’, sections of 3 to 5  $\mu\text{m}$  thickness were cut and floated onto warm distilled water ( $47$  to  $50^{\circ}\text{C}$ ), and picked up onto a clean glass slide pre-labelled with study, animal and block identification numbers.

The sections were stained with haematoxylin and eosin according to an automated sequence as follows: warming in the respective fixative (five minutes; oven maintained at  $60^{\circ}\text{C}$ ) to melt the paraffin wax; immersion in xylene (1 $\times$  five minutes; 3 $\times$  three minutes), IMS (3 $\times$  one minute), water (1 $\times$  one minute), haematoxylin (2 $\times$  three minutes; 1 $\times$  two minutes), water (2 $\times$  two minutes; 1 $\times$  one minute), eosin (2 $\times$  2.5 minutes), water (1 $\times$  30 seconds), IMS (3 $\times$  30 seconds) and xylene (2 $\times$  30 seconds; 3 $\times$  one minute).

Occasionally, at the request of the study pathologist, immunohistochemical staining was performed to confirm the phenotype of leukocytes observed in the lung sections (CD68, CD3 or CD79 glycoproteins for monocytes/macrophages, T-lymphocytes and

B-lymphocytes respectively). A coverslip was then applied and set using Entellan® rapid mounting medium (catalogue number 1079610100; Sigma Aldrich).

#### Microscopic examination of tissues

A pathologist examined selected tissues by light microscopy (up to ×40 magnification) and subjectively graded the incidence and severity of observations in rats administered the p38 MAPK inhibitors and control animals administered the vehicle alone. Histopathological findings were graded according to a qualitative scale of increasing severity as follows: minimal < mild < moderate < marked < very marked.

Selected tissues (Table 5.7) included the exposure route (respiratory tract for inhalation studies; injection site for subcutaneously administered GSK-899), macroscopic abnormalities observed at necropsy and potential target organs identified with reference to unpublished data (Freke, 2007, Freke, 2010, Rush, 2007). Tissues were examined for control rats and the highest dose administered. Tissues affected by treatment were then examined for animals of lower doses.

**Table 5.7: Summary of tissues examined by light microscopy after treatment of rats for 28 days**

Tissue type	Tissues	Studies examined
Respiratory tract	nasal cavities, nasopharynx, lungs	all studies
	larynx, trachea (+bifurcation), TBLN	all inhalation studies
Key organs	heart, kidney, liver	all studies
Reproductive organs	prostate	GSK-899 (R30662N, R31697N)
	testes	all studies
Miscellaneous	abnormalities and thymus	all studies
	adrenals	GSK-361 (R31035N, R31036N); GSK-899 (R31038N, R31039N, R31697N)
	eyes, optic nerve, jejunum, duodenum or colon	GSK-361 (R31035N, R31036N); GSK-899 (R31038N, R31039N)
	injection site (subcutis)	GSK-899 (R31697N)

#### Notes

TBLN tracheobronchial lymph node

### 5.3. Results and discussion

#### 5.3.1. *In vitro* analysis of cytotoxicity, cytokine release and morphology of cells incubated with particles

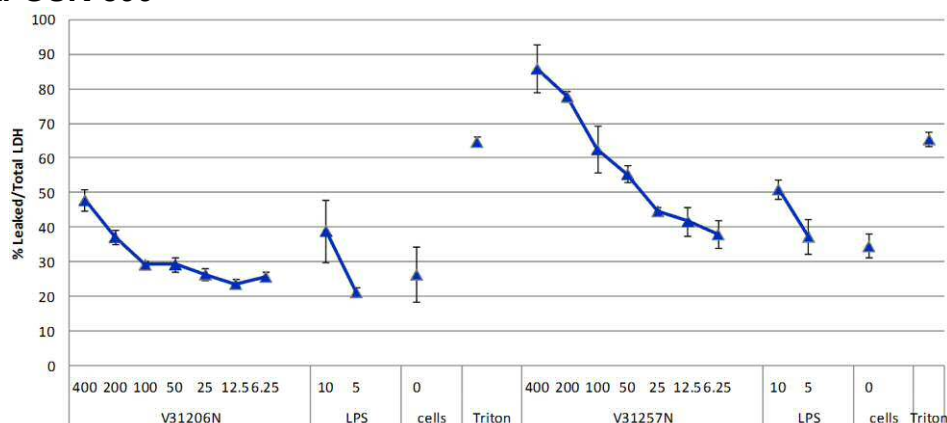
Results of *in vitro* investigations with NR8383 rat alveolar macrophage cells incubated with p38 MAPK inhibitors for 72 hours are detailed in Appendices 3 and 4 and reproduced below. High median effective concentrations ( $EC_{50}$ ) for particles of p38 MAPK inhibitors selected for subsequent *in vivo* investigations ranked GSK-361 > GSK-899 > GSK-677 (Table 5.8), and indicated a relatively low potential for cellular toxicity for the compounds ( $EC_{50} > 100 \mu\text{g/mL}$ ); criteria for categorisation of drugs are summarised in Section 5.2.2.2.

**Table 5.8: *In vitro* cytotoxicity ( $EC_{50}$ ) data for p38 MAPK inhibitors**

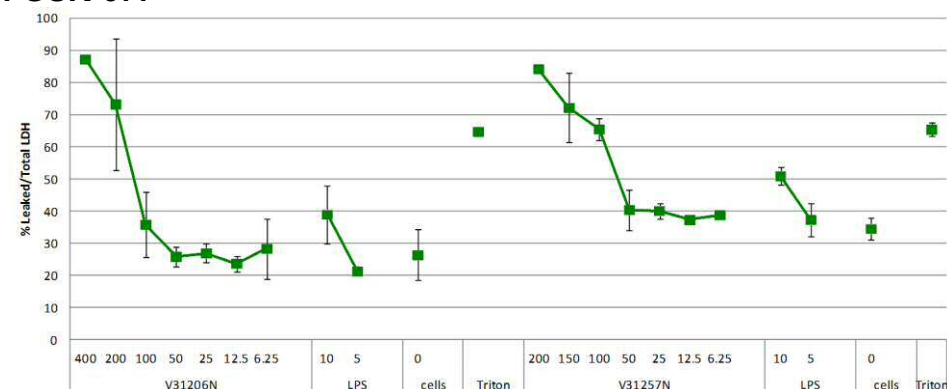
Test article	Lactate dehydrogenase $EC_{50}$ ( $\mu\text{g/mL}$ )	Study Numbers
GSK-899	316.2	V31206N, V31257N
GSK-677	144.2	
GSK-361	462.8	V31292N, V31307N
SB-323	93.74	

Variability in GSK-899 dose responses for duplicate assays to measure lactate dehydrogenase leakage (Figure 5.5A) was ascribed to relative insolubility of GSK-899. None of the p38 MAPK inhibitors induced release of cytokines *in vitro* (Appendices 3 and 4). This was expected given the anti-inflammatory pharmacology described for p38 MAPK inhibitors (Chung, 2011) and the compounds were thus considered to represent a relatively low potential for inflammatory mediator release *in vivo*. Morphological assessment of NR8383 rat alveolar macrophage cells by transmission electron microscopy after incubation with p38 MAPK inhibitor particles for 72 hours revealed endocytosed particles at 400  $\mu\text{g/ml}$  of GSK-899 (Figure 5.6A) and GSK-361 (Figure 5.6B). This was consistent with the high solubility of GSK-677 and low solubility of GSK-361 and GSK-899 (Chapter 2, Table 2.6).

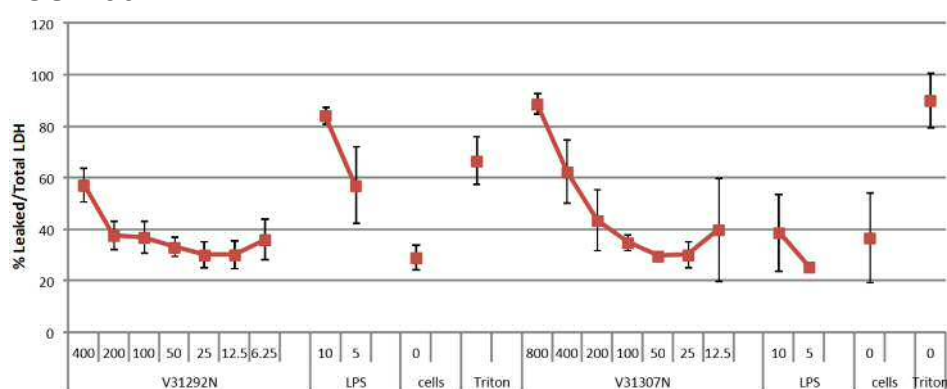
**5.5A: GSK-899**



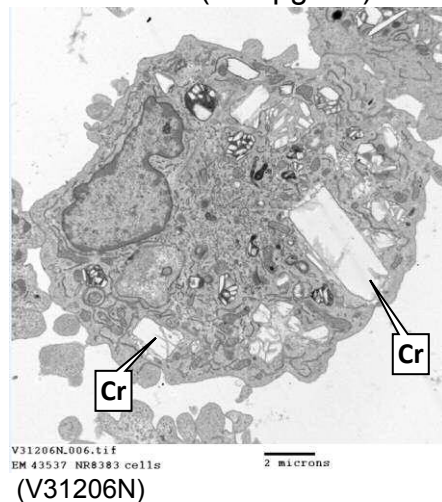
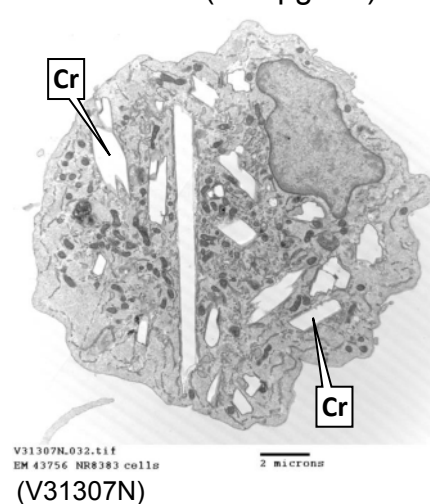
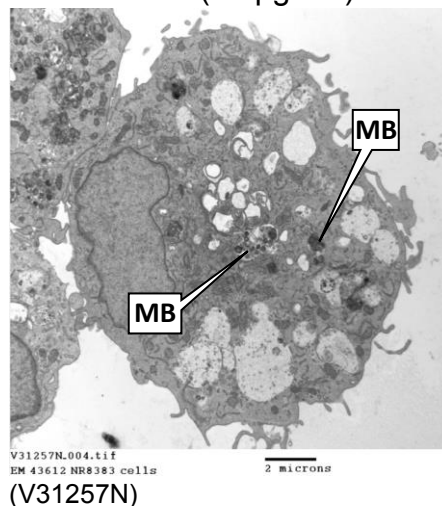
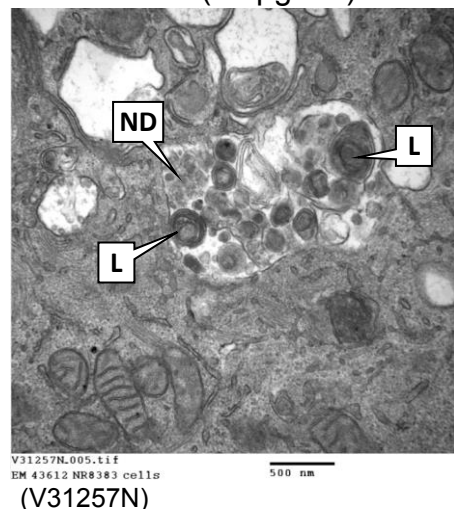
**5.5B: GSK-677**



**5.5C: GSK-361**



**Figure 5.5** Cytotoxicity assessed by leakage of lactate dehydrogenase (LDH) from NR8383 rat alveolar macrophage cells incubated with a p38 MAPK inhibitor. NR8383 cells in supplemented Kaighn’s modification of Ham’s F12 medium were incubated at 37°C in a humidified atmosphere containing 5% CO<sub>2</sub>. For LDH analysis, cells were seeded into wells, incubated for ≤4 hours and treated with an equal volume of the p38 MAPK inhibitor in medium for 72 hours. LDH leakage was expressed as a percentage of total with reference to media of control cells treated with Triton-X (to release LDH into media) at 71.5 hours. **5.5A:** GSK-899. **5.5B:** GSK-677. **5.5C:** GSK-361.

**5.6A:** GSK-899 (400 µg/mL)**5.6B:** GSK-361 (400 µg/mL)**5.6C:** GSK-677 (50 µg/mL)**5.6D:** GSK-677 (50 µg/mL)

**Figure 5.6:** Transmission electron microscopy of NR8383 rat alveolar macrophage cells incubated with a p38 MAPK inhibitor. NR8383 cells in supplemented Kaighn's modification of Ham's F12 medium were incubated at 37°C in a humidified atmosphere containing 5% CO<sub>2</sub>. For particulate exposure, cells were seeded into wells, incubated for ≤4 hours and treated with an equal volume of p38 MAPK inhibitor in medium for 72 hours. Cells were then harvested and processed for transmission electron microscopy. **5.6A:** GSK-899 (400 µg/mL); crystalline inclusions (Cr) were evident within macrophage cells. **5.6B:** GSK-361 (400 µg/mL); crystalline inclusions (Cr) were evident within macrophage cells. **5.6C:** GSK-677 (50 µg/mL); membrane-bound bodies (MB) containing lamellar material, vesicles or nondescript material lacking a clear shape or structure were evident within the cell. **5.6D:** GSK-677; higher magnification of membrane-bound body showing concentric lamellar (L) and nondescript (ND) material.

Crystalline inclusions were not seen in NR8383 cells incubated with GSK-677, but there was evidence (50 and 400 µg/ml) of secondary lysosomes containing lamellar or vesicular material that occasionally appeared to be developing lysosomal lamellar bodies (Figures 5.6C and 5.6D). This is consistent with lysosomal storage disorders such as drug-induced phospholipidosis (Anderson and Borlak, 2006, Dake *et al.*, 1985), an accumulation of phospholipid in lamellar bodies, or Niemann-Pick disease, an inherited disease causing accumulation of sphingolipid or cholesterol (Ikonen and Hölttä-Vuori, 2004).

### 5.3.2. Toxicopathology of p38 MAPK inhibitors in rats following 28 days of inhalation exposure

Lung and plasma concentration profiles, transmission electron microscopy (TEM) of macrophages and representative sections of toxicopathology findings (viewed by light microscopy) are presented for each p38 MAPK inhibitor and aerosol form (indexed in Table 5.9).

**Table 5.9: Index of figures and tables for dosimetry, drug-lung and plasma concentrations and representative microscopy images in rats**

p38 MAPK inhibitor and particle/dose form			Figure/table numbers				
			Inhaled doses	Concentration		Macro-phages	Toxico-pathology
				Lung	Plasma		
GSK-899	crystalline	Figures	-	5.7	5.8	5.10	5.11 - 5.13
		Tables	5.10	-	5.12	-	5.13
	amorphous	Figures	-	5.14	5.15	5.16	5.17 - 5.18
		Tables	5.10	-	5.14	-	5.15
nebulised	Figures	-	5.19	5.20	5.21	5.22 - 5.23	
	Tables	5.11	-	5.16	-	5.17	
Injection (subcutis)	Figures	-	5.24	5.25	-	5.26 - 5.29	
	Tables	-	-	5.18	-	5.19	
GSK-677	crystalline	Figures	-	5.30	5.31	5.32	-
		Tables	5.10	-	5.20	-	5.21
nebulised	Figures	-	5.33	5.34	5.35	5.36 - 5.39	
	Tables	5.11	-	5.22	-	5.23	
GSK-361	crystalline	Figures	-	5.40	5.41	5.42	5.43
		Tables	5.10	-	5.24	-	-
nebulised	Figures	-	5.44	5.45	-	5.46	
	Tables	5.11	-	5.25	-	-	

### 5.3.2.1. Inhalation exposure of rats to p38 MAPK inhibitors and estimation of the inhaled dose

Generally, achieved mean aerosol concentrations were in agreement with target ( $\pm 12\%$ ) and all groups were  $\pm 18\%$  of target. This was reflected in the estimated inhaled doses for each p38 MAPK inhibitor ( $\pm 11\%$  of respective targets), with all doses within  $\pm 20\%$  of target and clear separation between doses (Tables 5.10 and 5.11). The mass median aerodynamic diameter (MMAD) for all aerosols can be ranked: amorphous GSK-899 > crystalline GSK-677 > nebulised (study R31039N) and crystalline GSK-899 > crystalline GSK-361 and nebulised p38 MAPK inhibitors. The MMAD for nebulised aerosols and crystalline GSK-899 and GSK-361 were within the range recommended for repeat exposure studies, *i.e.* MMAD of 1 to 3  $\mu\text{m}$  (OECD[412], 2009, OECD[413], 2009, US-EPA[3645], 1998). Although slightly greater, the MMAD for amorphous GSK-899 and crystalline GSK-677 was within the range 1 to 4  $\mu\text{m}$  recommended for acute (single exposure) inhalation toxicity testing (US-EPA[1300], 1998, OECD[403], 2009), with the mid dose for amorphous GSK-899 on the cusp of this range (4.2  $\mu\text{m}$ ).

Estimates of fine particle fraction in Chapter 2 (Section 2.3.6.1) suggest minor differences ( $\leq 6\%$ ) in fine particle mass for MMAD of 2 to 3  $\mu\text{m}$  but a difference of approximately 20% of the aerosol between an MMAD of 3 and 4  $\mu\text{m}$  at the observed geometric standard deviations, and Raabe *et al.* (1988) described enhancement of nasal-pharyngeal deposition in rats for particles larger than 3  $\mu\text{m}$  in aerodynamic diameter. Whilst this has implications for the proportion of particulate likely to be deposited in rat lungs, the separation of achieved estimated inhaled doses was sufficient to permit investigation of the dose response of toxicopathology.

**Table 5.10: Estimated inhaled doses and characterisation of dry powder aerosols administered to rats over 28 days**

Test article (bold) and aerosol form	Study number	Test article concentration (% w/w in lactose)	Estimated inhaled dose (mg/kg) <sup>A</sup>	Mean aerosol concentration (µg/L) <sup>B</sup>	Particle size distribution <sup>C</sup>	
					MMAD (µm)	σg
<b>GSK-899</b>						
Crystalline	R29413	44%	1.06	25.6	2.9	2.1
	R30662N	44%	14.5	358	3.0	2.0
Amorphous	R30662N	0.50%	0.024	0.592	3.9	2.0
		5.0%	1.10	26.9	4.2	1.9
		39%	15.6	380	3.7	2.3
<b>GSK-677</b>						
Crystalline	R31037N	4.4%	1.04	25.0	3.3	2.1
		38%	7.28	175	3.5	1.7
		38%	16.7	403	3.3	2.2
<b>GSK-361</b>						
Crystalline	R31035N	0.95%	0.222	5.26	1.7	2.7
		5.0%	1.04	24.7	1.6	2.4
		43%	15.2	358	1.8	2.2

**Notes**

MMAD mass median aerodynamic diameter

σg geometric standard deviation

A Estimated inhaled doses calculated for a 60-minute exposure period using mean data (aerosol concentration and body weight) and a body-weight derived estimate of respired minute volume (Alexander *et al.*, 2008). Estimation of mean inhaled doses of GSK-899, GSK-677 and GSK-361 are summarised in Appendices 163 to 165 respectively.

B Aerosol concentration: aerosols were typically analysed twice per exposure on representative days of the 28-day treatment period (Study R29413 sampled daily).

C Particle size distribution: aerosols containing a p38 MAPK inhibitor (analyte) were sampled using a cascade impactor on two to four occasions per dose during the 28-day treatment period (median values presented).

**Table 5.11: Estimated inhaled doses and characterisation of nebulised aerosols administered to rats over 28 days**

Formulation vehicle (bold) and test article	Study number	Test article concentration in vehicle (mg/mL)	Estimated inhaled dose (mg/kg) <sup>A</sup>	Mean aerosol concentration (µg/L) <sup>B</sup>	Particle size distribution <sup>C</sup>	
					MMAD (µm)	σg
<b>3% (v/v) Solutol HS 15 in 10% (w/v) Aqueous 2-Hydroxypropyl-B-Cyclodextrin</b>						
GSK-899	R31039N	1.8 to 2.5	1.10	26.3	3.1	2.2
<b>3% (v/v) Solutol HS 15 in 0.9% (w/v) aqueous sodium chloride</b>						
GSK-899	R31038N	1.4 to 2.9	0.842	20.0	2.1	2.0
GSK-677	R31038N	1.4 to 2.3	1.08	25.7	1.8	2.1
		8.6 to 14	4.92	118	1.9	2.1
		25 to 35	14.8	352	1.8	2.1
<b>20:20:60 (v/v/v) Solutol:EtOH:60 mM phosphate buffer</b>						
GSK-361	R31036N	0.79 to 1.0	0.248	5.88	1.8	2.4
		1.8	1.18	28.0	1.9	2.5

**Notes**

MMAD mass median aerodynamic diameter

σg geometric standard deviation

A Estimated inhaled doses calculated for a 60-minute exposure period using mean data (aerosol concentration and body weight) and a body-weight derived estimate of respired minute volume (Alexander *et al.*, 2008). Estimation of mean inhaled doses of GSK-899, GSK-677 and GSK-361 are summarised in Appendices 163 to 165 respectively.

B Aerosol concentration: aerosols were typically analysed twice per exposure on representative days of the 28-day treatment period.

C Particle size distribution: aerosols containing a p38 MAPK inhibitor (analyte) were sampled using a cascade impactor on two or three occasions per dose during the 28-day treatment period (median values presented).

**5.3.2.2. Pulmonary and systemic exposure of rats to GSK-899 and toxicopathology after 28 days**

GSK-899 concentrations in lung homogenate showed persistence of the analyte in lungs of rats administered crystalline GSK-899, with no significant reduction from 1 to 24 hours relative to the start of aerosol administration (Figure 5.7). Accumulation of GSK-899 in lungs was evident after repeated exposure, with an approximate 10-fold increase in trough concentrations (24 hours) from Days 1 to 28 of treatment, which by inference indicated approximately 60% of the lung deposited dose of GSK-899 was cleared from the lungs during this period.

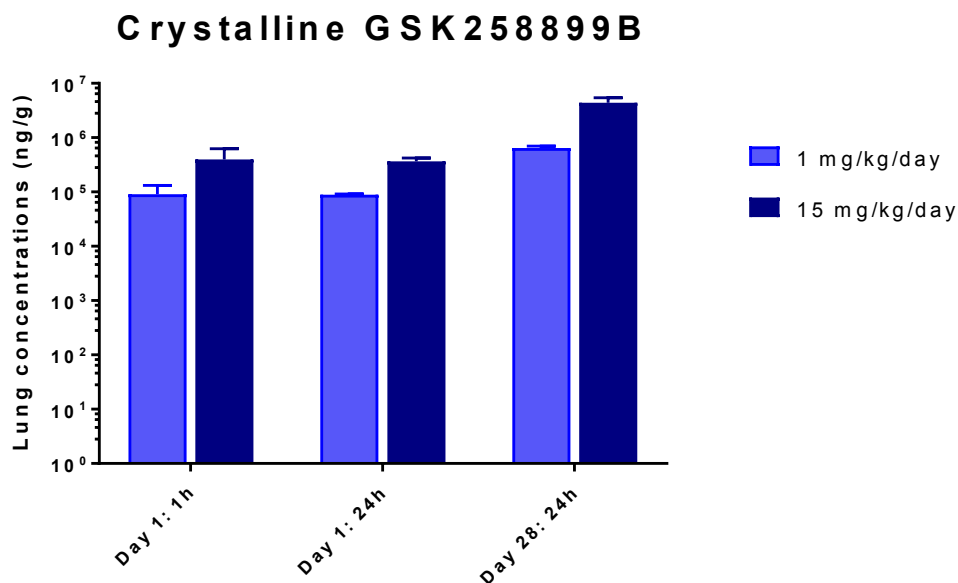
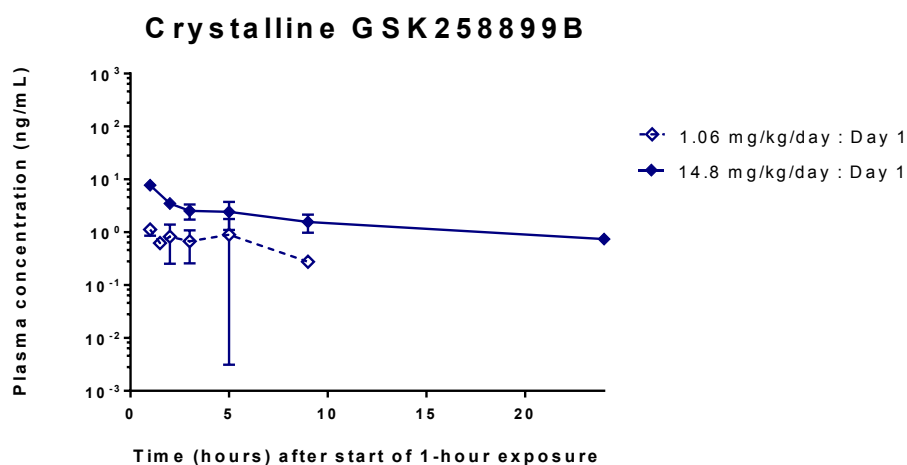


**Figure 5.7:** Drug-lung concentrations in rats following inhaled administration of crystalline GSK-899 for one or 28 days. Mean GSK-899 concentrations with standard deviations (error bars; n=3) are shown for rat lung homogenate data for samples taken immediately after a single 1-hour exposure and at 24 hours after single or repeat doses. Statistical analysis (2-way ANOVA with post hoc analysis using Tukey's honestly significant difference test (Abdi and Williams, 2010[B])) of log<sub>10</sub>-transformed data achieved significance (p<0.01) for Days 1 vs 28 (24 hours); no statistical difference achieved between 1 and 24 hours.

Mean drug-plasma concentrations were generally similar for a given dose after inhaled administration of crystalline GSK-899 to rats on Days 1 and 28 of treatment (Figure 5.8). A relatively high degree of variability was apparent for rats administered 1 mg/kg on Day 1, which was reflected in wide error bars representing standard deviation for each timepoint (Figure 5.8A).

## 5.8A



## 5.8B

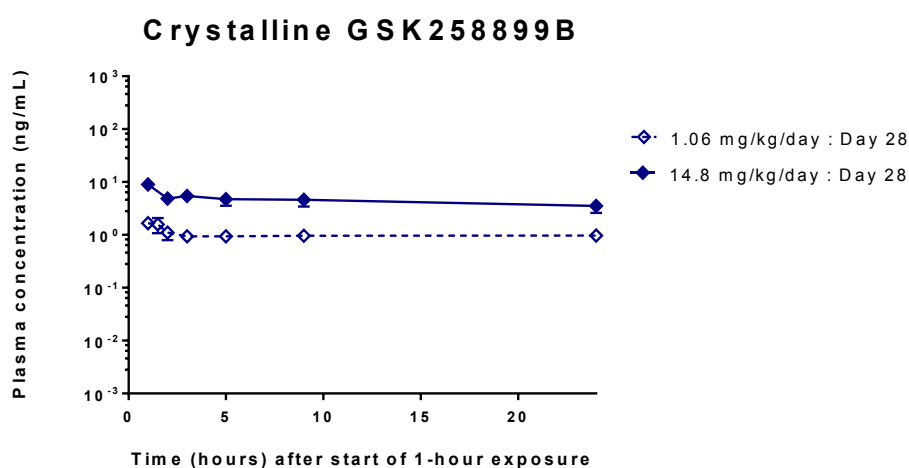


**Figure 5.8:** GSK-899 concentrations in rat plasma up to 24 hours after inhaled doses of crystalline GSK-899 on Days 1 and 28. Rats inhaled an aerosol of crystalline GSK-899 once daily (1-hour exposure) for up to 28 days; mean plasma concentrations with standard deviations (error bars; n=3) are shown for samples taken up to 24 hours after the start of inhalation exposure. **5.8A:** plasma concentrations after a single exposure (Day 1). **5.8B:** plasma concentrations after repeated administration (Day 28). Statistical analysis (MANOVA with post hoc analysis using Tukey's honestly significant difference test (Abdi and Williams, 2010[B])) of log<sub>10</sub>-transformed data achieved significance (p<0.01) for Days 1 vs 28.

Systemic exposure to GSK-899 was higher on Day 28, with AUC<sub>0-t</sub> increasing five-fold and three-fold for crystalline doses of 1 and 15 mg/kg/day respectively (Table 5.12) and minor differences in peak plasma concentration (C<sub>max</sub>), which occurred at the first sampled

timepoint immediately post exposure. Increases in systemic exposure were under proportional for an increase in dose, *i.e.*  $AUC_{0-t}$  increased  $\leq 7$ -fold for a 15-fold increase in the estimated inhaled dose, suggesting saturation of mechanisms for absorption.

**Table 5.12: Pharmacokinetics of GSK-899 in plasma after inhaled administration of micronised crystals (n=3)**

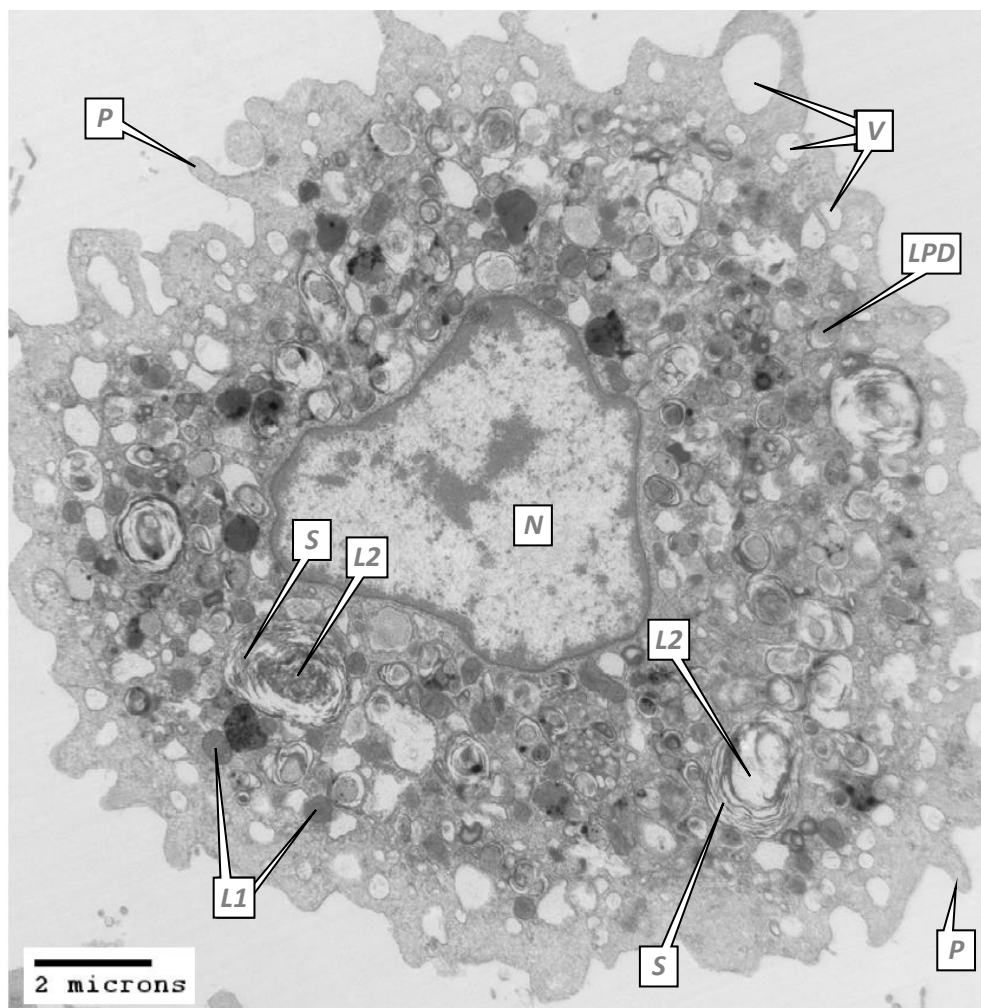
Study No.	Estimated Inhaled Dose (mg/kg/day) <sup>A</sup>	Period (Day)	Statistical parameter	Pharmacokinetics (plasma)		
				$AUC_{0-t}$ (h.ng/mL) <sup>B</sup>	$C_{max}$ (ng/mL) <sup>B</sup>	$T_{max}$ (h) <sup>C</sup>
R29413	1.06	D1	Mean	6.34	1.60	2
			sd	2.77	0.60	-
			CV (%)	44%	38%	-
		D28	Mean	32.5	2.28	1
			sd	1.08	0.35	-
			CV (%)	3%	15%	-
R30662N	14.6	D1	Mean	41.5	7.74	1
			sd	12.6	1.25	-
			CV (%)	30%	16%	-
	16.2	D28	Mean	106	9.00	1
			sd	25.2	1.91	-
			CV (%)	24%	21%	-

**Notes**

- A Overall estimated inhaled dose for toxicopathology animals over the 28-day treatment period.
- B Mean calculated from parameter for each rat (n=3): parameter dose-normalised (division by estimated inhaled dose on day of sampling) and re-normalised with the overall estimated inhaled dose<sup>A</sup>.
- C Median time presented relative to start of the 1-hour exposure period.
- CV Coefficient of variation (%) =  $sd/mean$

TEM of macrophages sampled from control rats administered lactose alone revealed normal cells with no evidence of particle uptake (Figure 5.9). The control macrophages were of normal appearance, typically spherical with lamellipodia at their surface and a large pleomorphic nucleus (size and shape varied). Many primary lysosomes were present (medium electron density and highly pleomorphic), with fewer secondary lysosomes that were generally larger and often contained lamellar-like material considered likely to be derived from pulmonary surfactant. Lipid was often present (seen as an electron

dense core with an electron lucent periphery, representing artefactual extraction of lipid during sample processing) and other features included frequent prominent Golgi and mitochondria (typically spherical to ovoid and containing well defined cristae).



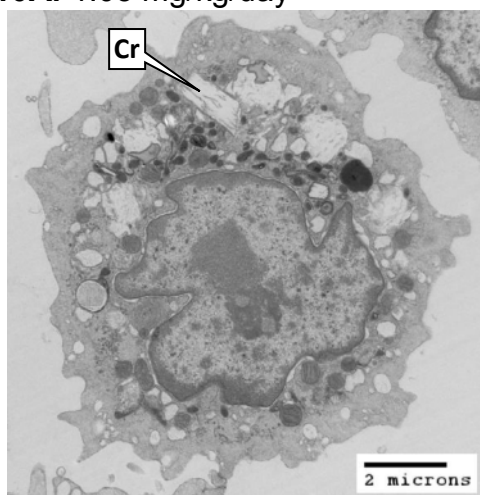
(R29413; Rat 026)

**Figure 5.9:** Normal macrophage sampled from a rat (control) after inhaled administration of lactose vehicle for 3 days. Rats were exposed to lactose vehicle alone for 3 days. Macrophages were harvested *post mortem* in saline by bronchoalveolar lavage and processed for transmission electron microscopy. The image shows a normal macrophage containing primary (L1) and secondary (L2) lysosomes, partly extracted lipid droplets (LPD) and lamellar bodies (S) likely to be lung surfactant. Additional features include the nucleus (N), vacuoles (V) and lamellipodia (P).

TEM of macrophages harvested from rats administered crystalline GSK-899 (1.05 or 45.3 mg/kg/day) revealed a dose-related increase in rectangular inclusions (Figure 5.10). The shapes of inclusions were

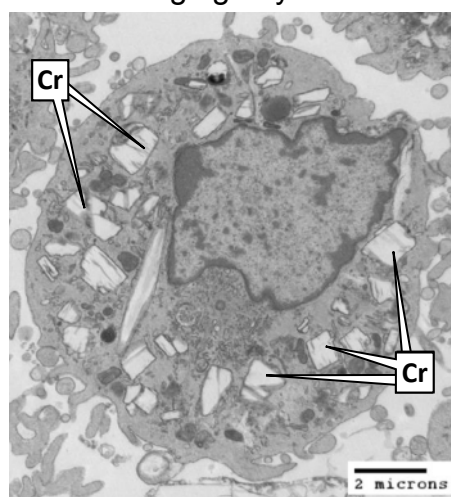
consistent with the cross section of micronised crystals imaged by scanning electron microscopy (SEM) in Chapter 2 (Figure 2.16A) and phagocytosed inclusions seen *in vitro* (Figure 5.6A). The ultrastructure of macrophages from rats administered crystalline GSK-899 was otherwise similar to controls administered the vehicle (lactose) alone.

**5.10A:** 1.05 mg/kg/day



(R29413; Rat 043)

**5.10B:** 45.3 mg/kg/day



(R29413; Rat 056)

**Figure 5.10: Macrophages containing crystalline particles after inhalation of GSK-899 for 3 days.** Rats were exposed to lactose vehicle alone or in combination with crystalline GSK-899 for 3 days. Macrophages were harvested *post mortem* in saline by bronchoalveolar lavage and processed for transmission electron microscopy. **5.10A:** macrophage containing partly extracted lipid droplets and a few crystal-like 'rectangular' inclusions (Cr). **5.10B:** macrophage containing numerous crystal-like inclusions (Cr) consistent with a dose dependent increase for a higher GSK-899 dose.

Rats administered micronised crystalline GSK258899B for 28 days presented dose-dependent increases in the incidence and severity of multifocal foamy macrophage aggregates (Table 5.13 and Figure 5.11) at administered doses (mild at 1.06 mg/kg/day and minimal to marked at 14.5 mg/kg/day) with foamy macrophage degeneration/necrosis and intra-alveolar neutrophils (minimal at 14.5 mg/kg/day; a few aggregates at 1.06 mg/kg/day). At 14.5 mg/kg/day, the macrophage aggregates were associated with inflammatory changes characterised by interstitial mononuclear inflammatory cell infiltration (mild to marked); immunohistochemical staining confirmed the inflammatory cells were

macrophages (CD68 positive) and T lymphocytes (CD3-positive) and, in 2/6 animals, B-lymphocytes (CD79 positive).

**Table 5.13: Histopathology of the respiratory tract of rats exposed to micronised crystalline GSK-899 for 28 days**

Vehicle for powder dispersal: lactose		Incidence of findings				
Study Numbers		R29413		R30662N		
Estimated inhaled dose (mg/kg/day)		0 (control)	1.06	0 (control)	14.5	
Number of rats on study	Grading of observation	6	6	6	6	
		6	0 <sup>A</sup>	6	6	
Lung	<i>No finding</i>	5	3	4	0	
	Aggregate, foamy macrophage; multifocal	Minimal	1	1	2	0
		Mild	0	2	0	3
		Moderate	0	0	0	2
		Marked	0	0	0	1
		Inflammatory cell infiltrate; alveolus; neutrophilic, multifocal	Minimal	0	0	0
	interstitium; mononuclear cell, multifocal	Mild	0	0	0	4
		Moderate	0	0	0	1
		Marked	0	0	0	1
	Degeneration/necrosis; foamy macrophage, multifocal	Minimal	0	0	0	6
	Cellularity increased; BALT (bronchus-associated lymphoid tissue)	Minimal	0	0	0	1
		Mild	0	0	0	2
Lymph node, tracheo-bronchial	<i>No finding</i>	3	3	4	0	
	<i>(no section)</i>	(0)	(1)	(1)	(1)	
	Cellularity increased; paracortex	Mild	0	0	0	5
		Aggregate; macrophage; paracortex; multifocal	Minimal	0	0	0
Mild	0		0	0	3	
Larynx	<i>No finding</i>	6	6	6	1	
	Squamous metaplasia	Minimal	0	0	5	

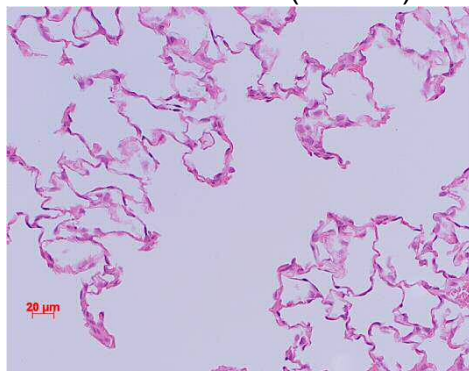
#### Notes

No treatment related findings: trachea and nasopharynx (animals of study R30662N only examined), tracheal bifurcation, nasal cavity.

A Study R29413: target doses of 0, 1 and 45 mg/kg/day administered; tissues of rats administered 1 mg/kg/day examined if findings were seen at 45 mg/kg/day.

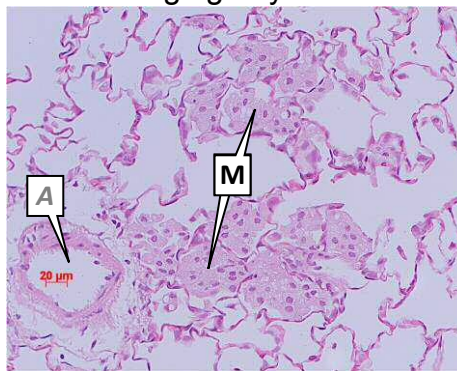
Increased cellularity of bronchus-associated lymphoid tissue (BALT) was seen at 14.5 mg/kg/day, with multifocal macrophage aggregates (minimal or mild) and increased cellularity (mild) of BALT (Table 5.13 and Figure 5.12). In the tracheobronchial lymph node, there was mild increased cellularity of the paracortex and minimal or mild multifocal macrophage aggregates with mild enlargement of the nodes.

**5.11A:** Vehicle control (lactose)



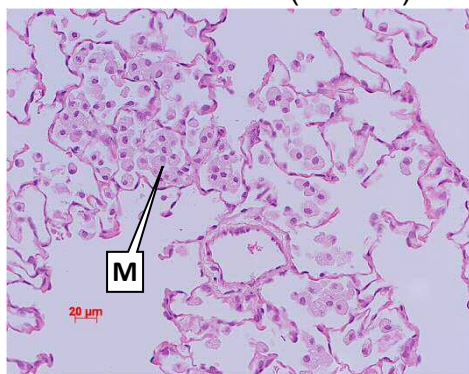
(R29413; Rat 001)

**5.11B:** 1.06 mg/kg/day



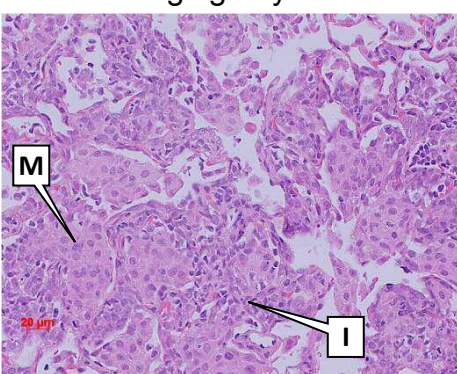
(R29413; Rat 010)

**5.11C:** Vehicle control (lactose)



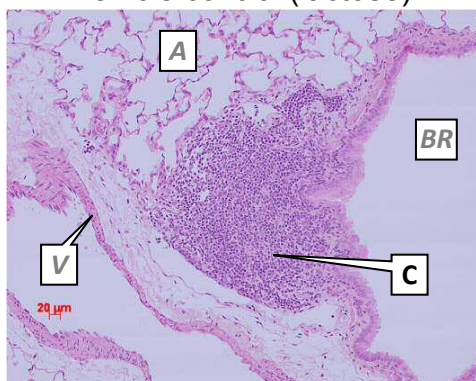
(R30662N; Rat 002)

**5.11D:** 14.5 mg/kg/day

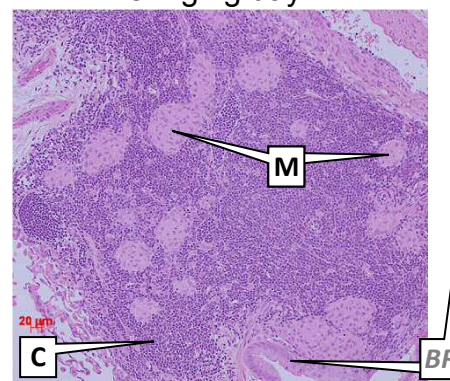


(R30662N; Rat 025)

**Figure 5.11: Representative histology of control rat lung and treatment related changes after inhalation of crystalline GSK-899 for 28 days.** Rats were exposed to lactose vehicle alone or in combination with crystalline GSK-899 for 28 days. Sections of tissue (3 µm thick) were stained with haematoxylin and eosin; *anatomical features are described in italics*. **5.11A:** histologically normal rat lung showing alveolar duct and alveoli. **5.11B:** mild macrophage aggregates (M) larger than those typically seen in concurrent controls. *A cross-section of a small airway (A) is also evident in section.* **5.11C:** control rat lung showing minimal macrophage aggregates (M). **5.11D:** moderate macrophage aggregates (M) and marked interstitial macrophages, T and B-lymphocytes (I); phenotype of inflammatory cells was confirmed by immunohistochemical staining for CD68, CD3 or CD79 glycoproteins.

**5.12A: Vehicle control (lactose)**

(R30662N; Rat 002)

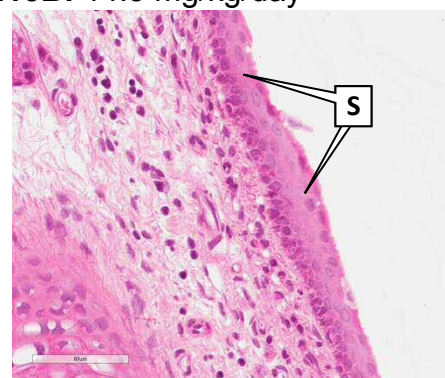
**5.12B: 14.5 mg/kg/day**

(R30662N; Rat 025)

**Figure 5.12:** Representative histology of control rat bronchus associated lymphoid tissue (BALT) and increased cellularity after inhalation of crystalline GSK-899 for 28 days. Rats were exposed to lactose vehicle alone or in combination with crystalline GSK-899. Tissue sections (3 µm thick) were stained with haematoxylin and eosin; *anatomical features are described in italics*. **5.12A:** normal cellularity (C) showing alveoli (A), bronchus (BR) and vein (V) in cross-section. **5.12B:** cellularity (C) increased relative to control with multifocal macrophage aggregates (M). Bronchus (BR) in cross-section.

**5.13A: Vehicle control (lactose)**

(R30662N; Rat 001)

**5.13B: 14.5 mg/kg/day**

(R30662N; Rat 025)

**Figure 5.13:** Representative histology of control rat larynx and changes after inhalation of crystalline GSK-899 for 28 days. Rats were exposed to lactose vehicle alone or in combination with crystalline GSK-899. Tissue sections (3 µm thick) were stained with haematoxylin and eosin; an *artefactual feature is described in italics*. **5.13A:** normal respiratory epithelium (RE); *haemorrhage (H) was agonal (post mortem artefact)*. **5.13B:** minimal squamous metaplasia.

In the larynx, squamous metaplasia (minimal) was evident for most rats administered 14.5 mg/kg/day. The rodent larynx is more susceptible to aerosol damage than primates and metaplastic changes are likely to

represent a defence mechanism in which a susceptible epithelium is replaced by more durable cell types (Gopinath and Mowat, 1987).

Amorphous GSK-899 was cleared from lung tissue after a single inhalation exposure (Figure 5.14). The mean lung concentration for rats administered 14.6 mg/kg at 24 hours (relative to the start of exposure) was approximately 0.7% of that determined immediately post exposure, and lung concentrations at 24 hours for rats administered 0.024 or 1.04 mg/kg were not quantifiable (<120 ng/g). GSK-899 concentrations were not quantifiable in lungs at 24 hours following completion of the 28-day treatment period for doses  $\leq 1.09$  mg/kg/day. This contrasted with lung concentrations following administration of crystalline GSK-899, which were approximately seven-fold higher immediately post exposure and persisted at 24 hours.

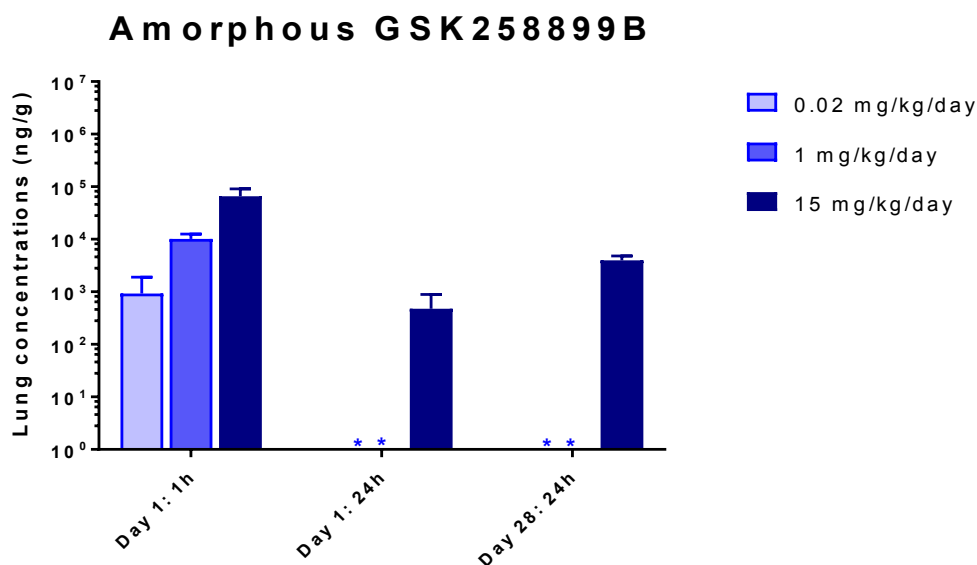


**Figure 5.14:** Drug-lung concentrations in rats following inhaled administration of amorphous GSK-899 for one or 28 days. Mean GSK-899 concentrations with standard deviations (error bars; n=3) are shown for rat lung homogenate data for samples taken immediately after a single 1-hour exposure and 24 hours after single or repeat exposures. Lung concentrations at 24 hours for doses of  $\leq 1$  mg/kg/day (\*) were below the limit of quantification (<120 ng/g lung tissue). Statistical analysis (2-way ANOVA with post hoc analysis using Tukey's honestly significant difference test (Abdi and Williams, 2010[B])) of  $\log_{10}$ -transformed data achieved significance for 1 vs 24 hours ( $p < 0.01$ ) and Days 1 vs 28 (24 hours;  $p < 0.05$ ).

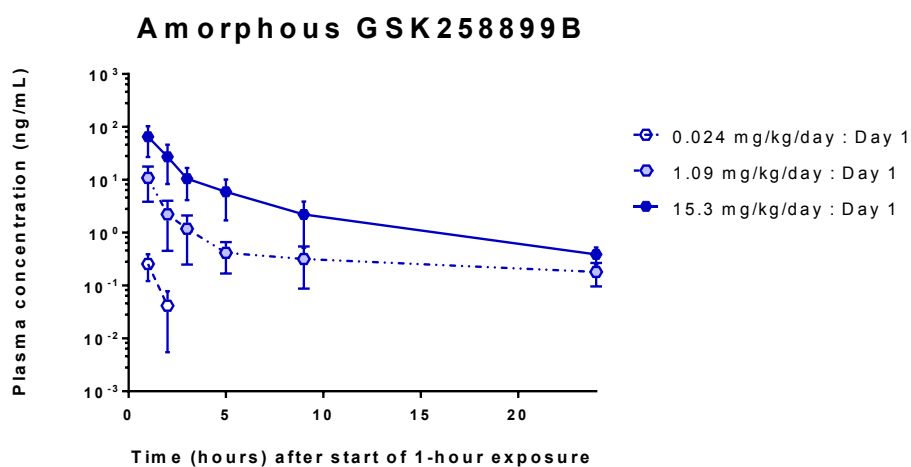
These findings are in line with expectations based on results summarised in Chapter 2 for *in vitro* dissolution (Figure 2.14) and *in vivo* lung concentration data (Figure 2.21). However, accumulation of GSK-899 in lungs was evident after repeated administration of 14.6 mg/kg/day, with an approximate nine-fold increase in trough concentrations from Days 1 to 28 of treatment. Although the degree of apparent accumulation was similar to that observed for crystalline GSK-899 at this dose, the absolute mean lung concentration following the last exposure to amorphous GSK-899 was <0.1% that measured after exposure to crystalline GSK-899. The apparent accumulation and the magnitude of difference between the particle forms of GSK-899 suggests sequestration of amorphous particles, for example lysosomal trapping, rather than saturation of clearance mechanisms *per se*.

Mean plasma concentrations of GSK-899 were similar on Days 1 and 28 of treatment for a given dose following inhaled administration of amorphous GSK-899 (Figure 5.15) and approximately three-fold higher than following administration of crystalline GSK-899 on Day 1 (Figure 5.8A). The plasma concentration profile on Day 28 for animals administered 0.02 mg/kg/day was lower at two hours than at subsequent timepoints (Figure 5.15B), which was probably a consequence of data variability exacerbated when 2/3 values at two hours were not quantifiable (<0.05 ng/mL), skewing calculation of the mean (zero values were entered for non-quantifiable sample results).

Systemic exposure ( $AUC_{0-t}$  and  $C_{max}$ ) of rats administered amorphous GSK-899 at 15 mg/kg/day was similar for Days 1 and 28 of treatment but approximately two-fold lower on Day 28 for animals administered 1 mg/kg/day (Table 5.14). For animals receiving 0.02 mg/kg/day, insufficient data were quantifiable on Day 1 (plasma concentrations <0.05 ng/mL from three hours) to enable determination of  $AUC_{0-t}$ . Although more samples were quantifiable on Day 28 for animals administered 0.02 mg/kg/day, permitting estimation of an  $AUC_{0-t}$ , the paucity of data precludes assessment of any changes between Days 1

and 28 at the low dose. Nevertheless, there was no evidence for systemic accumulation at higher doses ( $\geq 1$  mg/kg/day).

### 5.15A



### 5.15B

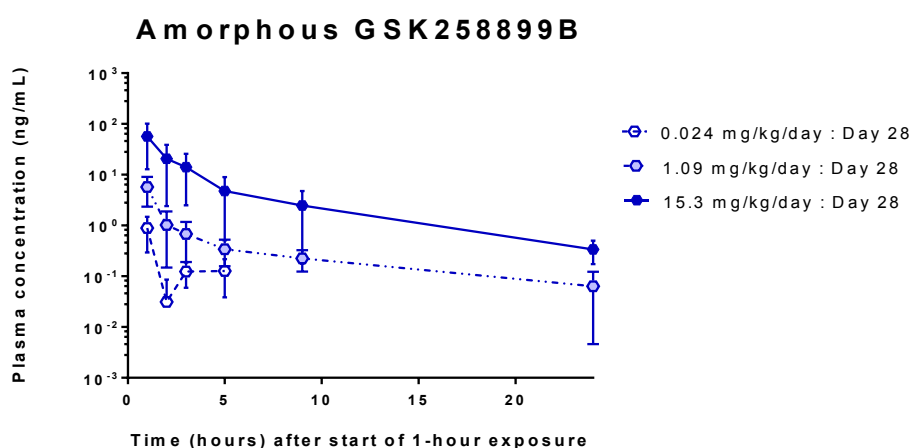


**Figure 5.15:** GSK-899 concentrations in rat plasma up to 24 hours after inhaled doses of amorphous GSK-899 on Days 1 and 28. Rats inhaled an aerosol of amorphous GSK-899 once daily (1 hour) for up to 28 days; mean plasma concentrations with standard deviations (error bars;  $n=3$ ) are shown for samples taken up to 24 hours after the start of inhalation exposure. **5.15A:** plasma concentrations after a single exposure (Day 1). **5.15B:** plasma concentrations after repeated administration (Day 28). Statistical analysis (MANOVA with post hoc analysis using Tukey's honestly significant difference test (Abdi and Williams, 2010[B])) of  $\log_{10}$ -transformed data indicated no statistical difference between Days 1 and 28.

Systemic exposure ( $AUC_{0-t}$  and  $C_{max}$ ) generally increased under proportionally for an increase in dose in line with data for crystalline GSK-899 at these doses.

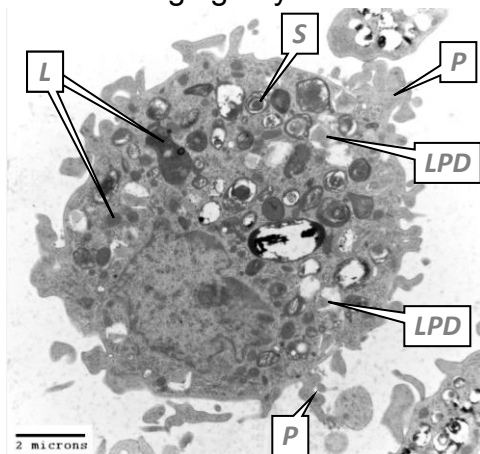
**Table 5.14: Pharmacokinetics of GSK-899 in plasma after inhaled administration of amorphous powder (n=3)**

Study No.	Estimated Inhaled Dose (mg/kg/day) <sup>A</sup>	Period (Day)	Statistical parameter	Pharmacokinetics (plasma)		
				AUC <sub>0-t</sub> (h.ng/mL) <sup>B</sup>	C <sub>max</sub> (ng/mL) <sup>B</sup>	T <sub>max</sub> (h) <sup>C</sup>
R30662N	0.022	D1	Mean	ND <sup>D</sup>	0.27	1
			sd	-	0.14	-
			CV (%)	-	52%	-
	0.024	D28	Mean	1.24	0.89	1
			sd	0.4	0.57	-
			CV (%)	35%	65%	-
1.30	D1	Mean	16.7	9.10	1	
		sd	10.9	5.88	-	
		CV (%)	65%	65%	-	
1.05	D28	Mean	10.5	5.93	1	
		sd	6.39	3.49	-	
		CV (%)	61%	59%	-	
15.9	D1	Mean	134	62.6	1	
		sd	82.0	36.7	-	
		CV (%)	61%	59%	-	
14.6	D28	Mean	134	59.5	1	
		sd	110	46.1	-	
		CV (%)	82%	78%	-	

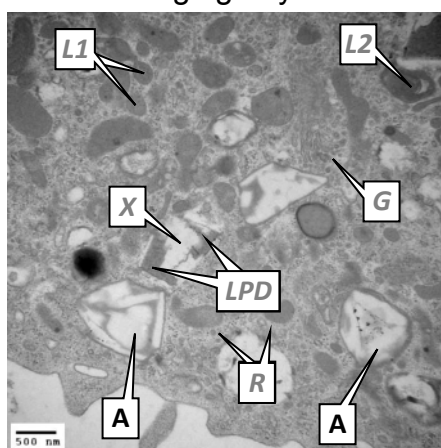
**Notes**

- A Overall estimated inhaled dose for toxicopathology animals over the 28-day treatment period.
- B Mean calculated from parameter for each rat (n=3): parameter dose-normalised (division by estimated inhaled dose on day of sampling) and re-normalised with the overall estimated inhaled dose<sup>A</sup>.
- C Median time presented relative to start of the 1-hour exposure period.
- D Not determined: insufficient data were available to permit calculation of the AUC<sub>0-t</sub> (concentrations for only two timepoints >0.05 ng/mL)
- CV Coefficient of variation (%) = sd/mean

TEM imaging of macrophages obtained from rats administered amorphous GSK-899 (10.9 mg/kg/day) revealed angular inclusions in a small proportion of macrophages (Figure 5.16B) consistent with the cross section of the dimpled spheres characterised by SEM in Chapter 2 (Figure 2.17A). Lamellar material and other inclusions were present but the shape was less distinct and these probably represent neutral lipid partially extracted during processing of the samples and similar to that seen in the lactose control (Figure 5.9).

**5.16A:** 10.9 mg/kg/day

(R30662N; Rat 034)

**5.16B:** 10.9 mg/kg/day

(R30662N; Rat 034)

**Figure 5.16: Macrophages containing amorphous particles after inhalation of GSK-899 for 3 days.** Rats were exposed to lactose vehicle alone or in combination with amorphous GSK-899 for 3 days. Macrophages were harvested *post mortem* in saline by bronchoalveolar lavage and processed for transmission electron microscopy. **5.16A:** macrophage showing evidence of artefactually extracted neutral lipid (LPD) and numerous lysosomes (L) of which some contain lamellar material likely to be lung surfactant (S). **5.16B:** macrophage with angular inclusions (A) likely to be amorphous GSK-899. Additional features in section include the Golgi body (G), primary lysosomes (L1), secondary lysosomes (L2) containing lamellar material, neutral lipid (LPD) with artefactual extraction (X), and ribosomes (R) that appear granular.

Rats administered amorphous GSK-899 for 28 days presented dose-dependent increases in the incidence and severity (minimal or mild) of multifocal foamy macrophage aggregates at  $\geq 0.024$  mg/kg/day (Table 5.15). Aggregates were associated with minimal interstitial mononuclear inflammatory cell infiltration in a proportion of animals receiving  $\geq 1.10$  mg/kg/day (Figure 5.17); immunohistochemical staining confirmed that inflammatory cells were macrophages (CD68-positive) at  $\geq 1.10$  mg/kg/day with T-lymphocytes (CD3-positive) also present at 15.6 mg/kg/day. The aggregates occurred in alveolar lumens bordering terminal bronchioles/alveolar ducts. Although the severity of the inflammatory cell infiltration was minimal following administration of amorphous GSK-899 (compared with mild to severe for crystalline GSK-899), the presence, incidence and nature of the finding were

sufficient for a dose of 14.6 mg/kg/day to be considered adverse, *i.e.* detrimental to the health status of the treated animals.

Squamous metaplasia (minimal) was observed in the larynx of most rats administered amorphous GSK-899 at  $\geq 1.10$  mg/kg/day (Figure 5.18), indicating that rats were more sensitive to irritation by the amorphous particle form.

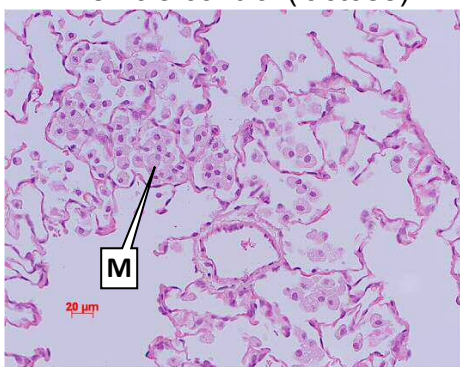
**Table 5.15: Histopathology of the respiratory tract of rats exposed to amorphous GSK-899 for 28 days**

Vehicle for powder dispersal: lactose		Incidence of findings (Study R30662N)			
Estimated inhaled dose (mg/kg/day)		0 (control)	0.024	1.10	15.6
Number of rats on study	Grading of observation	6	6	6	6
	Initial examination	6	0	0	6
Lung	<i>No findings</i>	4	2	2	1
	Aggregate, foamy macrophage; multifocal	2	3	3	2
	Mild	0	1	1	3
	Inflammatory cell infiltrate; interstitium; mononuclear cell, multifocal	0	0	2	4
Larynx	<i>No findings</i>	6	6	1	1
	Squamous metaplasia	0	0	5	5

**Notes**

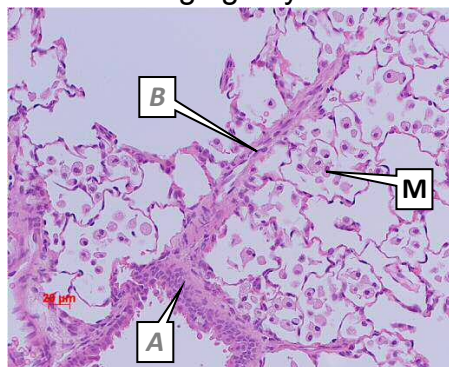
No treatment related findings (control and high dose animals examined): lymph node (tracheobronchial), tracheal bifurcation, trachea, nasopharynx, nasal cavity.

**5.17A:** Vehicle control (lactose)



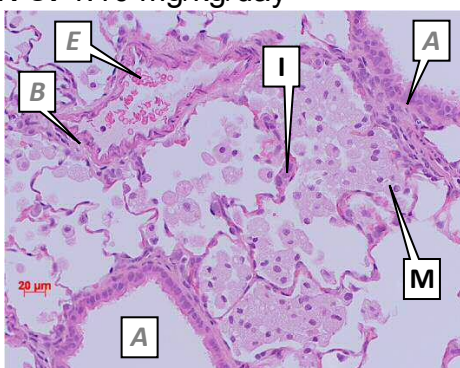
(R30662N; Rat 001)

**5.17B:** 0.024 mg/kg/day



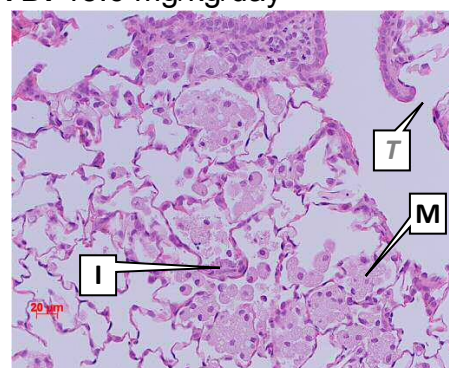
(R30662N; Rat 009)

**5.17C:** 1.10 mg/kg/day



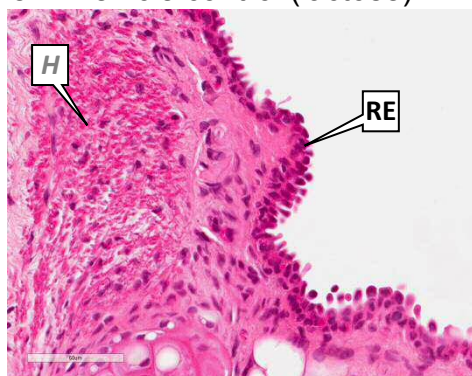
(R30662N; Rat 015)

**5.17D:** 15.6 mg/kg/day

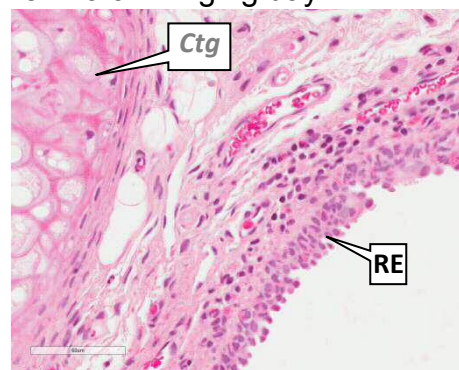


(R30662N; Rat 021)

**Figure 5.17:** Representative histology of control rat lung and treatment related changes after inhalation of amorphous GSK-899 for 28 days. Rats were exposed to lactose vehicle alone or in combination with amorphous GSK-899 for 28 days. Sections of tissue (3 µm thick) were stained with haematoxylin and eosin; *anatomical features are described in italics*. **5.17A:** normal rat lung showing minimal macrophage aggregates (M). **5.17B:** minimal macrophage aggregates (M). *An airway (A) in cross-section and a blood vessel (B) cut longitudinally are shown*. **5.17C:** mild macrophage aggregates (M); several aggregates seen in the plane of the section were bigger than those seen in concurrent controls. Minimal interstitial accumulation of macrophages (I) was confirmed by immunohistochemical staining for CD68 glycoprotein. *Airways (A) and a blood vessel (B) containing erythrocytes (E) are visible in cross-section*. **5.17D:** mild macrophage aggregates (M) and minimal interstitial accumulation of macrophages and T lymphocytes (I) (immunohistochemical staining for CD68, CD3 or CD79 glycoproteins confirmed interstitial cell phenotypes). *Terminal bronchioles were evident opening up into alveolar ducts (T)*.

**5.18A:** Vehicle control (lactose)

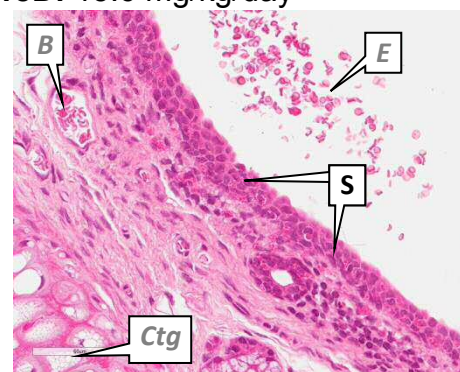
(R30662N; Rat 001)

**5.18B:** 0.024 mg/kg/day

(R30662N; Rat 009)

**5.18C:** 1.10 mg/kg/day

(R30662N; Rat 015)

**5.18D:** 15.6 mg/kg/day

(Study R30662N; Rat 020)

**Figure 5.18: Representative histology of control rat larynx and treatment related changes after inhalation of amorphous GSK-899 for 28 days.** Rats were exposed to lactose vehicle alone or in combination with amorphous GSK-899 for 28 days. Sections of tissue (3  $\mu$ m thick) were stained with haematoxylin and eosin; *artefactual and anatomical features are described in italics*. **5.18A:** rat larynx showing normal respiratory epithelium (RE); the haemorrhage (H) evident in section was agonal (post mortem artefact). **5.18B:** rat larynx showing normal cartilage (Ctg) and respiratory epithelium (RE); no GSK-899 related changes evident. **5.18C:** minimal squamous metaplasia (S). Separation of the tissue layers (X) was an artefact of the sectioning process post mortem. **5.18D:** minimal squamous metaplasia (S). Cartilage (Ctg and erythrocytes in a blood vessel (B) are visible in-section; erythrocytes in the lumen were agonal in origin.

Mean concentrations of GSK-899 in rat lung after a single exposure (one hour) were similar for nebulised aerosols using either vehicle (Figure 5.19) and approximately half that of rats administered amorphous GSK-899 at this dose. Lung clearance of GSK-899 was evident at 24 hours (mean concentration  $\leq$ 8% of that at one hour), with

an increase in trough concentrations from Days 1 to 28 (eight-fold when concentrations were also quantifiable at 24 hours on Day 1).

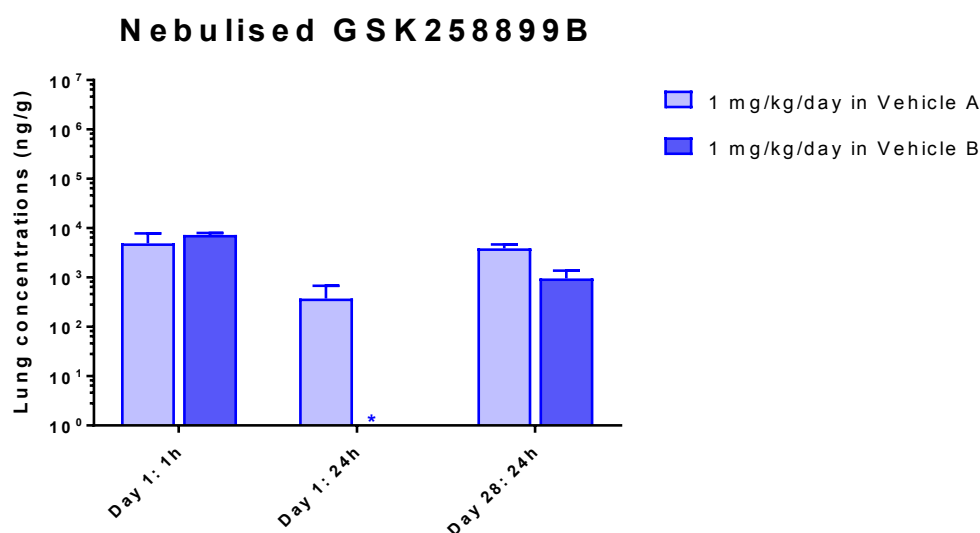


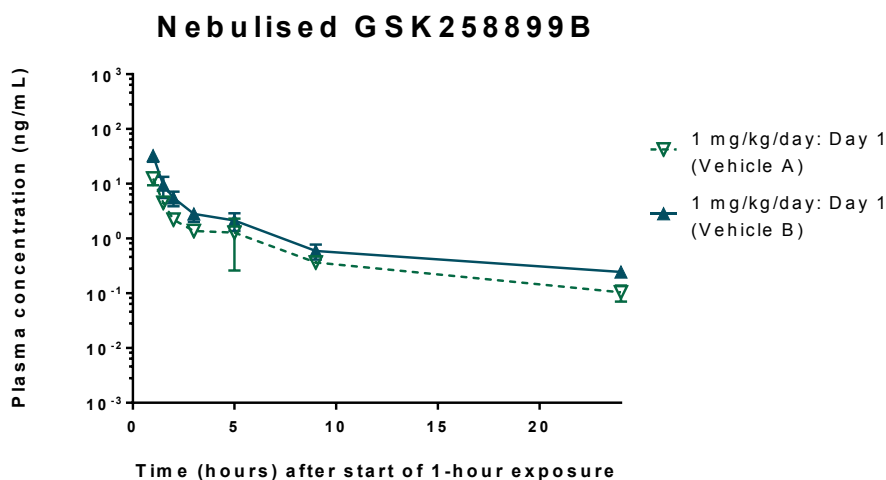
**Figure 5.19:** Drug-lung concentrations in rats following inhaled administration of nebulised GSK-899 for one or 28 days. Rats inhaled a nebulised aerosol of GSK-899 once daily (1 hour) for up to 28 days; mean dose normalised GSK-899 concentrations with standard deviations (error bars; n=3) are shown for rat lung homogenate data of samples taken immediately after a single exposure (1 hour) and at 24 hours after single or repeat exposures. Lung concentrations for a dose of 1 mg/kg/day in Vehicle B (\*) were below the limit of quantification (<120 ng/g lung tissue) 24 hours after a single exposure. Statistical analysis (2-way ANOVA with post hoc analysis using Tukey's honestly significant difference test (Abdi and Williams, 2010[B])) of log<sub>10</sub>-transformed data achieved significance for 1 vs 24 hours (p<0.01) and Days 1 vs 28 (24 hours; p<0.05); no statistical difference between the two nebulised formulations of GSK-899.

- Vehicle A = 3% (v/v) Solutol HS 15 in 0.9% (w/v) aqueous sodium chloride.
- Vehicle B = 3% (v/v) Solutol HS 15 in 10% (w/v) aqueous 2-hydroxypropyl-β-cyclodextrin.

Mean concentrations of GSK-899 in rat plasma were similar on Days 1 and 28 of treatment for each of the nebulised formulations, with  $T_{max}$  observed immediately post exposure (Figure 5.20 and Table 5.16). Plasma  $AUC_{0-t}$  following exposure of rats to GSK-899 nebulised in Solutol-NaCl was similar to that achieved following administration of amorphous powder (Table 5.14), but was approximately half that of the dose normalised  $AUC_{0-t}$  achieved with nebulisation of GSK-899 in Solutol-HPβCD. This confirmed that inclusion of the hydrophilic

cyclodextrin in the vehicle enhanced systemic uptake of GSK-899 (Chapter 2, Section 2.2.5.3).

### 5.20A



### 5.20B

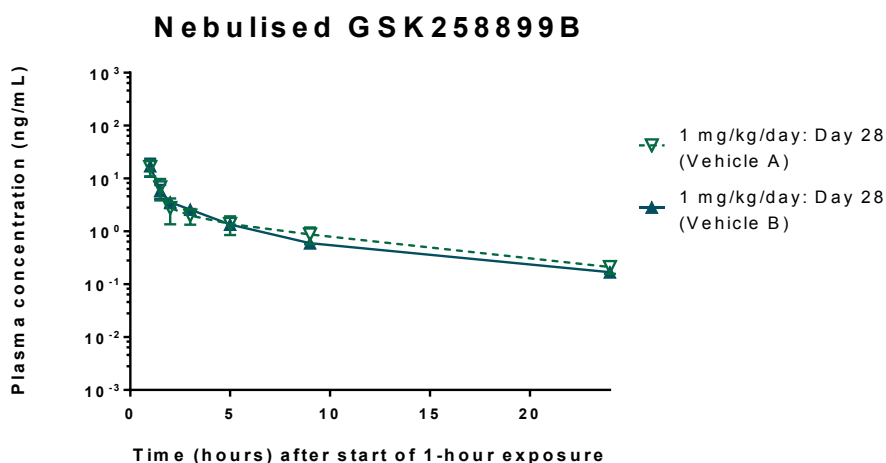


**Figure 5.20:** GSK-899 concentrations in rat plasma up to 24 hours after inhalation of nebulised doses on Days 1 and 28. Rats inhaled a nebulised aerosol of GSK-899 once daily (1 hour) for up to 28 days; mean dose normalised plasma concentrations with standard deviations (error bars; n=3) are shown for samples taken up to 24 hours after the start of inhalation exposure. **5.20A:** plasma concentrations after a single exposure (Day 1). **5.20B:** plasma concentrations after repeated administration (Day 28). Statistical analysis (MANOVA with post hoc analysis using Tukey's honestly significant difference test (Abdi and Williams, 2010[B])) of log<sub>10</sub>-transformed data achieved significance between the two nebulised formulations (p<0.01); no statistical difference between the Days 1 and 28 when dose normalised.

- Vehicle A = 3% (v/v) Solutol HS 15 in 0.9% (w/v) aqueous sodium chloride.
- Vehicle B = 3% (v/v) Solutol HS 15 in 10% (w/v) aqueous 2-hydroxypropyl-β-cyclodextrin.

**Table 5.16: Pharmacokinetics of GSK-899 in plasma after inhaled administration of nebulised solutions (n=3)**

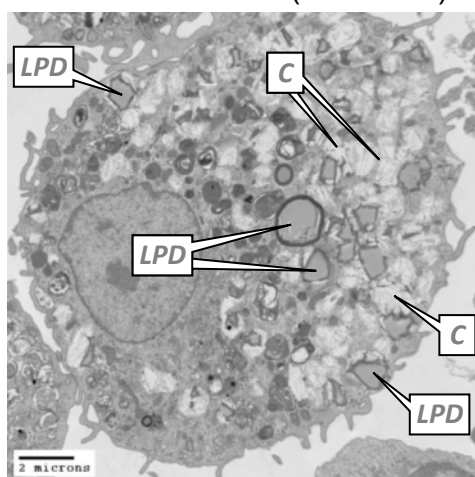
Study No.	Estimated Inhaled Dose (mg/kg/day) <sup>A</sup>	Period (Day)	Statistical parameter	Pharmacokinetics (plasma)		
				AUC <sub>0-t</sub> (h.ng/mL) <sup>B</sup>	C <sub>max</sub> (ng/mL) <sup>B</sup>	T <sub>max</sub> (h) <sup>C</sup>
R31038N	0.842	D1	Mean sd CV (%)	18.5 3.88 21%	10.5 2.40 23%	1 - -
		D28	Mean sd CV (%)	21.5 7.37 34%	10.7 3.65 34%	1 - -
R31039N	1.099	D1	Mean sd CV (%)	53.1 9.58 18%	35.5 7.84 22%	1 - -
		D28	Mean sd CV (%)	57.7 11.69 20%	31.0 11.76 38%	1 - -

**Notes**

- A Overall estimated inhaled dose for toxicopathology animals over the 28-day treatment period.
- B Mean calculated from parameter for each rat (n=3): parameter dose-normalised (division by estimated inhaled dose on day of sampling) and re-normalised with the overall estimated inhaled dose <sup>A</sup>.
- C Median time presented relative to start of the 1-hour exposure period.
- CV Coefficient of variation (%) = sd/mean

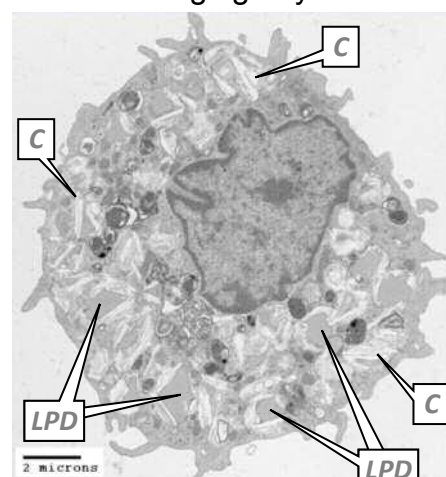
Examination of macrophages from rats administered nebulised GSK-899 (0.842 mg/kg/day) by TEM showed no evidence of particulate GSK-899. The appearance of these macrophages was similar to those of the vehicle control (Solutol-NaCl). A proportion of cells contained neutral lipid droplets or angular clefts (Figure 5.21) that were artefactual and ascribed to extraction of lipid during processing and/or cholesterol crystals (Lupu *et al.*, 1987).

5.21A: Vehicle control (nebulised)



(R31038N; Rat 067)

5.21B: 0.65 mg/kg/day



(R31038N; Rat 068)

**Figure 5.21: Macrophages after inhalation of nebulised vehicle or GSK-899 for 3 days.** Rats were exposed to vehicle alone (3% (v/v) Solutol HS 15 in 0.9% (w/v) aqueous sodium chloride) or a solution of GSK-899 for 3 days. Macrophages were harvested *post mortem* in saline by bronchoalveolar lavage and processed for transmission electron microscopy. **5.21A:** macrophage containing lipid droplets (LPD). Angular electron lucent crystal-like areas (C) associated with lipid droplets were consistent with extracted neutral lipid or cholesterol clefts (Lupu *et al.*, 1987). **5.21B:** macrophage containing lipid droplets (LPD) and crystal-like inclusions (C); no GSK-899 related ultrastructural changes were evident.

Multifocal bronchioloalveolar aggregates of macrophages (minimal or mild) were seen in the lungs of most rats administered 1 mg/kg/day GSK-899 nebulised in Solutol-NaCl (Table 5.17). In one rat, some macrophage aggregates were associated with alveolar wall thickening and scattered rare neutrophils. The macrophage aggregates were of similar grading to those seen following administration of crystalline or amorphous GSK-899 at this dose.

The macrophage aggregates (mild) were also seen in the lungs of all control rats exposed to Solutol-HP $\beta$ CD, and were associated with neutrophils and interstitial mononuclear inflammatory cells (minimal) and macrophage degeneration/necrosis (minimal in 5/6 rats; mild in one rat). The same lung pathology changes were seen in rats administered GSK-899 in Solutol-HP $\beta$ CD but the macrophage degeneration/necrosis was more pronounced (minimal in one rat; mild

in five rats) indicating exacerbation of the vehicle-related finding by GSK-899 (Table 5.18).

At the tracheal bifurcation of one rat administered 1 mg/kg/day nebulised in Solutol-NaCl, epithelial degeneration (minimal), characterised by deciliation and basophilia, was noted. However, the larynx showed no evidence of irritancy unlike that of rats exposed to crystalline or amorphous powders of GSK-899.

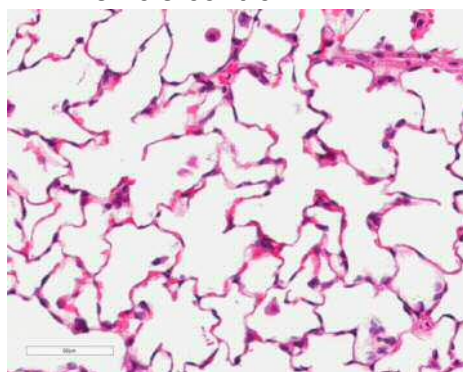
**Table 5.17: Histopathology of the respiratory tract of rats exposed to nebulised GSK-899 for 28 days**

Study Numbers		Incidence of findings			
		R31038N		R31039N	
Vehicle for nebulised solution		3% (v/v) Solutol HS 15 in 0.9% (w/v) aqueous sodium chloride		3% (v/v) Solutol HS 15 in 10% (w/v) aqueous 2-hydroxypropyl- $\beta$ -Cyclodextrin	
Estimated inhaled dose (mg/kg/day)		0 (control)	0.84	0 (control)	0.84
Number of rats on study Initial examination	Grading of observation	6	6	6	6
		6	6	6	6
Lung	<i>No finding</i>	5	2	0	0
Aggregate, foamy macrophage; multifocal; † bronchioloalveolar	Minimal	1†	2†	0	0
	Mild	0	2†	6	6
Inflammatory cell infiltrate; alveolus; neutrophilic, multifocal	Minimal	0	0	6	6
	Minimal	0	0	6	6
Degeneration/necrosis; macrophage	Minimal	0	0	5	1
	Mild	0	0	1	5
Tracheal bifurcation	<i>No finding</i>	5	5	6	6
	(no section)	(1)	(0)	(0)	(0)
Degeneration; epithelium	Minimal	0	1	0	0
Liver	<i>No finding</i>	6	6	6	3
Cytoplasmic rarefaction; hepatocellular	Mild	0	0	0	3

#### Notes

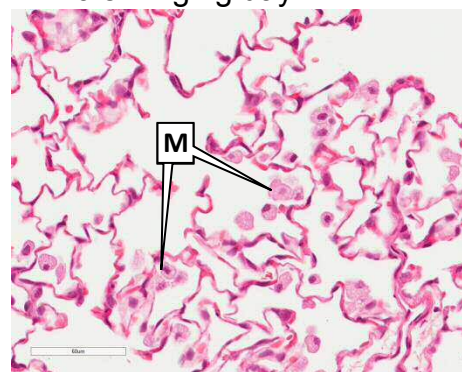
No treatment related findings (control and high dose animals examined): larynx, lymph node (tracheobronchial, mandibular), trachea, nasopharynx, nasal cavity.

5.22A: Vehicle control



(R31038N; Rat 001)

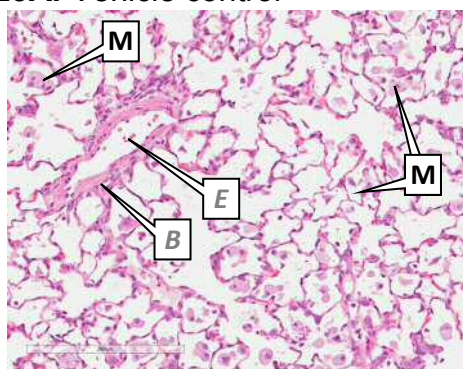
5.22B: 0.84 mg/kg/day



(R31038N; Rat 010)

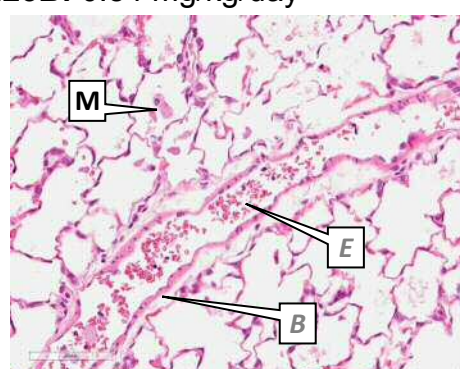
**Figure 5.22:** Representative histology of control rat lung and treatment related changes after inhalation of nebulised GSK-899 for 28 days. Rats were exposed to the vehicle alone (3% (v/v) Solutol HS 15 in 0.9% (w/v) aqueous sodium chloride) or as a solution of GSK-899 for 28 days. Sections of tissue (3  $\mu$ m thick) were stained with haematoxylin and eosin; *anatomical features are described in italics*. **5.22A:** normal rat lung showing alveolar duct and alveoli. **5.22B:** minimal bronchioloalveolar foamy macrophage aggregates (M).

5.23A: Vehicle control



(R31039N; Rat 001)

5.23B: 0.84 mg/kg/day



(R31039N; Rat 007)

**Figure 5.23:** Representative histology of rat lung and treatment related changes after inhalation of nebulised GSK-899 and/or vehicle for 28 days. Rats were exposed to the vehicle alone (3% (v/v) Solutol HS 15 in 10% (w/v) aqueous 2 hydroxypropyl-B-cyclodextrin) or as a solution of GSK-899 for 28 days. Sections of tissue (3  $\mu$ m thick) were stained with haematoxylin and eosin; *anatomical features are described in italics*. **5.23A:** lung of a control rat showing mild foamy macrophage aggregates (M) ascribed to administration of the nebulised vehicle. A blood vessel (B) is also evident, this time in cross-section. **5.23B:** mild foamy macrophage aggregates (M). A blood vessel (B) is also evident, this time in longitudinal-section.

The mean lung concentration of GSK-899 in lungs taken one hour after a single subcutaneous dose of 5 mg/kg was approximately half that

achieved after administration of a single nebulised dose of 1 mg/kg. A reduction in lung concentration was evident at 24 hours (10% of mean value at one hour) with a two-fold increase in trough concentrations from Days 1 to 28 of treatment (Figure 5.24).

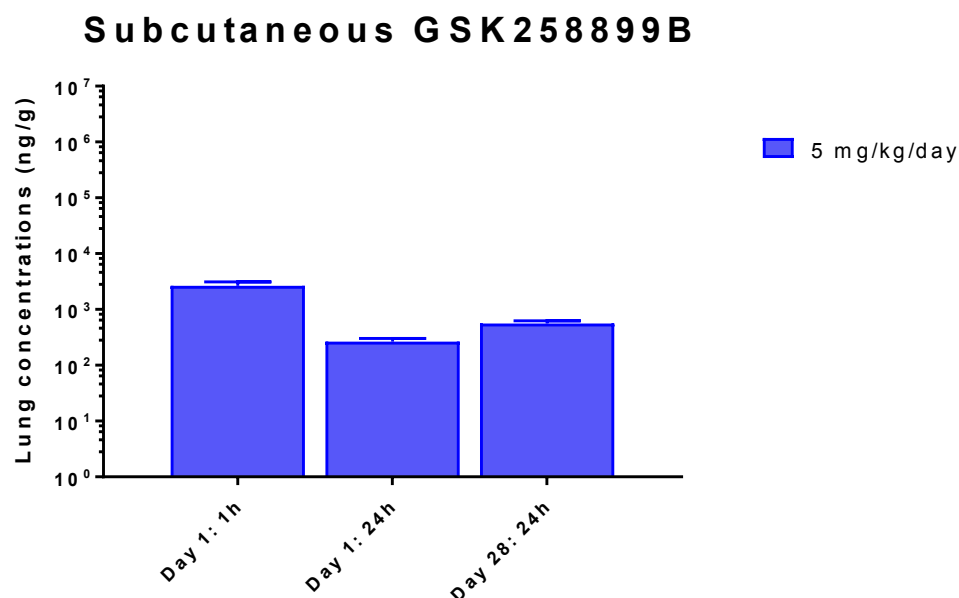
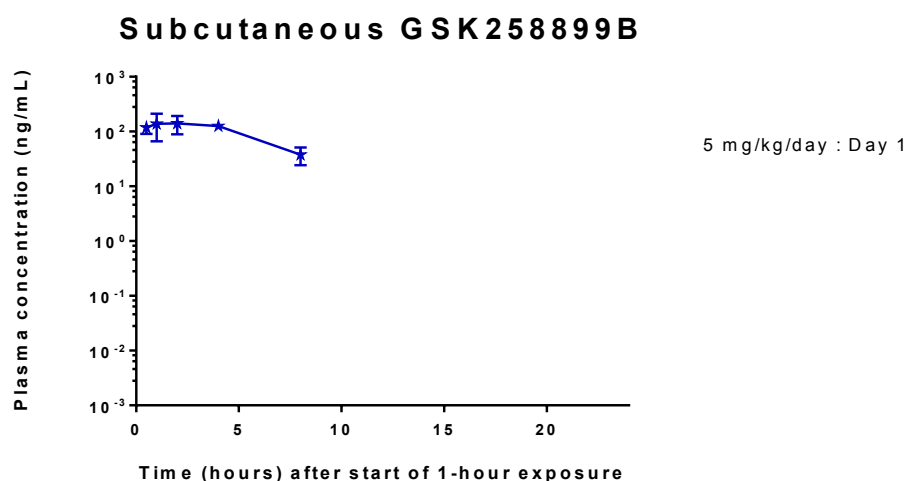


**Figure 5.24:** Drug-lung concentrations in rats after subcutaneous administration of GSK-899 for one or 28 days. Mean GSK-899 concentrations with standard deviations (error bars; n=3) are shown for rat lung homogenate data for samples taken 1 and 24 hours after a single dose and 24 hours after repeated administration. Statistical analysis (1-way ANOVA with post hoc analysis using Tukey's honestly significant difference test (Abdi and Williams, 2010[B])) of  $\log_{10}$ -transformed data achieved significance ( $p < 0.01$ ) between 1 and 24 hours, and between Days 1 and 28 (24 hours).

$C_{max}$  of GSK-899 in plasma was observed at one or two hours after subcutaneous injection of 5 mg/kg on Days 1 and 28 respectively, with elimination of the analyte from plasma at 24 hours and no obvious accumulation over the 28-day treatment period (Figure 5.25).

## 5.25A



## 5.25B

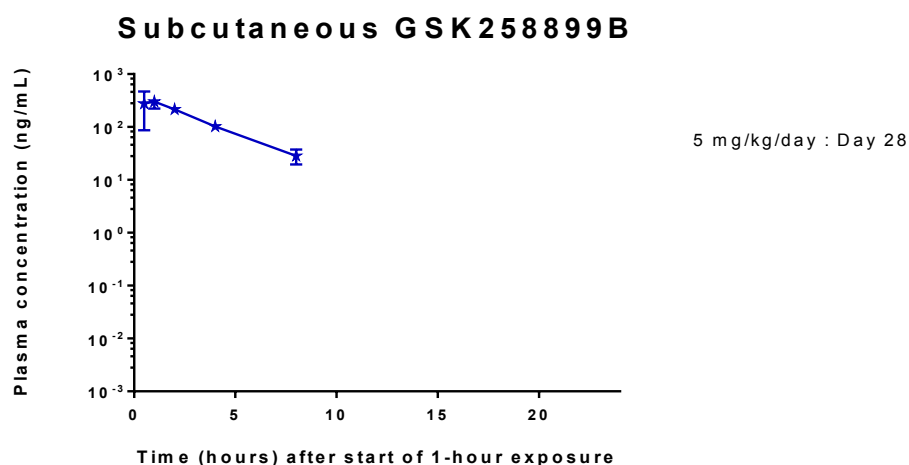


**Figure 5.25: GSK-899 concentrations in rat plasma up to 24 hours after subcutaneous administration on Days 1 and 28.** Mean GSK-899 concentrations in plasma with standard deviations (error bars; n=3) are shown for plasma samples taken up to 24 hours post dose. **5.25A:** plasma concentrations after a single dose (Day 1). **5.25B:** plasma concentrations after the final dose (Day 28). Statistical analysis (2-way ANOVA with post hoc analysis using Tukey's honestly significant difference test (Abdi and Williams, 2010[B])) of log<sub>10</sub>-transformed data achieved significance (p<0.05) between Days 1 and 28.

Systemic exposure (AUC<sub>0-t</sub>) in plasma was similar on Days 1 and 28, and at least six-fold higher than that achieved with inhaled administration of 15 mg/kg/day crystalline or amorphous GSK-899 (Table 5.18).

**Table 5.18: Pharmacokinetics of GSK-899 in plasma after subcutaneous administration of a solution (n=3)**

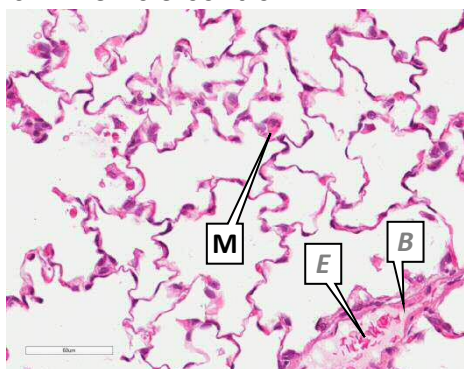
Study No.	Estimated Inhaled Dose (mg/kg/day)	Period (Day)	Statistical parameter	Pharmacokinetics (plasma)		
				AUC <sub>0-t</sub> (h.ng/mL)	C <sub>max</sub> (ng/mL)	T <sub>max</sub> (h) <sup>A</sup>
R31697N	5	D1	Mean	803	157	2
			sd	197	46	-
			CV (%)	24%	30%	-
		D28	Mean	920	333	1
			sd	277	133	-
			CV (%)	30%	40%	-

**Notes**

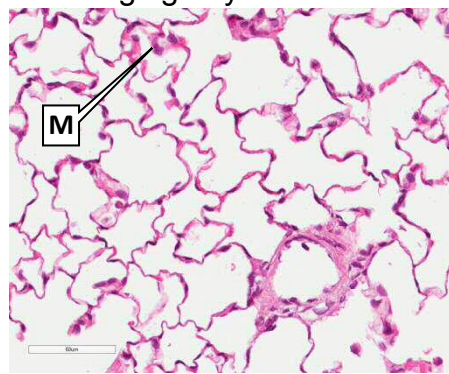
A Median time

CV Coefficient of variation (%) = sd/mean

There were no toxicopathology changes in the lungs of rats subcutaneously administered GSK-899 for 28 days (Table 5.19 and Figure 5.26). Minimal focal inflammatory cell infiltrate within the interstitium is a common background finding in CrI:CD(SD) rats; given the infiltration was not multifocal and also minimal, it was considered (in consultation with the study pathologist) not to be GSK-899-related.

**5.26A: Vehicle control**

(R31697N; Rat 002)

**5.26B: 5 mg/kg/day**

(R31697N; Rat 009)

**Figure 5.26: Representative histology of control rat lung and after subcutaneous administration of GSK-899 for 28 days.** Rats were dosed the vehicle alone (3% (v/v) Solutol HS 15 in 0.9% (w/v) aqueous sodium chloride) or as a solution of GSK-899 for 28 days. Sections of tissue (3 µm thick) were stained with haematoxylin and eosin; *anatomical features are described in italics*. **5.26A:** control rat lung showing occasional macrophages (M); a blood vessel (B) with erythrocytes (E) is evident in cross-section. **5.26B:** lung of rat administered nebulised GSK-899 showing normal lung with occasional macrophages (M).

**Table 5.19: Histopathology of lungs and injection sites of rats dosed subcutaneously with GSK-899 for 28 days**

Vehicle for dosing: 3% (v/v) Solutol HS 15 in 0.9% (w/v) aqueous sodium chloride		Incidence of findings (Study R31697N)	
Estimated inhaled dose (mg/kg/day)		0 (control)	5
Number of rats on study	Grading of observation	5	6
	Initial examination	6	0
Lung	<i>No findings</i>	3	0
Aggregate, foamy macrophage; BALT; multifocal	Minimal	0	5
Aggregate, macrophage; alveolar; focal	Minimal	0	1
Inflammatory cell infiltrate; interstitium; mixed cell, focal	Minimal	2	4
Thymus			
Haemorrhage; corticomedullary junction; focal	Minimal	1	1
Vacuolation, macrovesicular; cortex and medulla; multifocal	Minimal	1	1
	Mild	2	3
	Moderate	2	2
Injection sites (x4): <i>28 doses were injected subcutaneously at four dorsal sites rotated daily (7 injections/site); severity of findings were higher for GSK-899 than vehicle</i>			
Degeneration/regeneration; panniculus muscle; focal or multifocal		5 +	6 +++
Inflammation; subcutis; lymphohistiocytic (lymphocytes and macrophages, predominantly the latter with GSK-899 doses); multifocal		5 ++	6 ++++
Fibroplasia; subcutis; diffuse		5 +++	6 +++
Degeneration; subcutis (multifocal or diffuse)		4 +++	6 ++++
Haemorrhage; subcutis; localised		2 ++	6 +++
Pigmented macrophages; subcutis; focal at site 1 and multifocal at sites 2 to 4		1 +	5 ++
Inflammatory (mononuclear) cell infiltrate; dermis; focal		1 +	0
Granuloma; dermis; focal		0	1 +

**Notes**

Injection sites: the highest severity scored for observations in any animal and at any site is shown, graded as minimal (+), mild (++) , moderate (+++) or marked (++++).

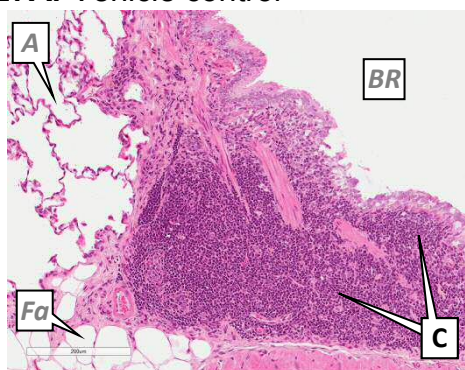
No treatment related findings (control and high dose animals examined): lymph node (tracheobronchial), nasopharynx, nasal cavity.

BALT bronchus associated lymphoid tissue

A Injection sites: a summary of the incidence and severity of findings at the injection sites is presented in Appendix 9.

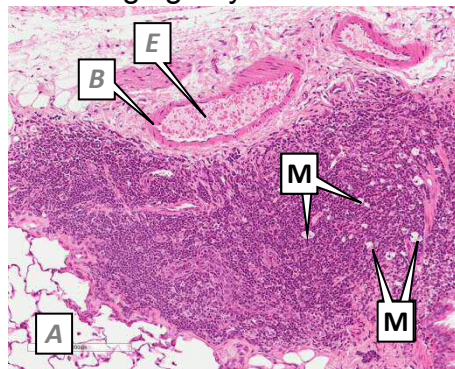
Foamy alveolar macrophages in the BALT of rats dosed with GSK-899 (Figure 5.27B) were considered unlikely to be treatment related given the minimal grade (Table 5.19), variability in amount of BALT between rats and incidence of this finding in the hepatocytes and thymus (Figure 5.28A) of both control and GSK-899 treated rats.

**5.27A:** Vehicle control



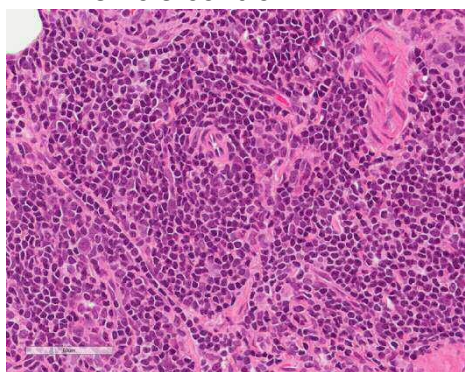
(R31697N; Rat 002)

**5.27B:** 5 mg/kg/day



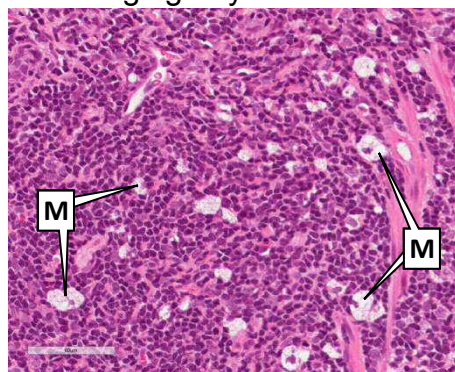
(R31697N; Rat 009)

**5.27C:** Vehicle control



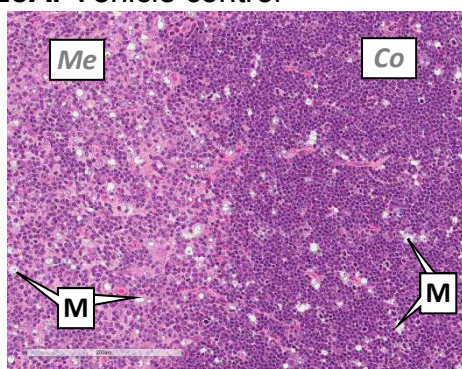
(R31697N; Rat 002)

**5.27D:** 5 mg/kg/day

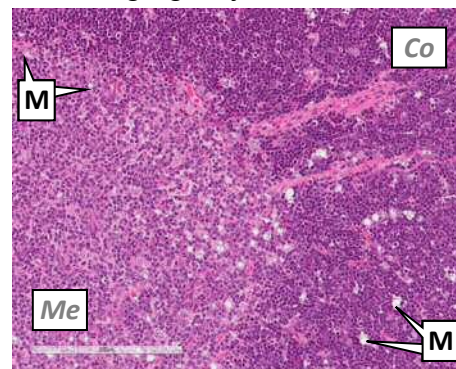


(R31697N; Rat 009)

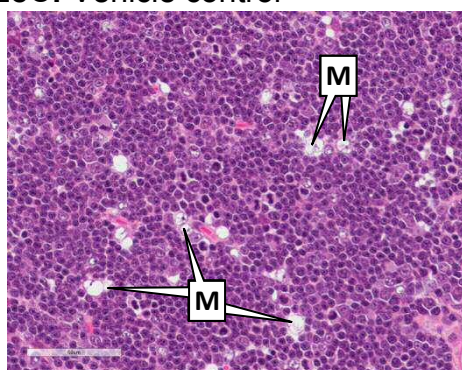
**Figure 5.27: Representative histology of bronchus associated lymphoid tissue (BALT) after subcutaneous administration of GSK-899 and/or vehicle for 28 days.** Rats were dosed the vehicle alone (3% (v/v) Solutol HS 15 in 0.9% (w/v) aqueous sodium chloride) or as a solution of GSK-899 for 28 days. Sections of tissue (3  $\mu$ m thick) were stained with haematoxylin and eosin; *anatomical features are described in italics*. **5.27A:** normal cellularity of rat BALT (C) showing alveoli (A) and a bronchus (BR) in cross-section; fat (Fa) appears as artefactual spaces due to depletion of fat from tissue during processing. **5.27B:** BALT of rat administered GSK-899 showing minimal, multifocal aggregates of foamy macrophages (M); alveoli (A) and a blood vessel (B) with erythrocytes (E) are evident in cross-section. **5.27C:** higher magnification showing normal cellularity of rat BALT. **5.27D:** higher magnification of rat BALT showing aggregates of foamy macrophages (M).

**5.28A:** Vehicle control

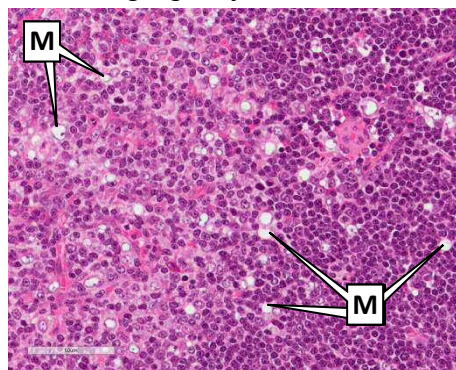
(R31697N; Rat 002)

**5.28B:** 5 mg/kg/day

(R31697N; Rat 009)

**5.28C:** Vehicle control

(R31697N; Rat 002)

**5.28D:** 5 mg/kg/day

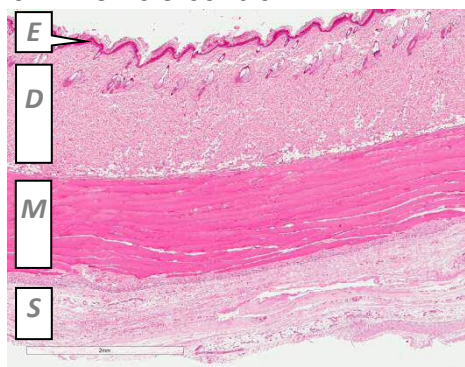
(R31697N; Rat 009)

**Figure 5.28:** Representative histology of thymus after subcutaneous administration of GSK-899 and/or vehicle for 28 days. Rats were dosed the vehicle alone (3% (v/v) Solutol HS 15 in 0.9% (w/v) aqueous sodium chloride) or as a solution of GSK-899 for 28 days. Sections of tissue (3  $\mu$ m thick) were stained with haematoxylin and eosin; *anatomical features are described in italics*. **5.28A:** thymus of a control rat showing occasional macrophages (M) in the *medulla (Me)* and *cortex (Co)*. **5.28B:** thymus of rat administered GSK-899 also showing occasional macrophages (M) in the *medulla (Me)* and *cortex (Co)*. **5.28C:** higher magnification of cortex showing macrovesicular vacuolation of macrophages (M). **5.28D:** higher magnification of rat medulla and cortex also showing vacuolated macrophages (M).

Injection sites were characterized by areas of localised haemorrhage and/or pigmented macrophages (stained for haemosiderin by Perl's Prussian Blue) due to trauma of the dose route. These observations occurred within areas of multifocal or diffuse degeneration of the subcutis associated with varying degrees of lymphohistiocytic (T-cell predominant) inflammation and fibroplasia (Figure 5.29). Findings were consistent with local irritancy and seen in controls (Solutol-NaCl) but increased in severity and incidence for rats dosed GSK-899.

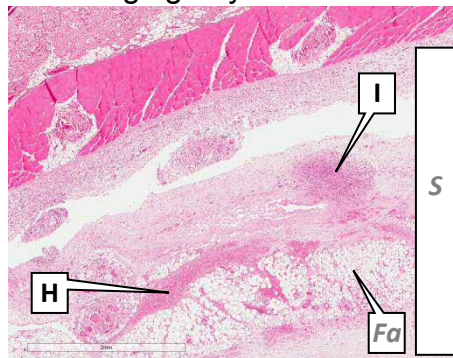
Degeneration and regeneration of the panniculus muscle in control and GSK-899 treated rats, and focal dermal granuloma in one GSK-899 treated rat, were also related to needle trauma and post dose healing.

**5.29A:** Vehicle control



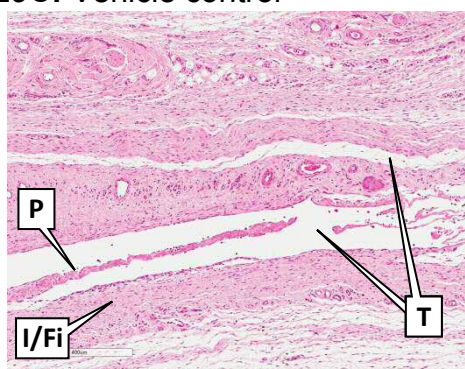
(R31697N; Rat 005)

**5.29B:** 5 mg/kg/day



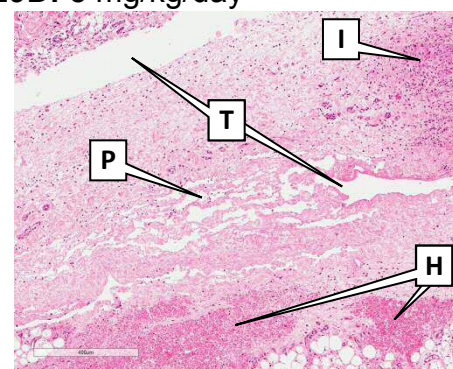
(R31697N; Rat 012)

**5.29C:** Vehicle control



(R31697N; Rat 005)

**5.29D:** 5 mg/kg/day



(R31697N; Rat 012)

**Figure 5.29: Representative histology of subcutaneous injection site after administration of GSK-899 and/or vehicle for 28 days.** Rats were dosed the vehicle alone (3% (v/v) Solutol HS 15 in 0.9% (w/v) aqueous sodium chloride) or as a solution of GSK-899 for 28 days using four dorsal injection sites in rotation. Tissue sections (3 µm thick) were stained with haematoxylin and eosin; *anatomical features are described in italics*. **5.29A:** skin of vehicle control rat showing the *epidermis (E)*, *dermis (D)*, *panniculus muscle (M)* and *subcutis (S)*. **5.29B:** GSK-899 treated rat skin showing areas of haemorrhage (H) and lymphohistiocytic inflammation (I) in the *subcutis (S)*. *Fat (Fa)* appears as *artefactual spaces in tissue due to its depletion during processing*. **5.29C:** high magnification of subcutis from a vehicle control rat showing lymphohistiocytic inflammation (I), characterized by macrophages and lymphocytes, and fibroplasia (Fi). Degeneration of subcutis is characterized by pale beaded collagen (P) and the formation of tracts (T). **5.29D:** high magnification of subcutis of GSK-899 treated rat showing erythrocytes indicative of haemorrhage (H) and lymphohistiocytic inflammation (I), characterized mainly by macrophages. Degeneration of the subcutis is characterized by pale beaded collagen (P) and formation of tracts (T).

### 5.3.2.3. Pulmonary and systemic exposure of rats to GSK-677 and toxicopathology after 28 days

Lung clearance of GSK-677 was evident after a single inhalation exposure of rats to the crystalline drug (Figure 5.30). The mean lung concentration for rats sampled at 24 hours (relative to the start of exposure) was less than 2% of that determined immediately post exposure. Slight accumulation of GSK-677 over the treatment period was evident (approximately two-fold increases in trough concentrations from Days 1 to 28), which contrasted slightly with expectations based on results summarised in Chapter 2 for *in vitro* dissolution (Figure 2.14) and *in vivo* lung concentration data (Figure 2.26) insofar as lung concentrations at 24 hours were not quantifiable and accumulation of GSK-677 in lung tissue was not anticipated.

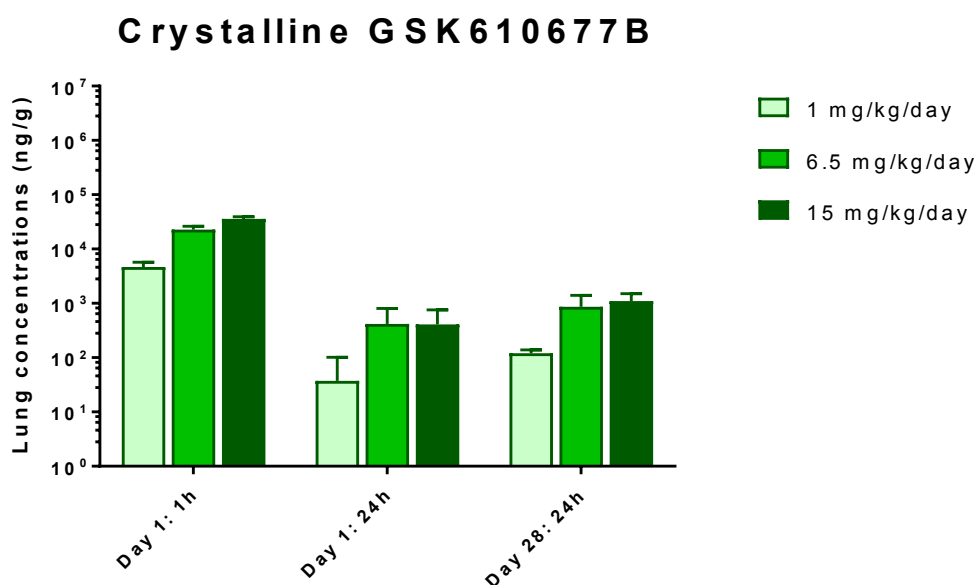
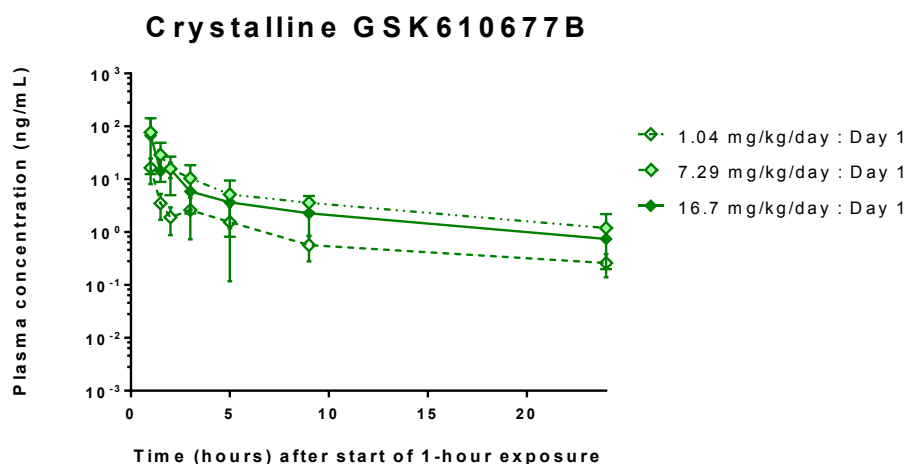


**Figure 5.30:** Drug-lung concentrations in rats following inhaled administration of crystalline GSK-677 for one or 28 days. Mean GSK-677 concentrations with standard deviations (error bars; n=3) are shown for rat lung homogenate data for samples taken immediately after a single 1-hour exposure and at 24 hours after single or repeat exposures. Statistical analysis (2-way ANOVA with post hoc analysis using Tukey's honestly significant difference test (Abdi and Williams, 2010[B])) of log<sub>10</sub>-transformed data achieved significance between 1 and 24 hours ( $p < 0.01$ ); no significant difference for Days 1 vs 28 (24 hours).

Plasma concentration (Figure 5.31),  $AUC_{0-t}$  and  $C_{max}$  (Table 5.20) were similar for doses  $\geq 7.29$  mg/kg/day and lower at 1.04 mg/kg/day, with  $T_{max}$  immediately post exposure. Differences in systemic exposure between Days 1 and 28 were minor, albeit statistically significant.

### 5.31A



### 5.31B

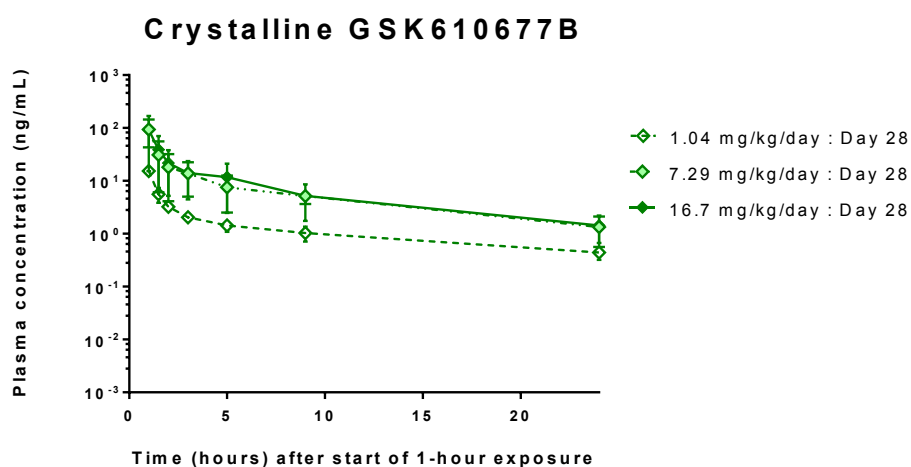


**Figure 5.31:** GSK-677 concentrations in rat plasma up to 24 hours after inhaled doses of crystalline GSK-677 on Days 1 and 28. Rats inhaled an aerosol of crystalline GSK-677 once daily (1-hour exposure) for up to 28 days; mean plasma concentrations with standard deviations (error bars;  $n=3$ ) are shown for samples taken up to 24 hours after the start of inhalation exposure. **5.31A:** plasma concentrations after a single exposure (Day 1). **5.31B:** plasma concentrations after repeated administration (Day 28). Statistical analysis (MANOVA with post hoc analysis using Tukey's honestly significant difference test (Abdi and Williams, 2010[B])) of  $\log_{10}$ -transformed data achieved significance between Days 1 and 28 ( $p<0.05$ ).

**Table 5.20: Pharmacokinetics of GSK-677 in plasma after inhaled administration of micronised crystals (n=3)**

Study No.	Estimated Inhaled Dose (mg/kg/day) <sup>A</sup>	Period (Day)	Statistical parameter	Pharmacokinetics (plasma)		
				AUC <sub>0-t</sub> (h.ng/mL) <sup>B</sup>	C <sub>max</sub> (ng/mL) <sup>B</sup>	T <sub>max</sub> (h) <sup>C</sup>
R31035N	1.04	D1	Mean	32.1	17.9	1
			sd	11.4	9.0	-
			CV (%)	36%	51%	-
		D28	Mean	38.0	16.2	1
			sd	7.3	1.3	-
			CV (%)	19%	8%	-
	7.29	D1	Mean	141.9	73.2	1
			sd	103.4	60.3	-
			CV (%)	73%	82%	-
		D28	Mean	180.5	88.8	1
			sd	94.3	48.3	-
			CV (%)	52%	54%	-
16.7	D1	Mean	98.6	62.1	1	
		sd	68.9	64.3	-	
		CV (%)	70%	104%	-	
	D28	Mean	188.1	81.7	1	
		sd	139.0	68.1	-	
		CV (%)	74%	83%	-	

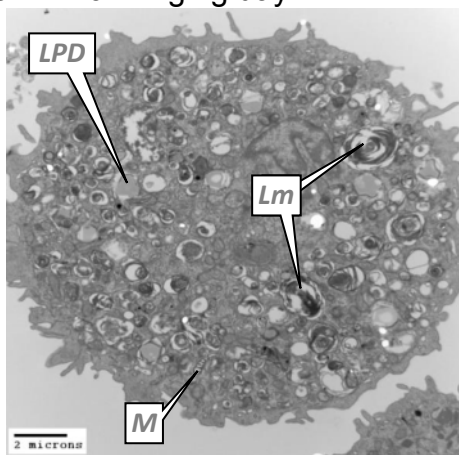
**Notes**

- A Overall estimated inhaled dose for toxicopathology animals over the 28-day treatment period.
- B Mean calculated from parameter for each rat (n=3): parameter dose-normalised (division by estimated inhaled dose on day of sampling) and re-normalised with the overall estimated inhaled dose <sup>A</sup>.
- C Median time presented relative to start of the 1-hour exposure period.
- CV Coefficient of variation (%) = sd/mean

TEM imaging of macrophages from rats administered crystalline GSK-677 (19.2 mg/kg/day) showed crystal-like structures associated with neutral lipid droplets (Figure 5.32). The inclusions were unlikely to be crystalline drug substance because similar 'structures' were not evident in phagosomes (vacuoles containing phagocytosed material) or secondary lysosomes. Given their association with neutral lipid, it is considered likely these inclusions are cholesterol clefts similar to those described by Lupu *et al.* (1987) for lipid laden cells in atherosclerotic lesions. This is in line with *in vitro* results, which also showed lamellar

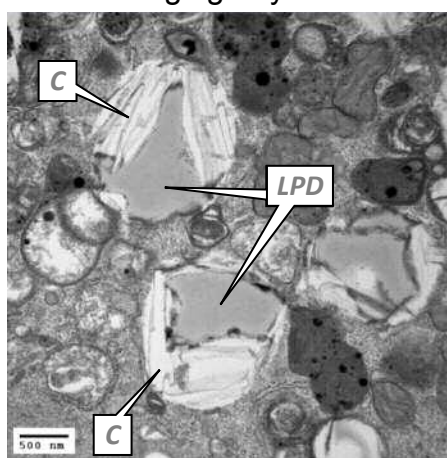
material but no obvious particulate drug substance within the macrophages (Figures 5.6C/D).

**5.32A:** 19.2 mg/kg/day



(R31037N; Rat 028)

**5.32B:** 19.2 mg/kg/day



(R31037N; Rat 028)

**Figure 5.32: Macrophages after inhalation of crystalline GSK-677 for 3 days.** Rats were exposed to lactose vehicle alone or in combination with crystalline GSK-677 for 3 days. Macrophages were harvested *post mortem* in saline by bronchoalveolar lavage and processed for transmission electron microscopy. **5.32A:** vacuolated macrophage with lamellar material (Lm) considered to be phagocytosed surfactant; neutral lipid (LDP) and mitochondrion (M) also shown. **5.32B:** higher magnification of macrophage showing neutral lipid (LPD) and associated crystal-like structures (C) considered consistent with extracted neutral lipid or cholesterol clefts (Lupu *et al.*, 1987).

Unpublished data (Freke, 2007) showed rats administered crystalline GSK-677 for 28 days presented dose-dependent increases in the incidence and severity (minimal or mild) of multifocal foamy bronchioloalveolar macrophage aggregates at  $\geq 2.25$  mg/kg/day (Table 5.21). In 3/10 rats administered 67.8 mg/kg/day, this finding was associated with mononuclear cell infiltration (mostly lymphocytic; minimal) and epithelial hyperplasia at the bronchioloalveolar junction. These findings are similar to those observed in rats administered GSK-899 at 1.1 mg/kg/day.

A dose-related increase in the incidence of squamous metaplasia (minimal) was observed ventrally in the larynx of rats administered crystalline GSK-677 at  $\geq 2.25$  mg/kg/day (Table 5.21) indicating slight irritancy of crystalline GSK-677 in this tissue.

**Table 5.21: Histopathology of the respiratory tract of rats exposed to micronised crystalline GSK-677 for 28 days**

Vehicle for powder dispersal: lactose		Incidence of findings (unpublished data: study R27090)				
Estimated inhaled dose (mg/kg/day)		0 (control)	0.016	0.20	2.25	67.8
Number of rats on study	Grading of observation	10	10	10	10	10
Initial examination		10	10	10	10	10
Lung	<i>No finding</i>	9	8	8	6	0
Aggregate, foamy macrophage; bronchioloalveolar; multifocal	1 (minimal)	1	2	2	3	3
	2 (mild)	0	0	0	1	7
Infiltration, mononuclear cell	1 (minimal)	0	0	0	0	3
Hyperplasia, bronchioloalveolar	1 (minimal)	0	0	0	0	3
Larynx	<i>No finding</i>	10	10	9	5	2
Squamous metaplasia	1 (minimal)	0	0	1	5	8

**Notes**

Study performed at Charles River Laboratories, Montreal, Canada (Freke, 2007).

No treatment related findings: bronchus, trachea, tracheal bifurcation, nasopharynx, nasal cavity.

Mean GSK-677 concentrations in lungs of rats administered nebulised solutions were approximately half that of rats administered similar doses of crystalline GSK-677.

Lung clearance of GSK-677 was evident after a single inhalation exposure of rats to nebulised solutions (Figure 5.33). The mean lung concentration at 24 hours (relative to the start of exposure) was less than 1% of that determined immediately post exposure. Accumulation of GSK-677 was evident from Days 1 to 28 of treatment (six or 14-fold increases in trough concentrations for mid and high doses respectively) in line with observations for crystalline GSK-677.

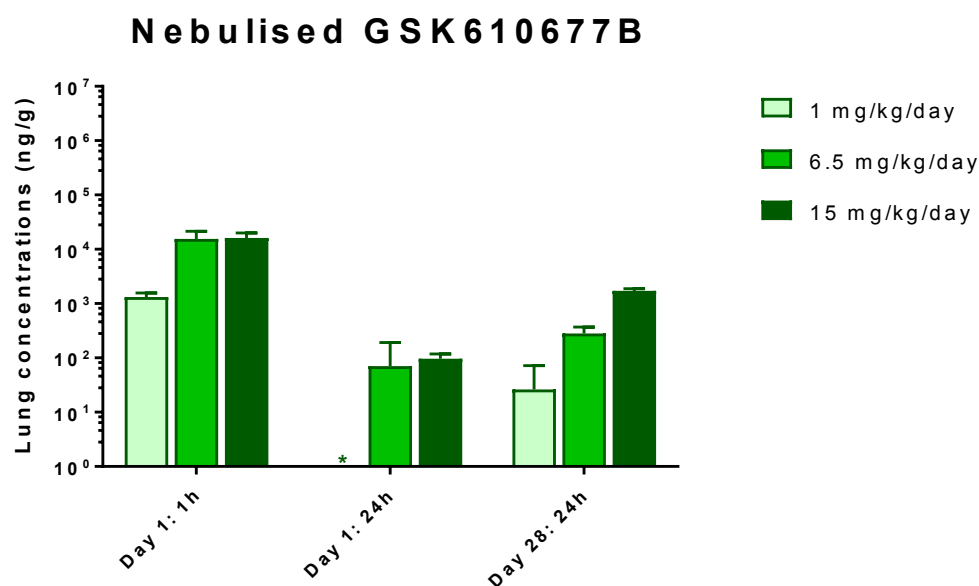
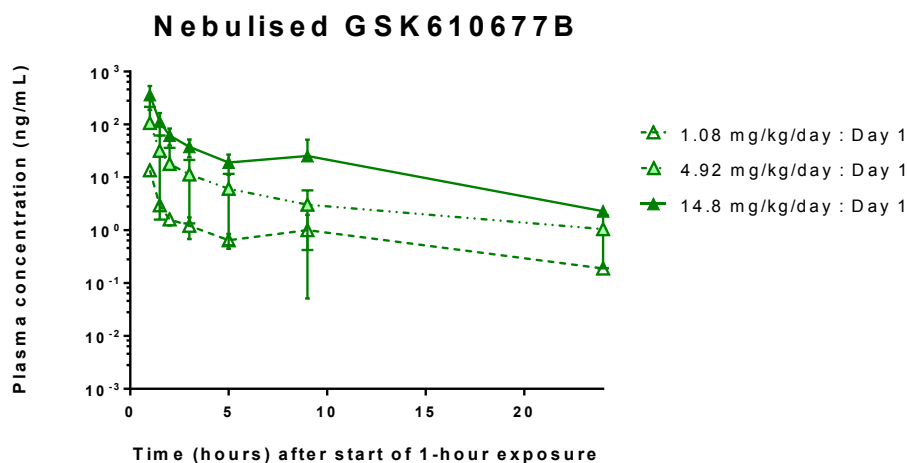


**Figure 5.33:** Drug-lung concentrations in rats following inhaled administration of nebulised GSK-677 for one or 28 days. Mean GSK-677 concentrations with standard deviations (error bars; n=3) are shown for rat lung homogenate data for samples taken immediately after a single 1-hour exposure and at 24 hours after single or repeat exposures. Lung concentrations for a dose of 1 mg/kg/day (\*) were below the limit of quantification (<120 ng/g lung tissue) 24 hours after a single exposure. Statistical analysis (2-way ANOVA with post hoc analysis using Tukey's honestly significant difference test (Abdi and Williams, 2010[B])) of log<sub>10</sub>-transformed data achieved significance (p<0.01) for 1 vs 24 hours and Days 1 vs 28 (24 hours).

Median T<sub>max</sub> was immediately post exposure. GSK-677 concentrations in plasma increased with an increase in the nebulised dose (Figure 5.34). There was no obvious or consistent change in systemic exposure between Days 1 and 28 of treatment (Table 5.22).

## 5.34A



## 5.34B

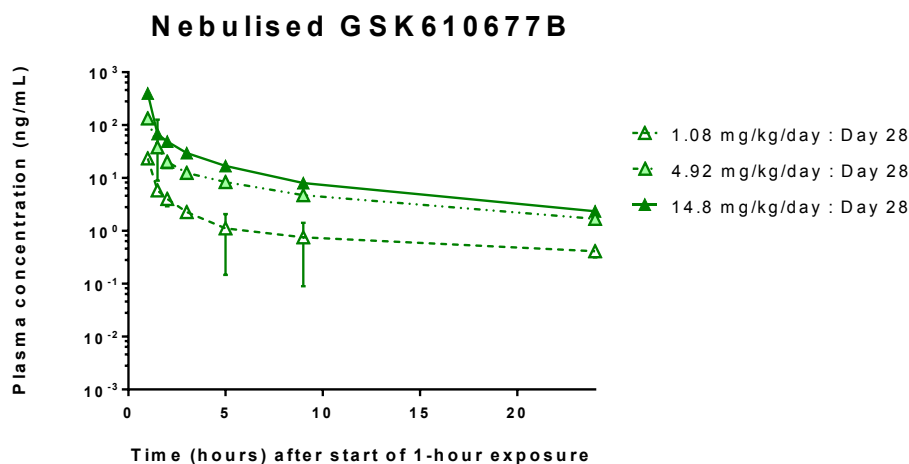


**Figure 5.34:** GSK-677 concentrations in rat plasma up to 24 hours after nebulised doses on Days 1 and 28. Rats inhaled a nebulised aerosol of GSK-677 once daily (1 hour) for up to 28 days; mean plasma concentrations with standard deviations (error bars;  $n=3$ ) are shown for samples taken up to 24 hours after the start of inhalation exposure. **5.34A:** plasma concentrations after a single exposure (Day 1). **5.34B:** plasma concentrations after repeated exposure (Day 28). Statistical analysis (MANOVA with post hoc analysis using Tukey's honestly significant difference test (Abdi and Williams, 2010[B])) of  $\log_{10}$ -transformed data achieved significance ( $p<0.01$ ) between Days 1 and 28.

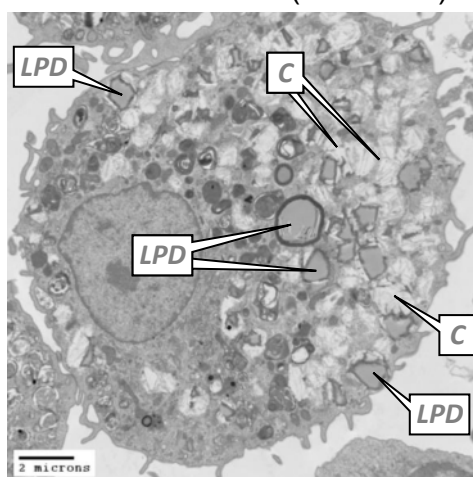
**Table 5.22: Pharmacokinetics of GSK-677 in plasma after inhaled administration of a nebulised solution (n=3)**

Study No.	Estimated Inhaled Dose (mg/kg/day) <sup>A</sup>	Period (Day)	Statistical parameter	Pharmacokinetics (plasma)		
				AUC <sub>0-t</sub> (h.ng/mL) <sup>B</sup>	C <sub>max</sub> (ng/mL) <sup>B</sup>	T <sub>max</sub> (h) <sup>C</sup>
R31038N	1.08	D1	Mean	18.9	10.4	1
			sd	3.32	2.16	-
	CV (%)		18%	21%	-	
	D28	Mean	33.2	17.7	1	
		sd	2.15	1.65	-	
		CV (%)	6%	9%	-	
4.92	D1	Mean	254	157	1	
		sd	239.8	159.6	-	
CV (%)		94%	101%	-		
D28	Mean	320	191	1		
	sd	48.3	32.7	-		
	CV (%)	15%	17%	-		
14.8	D1	Mean	481	232	1	
		sd	152.7	145.3	-	
CV (%)		32%	63%	-		
D28	Mean	345	225	1		
	sd	143.5	160.8	-		
	CV (%)	42%	72%	-		

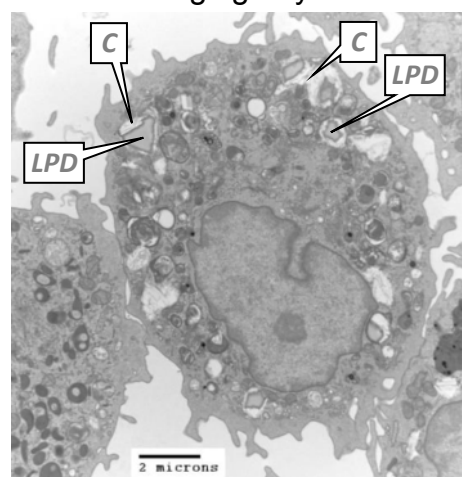
**Notes**

- A Overall estimated inhaled dose for toxicopathology animals over the 28-day treatment period.
- B Mean calculated from parameter for each rat (n=3): parameter dose-normalised (division by estimated inhaled dose on day of sampling) and re-normalised with the overall estimated inhaled dose <sup>A</sup>.
- C Median time presented relative to end of the 1-hour exposure period.
- CV Coefficient of variation (%) = sd/mean

Examination of macrophages by TEM from rats administered nebulised GSK-677 (12.6 mg/kg/day) revealed no evidence of particulate drug substance within the cells in line with results for crystalline GSK-677. Macrophages appeared similar to the vehicle control (Solutol-NaCl) with a proportion of cells containing neutral lipid droplets or angular clefts (Figure 5.35) ascribed to lipid extraction during processing and/or cholesterol clefts (Lupu *et al.*, 1987).

**5.35A:** Vehicle control (nebulised)

(R31038N; Rat 067)

**5.35B:** 12.6 mg/kg/day

(R31038N; Rat 068)

**Figure 5.35: Macrophages after inhalation of nebulised vehicle or GSK-677 for 3 days.** Rats were exposed to nebulised vehicle alone (3% (v/v) Solutol HS 15 in 0.9% (w/v) aqueous sodium chloride) or a solution of GSK-899 for 3 days. Macrophages were harvested *post mortem* in saline by bronchoalveolar lavage and processed for transmission electron microscopy. **5.35A:** macrophage containing lipid droplets (LPD). Angular shaped electron lucent areas (C) associated with the lipid droplets are considered consistent with extracted neutral lipid or cholesterol clefts (Lupu *et al.*, 1987). **5.35B:** macrophage containing lipid droplets (LPD) and crystal-like inclusions (C) consistent with extracted neutral lipid or cholesterol clefts; no GSK-677 related ultrastructural changes were evident.

Multifocal bronchioloalveolar aggregates of macrophages (minimal to mild) were seen in most rats at all doses of nebulised GSK-677 (Table 5.23 and Figure 5.36), in line with lung findings seen following administration of the crystalline aerosol form.

Toxicopathology findings seen mainly at doses  $\geq 4.92$  mg/kg/day in the nasal cavity, larynx and tracheal bifurcation, a 'hot spot' for impaction of particulates, were indicative of chemical irritancy (Gopinath and Mowat, 1987). In the nasal cavity (Figure 5.37), a dose dependent increase in the frequency of respiratory epithelial degeneration was seen in sections at levels 1 and 2 (Figure 5.4A) of most rats administered  $\geq 4.92$  mg/kg/day (minimal; mild for one rat administered 15 mg/kg/day). This finding was accompanied by focal squamous metaplasia (minimal) in a rat administered 15 mg/kg/day (Table 5.23).

**Table 5.23: Histopathology of the respiratory tract of rats exposed to nebulised GSK-677 for 28 days**

Vehicle for nebulised solution: 3% (v/v) Solutol HS 15 in 0.9% (w/v) aqueous sodium chloride		Incidence of findings (Study R31038N)			
Target dose (mg/kg/day)		0 (control)	1.08	4.92	14.8
Number of rats on study	Grading of observation	6	6	6	6
		6	0	0	6
Lung Aggregate, foamy macrophage; bronchiolo-alveolar; multifocal	<i>No finding</i>	5	1	2	1
	Minimal	1	4	3	4
	Mild	0	1	1	1
Larynx Squamous metaplasia Necrosis; ventral pouch cartilage Inflammatory cell infiltrate; submucosa; mononuclear cell Epithelial alteration	<i>No finding</i>	6	5	0	0
	Mild	0	0	4	4
	Moderate	0	0	2	2
	Present	0	0	5	6
	Minimal	0	0	2	2
	Mild	0	0	4	4
Tracheal bifurcation	<i>No finding</i>	5	5	5	2
	(no section)	(1)	(0)	(0)	(0)
Degeneration; epithelium	Minimal	0	1	1	4
Nasal cavity Degeneration; respiratory epithelium Squamous metaplasia; respiratory epithelium; focal	<i>No finding</i>	6	6	4	0
	Minimal	0	0	2	5
	Mild	0	0	0	1
	Minimal	0	0	0	1

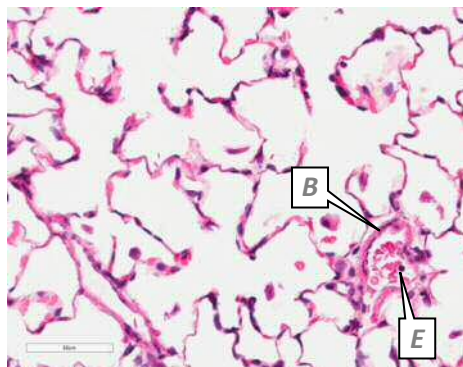
**Notes**

No treatment related findings (control and high dose animals examined): trachea, lymph node (tracheobronchial), nasopharynx; adrenals, colon, eyes and optic nerve, heart, jejunum, kidneys, liver, lymph node (mandibular), pancreas, testes, thymus.

In the larynx (Figures 5.38), squamous metaplasia (mild or moderate) was seen ventrolaterally in all rats administered  $\geq 4.92$  mg/kg/day and was accompanied by necrosis of the ventral pouch cartilage (Figure 5.39) and submucosal mononuclear inflammatory cell infiltration (minimal or mild) for most animals at these doses (Table 5.23). Epithelial alteration (minimal), characterised by focal flattening and stratification of the epithelium, was noted ventrolaterally in one rat administered 1 mg/kg/day. At the tracheal bifurcation of most

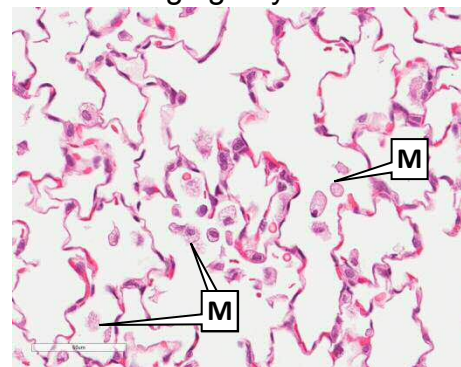
rats given 14.8 mg/kg/day and one rat at each dose  $\geq 4.92$  mg/kg/day, epithelial degeneration (minimal) was characterised by deciliation and basophilia (increased frequency of basophils).

**5.36A:** Vehicle control



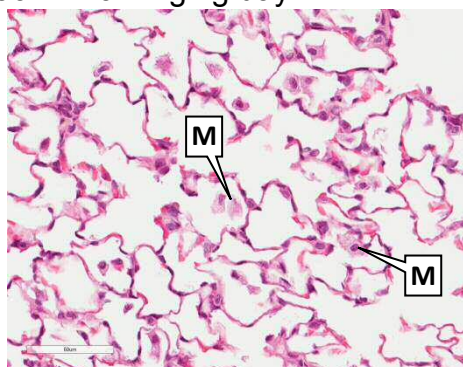
(R31038N; Rat 001)

**5.36B:** 1.08 mg/kg/day



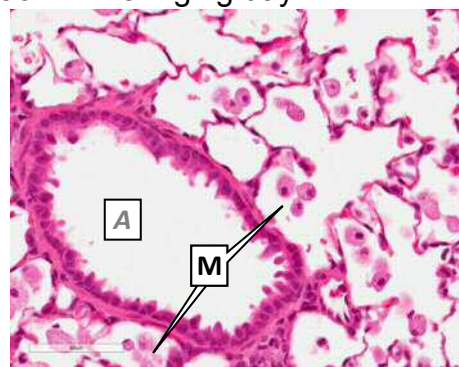
(R31038N; Rat 015)

**5.36C:** 4.92 mg/kg/day



(R31038N; Rat 024)

**5.36D:** 14.8 mg/kg/day



(R31038N; Rat 028)

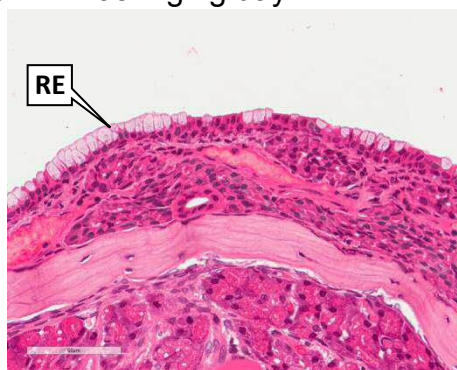
**Figure 5.36: Representative histology of control rat lung and treatment related changes after inhalation of nebulised GSK-677 for 28 days.** Rats were exposed to the vehicle alone (3% (v/v) Solutol HS 15 in 0.9% (w/v) aqueous sodium chloride) or as a solution of GSK-677 for 28 days. Sections of tissue (3  $\mu$ m thick) were stained with haematoxylin and eosin; *anatomical features are described in italics*. **5.36A:** normal rat lung showing alveolar duct and alveoli. A blood vessel (B) with erythrocytes (E) is also evident in cross-section. **5.36B:** minimal foamy bronchioloalveolar macrophage aggregates (M). **5.36C:** minimal foamy bronchioloalveolar macrophage aggregates (M). **5.36D:** mild foamy bronchioloalveolar macrophage aggregates (M). An airway (A) is evident in cross-section.

**5.37A:** Vehicle control



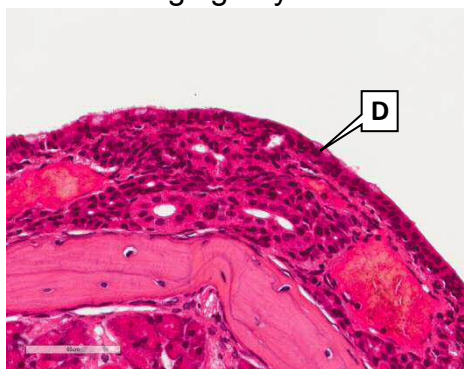
(R31038N; Rat 001)

**5.37B:** 1.08 mg/kg/day



(Study R31038N; Rat 015)

**5.37C:** 4.92 mg/kg/day



(R31038N; Rat 022)

**5.37D:** 14.8 mg/kg/day

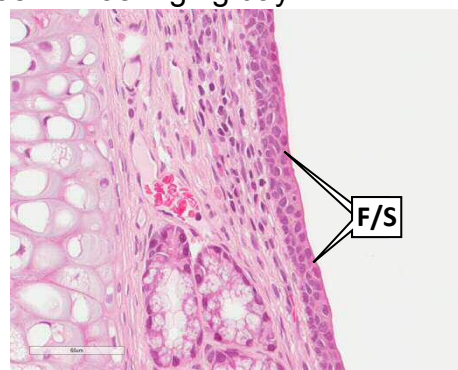


(R31038N; Rat 030)

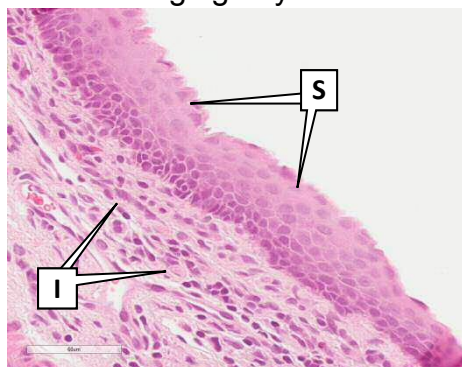
**Figure 5.37: Representative histology of control rat nasal cavity and mild irritancy after inhalation of nebulised GSK-677 for 28 days.** Rats were exposed to the vehicle alone (3% (v/v) Solutol HS 15 in 0.9% (w/v) aqueous sodium chloride) or as a solution of GSK-677 for 28 days. Sections of tissue (3  $\mu$ m thick) were stained with haematoxylin and eosin; *anatomical features are described in italics*. **5.37A:** control rat nasal cavity showing respiratory epithelium (RE). **5.37B:** rat nasal cavity at higher magnification showing respiratory epithelium (RE); no GSK-677 related changes evident. **5.37C:** rat nasal cavity at higher magnification showing minimal degeneration of the respiratory epithelium (D) characterised by deciliation and basophilia. **5.37D:** rat nasal cavity showing minimal degeneration and squamous metaplasia (S) of respiratory epithelium.

**5.38A:** Vehicle control

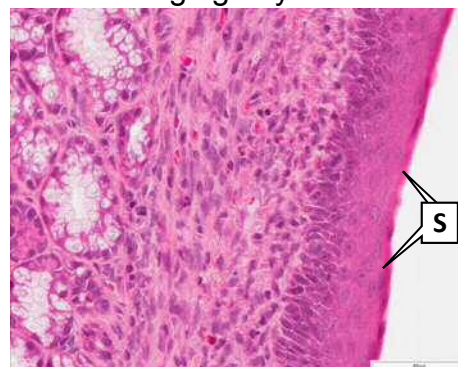
(R31038N; Rat 001)

**5.38B:** 1.08 mg/kg/day

(R31038N; Rat 015)

**5.38C:** 4.92 mg/kg/day

(R31038N; Rat 022)

**5.38D:** 14.8 mg/kg/day

(Study R31038N; Rat 030)

**Figure 5.38:** Representative histology of control rat larynx and mild irritancy after inhalation of nebulised GSK-677 for 28 days. Rats were exposed to the vehicle alone (3% (v/v) Solutol HS 15 in 0.9% (w/v) aqueous sodium chloride) or as a solution of GSK-677 for 28 days. Sections of tissue (3  $\mu$ m thick) were stained with haematoxylin and eosin; *anatomical features are described in italics*. **5.38A:** rat larynx showing transitional epithelium typical for this location (TE). **5.38B:** minimal alteration characterised by focal flattening and stratification of the epithelium (F/S). **5.38C:** mild inflammatory cell infiltrate (I), characterised by mononuclear cells in the submucosa, and moderate squamous metaplasia (S). **5.38D:** mild squamous metaplasia (S) of respiratory epithelium.

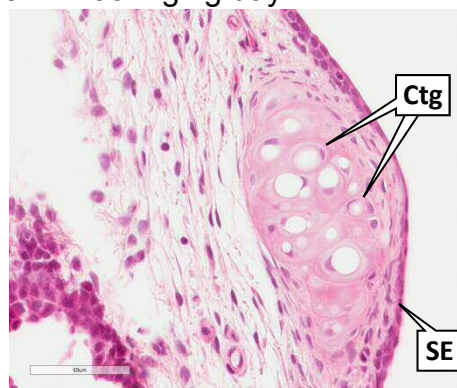
The toxicopathology findings seen in the respiratory tract indicated that GSK-677 was more irritant when presented as an aqueous (nebulised) formulation. This was corroborated by observations at the injection site of rats dosed subcutaneously with GSK-677 during an enabling study, in which the severity of degenerative changes (mild necrosis) and inflammation of the dermis and subcutis precluded subcutaneous administration of GSK-677 for 28 days (Appendix 8).

**5.39A:** Vehicle control



(R31038N; Rat 001)

**5.39B:** 1.08 mg/kg/day



(R31038N; Rat 015)

**5.39C:** 4.92 mg/kg/day



(R31038N; Rat 022)

**5.39D:** 14.8 mg/kg/day



(R31038N; Rat 030)

**Figure 5.39: Representative histology of control ventral pouch of rat larynx and mild irritancy after inhalation of nebulised GSK-677 for 28 days.** Rats were exposed to the vehicle alone (3% (v/v) Solutol HS 15 in 0.9% (w/v) aqueous sodium chloride) or as a solution of GSK-677 for 28 days. Sections of tissue (3 µm thick) were stained with haematoxylin and eosin; *anatomical features are described in italics*. **5.39A:** ventral pouch of rat larynx showing normal cartilage (Ctg) and typical squamoid epithelium (SE). **5.39B:** ventral pouch showing histologically normal cartilage (Ctg) and squamoid epithelium (SE); no GSK-678 related changes evident. **5.39C:** necrosis of ventral pouch cartilage (N) characterised by absence of cell nuclei. **5.39D:** necrosis of ventral pouch cartilage (N), with overlying mild squamous metaplasia (S) of respiratory epithelium.

#### **5.3.2.4. Pulmonary and systemic exposure of rats to GSK-361 and toxicopathology after 28 days**

Lung clearance of GSK-361 was evident after a single inhalation exposure of rats to the crystalline drug (Figure 5.40); lung concentrations of rats administered 0.22 mg/kg were not quantifiable at 24 hours, and mean lung concentrations for rats administered  $\geq 1.04$  mg/kg were  $<0.1\%$  of that determined immediately post

exposure. There was no obvious increase in trough lung concentrations of GSK-361 from Days 1 to 28, although statistical significance was achieved due to one of three rats returning a non-quantifiable result at the mid dose. Clearance of GSK-361 with repeated administration was consistent with expectations based on *in vivo* lung concentration data summarised in Chapter 2 (Figure 2.30).

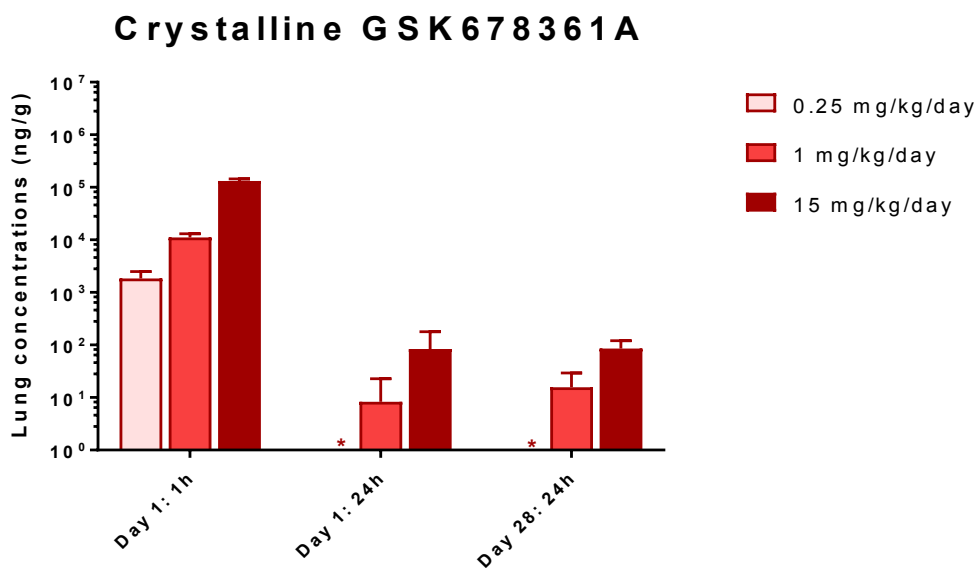
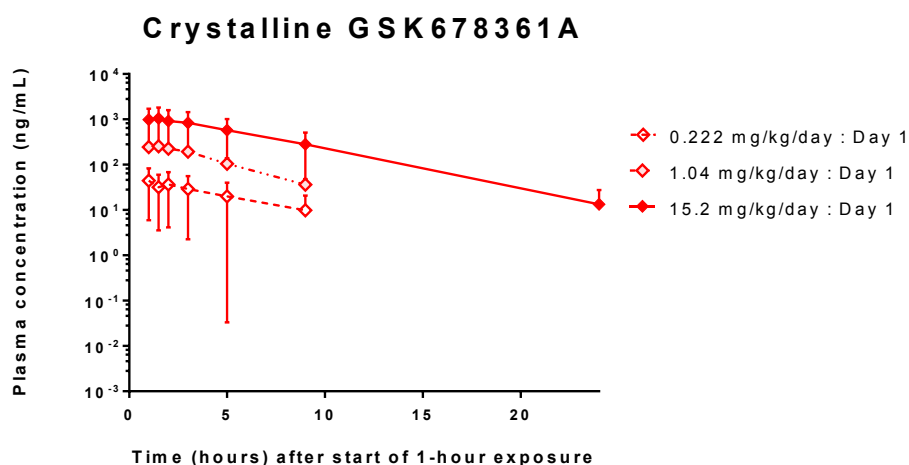


**Figure 5.40:** Drug-lung concentrations in rats following inhaled administration of crystalline GSK-361 for one or 28 days. Mean GSK-361 concentrations with standard deviations (error bars; n=3) are shown for rat lung homogenate data for samples taken immediately after a single 1-hour exposure and at 24 hours after single or repeat exposures. Lung concentrations for a dose of 0.25 mg/kg/day were below the limit of quantification (<30 ng/g lung tissue) 24 hours after single or repeat exposure. Statistical analysis (2-way ANOVA with post hoc analysis using Tukey's honestly significant difference test (Abdi and Williams, 2010[B])) of log<sub>10</sub>-transformed data achieved significance (p<0.01) for 1 vs 24 hours and Days 1 vs 28 (24 hours).

Plasma-drug concentrations were similar for a given dose of crystalline GSK-361 on Days 1 and 28, and were not quantifiable at 24 hours for doses ≤1.04 mg/kg/day (Figure 5.41). Systemic exposure (AUC<sub>0-t</sub> and C<sub>max</sub>) to GSK-361 was similar on Days 1 and 28 for a given dose, and increased proportionally with increasing dose between 0.222 and 1.04 mg/kg/day, less than proportionally between 1.04 and

15.2 mg/kg/day (Table 5.24), with median  $T_{max}$  generally observed at 1.5 hours, i.e. 30 minutes after the end of exposure.

### 5.41A



### 5.41B

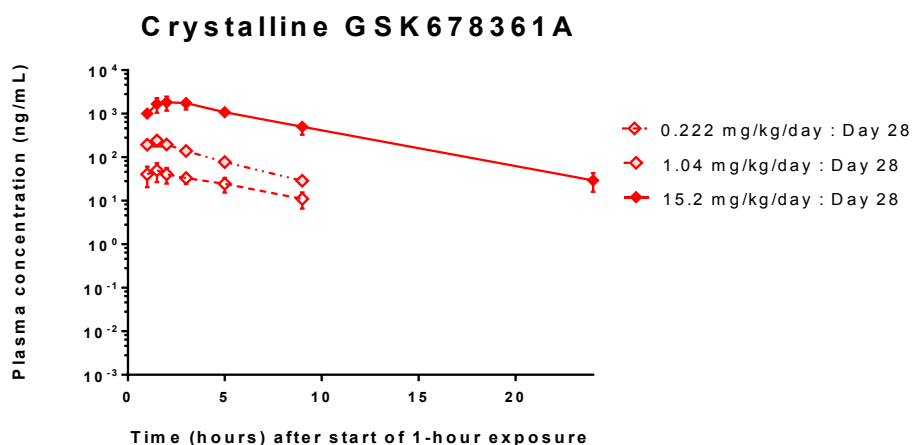


**Figure 5.41:** GSK-361 concentrations in rat plasma up to 24 hours after inhaled doses of crystalline GSK-361 on Days 1 and 28. Rats inhaled an aerosol of crystalline GSK-361 once daily (1-hour exposure) for up to 28 days; mean plasma concentrations with standard deviations (error bars; n=3) are shown for samples taken up to 24 hours after the start of inhalation exposure. **5.41A:** plasma concentrations after a single exposure (Day 1). **5.41B:** plasma concentrations after repeated administration (Day 28). Statistical analysis (MANOVA with post hoc analysis using Tukey's honestly significant difference test (Abdi and Williams, 2010[B])) of  $\log_{10}$ -transformed data achieved significance ( $p < 0.05$ ) between Days 1 and 28.

**Table 5.24: Pharmacokinetics of GSK-361 in plasma after inhaled administration of micronised crystals (n=3)**

Study No.	Estimated Inhaled Dose (mg/kg/day) <sup>A</sup>	Period (Day)	Statistical parameter	Pharmacokinetics (plasma)		
				AUC <sub>0-t</sub> (h.ng/mL) <sup>B</sup>	C <sub>max</sub> (ng/mL) <sup>B</sup>	T <sub>max</sub> (h) <sup>C</sup>
R31035N	0.222	D1	Mean	202	45.6	1
			sd	188.1	39.47	-
	CV (%)		93%	87%	-	
	D28	Mean	230	52.4	1.5	
		sd	86.1	20.90	-	
		CV (%)	37%	40%	-	
1.04	D1	Mean	1157	266	1.5	
		sd	115.0	59.5	-	
CV (%)		10%	22%	-		
D28	Mean	899	267	1.5		
	sd	32.3	34.4	-		
	CV (%)	4%	13%	-		
15.2	D1	Mean	7134	1126	1.5	
		sd	5588	829.2	-	
CV (%)		78%	74%	-		
D28	Mean	12707	1977	3		
	sd	3430	595.0	-		
	CV (%)	27%	30%	-		

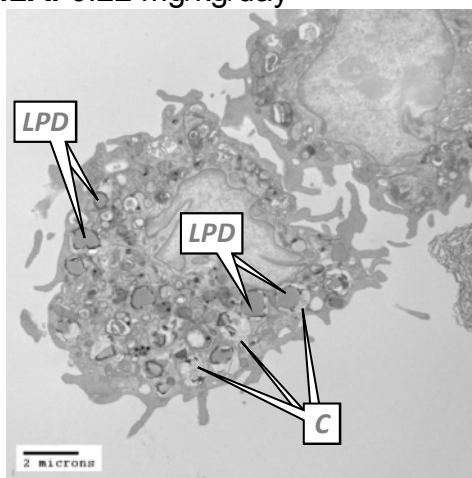
**Notes**

- A Overall estimated inhaled dose for toxicopathology animals over the 28-day treatment period.
- B Mean calculated from parameter for each rat (n=3): parameter dose-normalised (division by estimated inhaled dose on day of sampling) and re-normalised with the overall estimated inhaled dose <sup>A</sup>.
- C Median time presented relative to start of the 1-hour exposure period.
- CV Coefficient of variation (%) = sd/mean

At all doses, examination of harvested macrophages by TEM revealed no evidence of phagocytosed crystalline GSK-361. This contrasted with the crystalline inclusions seen *in vitro* (Figure 5.6B). The appearance of macrophages was normal but varied, with some cells containing neutral lipid droplets or angular clefts (Figure 5.42B) that were and ascribed to artefactual lipid extraction during processing and/or cholesterol crystals (Lupu *et al.*, 1987). Other macrophages presented fewer lipid droplets but more dense primary lysosomes (Figure 5.42C), phagosomes (vacuoles

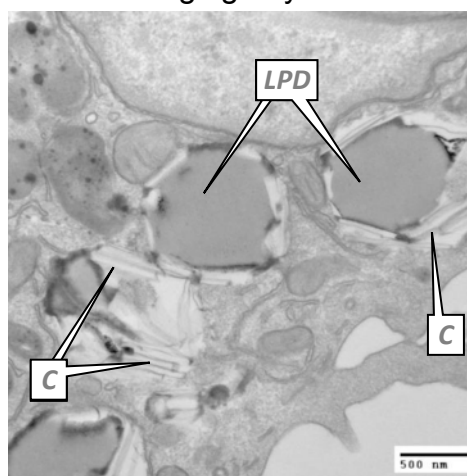
containing phagocytosed material) or secondary lysosomes containing nondescript or lamellar surfactant (Figure 5.42D).

**5.42A:** 0.22 mg/kg/day



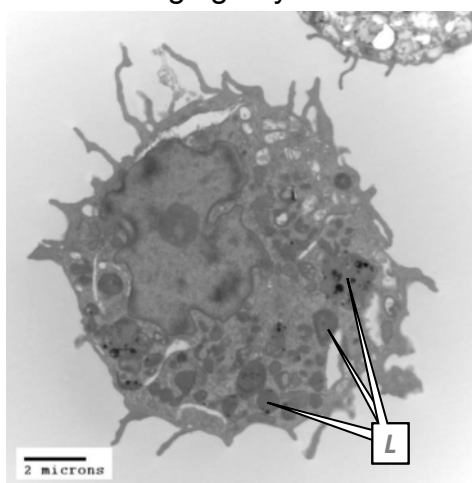
(R31035N; Rat 025)

**5.42B:** 0.22 mg/kg/day



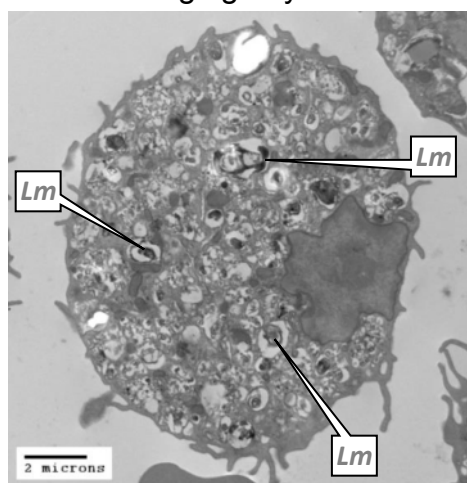
(R31035N; Rat 025)

**5.42C:** 1.04 mg/kg/day



(R31035N; Rat 028)

**5.42D:** 15.3 mg/kg/day



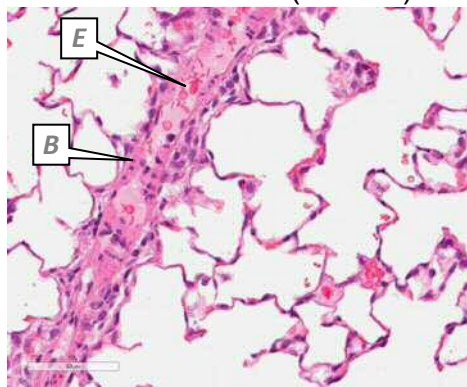
(R31035N; Rat 031)

**Figure 5.42: Macrophages after inhalation of lactose vehicle or crystalline GSK-361 for 28 days.** Rats were exposed to lactose vehicle alone or in combination with crystalline GSK-361 for 28 days. Macrophages were harvested *post mortem* in saline by bronchoalveolar lavage of the left lung and processed for transmission electron microscopy; no GSK-361 related ultrastructural changes were evident. **5.42A:** macrophage containing lipid droplets (LPD). Angular electron lucent areas (C) associated with these droplets were consistent with extracted neutral lipid or cholesterol clefts (Lupu *et al.*, 1987). **5.42B:** macrophage containing lipid droplets (LPD). Angular electron lucent areas (C) associated with these droplets were consistent with extracted neutral lipid or cholesterol clefts. **5.42C:** macrophage containing dense lysosomes (L). **5.42D:** macrophage containing vacuoles containing lamellar surfactant material (Lm).

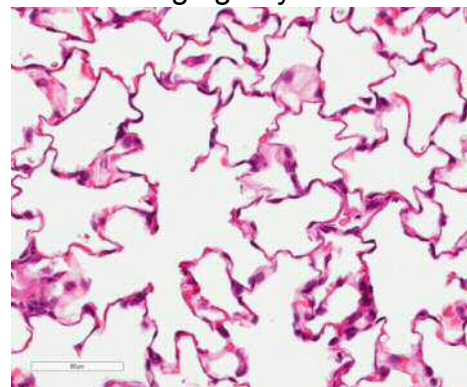
Histopathological examination of tissues by light microscopy revealed no treatment related findings after inhaled administration of crystalline GSK-361 at  $\leq 15.2$  mg/kg/day to rats for 28 days (Figure 5.43).

**5.43A:** Vehicle control (lactose)

**5.43B:** 15.2 mg/kg/day



(R31035N; Rat 002)



(R31035N; Rat 019)

**Figure 5.43:** Representative histology of control rat lung and after inhalation of crystalline GSK-361 for 28 days. Rats were exposed to lactose vehicle alone or in combination with crystalline GSK-899 for 28 days. Sections of tissue (3  $\mu$ m thick) were stained with haematoxylin and eosin; *anatomical features are described in italics*. **5.43A:** histologically normal rat lung showing alveolar duct and alveoli. A *longitudinal-section of a blood vessel (B) and erythrocytes (E)* is also evident in section. **5.43B:** histologically normal rat lung; no GSK-361 related changes evident (lower doses not examined).

GSK-361 concentrations in lungs sampled immediately post exposure from rats administered nebulised solutions were quantifiable for 2/3 rats at each dose but were less than 5% of mean values for rats administered corresponding doses of crystalline GSK-361. GSK-361 was not quantifiable at 24 hours on Day 1 or Day 28.

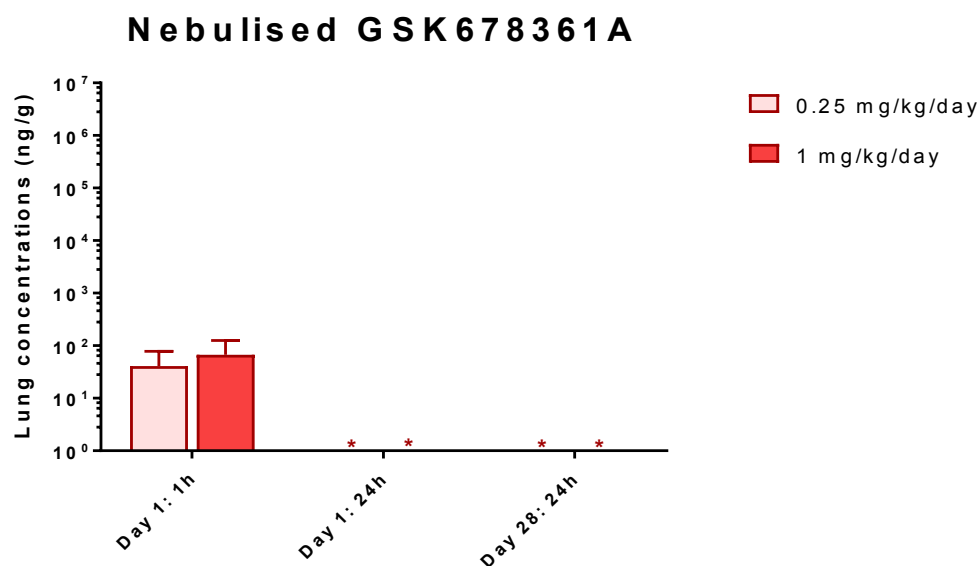
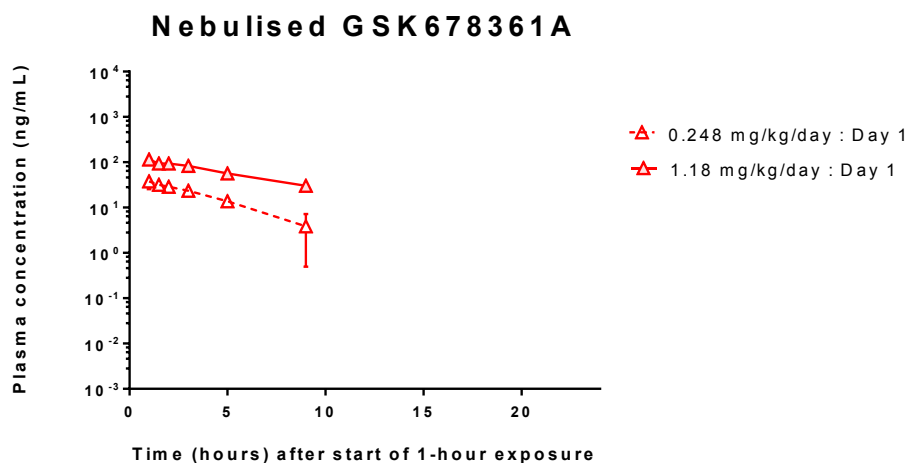


**Figure 5.44: Drug-lung concentrations in rats following inhaled administration of nebulised GSK-361 for one or 28 days.** Mean GSK-361 concentrations with standard deviations (error bars; n=3) are shown for rat lung homogenate data for samples taken immediately after a single 1-hour exposure. Lung concentrations at 24 hours post exposure (\*) were below the limit of quantification (<30 ng/g lung tissue); insufficient quantifiable data for log<sub>10</sub>-transformation of data for statistical analysis (2-way ANOVA).

Mean systemic exposure ( $AUC_{0-t}$  and  $C_{max}$ ) to GSK-361 was similar on Days 1 and 28 at a dose of 0.25 mg/kg/day, but was approximately three-fold higher on Day 28 at a nebulised dose of 1.18 mg/kg/day (Table 5.25). Mean systemic exposure increased approximately proportionally with increasing dose on Day 1 and greater than proportionally on Day 28. Median  $T_{max}$  was immediately post exposure.

There were no treatment related histopathological findings in rats administered nebulised GSK-361 at  $\leq 1.18$  mg/kg/day for 28 days (Figure 5.46).

## 5.45A



## 5.45B

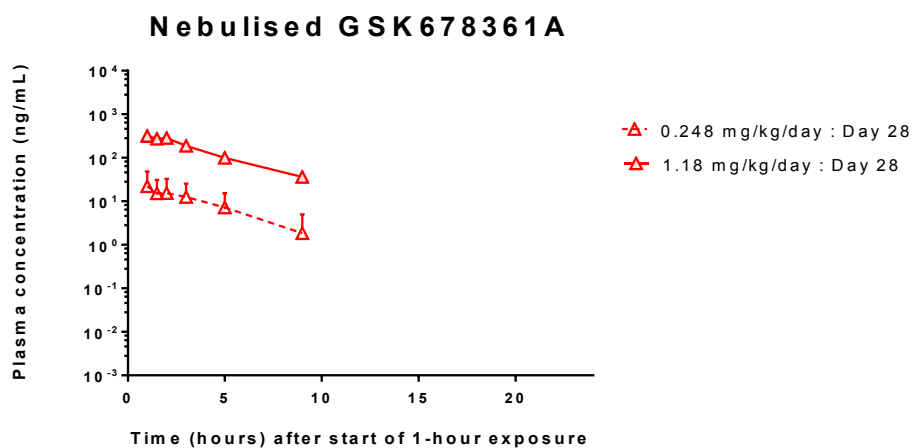


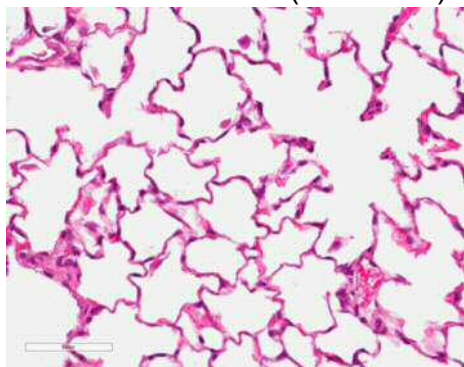
**Figure 5.45: GSK-361 concentrations in rat plasma up to 24 hours after nebulised doses on Days 1 and 28.** Rats inhaled a nebulised aerosol of GSK-361 once daily (1 hour) for up to 28 days; mean plasma concentrations with standard deviations (error bars; n=3) are shown for samples taken up to 24 hours after the start of inhalation exposure. **5.45A:** plasma concentrations after a single exposure (Day 1). **5.45B:** plasma concentrations after repeated exposure (Day 28). Statistical analysis (1-way ANOVA) of log<sub>10</sub>-transformed data indicated no significant difference between Days 1 and 28.

**Table 5.25: Pharmacokinetics of GSK-361 in plasma after inhaled administration of nebulised solution (n=3)**

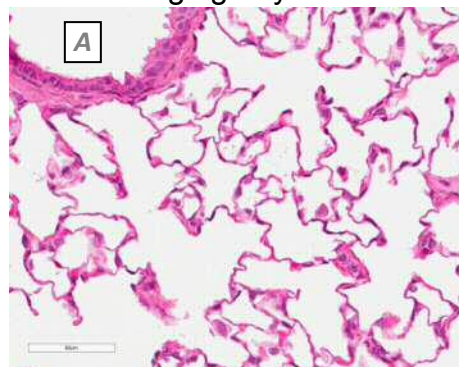
Study No.	Estimated Inhaled Dose (mg/kg/day) <sup>A</sup>	Period (Day)	Statistical parameter	Pharmacokinetics (plasma)		
				AUC <sub>0-t</sub> (h.ng/mL) <sup>B</sup>	C <sub>max</sub> (ng/mL) <sup>B</sup>	T <sub>max</sub> (h) <sup>C</sup>
R31036N	0.248	D1	Mean	119	32.3	1
			sd	10.5	10.47	-
			CV (%)	9%	32%	-
	D28	Mean	62	18.6	1	
		sd	74.6	22.20	-	
		CV (%)	120%	119%	-	
1.18	D1	Mean	435	91	1	
		sd	49.4	13.1	-	
		CV (%)	11%	14%	-	
D28	Mean	955	254	1		
	sd	121.3	65.9	-		
	CV (%)	13%	26%	-		

**Notes**

- A Overall estimated inhaled dose for toxicopathology animals over the 28-day treatment period.
- B Mean calculated from parameter for each rat (n=3): parameter dose-normalised (division by estimated inhaled dose on day of sampling) and re-normalised with the overall estimated inhaled dose <sup>A</sup>.
- C Median time presented relative to start of the 1-hour exposure period.
- CV Coefficient of variation (%) = sd/mean

**5.46A: Vehicle control (nebulised) 5.46B: 1.18 mg/kg/day**

(R31036N; Rat 004)



(R31036N; Rat 017)

**Figure 5.46: Representative histology of control rat lung and after inhalation of nebulised GSK-361 for 28 days.** Rats were exposed to nebulised vehicle alone (20:20:60 (v/v/v) Solutol HS 15, ethanol and 60mM phosphate buffer) or a solution of GSK-361 for 28 days. Sections of tissue (3 µm thick) were stained with haematoxylin and eosin; *anatomical features are described in italics*. **5.46A:** histologically normal rat lung showing alveolar duct and alveoli. **5.46B:** histologically normal rat lung; no GSK-361 related changes evident. An airway (A) is evident in cross-section.

## 5.4. Conclusion

The objectives of this chapter were to assess the pulmonary toxicopathology of three p38 MAPK inhibitors in the context of their systemic and pulmonary exposure. Differences in the resultant *in vivo* findings were to be considered with respect to each drug's physicochemical properties, aerosol presentation and correlation with *in vitro* endpoints. Key findings are summarised in Table 5.26.

**Table 5.26: Key findings for *in vitro* and *in vivo* assessment of toxicopathology and exposure of p38 MAPK inhibitors**

<b><i>In vitro</i> particles</b>	GSK-899			GSK-677		GSK-361	
Cellular toxicity	low risk			low risk		low risk	
Endocytosed particles	present			no		present	
Cytokine release	no			no		no	
<b><i>In vivo</i> data</b>							
Aerosol form	Crys	Am	Neb	Crys	Neb	Crys	Neb
Target doses <sup>A</sup>	1, 15	0.02 - 15	1	1 - 15	1 - 15	0.25 - 15	0.25, 1
Lung concentration							
D1: 24h vs 1h	≤26% ↓	≥99% ↓	≥92% ↓	≥98% ↓	>99% ↓	>99.9% ↓	100% ↓
D28 vs D1 <sup>A</sup>	≥ x10 ↑	x9 ↑ (14.6)	X8 ↑ (1)	≥ x2 ↑	≥ x6 ↑ (≥4.92)	similar	NQ
Plasma AUC <sub>0-t</sub>							
D28 vs D1	≥ x3 ↑	similar	similar	similar	similar	similar	NQ
Endocytosed particles	present	present	no	no	no	no	-
Lung <sup>AB</sup>							
Macrophage aggregates	≤ mkd (≥1)	≤ mild (≥0.024)	≤ mild (1)	≤ mild (≥2.25)	≤ mild (≥1.08)	-	-
Inflammation	≤ mkd (14.5)	min (14.6)	-	min (67.8)	-	-	-
Larynx <sup>AB</sup>							
Squamous metaplasia	min (14.5)	min (≥1.10)	-	min (≥2.25)	≤ mod (≥4.92)	-	-
Inflammation	-	-	-	-	≤ mild (≥4.92)	-	-
Necrosis <sup>VPC</sup>	-	-	-	-	≥4.92	-	-
Nasal <sup>AB</sup>							
Epithelial degeneration	-	-	-	-	min (≥4.92)	-	-

### Notes

- A Estimated inhaled doses in parentheses expressed as mg/kg/day  
 B Findings graded minimal (min) < mild < moderate (mod) < marked (mkd)  
 NQ Lung and plasma concentrations at 24 hours were non-quantifiable  
 VPC Ventral pouch cartilage of larynx

Trends for differences in measured lung exposure between aerosol forms and p38 MAPK inhibitors following a single one-hour inhalation exposure were consistent with *in vivo* results described in Chapter 2, but were more pronounced (GSK-361 lung concentrations notably lower for nebulised solution than crystalline aerosol). This is probably associated with the longer exposure period applied and hence a broader range of lung residence times (20 to 80 minutes) for deposited particles undergoing solvation, dissolution and then absorption, as opposed to droplets undergoing absorption alone prior to isolation of lungs post exposure. Increases in trough concentrations were evident for GSK-899 and GSK-677 from Days 1 to 28, although only crystalline GSK-899 persisted to a significant extent in terms of the proportion of analyte in lungs at one hour remaining at 24 hours (Table 5.26).

An increased incidence of multifocal foamy macrophage aggregates was observed for all aerosol forms of GSK-899 and GSK-677 (minimal to mild for all aerosol forms; mild to marked for crystalline GSK-899 at 14.5 mg/kg/day) but was not seen in rats administered GSK-361 by inhalation or GSK-899 by subcutaneous injection. Alveolar macrophages play a key role in clearance of particles from the alveolar spaces of lungs, and migrate towards deposition sites and phagocytosed particles (Warheit and Hartsky, 1993). The increased incidence of macrophage aggregates is consistent with an adaptive response in rats to clear particulate GSK-899 and GSK-677, with the more pronounced grading (mild to marked) correlating with the highest and most persistent lung concentrations evident for crystalline GSK-899 at 14.5 mg/kg/day. Given that almost 100% of micron-sized particles are endocytosed at 24 hours (Geiser, 2010), it is likely that most of the GSK-899 accumulating in rat lungs was trapped as crystals within macrophages and not available for solvation and dissolution in the epithelial lung fluid. Toxicopathological implications for particle overload include impairment of particle clearance and tumourigenesis (Morrow, 1988). Under such extreme circumstances, it is plausible that

a higher proportion of free crystals may be present in the epithelial lung fluid at high doses. Ultrastructural investigation of lung sections using the high resolution possible by secondary ion mass spectrometry (SIMS; (Benabdellah *et al.*, 2010, Guerquin-Kern *et al.*, 2004)) would enable determination of the precise location of p38 MAPK inhibitors within cell types or fluid compartments in frozen rat lung sections.

However, unlike reported findings for nuisance particles, aggregates of alveolar macrophages in rats administered GSK-899 (mainly at 15 mg/kg/day) or GSK-677 (67.8 mg/kg/day) were associated with infiltration of macrophages in the lung interstitium, graded “marked” for crystalline GSK-899 and “minimal” for amorphous GSK-899 or crystalline GSK-677. The incidence and severity of this inflammatory change was considered (in consultation with the study pathologist) adverse for GSK-899 only and was not predicted *in vitro* (low risk of cellular toxicity indicated, with no treatment-related release of inflammatory cell mediators). Although macrophages were exposed to GSK-899 *in vitro* for up to 72 hours, it is noteworthy that cells were not in their natural (*in vivo*) environment and the 28-day treatment period for rats inhaling GSK-899 was significantly longer. Such *in vitro* investigations provide a means of identifying candidate drugs with a potential *in vivo* liability, and perhaps screening out compounds considered “high risk”. However, the differences *in vitro* and *in vivo* still support an assertion that the complexity of respiratory drug delivery and the biological responses of intact animals to pharmaceuticals are such that the most complete assessment of pulmonary drug delivery and toxicity is currently achieved *in vivo* (Fernandes and Vanbever, 2009, Holländer, 1988).

Adaptive lung changes and adverse lesions associated with lung burden have been described in detail for nuisance particulates such as titanium dioxide (TiO<sub>2</sub>), a white pigment of low toxicity commonly used for investigating lung clearance of particulate (Lee *et al.*, 1985). Warheit *et al.* (1997) conducted a four-week inhalation toxicology study

in which groups of rats were exposed to TiO<sub>2</sub> or iron particles at aerosol concentrations of 5, 50 or 250 mg/m<sup>3</sup> but of differing particle size distributions for each test material (TiO<sub>2</sub>-MMAD of 1.4 to 1.9 μm; iron-MMAD of 2.9 to 3.4 μm), which were similar to the range of MMAD achieved for the p38 MAPK inhibitors (1.6 to 4.2 μm). Such toxicity studies with industrial materials are typically performed to facilitate risk assessment of potential occupational exposure and the experimental design thus reflected guidelines for the testing of chemicals in rodents including longer exposure periods (6 hours/day), a 'working week' (exposure 5 days/week) and targeting aerosol concentrations instead of inhaled doses (OECD[413], 2009, OECD[412], 2009, US-EPA[3645], 1998). Nevertheless, doses of 0.9, 9 and 45 mg/kg/day could be approximated for an assumed body weight (350 g) and the published aerosol concentrations of TiO<sub>2</sub> or iron adjusted for frequency and duration of exposure. These doses covered a similar range to those investigated for p38 MAPK inhibitors. Histopathological lung changes seen at 5 mg/m<sup>3</sup> (approximately 0.9 mg/kg/day) were minimal and similar to those observed in rats administered amorphous or crystalline GSK-899 at 1 mg/kg/day. Lung lesions described at the higher exposure concentrations of 50 or 250 mg/m<sup>3</sup> (approximately 9 or 45 mg/kg/day) were 'dose-related' in severity and included aggregates of particle-laden macrophages adjacent to focal cellular hypertrophy and hyperplasia, but appeared less severe than the infiltration of inflammatory cells observed in the lung interstitium after inhaled administration of crystalline and, to a lesser extent, amorphous GSK-899 at 15 mg/kg/day.

*In vitro*, endocytosed particles of GSK-899 (low solubility; low passive membrane permeability) and GSK-361 (low solubility; high passive membrane permeability) were seen in macrophages incubated in aqueous media with the particles for 72 hours; rectangular inclusions were not evident for macrophages incubated with GSK-677 (high solubility; low passive membrane permeability). However, only particles

of GSK-899 (both crystalline and amorphous) were evident in macrophages harvested from the lungs of rats administered dry powder aerosols (24 hours post exposure). Given that GSK-899 and GSK-361 were both of relatively low solubility, it appears likely the lung clearance of GSK-361 and the apparent absence of crystalline particles *in vivo* is attributable to its lipophilic properties facilitating absorption. The composition of the principal fluid lining the respiratory tract changes with anatomical location. Mucous, which is 95% water (Eixarch *et al.*, 2010), lines the conductive airways (trachea and extrapulmonary bronchi in rats (Harkema *et al.*, 2013)) and contrasts with lung surfactant prevalent in the distal respiratory region (terminal bronchioles and alveoli) consisting of 85% phospholipid, 5% cholesterol and 10% surfactant proteins (Eixarch *et al.*, 2010). Dissolution of the p38 MAPK inhibitors was assessed *in vitro* using simulated lung fluid (Section 2.2.3.2), which is approximately 95% water and consistent with mucous found in the conductive airways. Mucous secreting cells extend into the tracheobronchial airways of primates and dogs (Harkema *et al.*, 2013) and the mucous-like medium may be pertinent when considering the fate of particles in these species and the clinical context in particular. However, drug solubility in the respiratory tract is likely to be affected by significant differences in composition of the media onto which particles are deposited. Whilst transporter systems and efflux pumps potentially have a role in the pulmonary pharmacokinetics of the p38 MAPK inhibitors investigated in this thesis, the high lipophilicity of GSK-361 compared with GSK-899 is noteworthy and underpins its high passive membrane permeability measured *in vitro*. It can therefore be hypothesised that the composition of lung surfactant in rat lungs in combination with the transmembrane migration of GSK-361 from the 'lung fluid compartment' may have facilitated sink conditions for *in vivo* dissolution of GSK-361 particles deposited in the pulmonary region as opposed to non-sink conditions for GSK-899. Approximately 50% to 75% of

particles are typically endocytosed within 2 to 3 hours of deposition (Geiser, 2010) and a faster lung clearance rate for GSK-361 *in vivo* may explain, at least in part, absence of endocytosed particles in the examined macrophages harvested from lungs 24 hours post exposure.

Squamous metaplasia, an adaptive response to irritancy (Gopinath and Mowat, 1987), was evident in the larynx of rats administered GSK-677 (crystalline at  $\geq 2.25$  mg/kg/day; nebulised  $\geq 4.92$  mg/kg/day) or dry powder aerosols of GSK-899 (amorphous  $\geq 1.10$  mg/kg/day; crystalline 14.5 mg/kg/day). This finding was associated with inflammation and necrosis in the larynx and degeneration of the nasal epithelium of rats administered nebulised GSK-677 ( $\geq 4.92$  mg/kg/day). This is consistent with the irritancy observed at the injection sites of rats administered GSK-899 or GSK-677. It was anticipated that administration of nebulised solutions of the p38 MAPK inhibitors would not induce lung pathology changes due to presentation of a solution facilitating a faster rate of absorption from lungs. The absence of macrophage aggregates from the lungs of rats administered GSK-899 subcutaneously for 28 days (to perfuse lungs with solubilised GSK-899 *in situ*) suggests that this finding was not due to the chemical activity of the molecule *per se*, but may be a response to deposited droplets containing mild irritants.

The test article-related lung changes were clearly more severe in rats administered crystalline GSK-899 at 14.5 mg/kg/day compared to a similar dose of amorphous GSK-899 or GSK-677 at 67.8 mg/kg/day. The severity of findings was more pronounced than that reported for TiO<sub>2</sub> or iron Warheit *et al.* (1988) at comparable doses. It is therefore likely that the inflammatory changes observed in the lungs of rats administered GSK-899 is a function of the persistence of nuisance particles in combination with a mildly irritant effect of GSK-899.

This chapter characterised the pulmonary toxicopathology of three p38 MAPK inhibitors administered to rats as nebulised solutions, amorphous (GSK-899) or crystalline dry powder formulations. Key conclusions of experiments described in this chapter are:

- Differences in aerosol presentation of the evaluated drugs modulated the incidence and severity of toxicopathology findings (shift in dose response), but did not change the nature of the findings *per se*.
- Administering nebulised solutions of compounds of relatively low solubility may preclude detection of findings at higher doses exceeding the maximum practicable dose for limited solubility.
- Lung pathology changes after 28 days of treatment correlated with persistence and/or accumulation of the drug in lung tissue, which wasn't always predicted *in vitro*.
- Passive membrane permeability *in vitro* may be more predictive than solubility for predicting the potential for lung clearance and pulmonary toxicology.

These *in vivo* data indicate a clear relationship between drug accumulation and the onset of inflammation at higher doses that overpowered the anti-inflammatory pharmacology of p38 MAPK inhibition. The clinical relevance of adverse changes at high doses associated with particle overloading of alveolar macrophages should be considered when evaluating results of inhalation toxicity studies.



# **CHAPTER SIX**

## **General discussion**

## 6.1. General discussion

Chronic obstructive pulmonary disease (COPD) accounted for 3.2 million deaths worldwide in 2015, with lower respiratory tract infections, the most deadly communicable disease, accounting for a further 3.2 million deaths (WHO, 2017). GSK was the market leader in terms of revenue (\$9.4 billion) from respiratory disease products in 2015, accounting for 33.6% of this drug market (Research-Markets, 2016). Despite such commercial and therapeutic successes since the launch of the first pressurised metered dose inhaler 60 years ago (Anderson, 2005), there is still an unmet need for inhaled medicines, particularly in the developing world where general access to healthcare is poor and resources are limited (Aït-Khaled *et al.*, 2001). The cost and time required to develop and release a new drug onto the market varies, with estimates of seven to 12 years (Shankar *et al.*, 2006) and costs of up to \$2.0 billion (Adams and Brantner, 2006) cited in the literature. However, just one in 40,000 compounds tested in animals reaches the clinical market (Kapetanovic, 2008). Therefore, in addition to an ethical obligation to minimise the use of animals in medical research, pharmaceutical companies are under increasing pressure to reduce the price of new drugs to meet the need for lower costs in healthcare.

For chronic pulmonary diseases like asthma or COPD, it is desirable to develop drugs with a prolonged duration of action and to combine therapies to simplify and minimise the frequency of administration (Buhl *et al.*, 2003, RNS-LSE#1, 2017). Reducing the frequency of dosing can be achieved through a variety of mechanisms to prolong the duration of action. Drug design strategies include very low aqueous solubility (e.g. inhaled corticosteroids), tissue retention due to hydrophobicity (e.g. salmeterol) or particle engineering and/or encapsulation to slow dissolution (Patton and Byron, 2007). However, this has potential implications for safety as accumulation of insoluble material at the respiratory epithelium may impair lung function (Fröhlich, 2017).

Adaptive lung changes and adverse lesions associated with lung burden have also been described in detail for nuisance particulates such as minerals (Pauluhn, 2008), environmental pollutants (Miller, 2000) and pigments (Lee *et al.*, 1986), the mechanisms of which are independent of pharmacology-mediated toxicology. Differences in toxic potency of relatively inert materials may be associated with differences in particle clearance, dissolution rate in lung fluid or initiation of a self-perpetuating inflammation (Pauluhn, 2008).

Many inhaled drugs have been developed as dry powder formulations, notably micronised crystals, to prolong physical stability and improve the control of drug delivery (Crompton, 1991). Combining the molecule with a salt facilitates modulation of the physicochemical properties and resultant biological activity of the drug (Gould, 1986). Characterisation and selection of the salt can take time and development programmes for inhaled compounds also consume high masses of drug, relative to other exposure routes (primarily due to impaction or sedimentation of test article within exposure systems and the drug-lung deposition fraction in animals). Consequently, there is a balance between selecting the appropriate salt form and pharmacokinetic-pharmacodynamic (PK/PD) profile, and discharging liabilities such as toxicity or human efficacy. Use of surrogate exposure routes and/or formulations (differing from intended clinical presentation) to reduce drug requirements and expedite early non-clinical experiments may be attractive but is potentially at odds with developing drugs with an extended duration of action. This is because such strategies may significantly alter the pharmacokinetics and defer de-risking of potentially altered efficacy, tolerability or toxicopathology of the final formulation until later in development.

Leukocyte recruitment to sites of tissue injury and activation of inflammatory and immune cells are common features of inflammatory diseases such as COPD (Herlaar and Brown, 1999). p38 mitogen activated protein kinase (MAPK) performs a central regulatory function

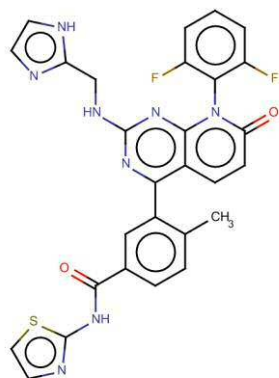
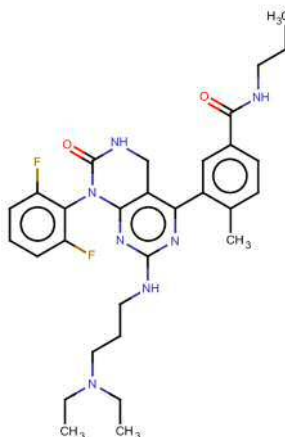
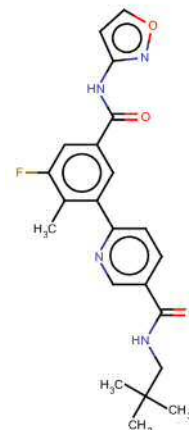
in the synthesis and modulation of proinflammatory mediators. The p38 $\alpha$  MAPK isoform is expressed in the cytoplasm and nucleus of cells (Cuenda and Rousseau, 2007) in the airway smooth muscle, respiratory epithelium and immune system (Williams *et al.*, 2008, Mayer and Callahan, 2006). Given the ubiquitous distribution of this pharmacological target in the respiratory tract, p38 MAPK inhibitors can be administered prophylactically by inhalation (diffuse pulmonary deposition pattern) before administering an antigen by intratracheal instillation (more focal) to investigate inhibition of acute inflammation. In addition, the pulmonary toxicopathology of micronised crystalline GSK-899 and GSK-677 in rats was known to the sponsor (Freke, 2007, Freke, 2010). p38 MAPK inhibitors were therefore selected as tool compounds to investigate the implications of changing aerosol presentation for *in vivo* endpoints of efficacy and toxicopathology. By administering aerosols of p38 MAPK inhibitors to rats, by snout-only inhalation exposure, the experimental objectives of this thesis were to:

- Measure systemic exposure (plasma) and lung exposure (tissue homogenate) in rats administered a single inhaled 'dose' of a dry powder aerosol or nebulised solution of each test article.
- Rank the median effective doses (ED<sub>50</sub>) of three inhaled drugs presented as a dry powder formulation or nebulised solution using a rat model to assess acute lung inflammation.
- Determine the pulmonary toxicopathology of three compounds presented as dry powder or nebulised aerosols for 28 days.

Principal component analysis was used to select p38 MAPK inhibitors of differing physicochemical properties for evaluation of efficacy and pulmonary toxicopathology *in vivo*. The most diverse compounds within the 'physicochemical space' (Figure 6.1) were:

- GSK-899, which had the most aromatic molecular structure (Figure 6.1A), was of relatively low aqueous solubility and had a propensity for protein binding;

- GSK-677, a polar, basic molecule of high aqueous solubility;
- GSK-361, a lipophilic molecule of relatively low aqueous solubility but high passive membrane permeability.

**A: GSK-899****B: GSK-677****C: GSK-361**

**Figure 6.1:** Chemical structures of three p38 MAPK inhibitors selected for investigation of *in vivo* endpoints. Figures **6.1A** to **6.1C** show molecular structures for the parent compounds (free base).

By administering micronised crystals, amorphous powder (GSK-899) or nebulised solutions of the three most diverse p38 MAPK inhibitors, with respect to their physicochemical properties, the following hypotheses were evaluated *in vivo*:

- physicochemical properties influence lung or systemic (plasma) exposure, and hence resultant efficacy and/or toxicopathology.
- changing presentation of a drug to rats will affect its absorption and hence alter the resultant efficacy and/or toxicopathology.

Addressing these hypotheses was expected to increase understanding of the relationship between physicochemical properties and the therapeutic index, *i.e.* the margin between doses of non-clinical efficacy (ED<sub>50</sub>) and no observed adverse effects in animals (toxicopathology).

The cost of equipping and maintaining research facilities for inhalation exposure of laboratory species is expensive and such laboratories are often operated by contract research organisations, pharmaceutical corporations or publicly funded agencies. Given the confidential nature

of research undertaken by such institutions, much of the work remains unpublished. In addition, pharmaceutical companies often progress a pre-selected salt form of a drug through the non-clinical and clinical development programmes. In the event of adverse findings, the development programme is often terminated with no further work undertaken and no data published. Consequently, it is unusual to find published data comparing *in vivo* efficacy or toxicity of different formulations of the same drug. This thesis thus represents an original contribution to the field by characterising the *in vivo* efficacy and respiratory toxicopathology of three compounds administered to rats as dry powder and aqueous aerosol forms.

The seminal publication of Snipes (1989) describing a lung deposition fraction of 7% in rats is still cited today. This article referenced historical data for laboratory species exposed to industrial materials such as inorganic nuisance particles and radionuclides, which differ to the small organic molecules and biopharmaceuticals developed by pharmaceutical companies. Approximately 85% of particles of aerodynamic diameter 2  $\mu\text{m}$  are “inhalable” to rats (Miller, 2000) but most particles are deposited in the nasal cavities or exhaled (Snipes, 1994). Persistence of crystalline GSK-899 in rat lung tissue post exposure made it suitable as a tool compound for investigating lung deposition of a small organic molecule (minimal drug clearance likely before isolation of the lungs). The mean lung deposited dose of GSK-899 (mass median aerodynamic diameter of  $2.1 \pm 0.4 \mu\text{m}$ ) was 12% of the inhaled dose estimated from the measured minute volume (MV). This was consistent with the deposition fraction used by the US-FDA for reviewing regulatory submissions of inhaled drug safety data (Jones and Baldrick, 2013, Owen, 2013, Forbes *et al.*, 2011).

Ranking of lung exposure, in terms of AUC (area under the drug concentration-time curve), after single inhalation exposure of crystalline p38 MAPK inhibitors was consistent with ranking of *in vitro* dissolution rates (Table 6.1). Lung exposure of the two p38 MAPK inhibitors of

lowest aqueous solubility was highest for crystalline aerosols and lowest for nebulised droplets, with amorphous GSK-899 ranked between these two particulate forms. Lung exposure of GSK-677, the most soluble drug, was similar for crystalline and nebulised aerosols.

**Table 6.1: Ranking of key findings for *in vitro* and *in vivo* assessment of p38 MAPK inhibitors**

<b><i>In vitro</i> data</b>					
Dissolution rate	GSK 677(c) > GSK 899(a) > GSK 361(c) > GSK 899(c)				
Potency	GSK-677	≈	GSK-899	≈	GSK-361
Pgp substrate <sup>A</sup>	GSK-677	>	GSK-899	>	GSK-361
Cellular toxicity <sup>B</sup>	low risk		low risk		low risk
Endocytosed particles <sup>B</sup>	no		present		present
Cytokine release <sup>B</sup>	no		no		no
<b><i>In vivo</i> data</b>					
Lung exposure					
crystalline	GSK-677	<	GSK-361	<	GSK-899
nebulised	GSK-361	<	GSK-677	<	GSK-899
GSK-899	<i>nebulised</i>	<	<i>amorphous</i>	<	<i>crystalline</i>
GSK-361	<i>nebulised</i>	<			<i>crystalline</i>
GSK-677	<i>nebulised</i>	≈			<i>crystalline</i>
Systemic (plasma) exposure	GSK-677	≤	GSK 899	<	GSK-361
Efficacy: ED <sub>50</sub>	GSK-677 (least effective)	>	GSK-361	>	GSK-899 (most effective)
'Safety margin' <sup>C</sup>	GSK-361 (NEL)	>	GSK-677 (NOAEL)	>	GSK-899 (NOAEL)
Endocytosed particles	no		no		present (c/a)
Drug-lung accumulation	GSK-361	<	GSK-677	<	GSK-899

**Notes**

- A Flux of compound measured across hMDR1-MDCK (type II) cell monolayer (Pgp expressed at apical surface of cells)
- B Incubation of particles with NR8383 rat alveolar macrophage cell line
- C Ratio of rat:human lung doses ranked (see Table 6.2), with presence or absence of non-adverse rat lung findings taken into account; NEL = No Effect Level; NOAEL = No Observed Adverse Effect Level
- ED<sub>50</sub> Extrapolated from dose response for reduction of neutrophils in bronchoalveolar lavage fluid taken four hours after LPS-challenge
- (c/a) crystalline / amorphous

In these experiments, rats were exposed to an aerosol for 30 minutes. An additional period of 20 minutes elapsed (logistics of animal transfer and euthanasia) before lungs could be removed from the carcass for drug analysis. Particulates thus resided in lungs for 20 to 50 minutes before tissue samples were disconnected from the systemic circulation. Solubilisation of crystalline solutes first requires disruption of the crystal lattice (Van den Mooter, 2012). A faster dissolution rate for amorphous powder was observed *in vitro* due to the disrupted, random organisation of molecules in the inhaled particles requiring less energy to facilitate solvation and subsequent absorption from the lung surface. Presentation of GSK-361 and GSK-899 in solution eliminated solvation, expediting absorption of these compounds from the lung. The potential for underestimating the achieved drug-lung exposure is therefore greatest for the nebulised aerosols and higher for amorphous GSK-899 than crystalline GSK-899 because a proportion of the lung-deposited drug was absorbed systemically before the lungs could be isolated for analysis of the drug-lung concentration at the first timepoint.

Ranking of lung exposure (AUC) for nebulised aerosols of each compound differed to that of crystalline aerosols, with GSK-361 achieving the lowest apparent exposure. This is again consistent with drug absorption during the particulate-lung residence period before the first timepoint resulting in an underestimate of lung exposure and a relatively higher systemic exposure (Table 6.1). GSK-361 was the most lipophilic compound and, *in vitro*, exhibited greatest transmembrane permeability. It therefore appears that GSK-361 in solution (nebulised aerosol) crossed the respiratory epithelium faster than aqueous GSK-677, resulting in a lower measured lung exposure. However, lung exposure following administration of crystalline GSK-361 was higher than for crystalline GSK-677, consistent with a slower dissolution rate, which resulted in reversal of the ranking for measured lung exposure.

Ranking of the median effective doses ( $ED_{50}$ ) indicated GSK-899, a drug of relatively low solubility and persistent in lung tissue, most effectively inhibited lung inflammation at four hours post challenge. GSK-677 was least effective, indicating high aqueous solubility presented a physicochemical barrier between the drug and intracellular pharmacological target (due to reduced transmembrane movement) and/or expedite elimination of the drug from the lungs. There was no obvious difference in efficacy for presentation of the p38 MAPK inhibitors as crystalline or nebulised aerosols. Although  $ED_{50}$  values appeared close for each compound, a more robust (less variable) endpoint for inflammation and/or improved precision of dose delivery would increase the confidence (statistical significance) of this result. The distribution and extent of particle deposition in the respiratory tract is size dependant (Snipes, 1994). Differences in particle size and, by inference, the lung deposited dose of amorphous GSK-899 correlated with modulation of the dose response for neutrophil counts in bronchoalveolar lavage fluid (BALF), *i.e.* an increase in median particle size was concurrent with a decrease in  $ED_{50}$ .

Presentation of p38 MAPK inhibitors to rats in different aerosol forms modulated the incidence and severity of pulmonary toxicopathology findings (shift in dose response for GSK-899), but did not change the nature of the findings *per se*. Lung toxicopathology changes seen after 28 days of treatment correlated with the persistence and/or accumulation of GSK-899 in rat lung tissue and presence of endocytosed particles in macrophages viewed by scanning electron microscopy. Warheit *et al.* (1997) administered  $TiO_2$  or iron particles to rats for four weeks, using a protocol based on guidelines designed for risk assessment of occupational exposure (OECD[412], 2009, OECD[413], 2009, US-EPA[3645], 1998) at inhaled doses (body weight not published; 350 g used for calculation) similar to those administered for the p38 MAPK inhibitors. Toxicopathology lung changes at approximately 0.9 mg/kg/day  $TiO_2$ /iron were similar to those seen in

rats administered amorphous or crystalline GSK-899 at 1 mg/kg/day. Lung lesions at inhaled TiO<sub>2</sub>/iron doses of 9 or 45 mg/kg/day were dose-related in severity and included aggregates of particle-laden macrophages adjacent to focal cellular hypertrophy and hyperplasia (Warheit *et al.*, 1997). However, the published findings for TiO<sub>2</sub> and iron appeared less severe than the infiltration of inflammatory cells observed in rat lung interstitium after inhaled administration of crystalline or amorphous GSK-899 at 15 mg/kg/day. Squamous metaplasia, an adaptive response to irritancy (Gopinath and Mowat, 1987), was evident in the larynx of rats administered high doses of GSK-677 or GSK-899. The absence of macrophage aggregates from lungs of rats subcutaneously administered GSK-899 (perfusing lungs *in situ*) for 28 days and the inflammation observed at injection sites suggests the inflammatory changes seen in the lungs of rats inhaling GSK-899 were not due to the pharmacology of the molecule but may be a function of the persistence of nuisance particles in combination with a mildly irritant effect of GSK-899.

In contrast to GSK-899, there were no treatment-related changes in the respiratory tract of rats administered similar doses of GSK-361, correlating with no drug accumulation in lung and an apparent absence of endocytosed particles in macrophages (contrary to *in vitro* data). Passive membrane permeability *in vitro* may therefore be more predictive than aqueous solubility for predicting the potential for liabilities associated with lung clearance and toxicopathology.

Taken together, the single dose efficacy and repeat dose toxicity data indicate designing molecules of relatively low aqueous solubility (GSK-899) results in persistence of the drug in lung tissue concurrent with an increase in single-dose efficacy (lower ED<sub>50</sub>) for suppression of neutrophils in BALF (Table 6.2). However, there is a trade-off insofar as repeated once-daily administration of the drug at high doses resulted in accumulation of the drug in lung tissue concurrent with a

pulmonary toxicopathology that overwhelmed the anti-inflammatory pharmacology of p38 MAPK inhibition.

For regulatory submissions, 'lung safety margins' are based on a ratio of lung dose in animals relative to that of humans for a given dose; the US-FDA assumes 10% deposition in rat lungs and 100% deposition in human lungs (Forbes *et al.*, 2011, Jones and Baldrick, 2013, Owen, 2013). If the lung dose ratio was based upon a no effect level (NEL), *i.e.* a dose at which no treatment-related findings were seen in animals, this 10-fold ratio would normally suffice for the 'lung safety margin'. However, if ratios were submitted to a regulatory agency based upon no observed adverse effect levels in animals (NOAEL; non-harmful treatment-related findings evident), further adjustments may be applied (Degeorge *et al.*, 1997) including an additional margin if the findings could not be monitored clinically; the US-FDA historically require a 10-fold margin for unmonitorable histopathological changes in rats. For worked examples of the p38 MAPK inhibitors (Table 6.2), crystalline GSK-677 achieved the highest rat:human lung ratio (1806) based on a NOAEL. However, crystalline GSK-361 achieved a margin based on a NEL (350), which would be unlikely to incur a 10-fold reduction in 'safety margin' due to the absence of GSK-361-related findings in the respiratory tract. It is noteworthy these ratios are driven by the NEL or NOAEL established at the evaluated doses, which were dose limiting for nebulised GSK-361. These data suggest 'lung safety margins' for different aerosol forms of the p38 MAPK inhibitors were influenced more by technical limitations than biological effects of the aerosol forms *per se*. It would therefore be prudent to use the intended clinical aerosol form (*e.g.* micronised crystals or nebulised solution with excipients as appropriate) for early non-clinical evaluations of general toxicology. For preclinical safety programmes, the exposure route and aerosol form may not always be critical for specific investigations, such as reproductive toxicology in which test subjects are exposed to the

drug *in utero* and the method of drug administration to the dam is therefore less important.

**Table 6.2: Median effective dose (ED<sub>50</sub>; single exposure) and non-effect levels (28 days) for inhaled p38 MAPK inhibitors administered to rats**

Compound	Aerosol form	ED <sub>50</sub> estimate (µg/kg) <sup>A</sup>	Effect level <sup>B</sup>	Dose of effect level (µg/kg/day)	Ratio of ED <sub>50</sub> to effect level	Ratio of rat to human lung dose <sup>C</sup>
GSK-899	crystalline	23.38	NOAEL	1058	2.2%	27.1
	amorphous-1	65.88	NOAEL	1102	6.0%	31.9
	amorphous-2	10.08	-	-	-	-
	nebulised	44.66	NOAEL	844	5.3%	20.8
GSK-361	crystalline	172	NEL	15200	1.1%	350
	nebulised	165	NEL	1180	14%	27.6
GSK-677	crystalline	366	NOAEL	67800	0.54%	1806
	nebulised	356	NOAEL	14800	2.4%	351

#### Notes

- A ED<sub>50</sub> from dose response for neutrophil counts in bronchoalveolar lavage fluid sampled four hours after intratracheal LPS-challenge.
- B NOAEL (no observed adverse effect level) or NEL (no effect level) in rats after 28 days of treatment.
- C Ratio of rat lung dose at N(OA)EL to human lung dose (for an inhaled dose of 1000 µg).

Lung accumulation from Days 1 to 28 presents a liability for a drug intended for chronic clinical administration. Further work could determine the dose threshold and time taken to achieve steady state (the point at which lung deposition is matched by clearance) and the progression of pulmonary toxicopathology. In addition, efficacy could be evaluated after repeated administration of p38 MAPK inhibitors since potential drug-lung accumulation at pharmacologically relevant doses may affect the dose response. However, demonstrating drug efficacy in humans is the primary objective (proof of concept) in drug development, as opposed to further investigating efficacy in animal models. In the pharmaceutical industry, the decision to use an animal model to investigate efficacy following repeated administration and/or other liabilities (or to terminate development) would depend upon a risk-benefit analysis for the drug development programme based on pertinent factors including therapeutic indication (disease, clinical dose

regimen *etc*), non-clinical findings and their relevance to humans, and ethical review of further *in vivo* experiments. In an industrial context, it is unlikely drug efficacy would be evaluated as a principal endpoint in animals after repeated administration of the inhaled drug.

Nebulised doses of GSK-899 and GSK-361 were limited by the relatively low solubility of these compounds in aqueous vehicles. It was therefore not possible to investigate the pulmonary toxicopathology at a nebulised dose of 15 mg/kg/day for 28 days to confirm if inflammatory changes were confined to dry powder aerosols (crystalline or amorphous GSK-899) at this dose. Failure to identify toxicopathology liabilities in preliminary non-clinical studies may have significant implications for later development, such as development of an alternate salt form or formulation, or termination of the development programme. This reaffirms the conclusion that aerosol forms anticipated for clinical administration should be used in early non-clinical drug development.

Optimisation of the challenge using small numbers of rats (n=3/treatment) suggested intratracheal instillation of lipopolysaccharide (LPS) produced a higher neutrophil count in BALF and a more consistent proportion of neutrophils in leukocytes than inhalation exposure (Appendix 1). The variability of this biological response could be interpreted in part as an indication of the precision of dose delivery and infer that intratracheal instillation leads to more consistent results. However, neutrophil counts were also more variable after intratracheal instillation of dry powders of GSK-899 or GSK-677 and an aqueous suspension of GSK-677, suggesting differences in data variability between experiments utilising intratracheal administration may be associated with the paucity of data.

Whilst inhalation exposure may be the most relevant exposure route to that intended for clinical administration of a drug, there are technical limitations for the precision of dose administration to animals. Animals were not “dosed” *per se* but passively inhaled the p38 MAPK inhibitors

mixed with air. In line with industry practices, inhaled “doses” were calculated using an equation that includes an algorithm for estimating the volume of air inhaled by the animals (Alexander *et al.*, 2008). Measurement of MV by head-out plethysmography indicated this algorithm, under the experimental conditions, may have underestimated mean inhaled doses by approximately 15%. Additional plethysmography data generated in this thesis showed this can be mitigated by allowing rats to settle in restraint tubes for approximately 15 minutes prior to initiating aerosol generation; local (GSK) practices for inhalation exposure of rodents have been adapted accordingly. With adequate animal handling (settling period before each exposure and (re)acclimatisation of rats to plethysmograph restraint over two consecutive days), changes in MV were in line with normal body weight development over a 28-day period. This supports the general application of the algorithm of Alexander *et al.* (2008) for estimating inhaled doses in healthy rats. However, the relationship between MV and body weight concurrent with an adverse effect of treatment (weight loss or reduced gain due to toxicity) was not established since the body weight development of rats was unaffected by p38 MAPK inhibitors at the evaluated doses.

The overall proportion of BALF recovered from whole rat lung ( $71\pm 10\%$ ) was consistent with reported values for lavage of human lungs (Ettensohn *et al.*, 1988). However, it is noteworthy that mean recoveries of 58%, 76% and 80% were achieved for successive BAL cycles in rats. It is plausible the second and third washes did not adequately mix with residual fluid from the first wash, compromising sampling of the alveolar region. Completion of image analysis for CAE-stained sections of lungs (Design D) from rats administered GSK-361 with or without being sampled for BALF would indicate the extent to which neutrophils were harvested from lungs by bronchoalveolar lavage. In addition, results of image analysis (Designs C and D) of lung sections stained for CAE would indicate if

data variability was consistent with that evident for neutrophil counts across three experiments and aerosol forms, *i.e.* for a larger dataset. If confidence limits for neutrophil counts and lung image analysis data were similar, further investigations could consider potential sources of inter-animal variability such as the immune status of rats (monitoring for sub-clinical infections) and pulmonary dosimetry following intratracheal instillation or inhalation exposure of drugs to rats. If the confidence limits for lung image analysis were narrower, a more robust ranking may be possible for the efficacy of p38 MAPK inhibitors and their aerosol forms. Furthermore, if results showed neutrophil counts in BALF lacked precision or did not correlate with inflammatory changes in lung sections, then automated histological processing and image analysis may provide advantages for investigating inhibition of inflammation provided lung sections can be prepared consistently and of sufficient quality for software to accurately distinguish between the biomarker for inflammation and the lung tissue.

## **6.2. Limitations and future work**

Drug-lung deposition: matrix assisted laser desorption/ionization of lung sections with mass spectrometry imaging (MALDI-MSI) demonstrated an even distribution of GSK-361 and GSK-899 across lung sections and concentration of GSK-677 in the main airways. However, this lacked the resolution required to differentiate between compartments within the lung section ( $\leq 13 \mu\text{m}$ ) such as the epithelium, fluid and macrophages (Krombach *et al.*, 1997, Patton and Byron, 2007)). Ultrastructural investigation of lung sections using a higher resolution technique such as secondary ion mass spectrometry (SIMS; (Benabdellah *et al.*, 2010, Guerquin-Kern *et al.*, 2004)) in concert with MALDI-MSI (to identify areas of interest for SIMS analysis) may identify precise locations of p38 MAPK inhibitors within cell types or fluid compartments in frozen rat lung sections. Higher resolution mapping of drug-lung distribution would improve understanding of the

compartmentalisation of p38 MAPK inhibitors after inhalation exposure and how this affects efficacy or pulmonary toxicopathology.

Drug-lung concentrations: differences in the rate of lung clearance were evident between compounds and aerosol forms, with different drug-lung concentrations evident in lungs taken as soon as practicable post exposure. However, a period of 20 minutes elapsed between cessation of aerosol generation and isolation of the lungs from the rat's circulatory system, during which time different proportions of GSK-899 (low solubility), GSK-677 (high solubility) and GSK-361 (lipophilic) were absorbed from lungs. The logistics and proximity of procedures for inhalation exposure and euthanasia should be considered with a view to minimizing the interval elapsing between these procedures for rats sampled 'immediately post exposure' without compromising animal welfare. For example, animals are handled carefully before euthanasia to minimize anxiety, and euthanasia should be performed "away from the immediate presence of other animals" to minimize stress (Home Office, 2014). In practice, euthanasia is normally performed in a dedicated room but transit time could be reduced if suitable apparatus were available in a room adjacent to the inhalation exposure systems. In addition, reducing the duration of inhalation exposure (by increasing aerosol concentration if practicable) would reduce the 'lung residence period' for deposited particles prior to isolation of the lung samples.

The potential underestimation of mean inhaled doses by approximately 15% due to excitability of animals prior to aerosol administration do not fully account for the observed variability in neutrophil data determined in the LPS model or generally in lung concentration data. For logistical reasons (sample size and apparatus), it was local practice to homogenise right lung lobes and omit the left lung. Further work could determine potential heterogeneity in lung deposition between the lobes or quantify potential sources of experimental error for drug-lung measurements such as incomplete homogenisation of lung tissue, which may potentially affect extraction of the analyte for analysis.

However, these potential sources of error in drug-lung concentration analyses did not affect biomarkers for neutrophils in the efficacy model.

Efficacy: neutrophil counts in BALF for rats administered prophylactic doses of p38 MAPK inhibitors were variable, as indicated by the range of 95% confidence limits for each compound and aerosol form. Whilst ED<sub>50</sub> values for GSK-899 treated rats were significantly lower than for GSK-361 and GSK-677, it was not possible to distinguish between the latter compounds or different aerosol forms with confidence. Completion of experiments described in Chapter 4 (Designs C and D) indicated staining of chloroacetate esterase lacked the specificity required to assess histological sections of rat lung for LPS-induced neutrophil infiltration. Identification of an alternative biomarker of neutrophils or refinement of existing methodology to increase the contrast between stained neutrophils and background cells or tissue would be required before the viability of image analysis of lung sections as an alternative method to BALF-neutrophil counts for evaluation of lung inflammation could be evaluated. Similarly, with identification of a robust biomarker for neutrophils, the efficiency of bronchoalveolar lavage for harvesting neutrophils and implications for variability in cell count data could be investigated.

The animal model used for assessing efficacy required construction of a dose response for single prophylactic doses inhibiting an infiltration of neutrophils into the lungs after LPS-challenge. COPD is a chronic lung disease requiring repeated administration of inhaled medicines. Although adverse lung changes in rats administered GSK-899 for 28 days were confined to the high dose of 15 mg/kg/day, further work could be conducted to investigate how efficacy is affected by repeated inhaled administration and potential drug accumulation in lungs.

Pulmonary toxicopathology: relatively low aqueous solubility of GSK-899 and GSK-361 precluded inhalation exposure of rats to nebulised solutions of the test articles, precluding evaluation of an

inhaled dose of 15 mg/kg/day. Although it was not possible to confirm if administration of this dose would have induced the adverse inflammatory changes observed following administration of amorphous (graded “minimal”) or crystalline (“marked”) GSK-899, it nevertheless illustrated a technical complication for evaluating the dose response of a compound by changing the aerosol form.

### 6.3. Summary

This thesis describes results of experiments conducted using dry powder and nebulised aerosols of three anti-inflammatory drugs of common pharmacology but different physicochemical properties. These experiments were conducted to test the following hypotheses:

1. The physicochemical properties of a drug influence its lung or systemic exposure *in vivo*, and hence the resultant efficacy and/or toxicopathology.
2. Changing the presentation of a drug to rats will affect its absorption and hence alter the resultant efficacy and/or toxicopathology *in vivo*.

The first hypothesis was accepted. Of the crystalline forms of the three p38 MAPK inhibitors investigated, GSK-899 (low aqueous solubility) was the most persistent in rat lung tissue after inhaled administration and GSK-361 (low solubility; high passive membrane permeability) was the least. The longer lung residence time for GSK-899, relative to GSK-677 (high solubility; low passive membrane permeability) or GSK-361, correlated with a more effective dose (lower ED<sub>50</sub>) for inhibition of LPS-induced pulmonary infiltration by neutrophils at four hours post challenge. However, at higher doses, this ‘improved’ efficacy was overpowered with repeated administration resulting in accumulation of GSK-899 in lung and adverse pulmonary inflammation.

The second hypothesis was accepted given the severity of respiratory tract toxicopathology for two of three p38 MAPK inhibitors differed with a change in aerosol form. Irritancy of the upper respiratory tract (larynx

and nasal cavity) was more pronounced in rats administered a nebulised solution of GSK-677 than those administered crystalline GSK-677. Conversely, pulmonary inflammation seen after administration of crystalline GSK-899 (15 mg/kg/day) was more pronounced than that seen in rats administered the more readily soluble amorphous aerosol form; evaluation of this dose as a nebulised solution of GSK-899 was precluded by low aqueous solubility of this compound. Furthermore, an increase in aerosol particle size and, by inference, a decrease in lung deposited dose diminished the effectiveness of amorphous GSK-899 to inhibit LPS-induced acute lung inflammation (evident as a higher ED<sub>50</sub> value). However, for GSK-361 and GSK-677, there was no obvious difference between ED<sub>50</sub> values for the respective crystalline and nebulised aerosol forms. Dose responses for nebulised or dry powder aerosol forms of GSK-899 (for similar median particle sizes) were also statistically indistinguishable.

Although much has been published about nuisance particulates in relation to adaptive and adverse pulmonary changes, the described experiments were largely undertaken during the late twentieth century using industrial materials or environmental pollutants that are strikingly different from organic molecules developed as inhaled medicines. Laboratories performing inhalation exposure of laboratory species are typically found within industry or publicly funded agencies undertaking commercially or strategically sensitive research. In addition, pharmaceutical companies expedite termination of programmes (to optimise resources) when drug developability is jeopardised; such laboratories normally archive unpublished data and rarely undertake empirical research. This thesis therefore represents an original contribution to the field by utilising industrial laboratories in support of academic research investigating the *in vivo* efficacy and respiratory toxicopathology of three drugs of common pharmacology when administered to rats as dry powder or aqueous aerosol formulations. This thesis supports the conservative approach of using an aerosol

formulation during early non-clinical development that is as near to the anticipated medicine as possible, and to eschew expediting strategies that potentially necessitate mitigation of liabilities identified when bridging data to the final clinical formulation (delaying timings and using additional animals). Changing aerosol form or particle size resulted in a shift in the dose response and/or severity of toxicopathology for two of the three p38 MAPK inhibitors investigated. Furthermore, technical limitations (dose limited by low solubility) precluded characterisation of toxicity for nebulised aqueous solutions at a higher dose, which had implications for defining the NOAEL and thereby reduced the safety margin for a nebulised clinical dose.

The seminal publication of Snipes (1989) describing a lung deposition fraction of 7% in rats, which is still cited today, referenced *in vivo* data for airborne inorganic nuisance particles and radionuclides. For regulatory review of non-clinical safety, the US-FDA assumes 10% of an aerosol is deposited in rat lungs. This thesis presents data confirming 12% of an inhaled organic molecule (crystalline GSK-899; MMAD  $2.1 \pm 0.4 \mu\text{m}$  and GSD  $2.0 \pm 0.1$ ) was retained in rat lungs, which corroborated the deposition fraction used by the US-FDA.

Minute volume measurements of rats restrained in tubes supported use of an allometric equation to estimate inhaled doses of compounds in healthy rats, provided the animals were adequately acclimatised to the restraint procedure and allowed to settle prior to aerosol administration; implications of toxicity (including body weight loss) or drug-induced changes in respiratory pharmacology were not investigated. Based on these data, the sponsor now applies a 15-minute pre-exposure period to allow rodents to settle in restraint tubes before the start of aerosol administration. Lung function data can also be interpreted as a surrogate indicator of activity or stress and the sponsor refined tube restraint protocols at their laboratory following a review of lung function data presented in this thesis. Acclimatisation of rodents for inhalation exposure (30 to 60 minutes) or intravenous infusion (up to four hours)

have been harmonised such that rats are now subjected to tube restraint for a 30-minute period on each of two consecutive days before the first dose, irrespective of the dose route or duration of dose administration. The data in this thesis demonstrated that 30 minutes was sufficient time to ensure rats achieved a calm state before their removal from the restraint tube. Longer restraint periods were shown to be of no obvious benefit before the first dose and were discontinued, representing benefits for animals and technical resources (protocols formerly applied incremental restraint periods over five days).

In conclusion, administration of three anti-inflammatory drugs with similar *in vitro* potencies but differing physicochemical properties resulted in a range of biological outcomes. Increasing lung persistence improved efficacy at four hours post LPS-challenge but also resulted in the onset of pulmonary toxicopathology with repeated administration of the drug. Similar work to investigate non-clinical efficacy and toxicity of other pharmacological classes of inhaled drugs would expand this dataset and establish the extent to which these findings are generic for inhaled drugs or standalone results for the investigated compounds. Results of this thesis also underpinned refinement of the restraint procedure for rodents during dose administration and considerations for experimental design for non-clinical development of inhaled drugs.



# **REFERENCES**

## References

- ABDI, H. & WILLIAMS, L. J. 2010[A]. Principal component analysis. *Wiley Interdisciplinary Reviews: Computational Statistics*, 2, 433-459.
- ABDI, H. & WILLIAMS, L. J. 2010[B]. Tukey's honestly significant difference (HSD) test. *Encyclopedia of Research Design*. Thousand Oaks, CA: Sage, 1-5.
- ABELLA, B. S., ZHAO, D., ALVARADO, J., HAMANN, K., HOEK, T. L. V. & BECKER, L. B. 2004. Intra-arrest cooling improves outcomes in a murine cardiac arrest model. *Circulation*, 109, 2786-2791.
- ABRAHAM, M. H. 1993. Scales of solute hydrogen-bonding: their construction and application to physicochemical and biochemical processes. *Chemical Society Reviews*, 22, 73-83.
- ADAMS, C. P. & BRANTNER, V. V. 2006. Estimating the cost of new drug development: is it really \$802 million? *Health Affairs*, 25, 420-428.
- AGARWAL, S., JAIN, R., PAL, D. & MITRA, A. K. 2007. Functional characterization of peptide transporters in MDCKII-MDR1 cell line as a model for oral absorption studies. *International journal of pharmaceuticals*, 332, 147-152.
- AÏT-KHALED, N., ENARSON, D. & BOUSQUET, J. 2001. Chronic respiratory diseases in developing countries: the burden and strategies for prevention and management. *Bulletin of the World Health Organization*, 79, 971-979.
- ALANI, A. W., RAO, D. A., SEIDEL, R., WANG, J., JIAO, J. & KWON, G. S. 2010. The effect of novel surfactants and Solutol® HS 15 on paclitaxel aqueous solubility and permeability across a Caco 2 monolayer. *Journal of Pharmaceutical Sciences*, 99, 3473-3485.
- ALBERTS, B., JOHNSON, A., LEWIS, J., RAFF, M., ROBERTS, K. & WALTER, P. 2002. Carrier proteins and active membrane transport. *Molecular Biology of the Cell*, 4th ed. Garland Science.
- ALEXANDER, D. J., COLLINS, C. J., COOMBS, D. W., GILKISON, I. S., HARDY, C. J., HEALEY, G., KARANTABIAS, G., JOHNSON, N., KARLSSON, A. & KILGOUR, J. D. 2008. Association of Inhalation Toxicologists (AIT) working party recommendation for standard delivered dose calculation and expression in non-clinical aerosol inhalation toxicology studies with pharmaceuticals. *Inhalation Toxicology*, 20, 1179-1189.
- ANDERSON, N. & BORLAK, J. 2006. Drug induced phospholipidosis. *FEBS letters*, 580, 5533-5540.
- ANDERSON, P. J. 2005. History of aerosol therapy: liquid nebulization to MDIs to DPIs. *Respiratory Care*, 50, 1139-1150.
- ANDREWS, P., CRAIK, D. & MARTIN, J. 1984. Functional group contributions to drug-receptor interactions. *Journal of Medicinal Chemistry*, 27, 1648-1657.
- ARMSTRONG, R., RODGERS, D., GUTTERIDGE, C., PAUL, G., MOORE, S., JORDAN, S. & MEECHAM, K. 2015. Efficacy of an inhaled PDE4 inhibitor, GSK256066, delivered by a novel dry powder pre-clinical inhalation delivery system in the acute cigarette smoke induced pulmonary inflammation model. *C35. Asthma Therapy I*. Am Thoracic Soc.
- ASHURST, I., MALTON, A., PRIME, D. & SUMBY, B. 2000. Latest advances in the development of dry powder inhalers. *Pharmaceutical Science and Technology Today*, 3, 246-256.

- BANCROFT, J. D. & COOK, H. C. 1994. *Manual of histological techniques and their diagnostic application*, Churchill Livingstone.
- BANERJEE, A., KOZIOL-WHITE, C. & PANETTIERI, R. 2012. p38 MAPK inhibitors, IKK2 inhibitors, and TNF $\alpha$  inhibitors in COPD. *Current Opinion in Pharmacology*, 12, 287-292.
- BARNES, P. J. & ADCOCK, I. M. 2009. Glucocorticoid resistance in inflammatory diseases. *The Lancet*, 373, 1905-1917.
- BARONE, F., DEEGAN, J., PRICE, W., FOWLER, P., FONDACARO, J. & ORMSBEE, H. R. 1990. Cold-restraint stress increases rat fecal pellet output and colonic transit. *American Journal of Physiology: Gastrointestinal and Liver Physiology*, 258, G329-G337.
- BATES, S., ZOGRAFI, G., ENGERS, D., MORRIS, K., CROWLEY, K. & NEWMAN, A. 2006. Analysis of amorphous and nanocrystalline solids from their X-ray diffraction patterns. *Pharmaceutical Research*, 23, 2333-2349.
- BEARDMORE, V. A., HINTON, H. J., EFTYCHI, C., APOSTOLAKI, M., ARMAKA, M., DARRAGH, J., MCILRATH, J., CARR, J. M., ARMIT, L. J. & CLACHER, C. 2005. Generation and characterization of p38 $\beta$  (MAPK11) gene-targeted mice. *Molecular and Cellular Biology*, 25, 10454-10464.
- BELLAMY, W. T. 1996. P-glycoproteins and multidrug resistance. *Annual Review of Pharmacology and Toxicology*, 36, 161-183.
- BENABDELLAH, F., SEYER, A., QUINTON, L., TOUBOUL, D., BRUNELLE, A. & LAPRÉVOTE, O. 2010. Mass spectrometry imaging of rat brain sections: nanomolar sensitivity with MALDI versus nanometer resolution by TOF-SIMS. *Analytical and Bioanalytical Chemistry*, 396, 151-162.
- BENNETT, J., HARRISON, T. & TATTERSFIELD, A. 1999. The contribution of the swallowed fraction of an inhaled dose of salmeterol to its systemic effects. *European Respiratory Journal*, 13, 445-448.
- BIDE, R., ARMOUR, S. & YEE, E. 2000. Allometric respiration/body mass data for animals to be used for estimates of inhalation toxicity to young adult humans. *Journal of Applied Toxicology*, 20, 273-290.
- BUHL, R., CREEMERS, J., VONDRA, V., MARTELLI, N., NAYA, I. & EKSTRÖ, T. 2003. Once-daily budesonide/formoterol in a single inhaler in adults with moderate persistent asthma. *Respiratory Medicine*, 97, 323-330.
- BURN, C. C. 2008. What is it like to be a rat? Rat sensory perception and its implications for experimental design and rat welfare. *Applied Animal Behaviour Science*, 112, 1-32.
- CAZZOLA, M. & MATERA, M. 2008. Novel long acting bronchodilators for COPD and asthma. *British Journal of Pharmacology*, 155, 291-299.
- CELLI, B. R., MACNEE, W., AGUSTI, A., ANZUETO, A., BERG, B., BUIST, A. S., CALVERLEY, P. M., CHAVANNES, N., DILLARD, T. & FAHY, B. 2004. Standards for the diagnosis and treatment of patients with COPD: a summary of the ATS/ERS position paper. *European Respiratory Journal*, 23, 932-946.
- CHALLA, R., AHUJA, A., ALI, J. & KHAR, R. 2005. Cyclodextrins in drug delivery: an updated review. *AAPS PharmSciTech*, 6, E329-E357.
- CHAURAND, P., SCHRIVER, K. E. & CAPRIOLI, R. M. 2007. Instrument design and characterization for high resolution MALDI MS imaging of tissue sections. *Journal of Mass Spectrometry*, 42, 476-489.

## References

- CHENG, P.-W., BOAT, T. F., SHAIKH, S., WANG, O.-L., HU, P.-C. & COSTA, D. L. 1995. Differential effects of ozone on lung epithelial lining fluid volume and protein content. *Experimental Lung Research*, 21, 351-365.
- CHENG, Y.-S., BARR, E. & YEH, H. 1989. A venturi disperser as a dry powder generator for inhalation studies. *Inhalation Toxicology*, 1, 365-371.
- CHRISTOPHER, D., DEY, M., LYAPUSTINA, S., MITCHELL, J., STEIN, S., TOUGAS, T., VAN OORT, M., STRICKLAND, H. & WYKA, B. Generalized simplified approaches for MMAD determination. *Pharm Forum*, 2010. 812-823.
- CHUNG, K. F. 2011. p38 mitogen-activated protein kinase pathways in asthma and COPD. *Chest*, 139, 1470-1479.
- CHURG, A., COSIO, M. & WRIGHT, J. L. 2008. Mechanisms of cigarette smoke-induced COPD: insights from animal models. *American Journal of Physiology: Lung Cellular and Molecular Physiology*, 294, L612-L631.
- COLE, S. P. 2014. Multidrug resistance protein 1 (MRP1, ABCC1), a "multitasking" ATP-binding cassette (ABC) transporter. *Journal of Biological Chemistry*, 289, 30880-30888.
- CRL. 2017. *LPS-induced pulmonary neutrophilia model* [Online]. Charles River. Available: <https://www.criver.com/products-services/discovery-services/vivo-pharmacology/respiratory-disease-pharmacology-models/lps-induced-pulmonary-neutrophilia-model?region=3696z> [Accessed].
- CROMPTON, G. K. 1991. Dry powder inhalers: advantages and limitations. *Journal of Aerosol Medicine*, 4, 151-156.
- CUDDIHY, R. & YEH, H. 1988. Respiratory tract clearance of particles and substances dissociated from particles. *Inhalation Toxicology*. Springer.
- CUENDA, A. & ROUSSEAU, S. 2007. p38 MAP-kinases pathway regulation, function and role in human diseases. *Biochimica et Biophysica Acta (BBA): Molecular Cell Research*, 1773, 1358-1375.
- DAKE, M. D., MADISON, J. M., MONTGOMERY, C. K., SHELLITO, J. E., HINCHCLIFFE, W. A., WINKLER, M. L. & BAINTON, D. F. 1985. Electron microscopic demonstration of lysosomal inclusion bodies in lung, liver, lymph nodes, and blood leukocytes of patients with amiodarone pulmonary toxicity. *The American Journal of Medicine*, 78, 506-512.
- DANIEL, W. A. & WÓJCIKOWSKI, J. 1999. Lysosomal trapping as an important mechanism involved in the cellular distribution of perazine and in pharmacokinetic interaction with antidepressants. *European Neuropsychopharmacology*, 9, 483-491.
- DANIEL, W. A. & WÓJCIKOWSKI, J. 1997. Contribution of lysosomal trapping to the total tissue uptake of psychotropic drugs. *Basic and Clinical Pharmacology and Toxicology*, 80, 62-68.
- DATESAND. 2017. *Nesting and enrichment (reusable): polycarbonate huts* [Online]. Available: <http://datesand.com/index.php/product/polycarbonate-huts/> [Accessed].
- DAWSON, S. 2014. History of UK food law. *Food Sci Technol*, 28, 37-9.
- DE BOER, A., HAGEDOORN, P., HOPPENTOCHT, M., BUTTINI, F., GRASMEIJER, F. & FRIJLINK, H. 2017. Dry powder inhalation: past, present and future. *Expert Opinion on Drug Delivery*, 14, 499-512.

- DEGEORGE, J. J., AHN, C. H., ANDREWS, P. A., BROWER, M. E., CHOI, Y. S., CHUN, M. Y., DU, T., LEE-HAM, D. Y., MCGUINN, W. D. & PEI, L. 1997. Considerations for toxicology studies of respiratory drug products. *Regulatory Toxicology and Pharmacology*, 25, 189-193.
- DERENDORF, H., NAVE, R., DROLLMANN, A., CERASOLI, F. & WURST, W. 2006. Relevance of pharmacokinetics and pharmacodynamics of inhaled corticosteroids to asthma. *European Respiratory Journal*, 28, 1042-1050.
- DEWAR, M., JAMIESON, A., MCLEAN, A. & CROMPTON, G. 1999. Peak inspiratory flow through Turbuhaler® in chronic obstructive airways disease. *Respiratory Medicine*, 93, 342-344.
- DIEHL, K. H., HULL, R., MORTON, D., PFISTER, R., RABEMAMPIANINA, Y., SMITH, D., VIDAL, J. M. & VORSTENBOSCH, C. V. D. 2001. A good practice guide to the administration of substances and removal of blood, including routes and volumes. *Journal of Applied Toxicology*, 21, 15-23.
- DOTSON, M. J. & HYATT, E. M. 2008. Understanding dog-human companionship. *Journal of Business Research*, 61, 457-466.
- DRISCOLL, C. A., MACDONALD, D. W. & O'BRIEN, S. J. 2009. From wild animals to domestic pets, an evolutionary view of domestication. *Proceedings of the National Academy of Sciences*, 106, 9971-9978.
- EEC 1965. Council Directive 65/65/EEC of 26 January 1965 on the approximation of provisions laid down by law, regulation or administrative action relating to proprietary medicinal products. *Official Journal of the European Communities* nE, 22.
- EIXARCH, H., HALTNER-UKOMADU, E., BEISSWENGER, C. & BOCK, U. 2010. Drug delivery to the lung: permeability and physicochemical characteristics of drugs as the basis for a pulmonary biopharmaceutical classification system (pBCS). *Journal of Epithelial Biology & Pharmacology*, 3.
- EMA-1. 2017. *History of EMA (European Medicines Agency)* [Online]. European Medicines Agency. Available: [http://www.ema.europa.eu/ema/index.jsp?curl=pages/about\\_us/general/general\\_content\\_000628.jsp&mid=WC0b01ac058087add](http://www.ema.europa.eu/ema/index.jsp?curl=pages/about_us/general/general_content_000628.jsp&mid=WC0b01ac058087add) [Accessed].
- EMA-2. 2017. *United Kingdom's withdrawal from the European Union ('Brexit')* [Online]. European Medicines Agency. Available: [http://www.ema.europa.eu/ema/index.jsp?curl=pages/news\\_and\\_events/general/general\\_content\\_001707.jsp&mid=WC0b01ac0580a809a7](http://www.ema.europa.eu/ema/index.jsp?curl=pages/news_and_events/general/general_content_001707.jsp&mid=WC0b01ac0580a809a7) [Accessed].
- EMA-3 2006. Guideline on the pharmaceutical quality of inhalation and nasal products. In: USE, C. F. M. P. F. H. (ed.). London: European Medicines Agency.
- ERTL, P., ROHDE, B. & SELZER, P. 2000. Fast calculation of molecular polar surface area as a sum of fragment-based contributions and its application to the prediction of drug transport properties. *Journal of Medicinal Chemistry*, 43, 3714-3717.
- ETTENSCHN, D. B., JANKOWSKI, M. J., REDONDO, A. A. & DUNCAN, P. G. 1988. Bronchoalveolar lavage in the normal volunteer subject: 2. safety and results of repeated BAL, and use in the assessment of intrasubject variability. *Chest*, 94, 281-285.

## References

- EUTAMENE, H., THEODOROU, V., SCHMIDLIN, F., TONDEREAU, V., GARCIA-VILLAR, R., SALVADOR-CARTIER, C., CHOVEL, M., BERTRAND, C. & BUENO, L. 2005. LPS-induced lung inflammation is linked to increased epithelial permeability: role of MLCK. *European Respiratory Journal*, 25, 789-796.
- FDA. 2017. *U.S. Food and Drug Administrations: History* [Online]. Available: <https://www.fda.gov/aboutfda/whatwedo/history/> [Accessed].
- FEHRENBACH, H., ZISSEL, G., GOLDMANN, T., TSCHERNIG, T., VOLLMER, E., PABST, R. & MÜLLER-QUERNHEIM, J. 2003. Alveolar macrophages are the main source for tumour necrosis factor  $\alpha$  in patients with sarcoidosis. *European Respiratory Journal*, 21, 421-428.
- FERNANDES, C. A. & VANBEVER, R. 2009. Preclinical models for pulmonary drug delivery. *Expert Opinion on Drug Delivery*, 6, 1231-1245.
- FESTING, S. & WILKINSON, R. 2007. The ethics of animal research. *EMBO Reports*, 8, 526-530.
- FIELD, K. & LANG, C. 1988. Hazards of urethane (ethyl carbamate): a review of the literature. *Laboratory Animals*, 22, 255-262.
- FINNEY, D. J. 1952. *Probit analysis: a statistical treatment of the sigmoid response curve*, Cambridge University Press.
- FORBES, B., ASGHARIAN, B., DAILEY, L. A., FERGUSON, D., GERDE, P., GUMBLETON, M., GUSTAVSSON, L., HARDY, C., HASSALL, D. & JONES, R. 2011. Challenges in inhaled product development and opportunities for open innovation. *Advanced Drug Delivery Reviews*, 63, 69-87.
- FREKE, M. 2007. GSK610677B: A 28-day inhalation toxicity study of a powder aerosol formulation in the Sprague-Dawley rat (GSK Study No. R27090; GSK Document Number WD2006/03386/00). Charles River Laboratories (Montreal), Canada.
- FREKE, M. 2010. GSK258899B: 28-day inhalation toxicity study of a powder formulation in the Sprague-Dawley rat (Study No. G05157; GSK Document No. CD2005/01071/00). Charles River Laboratories (Montreal), Canada.
- FRÖHLICH, E. 2017. Toxicity of orally inhaled drug formulations at the alveolar barrier: parameters for initial biological screening. *Drug Delivery*, 24, 891-905.
- FUKAMI, T. & YOKOI, T. 2012. The emerging role of human esterases. *Drug Metabolism and Pharmacokinetics*, 27, 466-477.
- GEBERT, A., ROTHKÖTTER, H.-J. & PABST, R. 1996. M cells in Peyer's patches of the intestine. *International Review of Cytology*, 167, 91-159.
- GEISER, M. 2010. Update on macrophage clearance of inhaled micro- and nanoparticles. *Journal of Aerosol Medicine and Pulmonary Drug Delivery*, 23, 207-217.
- GELLER, D. E. 2005. Comparing clinical features of the nebulizer, metered-dose inhaler, and dry powder inhaler. *Respiratory Care*, 50, 1313-1322.
- GERDE, P. M. 1999. Dust gun - aerosol generator and generation. Google Patents.

- GI-GOLD 2006. Global strategy for the diagnosis, management, and prevention of chronic obstructive pulmonary disease. *In: A COLLABORATIVE PROJECT OF THE NATIONAL HEALTH, L., AND BLOOD INSTITUTE, NIH AND THE WORLD HEALTH ORGANISATION (ed.)*. Global initiative for chronic obstructive lung disease (GOLD).
- GLAAB, T., DASER, A., BRAUN, A., NEUHAUS-STEINMETZ, U., FABEL, H., ALARIE, Y. & RENZ, H. 2001. Tidal midexpiratory flow as a measure of airway hyperresponsiveness in allergic mice. *American Journal of Physiology: Lung Cellular and Molecular Physiology*, 280, L565-L573.
- GOPINATH, C. & MOWAT, V. 1987. *Atlas of toxicological pathology*, Springer.
- GOULD, P. L. 1986. Salt selection for basic drugs. *International Journal of Pharmaceutics*, 33, 201-217.
- GRAY, V. A. 2015. Meeting Report: AAPS workshop on inhalation product biopharmaceutical classification system development: Challenges and opportunities. Dissolution Technologies, Inc 9 Yorkridge Trail, Hockessin, DE 19707-9633 USA.
- GUERQUIN-KERN, J.-L., HILLION, F., MADELMONT, J.-C., LABARRE, P., PAPON, J. & CROISY, A. 2004. Ultra-structural cell distribution of the melanoma marker iodobenzamide: improved potentiality of SIMS imaging in life sciences. *Biomedical Engineering Online*, 3, 10.
- GULLAND, A. 2016. How "Brexit" might affect the pharmaceutical industry. *BMJ: British Medical Journal (Online)*, 353.
- GURTOVENKO, A. A. & ANWAR, J. 2009. Interaction of ethanol with biological membranes: the formation of non-bilayer structures within the membrane interior and their significance. *The Journal of Physical Chemistry B*, 113, 1983-1992.
- GUYTON, A. C. 1947. Measurement of the respiratory volumes of laboratory animals. *American Journal of Physiology: Legacy Content*, 150, 70-77.
- HADDAD, E. B., BIRRELL, M., MCCLUSKIE, K., LING, A., WEBBER, S. E., FOSTER, M. L. & BELVISI, M. G. 2001. Role of p38 MAP kinase in LPS induced airway inflammation in the rat. *British Journal of Pharmacology*, 132, 1715-1724.
- HANCOCK, B. C. & PARKS, M. 2000. What is the true solubility advantage for amorphous pharmaceuticals? *Pharmaceutical Research*, 17, 397-404.
- HARKEMA, J. R., NIKULA, K. J. & HASCHEK, W. M. 2013. "Respiratory system" in *Haschek and Rousseaux's handbook of toxicologic pathology*, Academic Press.
- HASTEDT, J. E., BÄCKMAN, P., CLARK, A. R., DOUB, W., HICKEY, A., HOCHHAUS, G., KUEHL, P. J., LEHR, C.-M., MAUSER, P. & MCCONVILLE, J. 2016. Scope and relevance of a pulmonary biopharmaceutical classification system AAPS/FDA/USP Workshop March 16-17th, 2015 in Baltimore, MD. *AAPS Open*, 2.
- HEALY, A. M., AMARO, M. I., PALUCH, K. J. & TAJBER, L. 2014. Dry powders for oral inhalation free of lactose carrier particles. *Advanced Drug Delivery Reviews*, 75, 32-52.

## References

- HELMKE, R. J., BOYD, R. L., GERMAN, V. F. & MANGOS, J. A. 1987. From growth factor dependence to growth factor responsiveness: the genesis of an alveolar macrophage cell line. *In Vitro Cellular and Developmental Biology-Plant*, 23, 567-574.
- HELMKE, R. J., GERMAN, V. F. & MANGOS, J. A. 1989. A continuous alveolar macrophage cell line: comparisons with freshly derived alveolar macrophages. *In Vitro Cellular and Developmental Biology-Plant*, 25, 44-48.
- HENDERSON, R., BENSON, J., HAHN, F., HOBBS, C., JONES, R., MAUDERLY, J., MCCLELLAN, R. & PLCKRELL, J. 1985. New approaches for the evaluation of pulmonary toxicity: bronchoalveolar lavage fluid analysis. *Toxicological Sciences*, 5, 451-458.
- HENDERSON, R. F. 1984. Use of bronchoalveolar lavage to detect lung damage. *Environmental Health Perspectives*, 56, 115.
- HENDERSON, R. F. 2005. Use of bronchoalveolar lavage to detect respiratory tract toxicity of inhaled material. *Experimental and Toxicologic Pathology*, 57, 155-159.
- HERLAAR, E. & BROWN, Z. 1999. p38 MAPK signalling cascades in inflammatory disease. *Molecular Medicine Today*, 5, 439-447.
- HERTEL, S. P., WINTER, G. & FRIESS, W. 2015. Protein stability in pulmonary drug delivery via nebulization. *Advanced drug delivery reviews*, 93, 79-94.
- HNIZDO, E. & VALLYATHAN, V. 2003. Chronic obstructive pulmonary disease due to occupational exposure to silica dust: a review of epidemiological and pathological evidence. *Occupational and Environmental Medicine*, 60, 237-243.
- HOLLÄNDER, W. 1988. Exposure facilities and aerosol generation and characterization for inhalation experiments. *Inhalation Toxicology*. Springer.
- HOME OFFICE 2013. Animals (Scientific Procedures) Act 1986. *In*: HOME OFFICE (ed.). London: HM Stationery Office.
- HOME OFFICE 2014. Home Office code of practice for the housing and care of animals bred, supplied or used for scientific procedures. *In*: HOME OFFICE (ed.). London: HM Stationery Office.
- HOME OFFICE 2017. Annual statistics of scientific procedures on living animals: Great Britain 2016. *In*: OFFICE, H. (ed.). London: Williams Lea Group on behalf of the Controller of Her Majesty's Stationery Office
- HOSHINO, H., LOTVALL, J., SKOOGH, B.-E. & LINDÉN, A. 1999. Neutrophil recruitment by interleukin-17 into rat airways in vivo: role of tachykinins. *American Journal of Respiratory and Critical Care Medicine*, 159, 1423-1428.
- HOYMANN, H. G. 2012. Lung function measurements in rodents in safety pharmacology studies. *Frontiers in pharmacology*, 3, 156.
- ICH. 2017. *History; about ICH* [Online]. Available: <http://www.ich.org/about/history.html> [Accessed].
- IKONEN, E. & HÖLTTÄ-VUORI, M. Cellular pathology of Niemann-Pick type C disease. *Seminars in cell and developmental biology*, 2004. Elsevier, 445-454.
- IOANNOU, C. 2005. Pharmacokinetics of GSK678361A in male CD rats following intravenous (1 mg/kg) and oral administration (1, 10 and 100 mg/kg); (GSK Study No. CMD/05/089). GSK R&D (Stevenage), UK.

- JONES, D. R. & BALDRICK, P. 2013. Association of Inhalation Toxicologists' (AIT) review of regulatory aspects for inhalation toxicology studies. *Inhalation Toxicology*, 25, 84-90.
- JONES, J. B., WATHES, C. M., PERSAUD, K. C., WHITE, R. P. & JONES, R. B. 2001. Acute and chronic exposure to ammonia and olfactory acuity for n-butanol in the pig. *Applied animal behaviour science*, 71, 13-28.
- JONES, R. M. & NEEF, N. 2012. Interpretation and prediction of inhaled drug particle accumulation in the lung and its associated toxicity. *Xenobiotica*, 42, 86-93.
- KAIGHN, M. E., KIRK, D., SZALAY, M. & LECHNER, J. F. 1981. Growth control of prostatic carcinoma cells in serum-free media: interrelationship of hormone response, cell density, and nutrient media. *Proceedings of the National Academy of Sciences*, 78, 5673-5676.
- KANSY, M., SENNER, F. & GUBERNATOR, K. 1998. Physicochemical high throughput screening: parallel artificial membrane permeation assay in the description of passive absorption processes. *Journal of medicinal chemistry*, 41, 1007-1010.
- KAPETANOVIC, I. 2008. Computer-aided drug discovery and development (CADD): in silico-chemico-biological approach. *Chemico-biological Interactions*, 171, 165-176.
- KAZMI, F., HENSLEY, T., POPE, C., FUNK, R. S., LOEWEN, G. J., BUCKLEY, D. B. & PARKINSON, A. 2013. Lysosomal sequestration (trapping) of lipophilic amine (cationic amphiphilic) drugs in immortalized human hepatocytes (Fa2N-4 cells). *Drug Metabolism and Disposition*, 41, 897-905.
- KERLIN, R., BOLON, B., BURKHARDT, J., FRANCKE, S., GREAVES, P., MEADOR, V. & POPP, J. 2016. Scientific and regulatory policy committee: recommended ("best") practices for determining, communicating, and using adverse effect data from nonclinical studies. *Toxicologic Pathology*, 44, 147-162.
- KILLE, J. W. 2013. *Chapter 28 - Regulatory toxicology; a comprehensive guide to toxicology in preclinical drug development*, Academic Press.
- KIM, D. D. & CHIEN, Y. W. 1996. Transdermal delivery of dideoxynucleoside type anti HIV drugs. 2. The effect of vehicle and enhancer on skin permeation. *Journal of Pharmaceutical Sciences*, 85, 214-219.
- KOMAROV, P. G., SHTIL, A. A., BUCKINGHAM, L. E., BALASUBRAMANIAN, M., PIRANER, O., EMANUELE, R. M., RONINSON, I. B. & COON, J. S. 1996. Inhibition of cytarabine induced MDR1 (P glycoprotein) gene activation in human tumor cells by fatty acid polyethylene glycol fatty acid diesters, novel inhibitors of P glycoprotein function. *International Journal of Cancer*, 68, 245-250.
- KOREN, E., SMITH, H. W., SHORES, E., SHANKAR, G., FINCO-KENT, D., RUP, B., BARRETT, Y.-C., DEVANARAYAN, V., GOROVITS, B. & GUPTA, S. 2008. Recommendations on risk-based strategies for detection and characterization of antibodies against biotechnology products. *Journal of Immunological Methods*, 333, 1-9.
- KROMBACH, F., MÜNZING, S., ALLMELING, A.-M., GERLACH, J. T., BEHR, J. & DÖRGER, M. 1997. Cell size of alveolar macrophages: an interspecies comparison. *Environmental Health Perspectives*, 105, 1261.

## References

- LARSON, J. E. & HERRING, S. W. 1996. Movement of the epiglottis in mammals. *American Journal of Physical Anthropology: The Official Publication of the American Association of Physical Anthropologists*, 100, 71-82.
- LEE, J. C., KASSIS, S., KUMAR, S., BADGER, A. & ADAMS, J. L. 1999. p38 mitogen-activated protein kinase inhibitors - mechanisms and therapeutic potentials. *Pharmacology and Therapeutics*, 82, 389-397.
- LEE, K., HENRY, N. W., TROCHIMOWICZ, H. & REINHARDT, C. 1986. Pulmonary response to impaired lung clearance in rats following excessive TiO<sub>2</sub> dust deposition. *Environmental Research*, 41, 144-167.
- LEE, K., TROCHIMOWICZ, H. & REINHARDT, C. 1985. Pulmonary response of rats exposed to titanium dioxide (TiO<sub>2</sub>) by inhalation for two years. *Toxicology and Applied Pharmacology*, 79, 179-192.
- LEWIS, D. J. & MCKEVITT, T. P. 2013. "Respiratory system" in *toxicologic pathology: nonclinical safety assessment*, CRC press.
- LIPINSKI, C. A., LOMBARDO, F., DOMINY, B. W. & FEENEY, P. J. 1997. Experimental and computational approaches to estimate solubility and permeability in drug discovery and development settings. *Advanced Drug Delivery Reviews*, 23, 3-25.
- LOFTSSON, T., VOGENSEN, S. B., BREWSTER, M. E. & KONRÁÐSDÓTTIR, F. 2007. Effects of cyclodextrins on drug delivery through biological membranes. *Journal of Pharmaceutical Sciences*, 96, 2532-2546.
- LOUKAS, C. G., WILSON, G. D., VOJNOVIC, B. & LINNEY, A. 2003. An image analysis based approach for automated counting of cancer cell nuclei in tissue sections. *Cytometry Part A*, 55, 30-42.
- LUPU, F., DANARICU, I. & SIMIONESCU, N. 1987. Development of intracellular lipid deposits in the lipid-laden cells of atherosclerotic lesions: a cytochemical and ultrastructural study. *Atherosclerosis*, 67, 127-142.
- MACFARLAND, H. N. 1983. Designs and operational characteristics of inhalation exposure equipment - a review. *Fundamental and Applied Toxicology*, 3, 603-613.
- MARPLE, V. A., ROBERTS, D. L., ROMAY, F. J., MILLER, N. C., TRUMAN, K. G., VAN OORT, M., OLSSON, B., HOLROYD, M. J., MITCHELL, J. P. & HOCHRAINER, D. 2003. Next generation pharmaceutical impactor (a new impactor for pharmaceutical inhaler testing). Part I: Design. *Journal of Aerosol Medicine*, 16, 283-299.
- MARTINEZ, F. O. & GORDON, S. 2014. The M1 and M2 paradigm of macrophage activation: time for reassessment. *F1000prime reports*, 6.
- MATTHAY, M. A. & ZEMANS, R. L. 2011. The acute respiratory distress syndrome: pathogenesis and treatment. *Annual Review of Pathology: Mechanisms of Disease*, 6, 147-163.
- MAYER, R. J. & CALLAHAN, J. F. 2006. p38 MAP kinase inhibitors: a future therapy for inflammatory diseases. *Drug Discovery Today: Therapeutic Strategies*, 3, 49-54.
- MCCORMICK, J. J., LARSON, L. J. & RICH, M. A. 1974. RNase inhibition of reverse transcriptase activity in human milk. *Nature*, 251, 737-740.
- MCGOWAN, J. C. 1978. Estimates of the properties of liquids. *Journal of Chemical Technology and Biotechnology*, 28, 599-607.

- MCMAHON, T., BRAIN, J. & LEMOTT, S. 1975. Species differences in aerosol deposition. *Inhaled Particles*, 4, 23-33.
- MHRA. 2012. *Medicines and medical devices regulation: what you need to know* [Online]. The Medicines and Healthcare Products, Regulatory Agency, UK. Available: <http://www.mhra.gov.uk/home/groups/comms-ic/documents/websiteresources/con2031677.pdf> [Accessed].
- MILLAN, D. S., BUNNAGE, M. E., BURROWS, J. L., BUTCHER, K. J., DODD, P. G., EVANS, T. J., FAIRMAN, D. A., HUGHES, S. J., KILTY, I. C. & LEMAITRE, A. 2011. Design and synthesis of inhaled p38 inhibitors for the treatment of chronic obstructive pulmonary disease. *Journal of Medicinal Chemistry*, 54, 7797-7814.
- MILLER, F. J. 2000. Dosimetry of particles in laboratory animals and humans in relationship to issues surrounding lung overload and human health risk assessment: a critical review. *Inhalation Toxicology*, 12, 19-57.
- MILLONIG, G. 1961. Advantages of a phosphate buffer for OsO<sub>4</sub> solutions in fixation. *Journal of Applied Physiology*, 32, 1-10.
- MIRZA, A., DESAI, R. & REYNISSON, J. 2009. Known drug space as a metric in exploring the boundaries of drug-like chemical space. *European Journal of Medicinal Chemistry*, 44, 5006-5011.
- MOELLER, A., ASK, K., WARBURTON, D., GAULDIE, J. & KOLB, M. 2008. The bleomycin animal model: a useful tool to investigate treatment options for idiopathic pulmonary fibrosis? *The International Journal of Biochemistry and Cell Biology*, 40, 362-382.
- MOON, P. F. & SMITH, L. J. 1996. General anesthetic techniques in swine. *Veterinary Clinics: Food Animal Practice*, 12, 663-691.
- MORROW, P. 1988. Possible mechanisms to explain dust overloading of the lungs. *Fundamental and Applied Toxicology*, 10, 369-384.
- MORTON, D. B. 1999. *Humane endpoints in animal experimentation for biomedical research: ethical, legal and practical aspects*. London: Royal Society of Medicine Press.
- MOSSER, D. M. & EDWARDS, J. P. 2008. Exploring the full spectrum of macrophage activation. *Nature reviews immunology*, 8, 958.
- MUDGE, J. 1779. *A radical and expeditious cure for a recent catarrhus cough: preceded by some observations on respiration, with occasional and practical remarks on some other diseases of the lungs; to which is added a chapter on the vis vitae, so far as it is concerned in preserving and reinstating the health of an animal; accompanied with some strictures on the treatment of compound fractures*.  
, E. Allen, and sold by J. Walter, B. Thorn and M. Haydon.
- MURRAY, P. J. & WYNN, T. A. 2011. Protective and pathogenic functions of macrophage subsets. *Nature Reviews Immunology*, 11, 723-737.
- NEGUS, V. 1927. The function of the epiglottis. *Journal of Anatomy*, 62, 1.
- NHS. 2017. *Chronic obstructive pulmonary disease (COPD)* [Online]. Available: <https://www.nhs.uk/conditions/chronic-obstructive-pulmonary-disease-copd/> [Accessed].
- NICE. 2010. *Chronic obstructive pulmonary disease in over 16s: diagnosis and management* [Online]. Available: <https://www.nice.org.uk/guidance/cg101> [Accessed].

## References

- NICK, J. A., YOUNG, S. K., ARNDT, P. G., LIEBER, J. G., SURATT, B. T., POCH, K. R., AVDI, N. J., MALCOLM, K. C., TAUBE, C. & HENSON, P. M. 2002. Selective suppression of neutrophil accumulation in ongoing pulmonary inflammation by systemic inhibition of p38 mitogen-activated protein kinase. *The Journal of Immunology*, 169, 5260-5269.
- NIKANDER, K. & SANDERS, M. 2010. The early evolution of nebulizers. *Medicamundi*, 54, 47-53.
- NIROGI, R., SHANMUGANATHAN, D., JAYARAJAN, P., ABRAHAM, R. & KANCHARLA, B. 2012. Comparison of whole body and head out plethysmography using respiratory stimulant and depressant in conscious rats. *Journal of Pharmacological and Toxicological Methods*, 65, 37-43.
- NRC 2006. *Overcoming challenges to develop countermeasures against aerosolized bioterrorism agents: appropriate use of animal models (generation and characterization of aerosolized agents)*, National Academies Press.
- OECD[403] 2009. Test No. 403: acute inhalation toxicity. OECD Publishing.
- OECD[412] 2009. Test No. 412: subacute inhalation toxicity: 28-day study. OECD Publishing.
- OECD[413] 2009. Test No. 413: subchronic inhalation toxicity: 90-day study. OECD Publishing.
- OECD[TG412] 2017. Test No. 412: 28-day (subacute) inhalation toxicity study. OECD Publishing.
- OECD[TG413] 2017. Test No. 413: 90-day (subchronic) inhalation toxicity study. OECD Publishing.
- OSIER, M. & OBERÖRSTER, G. 1997. Intratracheal inhalation vs intratracheal instillation: differences in particle effects. *Toxicological Sciences*, 40, 220-227.
- OWEN, K. 2013. Regulatory toxicology considerations for the development of inhaled pharmaceuticals. *Drug and Chemical Toxicology*, 36, 109-118.
- PATTON, J. S. 1996. Mechanisms of macromolecule absorption by the lungs. *Advanced Drug Delivery Reviews*, 19, 3-36.
- PATTON, J. S., BRAIN, J. D., DAVIES, L. A., FIEGEL, J., GUMBLETON, M., KIM, K.-J., SAKAGAMI, M., VANBEVER, R. & EHRHARDT, C. 2010. The particle has landed - characterizing the fate of inhaled pharmaceuticals. *Journal of Aerosol Medicine and Pulmonary Drug Delivery*, 23, S-71-S-87.
- PATTON, J. S. & BYRON, P. R. 2007. Inhaling medicines: delivering drugs to the body through the lungs. *Nature Reviews: Drug Discovery*, 6, 67.
- PATTON, J. S., FISHBURN, C. S. & WEERS, J. G. 2004. The lungs as a portal of entry for systemic drug delivery. *Proceedings of the American Thoracic Society*, 1, 338-344.
- PAUL, G. R., SOMERS, G. I., MOORE, S. A. & GOODWAY, R. E. 2012. The capsule based aerosol generator - conserving test article in small scale inhalation exposures. *Respiratory Drug Delivery*, 2, 525-530.
- PAULUHN, J. 2008. Inhalation toxicology: methodological and regulatory challenges. *Experimental and Toxicologic Pathology*, 60, 111-124.
- PAULUHN, J. & MOHR, U. 2000. Inhalation studies in laboratory animals - current concepts and alternatives. *Toxicologic Pathology*, 28, 734-753.

- PAUWELS, M. & ROGIERS, V. 2007. EU legislations affecting safety data availability of cosmetic ingredients. *Regulatory Toxicology and Pharmacology*, 49, 308-315.
- PEIRCE, G. 1913. The compound formed between esterase and sodium fluoride. *Journal of Biological Chemistry*, 16, 5-18.
- PENNOCK, B., COX, C., ROGERS, R., CAIN, W. & WELLS, J. 1979. A noninvasive technique for measurement of changes in specific airway resistance. *Journal of Applied Physiology*, 46, 399-406.
- PETRI, C. 2004. PK [pharmacokinetics] of GSK258899A and GSK618121A following intravenous and oral administration of GSK258899A to male rats (GSK Study No. RI04079). GSK R&D (King of Prussia, PA), USA.
- POINTEL, J., GIN, H., DROUIN, P., VERNHES, G. & DEBRY, G. 1981. Venous plethysmography: measuring techniques and normal values. *Angiology*, 32, 145-154.
- PRINCI, F., CHURCH, F. & MCGILVRAY, W. 1949. An improved animal dusting apparatus. *Journal of Industrial Hygiene and Toxicology*, 31, 106-12.
- RAABE, O. G., AL-BAYATI, M. A., TEAGUE, S. V. & RASOLT, A. 1988. Regional deposition of inhaled monodisperse coarse and fine aerosol particles in small laboratory animals. *Annals of Occupational Hygiene*, 32, 53-63.
- RENNARD, S., BASSET, G., LECOSSIER, D., O'DONNELL, K., PINKSTON, P., MARTIN, P. & CRYSTAL, R. 1986. Estimation of volume of epithelial lining fluid recovered by lavage using urea as marker of dilution. *Journal of Applied Physiology*, 60, 532-538.
- RENNINGER, J. P. 2006. Head out plethysmography in safety pharmacology assessment. *Current Protocols in Pharmacology*, 10.11. 1-10.11. 18.
- RESEARCH-MARKETS. 2016. *Global respiratory drugs market to 2022 - pipeline and market characterized by growing prominence of targeted therapies, with asthma and cystic fibrosis leading the way* [Online]. Research and Markets. Available: <https://www.researchandmarkets.com/research/fmz5wv/global> [Accessed].
- RESSLER, K. J., SULLIVAN, S. L. & BUCK, L. B. 1993. A zonal organization of odorant receptor gene expression in the olfactory epithelium. *Cell*, 73, 597-609.
- RESTREPO, R. D., ALVAREZ, M. T., WITTNEBEL, L. D., SORENSON, H., WETTSTEIN, R., VINES, D. L., SIKKEMA-ORTIZ, J., GARDNER, D. D. & WILKINS, R. L. 2008. Medication adherence issues in patients treated for COPD. *International Journal of Chronic Obstructive Pulmonary Disease*, 3, 371.
- RITCHIE, T. J., LUSCOMBE, C. N. & MACDONALD, S. J. 2009. Analysis of the calculated physicochemical properties of respiratory drugs: can we design for inhaled drugs yet? *Journal of Chemical Information and Modeling*, 49, 1025-1032.
- RITCHIE, T. J. & MACDONALD, S. J. 2009. The impact of aromatic ring count on compound developability—are too many aromatic rings a liability in drug design? *Drug discovery today*, 14, 1011-1020.

## References

- RNS-LSE#1 2017. GSK and Innoviva report positive headline results from IMPACT study showing single inhaler triple therapy Trelegy Ellipta reduced COPD exacerbations. Regulatory News Service (London Stock Exchange).
- RNS-LSE#2 2017. GSK submits landmark IMPACT data to US regulatory authority to support expanded label for Trelegy Ellipta. Regulatory News Service (London Stock Exchange).
- ROCHE. 2016. *Cytotoxicity detection kit (LDH)* [Online]. Available: <https://www.sigmaaldrich.com/content/dam/sigma-aldrich/docs/Roche/Bulletin/1/11644793001bul.pdf> [Accessed Cat. No. 11 644 793 001].
- ROSS, N. E., PRITCHARD, C. J., RUBIN, D. M. & DUSE, A. G. 2006. Automated image processing method for the diagnosis and classification of malaria on thin blood smears. *Medical and Biological Engineering and Computing*, 44, 427-436.
- ROUX, P. P. & BLENIS, J. 2004. ERK and p38 MAPK-activated protein kinases: a family of protein kinases with diverse biological functions. *Microbiology and Molecular Biology Reviews*, 68, 320-344.
- ROWLAND, M. & TOZER, T. N. 1995. *Clinical pharmacokinetics: concepts and applications (Chapter 19: distribution kinetics)*, Williams & Wilkins.
- RUBOW, K. L., MARPLE, V. A., OLIN, J. & MCCAWLEY, M. A. 1987. A personal cascade impactor: design, evaluation and calibration. *The American Industrial Hygiene Association Journal*, 48, 532-538.
- RUSH, K. V. G., P.S. 2007. GSK678361A : 4-week oral toxicity study in Sprague-Dawley rats (GSK Study No. R27314; GSK Document No. WD2007/00579/00). GSK R&D (Ware), UK.
- RUSSEL, W. & BURCH, R. 1959. *The principles of humane experimental technique*, Methuen and Co Ltd, London.
- SAETTA, M., BARALDO, S., CORBINO, L., TURATO, G., BRACCIONI, F., REA, F., CAVALLESCO, G., TROPEANO, G., MAPP, C. E. & MAESTRELLI, P. 1999. CD8+ve cells in the lungs of smokers with chronic obstructive pulmonary disease. *American Journal of Respiratory and Critical Care Medicine*, 160, 711-717.
- SAETTA, M., TURATO, G., MAESTRELLI, P., MAPP, C. E. & FABBRI, L. M. 2001. Cellular and structural bases of chronic obstructive pulmonary disease. *American Journal of Respiratory and Critical Care Medicine*, 163, 1304-1309.
- SCANBUR. 2017. *Bedding and nesting: polycarbonate enrichment* [Online]. Available: <http://www.scanbur.com/consumables/enrichment/polycarbonate/#prettyPhoto> [Accessed].
- SCHLESINGER, R. B. 1985. Comparative deposition of inhaled aerosols in experimental animals and humans: a review. *Journal of Toxicology and Environmental Health, Part A Current Issues*, 15, 197-214.
- SCHNEIDER, T. & ISSEKUTZ, A. C. 1996. Quantitation of eosinophil and neutrophil infiltration into rat lung by specific assays for eosinophil peroxidase and myeloperoxidase Application in a Brown Norway rat model of allergic pulmonary inflammation. *Journal of Immunological Methods*, 198, 1-14.

- SCHNEIDER, T., VAN VELZEN, D., MOQBEL, R. & ISSEKUTZ, A. C. 1997. Kinetics and quantitation of eosinophil and neutrophil recruitment to allergic lung inflammation in a brown Norway rat model. *American Journal of Respiratory Cell and Molecular Biology*, 17, 702-712.
- SCHREIDER, J. P. & RAABE, O. G. 1981. Anatomy of the nasal pharyngeal airway of experimental animals. *The Anatomical Record*, 200, 195-205.
- SHANKAR, R., FRAPAISE, X. & BROWN, B. 2006. LEAN drug development in R&D. *Drug Discovery and Development*, 9, 57-60.
- SHANLEY, T. P., SCHMAL, H., FRIEDL, H. P., JONES, M. L. & WARD, P. A. 1995. Role of macrophage inflammatory protein-1 alpha (MIP-1 alpha) in acute lung injury in rats. *The Journal of Immunology*, 154, 4793-4802.
- SHAPIRO, S. D. 2000. Animal models for chronic obstructive pulmonary disease: age of klothe and marlboro mice. *American Journal of Respiratory Cell and Molecular Biology*, 22, 4-7.
- SHARGEL, L., ANDREW, B. & WU-PONG, S. 2005. *Applied biopharmaceutics and pharmacokinetics*, McGraw-Hill New York:.
- SHEHATA, M. 2008. History of inhalation therapy. *Internet J Health*, 9, 1-9.
- SIMARD, J. R., ZUNSZAIN, P. A., HAMILTON, J. A. & CURRY, S. 2006. Location of high and low affinity fatty acid binding sites on human serum albumin revealed by NMR drug-competition analysis. *Journal of molecular biology*, 361, 336-351.
- SINHA, V. & KAUR, M. P. 2000. Permeation enhancers for transdermal drug delivery. *Drug Development and Industrial Pharmacy*, 26, 1131-1140.
- SNIPES, M. 1989. Species comparisons for pulmonary retention of inhaled particles. *Concepts in Inhalation Toxicology*, 193-227.
- SNIPES, M. B. 1994. Biokinetics of inhaled radionuclides. *Internal Radiation Dosimetry*, 181-196.
- SNYDER, W. S., COOK, M. J., KARHAUSEN, L. R., NASET, E. S., HOWELLS, G. P. & TIPTON, I. H. 1975. International commission of radiological protection No. 23: report of the task group on reference man. . In: OXFORD: (ed.). Oxford: Pergamon Press.
- SPOND, J., BILLAH, M., CHAPMAN, R., EGAN, R., HEY, J., HOUSE, A., KREUTNER, W. & MINNICOZZI, M. 2004. The role of neutrophils in LPS-induced changes in pulmonary function in conscious rats. *Pulmonary Pharmacology and Therapeutics*, 17, 133-140.
- STEIN, S. W. & THIEL, C. G. 2017. The history of therapeutic aerosols: a chronological review. *Journal of Aerosol Medicine and Pulmonary Drug Delivery*, 30, 20-41.
- SUGIYAMA, S., OKADA, Y., SUKHOVA, G. K., VIRMANI, R., HEINECKE, J. W. & LIBBY, P. 2001. Macrophage myeloperoxidase regulation by granulocyte macrophage colony-stimulating factor in human atherosclerosis and implications in acute coronary syndromes. *The American Journal of Pathology*, 158, 879-891.
- SUNG, J. H., JI, J. H., YOON, J. U., KIM, D. S., SONG, M. Y., JEONG, J., HAN, B. S., HAN, J. H., CHUNG, Y. H. & KIM, J. 2008. Lung function changes in Sprague-Dawley rats after prolonged inhalation exposure to silver nanoparticles. *Inhalation Toxicology*, 20, 567-574.

## References

- SZÉL, Á. & RÖHLICH, P. 1992. Two cone types of rat retina detected by anti-visual pigment antibodies. *Experimental Eye Research*, 55, 47-52.
- TAYAB, Z. R. & HOCHHAUS, G. 2005. Pharmacokinetic/pharmacodynamic evaluation of inhalation drugs: application to targeted pulmonary delivery systems. *Expert Opinion on Drug Delivery*, 2, 519-532.
- TELKO, M. J. & HICKEY, A. J. 2005. Dry powder inhaler formulation. *Respiratory Care*, 50, 1209-1227.
- TITFORD, M. 2005. The long history of hematoxylin. *Biotechnic and Histochemistry*, 80, 73-78.
- TRIPLETT, J., HAYDEN, T., MCWHORTER, L., GAUTAM, S., KIM, E. & BOURNE, D. 1985. Determination of gallium concentration in "blood free" tissues using a radiolabeled blood marker. *Journal of Pharmaceutical Sciences*, 74, 1007-1009.
- TURATO, G., ZUIN, R. & SAETTA, M. 2001. Pathogenesis and pathology of COPD. *Respiration*, 68, 117-128.
- UAR. 2017. *What is animal research? => Numbers of animals* [Online]. Understanding Animal Research. Available: <http://www.understandinganimalresearch.org.uk/animals/numbers-animals/> [Accessed].
- ULICH, T. R., EUNHEE, S. Y., YIN, S., SMITH, C. & REMICK, D. 1994. Intratracheal administration of endotoxin and cytokines: VII. The soluble interleukin-1 receptor and the soluble tumor necrosis factor receptor II (p80) inhibit acute inflammation. *Clinical Immunology and Immunopathology*, 72, 137-140.
- UMBRECHT, S. 2007. Pharmacokinetics of GSK610677A in the male Sprague-Dawley rat (GSK Study No. RI05042; GSK Document No. CH2007/00133/00). GSK R&D (King of Prussia, PA), USA.
- UMETRICS. 2013. *How it works: multivariate data analysis (MVDA)* [Online]. Sartorius Stedim Biotech. Available: <http://www.umetrics.com/how-it-works/mva> [Accessed].
- UNDERWOOD, D. C., OSBORN, R. R., BOCHNOWICZ, S., WEBB, E. F., RIEMAN, D. J., LEE, J. C., ROMANIC, A. M., ADAMS, J. L., HAY, D. W. & GRISWOLD, D. E. 2000. SB 239063, a p38 MAPK inhibitor, reduces neutrophilia, inflammatory cytokines, MMP-9, and fibrosis in lung. *American Journal of Physiology: Lung Cellular and Molecular Physiology*, 279, L895-L902.
- URIEN, S., BREE, F., TESTA, B. & TILLEMENT, J. 1993. pH-dependence of warfarin binding to  $\alpha$ 1-acid glycoprotein (orosomucoid). *Biochemical Journal*, 289, 767-770.
- US-EPA[1300] 1998. Health effects test guidelines: OPPTS 870. 1300 acute inhalation toxicity. *In: AGENCY, U. S. E. P. (ed.)*.
- US-EPA[3645] 1998. Health effects test guidelines: OPPTS 870.3465 90-day inhalation toxicity. *In: AGENCY, U. S. E. P. (ed.)*.
- VALKÓ, K., BEVAN, C. & REYNOLDS, D. 1997. Chromatographic hydrophobicity index by fast-gradient RP-HPLC: a high-throughput alternative to log P/log D. *Analytical Chemistry*, 69, 2022-2029.

- VAN DEN MOOTER, G. 2012. The use of amorphous solid dispersions: a formulation strategy to overcome poor solubility and dissolution rate. *Drug Discovery Today: Technologies*, 9, e79-e85.
- VAN HELDEN, H., KUIJPERS, W., STEENVOORDEN, D., GO, C., BRUIJNZEEL, P., VAN EIJK, M. & HAAGSMAN, H. 1997. Intratracheal aerosolization of endotoxin (LPS) in the rat: a comprehensive animal model to study adult (acute) respiratory distress syndrome. *Experimental Lung Research*, 23, 297-316.
- VEBER, D. F., JOHNSON, S. R., CHENG, H.-Y., SMITH, B. R., WARD, K. W. & KOPPLE, K. D. 2002. Molecular properties that influence the oral bioavailability of drug candidates. *Journal of medicinal chemistry*, 45, 2615-2623.
- VEHRING, R. 2008. Pharmaceutical particle engineering via spray drying. *Pharmaceutical Research*, 25, 999-1022.
- VEISEH, O., TANG, B. C., WHITEHEAD, K. A., ANDERSON, D. G. & LANGER, R. 2015. Managing diabetes with nanomedicine: challenges and opportunities. *Nature Reviews Drug Discovery*, 14, 45-57.
- VIJAYARAGHAVAN, R., SCHAPER, M., THOMPSON, R., STOCK, M. & ALARIE, Y. 1993. Characteristic modifications of the breathing pattern of mice to evaluate the effects of airborne chemicals on the respiratory tract. *Archives of Toxicology*, 67, 478-490.
- WARD, K. W. & AZZARANO, L. M. 2004. Preclinical pharmacokinetic properties of the P-glycoprotein inhibitor GF120918A (HCl salt of GF120918, 9, 10-dihydro-5-methoxy-9-oxo-N-[4-[2-(1, 2, 3, 4-tetrahydro-6, 7-dimethoxy-2-isoquinolinyl) ethyl] phenyl]-4-acridine-carboxamide) in the mouse, rat, dog, and monkey. *Journal of Pharmacology and Experimental Therapeutics*, 310, 703-709.
- WARHEIT, D., HANSEN, J., YUEN, I., KELLY, D., SNAJDR, S. & HARTSKY, M. 1997. Inhalation of high concentrations of low toxicity dusts in rats results in impaired pulmonary clearance mechanisms and persistent inflammation. *Toxicology and Applied Pharmacology*, 145, 10-22.
- WARHEIT, D. B. & HARTSKY, M. A. 1993. Role of alveolar macrophage chemotaxis and phagocytosis in pulmonary clearance responses to inhaled particles: comparisons among rodent species. *Microscopy Research and Technique*, 26, 412-422.
- WARHEIT, D. B., HARTSKY, M. A. & STEFANIAK, M. S. 1988. Comparative physiology of rodent pulmonary macrophages: in vitro functional responses. *Journal of Applied Physiology*, 64, 1953-1959.
- WELLS, D. J. 2011. Animal welfare and the 3Rs in European biomedical research. *Annals of the New York Academy of Sciences*, 1245, 14-16.
- WHEELLOCK, Å. M. & WHEELLOCK, C. E. 2013. Trials and tribulations of 'omics data analysis: assessing quality of SIMCA-based multivariate models using examples from pulmonary medicine. *Molecular bioSystems*, 9, 2589-2596.
- WHO. 2017. *World Health Organisation fact sheet: the top 10 causes of death* [Online]. Available: <http://www.who.int/mediacentre/factsheets/fs310/en/> [Accessed].

## References

- WILLIAMS, A. S., ISSA, R., DURHAM, A., LEUNG, S.-Y., KAPOUN, A., MEDICHERLA, S., HIGGINS, L. S., ADCOCK, I. M. & CHUNG, K. F. 2008. Role of p38 mitogen-activated protein kinase in ozone-induced airway hyperresponsiveness and inflammation. *European Journal of Pharmacology*, 600, 117-122.
- WILLIAMS, C. L., VILLAR, R. G., PETERSON, J. M. & BURKS, T. F. 1988. Stress-induced changes in intestinal transit in the rat: a model for irritable bowel syndrome. *Gastroenterology*, 94, 611-621.
- WILLIS, B., BARTON, P., PEARMAN, P., BRYAN, S. & HYDE, C. 2005. Cervical screening programmes: can automation help? Evidence from systematic reviews, an economic analysis and a simulation modelling exercise applied to the UK. *NIHR Health Technology Assessment programme: Executive Summaries*.
- WOLD, S., ESBENSEN, K. & GELADI, P. 1987. Principal component analysis. *Chemometrics and Intelligent Laboratory Systems*, 2, 37-52.
- WRIGHT, B. 1950. A new dust-feed mechanism. *Journal of Scientific Instruments*, 27, 12.
- WRIGHT, J. L. & CHURG, A. 2002. Animal models of cigarette smoke-induced COPD. *Chest Journal*, 122, 301S-306S.
- WRIGHT, J. L., COSIO, M. & CHURG, A. 2008. Animal models of chronic obstructive pulmonary disease. *American Journal of Physiology: Lung Cellular and Molecular Physiology*, 295, L1-L15.
- ZHANG, J. 2003. SB 731445: investigation of the intravenous pharmacokinetic parameters and oral bioavailability of SB-731445 in the male Sprague-Dawley rat (GSK Study No. CD01821; GSK Document No. CH2002/00022/00). GSK R&D (King of Prussia, PA), USA.
- ZOSKY, G. & SLY, P. 2007. Animal models of asthma. *Clinical and Experimental Allergy*, 37, 973-988.

# **APPENDICES**

### **Appendix 1: Optimisation of exposure route for administration of lipopolysaccharide to induce acute lung inflammation**

In an experiment, two operators administered lipopolysaccharide (LPS) to groups of rats (n=6/group) via the trachea using a Portex<sup>®</sup> cannula. Neutrophil counts in BALF were inconsistent, with a significant proportion of rats (1/6 to 5/6) not responding to the LPS-lung challenge. This indicated the cannula had been misplaced and LPS discharged into the oesophagus in error. Subsequent investigations confirmed a difference between operators for the frequency of successful placement of the cannula into the trachea.

Before progressing with experiments summarised in Chapter 4, three methods for administering LPS were evaluated. Groups of rats (n=3) were dosed by intratracheal instillation (2 µg/rat; 0.2 mL/rat; 10 µg/mL LPS in phosphate buffered saline) using a Penn Century microsyringe (Figures A1A and A1B) or by inhalation of a nebulised aerosol for 15 minutes (150 µg/mL; airflow 9 L/min) in a whole-body chamber (Figure A1C) or restrained in tubes attached to a snout-only exposure chamber (Figure A1D). The aerosol concentration of LPS was not measured but the guesstimated inhaled dose was 100 µg/rat (based on knowledge of the apparatus) and equivalent to a lung dose of 10 µg/rat assuming 10% aerosol deposition. Neutrophil counts were determined in bronchoalveolar lavage fluid taken four hours post challenge.

#### **Methodological outcomes for LPS challenge**

Intratracheal instillation was selected as the preferred method for administration for LPS challenge. Under the experimental conditions, intratracheal instillation produced the highest neutrophil counts of the three methods (Figure A1E) and had the highest and most consistent proportion of neutrophils as a percentage of leukocytes (Figure A1F). However, careful placement of the cannula in the trachea was critical for successful dose administration of LPS.

## Appendix 1: Optimisation of exposure route for administration of lipopolysaccharide to induce acute lung inflammation (continued)

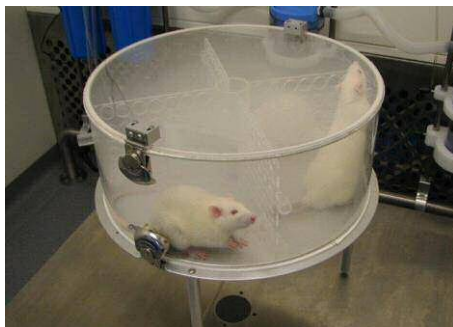
A1A



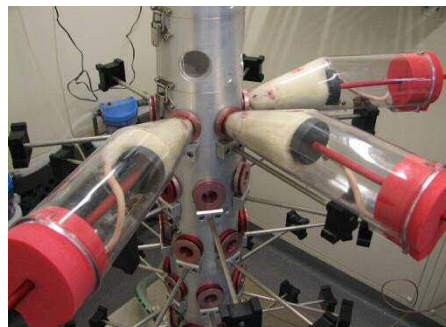
A1B



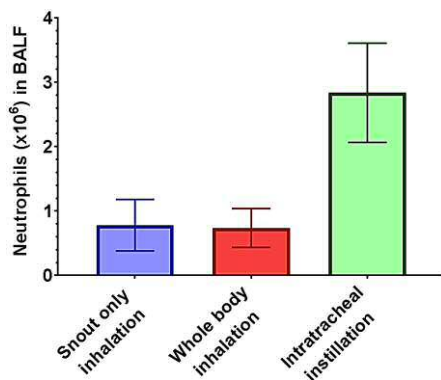
A1C



A1D

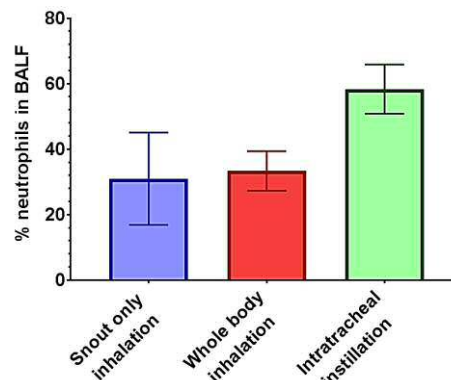


A1E



Method of LPS administration 4 hours before bronchoalveolar lavage of lungs

A1F

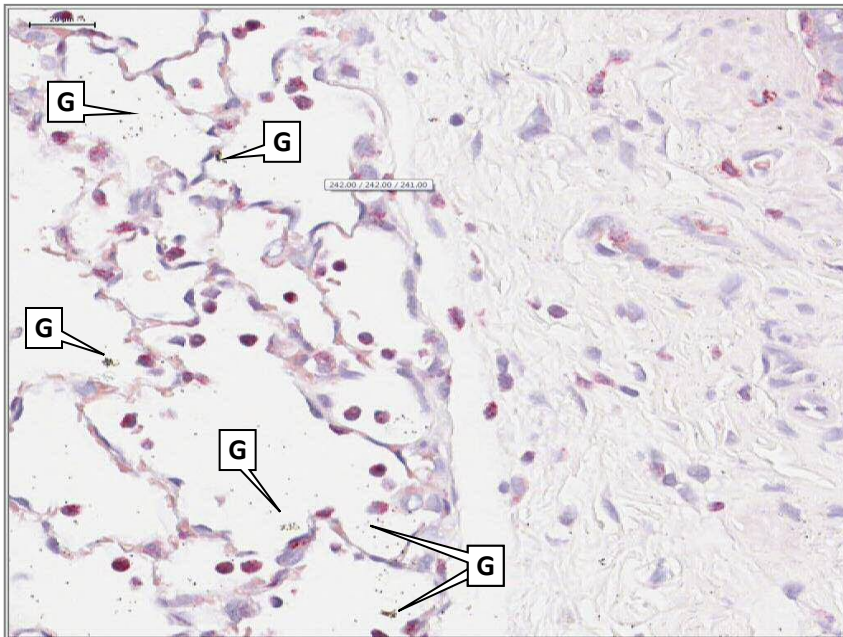


Method of LPS administration 4 hours before bronchoalveolar lavage of lungs

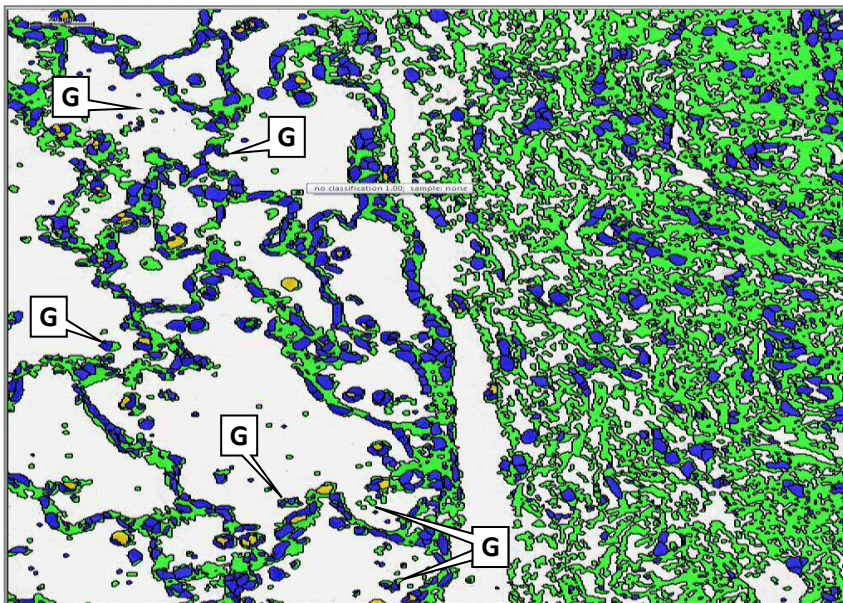
**Figure A1: Induction of inflammation in rat lungs after administration of lipopolysaccharide via three exposure routes.** Rats (n=3/group) were administered lipopolysaccharide in phosphate buffered saline by intratracheal instillation (2  $\mu\text{g}/\text{rat}$ ; bolus) or inhalation (150  $\mu\text{g}/\text{mL}$  nebulised; 15 minutes). Rats were euthanized four hours post dose and lungs lavaged for cell counts. **A1A:** Penn Century microsprayer (without syringe). **A1B:** intratracheal dosing of a rat under light anaesthesia; vocal folds were visualized by a cold light source to facilitate passage of the cannula into the trachea. **A1C:** whole body inhalation exposure of rats. **A1D:** snout-only inhalation exposure of rats. **A1E:** absolute neutrophil counts in bronchoalveolar lavage fluid (BALF). **A1F:** neutrophils as percentage of leukocytes in BALF.

## Appendix 2: Examples of technical issues that compromised image analysis of rat lungs

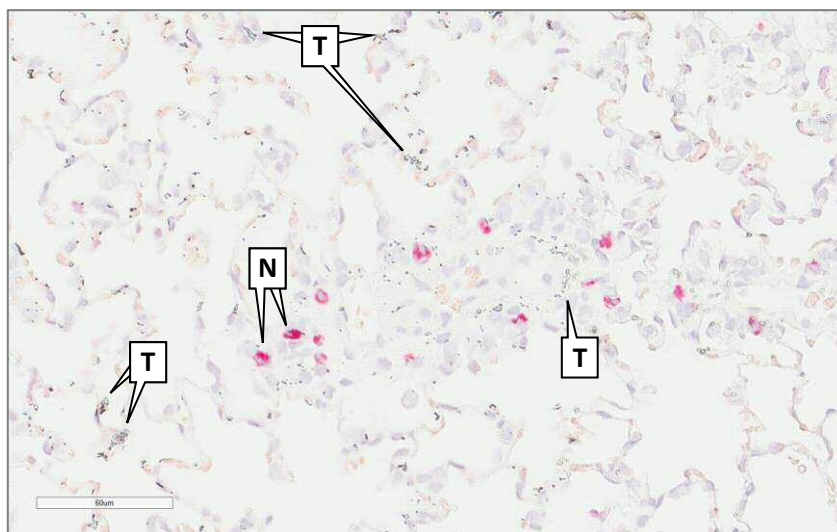
A2A



A2B



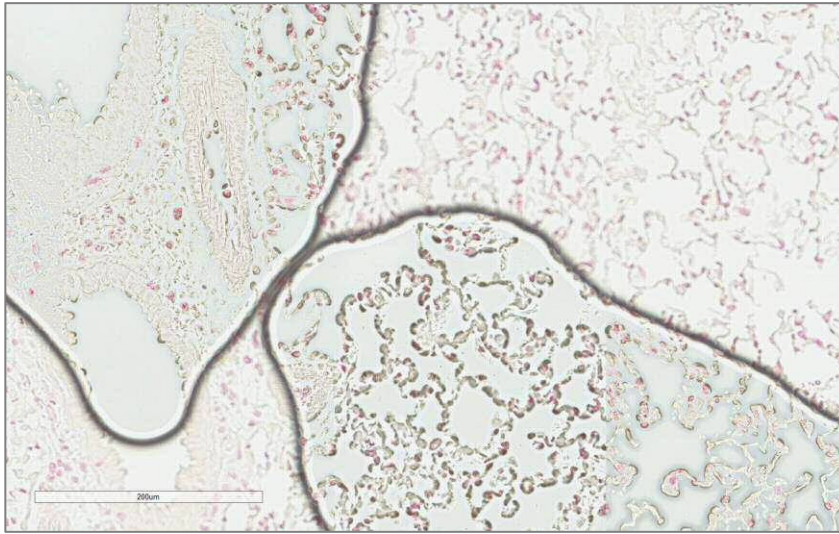
**Figure A2: Contaminant dust erroneously identified as lung tissue.** Rat lungs (formalin-fixed, paraffin wax-embedded) were sectioned and stained for chloroacetate esterase (CAE; biomarker of neutrophils); cell nuclei were counterstained blue with haematoxylin. **A2A:** fine particles (G) in empty areas of the slide and superimposed over tissue; the dust was generated during etching of the glass slide with sample identification details. **A2B:** colour overlay during image analysis identified fine particles (G) as part of the lung tissue (green) or cell nuclei (blue).

**Appendix 2: Examples of technical issues that compromised image analysis of rat lungs (continued)****A2C****A2D**

**Figure A2: Translucent structures erroneously identified as lung tissue.** Rat lungs (formalin-fixed, paraffin wax-embedded) were sectioned and stained for chloroacetate esterase (CAE; biomarker of neutrophils); cell nuclei were counterstained blue with haematoxylin. **A2C:** translucent structures (T) overlaying tissue were associated with the dehydration and drying of sections; CAE-stained neutrophils (N) also shown. **A2D:** translucent structures could be dissolved using an organic solvent (industrial methylated spirits or tertiary butanol used) but this depleted the CAE stain (red) and haematoxylin stain.

**Appendix 2: Examples of technical issues that compromised image analysis of rat lungs (continued)**

**A2E**



**A2F**

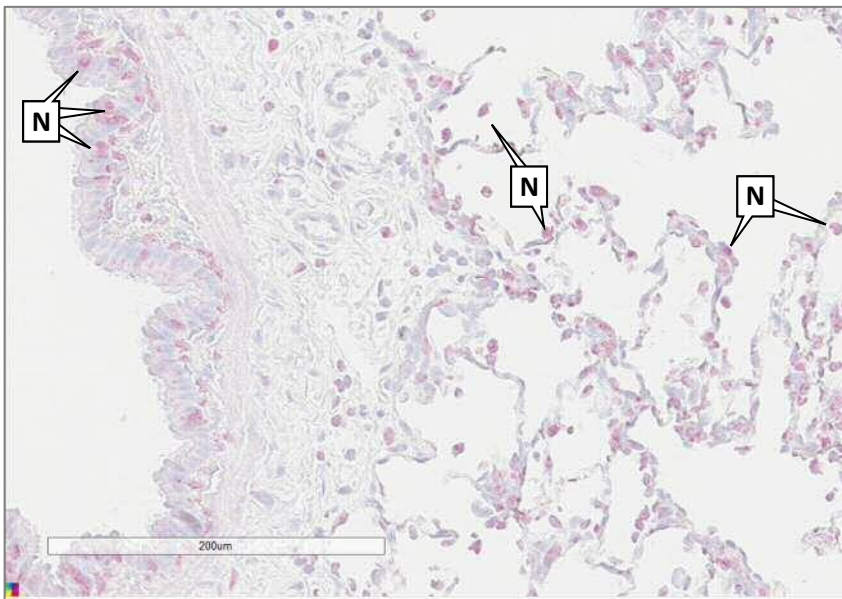


**Figure A2: Air bubbles trapped beneath a glass coverslip compromised image analysis of lung tissue.** Rat lungs (formalin-fixed, paraffin wax-embedded) were sectioned and stained for chloroacetate esterase (CAE; biomarker of neutrophils); cell nuclei were counterstained blue with haematoxylin. **A2E:** air bubbles trapped when a coverslip was applied and set using Entellan<sup>®</sup> rapid mounting medium (Sigma Aldrich). **A2F:** aqueous hard-setting mount warmed to 40°C and used to fix the coverslip eliminated bubbles. CAE-stained neutrophils (N) shown; staining of lung tissue is pale but sufficient for lung image analysis.

### Appendix 3: *In vitro* assessment of cytotoxicity, morphology and pro-inflammatory mediator release of NR8383 rat alveolar macrophage cells treated with GSK-899 or GSK-677

V31206N (eLNB: N27241-10) & V31257N (eLNB: N27241-11)

Investigative study to assess cytotoxicity, pro-inflammatory mediator release and morphology following treatment of NR8383 rat alveolar macrophage cells with GSK258899B and GSK610677B over 72 hours.

#### Introduction

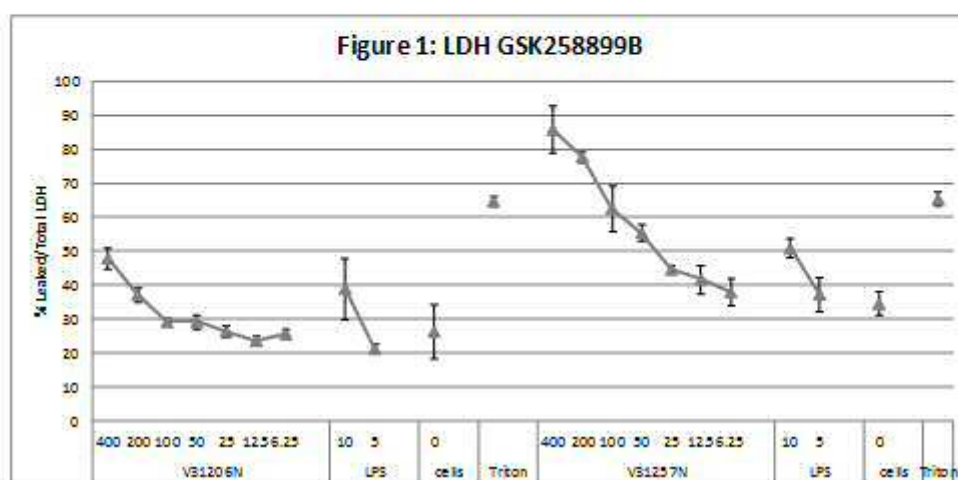
These studies were carried out to measure cytotoxicity and cytokine release of NR8383 cells following a concentration range of treatments with test compounds after 72 hours. The following endpoints were assessed in the study:

- General morphology by phase microscopy.
- Lactate dehydrogenase (LDH) leakage to assess cytotoxicity.
- TNF $\alpha$ , MCP-1, IL-1 $\alpha$ , CXCL1/rKC/GRO and IL-1 $\beta$  by MSD to assess inflammatory mediator release.
- TEM images analysed for morphological changes and evidence of toxicity.

#### Viability

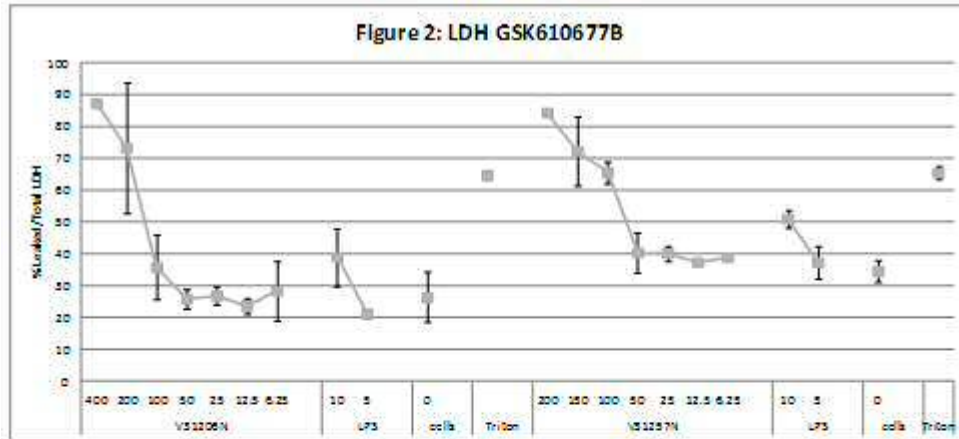
Cellular viability was quantified by measuring the % LDH leaked from the cells. The Triton X-100 positive control produced a response between 60-70% for both studies. The media treated cell negative control produced a response of between 20-40% for both studies. These were acceptable values for controls within this assay.

The LDH leakage data for GSK258899B in Figure 1 shows a concentration dependent increase but also a large difference between replicate studies. This is likely due to the known insolubility of the compound and difficulty in obtaining an accurate serial dilution. For GSK610677B, the leaked LDH levels were also shown to increase in a concentration dependent manner (Figure 2). In study V31257N, it was evident that the lower non-toxic concentrations gave slightly higher LDH leaked values compared to V31206N and overall the data in this study were shifted higher on the graph, however, the toxicity profiles in both studies were similar. ]



**Appendix 3: *In vitro* assessment of cytotoxicity, morphology and pro-inflammatory mediator release of NR8383 cells treated with GSK-899 or GSK-677 (continued)**

V31206N (eLNB: N27241-10) & V31257N (eLNB:N27241-11)



A signal window (0-100%) was calculated to determine the % cytotoxicity and the data was plotted in Graphpad to enable curves to be generated for curve comparison and EC50 values estimated (Figure 2.5).

The EC50 values were combined from both V31206N and V31257N. All the % cytotoxicity values from both studies were plotted together on one graph to give the overall EC50.

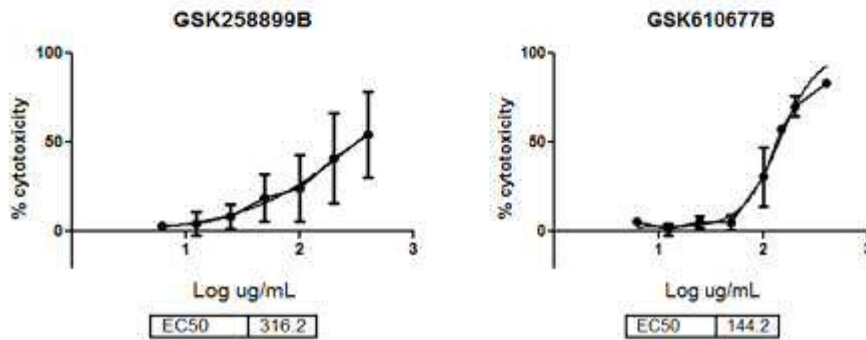


Figure 2.5

**Appendix 3: *In vitro* assessment of cytotoxicity, morphology and pro-inflammatory mediator release of NR8383 cells treated with GSK-899 or GSK-677 (continued)**

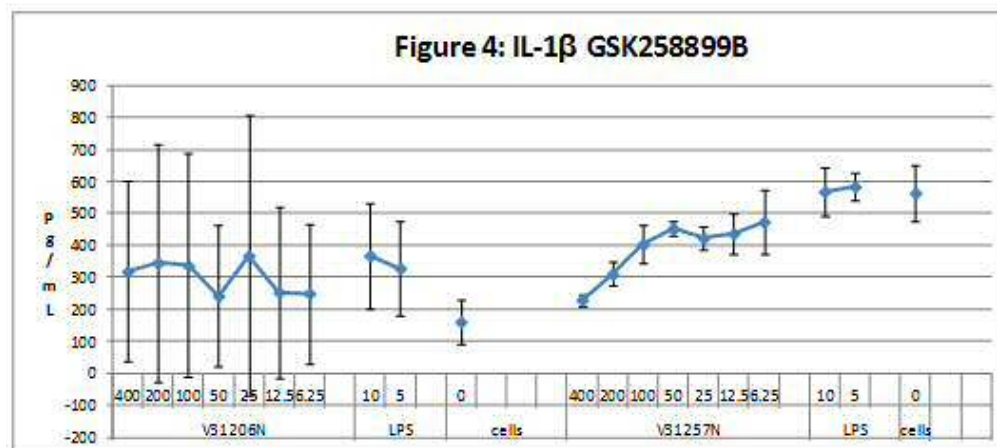
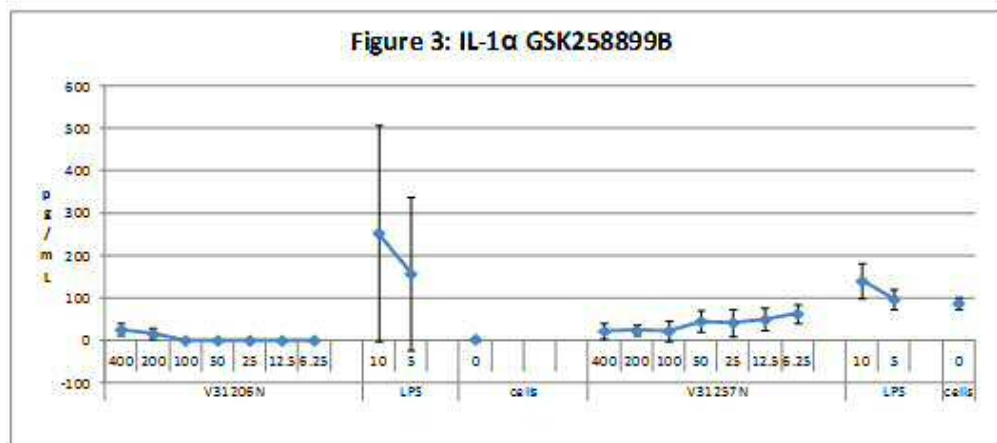
V31206N (eLNB: N27241-10) & V31257N (eLNB: N27241-11)

**Activation**

MSD analysis was carried out to measure the levels of cytokines and chemokines in the collected supernatant.

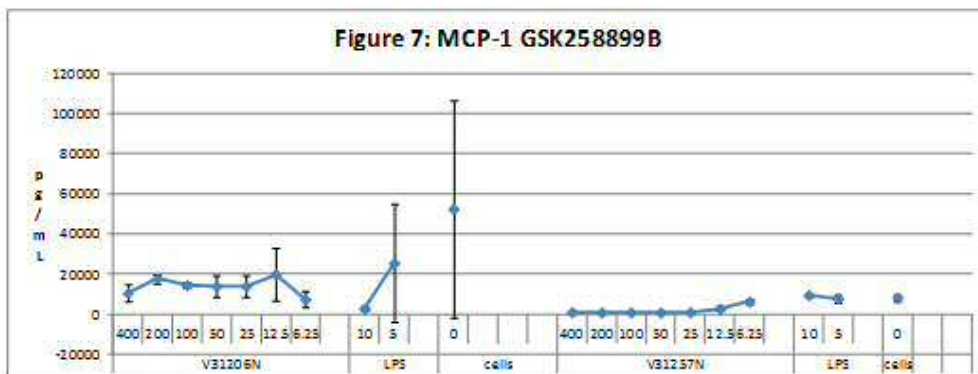
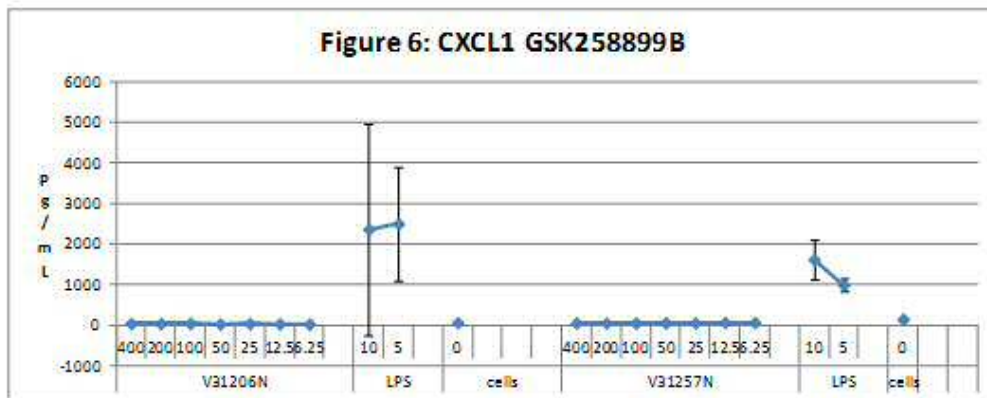
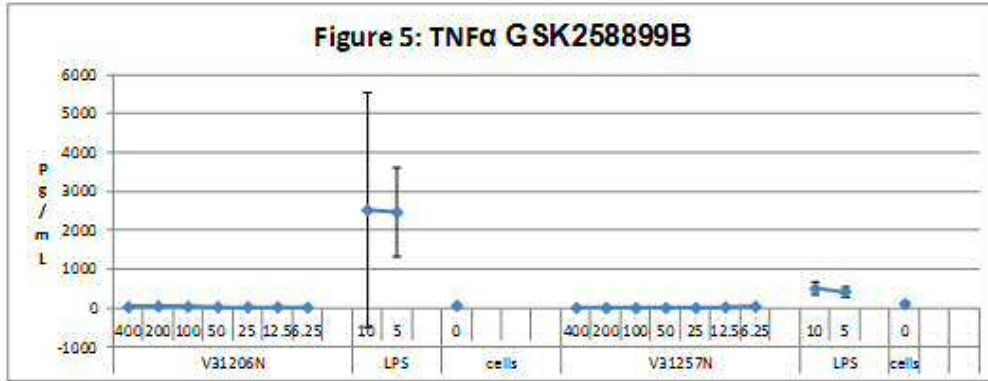
In both studies, there were no compound concentration dependent changes for GSK258899B or GSK610677B. For V31206N, LPS positive control values appeared variable indicated by the large error bars, which was not seen in the repeat study (V31257N).

It is considered there is minimal to no change in all cytokine levels for GSK258899B across both studies, although large error bars show the data is more variable in V31206N. IL-1b levels for GSK258899B (Figure 4) and MCP-1 levels for GSK610677B (Figure 12) were less variable in the repeat study V31257N compared to the first study with both compounds.



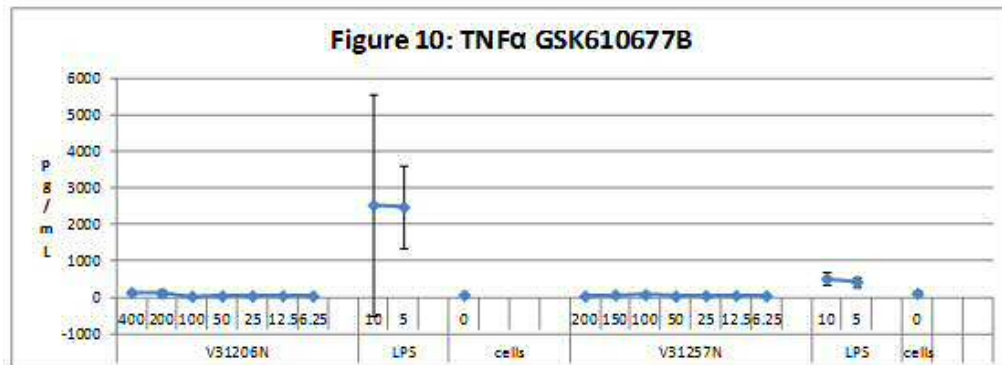
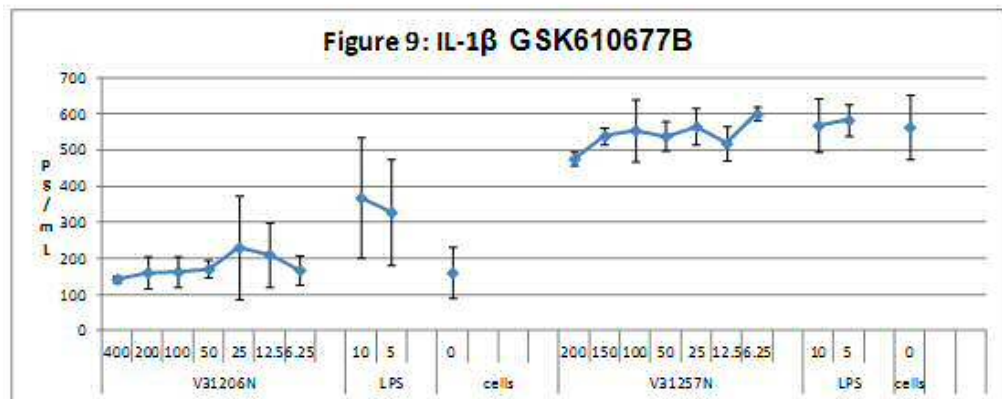
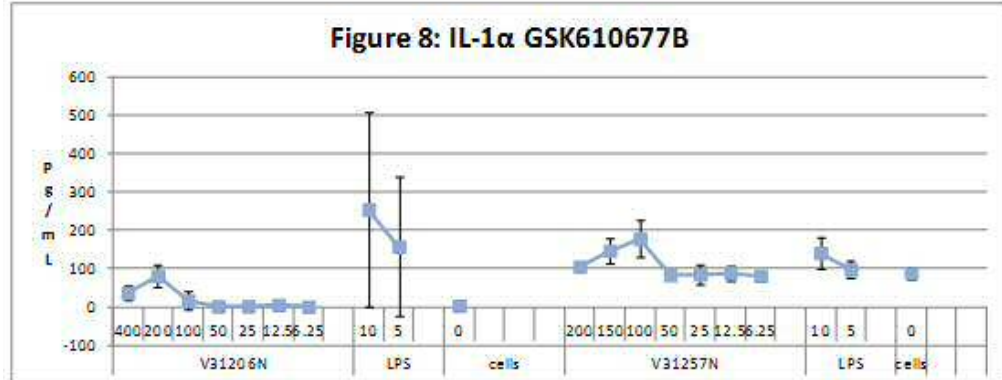
**Appendix 3: *In vitro* assessment of cytotoxicity, morphology and pro-inflammatory mediator release of NR8383 cells treated with GSK-899 or GSK-677 (continued)**

V31206N (eLNB: N27241-10) & V31257N (eLNB:N27241-11)



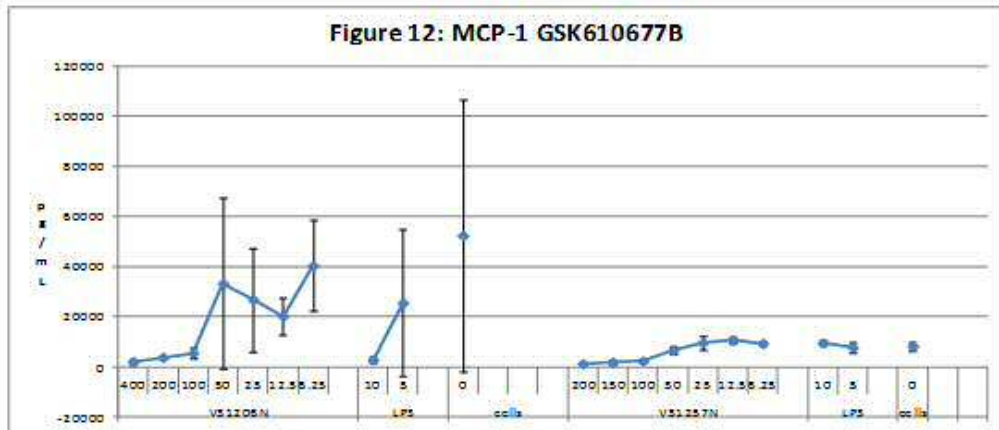
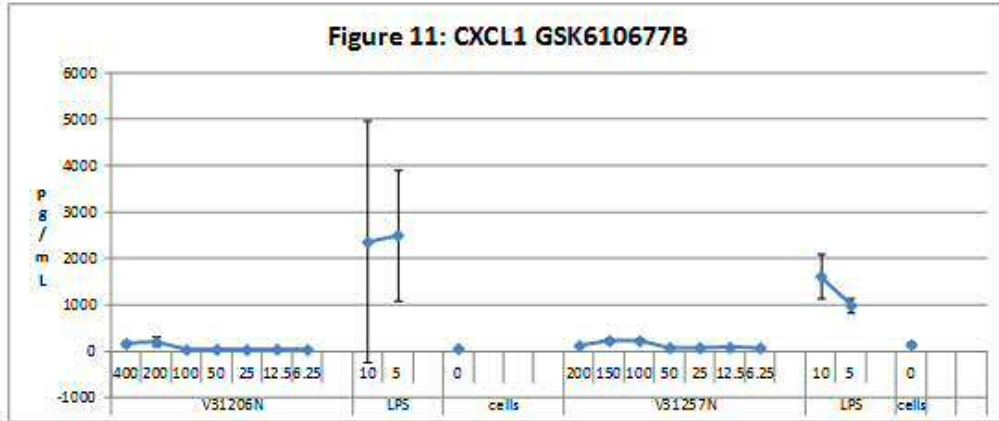
**Appendix 3: *In vitro* assessment of cytotoxicity, morphology and pro-inflammatory mediator release of NR8383 cells treated with GSK-899 or GSK-677 (continued)**

V31206N (eLNB: N27241-10) & V31257N (eLNB:N27241-11)



**Appendix 3: *In vitro* assessment of cytotoxicity, morphology and pro-inflammatory mediator release of NR8383 cells treated with GSK-899 or GSK-677 (continued)**

V31206N (eLNB: N27241-10) & V31257N (eLNB: N27241-11)



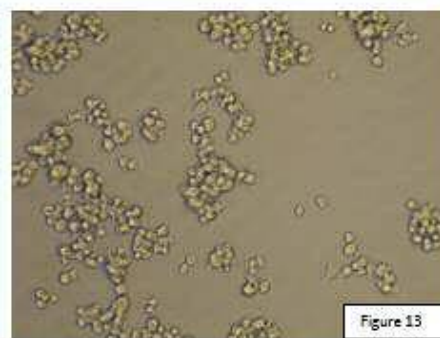
**Appendix 3: *In vitro* assessment of cytotoxicity, morphology and pro-inflammatory mediator release of NR8383 cells treated with GSK-899 or GSK-677 (continued)**

V31206N (eLNB: N27241-10) & V31257N (eLNB:N27241-11)

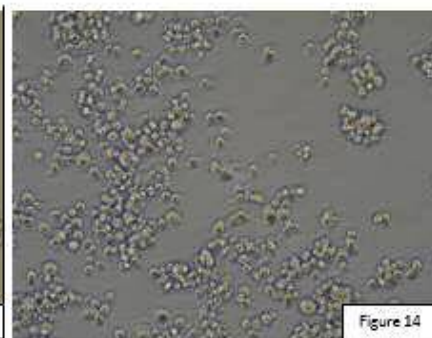
**Morphology**

Cells were visualised by phase contrast microscopy and in both studies. The cells only untreated images appeared the same across the plates in both studies, the regular morphology of the NR8383 cell appears spread fairly evenly across the wells, uniform in size and a clear/pale body with only a few small clusters of cells (Figures 13 & 14).

V31206N cells only (x200).

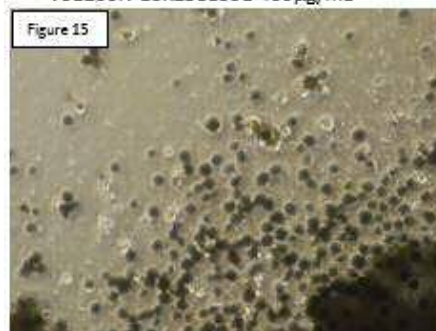


V31257N cells only (x200).



- GSK258899B. At the highest concentration of 400µg/mL (figures 15 & 16), in both studies the cells look swollen and there are large amounts of particulate visible in the well. Cells can be seen enlarged and darker in colour, having phagocytosed the test material. At 50µg/mL and below, cells appear normal in their morphology (Figures 17 & 18). All images are x200 magnification unless otherwise stated.

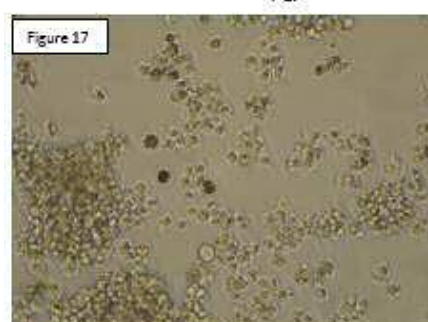
V31206N GSK258899B 400µg/mL



V31257N GSK258899B 400µg/mL



V31206N GSK258899B 25µg/mL



V31257N GSK258899B 25µg/mL

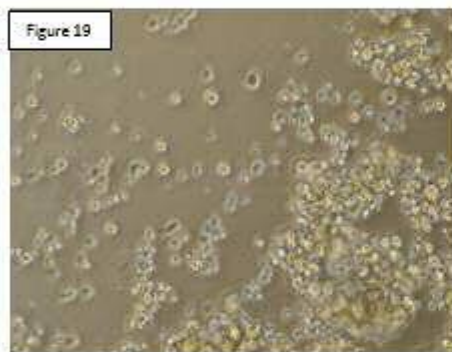


**Appendix 3: *In vitro* assessment of cytotoxicity, morphology and pro-inflammatory mediator release of NR8383 cells treated with GSK-899 or GSK-677 (continued)**

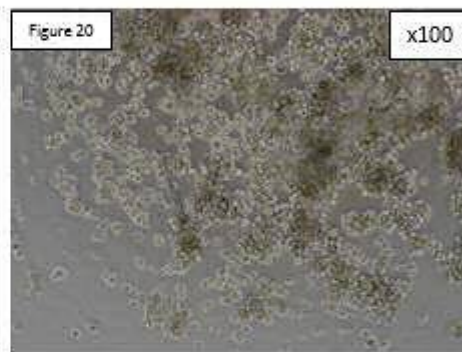
V31206N (eLNB: N27241-10) & V31257N (eLNB:N27241-11)

- GSK610677B. Cells appear to have been minimally affected morphologically at all concentrations, with some slight particulate visible (possibly insoluble test material) in the 200µg/mL sample in study V31206N (Figure 19). All images are taken at x200 magnification unless stated otherwise.

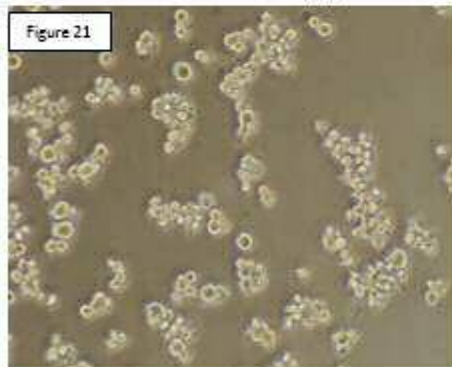
V31206N GSK610677B 200µg/mL



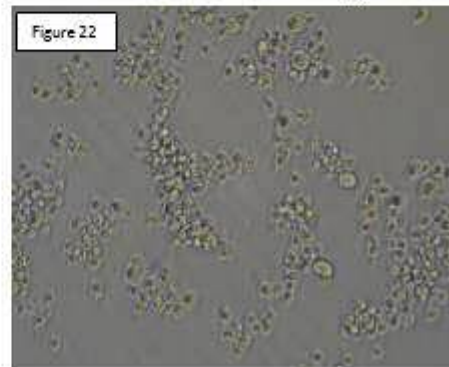
V31257N GSK610677B 150µg/mL



V31206N GSK610677B 12.5µg/mL



V31257N GSK610677B 12.5µg/mL



### Appendix 3: *In vitro* assessment of cytotoxicity, morphology and pro-inflammatory mediator release of NR8383 cells treated with GSK-899 or GSK-677 (continued)

V31206N (eLNB: N27241-10) & V31257N (eLNB:N27241-11)

#### Transition Electron Microscopy (TEM).

Cells were harvested after a 72 hr treatment with GSK258899B and GSK610677B and fixed for TEM, to assess ultrastructural effects of these compounds. Table 1 represents TEM data for GSK258899B which was carried out in study V31206N, while TEM for GSK610677B was carried out in study V31257N and results are represented in Table 2.

Table 1.

Cell Sample		% Cells (n=100) containing LLBs	% Necrotic cells (n=100)	Key Observations
Untreated		0	<1	
Chloroquine	5 µg/ml	100	6	
GSK258899B	50 µg/ml	0	1	
	400 µg/ml	0	8	All cells contained crystalline clefts consistent with endocytosed test material

In study V31206N, the untreated cells were of typical appearance consistent with that of untreated cells in previous studies. There were no Lysosomal Lamellar Bodies (LLB) present at the concentrations assessed for GSK258899B, which represents the highest concentration tested in these studies as well as one in the middle of the concentration range which is non-toxic based on the LDH leakage data. At 50µg/mL the numbers of cells containing cytoplasmic vacuoles and the incidence of these vacuoles was considered to be only slightly increased compared to the untreated cells. This may reflect an increase in endocytosis or a slowdown in membrane recycling. A small proportion of cells (8%) at 400µg/mL were necrotic, but the incidence of necrosis was low. All observed cells at 400µg/mL contained crystalline clefts within the cytoplasm, which represents endocytosed crystalline test material. A very small proportion of cells (6%) treated with the positive control (chloroquine 5 µg/ml) for LLBs were necrotic, but 100% of cells showed evidence of LLBs consistent with accumulation of phospholipid within lysosomes.

In study V31257N, the untreated cells were of a typical appearance consistent with that of untreated cells in previous studies. Two concentrations of GSK610677B were selected for TEM assessment in this study based on the LDH leakage results as well as phase contrast morphological images. Unfortunately at the highest concentration selected (200 µg/ml), all cells were necrotic and it was not possible to view LLBs in the necrotic cells. At the next highest non-cytotoxic concentration determined by LDH leakage (50 µg/ml), a small proportion of cells were necrotic (15%), and it was

**Appendix 3: *In vitro* assessment of cytotoxicity, morphology and pro-inflammatory mediator release of NR8383 cells treated with GSK-899 or GSK-677 (continued)**

V31206N (eLNB: N27241-10) & V31257N (eLNB:N27241-11)

possible to make an assessment on the ultrastructural morphology of the cells. A large proportion of these cells had membrane bound bodies containing vesicles and/or lamellar material or amorphous material. The bodies that contained lamellar material appeared to be developing into LLBs. Unfortunately all cells treated with the positive control for LLBs (chloroquine 5 µg/ml) were necrotic. This was an unexpected finding since in previous studies, and with historical data at this concentration, chloroquine had not caused a significant increase in necrosis. It was therefore not possible to recognise lysosomal lamellar bodies (LLBs) in the necrotic cells.

Table 2.

Cell Sample		% Necrotic cells (n=100)	Key Observations
Untreated		7%	
Chloroquine	5 µg/ml	100%	
GSK610677B	50 µg/ml	15%	41% cells contain secondary lysosomes containing lamellar or vesicular material that on occasions appeared to be developing LLBs
	200 µg/ml	100%	

**Conclusion.**

GSK258899B: The high EC50 value for cytotoxicity associated with GSK258899B over 72 hours in these studies indicated that it is a low hazard for cellular toxicity. Although a higher LDH leakage for GSK258899B was observed in one study only over the same concentration range, this is likely to be attributed to the known insolubility of the compound. GSK258899B did not elicit cytokine/chemokine activation after 72 hour treatment, therefore activation of the cells and inflammatory mediator release is considered to be a low hazard with this compound. After morphological assessment with GSK258899B, endocytosed particulate test material was evident at the higher concentrations by phase contrast morphology and observed as crystalline clefts in all cells at 400 µg/ml when assessed by TEM. Although results for GSK258899B indicates a low hazard for cytotoxicity and cell activation, it should however be classified as a moderate risk compound when considering compound particulate accumulation within the cells.

GSK610677B: The high EC50 value for cytotoxicity associated with GSK610677B over 72 hours in these studies indicated that it is a low hazard for cellular toxicity. GSK610677B did not elicit cytokine/chemokine activation after 72 hour treatment, therefore activation of the cells and inflammatory mediator release is also considered to be a low hazard with this compound. Although no obvious effects were seen morphologically by phase contrast microscopy, by TEM there was evidence of secondary lysosomes containing lamellar or vesicular material that on occasions appeared to be developing LLBs, and it is for this reason that GSK610677B is considered a moderate risk compound.

Signature: (Anita Naidoo)

*A. Naidoo*

Date:

*2nd July 2015*

### Appendix 3: *In vitro* assessment of cytotoxicity, morphology and pro-inflammatory mediator release of NR8383 cells treated with GSK-899 or GSK-677 (continued)

#### Transmission Electron Microscopy of NR8383 cells for Study V31206N.

Paul McGill 20<sup>th</sup> March 2015

#### Tabulated Summary

Cell Sample		% Cells (n=100) containing LLBs	% Necrotic cells (n=100)	Key Observations
Untreated		0	<1	
Chloroquine	5 µg/ml	100	6	
GSK258899B	50 µg/ml	0	1	
	400 µg/ml	0	8	All cells contained crystalline clefts consistent with endocytosed test material

LLBs= lysosomal lamellar bodies

#### Observations

##### Untreated Cells

The ultrastructural appearance of the cells (Figure 1 and Figure 2) was similar to that of NR8383 cells in previously examined untreated cell samples. This included the presence of a few small to medium sized membrane bound cytoplasmic vacuoles in a small proportion of cells. These vacuoles were largely electron lucent and were probably endocytic, endosomal or lysosomal in origin.

##### Chloroquine 5 µg/ml

All the observed cells contained lysosomal lamellar bodies (LLBs) (Figure 3 and Figure 4) consistent with accumulation of phospholipid within lysosomes. Otherwise, the cells did not show ultrastructural evidence of injury. There were fewer 'electron lucent' cytoplasmic vacuoles compared to the media control sample. This may be because these vacuoles had been utilised in the formation of the LLBs.

##### GSK258899B 50 µg/ml

The appearance of the cells (Figure 5 and Figure 6) was generally similar to that of the untreated cells. The numbers of cells containing cytoplasmic vacuoles and the incidence of these vacuoles was considered to be slightly increased compared to the media control. This may reflect an increase in endocytosis or a slowdown in membrane recycling. There was no ultrastructural evidence of cell injury.

##### GSK258899B 400 µg/ml

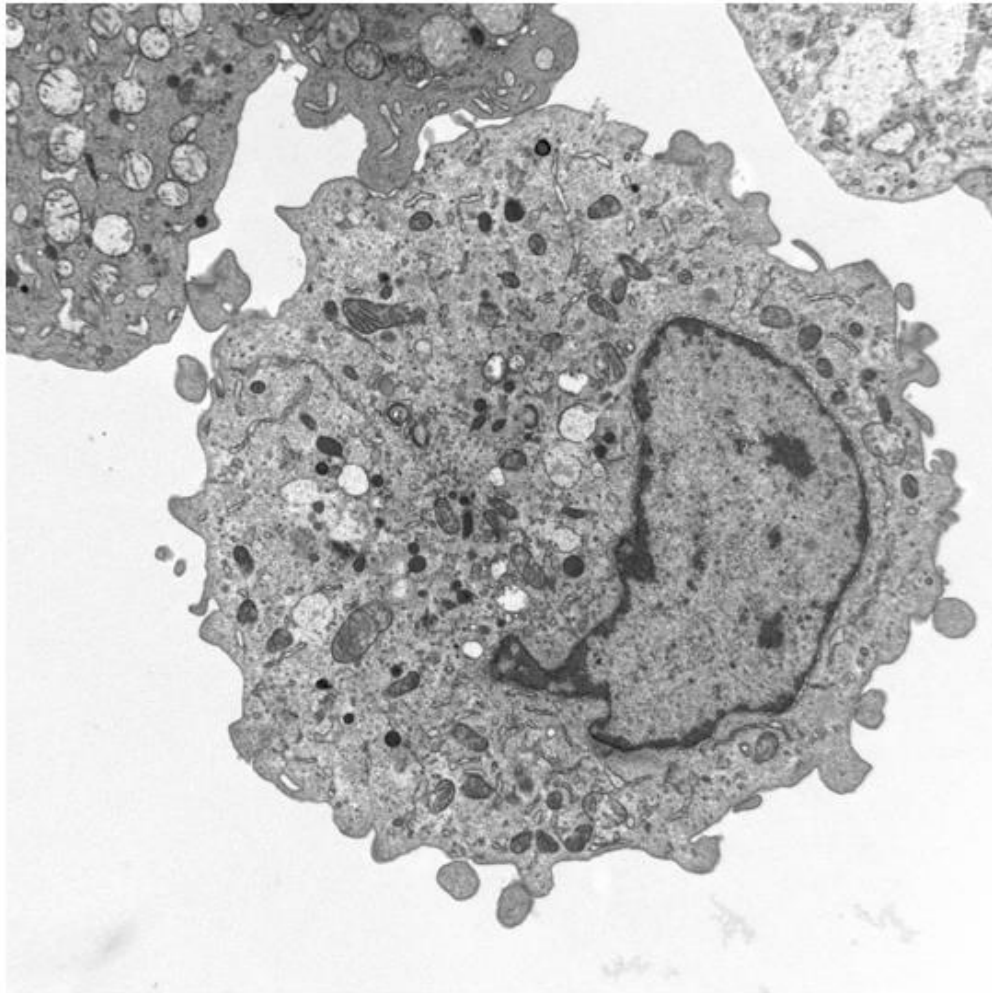
All observed cells contained crystalline clefts within the cytoplasm (Figure 7 to Figure 10 inclusive). These were considered to represent endocytosed crystalline test material and were often observed within medium electron dense cytoplasmic bodies (Figure 8 and Figure 9) that were considered to be

endocytic vacuoles and/or lysosomes. A small proportion of cells were necrotic, and all of these contained crystalline clefts consistent with the test material (Figure 10). The incidence of necrosis was low and not much, if at all, above normal levels.

**Appendix 3: *In vitro* assessment of cytotoxicity, morphology and pro-inflammatory mediator release of NR8383 cells treated with GSK-899 or GSK-677 (continued)**

**Figures**

Figure 1 Untreated Cell Sample



V31206N.010.tif  
EM 43534 NR8383 cells  
Untreated cells  
Print Mag: 10300x @ 7.0 in  
12:20 03/17/15  
Microscopist: pjm41508

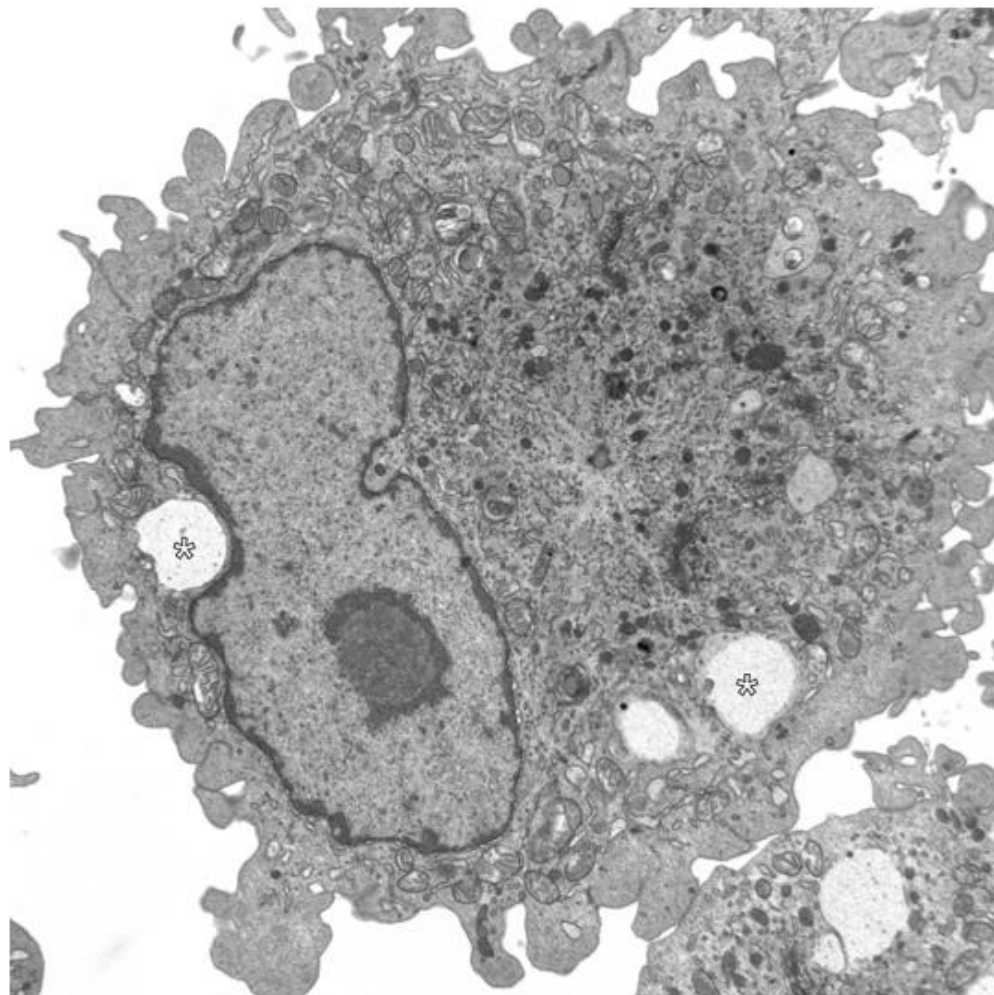
2 microns  
HV=80.0kV  
Direct Mag: 8000x  
GSK UK



Cell from the media control sample showing a typical appearance.

**Appendix 3: *In vitro* assessment of cytotoxicity, morphology and pro-inflammatory mediator release of NR8383 cells treated with GSK-899 or GSK-677 (continued)**

Figure 2 Untreated Cell Sample



V31206N.009.tif  
EM 43534 NR8383 cells  
Untreated cells  
Print Mag: 10300x @ 7.0 in  
12:19 03/17/15  
Microscopist: pjm41508

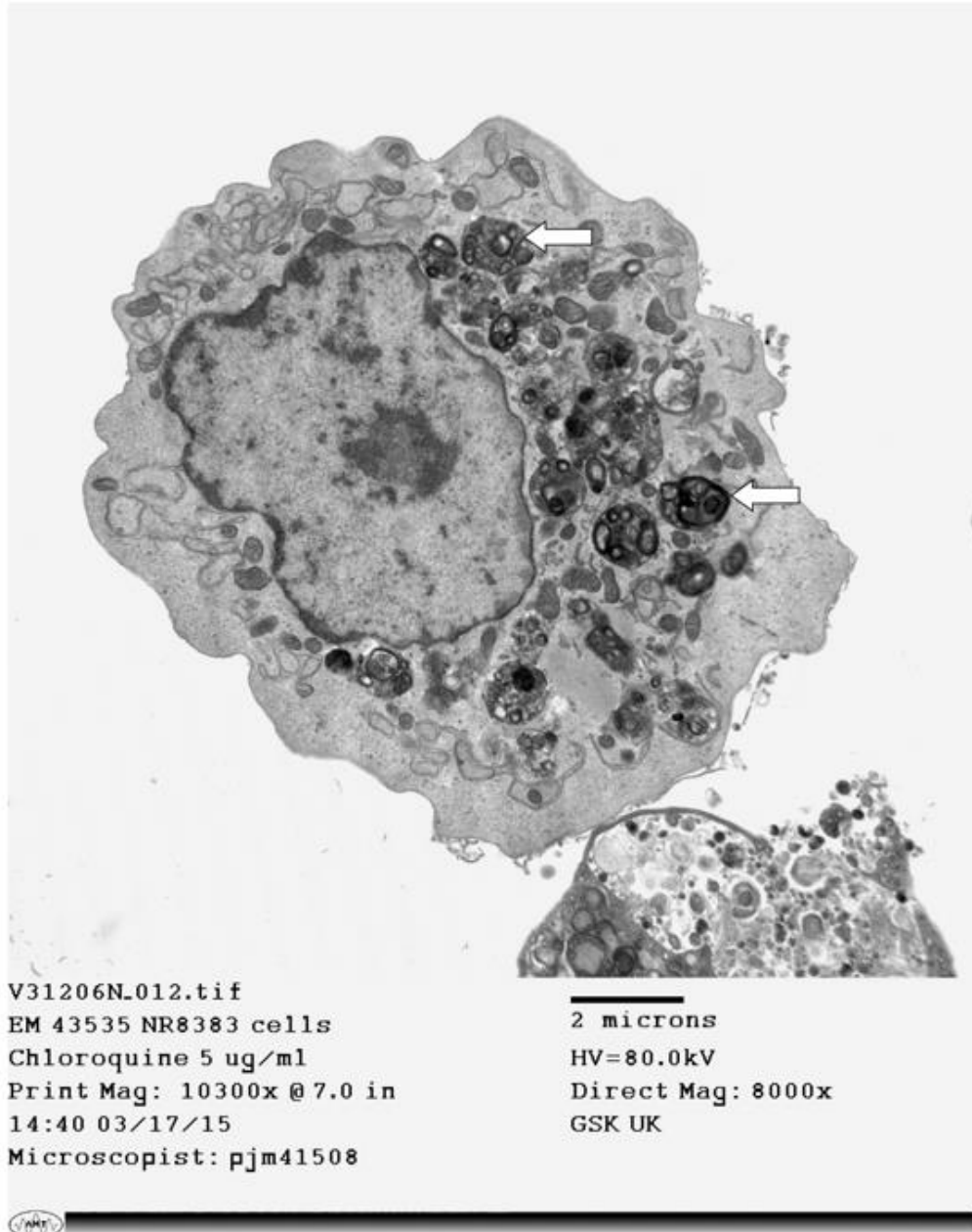
2 microns  
HV=80.0kV  
Direct Mag: 8000x  
GSK UK



Cell from the media control sample showing a typical appearance. The cytoplasm contains a few medium sized membrane-bound vacuoles (\*) of largely electron lucent appearance.

**Appendix 3: *In vitro* assessment of cytotoxicity, morphology and pro-inflammatory mediator release of NR8383 cells treated with GSK-899 or GSK-677 (continued)**

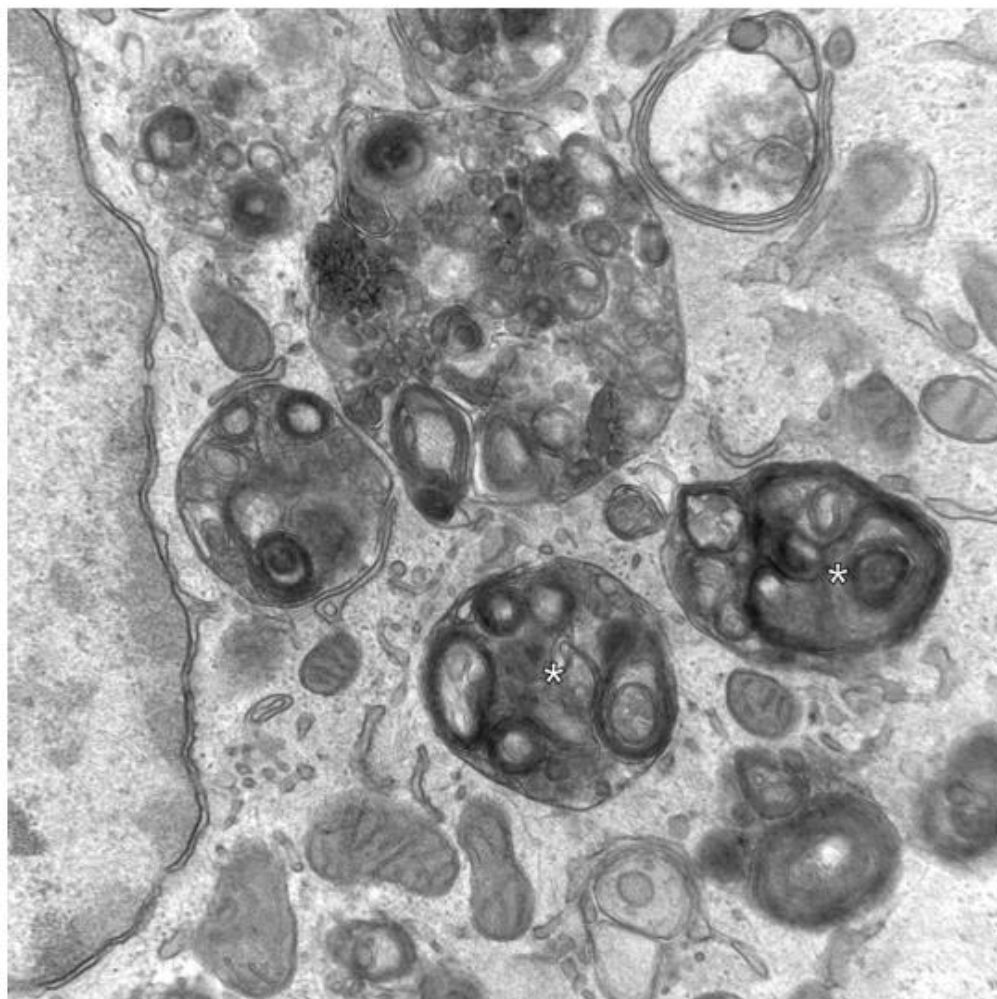
Figure 3 Chloroquine 5 µg/ml



Cell containing lysosomal lamellar bodies (LLBs) (arrows).

**Appendix 3: *In vitro* assessment of cytotoxicity, morphology and pro-inflammatory mediator release of NR8383 cells treated with GSK-899 or GSK-677 (continued)**

Figure 4 Chloroquine 5 µg/ml



V31206N.013.tif  
EM 43535 NR8383 cells  
Chloroquine 5 ug/ml  
Print Mag: 38600x @ 7.0 in  
14:43 03/17/15  
Microscopist: pjm41508

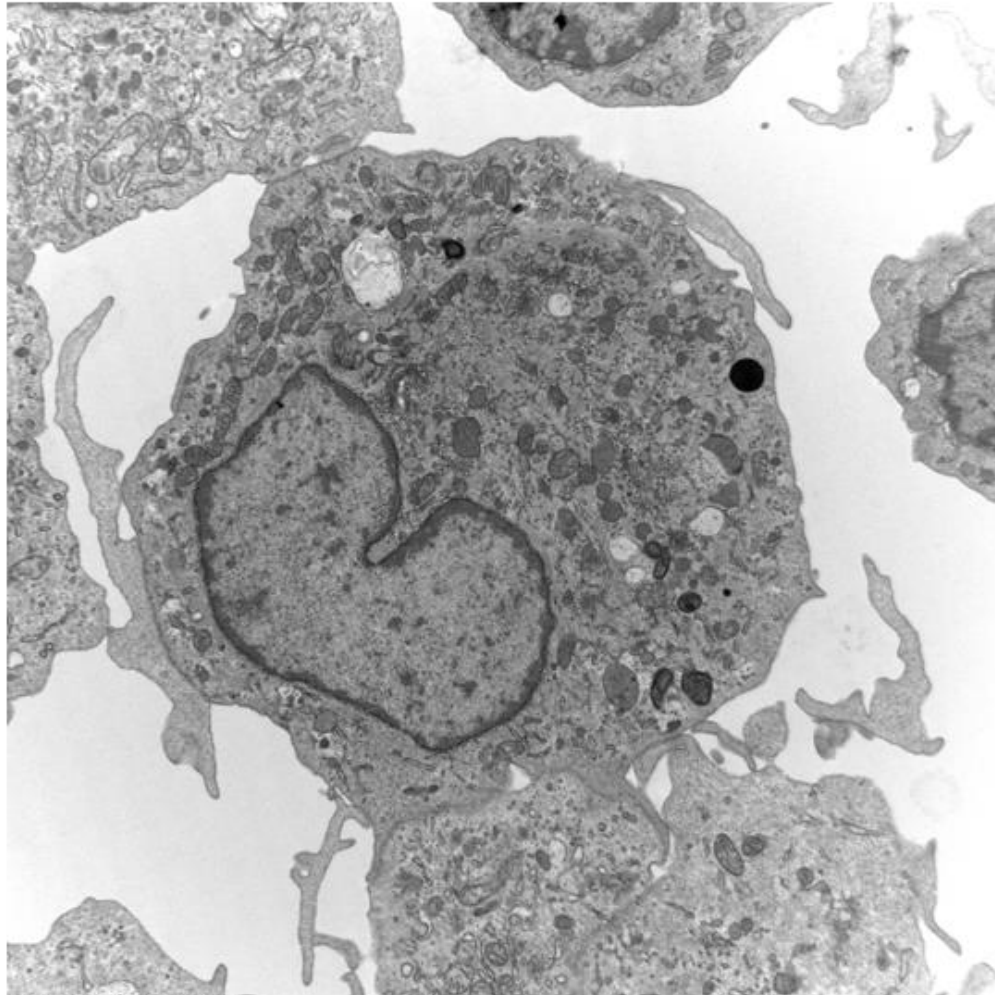
500 nm  
HV=80.0kV  
Direct Mag: 30000x  
GSK UK



Higher magnification of LLBs (\*) seen in Chloroquine treated cells.

**Appendix 3: *In vitro* assessment of cytotoxicity, morphology and pro-inflammatory mediator release of NR8383 cells treated with GSK-899 or GSK-677 (continued)**

Figure 5 GSK258899B 50 µg/ml



V31206N.017.tif

EM 43536 NR8383 cells

GSK258899B 50 ug/ml

Print Mag: 10300x @ 7.0 in

15:04 03/17/15

Microscopist: pjm41508

2 microns

HV=80.0kV

Direct Mag: 8000x

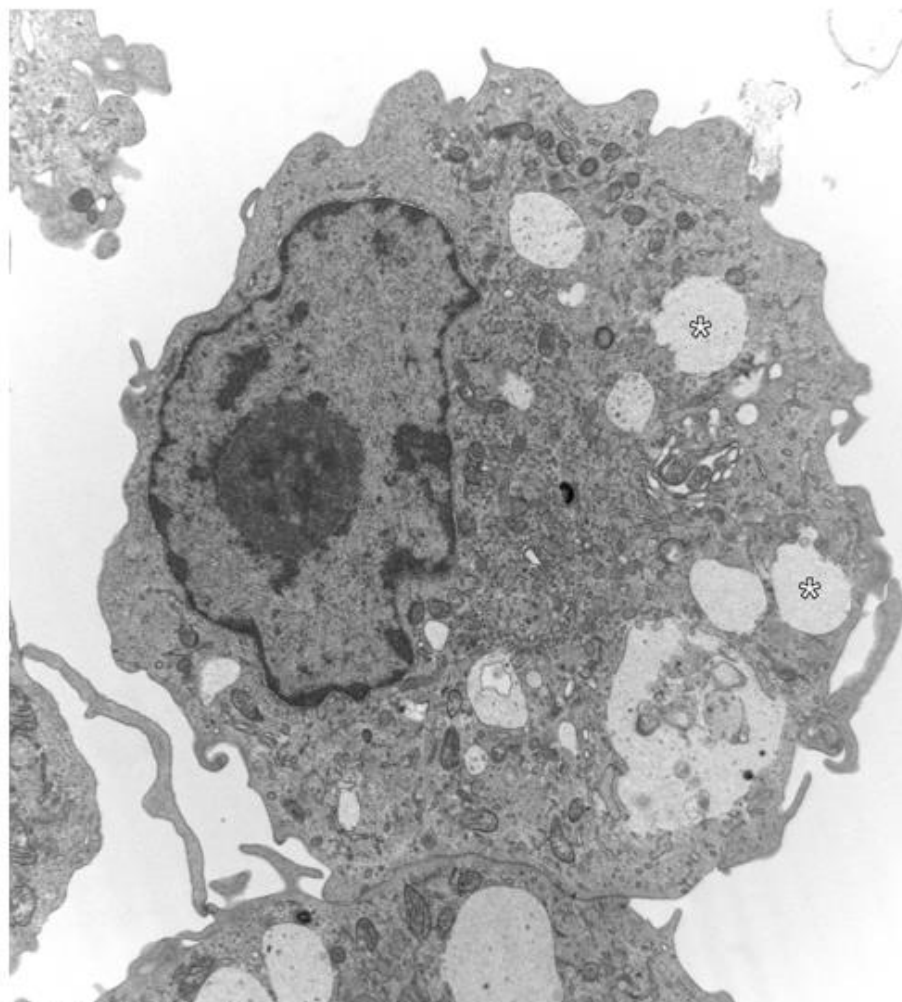
GSK UK



Typical appearance of cell from this sample, which was similar to that of the untreated cells.

**Appendix 3: *In vitro* assessment of cytotoxicity, morphology and pro-inflammatory mediator release of NR8383 cells treated with GSK-899 or GSK-677 (continued)**

Figure 6 GSK258899B 50 µg/ml



V31206N.018.tif

EM 43536 NR8383 cells

GSK258899B 50 µg/ml

Print Mag: 10300x @ 7.0 in

15:08 03/17/15

Microscopist: pj41508

2 microns

HV=80.0kV

Direct Mag: 8000x

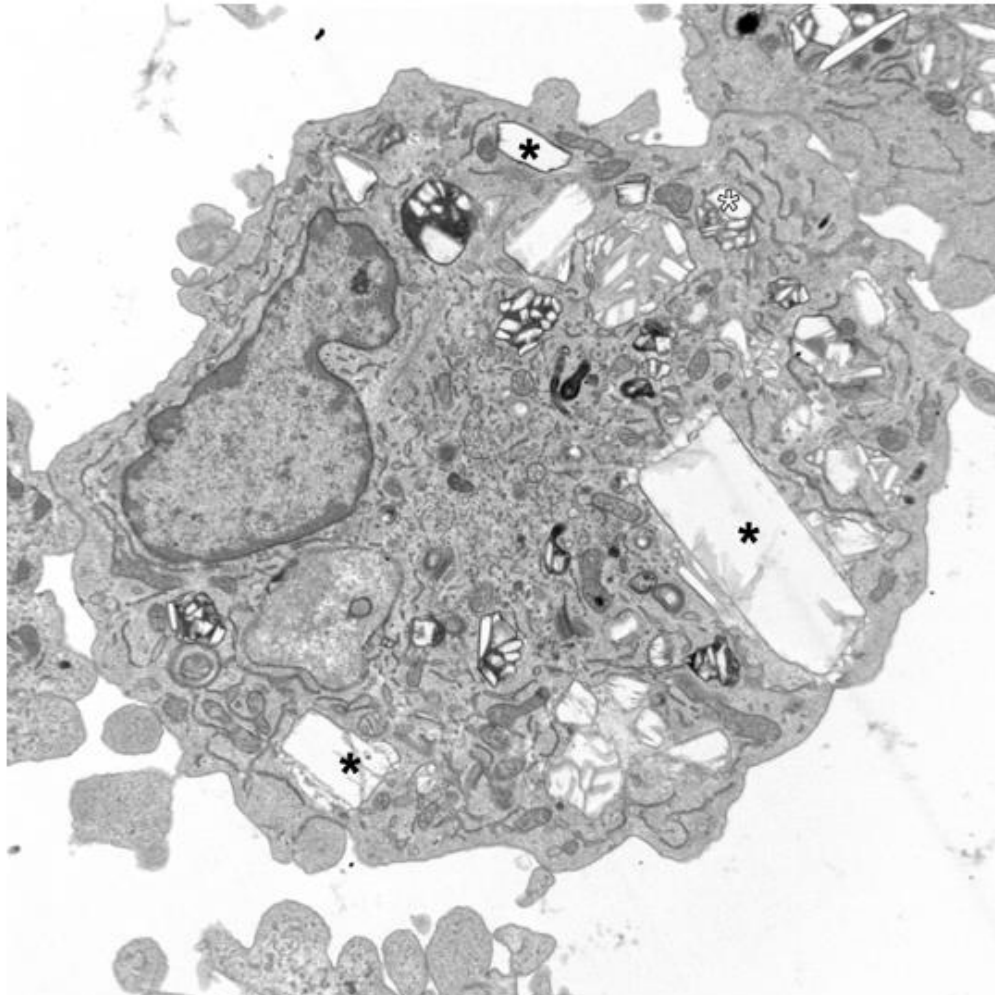
GSK UK



Typical appearance of cell from this sample. There were no apparent ultrastructural differences compared to the untreated cells. In agreement with the untreated cells, a small proportion of cells contained vacuoles of largely electron lucent appearance (\*).

**Appendix 3: *In vitro* assessment of cytotoxicity, morphology and pro-inflammatory mediator release of NR8383 cells treated with GSK-899 or GSK-677 (continued)**

Figure 7 GSK258899B 400 µg/ml



V31206N.006.tif

EM 43537 NR8383 cells

GSK258899B 400 ug/ml

Print Mag: 10300x @ 7.0 in

12:13 03/13/15

Microscopist: pjm41508

2 microns

HV=100.0kV

Direct Mag: 8000x

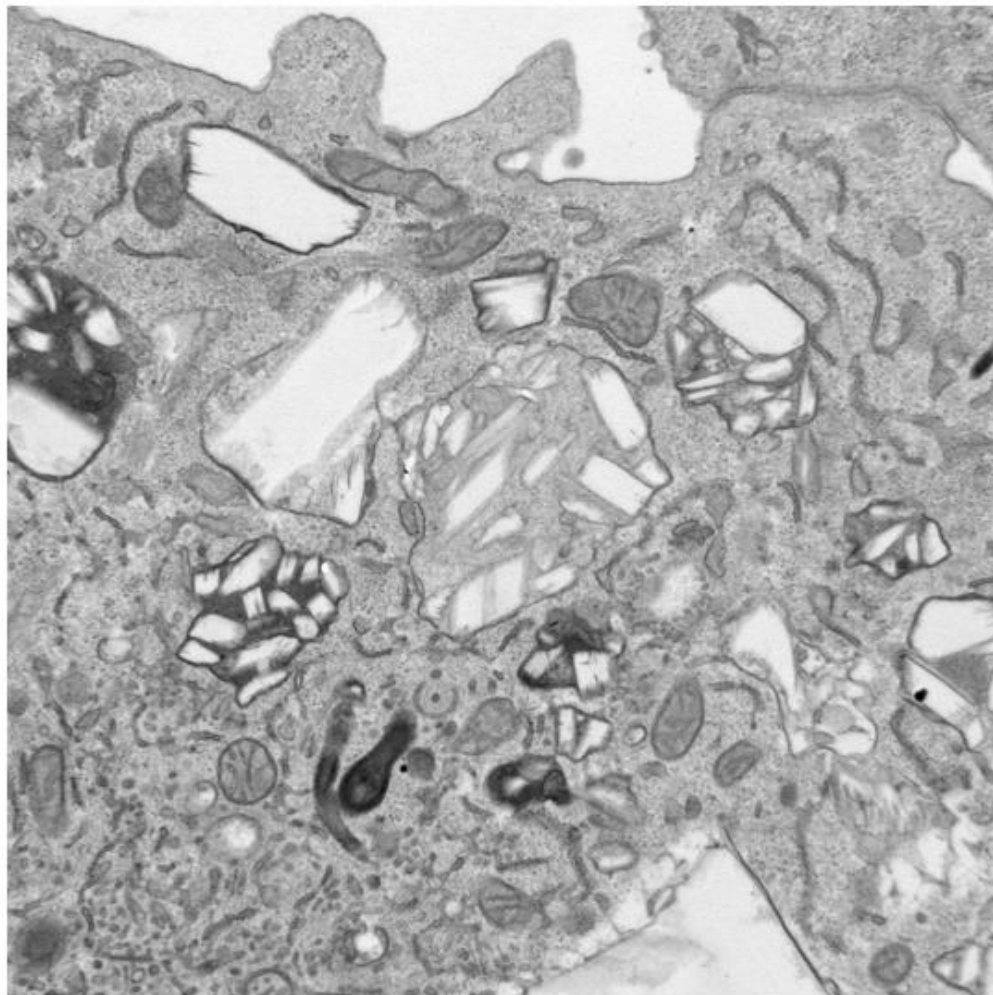
GSK UK



Cell containing electron lucent crystalloid clefts of variable size (\*) consistent with uptake of test article into the cell.

**Appendix 3: *In vitro* assessment of cytotoxicity, morphology and pro-inflammatory mediator release of NR8383 cells treated with GSK-899 or GSK-677 (continued)**

Figure 8 GSK258899B 400 µg/ml



V31206N.007.tif  
EM 43537 NR8383 cells  
GSK258899B 400 µg/ml  
Print Mag: 25700x @ 7.0 in  
12:20 03/13/15  
Microscopist: pjm41508

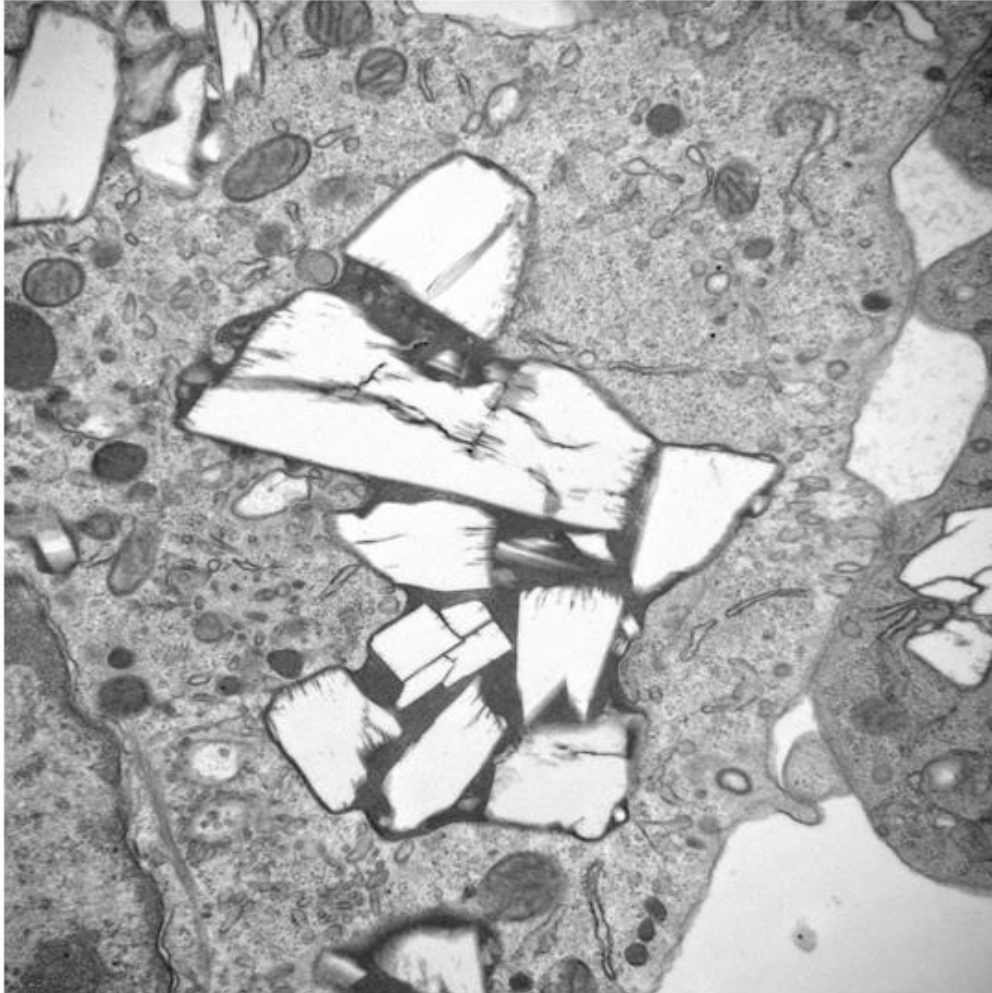
500 nm  
HV=100.0kV  
Direct Mag: 20000x  
GSK UK



Higher magnification of electron lucent crystalline clefts of variable size. The crystalline clefts are within membrane bound bodies probably consistent with lysosomes or endocytic vacuoles.

**Appendix 3: *In vitro* assessment of cytotoxicity, morphology and pro-inflammatory mediator release of NR8383 cells treated with GSK-899 or GSK-677 (continued)**

Figure 9 GSK258899B 400 µg/ml



V31206N.005.tif

EM 43537 NR8383 cells

GSK258899B 400 ug/ml

Print Mag: 25700x @ 7.0 in

12:09 03/13/15

Microscopist: pjm41508

500 nm

HV=100.0kV

Direct Mag: 20000x

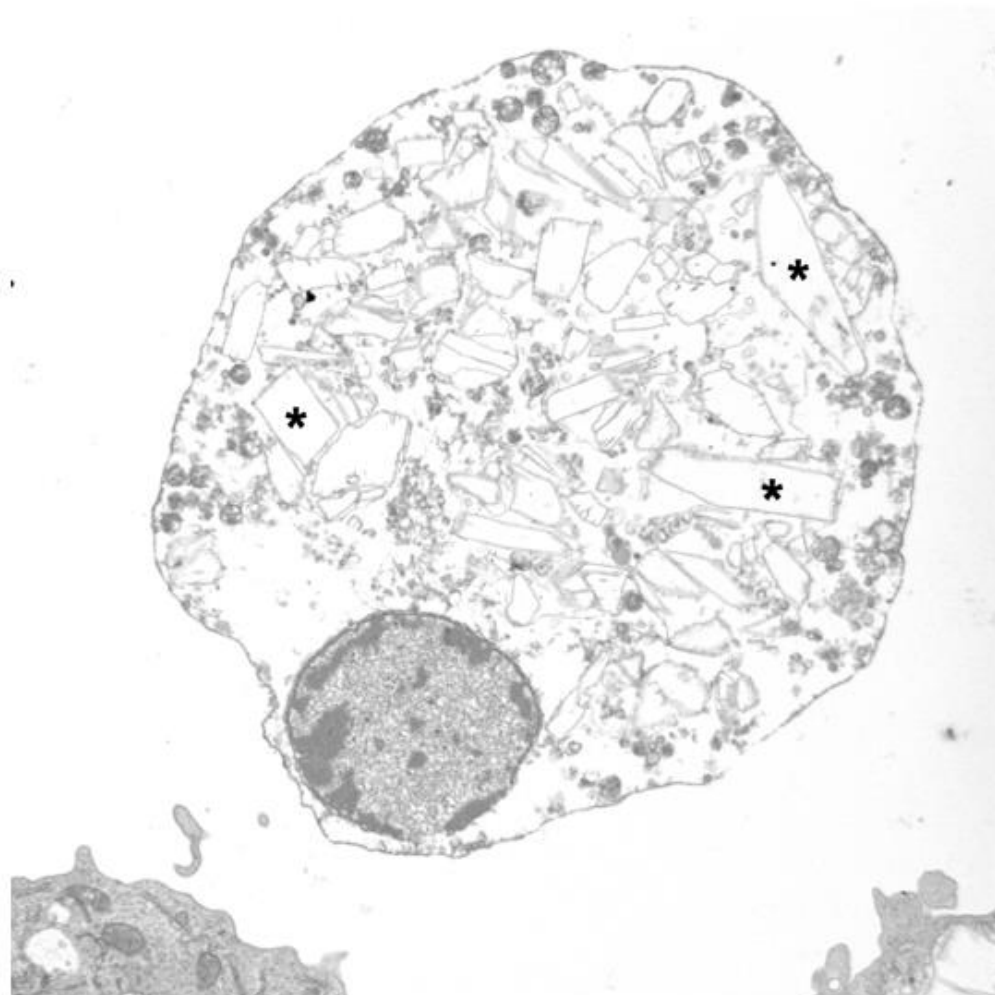
GSK UK



Higher magnification of electron lucent crystalline clefts of variable size. The crystalline clefts are within membrane bound bodies probably consistent with lysosomes or endocytic vacuoles.

**Appendix 3: *In vitro* assessment of cytotoxicity, morphology and pro-inflammatory mediator release of NR8383 cells treated with GSK-899 or GSK-677 (continued)**

Figure 10 GSK258899B 400 µg/ml



V31206N.003.tif  
EM 43537 NR8383 cells  
GSK258899B 400 ug/ml  
Print Mag: 10300x @ 7.0 in  
12:03 03/13/15  
Microscopist: pjm41508

2 microns  
HV=100.0kV  
Direct Mag: 8000x  
GSK UK



An example of a necrotic cell, within which the crystalline clefts (\*) of endocytosed test material are still evident.

### Appendix 3: *In vitro* assessment of cytotoxicity, morphology and pro-inflammatory mediator release of NR8383 cells treated with GSK-899 or GSK-677 (continued)

#### Transmission Electron Microscopy of NR8383 cells for Study V31257N.

Paul McGill 29<sup>th</sup> June 2015

#### Tabulated Summary

Cell Sample		% Necrotic cells (n=100)	Key Observations
Untreated		7%	
Chloroquine	5 µg/ml	100%	
GSK610677B	50 µg/ml	15%	41% cells contain secondary lysosomes containing lamellar or vesicular material that on occasions appeared to be developing LLBs
	200 µg/ml	100%	

LLBs= lysosomal lamellar bodies

#### Observations

##### Untreated Cells

The cells were of typical appearance (Figure 1) consistent with that of untreated cells in previous studies. This included the presence of a few small to medium sized membrane bound cytoplasmic vacuoles in a small proportion of cells.

##### Chloroquine 5 µg/ml

The cells were all necrotic (Figure 2). This was an unexpected finding since in previous studies, at this concentration, chloroquine had not caused a significant increase in necrosis. It was not possible to recognise lysosomal lamellar bodies (LLBs) in the necrotic cells.

##### GSK610677B 50 µg/ml

A large proportion of cells had membrane bound bodies containing vesicles and/or lamellar material or amorphous material (Figure 3 to Figure 8 inclusive). The bodies that contained lamellar material appeared to be developing into LLBs (Figures 3 and 4, 7 and 8).

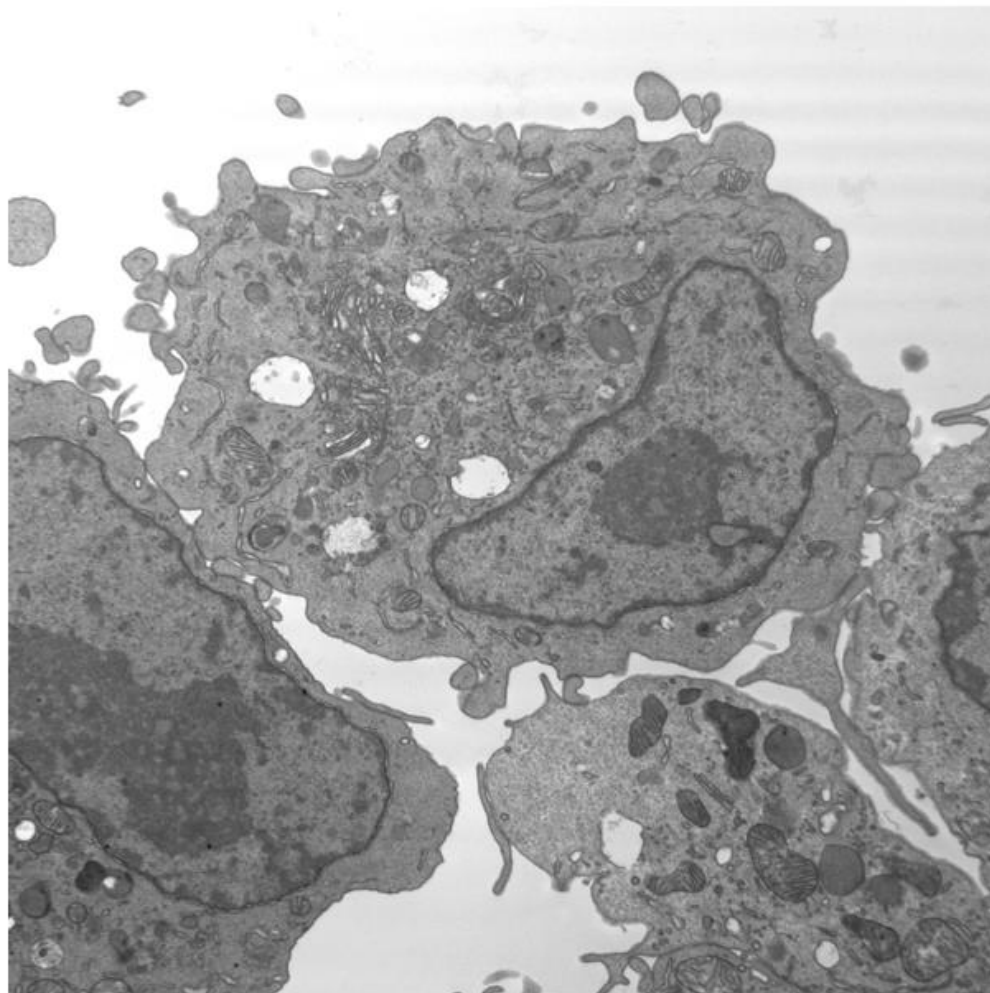
##### GSK610677B 200 µg/ml

Cells given 200 µg/ml GSK610677B were all necrotic (Figure 9 and Figure 10). It was not possible to recognise lysosomal lamellar bodies (LLBs) in the necrotic cells.

**Appendix 3: *In vitro* assessment of cytotoxicity, morphology and pro-inflammatory mediator release of NR8383 cells treated with GSK-899 or GSK-677 (continued)**

**Figures**

Figure 1 Untreated Cell Sample



V31257N.001.tif  
EM 43609 NR8383 cells  
Untreated cells  
Print Mag: 10300x @ 7.0 in  
11:38 06/19/15  
Microscopist: pjm41508

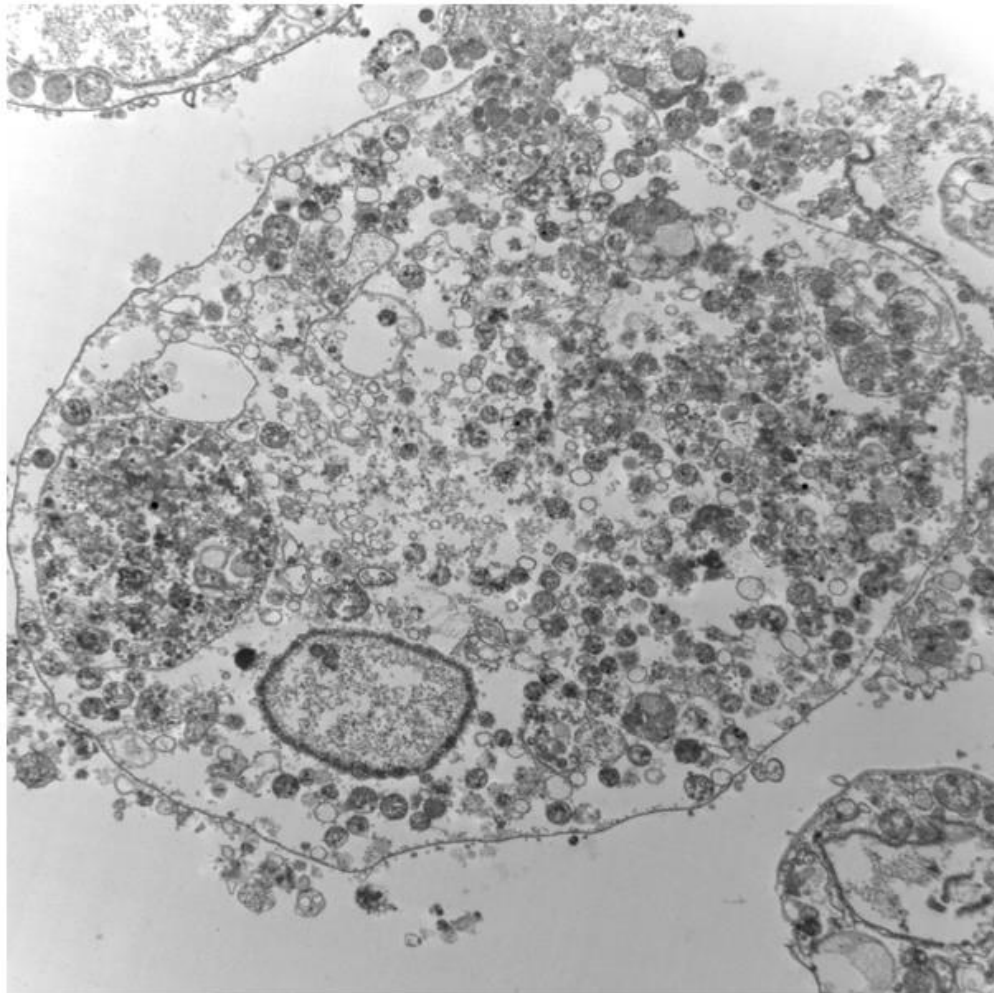
2 microns  
HV=80.0kV  
Direct Mag: 8000x  
GSK UK



Cells from the media control sample showing a typical appearance.

**Appendix 3: *In vitro* assessment of cytotoxicity, morphology and pro-inflammatory mediator release of NR8383 cells treated with GSK-899 or GSK-677 (continued)**

Figure 2 Chloroquine 5 µg/ml



V31257N.018.tif  
EM 43610 NR8383 cells  
Chloroquine 5 ug/ml  
Print Mag: 10300x @ 7.0 in  
14:48 06/26/15  
Microscopist: pjm41508

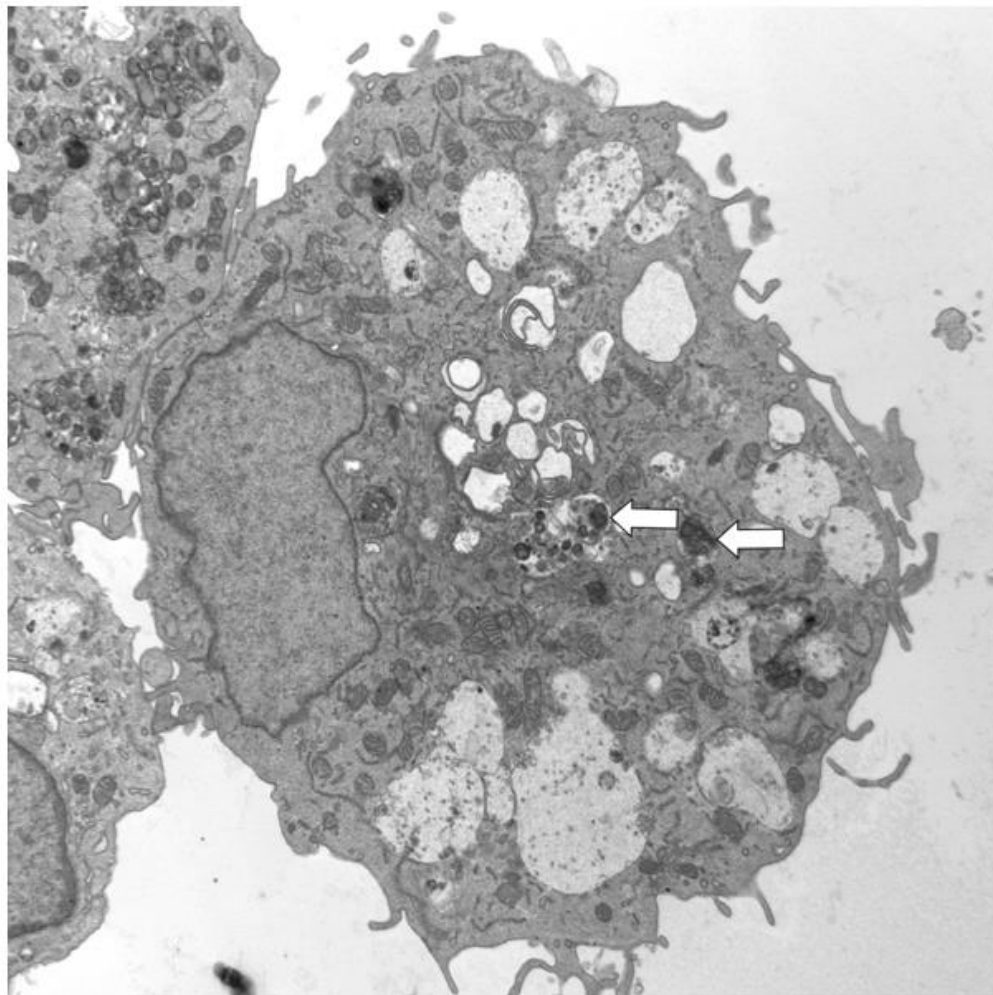
2 microns  
HV=80.0kV  
Direct Mag: 8000x  
GSK UK



Necrotic cell showing remnants of the nucleus, organellar debris and a lack of recognisable organelles.

**Appendix 3: *In vitro* assessment of cytotoxicity, morphology and pro-inflammatory mediator release of NR8383 cells treated with GSK-899 or GSK-677 (continued)**

Figure 3 GSK610677B 50 µg/ml



V31257N.004.tif  
EM 43612 NR8383 cells  
GSK610677B 50 ug/ml  
Print Mag: 10300x @ 7.0 in  
11:57 06/19/15  
Microscopist: pjm41508

2 microns  
HV=80.0kV  
Direct Mag: 8000x  
GSK UK

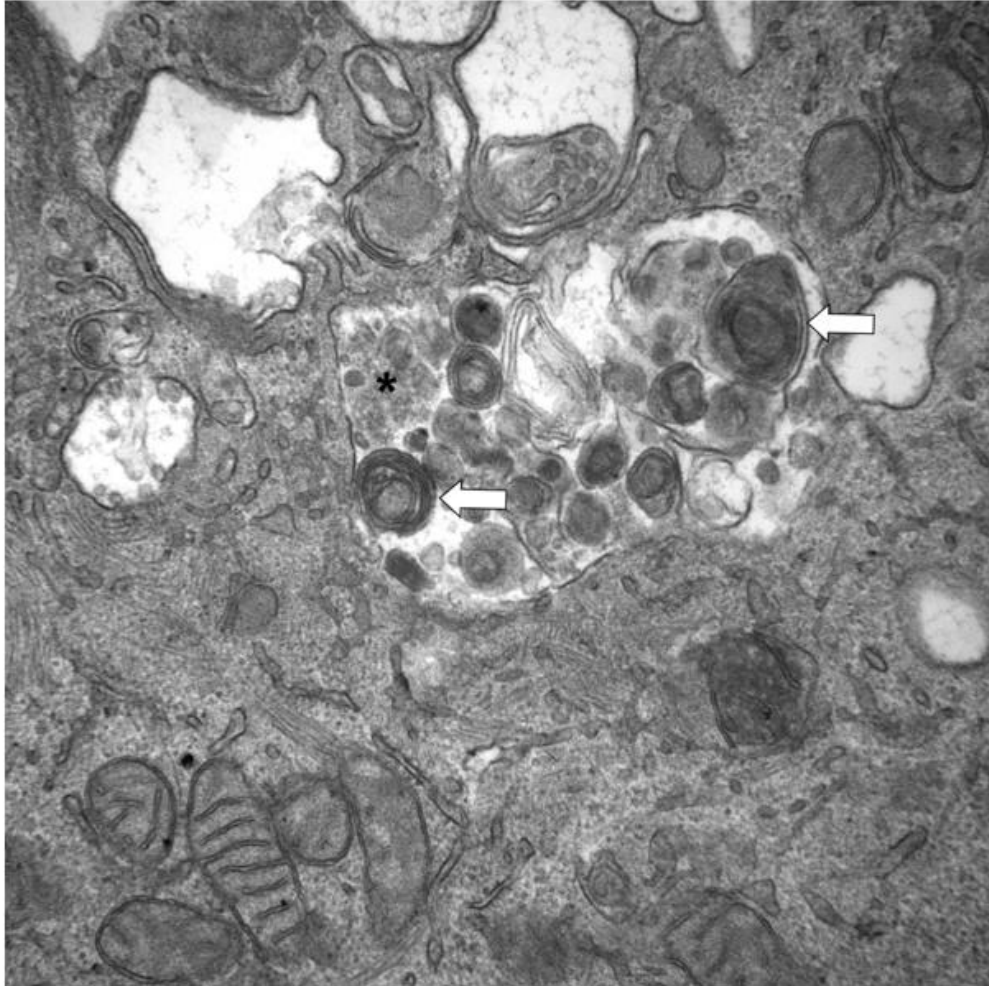
Image annotated  
File saved as V31257N\_004a  
Paul McGill  
29th Jun 2015



Membrane bound bodies containing lamellar material, vesicles and amorphous material.

**Appendix 3: *In vitro* assessment of cytotoxicity, morphology and pro-inflammatory mediator release of NR8383 cells treated with GSK-899 or GSK-677 (continued)**

Figure 4 GSK610677B 50 µg/ml



V31257N.005.tif  
EM 43612 NR8383 cells  
GSK610677B 50 ug/ml  
Print Mag: 51500x @ 7.0 in  
11:59 06/19/15  
Microscopist: pj41508

500 nm

HV=80.0kV

Direct Mag: 40000x

GSK UK

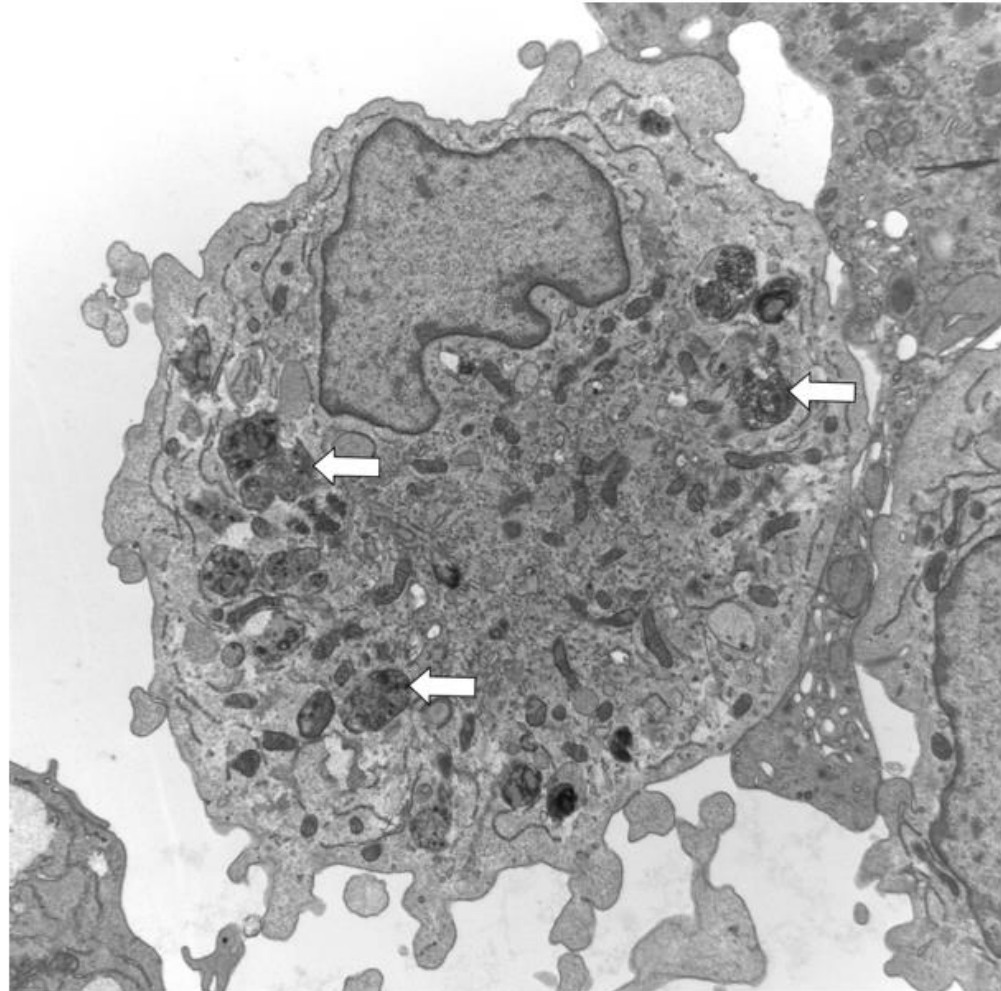
Image annotated  
File saved as V31257N\_005a  
Paul McGill  
29th Jun 2015



Higher magnification of membrane-bound body seen in the previous figure showing that it contains concentric lamellar material (arrows), vesicles and amorphous material (\*). This body appears to be a developing LLB.

**Appendix 3: *In vitro* assessment of cytotoxicity, morphology and pro-inflammatory mediator release of NR8383 cells treated with GSK-899 or GSK-677 (continued)**

Figure 5 GSK610677B 50 µg/ml



V31257N.008.tif  
EM 43612 NR8383 cells  
GSK610677B 50 µg/ml  
Print Mag: 10300x @ 7.0 in  
14:34 06/19/15  
Microscopist: pjm41508

2 microns  
HV=80.0kV  
Direct Mag: 8000x  
GSK UK

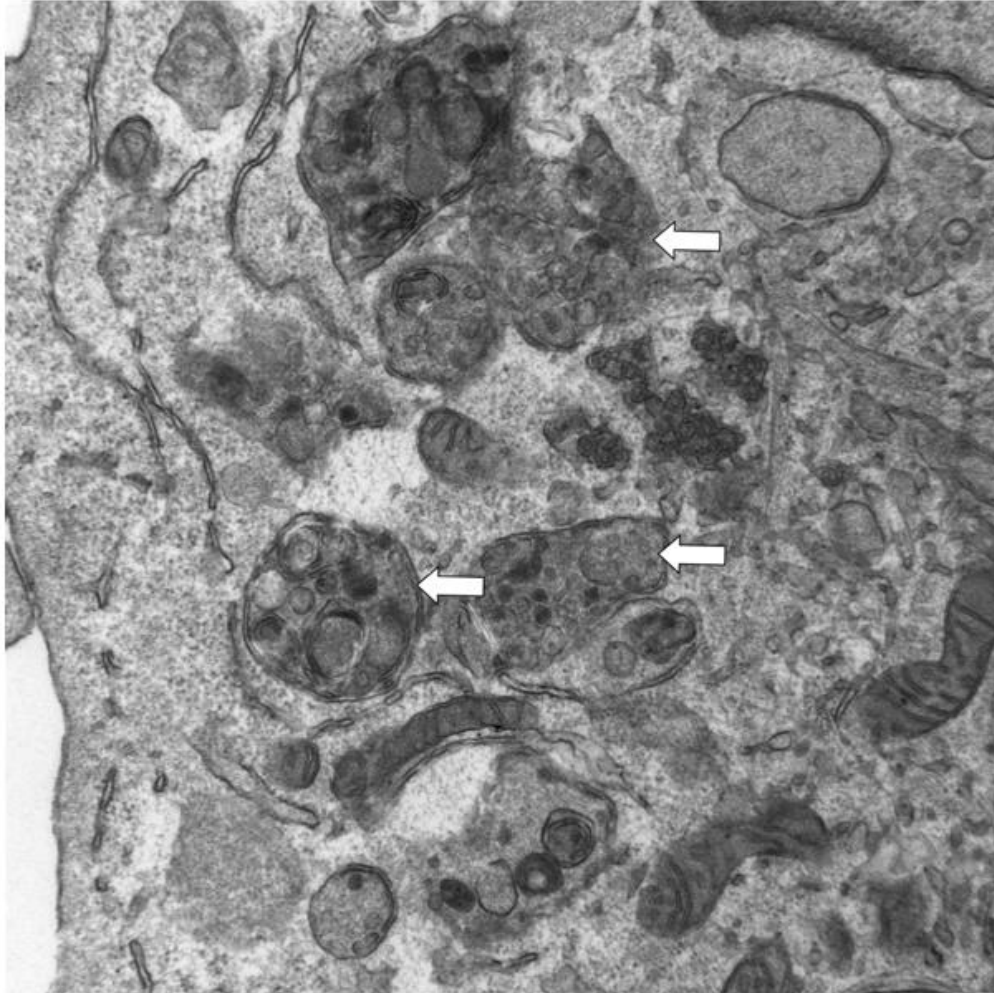
Image annotated  
File saved as V31257N\_008a  
Paul McGill  
29th Jun 2015



Cell containing heterogeneous membrane bound bodies (arrows).

**Appendix 3: *In vitro* assessment of cytotoxicity, morphology and pro-inflammatory mediator release of NR8383 cells treated with GSK-899 or GSK-677 (continued)**

Figure 6 GSK610677B 50 µg/ml



V31257N.009.tif  
EM 43612 NR8383 cells  
GSK610677B 50 ug/ml  
Print Mag: 38600x @ 7.0 in  
14:39 06/19/15  
Microscopist: pjm41508

500 nm  
HV=80.0kV  
Direct Mag: 30000x  
GSK UK

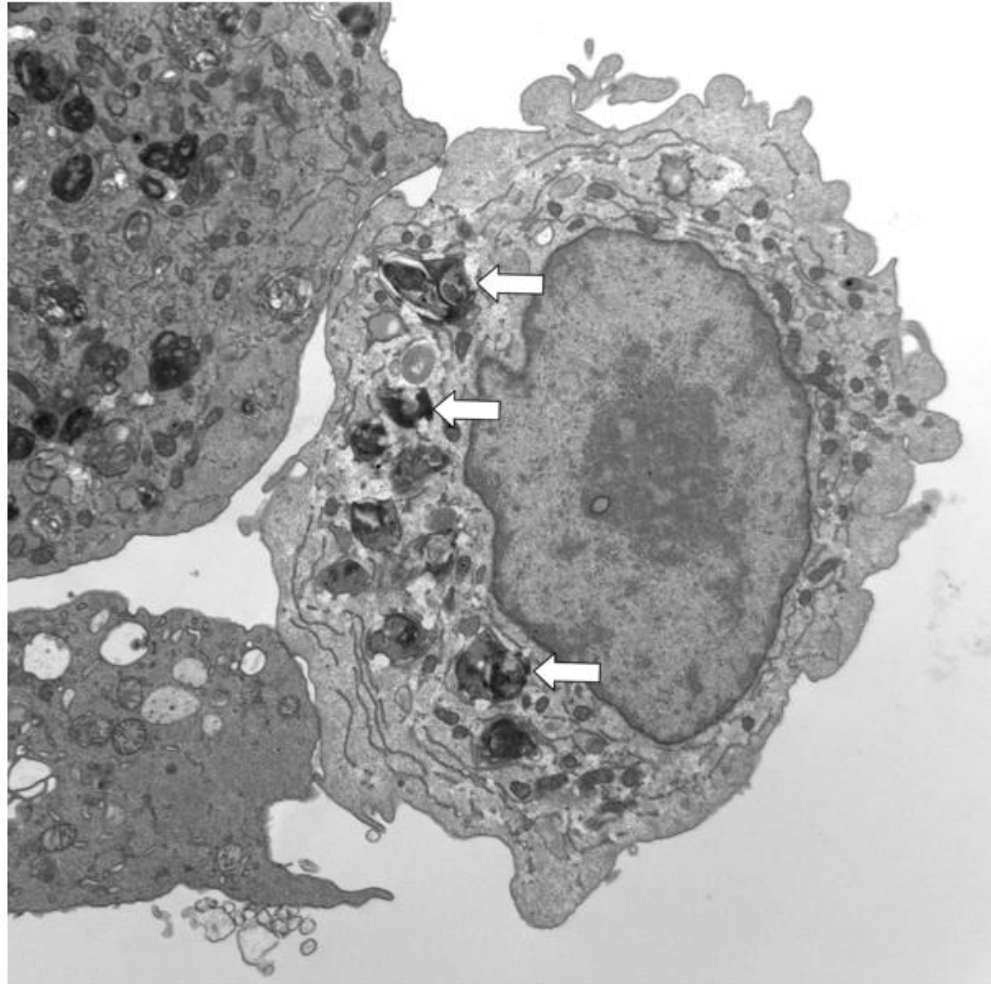
Image annotated  
File saved as V31257N\_009a  
Paul McGill  
29th Jun 2015



Membrane bound bodies (arrows) containing vesicles and amorphous material. It is unclear if these bodies will develop into LLBs, but they are probably lysosomal.

**Appendix 3: *In vitro* assessment of cytotoxicity, morphology and pro-inflammatory mediator release of NR8383 cells treated with GSK-899 or GSK-677 (continued)**

Figure 7 GSK610677B 50 µg/ml



V31257N.010.tif  
EM 43612 NR8383 cells  
GSK610677B 50 ug/ml  
Print Mag: 10300x @ 7.0 in  
14:47 06/19/15  
Microscopist: pjm41508

2 microns

HV=80.0kV

Direct Mag: 8000x

GSK UK

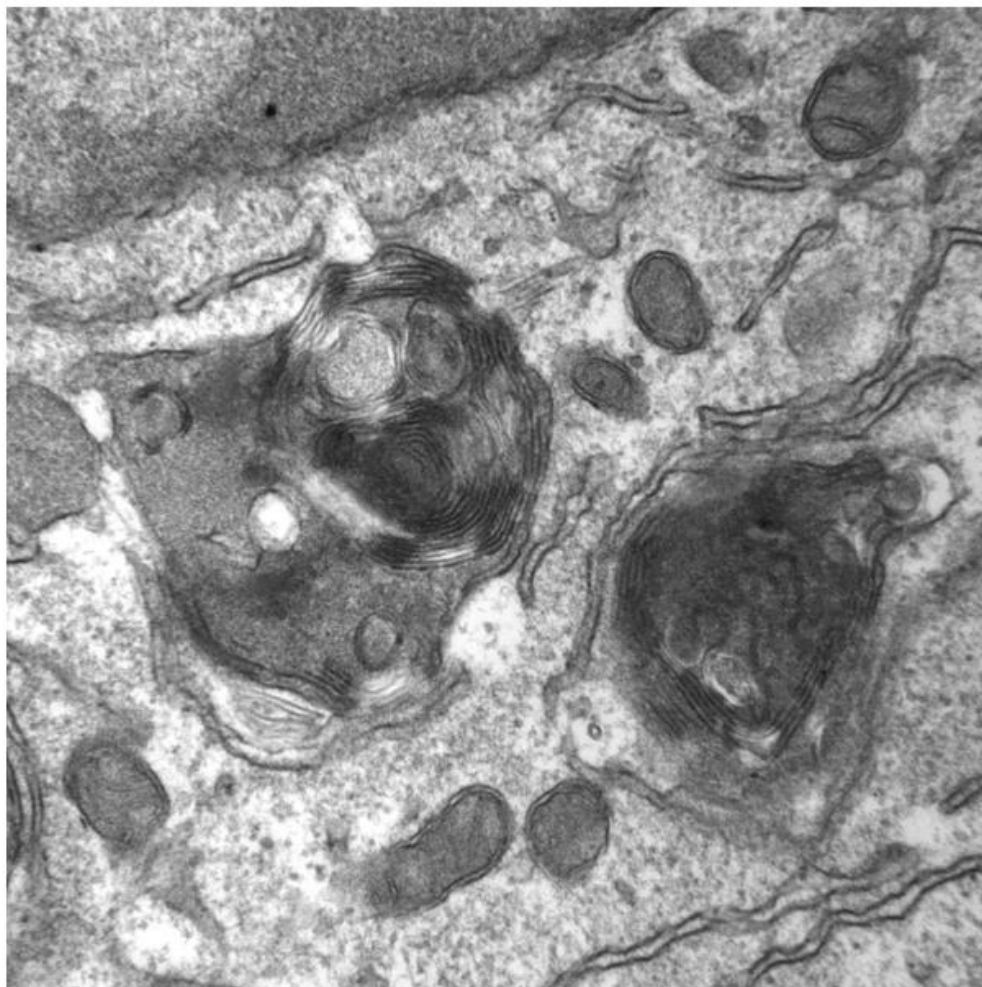
Image annotated  
File saved as V31257N\_010a  
Paul McGill  
20th Jun 2015



Cell containing heterogeneous membrane bound bodies (arrows).

**Appendix 3: *In vitro* assessment of cytotoxicity, morphology and pro-inflammatory mediator release of NR8383 cells treated with GSK-899 or GSK-677 (continued)**

Figure 8 GSK610677B 50 µg/ml



V31257N.011.tif

EM 43612 NR8383 cells

GSK610677B 50 ug/ml

Print Mag: 64400x @ 7.0 in

14:49 06/19/15

Microscopist: pjm41508

500 nm

HV=80.0kV

Direct Mag: 50000x

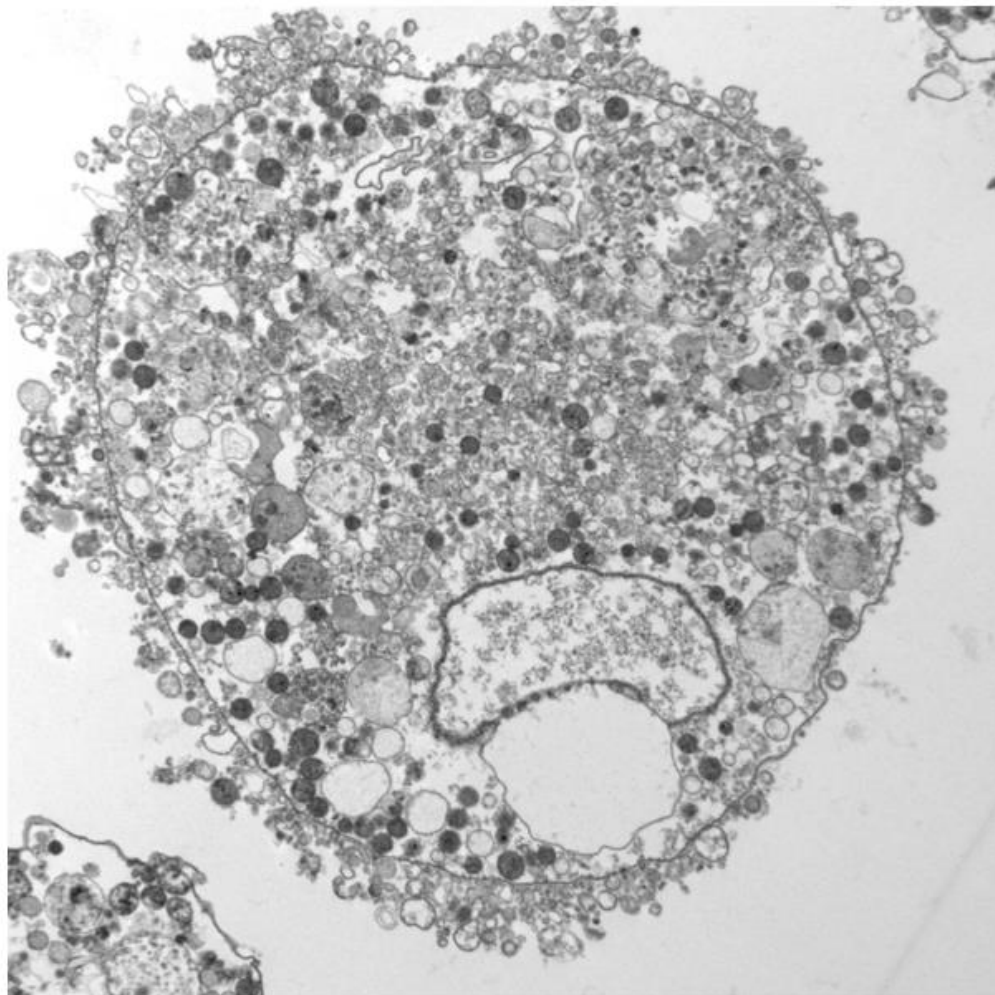
GSK UK



These examples of membrane-bound bodies appear to be LLBs, since they contain concentrically arranged lamellae.

**Appendix 3: *In vitro* assessment of cytotoxicity, morphology and pro-inflammatory mediator release of NR8383 cells treated with GSK-899 or GSK-677 (continued)**

Figure 9 GSK610677B 200 µg/ml



V31257N.015.tif  
EM 43611 NR8383 cells  
GSK610677B 200 ug/ml  
Print Mag: 10300x @ 7.0 in  
15:14 06/19/15  
Microscopist: pjm41508

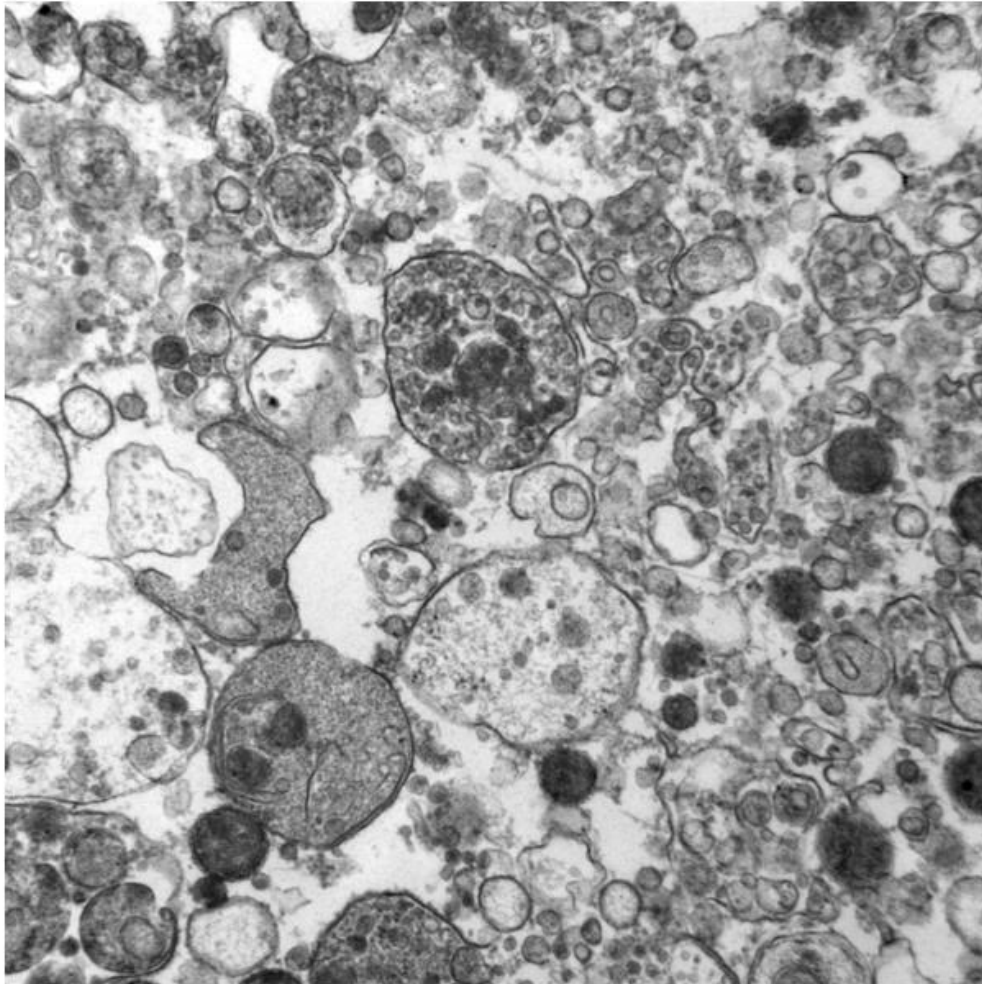
2 microns  
HV=80.0kV  
Direct Mag: 8000x  
GSK UK



Necrotic cell contain remnants of the nucleus, organellar debris and a lack of recognisable organelles.

**Appendix 3: *In vitro* assessment of cytotoxicity, morphology and pro-inflammatory mediator release of NR8383 cells treated with GSK-899 or GSK-677 (continued)**

Figure 10 GSK610677B 200 µg/ml



V31257N.016.tif

EM 43611 NR8383 cells

GSK610677B 200 µg/ml

Print Mag: 38600x @ 7.0 in

15:20 06/19/15

Microscopist: pjm41508

500 nm

HV=80.0kV

Direct Mag: 30000x

GSK UK



Higher magnification of a necrotic cell.

## Appendix 4: *In vitro* assessment of cytotoxicity, morphology and pro-inflammatory mediator release of NR8383 rat alveolar macrophage cells treated with GSK-361 or SB-323

V31292N (eLNB: N27241-13) & V31307N (eLNB:N27241-14)

Investigative study to assess cytotoxicity, pro-inflammatory mediator release and morphology following treatment of NR8383 rat alveolar macrophage cells with GSK678361A and SB-681323T over 72 hours.

### Introduction

These studies were carried out to measure cytotoxicity and cytokine release of NR8383 cells following a concentration range of treatments with test compounds after 72 hours. The following endpoints were assessed in the study:

- General morphology by phase microscopy.
- Lactate dehydrogenase (LDH) leakage to assess cytotoxicity.
- TNF $\alpha$ , MCP-1, IL-1 $\alpha$ , CXCL1/rKC/GRO and IL-1 $\beta$  by MSD to assess inflammatory mediator release.
- TEM images analysed for morphological changes and evidence of toxicity.

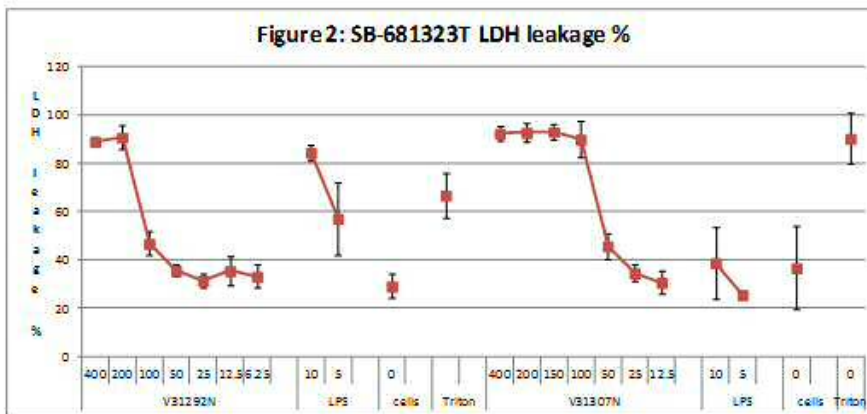
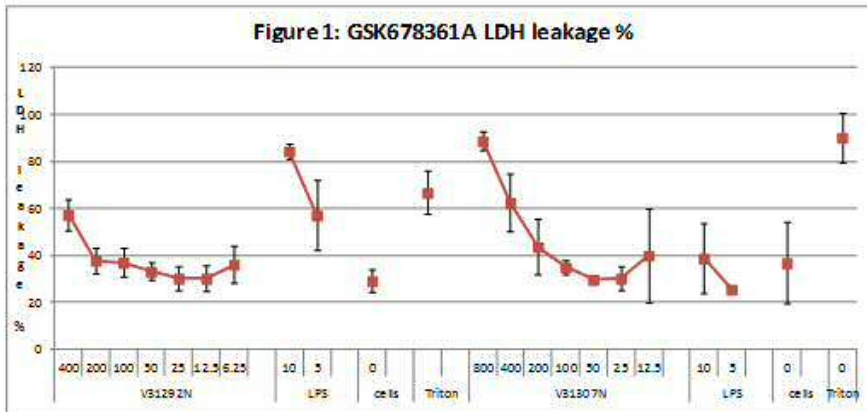
### Viability

Cellular viability was quantified by measuring the % LDH leaked from the cells. Following 72 hours treatment, only at the highest concentration (400 $\mu$ g/mL) in the first study, V31292N, did GSK678361A show a slight increase in LDH leakage levels (Figure1). The highest concentration was therefore raised to 800 $\mu$ g/mL for the repeat study (V31307N), where a concentration dependent increase was then seen, with consistent results between the two studies at 400 $\mu$ g/mL and lower. Triton X-100 produced a response between 60-100% in both studies, which was as expected for the positive control. The media treated cell negative control produced a response of between 20-40% in both studies, with some slight variability seen in the values for the second study, V31307N.

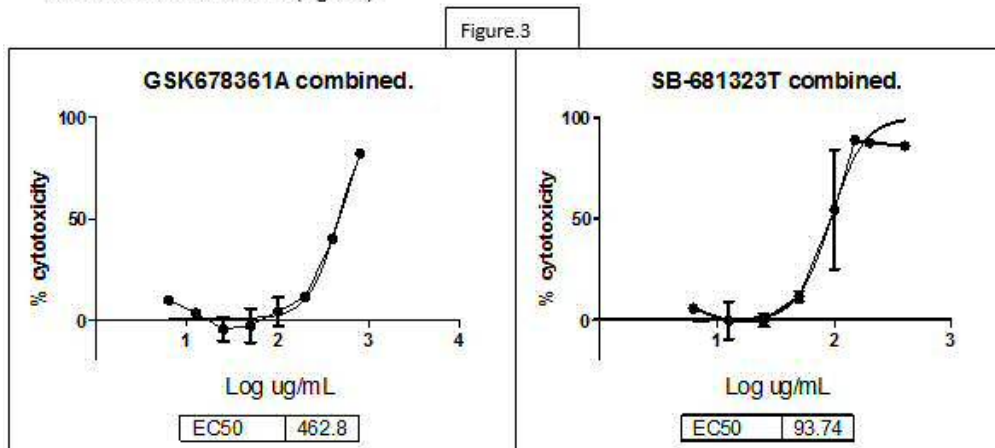
For SB-681323T, the two highest concentrations in both studies (200 $\mu$ g/mL and 400 $\mu$ g/mL) showed high levels of LDH leakage (Figure2). There was a sharp increase in leaked LDH levels in the first study between 100 $\mu$ g/mL and 200 $\mu$ g/mL, therefore a concentration of 150  $\mu$ g/mL was introduced in the repeat study. The results of the repeat study showed that 100 $\mu$ g/mL to 400 $\mu$ g/mL gave high LDH leakage values >80%.

**Appendix 4: *In vitro* assessment of cytotoxicity, morphology and pro-inflammatory mediator release of NR8383 cells treated with GSK-361 or SB-323 (continued)**

V31292N (eLNB: N27241-13) & V31307N (eLNB: N27241-14)



A signal window (0-100%) was calculated to determine the % cytotoxicity and the data was plotted in Graphpad to enable curve comparison and EC50 values to be generated from combined data from both V31292N and V31307N (Figure3).



## Appendix 4: *In vitro* assessment of cytotoxicity, morphology and pro-inflammatory mediator release of NR8383 cells treated with GSK-361 or SB-323 (continued)

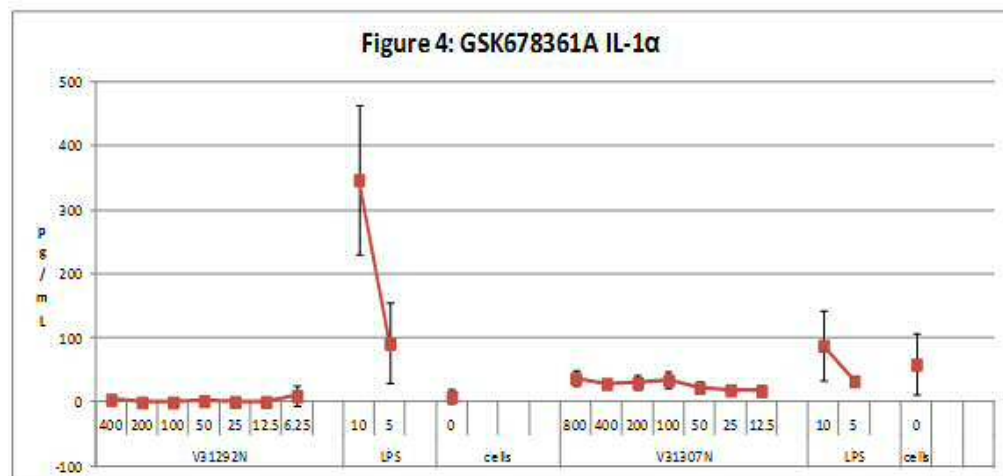
V31292N (eLNB: N27241-13) & V31307N (eLNB: N27241-14)

### Activation

For both GSK678361A and SB-681323T there was no activation of any of the cytokines/chemokines measured after a 72 hour treatment with these compounds compared to the control values. Data was also consistent between the two studies showing similar cytokine profiles with little variability. LPS positive control values were generally more variable in the first study V31292N, than in the repeat study.

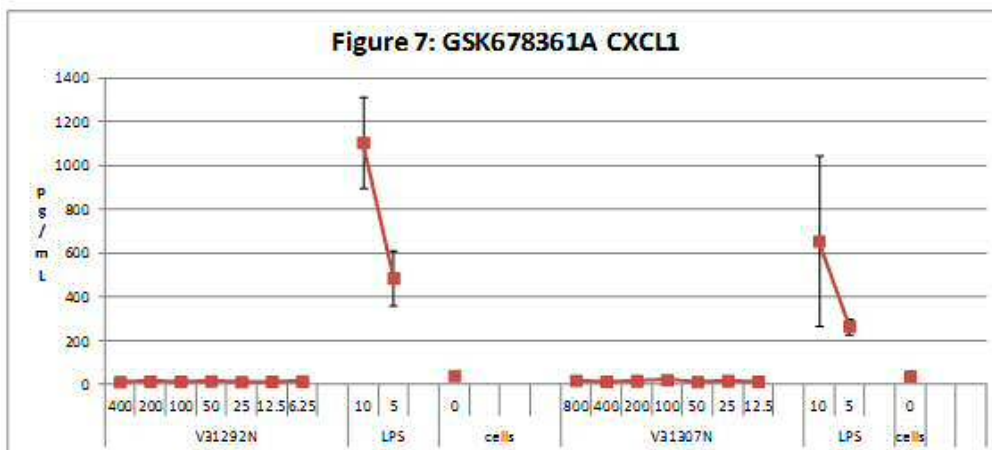
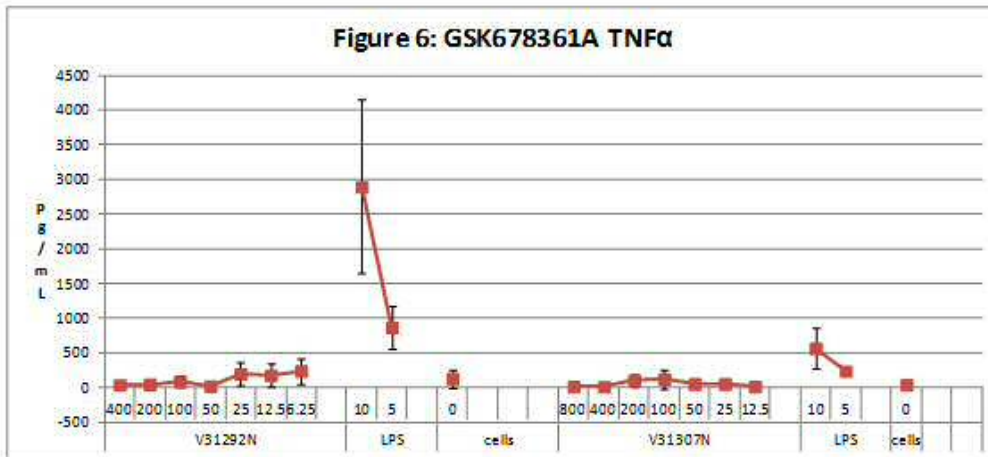
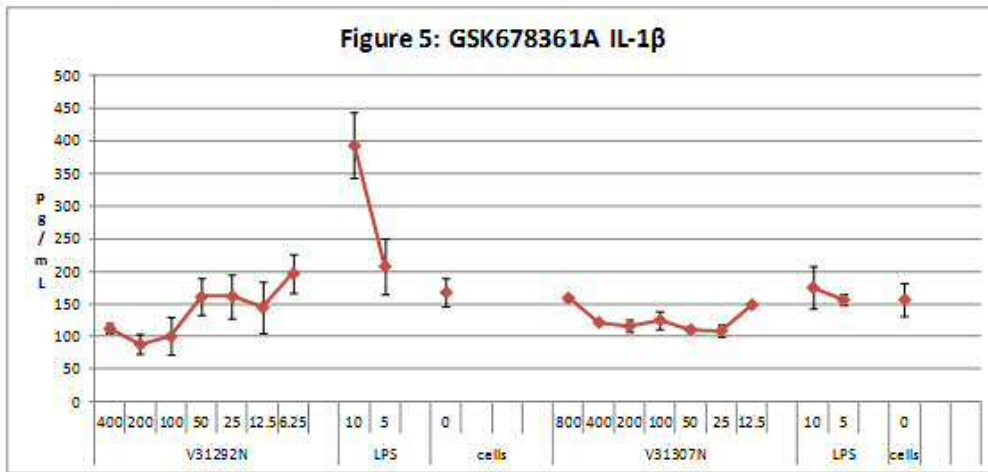
GSK678361A - There was minimal IL-1 $\alpha$  activity detected at all concentrations tested and was similar to that of the control values (Figure 4). IL-1 $\beta$  values remained almost identical over the 2 studies (Figure 5), and again there were with very low detectable levels similar to control values. For CXCL1 and TNF- $\alpha$  levels, the data is identical across both studies with very little variability and again at levels similar to control values (Figures 6 and 7). GSK678361A showed a concentration dependent decrease in levels of MCP-1 in both studies (Figure 8).

SB-681323T - IL-1 $\alpha$  induction was not seen in either study and levels remained below or the same as control values (Figure 9). SB-681323T IL-1 $\beta$  values were also very similar across both studies with levels either the same or below that of the control values, with the exception of a lower value seen for 200 $\mu$ g/mL in study V31292N, and some variability at the highest concentration of 400 $\mu$ g/mL (Figure 10). Although TNF- $\alpha$  levels appeared slightly more variable at the lowest 3 concentrations in study V31292N only (Figure 11), there was minimal activity detected across both studies and were similar to control values. SB-681323T did not elicit a CXCL1 response; this was observed in both studies (Figure 12). For MCP-1, all concentrations showed a notable concentration dependent decrease in both studies compared to control levels (Figure 13).



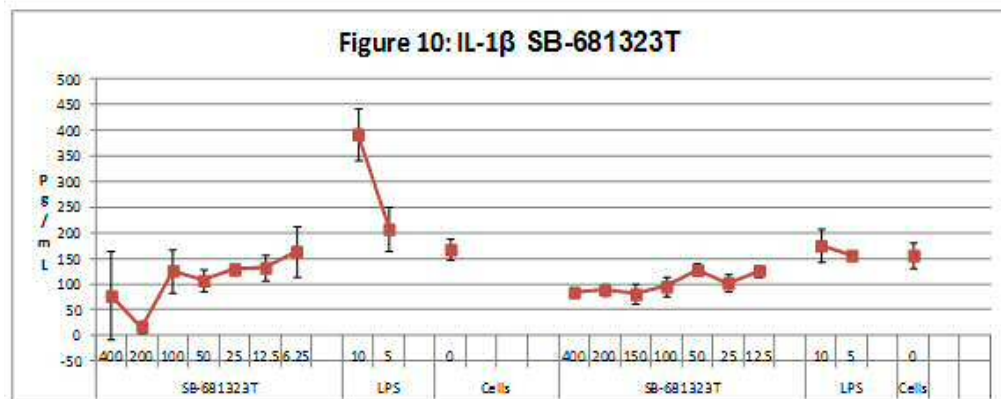
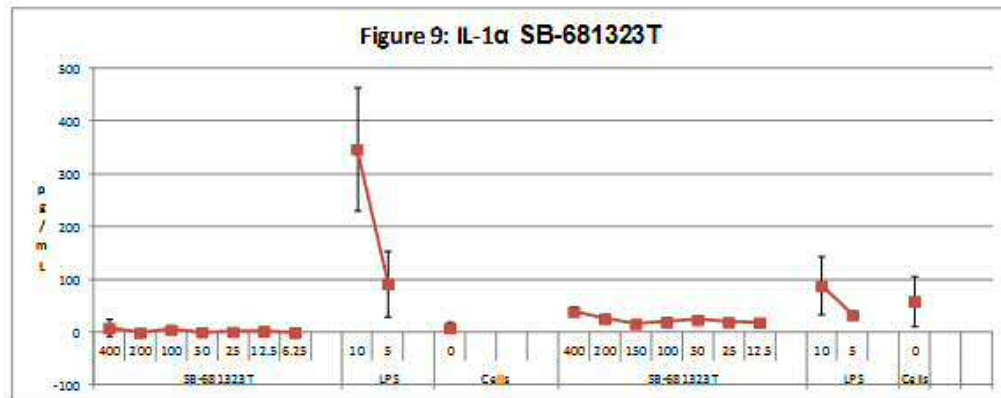
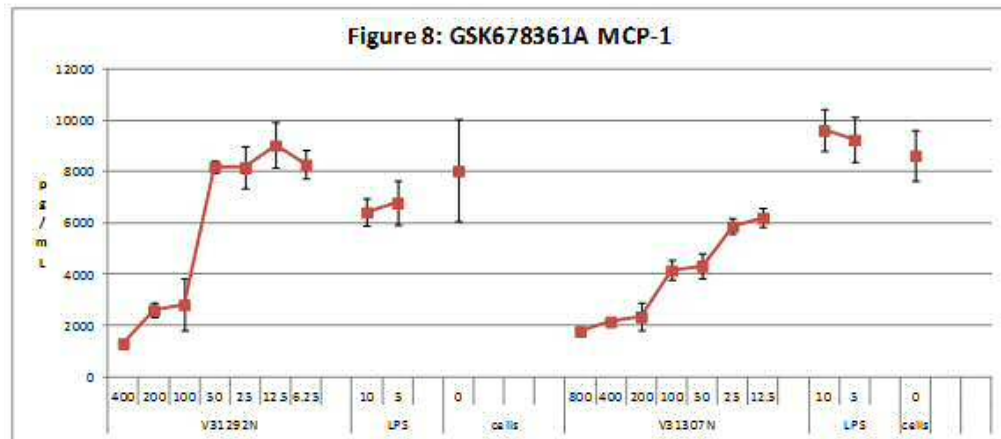
**Appendix 4: *In vitro* assessment of cytotoxicity, morphology and pro-inflammatory mediator release of NR8383 cells treated with GSK-361 or SB-323 (continued)**

V31292N (eLNB: N27241-13) & V31307N (eLNB: N27241-14)



**Appendix 4: *In vitro* assessment of cytotoxicity, morphology and pro-inflammatory mediator release of NR8383 cells treated with GSK-361 or SB-323 (continued)**

V31292N (eLNB: N27241-13) & V31307N (eLNB: N27241-14)



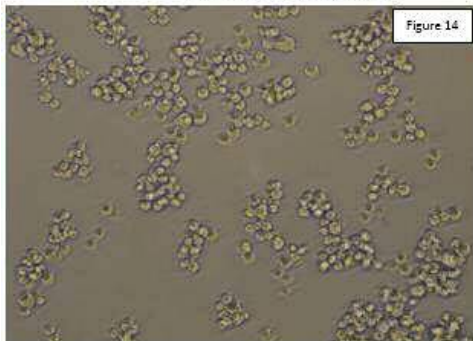
## Appendix 4: *In vitro* assessment of cytotoxicity, morphology and pro-inflammatory mediator release of NR8383 cells treated with GSK-361 or SB-323 (continued)

V31292N (eLNB: N27241-13) & V31307N (eLNB: N27241-14)

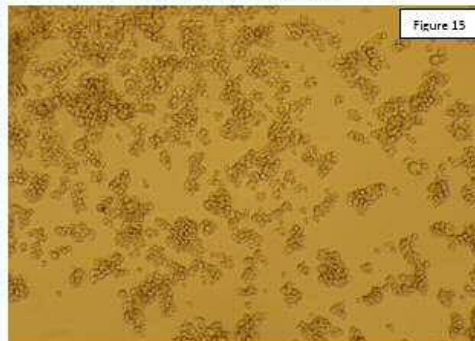
### Morphology

Cells were visualised by phase contrast microscopy. The untreated cells images appeared the same across the plates in both studies (Figures 14 & 15), showing the regular morphology of the NR8383 cell. Cells appeared healthy, round and uniform in size with only a few small clusters and spread evenly across the wells.

V31292N cells only (x200).

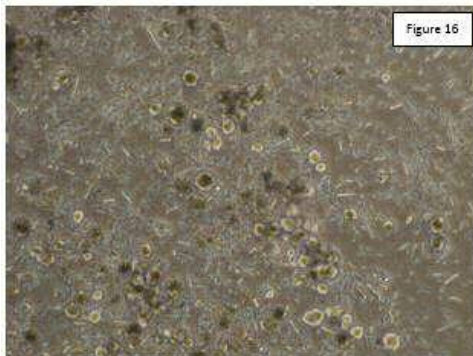


V31307N cells only (x100).

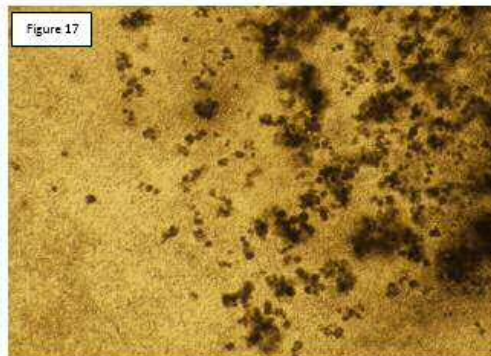


GSK678361A - At the higher doses a large amount of debris was visible throughout the well. At 400µg/mL treatment (Figures 16 & 17), the cells appeared to be fewer in number and clustered towards the centre of the well. The live cells were darker and more granular with what appeared to be test material inside the cell. GSK678361A test material particulate or cell debris was also seen in the wells. At lower concentrations down to 25µg/mL (Figures 18 and 19), cells appeared to be more populous and not so clustered to the centre of the well, similar to the 'untreated cells' image.

V31292N GSK678361A 400µg/mL (x200)



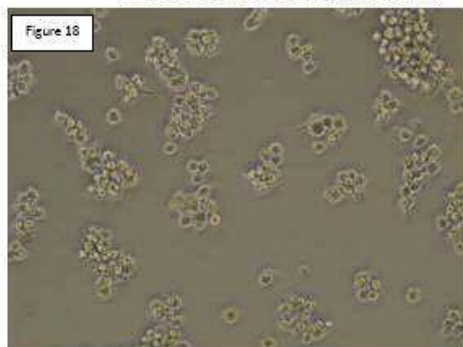
V31307N GSK678361A 400µg/mL (x100)



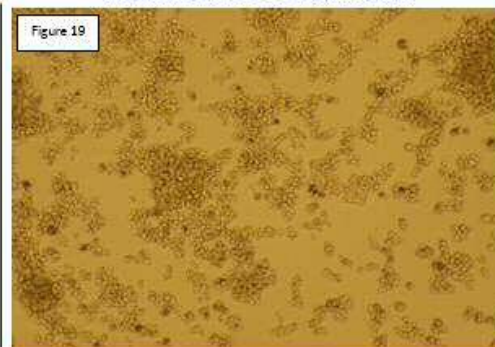
**Appendix 4: *In vitro* assessment of cytotoxicity, morphology and pro-inflammatory mediator release of NR8383 cells treated with GSK-361 or SB-323 (continued)**

V31292N (eLNB: N27241-13) & V31307N (eLNB:N27241-14)

V31292N GSK678361A 25µg/mL (x200)

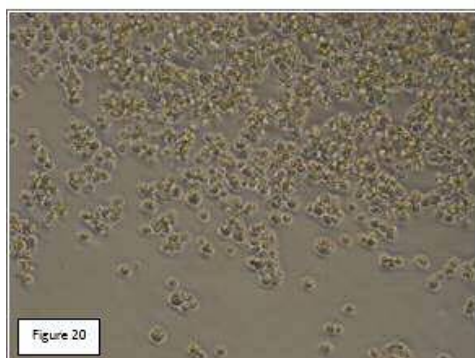


V31307N GSK678361A 25µg/mL (x100)

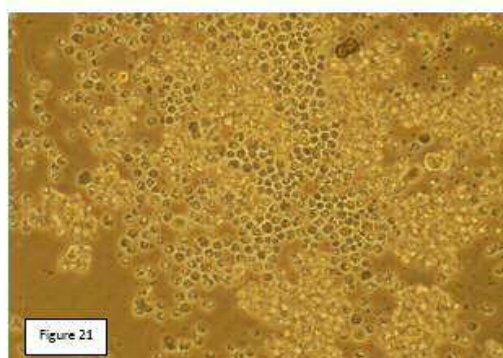


SB-681323T- Cells appeared to be morphologically affected at the higher concentrations down to 50µg/mL, where they showed signs of normal morphology. At 150µg/mL SB-681323T in the repeat study (Figure 21) cells on the inside of a cluster were darker and more granular in appearance than those on the outside of the same cluster, which appeared healthier. At 12.5µg/mL (Figures 22 & 23), cells appeared to have normal morphology of untreated NR8383 cells.

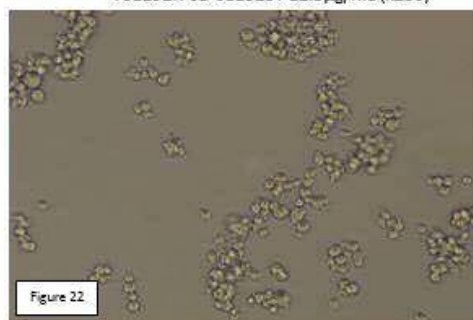
V31292N SB-681323T 200µg/mL (x200)



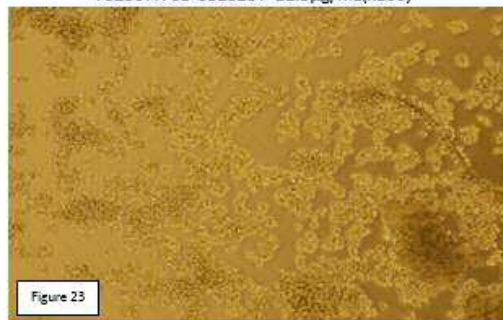
V31307N SB-681323T 150µg/mL (x200)



V31292N SB-681323T 12.5µg/mL (x200)



V31307N SB-681323T 12.5µg/mL(x100)



#### Appendix 4: *In vitro* assessment of cytotoxicity, morphology and pro-inflammatory mediator release of NR8383 cells treated with GSK-361 or SB-323 (continued)

V31292N (eLNB: N27241-13) & V31307N (eLNB:N27241-14)

##### Transition Electron Microscopy (TEM).

Cells were harvested after a 72 hr treatment with SB-681323T and GSK678361A, and fixed for TEM to assess ultrastructural effects of these compounds. Table 1 represents TEM data for both compounds which was carried out in study V31307N.

Table 1.

Cell Sample		% Necrotic cells (n=100)	Key Observations
Untreated		3	
Chloroquine	5 µg/ml	3	72% cells contained LLBs
SB-681323T	12.5 µg/ml	4	
	150 µg/ml	3	Observed increased incidence and severity of mitochondria that were swollen with pale matrix and disorganised or reduced numbers of cristae.
GSK678361A	50 µg/ml	8	58 % cells contained crystalline inclusions consistent with test article
	400 µg/ml	5	100 % cells contained crystalline inclusions consistent with test article

The untreated cells were of typical appearance consistent with that of untreated cells in previous studies, with a very low proportion of necrotic cells (3%). However in some cells the mitochondria appeared swollen with a pale matrix and few cristae.

For SB-681323T at 12.5 µg/mL, one of the higher concentrations in the lower part of the concentration curve which caused little effects by both phase contrast microscopy, and LDH leakage, a low proportion of necrotic cells (4%) were observed by TEM. There were also no outstanding ultrastructural observations different to the untreated control cells. At 150 µg/mL, where cells were observed to have a darker and more granular appearance by phase contrast morphology, there was an increase in the incidence and severity of swollen mitochondria with notable pale matrix and disorganised or reduced numbers of cristae. At this concentration, the proportion of necrotic cells seen by TEM was low (3%).

For GSK678361A at both concentrations selected for TEM (50 and 400 µg/mL) where there was a low proportion of necrotic cells for each (8 and 5% respectively), there was evidence of test material within the cells as crystalline inclusions, the severity of which increased with dose. In all other respects the cells appeared unaffected ultrastructurally. This observation corresponds with the phase contrast observations of particulate test material seen within the cells.

Although there were no LLBs identified with either compound by TEM, 72% LLBs were observed in the cells treated with the positive control for induction of LLBs (chloroquine at 5 µg/mL).

**Appendix 4: *In vitro* assessment of cytotoxicity, morphology and pro-inflammatory mediator release of NR8383 cells treated with GSK-361 or SB-323 (continued)**

V31292N (eLNB: N27241-13) &amp; V31307N (eLNB:N27241-14)

**Conclusion.**

GSK678361A: The high EC50 value for cytotoxicity associated with GSK678361A over 72 hours in these studies indicates that it is a low hazard for cellular toxicity. GSK678361A did not elicit cytokine/chemokine activation after 72 hour treatment, therefore activation of the cells and inflammatory mediator release is considered to be a low hazard with this compound. However, as phase contrast morphology showed evidence of a dose related increase in particulate accumulation within the cells, and TEM confirmed the presence of crystalline inclusions consistent with test material, it should be classified as a moderate hazard when considering compound particulate accumulation within the cells.

SB-681323T: The EC50 value for cytotoxicity associated with SB-681323T over 72 hours in these studies (93.74µg/mL) was less than the 100µg/mL threshold of the *in vitro* liability profile, and would be considered a moderate hazard for cellular toxicity. Although SB-681323T did not elicit cytokine/chemokine activation after 72 hour treatment, and would be considered a low hazard for inflammatory mediator release, it should be classified as a moderate hazard when considering the ultrastructural changes observed by both TEM and phase contrast microscopy.

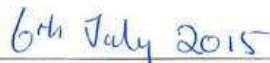
Signature:

(Anita Naidoo)



---

Date:



---

**Appendix 4: *In vitro* assessment of cytotoxicity, morphology and pro-inflammatory mediator release of NR8383 cells treated with GSK-361 or SB-323 (continued)**

Transmission Electron Microscopy of NR8383 cells for Study V31307N.

Paul McGill 29<sup>th</sup> June 2015

**Tabulated Summary**

Cell Sample		% Necrotic cells (n=100)	Key Observations
Untreated		3	
Chloroquine	5 µg/ml	3	72% cells contained LLBs
SB681323T	12.5 µg/ml	4	
	150 µg/ml	3	Observed increased incidence and severity of mitochondria that were swollen with pale matrix and disorganised or reduced numbers of cristae.
GSK678361A	50 µg/ml	8	58 % cells contained crystalline inclusions consistent with test article
	400 µg/ml	5	100 % cells contained crystalline inclusions consistent with test article

LLBs= lysosomal lamellar bodies

**Observations**

**Untreated Cells**

The cells were generally of typical appearance (Figure 1) consistent with that seen in previous studies. This included the presence of a few small to medium sized membrane bound cytoplasmic vacuoles in a small proportion of cells. However in some cells the mitochondria appeared swollen with a pale matrix and few cristae.

3% of cells were necrotic.

**Chloroquine 5 µg/ml**

The majority of cells contained lysosomal lamellar bodies (LLBs) (Figure 2 and Figure 3) consistent with accumulation of phospholipid. Mitochondria were of a similar appearance to those in the untreated cells

3% of cells necrotic.

**SB681323T 12.5 µg/ml**

The cells were of similar appearance to the untreated cells (Figure 4). Mitochondria were of a similar appearance to those in untreated cells. 4 % of cells necrotic.

**Appendix 4: *In vitro* assessment of cytotoxicity, morphology and pro-inflammatory mediator release of NR8383 cells treated with GSK-361 or SB-323 (continued)**

**SB681323T 150 µg/ml**

There appeared to be a greater incidence and severity of mitochondria that were swollen and had a pale matrix and showed disorganised or reduced numbers of cristae (Figure 5, Figure 6 and Figure 7) than in the untreated cells. However given that this change to a degree was seen in untreated cells, and because of the small sample size for comparison, its significance is uncertain.

3 % of cells necrotic.

**GSK678361A 50 µg/ml**

58 % cells contained a few crystalline inclusions consistent with test article (Figure 8 and Figure 9). In other respects the cells appeared unaffected ultrastructurally.

8% cells necrotic.

**GSK678361A 400 µg/ml**

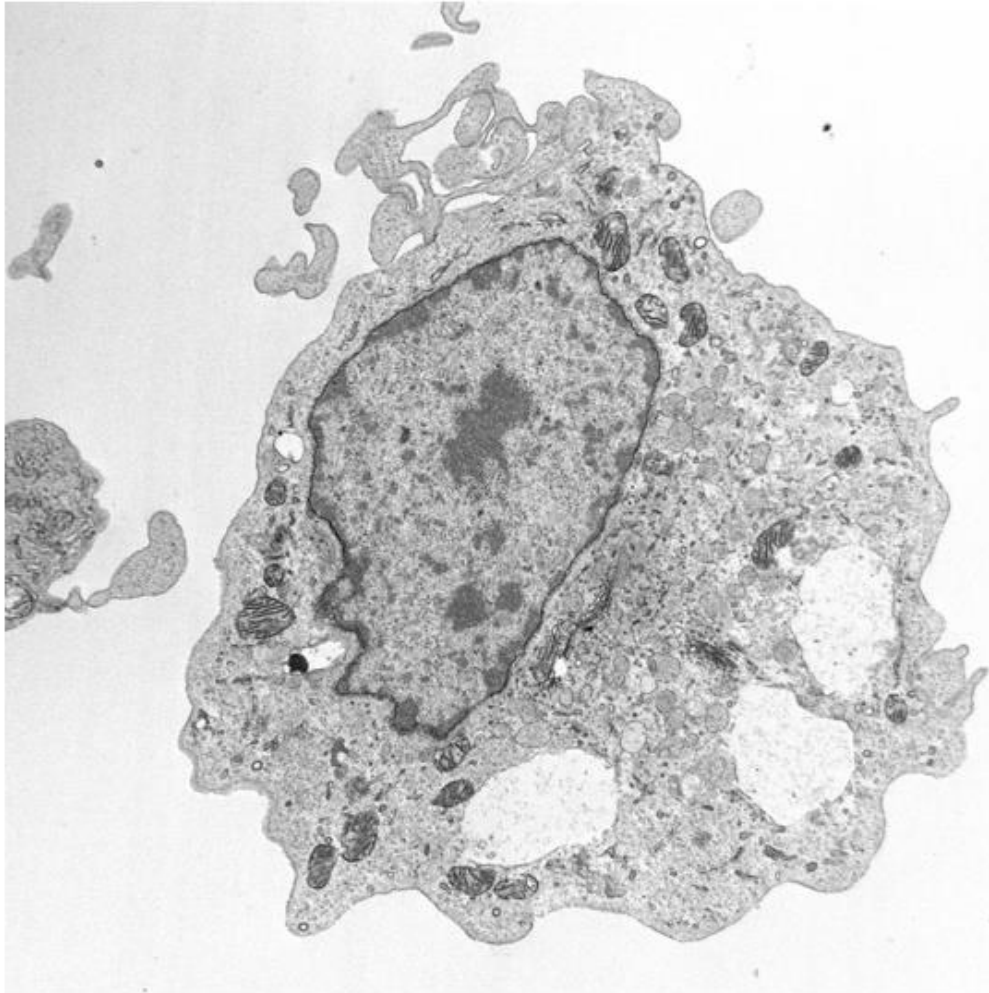
All examined cells contained numerous crystalline inclusions consistent with test article (Figure 10 to Figure 12 inclusive). On occasions the inclusions were >10 µm in length. In other respects the cells appeared unaffected ultrastructurally.

5% cells necrotic.

**Appendix 4: *In vitro* assessment of cytotoxicity, morphology and pro-inflammatory mediator release of NR8383 cells treated with GSK-361 or SB-323 (continued)**

**Figures**

Figure 1 Untreated Cell Sample



V31307N.003.tif  
EM 43753 NR8383 cells  
Untreated cells  
Print Mag: 10300x @ 7.0 in  
8:51 06/26/15  
Microscopist: pjm41508

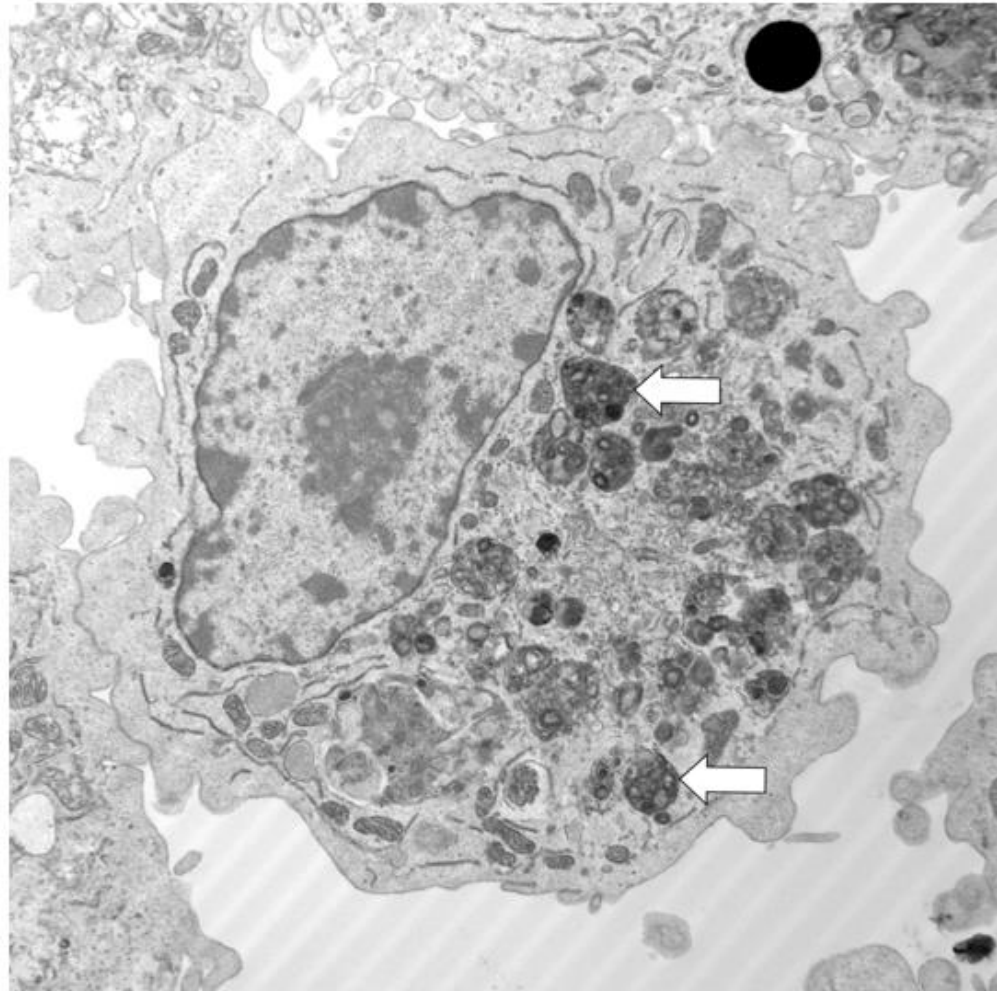
2 microns  
HV=80.0kV  
Direct Mag: 8000x  
GSK UK



Cell from the media control sample showing a typical appearance, though some of the mitochondria appear slightly swollen with reduced numbers of cristae.

**Appendix 4: *In vitro* assessment of cytotoxicity, morphology and pro-inflammatory mediator release of NR8383 cells treated with GSK-361 or SB-323 (continued)**

Figure 2 Chloroquine 5 µg/ml



V31307N.008.tif  
EM 43758 NR8383 cells  
5 ug/ml Chloroquine  
Print Mag: 10300x @ 7.0 in  
9:27 06/26/15  
Microscopist: pjm41508

2 microns

HV=80.0kV

Direct Mag: 8000x

GSK UK

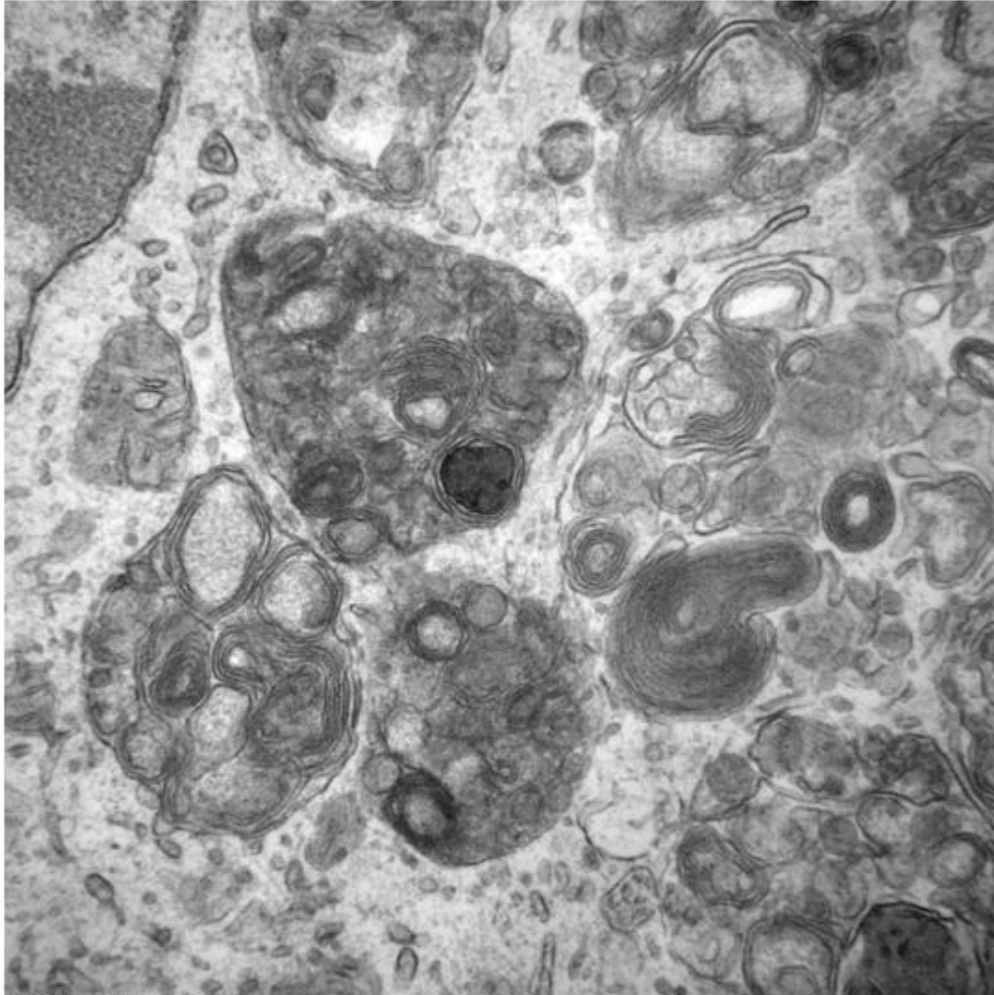
Image annotated  
File saved as V31307N\_008a  
Paul McGill  
29th June 2015



Cell containing LLBs (arrows)

**Appendix 4: *In vitro* assessment of cytotoxicity, morphology and pro-inflammatory mediator release of NR8383 cells treated with GSK-361 or SB-323 (continued)**

Figure 3 Chloroquine 5 µg/ml



V31307N.009.tif

EM 43758 NR8383 cells

5 ug/ml Chloroquine

Print Mag: 51500x @ 7.0 in

9:29 06/26/15

Microscopist: pjm41508

500 nm

HV=80.0kV

Direct Mag: 40000x

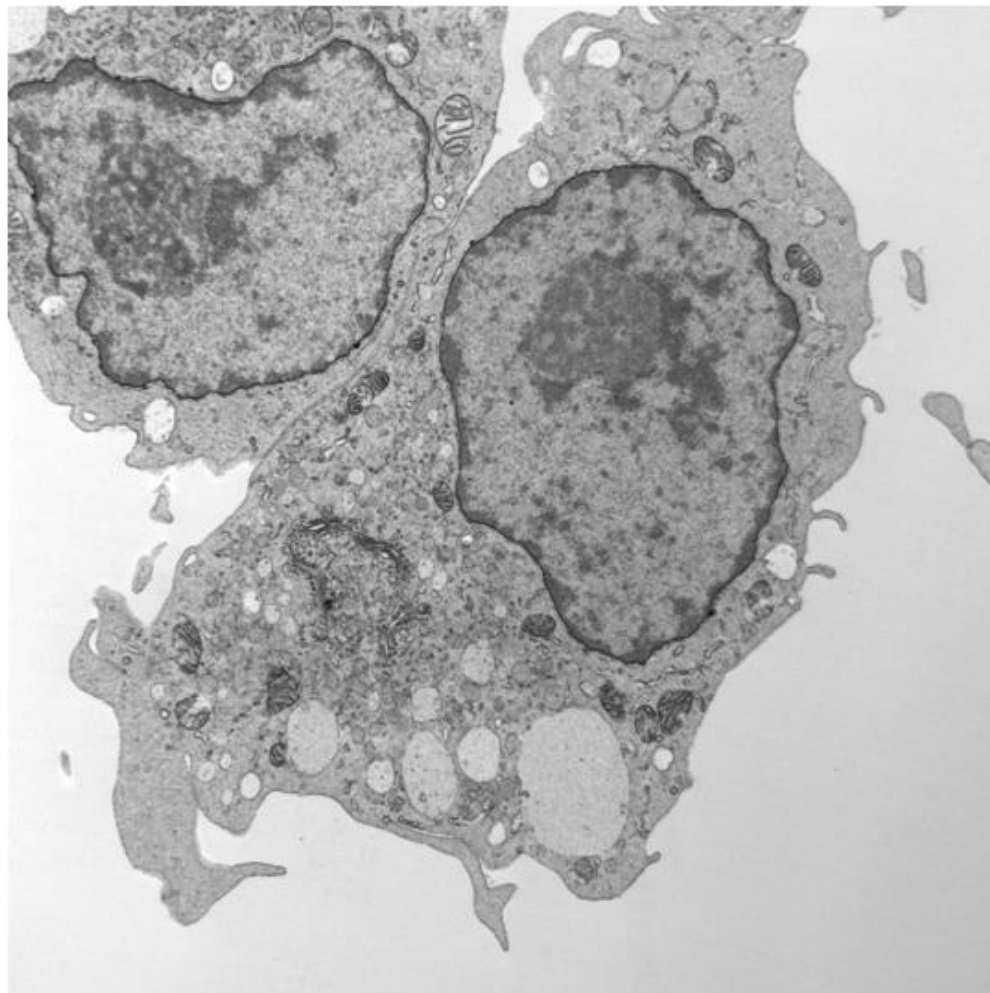
GSK UK



Higher magnification of LLBs.

**Appendix 4: *In vitro* assessment of cytotoxicity, morphology and pro-inflammatory mediator release of NR8383 cells treated with GSK-361 or SB-323 (continued)**

Figure 4 SB681323T 12.5 µg/ml



V31307N.025.tif  
EM 43755 NR8383 cells  
SB681323T 12.5 ug/ml  
Print Mag: 10300x @ 7.0 in  
13:05 06/26/15  
Microscopist: pjm41508

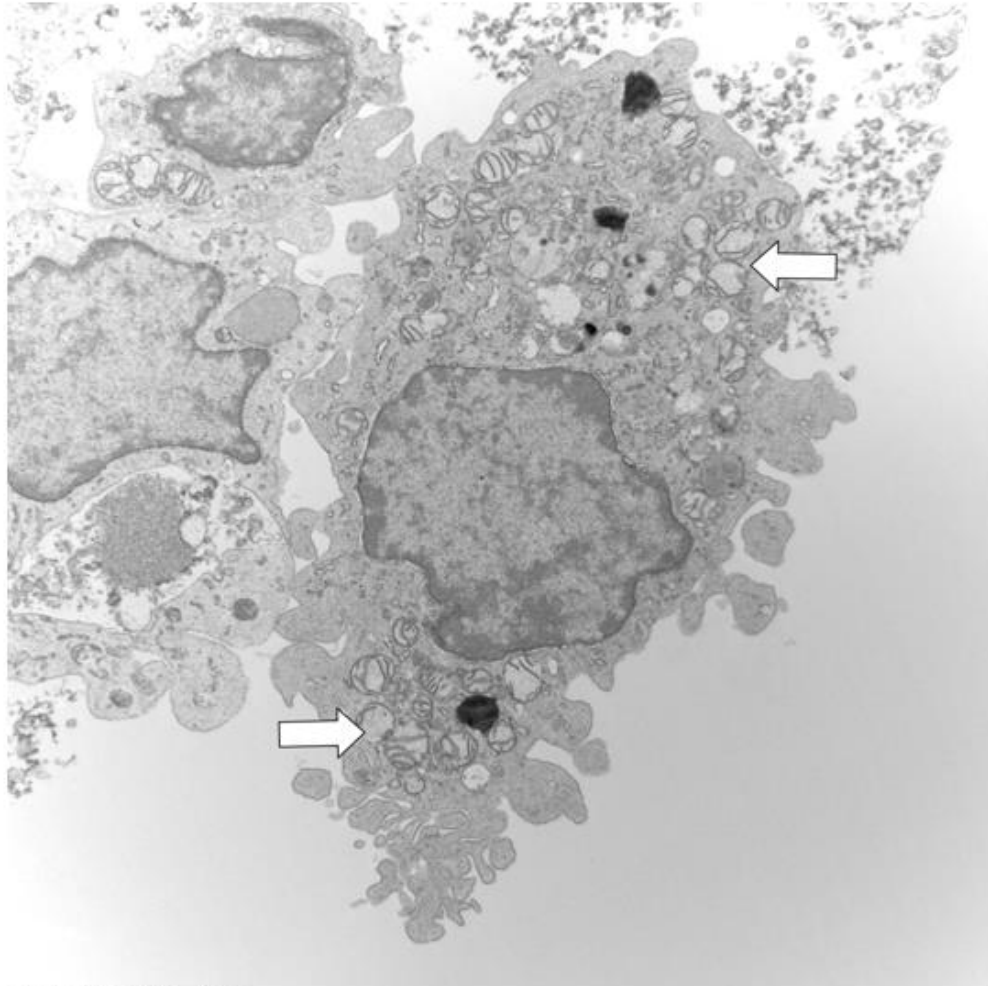
2 microns  
HV=80.0kV  
Direct Mag: 8000x  
GSK UK



Typical appearance of cell showing similarity to untreated cells.

**Appendix 4: *In vitro* assessment of cytotoxicity, morphology and pro-inflammatory mediator release of NR8383 cells treated with GSK-361 or SB-323 (continued)**

Figure 5 SB681323T 150 µg/ml



V31307N.021.tif  
EM 43754 NR8383 cells  
SB681323T 150 ug/ml  
Print Mag: 10300x @ 7.0 in  
12:38 06/26/15  
Microscopist: pjm41508

2 microns

HV=80.0kV

Direct Mag: 8000x

GSK UK

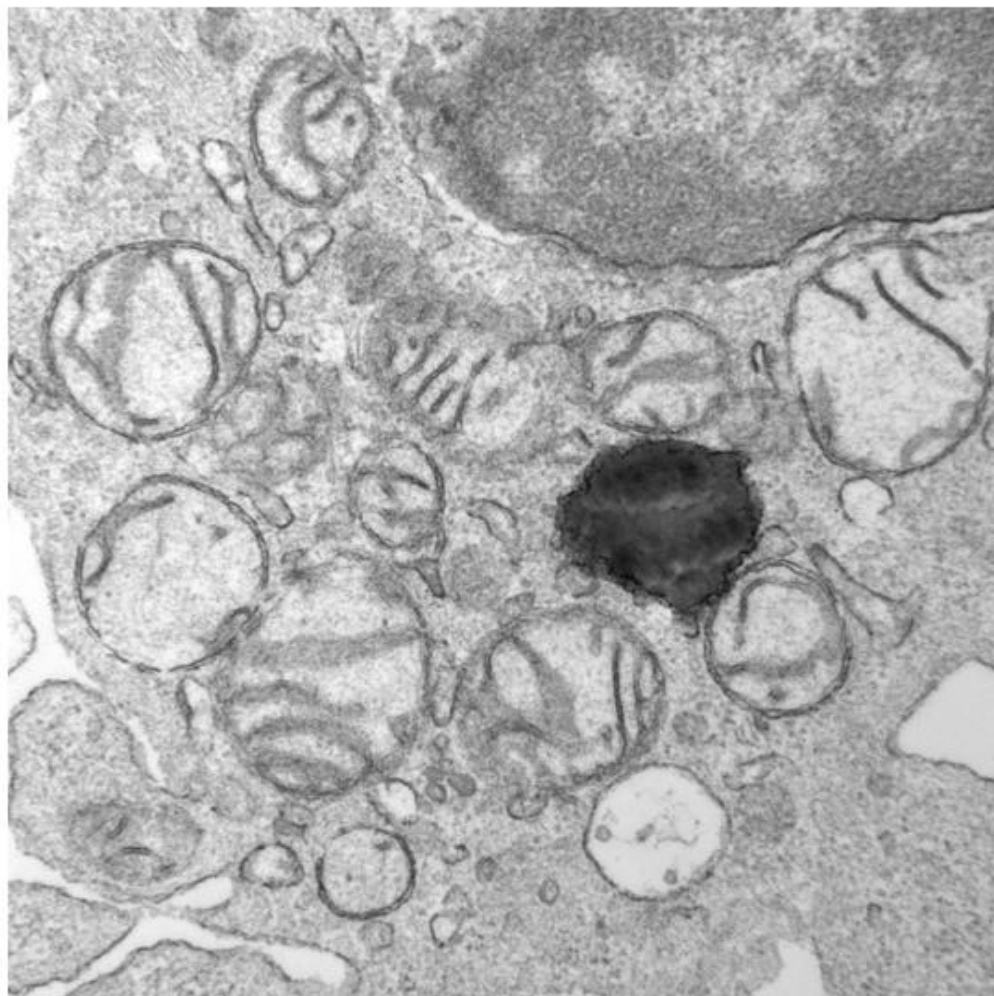
Image annotated  
File saved as V31307N\_021a  
Paul McGill  
29th June 2015



The mitochondria appear swollen with a pale matrix and reduced numbers of cristae (arrows). There appeared to be a greater incidence and severity of this change than in the untreated cells.

**Appendix 4: *In vitro* assessment of cytotoxicity, morphology and pro-inflammatory mediator release of NR8383 cells treated with GSK-361 or SB-323 (continued)**

Figure 6 SB681323T 150 µg/ml



V31307N.022.tif  
EM 43754 NR8383 cells  
SB681323T 150 µg/ml  
Print Mag: 51500x @ 7.0 in  
12:40 06/26/15  
Microscopist: pjm41508

500 nm  
HV=80.0kV  
Direct Mag: 40000x  
GSK UK



Examples of swollen mitochondria with pale matrix and cristae that appear disorganised and are reduced in numbers.

**Appendix 4: *In vitro* assessment of cytotoxicity, morphology and pro-inflammatory mediator release of NR8383 cells treated with GSK-361 or SB-323 (continued)**

Figure 7 SB681323T 150 µg/ml



V31307N.017.tif  
EM 43754 NR8383 cells  
SB681323T 150 ug/ml  
Print Mag: 77300x @ 7.0 in  
12:28 06/26/15  
Microscopist: pjm41508

500 nm  
HV=80.0kV  
Direct Mag: 60000x  
GSK UK

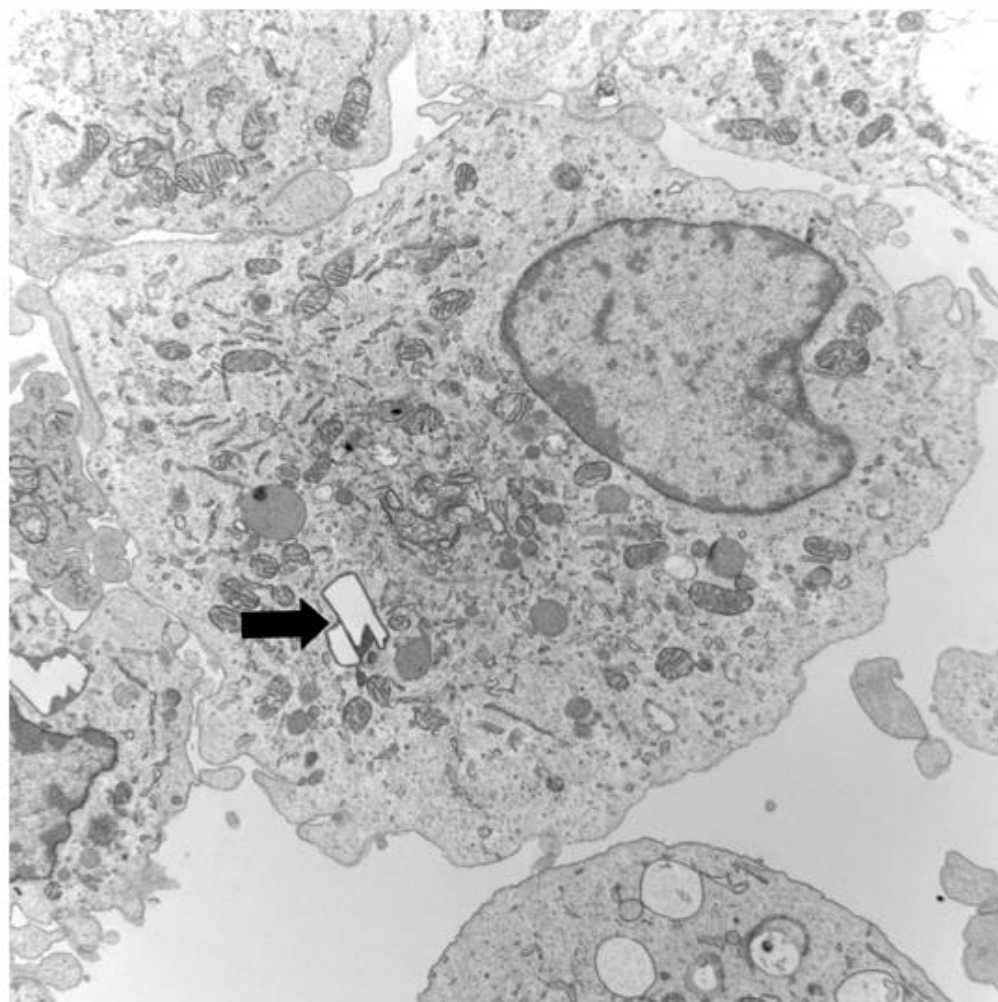
Image annotated  
File saved as V31307N\_017a  
Paul McGill  
29th June 2015



Mitochondrion (M) shows swelling and disorganisation and loss of cristae

**Appendix 4: *In vitro* assessment of cytotoxicity, morphology and pro-inflammatory mediator release of NR8383 cells treated with GSK-361 or SB-323 (continued)**

Figure 8 GSK678361A 50 µg/ml



V31307N.036.tif  
EM 43757 NR8383 cells  
GSK678361A 50 ug/ml  
Print Mag: 10300x @ 7.0 in  
13:58 06/26/15  
Microscopist: pjm41508

2 microns  
HV=80.0kV  
Direct Mag: 8000x  
GSK UK

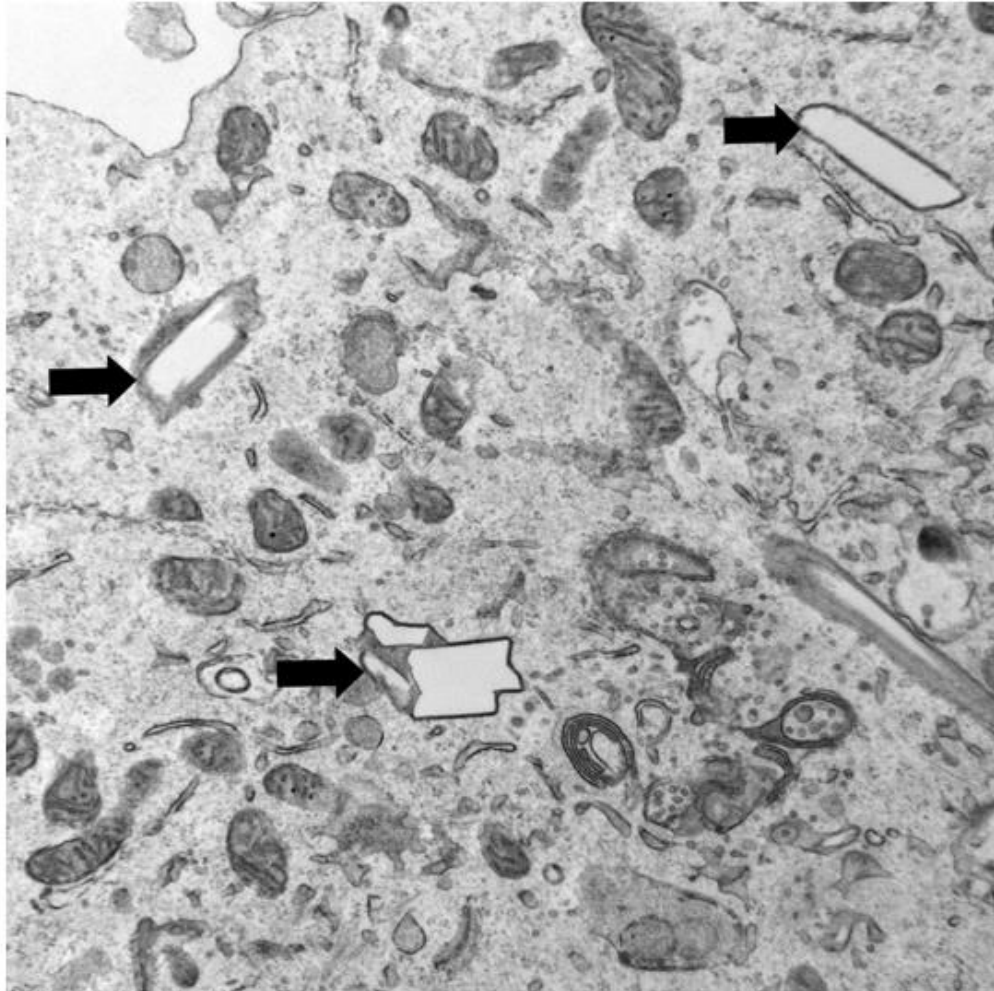
Image annotated  
File saved as V31307N\_036a  
Paul McGill  
29th June 2015



Cell containing a membrane bound crystalline inclusion (arrow)

**Appendix 4: *In vitro* assessment of cytotoxicity, morphology and pro-inflammatory mediator release of NR8383 cells treated with GSK-361 or SB-323 (continued)**

Figure 9 GSK678361A 50 µg/ml



V31307N.038.tif  
EM 43757 NR8383 cells  
GSK678361A 50 ug/ml  
Print Mag: 25700x @ 7.0 in  
14:12 06/26/15  
Microscopist: pjm41508

500 nm

HV=80.0kV

Direct Mag: 20000x

GSK UK

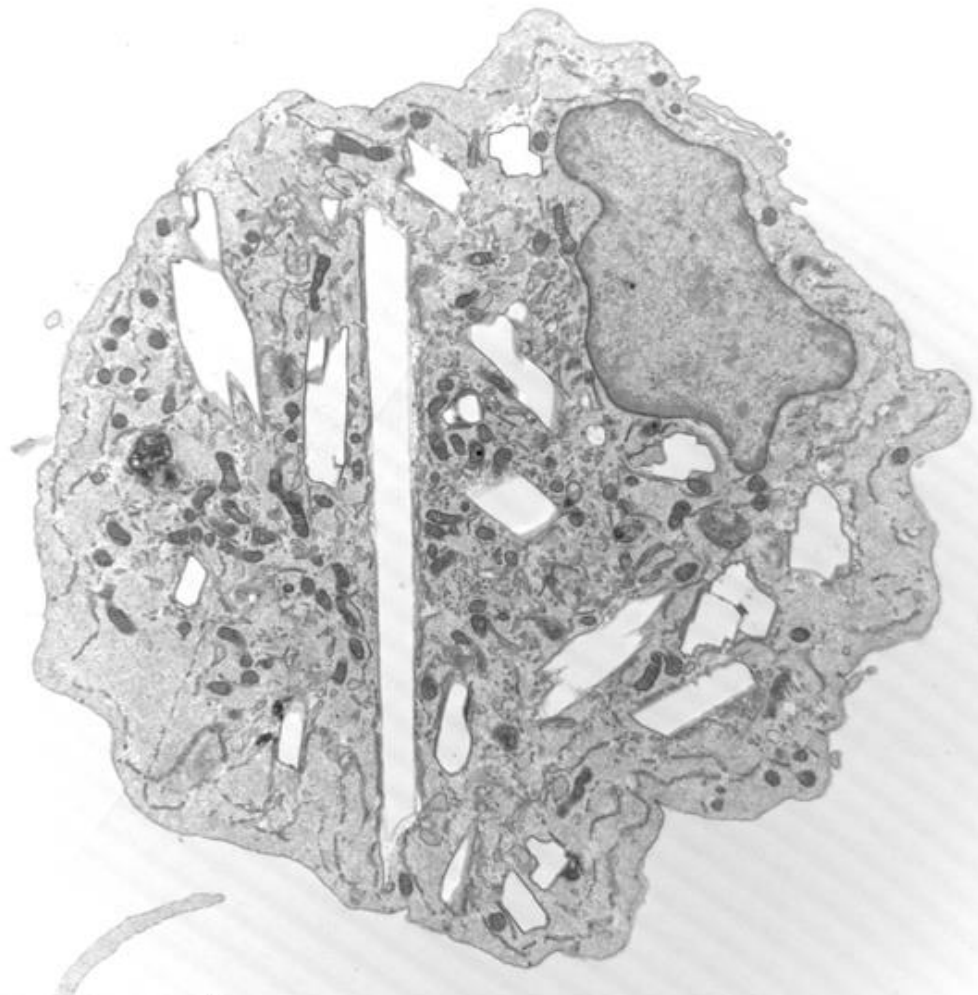
Image annotated  
File saved as V31307N\_038a  
Paul McGill  
29th June 2015



Higher magnification of crystalline inclusions (arrows) within the cell

**Appendix 4: *In vitro* assessment of cytotoxicity, morphology and pro-inflammatory mediator release of NR8383 cells treated with GSK-361 or SB-323 (continued)**

Figure 10 GSK678361A 400 µg/ml



V31307N.032.tif  
EM 43756 NR8383 cells  
GSK678361A 400 ug/ml  
Print Mag: 10300x @ 7.0 in  
13:42 06/26/15  
Microscopist: pjm41508

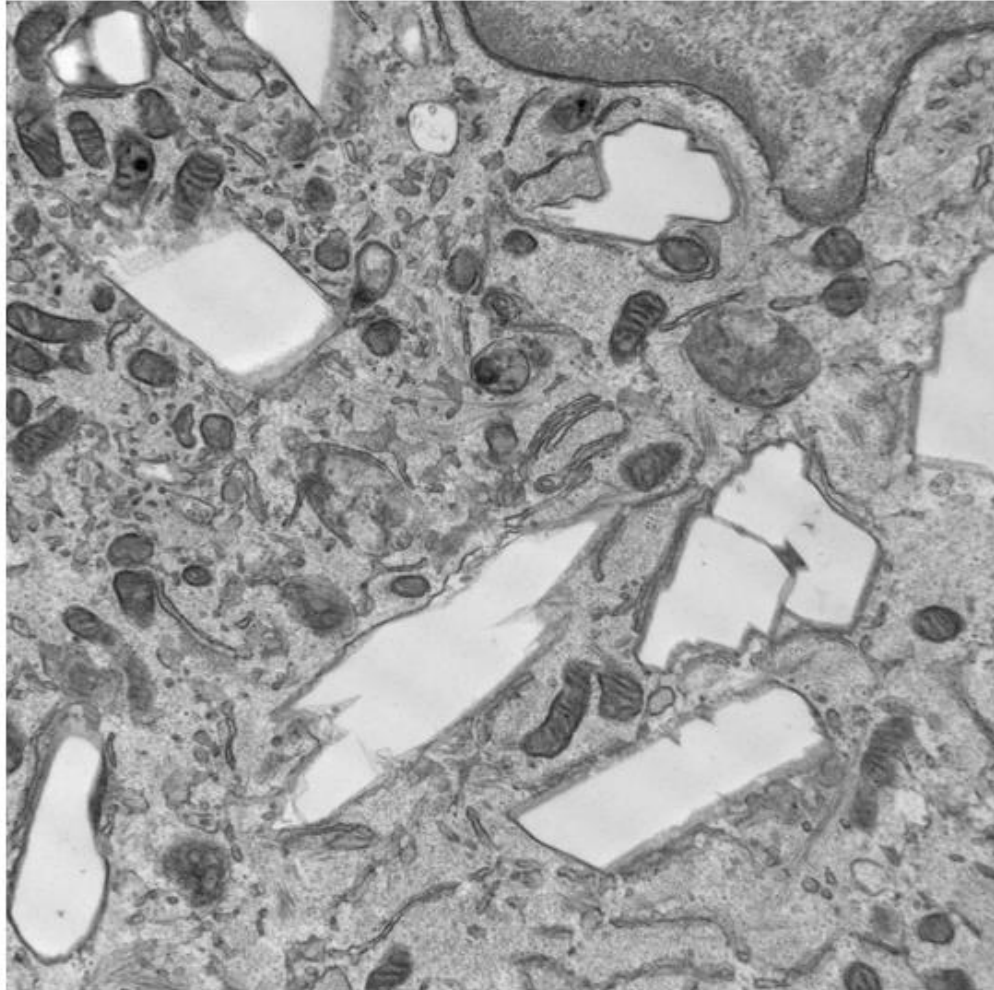
2 microns  
HV=80.0kV  
Direct Mag: 8000x  
GSK UK



Cell containing numerous crystalline inclusions

**Appendix 4: *In vitro* assessment of cytotoxicity, morphology and pro-inflammatory mediator release of NR8383 cells treated with GSK-361 or SB-323 (continued)**

Figure 11 GSK678361A 400 µg/ml



V31307N.033.tif

EM 43756 NR8383 cells

GSK678361A 400 ug/ml

Print Mag: 25700x @ 7.0 in

13:44 06/26/15

Microscopist: pjm41508

500 nm

HV=80.0kV

Direct Mag: 20000x

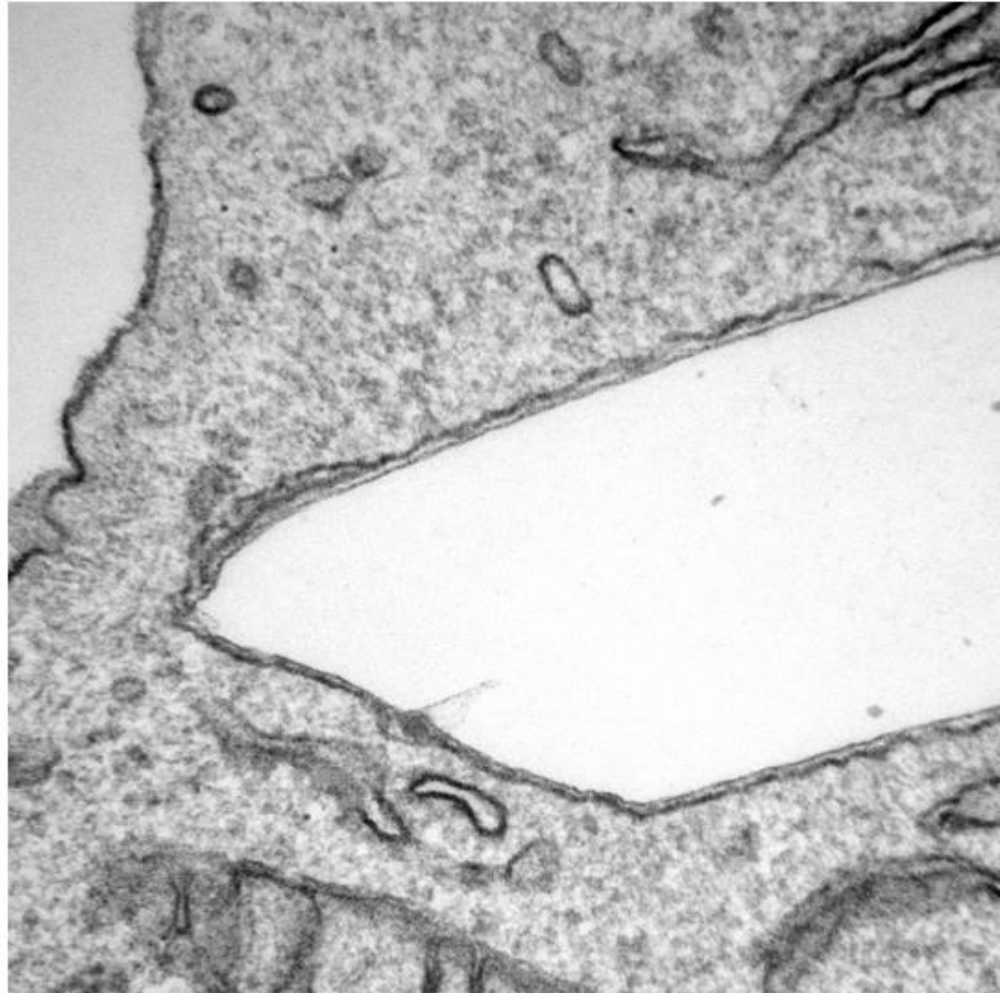
GSK UK



Higher magnification of crystalline inclusions within the cell. The mitochondria are of normal appearance.

**Appendix 4: *In vitro* assessment of cytotoxicity, morphology and pro-inflammatory mediator release of NR8383 cells treated with GSK-361 or SB-323 (continued)**

Figure 12 GSK678361A 400 µg/ml



V31307N.031.tif

EM 43756 NR8383 cells

GSK678361A 400 ug/ml

Print Mag: 103000x @ 7.0 in

13:34 06/26/15

Microscopist: pjm41508

500 nm

HV=80.0kV

Direct Mag: 80000x

GSK UK



Detail of an elongate crystalline inclusion showing that it is membrane bound.

**Appendix 5: Histopathology of the respiratory tract of rats exposed to micronised crystalline GSK-899 for 3 days**

		Incidence of observations		
Vehicle for powder dispersal		Lactose		
GSK Study Numbers		R29739		R30353N
Target dose (mg/kg/day)	Grading of observation	0 (control)	45	15
Number of rats on study		6	6	6
Initial examination		6	6	6
<b>Treatment-related findings (TRF)</b>				
Lung	NAD	3	0	0
Macrophage infiltration; interstitium; multifocal	Minimal	0	6	6
Degeneration/regeneration; bronchiole; epithelial, multifocal	Minimal	0	0	6
<b>Incidental findings (no affect of treatment)</b>				
Lung	(TRF only)			(5)
Aggregate; foamy macrophage; bronchioloalveolar	Minimal	1	0	0
Foamy alveolar macrophages	Minimal	1	1	0
Haemorrhage; alveolus; focal	Minimal	0	1	1
Hyperplasia; neuroendocrine cell; bronchiole; focal	Minimal	1	0	0
Inflammation; alveolus	Minimal	1	0	0
Lymph node, mandibular	(examined)	(2)	(0)	(2)
Cellularity increased	Minimal	0	-	1
	Mild	0	-	1
	Moderate	2	-	0

**Notes**

NAD no abnormality detected: unaffected tissues include tracheal bifurcation, lymph node (tracheobronchial)

TRF treatment-related findings

**Appendix 6: Histopathology observations in rats exposed to micronised crystalline GSK-361 for 14 days**

GSK Study No. R31034N		Incidence of observations	
Vehicle for powder dispersal		Lactose	
Target dose (mg/kg/day)	Grading of observation	5	15
Number of rats on study		4	4
Initial examination		0	4
<b>Treatment-related findings (TRF)</b>			
Lung	NAD/NTRF	1+1	1+1
Alveolar macrophages aggregate	Minimal	2	2
<b>Incidental findings (no affect of treatment)</b>			
Lung	NAD	1	1
	(TRF only)	(1)	(2)
Alveolar macrophages prominent; focal	Minimal	1	1
Haemorrhage; focal	Minimal	1	0
Larynx	NAD	-	3
Epithelial alteration; focal	Minimal	-	1
Lymph node (tracheobronchial)	NAD	-	2
	(no section)	-	(1)
Haemorrhage	Minimal	-	1
Heart	NAD	4	2
Necrosis/inflammatory cell infiltrate; multifocal	Minimal	0	2
Thymus	(examined)	-	(1 <sup>A</sup> )
Haemorrhage	Mild	-	1

**Notes**

NAD no abnormality detected: unaffected tissues include trachea, tracheal bifurcation, nasopharynx, nasal cavity; skeletal muscle

NTRF no treatment related findings

A Thymus: macroscopic abnormality (red discolouration on left lobe) seen at necropsy for one animal; tissue examined microscopically for affected animal

**Appendix 7: Systemic exposure of rats following a single subcutaneous dose of 5 mg/kg GSK-899 or GSK-677**

**Pharmacokinetic parameters (plasma) on Day 1**

Analyte	GSK-899			GSK-677		
Parameter	AUC <sub>0-t</sub> (ng.h/mL)	C <sub>max</sub> (ng/mL)	T <sub>max</sub> (h)	AUC <sub>0-t</sub> (ng.h/mL)	C <sub>max</sub> (ng/mL)	T <sub>max</sub> (h)
1 <sup>st</sup> rat	735	292	1	1260	399	0.5
2 <sup>nd</sup> rat	582	287	0.5	1630	604	1
3 <sup>rd</sup> rat	1070	366	0.5	1690	518	0.5
Mean	796	315	0.5 <sup>A</sup>	1530	507	0.5 <sup>A</sup>

**Drug concentrations in plasma (ng/mL) on Day 1**

Analyte	GSK-899			GSK-677		
Rat no.	001	002	003	004	005	006
<b>Time (h)</b>						
0.5	266	287	366	399	534	518
1	292	183	293	357	604	478
2	140	124	185	309	354	409
4	54.1	38.3	27.4	119	132	159
8	21.4	14.1	38.4	25.5	34.3	40.1
24	NQ	NQ	6.18	NQ	NQ	NQ

**Notes**

A Median T<sub>max</sub>

NQ Not quantifiable (<2.5 ng/mL)

**Appendix 8: Histopathology of injection sites in rats administered a single subcutaneous dose of GSK-899 or GSK-677**

Vehicle for dosing: 3% (v/v) Solutol HS 15 in 0.9% (w/v) aqueous sodium chloride		Incidence of observations (Study R31711N)	
Dose (mg/kg/day) <sup>A</sup>	Grading of observation	5 GSK-899	5 GSK-677
Number of rats on study		3	3
<b>Treatment-related findings (TRF)</b>			
Injection site	NAD	2	1
Necrosis; dermis; subcutis; multifocal	Mild	0	1
Inflammatory cell infiltrate; subcutis; dermis; mononuclear cell, multifocal	Mild	0	1
Inflammatory cell infiltrate; subcutis; mononuclear cell, localised	Minimal	1 <sup>B</sup>	1
<b>Procedural-related findings (injection)</b>			
Inflammatory cell infiltrate; dermis; neutrophilic, focal	Minimal	1	0
Haemorrhage; subcutis; dermis; multifocal	Minimal	0	1
Haemorrhage; subcutis; focal	Minimal	0	1

**Notes**

NAD no abnormality detected

A Animals were dosed (Day 1) and euthanized after completion of an off-dose period of four days (necropsy on Day 5)

B Observation may have been due to a combination of the needle passage, GSK-899 and/or formulation

**Appendix 9: Histopathology observations at injection sites of rats dosed subcutaneously with GSK-899 for 28 days**

Vehicle for dosing: 3% (v/v) Solutol HS 15 in 0.9% (w/v) aqueous sodium chloride		Incidence of observations (Study R31697N)							
Dose (mg/kg/day)		0 (control)				5			
Number of rats on study	Grading of observation	5 on study				6 on study			
Initial examination		5 examined				6 examined			
Injection sites (identified no. 1 to 4) <sup>A</sup>		1	2	3	4	1	2	3	4
Number of rats	Examined	5	0	1	5	6	3	3	6
	NAD	1	-	-	-	1	-	-	-
Degeneration/regeneration; panniculus muscle; focal	Minimal	1	-	0	0	3	0	0	0
	Mild	0	-	0	0	0	0	0	0
	Moderate	0	-	0	0	0	0	0	0
Degeneration/regeneration; panniculus muscle; multifocal	Minimal	0	-	0	3	0	1	2	1
	Mild	0	-	0	1	0	0	1	2
	Moderate	0	-	0	1	0	1	0	2
Inflammation; subcutis; lymphohistiocytic, multifocal	Minimal	1	-	1	3	1	0	1	0
	Mild	2	-	0	2	2	2	1	1
	Moderate	0	-	0	0	2	0	1	5
Fibroplasia; subcutis; diffuse	Minimal	2	-	0	4	2	3	1	1
	Mild	1	-	1	1	2	0	0	4
	Moderate	1	-	0	0	1	0	1	1
Degeneration; subcutis; multifocal	Minimal	3	-	0	0	0	2	0	0
	Mild	0	-	1	0	0	0	0	0
	Moderate	1	-	0	0	3	1	2	0
	Marked	0	-	0	0	1	0	1	0
Degeneration; subcutis; diffuse	Minimal	0	-	0	1	0	0	0	0
	Mild	0	-	0	2	0	0	0	1
	Moderate	0	-	0	1	0	0	0	2
	Marked	0	-	0	0	0	0	0	3
Haemorrhage; subcutis; localised	Minimal	0	-	1	2	2	2	2	4
	Mild	1	-	0	0	1	0	1	1
	Moderate	0	-	0	0	0	0	0	1
Pigmented macrophages; subcutis; focal (site 1) or multifocal (sites 2 and 4)	Minimal	0	-	0	1	2	2	0	4
	Mild	0	-	0	0	0	0	1	0
Inflammatory cell infiltrate; dermis; mononuclear cell, focal	Minimal	0	-	1	0	0	0	0	0
Granuloma; dermis; focal	Minimal	0	-	0	0	0	0	1	0

**Notes**

NAD no abnormalities detected

A Rats were dosed once daily using four sites in rotation, i.e. each site was injected 7 times with a 3-day interval between consecutive injections.

### Appendix 10: Image analysis of lung sections stained for chloroacetate esterase (new data available post submission)

**Table A1: Estimated inhaled dose of GSK-899 to achieve 50% reduction (ED<sub>50</sub>) in inflammation 4 hours after challenge of rats with LPS**

Parameter and medium	Presentation of GSK-899	ED <sub>50</sub> estimate (µg/kg) <sup>A</sup>	95% confidence interval (µg/kg)		ED <sub>50</sub> outside dose range?
			lower	upper	
CAE stain (4h) lung	crystalline	211	75.8	1046.7	No
	amorphous-1 <sup>B</sup>	15.8 x10 <sup>4</sup>	NC	NC	Yes
	amorphous-2	34.0	NC	518.1	No
	nebulised	14.7	NC	NC	No

**Notes**

A ED<sub>50</sub> values extrapolated from net data (mean value of PBS-challenged control deducted from result for LPS-challenged animal).

B ED<sub>50</sub> value 10-fold higher than dose inducing adverse lung toxicopathology after 28 days (Chapter 5).

NC Not calculable

**Table A2: Estimated inhaled dose of GSK-361 to achieve 50% reduction (ED<sub>50</sub>) in inflammation 4 hours after challenge of rats with LPS**

Parameter and medium	Presentation of GSK-361	ED <sub>50</sub> estimate (µg/kg) <sup>A</sup>	95% confidence interval (µg/kg)		ED <sub>50</sub> outside dose range?
			lower	upper	
CAE stain (4h) lung	Crystalline	60.3 x10 <sup>4</sup>	NC	NC	Yes
	Nebulised	1375	169.6	2.48 x10 <sup>12</sup>	Yes

**Notes**

A ED<sub>50</sub> values extrapolated from net data (mean value of PBS-challenged control deducted from result for LPS-challenged animal).

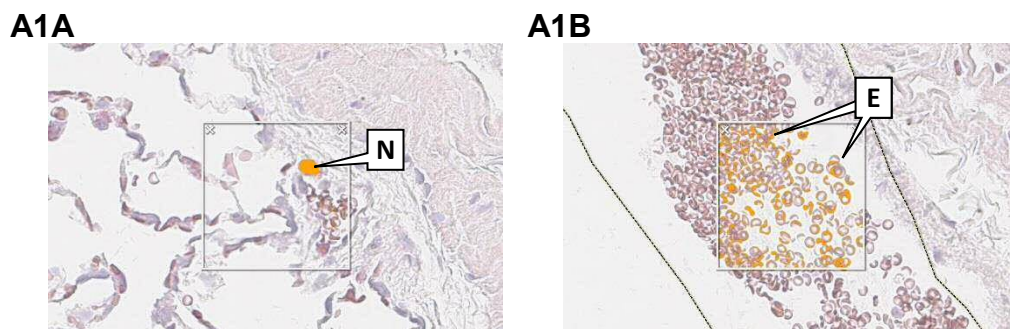
NC Not calculable

Image analysis to investigate the efficiency of bronchoalveolar lavage in harvesting neutrophils from GSK-361-treated rats was inconclusive, with no obvious dose response for inhibition of LPS-induced inflammation.

## Appendix 10: Image analysis of lung sections stained for chloroacetate esterase (continued)

### Methods: lung image analysis for CAE: Design C and D

Digitalized images of slides were imported into HALO software (version 2.1.1637.10; Indica Labs). Image analysis gave insufficient contrast to differentiate CAE-staining of neutrophils from erythrocytes (Figure A1).



**Figure A1:** Example of image analysis of rat lungs for chloroacetate esterase (CAE), a biomarker of inflammation. Rats (n=6/treatment) were administered lipopolysaccharide in phosphate buffered saline by intratracheal instillation (2  $\mu\text{g}/\text{rat}$ ; bolus). Lungs taken four hours later were fixed in 10% buffered formalin and embedded in paraffin wax. Lung sections were stained for CAE and lung tissue counterstained with haematoxylin and eosin. Colour overlays were applied to areas of interest: yellow indicated 'moderate intensity' of CAE-stain and red a 'strong intensity' of CAE-stain. The ratio of CAE-stained area to remaining tissue area was determined with exclusion of air spaces. **A1A:** lung section with CAE-stained neutrophil (N). **A1B:** lung section with erythrocytes 'stained' by CAE (E).

Three representative areas (1.5 mm square) proximal, mid and distal to a main airway were selected for quantification for each lung section (Figure A2A), avoiding clusters of erythrocytes; the first square was situated next to the most central bronchus with additional areas at 1 mm intervals. Most connective tissue (submucosa, lymphoid tissue, arteries and veins) were excluded from the region of interest using the HALO exclusion drawing tool (x3 magnification); a classifier layer ('train by example' algorithm with manual definition of pertinent or irrelevant textures or colours) was used to detect the tissue area omitting alveolar air spaces, glass and bubble artifacts (Figure A2B). Threshold intensity for detecting CAE stain was set at 0.138 (moderate) and 0.359 (strong); red-green-blue colour detection set at 0.142, 0.411 and 0.299.

## Appendix 10: Image analysis of lung sections stained for chloroacetate esterase (continued)

### A2A

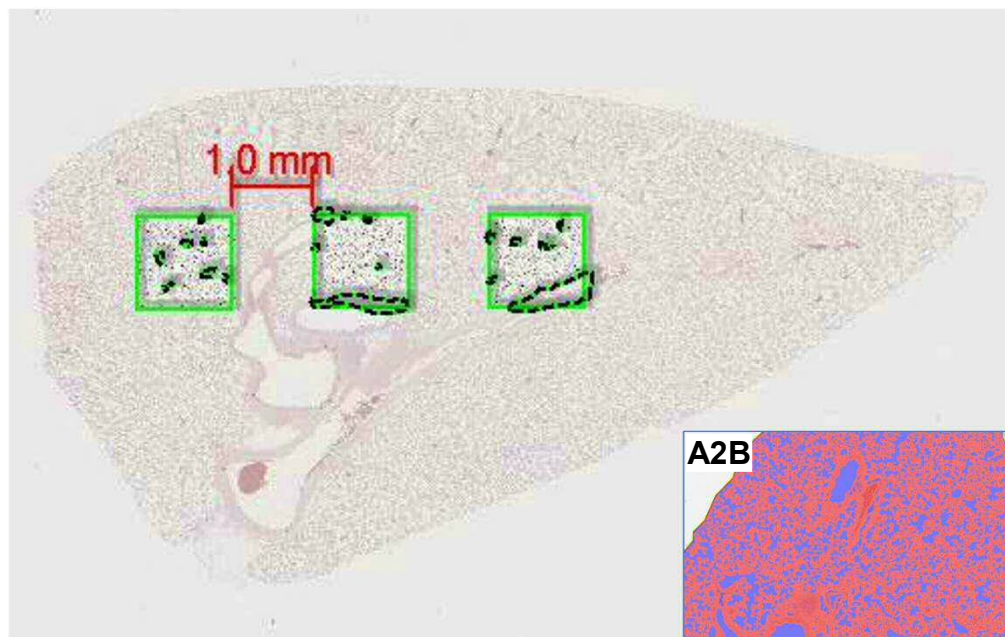


**Figure A2:** Processing of rat lung images for analysis of chloroacetate esterase (CAE), a biomarker of inflammation. Rats ( $n=6$ /treatment) were administered lipopolysaccharide in phosphate buffered saline by intratracheal instillation ( $2 \mu\text{g}/\text{rat}$ ; bolus). Formalin-fixed paraffin-embedded lungs were stained for CAE and the lung tissue counterstained with haematoxylin and eosin. A classifier layer was applied to define areas of interest. The ratio of CAE-stained area to remaining tissue (region of interest) was determined. **A2A:** definition of areas in lung section proximal, mid and distal to a main airway for quantification of CAE-staining area, relative to the evaluated region of interest. **A2B:** classifier layer applied to demarcate tissue area (pink) and exclude alveolar air spaces, glass and bubble artifacts (blue).

### Determination of 50% effective dose ( $\text{ED}_{50}$ ) for inhibition of LPS-induced lung inflammation

The baseline CAE-stain value (mean for PBS-challenged rats) was deducted from the datum for each LPS-challenged rat. Net values were plotted against  $\text{Log}_{10}$  of estimated inhaled doses of p38 MAPK inhibitor and a linear regression line was fitted. The regression line was then used to estimate the inhaled dose for a 50% response ( $\text{ED}_{50}$ ) of net mean LPS-control response and corresponding 95% confidence intervals of this estimate; analyses conducted using SAS (version 9.3).



# **ADDENDA**

**Publications and presentations**

## 1. External presentations

### 1.1. Oral presentations

Defining dosimetry & markers of exposure in inhalation drug development. *GSK Inhaled Sciences Symposium, 23-Nov-2011. Stevenage, Hertfordshire, UK.*

Influence of aerosol presentation on lung pathology changes induced in rats. *31<sup>st</sup> Annual Meeting of the British Society of Toxicological Pathology held jointly with the Association of Inhalation Toxicologists, 11-Nov-2016. Alderley Edge, Cheshire, UK. (Addendum 1)*

Head-out plethysmography and estimation of inhaled doses in rats. *31<sup>st</sup> Annual Meeting of the British Society of Toxicological Pathology held jointly with the Association of Inhalation Toxicologists, 11-Nov-2016. Alderley Edge, Cheshire, UK. (Addendum 2)*

Aerosol presentation and implications for non-clinical development of inhaled drugs. *Postgraduate Research Day, 28-Apr-2017. School of Pharmacy and Pharmaceutical Sciences, Cardiff University, UK. (Addendum 3)*

Multivariate-based selection of drugs and implications of aerosol presentation for inhalation toxicology in rats. *14<sup>th</sup> Annual Meeting of the Association of Inhalation Toxicologists, 27-Oct-2017. Copenhagen, Denmark. (Addendum 3)*

Cascade impaction data and the devil in the detail. *14<sup>th</sup> Annual Meeting of the Association of Inhalation Toxicologists, 27-Oct-2017. Copenhagen, Denmark. (Addendum 4)*

Cascade impaction data and *in silico* modelling of drug-lung deposition in rats. *Chemical Aspects of Toxicology (CHAOTIC70), 09-May-2018. Ware, Hertfordshire, UK.*

Aerosol characterisation of spray-dried constructs. *Chemical Aspects of Toxicology (CHAOTIC70), 09-May-2018. Ware, Hertfordshire, UK.*

### 1.2. Poster presentations and associated abstracts

Paul GR, Somers GI, Moore SA, Goodway RE (2012). The Capsule Based Aerosol Generator - Conserving Test Article in Small Scale Inhalation Exposures. *Respiratory Drug Delivery 2012, 2, 525-530. (Addendum 5)*

Paul GR (2015). Defining dosimetry & markers of inhaled exposure in drug development. *Society of Biology (Beds, Essex & Herts branch) early career biologist event, 29-Jun-2015. Ware, Hertfordshire, UK.*

Paul GR (2015). Inhalation dosimetry and environmental factors investigated in rats using head-out plethysmography. *12<sup>th</sup> Annual Meeting of the Association of Inhalation Toxicologists, 13-Oct-2015. Cambridge, UK.*

Paul GR, Somers GI and Taylor G (2016). Implications for Room Lighting and the Duration of Acclimation Protocols on the Dosimetry of Inhaled Drugs in Rats. *Respiratory Drug Delivery* 2016, 2, 327-332. (Addendum 6)

### **1.3. Journal articles**

Paul GR, Gumbleton M and Somers GI (2017). Effect of Conditioning on Rat Lung Function Measurements and Implications for Exposure and Dose Estimation of Inhaled Drugs. *Inhalation Magazine*. (Addendum 7)

## **2. Internal presentations for sponsor (GSK)**

### **2.1. Oral presentations**

Paul GR (2014). Permeability solubility data review: overview of non-clinical studies performed in rats to investigate pharmacokinetic profiles of 12 inhaled compounds in blood and lung. *Inhaled Sciences Forum, 26-Jun-2014. GSK R&D, Stevenage, Hertfordshire, UK.*

Paul GR (2015). Rats; inhalation dosimetry and environmental factors. *CPD event, 15-Sep-2015. GSK R&D, Ware, Hertfordshire, UK.*

Paul GR (2016). Feasibility and scale-up of spray drying to support safety studies: influence of aerosol presentation on lung exposure and pathology changes in rats. *Modelling Community Forum (Chemistry and Pharmaceutical Development), 22-Nov-2016. GSK R&D, Stevenage, Hertfordshire, UK.*

Paul GR (2017). Aerosol form and Pathology; experiences with GSK258899B in rats. *Inhaled Sciences Forum, 25-Jan-2017. GSK R&D, Stevenage, Hertfordshire, UK.*

Paul GR (2017). Head-out plethysmography and estimation of inhaled doses in rats. *Inhaled Sciences Forum, 22-Mar-2017. GSK R&D, Stevenage, Hertfordshire, UK.*

### **2.2. Abstracts**

Paul GR, 2015. Environmental factors and their implications for dosimetry of inhaled drugs in rats. *GSK 3Rs Quarterly Newsletter (Q3: September 2015); in house online publication.*

Paul GR (2016). Rat lung function, inhaled dose and refining tube restraint. *GSK 3Rs Quarterly Newsletter (Q1: March 2017); in house online publication.*

## Addendum 1

### Influence of Aerosol Presentation on Lung Pathology Changes Induced in Rats

**Graham R. Paul, GSK**

Many inhaled drugs are developed as crystalline dry powder formulations for prolonged stability and to improve clinical control of drug delivery. Pre-clinical development of inhaled drugs consumes large masses of material, relative to other dose routes. Surrogate formulations or administration routes are sometimes proposed to expedite evaluation (first time) in humans. Such strategies defer the discharging of liabilities such as altered PK/PD or tolerability of the final (particulate) formulation until later in development.

Male rats were administered GSK258899B by snout-only inhalation exposure for 28 consecutive days. The drug was presented as micronised crystals or amorphous powder blended in lactose ( $\leq 15$  mg/kg/day) or as a nebulised solution (1 mg/kg/day; limited by solubility) in 3% (v/v) Solutol HS15 in 0.9% (w/v) aqueous sodium chloride.

Dose dependent increases in severity and incidence of multifocal foamy macrophage aggregates were evident in rats administered all forms of GSK258899B, with changes in animals exposed to the crystalline aerosol form being most pronounced. This was associated with inflammatory changes characterised by minimal interstitial mononuclear inflammatory cell infiltration at amorphous doses of  $\geq 1$  mg/kg/day, and foamy macrophage degeneration/necrosis and intra-alveolar neutrophils (minimal), interstitial mononuclear inflammatory cell infiltration (mild to marked), and increased cellularity and enlargement of bronchus-associated lymphoid tissue (minimal or mild) at the crystalline dose of 15 mg/kg/day.

### **Addendum 1 (continued)**

Changes for all aerosol forms at 1 mg/kg/day were considered non-adverse. The crystalline form of GSK258899B was persistent in lung tissue and produced more severe lung changes at 15 mg/kg/day compared to the amorphous powder. Nonetheless, the changes were considered adverse for both aerosol forms at this dose and the NOAEL was not affected by changing the aerosol form.

*All animal studies were ethically reviewed and conducted in accordance with the Animals (Scientific Procedures) Act 1986 and GSK Policy on the Care, Welfare and Treatment of Animals.*

## Addendum 2

### Head-out Plethysmography and Estimation of Inhaled Doses in Rats

**Graham R. Paul, GSK**

Non-clinical studies often report 'doses' calculated using an equation to estimate respired minute volume (RMV) from bodyweight, which may overlook habituation of animals to procedures. The influence of bodyweight development and procedural conditioning on the breath frequency (BF) and minute volume (MV) of rats was investigated over a 28-day treatment period (1-hour snout-only inhalation exposure). Rats were allowed to settle in restraint tubes for 15 minutes before aerosol administration; BF and MV were measured using head-out plethysmography.

A reduction in mean BF and MV was evident during the 15-minute settling period. Animals appeared to take longer to settle when diaphragms used for maintaining a neck-seal during head-out plethysmography were omitted from restraint tubes for preceding days of aerosol administration.

Measured MV was more variable than corresponding bodyweight-derived estimates, especially for Day 1 of treatment (first exposure) or following several days of treatment when diaphragms were omitted during restraint. Omission of diaphragms for a prolonged period also resulted in lower MVs, relative to bodyweight-derived estimates. Parity of these parameters, and hence 'dose' estimates, was achieved after three days of reintroducing the diaphragms.

Results suggest a desire to minimize the degree of restraint applied to animals during inhalation exposures between days of lung function measurement needs to be weighed against a potential impact on parameters and the need for reconditioning animals.

*All animal studies were ethically reviewed and conducted in accordance with the Animals (Scientific Procedures) Act 1986 and GSK Policy on the Care, Welfare and Treatment of Animals.*

### Addendum 3

## Multivariate-based selection of drugs and implications of aerosol presentation for inhalation toxicology in rats

Graham R Paul

*GSK R&D, Park Road, Ware, Hertfordshire, SG12 0DP*

Many inhaled drugs have been developed as crystalline dry powder formulations for prolonged stability and to optimise clinical drug delivery. Inhalation exposure of animals requires large masses of drug, relative to other dose routes in pre-clinical development. Surrogate formulations or administration routes are sometimes proposed to expedite early clinical evaluation. Such strategies defer discharging of liabilities such as altered pharmacokinetics-pharmacodynamics (PK/PD) or tolerability of the final formulation until later in development. Using three compounds of common pharmacology but differing physicochemical properties, the aim of this work was to determine if altered presentation of an inhaled drug affected exposure or toxicology and hence if such shortcuts are prudent.

Rats (n=6/group) were administered GSK-899, GSK-677 or GSK-361 for up to 28 days by snout-only inhalation exposure (one hour daily) at target doses of  $\leq 15$  mg/kg/day. The compounds were administered to rats as aerosols generated from dry powder formulations of micronised crystals (all compounds) or amorphous powder (GSK-899 only) blended with lactose, or as nebulised aqueous solutions. Rats were euthanized after 28 days of treatment and the lungs were fixed in 10% buffered formalin, embedded in paraffin wax, sectioned and stained with haematoxylin and eosin for examination by light microscopy. Additional rats (n=3/group/timepoint) were exposed and the lungs taken following a single dose or 28 days of treatment for homogenisation and HPLC-MS/MS analysis of the parent compounds. Macrophages were also harvested from satellite animals (one rat per compound and aerosol form) by bronchoalveolar lavage using 0.9% (w/v) aqueous sodium chloride. The cells were fixed in 4% formaldehyde and 1% glutaraldehyde (v/v/v) in phosphate buffer, embedded in Agar 100 resin, sectioned and stained with uranyl acetate and lead citrate for examination by transmission electron microscopy.

*In vitro* dissolution rates in simulated lung fluid were relatively fast for amorphous GSK-899 and crystalline GSK-677, and relatively slow for crystalline GSK-899 and GSK-361. *In vivo*, crystalline GSK-899 (low solubility) was most persistent in rat lung tissue, with no appreciable decrease in drug-homogenate concentration at 24 hours and a 7-fold increase from Days 1 to 28. Post dose drug-lung concentrations for amorphous GSK-899, GSK-677 (crystalline and nebulised aerosols) and crystalline GSK-361 were similar and reduced at 24 hours. However, GSK-677 (most soluble) increased from Days 1 to 28 indicating a degree of accumulation. Conversely, crystalline GSK-361 was least persistent in lung tissue with no evidence of accumulation Days 1 to 28; drug-lung homogenate concentrations were lowest for nebulised GSK-361 ( $\leq 1$  mg/kg/day evaluated) and non quantifiable at 24 hours. This correlated with no GSK-361-related lung pathology. A non-adverse dose dependent increase in the severity and incidence of multifocal foamy macrophage aggregates was evident for nebulised and dry powder formulations of GSK-899 and GSK-677.

### Addendum 3 (continued)

Administration of GSK-899 at 15 mg/kg/day was also associated with adverse inflammatory changes characterised by interstitial mononuclear inflammatory cell infiltration, which was marked for the crystalline form. Transmission electron microscopy confirmed the presence of particles in macrophages harvested from rats administered amorphous or crystalline GSK-899 only.

Crystalline GSK-361, which was of low solubility but high membrane permeability *in vitro*, showed no drug-lung accumulation *in vivo* or pulmonary toxicity. Differences in dissolution rate for amorphous and crystalline GSK-899 correlated with drug-lung concentrations and a shift in the severity of lung pathology suggesting that the physical state of a drug can influence observed toxicity. However, inflammatory changes at 15 mg/kg/day were nevertheless adverse for both dry powder aerosol forms of GSK-899 and the safety margin between the no observed adverse effect level (NOAEL) and the hypothetical clinical exposure was thus unaffected. This suggests that membrane permeability may be a greater driver than *in vitro* solubility for mitigating toxicopathology when designing inhaled drugs.

*All animal studies were ethically reviewed and performed in accordance with the UK Animals (Scientific Procedures) Act 1986 and the GSK Policy on the Care, Welfare and Treatment of Animals.*

## Addendum 4

### Cascade impaction data and the devil in the detail

Graham R Paul

*GSK R&D, Park Road, Ware, Hertfordshire, SG12 0DP*

Formal guidelines for the testing of chemicals in rodents have been in place since the early 1980s. These stipulate a requirement to characterise aerosols for the particle size distribution, specifically the mass median aerodynamic diameter (MMAD) and geometric standard deviation (GSD). These parameters are commonly determined by linear regression analysis of the cumulative mass of test article collected by cascade impaction plotted against the log-transformed cut-point, assuming linearity of the data.

Samples (n=45) of dry powder and aqueous nebulised formulations of drugs collected using a Marple 296 cascade impactor illustrated that log-transformed data are often non-linear (device-specific calibrated cut points used for calculation). Whilst interpolation of two data points provides a pragmatic means of estimating the MMAD, this does not adequately describe the variability of the dataset and hence the particle size distribution. Mathematical methods of modelling a curved line to fit the non-linear data provide a means for determining MMAD. Although the Smoothed Spline method provided a means of determining the MMAD for study-specific samples, such mathematical methods are more complex and thus present challenges for the routine processing of data in preclinical studies.

*In silico* lung models can be used to predict lung deposition in various species. The drug deposition in rats was estimated using the MPPD model with reference to measured rat lung function (breath frequency and minute volume) and cascade impaction data (MMAD = 1.8 $\mu$ m; GSD = 2.0). The MPPD model predicted total lung deposition of 2.5% of the aerosol in rats, which was lower than the value published by Snipes in 1989 (7% for 2 $\mu$ m particles) and the proportion of the estimated inhaled dose of a drug measured in lung tissue by HPLC-MS/MS (11-13%). The results indicate refinement of *in silico* models and a good understanding of lung deposition through high resolution image analysis techniques are key to a holistic approach for understanding particle size distribution and implications for pulmonary exposure.

*All animal studies were ethically reviewed and performed in accordance with the UK Animals (Scientific Procedures) Act 1986 and the GSK Policy on the Care, Welfare and Treatment of Animals.*

## Addendum 5

*Respiratory Drug Delivery 2012 – Paul et al.*

---

# The Capsule Based Aerosol Generator – Conserving Test Article in Small Scale Inhalation Exposures

Graham R. Paul,<sup>1</sup> Graham I. Somers,<sup>1</sup> Simon A. Moore,<sup>2</sup>  
and Roger E. Goodway<sup>2</sup>

<sup>1</sup>*GlaxoSmithKline, Ware, Hertfordshire, UK*

<sup>2</sup>*Huntingdon Life Sciences, Alconbury, Cambridgeshire, UK*

**KEYWORDS:** capsule, actuation, powder, aerosol generator, rodents

### INTRODUCTION

Inhalation administration of powders to laboratory species is inefficient, consuming a disproportionate mass of material relative to that inhaled by test subjects. This limits the extent to which inhalation exposure is used in early drug development, where surrogate exposure routes such as intratracheal instillation are used, concurrent with preliminary inhalation toxicity studies before committing key resources in support of full development (unpublished data). GlaxoSmithKline (GSK) and Huntingdon Life Sciences (HLS) are collaborating to develop a non-commercial aerosol delivery system for 'dosing' rodents while utilizing small masses of powder. If successful, the device is expected to permit greater use of the inhaled route early in drug discovery to increase the quality of candidate drugs and reduce compound attrition precipitated by findings in later, more resource and animal intensive studies.

### METHODS

A prototype capsule-based aerosol generator (CBAG; Figure 1) was produced with design improvements including in-line (longitudinal) double piercing of restrained capsules with downward dispersal of powder by a pulse of air directed through a sealed capsule to optimize powder utilization, and dual feed of capsules to increase the actuation rate. Design advantages over commercially available devices included utilization of powder without compression and elimination of dead spaces.

Aerosol characterization trials were performed to assess the performance of the CBAG. Three compounds with markedly different physicochemical properties (soluble vs. lipophilic) were evaluated as micronized compound *per se* and as a 5% (w/w) blend in lactose; each capsule was filled with nominally 1 mg of powder.

## Addendum 5 (continued)

526

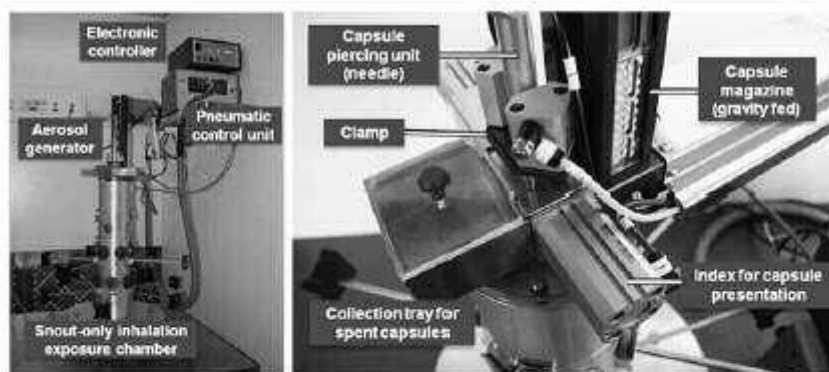
*The Capsule Based Aerosol Generator – Conserving Test Article in Small Scale... – Paul et al.*

Figure 1. The Capsule Based Aerosol Generator (CBAG) mounted on top of a flowthrough chamber for snout-only inhalation exposure of rodents.

- GSK-CMPD: 3-[8-(2,6-difluorophenyl)-2-[(1H-imidazol-2-yl methyl) amino-7-oxo-7, 8-dihydro-pyrido[2,3-D]pyrimidin-4-yl]-4-methyl-N-2-thiazolylbenzamide monomethanesulfonate
- Fluticasone propionate (FP)
- Tiotropium

In addition, FP was used to evaluate a broader range of formulations (0.01, 0.1, 1, 5, and 10% (w/w) micronized FP in lactose carrier; spray-dried FP with and without diluent excipient) and capsule fill weight (0.1, 0.3 and 1 mg FP/capsule; no lactose). Filling of HPMC capsules with 1 mg powder was automated using a Quantos dosing system; automated filling of 0.1 or 0.3 mg was not technically feasible and these fill weights were thus achieved manually.

Aerosol generation trials (normally in triplicate) were of 20 or 30 minutes duration (94 capsules actuated at 3 or 4.6 min<sup>-1</sup>); air supply and exhaust flows were balanced. Aerosols were sampled using an open faced filter holder and Marple 296 cascade impactor (2 L/min) to determine aerosol concentration and particle size distribution of parent compound (HPLC-UV analysis). The relative aerosol concentration of total particulate was monitored continuously using a real-time dust meter (qualitative analysis).

## RESULTS

Continuous monitoring of aerosol concentration indicated a distinct pulsatile delivery of powder for airflow of 10 L/min and capsule actuation rate of 3 min<sup>-1</sup> (Figure 2). The profile was characterized by peak concentrations typically 4- to 6-fold higher than baseline. Reduction of airflow (5 L/min) and accelerated actuation (4.6 min<sup>-1</sup>) softened the profile, with peak concentrations of 2- to 3-fold higher than baseline.

Aerosol concentrations of 0.07 to 119 µg/L (FP in air) were achieved by varying the proportion of FP in the formulation (Figure 3) and 20 to 119 µg/L were achieved by varying the mass of dispensed FP from 0.1 to 1 mg/capsule (Figure 4).

Addendum 5 (continued)

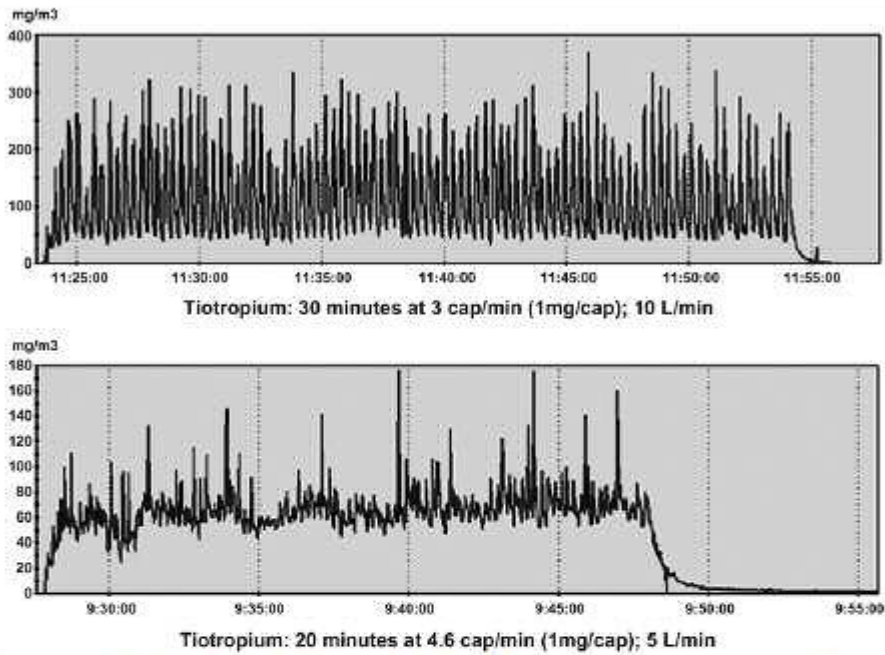


Figure 2. Mitigation of pulsatile delivery by reducing airflow and accelerating capsule actuation. Aerosol concentration was monitored using an optical particle meter.

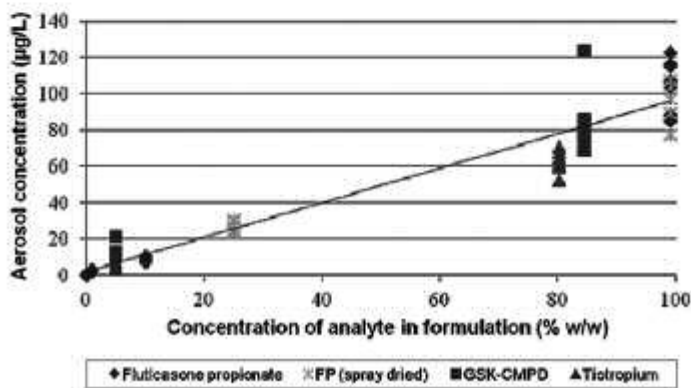


Figure 3. Aerosol concentration of analyte with a change in formulation concentration (w/w); 0.01% to 100% FP; 5% and undiluted GSK-CMPD and tiotropium.

## Addendum 5 (continued)

528

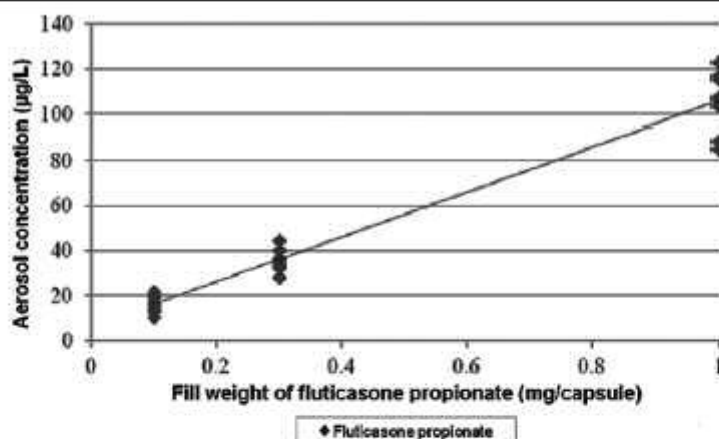
*The Capsule Based Aerosol Generator – Conserving Test Article in Small Scale... – Paul et al.*

Figure 4. Aerosol concentration of FP with a change in mass dispensed into capsules (no lactose present).

The mass median aerodynamic diameter (MMAD) for micronized GSK-CMPD, FP and tiotropium were 3.2, 4.2 and 5.0  $\mu\text{m}$  respectively. A static charge on capsules containing spray-dried FP formulations (evident by adhesion of capsules to a glass vessel) was concurrent with a higher MMAD compared with micronized FP (Table 1). No trends in particle size were evident for changes in formulation concentration or capsule loading.

Table 1.

Aerosol particle size distribution data for FP formulations  
(MMAD = mass median aerodynamic diameter; GSD = geometric standard deviation).

Formulation (1 mg/capsule)	Proportion of analyte in formulation	MMAD ( $\mu\text{m}$ )	GSD
FP-micronized	99.1%	4.8	2.59
	10%	4.1	2.40
	5%	4.2	2.41
	1%	4.9	2.65
	0.10%	3.7	2.67
	0.01%	4.5	2.87
FP-spray-dried	100%	5.8	3.33
	25%	5.6	3.00

## Addendum 5 (continued)

## CONCLUSIONS

The CBAG successfully generated aerosols from powders containing compounds with marked differences in physicochemical properties. Increases in aerosol concentration correlated with an increase in analyte concentration in formulations and the dispensed mass of powder (FP) used to fill HPMC capsules. A wide range of aerosol concentration (0.07 to 119 µg/L) was achieved by varying the proportion of analyte in the formulation in keeping with requirements for early inhalation studies. Technical limitations associated with handling low microgram quantities of powder precluded the use of undiluted drug alone to achieve lower aerosol concentrations.

The CBAG utilizes formulations without the need to compress the powder into a reservoir and its efficiency was similar to commercially available devices. However, it offers a saving in the mass of powder consumed due to elimination of dead spaces.

While early data are encouraging, further work is necessary to reduce the particle size of test aerosols in line with technical guidance (MMAD - 1 to 3 µm) pertaining to exposure of rodents for 'repeat dose' toxicity testing (1). An *in vivo* study will then be undertaken to demonstrate the suitability of the CBAG for anticipated applications.

## ACKNOWLEDGEMENTS

We would like to thank our colleagues at GlaxoSmithKline and Huntingdon Life Sciences for their logistical and technical support for development of the CBAG.

## REFERENCE

1. OECD (2009), Test No. 413: Subchronic Inhalation Toxicity: 90-day study, OECD Guidelines for the Testing of Chemicals, Section 4, OECD Publishing.

## Addendum 6

*Respiratory Drug Delivery 2016 – Paul et al.*

---

## Implications for Room Lighting and the Duration of Acclimation Protocols on the Dosimetry of Inhaled Drugs in Rats

Graham R. Paul,<sup>1</sup> Graham I. Somers,<sup>1</sup> and Glyn Taylor<sup>2</sup>

<sup>1</sup>*GlaxoSmithKline, Ware, Hertfordshire, UK*

<sup>2</sup>*School of Pharmacy and Pharmaceutical Sciences, Cardiff University, Cardiff, UK*

**KEYWORDS:** dosimetry, plethysmography, light, tube restraint, rat

### INTRODUCTION

Inhaled administration of test materials to animals has technical challenges for quantitative dosimetry. Inhaled “doses” reported in non-clinical studies are often calculated using an equation such as that of Alexander *et al.* [1] to estimate the respired minute volume (eRMV) from body weight data. This approach may overlook physiological effects on lung function associated with a formulation’s properties or habituation of animals to the “dosing” technique. Rats are insensitive to red light [2] and anecdotal data (unpublished) suggested red lighting may induce a calmer state in restrained rats. We hypothesized that the lighting color (red or white) and duration of restraint tube acclimation protocols may influence the breath frequency and minute volume of rats during inhalation exposure, representing a potential source of variability in achieved doses. Head-out plethysmography [3] was used to investigate this hypothesis concurrent with inhaled administration of an anti-inflammatory drug.

### METHODS

Male rats (CrI:WI(Han); n=8 per group; 11 weeks old) were acclimatized to restraint tubes for two or six days and administered a single inhaled “dose” (600 µg/kg; one hour exposure) of an anti-inflammatory drug under either normal fluorescent lighting or red-filtered lighting (≥600 nm). Rats were acclimatized by progressively increasing the period of tube restraint each day, up to a maximum of one hour; rats acclimatized over six days were first subjected to a neck-seal on the fourth day of tube restraint. The micronized drug, 5% (w/w) in lactose, was dispersed into a flow-through chamber using a Wright dust feed [4]. Rats were assessed for breath frequency (BF) and

## Addendum 6 (continued)

minute volume (MV) by head-out plethysmography during the snout-only inhalation exposure and euthanized immediately post-dose and sampled for drug analysis of lung homogenate (right and intermediate lobes pooled) by high performance liquid chromatography with mass spectrometry detection (HPLC-MS/MS).

For each rat, a mean BF and MV was calculated for the one hour exposure period and for five minute periods ending 5, 15, 30, 45, and 60 minutes from the start of exposure. Statistical analysis (2-way analysis of variance; ANOVA) was applied to the mean of animal-specific means pooled for acclimation periods or lighting conditions (n=16). A Latin square design was used for statistical analyses (2-way ANOVA) of acclimation period (red and white light data pooled) and lighting (two-day and six-day acclimation protocols pooled).

## RESULTS

BF and MV of rats during exposure were not affected by their illumination under red or white light. There was no statistical difference in mean values for the one hour exposure period (Tables 1 and 2), but an initial transient elevation in BF and MV was more pronounced for rats subjected to a two-day acclimatization protocol, relative to a six-day protocol (Figures 1 and 2).

Table 1.

Breath frequency (breaths/minute) of rats during a one hour inhalation exposure period.

	Acclimation <sup>A</sup>		Lighting conditions <sup>B</sup>	
	2 days	6 days	White	Red
Mean (bpm)	168.3	169.0	169.2	170.3
sd	17.9	19.2	15.7	5.93
CV	11%	11%	9%	10%
n	16	16	16	16

No differences of statistical difference (2-way ANOVA)

<sup>A</sup> Acclimation: data for white and red light pooled for statistical analysis

<sup>B</sup> Lighting: data for 2-day and 6-day acclimation protocols pooled for statistical analysis

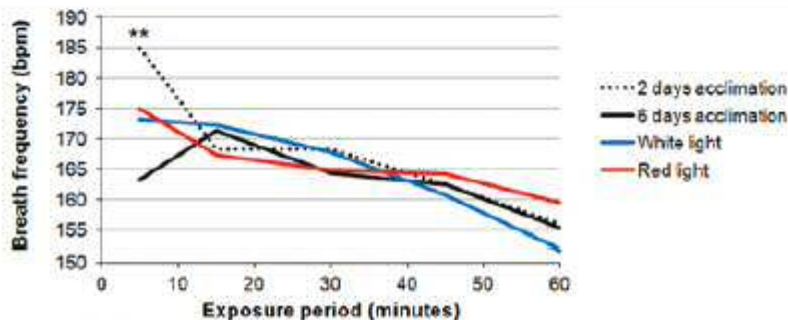


Figure 1. Breath frequency during a one hour inhalation exposure period. \*\*p<0.01 for six-day vs two-day acclimation protocols at five minutes of exposure.

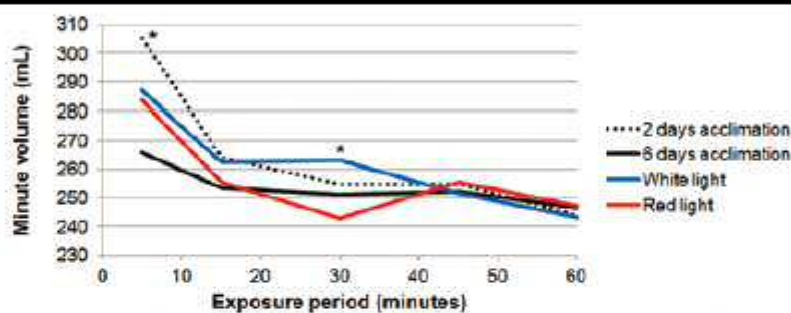
## Addendum 6 (continued)

Table 2.

Minute volume (mL) of rats during a one hour inhalation exposure period.

	Acclimation <sup>A</sup>		Lighting conditions <sup>B</sup>	
	2 days	6 days	White	Red
Mean (mL)	258.1	253.8	262.0	254.6
sd	18.4	25.2	22.2	25.4
CV	7%	10%	8%	10%
n	16	16	16	16

No differences of statistical difference (2-way ANOVA)

<sup>A</sup> Acclimation: data for white and red light pooled for statistical analysis<sup>B</sup> Lighting: data for 2-day and 6-day acclimation protocols pooled for statistical analysisFigure 2. Minute volume during a one hour inhalation exposure period. \* $p < 0.05$  for six-day vs two-day acclimation at five minutes; red vs white light at 30 minutes.

The measured MV of rats under the conditions of this study (no pre-exposure settling period) was generally higher and more variable than the body weight-derived estimate of respired minute volume (mean MV  $\approx 1.17x$  eRMV) suggesting a lack of relationship between body weight and MV, or a potential for eRMV to underestimate the "achieved inhaled dose" (Figure 3, Table 3).

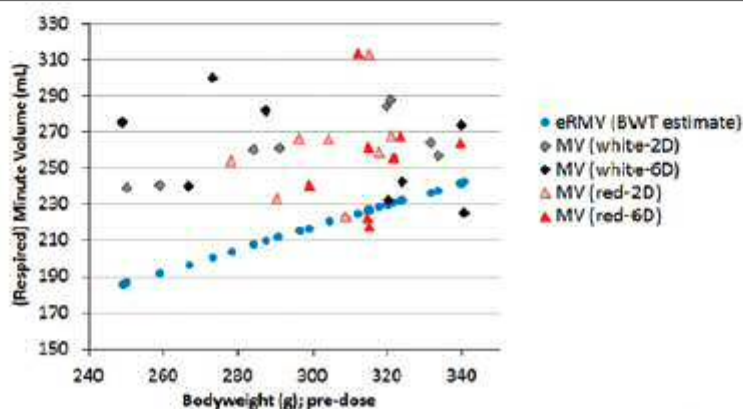


Figure 3. Comparison of the minute volume (MV; measured by head-out plethysmography) and body weight-derived respired minute volume (eRMV).

## Addendum 6 (continued)

330

*Room Lighting and the Duration of Acclimation: Impact on Rat Dosing Protocols – Paul et al.*

Table 3.

Comparison of measured and body weight-derived estimates of the minute volume (mL) of rats during a one hour inhalation exposure period.

	Respired minute volume (body weight derived estimate)	Minute volume (measured)
Mean	221	260**
sd	15.9	24.8
CV	7%	10%

\*\*MV vs eRMV;  $p < 0.01$  (2-way ANOVA)

Drug-lung homogenate concentrations (Table 4) were more variable than BF and MV. An apparent difference in lung concentrations for red versus white lighting was not corroborated by a similar trend in MV (Table 2) and hence “achieved lung dose.”

Table 4.

Lung homogenate concentrations ( $\mu\text{g/g}$ ) for groups and pooled for lighting conditions or duration of the acclimation protocol.

Pooled data	Acclimation		Lighting conditions	
	2 days	6 days	White	Red
Mean	39.0	35.2	33.5	40.7**
sd	8.19	4.69	4.75	6.81
CV	21%	13%	14%	17%
n	16	16	16	16

\*\* Red vs white light;  $p < 0.01$  (2-way ANOVA)

No statistical difference between 2-day and 6-day acclimation protocols

## CONCLUSIONS

Results of this study suggest a poor relationship between body weight and MV for relatively small numbers of animals, or a potential for body weight-derived “dose” estimates to underestimate the “achieved inhaled dose.” A more pronounced initial transient elevation of breath frequency and MV was evident for rats acclimatized for two days, which could be mitigated if animals are allowed to settle before inhalation exposure. MV and BF were unaffected by red or white lighting. Measurement of MV during non-clinical inhalation studies may refine anomalies in quantitative dosimetry, particularly if respiratory function is affected by treatment. Further work to investigate the relationship between measured MV and body weight increases of rats during repeat “dose” inhalation studies is ongoing.

## Addendum 6 (continued)

## ACKNOWLEDGEMENTS

The authors thank EMMS (UK) for loan of head-out plethysmography equipment; Charles River Edinburgh (UK; Elaine Rafferty and Steven Oag) for training in plethysmograph restraint; GSK (UK) for resourcing this work, including Mike Denham (statistical support) and Dorian Long. All animal studies were ethically reviewed and conducted in accordance with the Animals (Scientific Procedures) Act 1986 and the GSK Policy on the Care, Welfare and Treatment of Animals.

## REFERENCES

1. Alexander DJ, Collins CJ, Coombs DW, Gilkison IS, Hardy CJ, Healey G, Karantabias G, Johnson N, Karlsson A, Kilgour JD, McDonald P: Association of Inhalation Toxicologists (AIT) working party recommendation for standard delivered dose calculation and expression in non-clinical aerosol inhalation toxicology studies with pharmaceuticals. *Inhal Tox* 2008, 20: 1179-89.
2. Szel Á, Röhlich P: Two cone types of rat retina detected by anti-visual pigment antibodies, *Exp Eye Res* 1992, 55: 47-52.
3. Vijayaraghavan R, Schaper M, Thompson R, Stock MF, Alarie Y: Characteristic modifications of the breathing pattern of mice to evaluate the effects of airborne chemicals on the respiratory tract. *Arch Toxicol* 1993, 67: 478-90.
4. Wright BM: A new dust-feed mechanism. *J Sci Instrum* 1950, 27: 12-15.

## Addendum 7

AS APPEARED IN FEBRUARY 2017 Inhalation

Copyright CSC Publishing

WWW.INHAIIATIONMAG.COM

# Effect of conditioning on rat lung function measurements and implications for exposure and dose estimation of inhaled drugs

Measurement of minute volume may provide a tool for refining inhalation exposure procedures and understanding dosing anomalies or a test material's effect on dose, such as respiratory pharmacology or irritancy

**Graham R. Paul**  
GlaxoSmithKline

**Mark Gumbleton**  
School of Pharmacy and Pharmaceutical  
Sciences, Cardiff University

**Graham I. Somers**  
GlaxoSmithKline

## Introduction

Inhaled administration of substances to animals is technically challenging for quantitative dosimetry. Animals are not "dosed" *per se*, but are exposed to an atmosphere containing a test substance mixed with air. Non-clinical "doses" reported for animals inhaling such atmospheres are calculated using the following equation:

$$eID = \frac{C \times RMV \times T}{BW} \quad \dots\dots\dots \text{Equation 1}$$

where eID = estimated inhaled dose (mg/kg), C = concentration of a substance in air (mg/L), RMV = respired minute volume (L/min), T = time (minutes; duration of inhalation exposure) and BW = body weight (kg). The minute volume (MV) can be measured or estimated (eRMV) by calculation from body weight using a published algorithm such as that of Alexander, et al.<sup>1</sup>

$$eRMV = 0.608 \times BW^{0.852} \quad \dots\dots\dots \text{Equation 2}$$

Although the latter equation is derived from measurements of MV in conscious animals of relevant species (mice, rats, beagle dogs and cynomolgus monkeys) used for non-clinical research, this approach overlooks physiological effects on lung function that can be induced by a substance's properties.<sup>2,3</sup> Furthermore, MV measurements may vary due to differences in habituation of animals to procedures that also differ between species and protocols used by the 18 laboratories generating data used to derive Equation 2.<sup>1</sup>



*Snout-only inhalation exposure chamber with rat restraint tubes*

Lung-homogenate concentration data for rats attached to adjacent ports on a snout-only inhalation exposure chamber, and thus breathing from the same aerosol, can vary two- to three-fold (unpublished data). Little is known about the ways environmental factors may affect lung function and therefore inhaled dosimetry of individual animals subjected to "standard procedures" during non-clinical studies. For example, manipulation or disturbance of animals may excite them to varying degrees and the implications of this for lung dose are uncertain. In addition, rats are insensitive to red light<sup>4</sup> and anecdotal data suggested red light may induce a calmer state in restrained rats, which we hypothesized may be ascribed to rats perceiving darkness in an enclosed environment.

Plethysmography is a technique used for measuring changes in the volume of an organ or body, typically due to changes in the volume of blood<sup>5</sup> or air<sup>6</sup> contained therein. A head-out plethysmograph<sup>3,7</sup> is a vessel that encloses the body of a subject to facilitate

## Addendum 7 (continued)

Copyright CSC Publishing

lung function measurements derived from changes in ambient pressure due to changes in body volume as the subject breathes. Since the head of an animal is outside this compartment, its snout or head can be presented simultaneously to an atmosphere for inhaled administration of a test substance, e.g., aerosol, vapor or smoke.

The aims of this study were to measure MV in conscious rats using head-out plethysmography to determine:

- Whether the MV of rats subjected to a two-day acclimatization protocol was similar to that of rats acclimatized over six days;
- Whether there were differences in MV for rats acclimatized and exposed under normal fluorescent ("white") or red-filtered lighting;
- The effect of minimizing restraint on MV and, by inference, confirming requirements for reconditioning rats prior to data acquisition during repeat-dose inhalation studies;
- Whether MV correlated with body-weight-derived estimates (eRMV) and/or changes in body weight with maturation of rats over four weeks.

Results of these investigations were anticipated for refinement of restraint procedures for acclimatization and inhalation exposure of rats, to identify considerations for implementing lung function measurements during repeat-dose studies and to indicate the extent to which eRMV is representative of MV for the small group sizes of animals used in early drug development.

## Methods

### Measurement of minute volume in rats

Rats were accommodated under standard laboratory conditions<sup>8</sup> for at least five days before undertaking licensed procedures (tube restraint). MV of conscious rats was measured non-invasively using a body plethysmograph similar to that described by Glaab<sup>7</sup> but differing insofar as only the snout of the rat was presented to the test atmosphere. The animal's body was enclosed in the tube, using a rubber diaphragm to form a seal around its neck, and a sensor detected changes in pressure inside the tube as the animal breathed.

Using Boyle's law, lung function parameters derived from changes in pressure inside the body plethysmograph were captured using software that facilitated rejection of anomalous breath-wave signals ascribed to a compromised neck seal, typically during movement of animals in plethysmographs; approximately 700 to 1,000 breaths/hour were recorded for each animal. Plethysmographs were attached to a simple, flow-through design, snout-only, inhalation exposure chamber for aerosol administration.

For data analysis, a mean MV was calculated for each rat for 5-minute periods ending at minus 10 minutes (pre-dose) and/or 5, 15, 30, 45 and 60 minutes of exposure. All animal studies were ethically reviewed

and performed in accordance with the UK Animals (Scientific Procedures) Act 1986 and the GSK Policy on the Care, Welfare and Treatment of Animals.

### Estimation of minute volume from body weight

To investigate the influence of body weight on doses estimated using Equation 1, the mean minute volume was measured using head-out plethysmography and compared with an estimate of the respired minute volume calculated from the corresponding pre-dose body weight using Equation 2.<sup>1</sup>

### Experimental study designs

A preliminary study was performed to implement methodology and confirm satisfactory data capture by head-out plethysmography. Male Crl:WI(Han) rats were restrained in plethysmographs for data capture concurrent with snout-only exposure to air only. Results (unpublished data) were used to refine the design of two studies. Procedures evolved from study to study and key features are summarized in Figure 1.

A Latin square design was used to investigate the influence of lighting and duration of pre-treatment acclimatization periods on MV during inhalation exposure of rats to a dry powder aerosol;<sup>9</sup> the known pharmacology of the drug ("Compound 1") was not expected to affect lung function. Acclimatization periods of two days (applied to non-clinical studies at our laboratory) and six days (adopted by other laboratories using head-out plethysmography; unpublished communications) were investigated.

Male Crl:WI(Han) rats (4 groups; n = 8 per group; 11 weeks old) were acclimatized to plethysmographs under either normal fluorescent (white) lighting or red-filtered lighting ( $\lambda \geq 600$  nm) by progressively extending daily restraint periods over two days (20 and 40 minutes; neck seals present) or six days (20 to 60 minutes over three days without a neck seal, followed by 30 to 60 minutes over three days with a neck seal).

MV was measured during inhaled administration of a dry powder aerosol (600 µg/kg; 60 minutes) under white or red light. The micronized crystalline drug, blended 5% (w/w) in lactose, was dispersed into an inhalation exposure chamber using a Wright dust feed.<sup>10</sup> Rats were euthanized immediately post-exposure and the lungs removed (right and intermediate lobes pooled) and homogenized for drug extraction in a suitable solvent for analysis using a validated HPLC-MS/MS method.

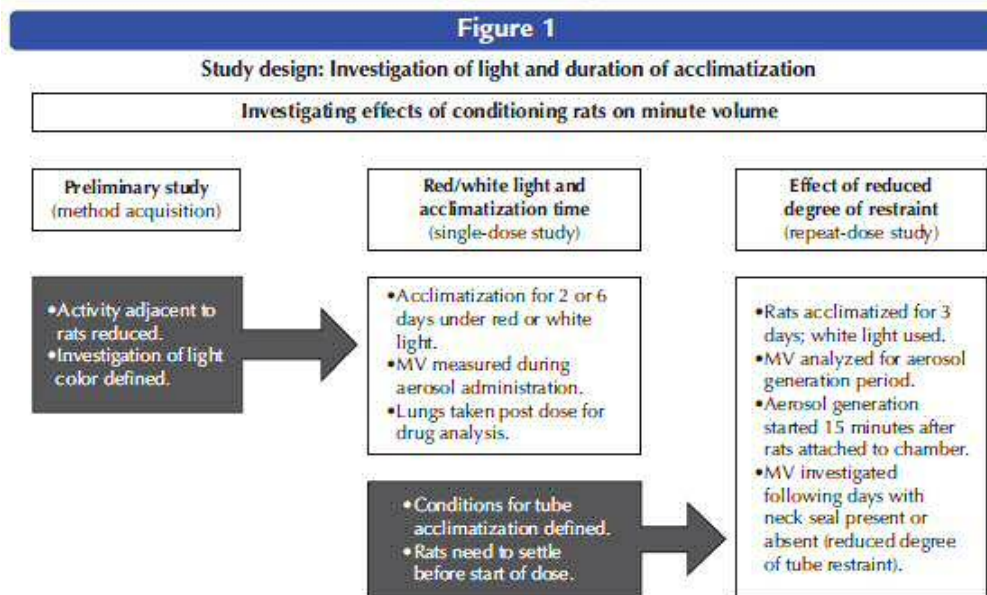
The crystalline form of Compound 1 was known to be of relatively low solubility in simulated lung fluid (unpublished *in vitro* data) and thus minimized drug/lung clearance prior to isolation of lung tissue; unpublished *in vivo* data demonstrated no appreciable decrease in drug/lung-homogenate concentrations up to 24 hours after a single inhaled dose.

Statistical analyses (two-way analysis of variance; ANOVA) was applied to individual drug/lung-homogenate concentrations and the mean MV of

## Addendum 7 (continued)

Copyright CSC Publishing

Figure 1



animal-specific mean data, which were each pooled for the acclimatization period or lighting conditions (n = 16).

#### **Study design: Investigation of restraint for repeat-dose inhalation studies**

There is an ethical desire to minimize the restraint of animals necessary to achieve the scientific objective. In view of the degree of restraint required for head-out plethysmography, a 28-day study was conducted to investigate the effect on MV measurements when neck seals were included or omitted on days of inhalation exposure preceding data capture, with a view to optimizing the degree of neck restraint when incorporating lung function measurements into repeat-dose studies.

For logistical reasons, MV was measured using satellite rats assigned to two toxicology studies, one administering a dry powder aerosol and the other a nebulized solution of the same drug ("Compound 2"). The known pharmacology of the drug (same class as Compound 1) was not expected to affect lung function parameters and no differences in MV were evident for the two aerosol forms.

Male CrI:CD(SD) rats (2 groups; n = 3 per group; 10 weeks old) were acclimatized to plethysmographs with a neck seal for three days by progressively increasing the restraint period each day from 20 to 60 minutes. Rats were exposed under normal fluorescent lighting to an atmosphere containing Compound 2. The dry powder formulation (5% crystalline drug (w/w) in lactose) was dispersed into the inhalation exposure chamber using a Wright dust feed<sup>10</sup> and solutions dispersed using an air jet nebulizer (Pari LC Sprint, Pari Pharma GmbH,

Munich, Germany). MV was measured pre-treatment (acclimatization) and Days 1, 4, 14 and 26 to 28 of treatment. On Days 5 to 13 and 15 to 25, rats were restrained without a neck seal and exposed to the test aerosol for 60 minutes.

## **Results and discussion**

### ***Effect on minute volume when rats are allowed to settle in plethysmographs***

Mean MV of rats decreased over the first 15 minutes of restraint for all experiments. Please click the link to see Figure 2, which presents representative data. It is common practice during non-clinical studies to perform visual checks on the condition of restrained animals for animal welfare reasons. Transient increases in MV were observed concurrently with this practice in the preliminary experiment or when repositioning a rat that had compromised its neck seal (unpublished data).

### ***Effects of light and acclimatization on minute volume and lung dose***

During the preliminary study, rats restrained in plethysmographs under red light appeared calmer (subjective observation) than under white light, with less soiling of fur with excreta. However, these observations were not verified by changes in MV when tested in a study designed to evaluate this.

The MV of rats was similar after illumination of restraint and exposure procedures under red or white light, with no statistical difference in mean values for the 60-minute exposure period (Table 1). Nevertheless, an initial transient elevation in MV was more pronounced for rats acclimatized over two days than six days (Figure 2).

## Addendum 7 (continued)

Copyright CSC Publishing

Table 1

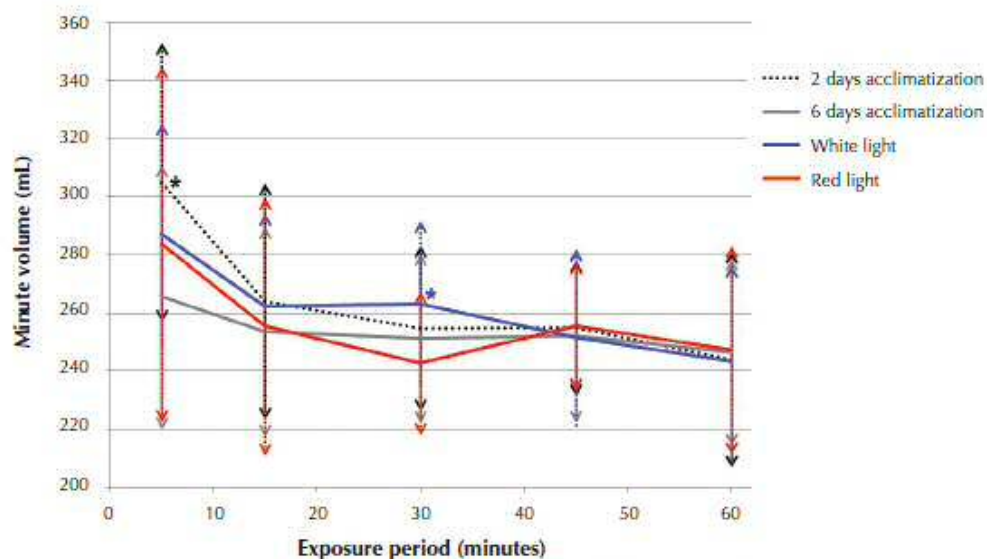
Minute volume during a single (60-minute) exposure and drug/lung-homogenate concentration post-exposure for rats acclimatized for two or six days under red or white light

Latin Square Design (data pooled)	Acclimatization <sup>A</sup>		Lighting Conditions <sup>B</sup>	
	2 Days	6 Days	White	Red
Minute volume of rats during inhalation exposure				
Mean (mL)	258.1	253.8	262	254.6
sd	18.4	25.2	22.2	25.2
CV	7%	10%	8%	10%
n	16	16	16	16
Lung-homogenate concentration after a single exposure				
Mean ( $\mu\text{g/g}$ )	39	35.2	33.5	40.7**
sd	8.19	4.69	4.75	6.81
CV	21%	13%	4%	17%
n	16	16	16	16

\*\* Red versus white light (drug/lung-homogenate concentration):  $p < 0.01$  (two-way ANOVA). Rats used for measurement of MV during inhaled administration of a crystalline drug were data-pooled ( $n = 16$ ) for statistical analysis of lighting (A) and duration of acclimatization (B).

Figure 2

Mean minute volume (with standard deviation) of rats during a single 60-minute inhalation exposure after two or six days of acclimatization under red or white light



$p < 0.05$  for six-day versus two-day acclimatization at 5 minutes; red versus white light at 30 minutes. Latin square design ( $n = 16$  per variable) with two-way ANOVA of acclimatization period (red and white light data pooled) and lighting (two- and six-day acclimatization protocols pooled).

## Addendum 7 (continued)

Copyright CSC Publishing

Drug concentrations for lungs taken immediately post-exposure (Table 1) were more variable than MV measured in the same animals and an apparent difference in lung-homogenate concentrations for red versus white lighting was in contrast to trends in MV and therefore “achieved lung dose.” Although the variability observed in lung-homogenate concentrations was not unexpected (unpublished data), the apparent differences between these data types suggest the reason for a difference in lung concentrations between rats maintained under red or white light cannot be ascribed to inter-animal differences of MV and therefore achieved lung dose *per se*. Possible explanations for discrepancies or imprecision in drug/lung-homogenate concentrations include processing of lung-homogenate samples for HPLC-UV analysis (e.g., non-uniform drug/lung deposition in conjunction with pooling selected lobes, degree of homogenization and incomplete solvent extraction of the drug).

**Effect of restraint on minute volume during repeat-dose inhalation studies**

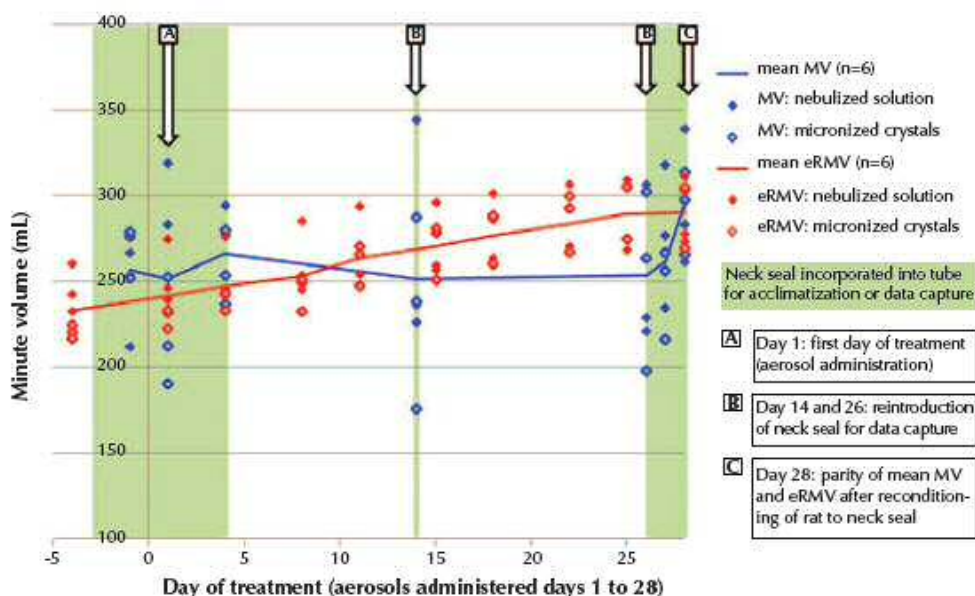
Interventions or activities near rats during inhalation exposure procedures can induce erratic increases in MV (unpublished data) and visual checks on the condition of restrained animals (routine for non-clinical inhalation safety studies) were minimized to avoid

excitation of the rats during this study. MV was most variable on Day 1, when rats were first exposed to an aerosol, and on Days 14 and 26 following a treatment period in which the neck seal was omitted from the body plethysmograph for aerosol administration (Figure 3). It is noteworthy that mean MV was similar to or slightly greater than eRMV when the neck seal was used during preceding days of restraint (pretreatment and Days 1, 4 and 28). However, with omission of the neck seal from Day 5 (excluding days of MV measurement), the mean MV decreased with an increase in eRMV (Days 14 and 26). With reintroduction of the neck seal from Day 26, the variability in measured MV progressively reduced and mean MV attained parity with eRMV (Day 28) suggesting rats may require at least two days of reacclimatization to the neck seal before the mean measured MV is representative of eRMV.

Alternatively, this raises the possibility of an observer effect, i.e., that minute volume may change as a consequence of using the neck seal to facilitate measurement of this parameter. Nirogi, et al.<sup>2</sup> published baseline minute volumes for male Wistar rats (body weight 250 to 300 g) of  $173 \pm 15.7$  mL when measured by whole body plethysmography and  $228 \pm 14.8$  mL when measured by head-out plethysmography, suggesting a potential for differences in

**Figure 3**

Minute volume (MV) and body-weight-derived estimate of respired minute volume (eRMV) in rats over a 28-day treatment period



Measured MV data are shown in blue, with corresponding body-weight-derived eRMV data in red. Mean data points are joined by a blue or red line, respectively. There was no obvious difference in MV or eRMV data for rats administered a crystalline or nebulized aerosol.

## Addendum 7 (continued)

Copyright CSC Publishing

lung function measurements between techniques with differing degrees of restraint.

#### **Relationship of measured minute volume and body weight**

There was no clear proportional relationship between body weight and measured MV of rats during a preliminary study (unpublished data) and the study examining the effect of light and acclimatization on lung function, when MV was also generally higher and considerably more variable than the body-weight-derived estimate (mean MV  $\approx 1.17 \times$  eRMV) (Figure 4). In contrast, when rats were allowed to settle in the plethysmographs for 15 minutes before the start of aerosol generation and had also been acclimatized to the neck seal in days preceding data capture, the MV and eRMV for a given body weight were similar (Figure 5) with a 23% increase in mean MV concurrent with a 30% increase in mean body weight from Days 1 to 28 of treatment.

#### **Conclusions**

This work illustrated the importance of considering the experimental design and procedural conduct for acclimatizing animals to restraint procedures and data acquisition by head-out plethysmography, a technique used for assessing lung function and estimating doses in non-clinical inhalation studies.

Key conclusions were:

- Two days of acclimatization of rats (or reacclimatization after a reduced level of restraint) to plethysmographs was sufficient to achieve parity of mean MV (measured) with mean eRMV (body-weight-derived estimate) when rats were allowed to settle for 15 minutes before initiating aerosol generation.
- There was no difference in MV for rats subjected to red or white light during acclimatization and inhalation exposure procedures.
- Minute volume (MV) measurements were more variable than corresponding body-weight-derived estimates (eRMV), especially when animals were exposed to an aerosol for the first time.

Although rats were successfully acclimatized for a 60-minute exposure period over two days, experiments requiring detection of more subtle changes in lung function (e.g., a dose response in respiratory pharmacology) may require a modified and possibly more prolonged approach for acclimatization. An ethical desire to minimize the degree of restraint applied to animals during repeat-dose inhalation studies must be weighed against a potentially deleterious effect on the precision and accuracy of lung function measurements.

These preliminary conclusions are limited by small group sizes that are nevertheless typical of those used during non-clinical studies in early drug development, where there is a desire to minimize the number of animals used. Measurement of MV during

non-clinical studies may therefore provide a tool for refining inhalation exposure procedures, understanding anomalies in quantitative lung doses and understanding potential effects on inhaled dosimetry associated with the properties of a test substance, such as respiratory pharmacology or irritancy.

#### **Acknowledgements**

The authors thank EMMS (UK) for the loan of head-out plethysmography equipment; Charles River Edinburgh (UK); Elaine Rafferty and Steven Oag for training in plethysmograph restraint and GSK R&D (UK) for resourcing this work.

#### **References**

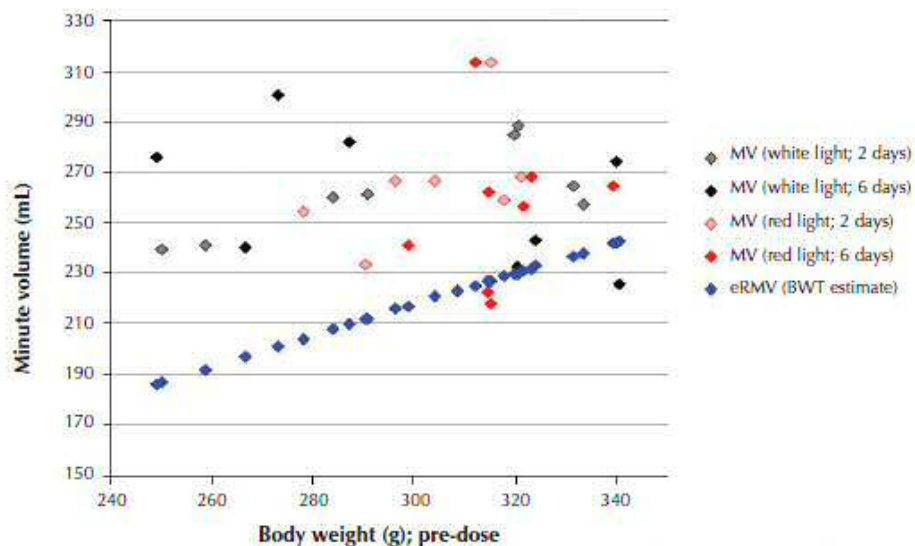
1. Alexander DJ, Collins CJ, Coombs DW, Gilkison IS, Hardy CJ, Healey G, Karantzas G, Johnson N, Karlsson A, Kilgour JD, McDonald P. Association of Inhalation Toxicologists (AIT) working party recommendation for standard delivered dose calculation and expression in non-clinical aerosol inhalation toxicology studies with pharmaceuticals. *Inhal Toxicol* 2008, 20:1179-1189.
2. Nirogi R, Shanmuganathan D, Jayarajan P, Abraham R, Kancharla B. Comparison of whole body and head out plethysmography using respiratory stimulant and depressant in conscious rats. *J Pharmacol Toxicol Methods* 2012, 65(1):37-43.
3. Vijayaraghavan R, Schaper M, Thompson R, Stock MF, Alarie Y. Characteristic modifications of the breathing pattern of mice to evaluate the effects of airborne chemicals on the respiratory tract. *Arch Toxicol* 1993, 67:478-490.
4. Széll A, Rohlich P. Two cone types of rat retina detected by anti-visual pigment antibodies. *Exp Eye Res* 1992, 55:47-52.
5. Pointel JP, Gin H, Drouin P, Vernhes G, Debry G. Venous plethysmography: Measuring techniques and normal values. *Angiology* 1981, 32:145-154.
6. Pennock BE, Cox CP, Rogers RM, Cain WA, Wells JH. A noninvasive technique for measurement of changes in specific airway resistance. *J Appl Physiol Respir Environ Exerc Physiol* 1979, 46(2):399-406.
7. Glaz T, Daser A, Braun A, Neuhaus-Steinmetz U, Fabel H, Alarie Y, Renz H. Tidal midexpiratory flow as a measure of airway hyperresponsiveness in allergic mice. *Am J Physiol Lung Cell Mol Physiol* 2001, 280:L565-L573.
8. Home Office: Code of Practice for the Housing and Care of Animals Bred, Supplied or Used for Scientific Purposes; Presented to Parliament pursuant to Section 21(5) of the Animal (Scientific Procedures) Act 1986. Stationery Office 2014, ISBN 9781474112390.
9. Paul GR, Somers CJ, Taylor G. Implications for room lighting and the duration of acclimation protocols on the dosimetry of inhaled drugs in rats. *Respiratory Drug Delivery* 2016, 2:327-332.
10. Wright BM. A new dust-feed mechanism. *J Sci Instrum* 1950, 27:12-15.

*Graham R. Paul is Investigator for Toxicology and Biometabolism, and Non-clinical Inhaled Delivery at GlaxoSmithKline, Ware, Hertfordshire, UK; Mark Gumbleton is Professor of Experimental Therapeutics and Associate Dean of Impact at the School of Pharmacy and Pharmaceutical Sciences, Cardiff University, Cardiff, UK and Graham I. Somers is Innovative Medicines Initiative Portfolio Director at GlaxoSmithKline, Stevenage, Hertfordshire, UK. Corresponding author: Graham R. Paul, GlaxoSmithKline, David Jack Centre for Research and Development, Park Road, Ware, Hertfordshire, SG12 0DP, UK, Tel.: +44 1992 502216, graham.r.paul@gsk.com. Website: www.gsk.com.*

## Addendum 7 (continued)

Figure 4

Minute volume (MV) and the body-weight-derived estimate of respired minute volume (eRMV) plotted against body weight; aerosol generation was started immediately after rats were attached to the chamber



Measured MV data were generally higher than the corresponding body-weight-derived estimates (eRMV; blue data points) irrespective of lighting color and days of acclimatization. Overall, mean MV (260 mL; sd = 24.8) was significantly higher ( $p < 0.01$ ; two-way ANOVA) than eRMV (221 mL; sd = 15.9).